

Microphotochemistry – a New Resources-Efficient Synthesis Tool Approach

PhD Thesis

Oksana Shvydkiv (M.Sc)

Supervisors:

Dr. Kieran Nolan

Dr. Michael Oelgemöller

The School of Chemical Sciences

Dublin City University

2012

The most important thing in science
is not so much to obtain new facts
as to discover new ways
of thinking about them

Sir William Bragg

I hereby certify that this material, which I now submit for assessment on the programme of study leading to the award of Doctor of Philosophy is entirely my own work, that I have exercised reasonable care to ensure that the work is original, and does not to the best of my knowledge breach any law of copyright, and has not been taken from the work of others save and to the extent that such work has been cited and acknowledged within the text of my work.

Signed: _____ ID No.: 58123351

Date: 19.10.2012

Abstract

Microphotochemistry, *i.e.* photochemistry in microstructured reactors, is a novel research area of the 21st century. It combines established techniques in organic photochemistry and continuous flow microsystem engineering with advances in light technology.

This research work aimed to develop a novel resource- and energy-efficient approach in synthetic chemistry and to demonstrate that microflow-photochemistry can serve as a compact, rapid and resource efficient R&D tool.

A series of *homogeneous* and *heterogeneous* photoreactions have been studied in microreactors to evaluate the potential of microphotochemistry. A range of acetone-sensitized photodecarboxylation reactions involving phthalimides was investigated in commercially available microreactor *dwell device* and a number of isopropanol additions to furanones were studied in newly designed within the project *LED-driven microchip*. All results were compared to analogous experiments in conventional Rayonet reactor. In all cases examined, the reactions performed in the chosen microreactors gave higher conversions or yields. This finding was explained by the generated data of light penetration, irradiated surface-to-volume ratio, energy efficiency and space-time yield. The numbers achieved for continuous flow systems were notably higher compared to the conventional setup. This finding nicely proved superiority of microphotochemistry concept.

Another commercially available device *falling film microreactor* was successfully adapted for the photooxygenation of α-terpinene and new safer methodology have been developed for the synthesis of potentially explosive endoperoxide ascaridole.

Major disadvantages of commercially available microreactors are, however, the fixed length of the reaction channel and the single-channel design. Although numbering-up can be achieved using an array of microreactors, which required significant costs investment. Flexible PTFE capillaries represent a cost-efficient alternative. Thus a simple continuous microflow *dual-capillary reactor* and its optimised version *multi-microcapillary tower* were developed. The tower design enables parallel operation of 10 experiments and it was successfully tested for reaction optimization, library synthesis and scale-up. The multi-capillary design may be easily transferred to other microflow applications such as parallel testing of biologically active compounds, process modeling, in situ analysis and combinatorial chemistry.

Consequently, micro-photochemistry may serve as a compact, rapid and resource efficient R&D tool and opens new approaches for synthetic chemistry.

Acknowledgements

It is my pleasure to thank the many people who made this thesis possible.

First of all, I would like to express my sincerest gratitude and appreciation to my PhD supervisors, Dr Kieran Nolan, from the School of Chemical Sciences in Dublin City University (Ireland) and Dr Michael Oelgemöller, from the School of Pharmacy and Molecular Sciences in James Cook University (Australia). Dr Kieran Nolan has supported me through my thesis with patience, encouragement and knowledge whilst allowing me the room to work in my own way. Dr Michael Oelgemöller showed his proficient and sophisticated support by providing regular feedback about my monthly reports and Skype meetings. His enthusiasm, inspiration and great efforts to explain things clearly and simply helped me to enjoy my research work.

Most of all I would like to thank my project manager Dr Alexander Yavorskyy, his wife Dr Oksana Yavorska and their family for the encouragement, efforts, support, understanding, advice, teaching, guidance, good company, and lots of good ideas. Their enthusiasm, passion, emotional support and 'entertainment' helped to make microphotochemistry fun for me. And a special thanks go to Dr Lidia Yavorska for belief in my capability.

I would like to acknowledge Dr Mirek Macka for giving me the chance to work on this project and Environmental Protection Agency of Ireland for funding.

My special thanks go to Timothy Sullivan and James Chapman for making my time in the lab enjoyable and unforgettable. Also, I would like to extend my warm gratitude to my colleagues and friends who accompanied me and contributed to my project, without them it would have never been the same. I would like to thank Sonia Gallagher, Kieran Joyce, Brian Murphy, Sharon Murphy, Declan Daly, Emma Coyle, Su Bee Tan, Rohitkumar Gore, Mukund Ghavre, Monika Gurbisz, Zeliha Ates, Lily He and Ana Almeida.

I am also grateful to Veronica Dobbyn, Ambrose May, Damien McGuirk, John McLoughlin, Brendan Twamley, Mary Ross, Vincent Hooper and Catherine Keogh for their technical assistance and support whenever required.

I would also like to thank Dr Patrick O'Malley for being supportive and encouraging during lab demonstrations.

I sincerely thank Dr Klaus Jähnisch for his invaluable help and professional support during this research work and for giving me the opportunity to enrich my professional experience in the laboratory of Micro Reaction Engineering at Leibniz-Institute for Catalysis in Rostock (Germany). Also, I want to thank the following people in his research group for their assistance and support during my stay: Dr Norbert Steinfeldt, Michael Sebek, Manuela Pritzkow, Dr Sandra Hübner, Anna-Maria Vogt, Dr Heike Ehrich, Dr Elka Kraleva and Hannes Alex.

My best regards go to Dr Norbert Hoffmann for being very helpful and supportive throughout the study of photoinduced addition reactions involving furanones and Dr Sylvie Lacombe for giving me the chance to visit the University of Pau and Pays de l'Adour (France) and spend three remarkable days in her laboratory. Also, I would like to thanks Dr Dmytro Korobko from the School of Pharmacy at Ternopil State Medical University for his encouragement.

This thesis would also not be possible without the understanding, love and support of my friends in Ukraine and Australia: Olena Kalushka, Olga Humnycka, Ana Karapolova, Tanja Melnyk, Olga Novakovska, Ksenia Chamula and Devagi Kanakaraju, who gave me a home away from home.

I am extremely grateful my parents Stefan and Anastasia Shvydkiv, my sister Natalia and my nephew Dmytro for supporting and encouraging me to pursue this degree. My father has never lost belief in me, he always reminded me that I could achieve anything I wanted to. He has been my guiding light and I thank him.

Oksana Shvydkiv

Table of Contents

Signature page ..... **iii**

Abstract ..... **iv**

Acknowledgements ..... **v**

Table of Contents ..... **vii**

List of Abbreviations ..... **xvii**

Chapter 1 Literature Review **1**

1.1 Introduction **2**

1.2 Microphotochemistry **3**

1.3 Photochemistry **4**

1.3.2 Principles of photochemistry 6

1.3.3 Distinctive features of photochemical reactions 9

1.4 Green chemistry **10**

1.5 Photoreactor technologies **12**

1.5.1 Conventional photochemistry 12

1.5.2 Photochemistry in microreactors 13

1.5.2.1 Microstructured reactors (MR) 15

1.5.2.1.1 Definition and special properties of MR 15

1.5.2.1.2 Microreactor technology (or Types of microreactors) 16

1.5.2.1.2.1 Glass microreactors 17

1.5.2.1.2.2 Stainless steel microreactors 18

1.5.2.1.2.3 Polymer-based microreactors 18

1.5.2.1.2.4 Silicon microreactors 20

1.5.2.1.2.5 Ceramic microreactors 20

1.5.2.1.3 Variety of reactor designs used in photochemistry and organic chemistry 20

1.5.3 Accessible light sources for photochemical reactions 20

1.5.3.1 Incandescent lamps 21

1.5.3.2 Mercury and xenon based lamps 21

1.5.3.3 Excimer lamps 22

1.5.3.4 Lasers 23

1.5.3.5 LEDs 23

Chapter 2 Photochemical model reactions in microreactors **25**

2.1 Homogeneous reactions **25**

2.1.1 Photopinacolisation 25

2.1.2 Barton reaction 26
2.1.3 Photocycloaddition reactions 27
2.1.3.1 Photochemical [2 + 2] cycloaddition of cyclohex-2-enone with vinyl acetate 27
2.1.3.2 Diastereoselective [2 + 2] photocycloaddition of a chiral cyclic enone with cyclopentene....29
2.1.3.3 Intramolecular [2 + 2] photocycloaddition of a 1-cyanonaphthalene derivative 30
2.1.3.4 Intramolecular [2 + 2] and [2 + 3] photocycloadditions of 2-(2-alkenyloxymethyl)-naphthalene-1-carbonitriles 31
2.1.3.5 Intramolecular [2 + 2] photocycloaddition of coumarin derivative ...32
2.1.3.6 Photochemical [2 + 2] cycloaddition of maleimide with 1-hexyne and intramolecular [5 + 2] photocycloaddition of 3,4-dimethyl-1-pent-4-enylpyrrole-2,5-dione 33
2.1.4 Photo dimerization of maleic anhydride....35
2.1.5 Diastereodifferentiating addition of methanol to (R)-(+)-(Z)-limonene 36
2.1.6 Continuous-flow synthesis of vitamin D_3 37
2.1.7 Photodecarboxylative benzylations of phthalimide....39
2.1.8 Photocyanation of pyrene....39
2.2 Heterogeneous reactions 40
2.2.1 Photooxygenation reactions 40
2.2.1.1 Photochemical generation and addition of singlet oxygen to α-terpinene 40
2.2.1.2 Photochemical generation and addition of singlet oxygen to cyclopentadiene....41
2.2.1.3 Photosensitized oxidation of citronellol 42
2.2.2 Photochlorination 44
2.2.2.1 Photochemical chlorination of alkylaromatics....44
2.2.2.2 Photo-radical chlorination of cycloalkanes....46
2.3 Catalytic reactions....47
2.3.1 Photocatalytic synthesis of L-pipecolinic acid 47
2.3.2 Photocatalytic *N*-alkylation of amines....48
2.3.3 Photocatalytic reduction in microreactors 50
2.4 Microphotochemistry in industry....51

2.4.1 Synthesis of 10-hydroxycamptothecin and 7-alkyl-10-hydroxycamptothec……..52
2.5 Concluding remarks.....53
3 Thesis proposal.....54
Chapter 4 Intra- and intermolecular transformations involving phthalimides ..57
4.1 Introduction.....58
4.2 Experimental set-ups.....58
4.2.1 Batch system – Rayonet reactor 58
4.2.2 Continuous flow system – dwell device 59
4.3 Model reactions and experimental results.....61
4.3.1 Intermolecular photoaddition of thioethers to N-methylphthalimide.....61
4.3.1.1 The addition of dimethyl sulphide to N-methylphthalimide.....61
4.3.1.2 The addition of ethylmethyl sulphide to N-methylphthalimide.....63
4.3.2 Intermolecular photodecarboxylative additions of carboxylates to NMP ...63
4.3.2.1 Intermolecular photodecarboxylative additions of sulphur-containing carboxylates to NMP 64
4.3.2.1.1 Procedure optimization in the batch system.....64
4.3.2.1.2 Residence time optimisation study in the batch system (Rayonet) and microsystem (Dwell device) 65
4.3.2.1.3 The efficiency of the addition reaction in Rayonet reactor operated with 5 lamps 66
4.3.2.1.4 Investigation of the effect of the sensitizer and irradiation wavelength on the reaction efficiency 67
4.3.2.1.5 Study of the N-methylphthalimide reactivity under direct excitation 69
4.3.2.1.6 The affect of the N_2 stream rate on the reaction efficiency in the batch system 69
4.3.2.2 Intermolecular photodecarboxylative addition of alkyl carboxylates to NMP 70
4.3.2.2.1 Comparison study of the reaction performance in the batch system (Rayonet) and microsystem (Dwell device) at various residence times……70
4.3.2.2.2 The effect of reagents concentration on the efficiency of addition……72
4.3.2.2.3 The DMBP sensitised PDC addition of phenylacetate to NMP..72

4.3.2.2.4 Study of PDC addition of phenylacetate to NMP under direct excitation by UVA light 73
4.3.3 Intramolecular PDC-cyclizations of phthalimide derivatives 73
4.3.3.1 Intramolecular PDC cyclization of potassium phthalimidomethylsulfanyl acetate 74
4.3.3.1.1 Reaction efficiency in the batch system (Rayonet) and microsystem (Dwell device) against to a range of residence time 74
4.3.3.1.2 Intramolecular PDC cyclization of phthalimidomethylsulfanyl acetate under DMBP sensitization 75
4.3.3.2 Intramolecular PDC cyclization of potassium phthaloyl-γ-aminobutyrate 75
4.3.3.2.1 Assessment study of the reaction efficiency in the batch system (Rayonet) and microsystem (Dwell device) at a series of residence times 76
4.3.3.2.2 Performance of the PDC cyclization of potassium phthaloyl-γ-aminobutyrate at UVA irradiation 76
4.3.4 Intramolecular PDC of phthaloyl glycine (Pht=Gly) 78
4.3.4.1 Effect of the residence time on the reaction efficiency in both systems 78
4.3.4.2 Effect of the sensitizer and irradiation wavelength on the reaction efficiency 79
4.4 Discussions 80
4.4.1 Intra- and intermolecular reactions involving phthalimides 80
4.4.1.1 Intermolecular photoaddition reactions involving phthalimides 80
4.4.1.2 Intramolecular PDC-cyclisation reactions involving phthalimide derivatives 85
4.4.2 Wavelength matching and light penetration for experiments involving phthalimides 87
4.4.3 Energy efficiencies of the used light sources in the experiments involving phthalimides 89
4.4.4 Reactors efficiencies used in the experiments involving phthalimides 90
4.5 Summary 93
Chapter 5 Highly efficient and stereoselective radical addition of secondary alcohols to electron-deficient alkenes in diverse manner experimental set-ups 94
5.1 Introduction 95
5.2 Photoinduced addition of isopropanol to 2(5*H*)-furanones 97

5.2.1 Photoinduced addition of isopropanol to 2(5*H*)-furanones in the Rayonet reactor 98
5.2.2 Photoinduced addition of isopropanol to 2(5*H*)-furanones in the Dwell device 99
5.2.3 Photoinduced addition of isopropanol to 2(5*H*)-furanones in the microchip....100
5.2.3.1 Microchip Micronit experimental set-up 101
5.2.3.2 Efficiency of photoinduced addition of isopropanol to 2(5*H*)-furanones in the microchip 102
5.2.4 Photoinduced addition of isopropanol to 2(5*H*)-furanones in the in-house made dual-capillary microreactor 103
5.2.4.1 Dual-capillary microreactor experimental set-up....104
5.2.4.2 Efficiency of photoinduced addition of isopropanol to 2(5*H*)-furanones in the dual-capillary microreactor 105
5.2.5 Comparison of the efficiency of photoinduced addition of isopropanol to 2(5*H*)-furanones in the applied experimental set-ups 108
5.3 Optimisation of photochemical processes in advanced and newly designed multi-microcapillary reactor....109
5.3.1 Multi-microcapillary tower experimental set-up....109
5.3.2 Benefits of multi-microcapillary reactor....112
5.3.2.1 Reactions residence time optimisation study 112
5.3.2.2 Reproducibility study 113
5.3.2.3 Scale-up product synthesis and energy efficiency of multi-microcapillary reactor....114
5.3.2.4 Effect of the sensitizer on the photoinduced addition of isopropanol to 2(5*H*)-furanone 84a 116
5.3.2.5 Effect of the sensitizer concentration on the photoinduced addition of isopropanol to 2(5*H*)-furanone 84a 117
5.3.2.6 Effect of the concentration of 2(5*H*)-furanone 84a on the reaction efficiency 119
5.3.2.7 Synthesis of small compound library 120
5.4 Discussions....127
5.4.1 Photosensitized addition of secondary alcohols to α,β-unsaturated esters 127
5.4.1.1 Photosensitized addition of secondary alcohols to furanones....127

5.4.1.2 Photosensitized addition of secondary alcohols to E/Z dimethyl esters of butenedioic acid 129
5.4.2 Wavelength matching and light penetration for experiments involving furanones and E/Z dimethyl esters of butenedioic acid 129
5.4.3 Irradiated area-to-volume ratio of experimental photoreactors..... 132
5.4.4 Energy efficiencies of the used light sources in the chosen experimental setups 133
5.4.5 Efficiencies of reactors used in the furanone involved experiments..... 134
5.5 Summary 136
Chapter 6 Rose bengal sensitised photooxygenation of α-terpinene – synthesis of ascaridole 137
6.1 Introduction..... 138
6.2 Falling film microreactor experimental set-up 140
6.3 Investigation of ascaridole synthesis in the falling film microreactor..... 142
6.3.1 Reaction residence time optimisation study..... 142
6.3.2 Reproducibility study..... 146
6.3.3 Effect of oxygen concentration on the ascaridole synthesis 148
6.3.4 Effect of solvent on the ascaridole synthesis 150
6.3.5 Effect of α-terpinene concentration on the ascaridole synthesis..... 151
6.3.6 Effect of rose bengal concentration on the ascaridole synthesis..... 154
6.3.7 Effect of oxygen flow rate on the ascaridole synthesis 159
6.3.8 Effect of temperature on ascaridole synthesis..... 161
6.3.9 Effect of the light source on the ascaridole synthesis..... 166
6.3.10 Stability study of the synthesised ascaridole..... 168
6.3.11 Optimised experimental procedure for ascaridole synthesis in the falling film microreactor 169
6.4 Investigation of ascaridole synthesis in the batch system 169
6.4.1 Experimental batch set-up..... 169
6.4.2 Efficiency of ascaridole synthesis in the batch set-up..... 170
6.5 Discussions..... 171
6.5.1 Rose bengal sensitised photooxygenation of α-terpinene (synthesis of ascaridole) 171
6.5.2 Wavelength matching and light penetration for the experiments of ascaridole synthesis..... 174

6.5.3 Irradiated area-to-volume ratio of experimental set-ups involved in ascaridole synthesis....176
6.5.4 Energy efficiencies of the light sources used for ascaridole synthesis in the falling film microreactor....177
6.5.5 Interfacial area of experimental set-ups involved in ascaridole synthesis.177
6.6 Summary....180
Chapter 7 Dye sensitised photooxygenation of 1,5-dihydroxynaphthalene – synthesis of Juglone....181
7.1 Introduction....182
7.2 Synthesis of Juglone in the falling film microreactor using fluorescent lamp....183
7.2.1 Experimental set-up....183
7.2.2 Efficiency of Juglone synthesis in the falling film microreactor....184
7.3 Synthesis of Juglone in the in-house made slug flow column reactor....186
7.3.1 Experimental set-up....186
7.3.2 Flow patterns in the in-house made glass column reactor....188
7.3.3 Assessment of the glass column reactor suitability for photooxygenation processes....190
7.3.3.1 Effect of solvent on the photooxygenation of 1,5-dihydroxynaphthalene....190
7.3.3.2 Effect of flow patterns on the photooxygenation of 1,5-dihydroxynaphthalene....191
7.3.3.3 Effect of sensitizer and its concentration on the photooxygenation of 1,5-dihydroxynaphthalene....192
7.3.3.4 Effect of the irradiation time and the air flow rate on the photooxygenation of 1,5-dihydroxynaphthalene....193
7.3.3.5 Optimised condition of Juglone synthesis and experimental scale-up....194
7.3.3.6 Suitability of slug flow column reactor for other photooxygenation reactions....195
7.4 Discussions....196
7.4.1 Dye-sensitised photooxygenation of 1,5-dihydroxynaphthalene (synthesis of Juglone)....196
7.4.2 Benefits of slug flow pattern for photooxygenation reactions....197

7.4.3 Wavelength matching and light penetration for the experiments in glass column reactor 197
7.4.4 Technical parameters of glass column reactor and its efficiency 198
7.6 Summary 200
8 Thesis conclusions 201
Chapter 9 Experimental 205
9.1 Chapter 4: Intra- and intermolecular transformations involving phthalimides 207
9.1.1 General procedure (GP-1) for the photoaddition of thioethers to N-methylphthalimide under batch conditions (Rayonet) 208
9.1.2 General procedure (GP-2) for photoaddition of thioethers to N-methylphthalimide in the dwell-microreactor 209
9.1.3 General procedure (GP-3) for photodecarboxylative additions of sulphur containing and alkyl carboxylates to N-methylphthalimide under batch conditions (Rayonet) 212
9.1.4 General procedure (GP-4) for photodecarboxylative additions of potassium 2-(methylthio) acetate or phenylacetate to N-methylphthalimide in the dwell-microreactor 217
9.1.5 General procedure (GP-5) for photodecarboxylative addition of potassium 2-(methylthio) acetate or phenylacetate to N-methylphthalimide under DMBP or 4-CBPH sensitisation in the batch system (Rayonet) 219
9.1.6 General procedure (GP-6) for photodecarboxylative addition of potassium 2-(methylthio) acetate or phenylacetate to N-methylphthalimide under DMBP sensitisation in the dwell-microreactor 221
9.1.7 General procedure (GP-7) for photodecarboxylative cyclizations of phthalimidomethylsulfanyl acetate and phthaloyl-γ-aminobutyrate under batch conditions (Rayonet) 234
9.1.8 General procedure (GP-8) for photodecarboxylative cyclizations of phthalimidomethylsulfanyl acetate and phthaloyl-γ-aminobutyrate in the dwell-microreactor 236
9.1.9 General procedure (GP-9) for photodecarboxylative cyclizations of phthalimidomethylsulfanyl acetate and phthaloyl-γ-aminobutyrate under DMBP or 4-CBPH sensitisation in the batch system (Rayonet) 238

9.1.10 General procedure (GP-10) for photodecarboxylative cyclizations of phthalimidomethylsulfanyl acetate and phthaloyl-γ-aminobutyrate under DMBP sensitisation in the dwell-microreactor 239
9.1.11 General procedure (GP-11) for α-photodecarboxylation of phthaloyl glycine under batch conditions (Rayonet) 246
9.1.12 General procedure (GP-12) for α-photodecarboxylation of phthaloyl glycine in the dwell-microreactor 248
9.2 Chapter 5: Highly efficient and stereoselective radical addition of secondary alcohols to electron-deficient alkenes in diverse manner experimental set-ups 253
9.2.1 General procedure (GP-13) for photosensitized addition of isopropanol to furanones 84a-c under batch conditions (Rayonet) 256
9.2.2 General procedure (GP-14) for photosensitized addition of isopropanol to furanones 84a-c in the dwell-microreactor 262
9.2.3 General procedure (GP-15) for photosensitized addition of isopropanol to furanones 84a-c in the LED-microchip 264
9.2.4 General procedure (GP-16) for photosensitized addition of isopropanol to furanones 84a-c in the dual-capillary microreactor 267
9.2.5 General procedure (GP-17) for photosensitized addition of secondary alcohols to furanones 84a-c and α,β-unsaturated esters 91a,b in the multi-capillary reactor 271
9.3 Chapter 6: Rose bengal sensitised photooxygenation of α-terpinene – synthesis of ascaridole 294
9.3.1 General procedure (GP-18) for rose bengal sensitised photooxygenation of α-terpinene 39 (synthesis of ascaridole 40) in the falling film microreactor 296
9.3.1.1 Details of the GC analytical method for products analysis of ascaridole synthesis 298
9.3.1.2 Analytical data of *1-methyl-4-(propan-2-yl)-2,3-dioxabicyclo[2.2.2]-oct-5-ene* (ascaridole 40) 301
9.3.2 General procedure (GP-19) for rose bengal sensitised photooxygenation of α-terpinene 39 (synthesis of ascaridole 40) in the falling film microreactor 310
9.3.3 General procedure (GP-20) for rose bengal sensitised photooxygenation of α-terpinene 39 (synthesis of ascaridole 40) in the conventional Schlenk flask 319
9.4 Chapter 7: Dye sensitised photooxygenation of 1,5-dihydroxynaphthalene – synthesis of Juglone 321

9.4.1 General procedure (GP-21) for rose bengal sensitised photooxygenation of 1,5-dihydroxynaphthalene 98 (synthesis of Juglone 99) in the falling film microreactor.....323
9.4.2 General procedure (GP-22) for rose bengal sensitised photooxygenation of 1,5-dihydroxynaphthalene 98 (synthesis of Juglone 99) in the slug flow column reactor 326
10 References.....340
Appendix 363

List of Abbreviations

%	percent
∅	diameter
Δ	heat
°C	degree Celsius
^{13}C-NMR	carbon nuclear magnetic resonance
1Cl-TDI	1-chloromethyl-2,4-diisocyanatobenzene
^{1}H-NMR	proton nuclear magnetic resonance
$^{1}O_2$	singlet oxygen
4-CBPH	4-Carboxybenzophenone
5Cl-TDI	toluene-5-chloro-2,4-diisocyanate
A	absorbance
Å	angstrom
AHPCS	allylhydridopolycarbosilane
BET	back electron transfer
c	concentration
C_2D_6CO	deuterated acetone
ca.	calculated
CBTA	cyclobutane tetracarboxylic dianhydride
$CDCl_3$	deuterated Chloroform
cGMP	current Good Manufacturing Practice
CH_2Cl_2	Chloroform
CH_3CN	acetonitrile
cm	centimeter
CO_2	carbon dioxide
conc.	concentrated
D	depth
DCB	1,4-dicyanobenzene
DCM	dichloromethane
DCU	Dublin City University
dd	doublet of a doublet
ddd	doublet of a doublet of a doublet
DHN	1,5-dihydroxynaphthalene
DMBP	4,4'-dimethoxybenzophenone

DMF	Dimethylformamide
DMSO	Dimethyl sulfoxide
DMSO-d_6	deuterated dimethyl sulphoxide
E	energy
e.e.	enantiomeric excess
e.g.	exempli gratia
EA	ethyl acetate
E_{ox}	oxidation potential
E_T (M)	triplet energy of the substrate
E_T (Z)	triplet energy of the sensitizer
et al.	and others
ET	electron transfer
etc	et cetera
eV	electrovolts
F	fluorescence
FEP	Fluorinated ethylene propylene
FFMR	Falling Film Microreactor
FFMR-cyl	Cylindrical Falling Film Microreactor
Fig.	figure
g	gram
g/mol	gram per mole
GC	Gas chromatography
GC-MS	Gas chromatography–mass spectrometry
GP	general procedure
H	height
h	hour
h	Planck's constant (in J·s)
H_2O	distilled water
H_2SO_4	sulphuric acid
$H_{arom.}$	aromatic proton
Hg	mercury
$H_{olef.}$	olefinic proton
HPLC	High-performance liquid chromatography
hrs	hour(s)
hv	photon's energy

i.e.	id est
IC	internal conversion
ID	inner diameter
IMM	Institut für Mikrotechnik in Mainz
IMTEK	Institut für Mikrosystemtechnik
IR	infrared
ISC	intersystem crossing
IUPAC	International Union of Pure and Applied Chemistry
J	coupling constant
K	Kelvin
K_2CO_3	potassium carbonate
kcal	kilocalories
kg	kilogram
kJ	kilojoules
Kr	krypton
kW	kilowatt
L	length
L	liter
L	pathlength
LED	Light Emitting Diode
Log	logarithm
L-PCA	L-pipecolinic acid
LTF	GmbH Little Things Factory *Gesellschaft mit beschränkter Haftung* (*company with limited liability*)
m	meter
M	molarities, i.e. mol L^{-1}
m	multiplet
M	substrate
M_0	ground state of the substrate molecule
m^2	square meter
m^3	cubic meter
max	maximum
MB	methylene blue
mbar	milibar
m-CR	multi-microcapillary reactor

MeCN	acetonitrile
Mfg	manufacturing
mg	milligram
$MgSO_4$	magnesium sulphate
MHz	megahertz
min	minute
MJ	megajoules
ml	milliliter
mm	millimeter
mmol	millimole
mol	mole
MR	Microstructured Reactor
mV	milivolt
mW	miliwatt
N	normality
n.r.	no reaction
N_2	nitrogen gas
NaCl	sodium chloride
nm	nanometres
NMP	N-methylphthalimide
NMR	nuclear magnetic resonance
No	number
n_R	amount of NMP or its derivative converted within the reactor volume
OD	outer diameter
OLED	Organic Light Emitting Diode
OS	Oksana Shvydkiv
P	phosphorescence
PC	Personal computer
PDC	photodecarboxylation
PDMS	poly(dimethylsiloxane)
PEEK	Polyether ether ketone
PET	Photoinduced Electron Transfer
Ph	phenyl
Pht=Gly	phthaloyl glycine

Pic.	Picture
PMMA	poly(methylmethacrylate)
ppm	parts per million
PROPHIS	parabolic trough-facility for organic photochemical syntheses in sunlight
PS	polystyrene
PTFE	Polytetrafluoroethylene
PVSZ	polyvinylsilazane
P_λ	transmitted radiation
P_λ^0	radiation
q	quartet
R	relaxation
R&D	Research and Development
RB	rose bengal
Ref.	reference
s	second
S	selectivity
s	singlet
S	singlet state
S^*	exited state of the molecule
S_0	ground singlet state of the molecule
S_0	ground state of the molecule
S_1	excited singlet state of the molecule
SCE	saturated calomel electrode
SET	single electron transfer
SG	Sonia Gallagher
SOC	Spin Orbit Coupling
STY	space-time yield
t	irradiation time
T	transmittance
t	triplet
T	triplet state
T_1	excited triplet state of the molecule
TDI	toluene-2,4-diisocyanate
THF	Tetrahydrofuran

TLC	Thin layer chromatography
TMC	titania-modified microchannel chip
UV	ultraviolet
UVA	Ultraviolet A, long wave, or black light
UVB	Ultraviolet B or medium wave
v	Frequency (in Hz)
VIS	visible
Vol-%	volume percent
V_R	reactor volume
vs.	versus
VUV	vacuum ultraviolet
W	Walt
W	watt
W	width
wt	weight
X	conversion
Z	sensitizer
Z_0	ground state of the sensitizer
Z_T	triplet state of the sensitizer
ε	molar absorption coefficient
λ	wavelength
µl	microliter
µm	micrometers
µmol	micromole
µ-TAS	Micro-Total Analytical Systems
π	pi
σ	sigma
Φ	photon efficiency
Φ	quantum yield

Chapter 1

Literature Review

1.1 Introduction

During the last two decades the development and application of new technologies directed to decrease environmental pollution significantly increased in all research areas. Organic chemistry is one of the main hazardous waste manufacturers as it forms the basis for pharmaceuticals, cosmetics, surfactants and agricultural products. It is estimated that between 25 and 100 kg waste are generated for every 1 kg of active pharmaceutical product manufactured.[1] Moreover every large-scale industrial process consumes vast amounts of energy and fossil fuels.[2] Consequently, the chemical industry is facing an unprecedented challenge. To survive, a sharp reduction in pollutant and greenhouse gas emissions must occur without harming the markets for its products. To reach this aim, innovative procedures have to be employed to change both the methods and the technology used throughout the production cycle.

Therefore, microtechnology has received a great deal of attention. The application of microtechnology has rapidly grown in many areas, such as electronics and engineering. The development of microstructured devices for chemical reactions was introduced only within the last ten years.

Miniaturisation of chemical reactors offers many fundamental and practical advantages of relevance to the pharmaceutical and fine chemicals industry. The industry is constantly searching for controllable, information rich, high throughput and environmentally friendly methods of producing products with a high degree of chemical selectivity. Indeed, for pharmaceutical companies an informatics-based approach, that microreactor chemistry can uniquely deliver, may be the trigger for a step change in processes. Also, the possibility of preparing chemicals in the required volume at point of use neglects the need to store and transport hazardous materials.

Since light is regarded as clean reagent in organic synthesis of new bioactive compounds and natural products photochemical procedures could serve as desirable synthetic methods compared to existing thermal copartners.

This report explores how miniaturisation may revolutionise photochemical synthesis, as a novel chemical technology and process in which the reactions generally produces the desired product in higher yield and purity, in shorter periods of time, compared with traditional batch reactions. In addition, the performance of photoreactions in micro reactors is subsequently highlighted regarding their environmental significance compared with traditional techniques.

1.2 Microphotochemistry

Microphotochemistry is a novel research area of the 21st century that arises from significant progress in chemical synthesis based on micro- and nanotechnologies. Interest in miniaturisation increased in all areas of science, technology and engineering due to the general tendency for greener industrial and academic research processes. Therefore, even 'molecular microreactors' such as nanoparticles[3], zeolites[4], dendrimers[5], capsules[6] and micelles[7] found widespread application in the screening of drugs and pharmacokinetic investigations of bioactive compounds. In chemistry, miniaturisation is especially linked to the analytical terms "Lab-on-a-chip" and "Micro-Total Analytical Systems (μ-TAS)."[8]

Microphotochemistry combines established techniques in organic photochemistry and continuous flow microsystem engineering with advances in LED technology (Figure 1). Also it can be consider as an environmentally conscious methodology that contributes to the rapidly expanding field of Green Chemistry, by reducing the volume of waste, improving energy efficiency and product selectivity.

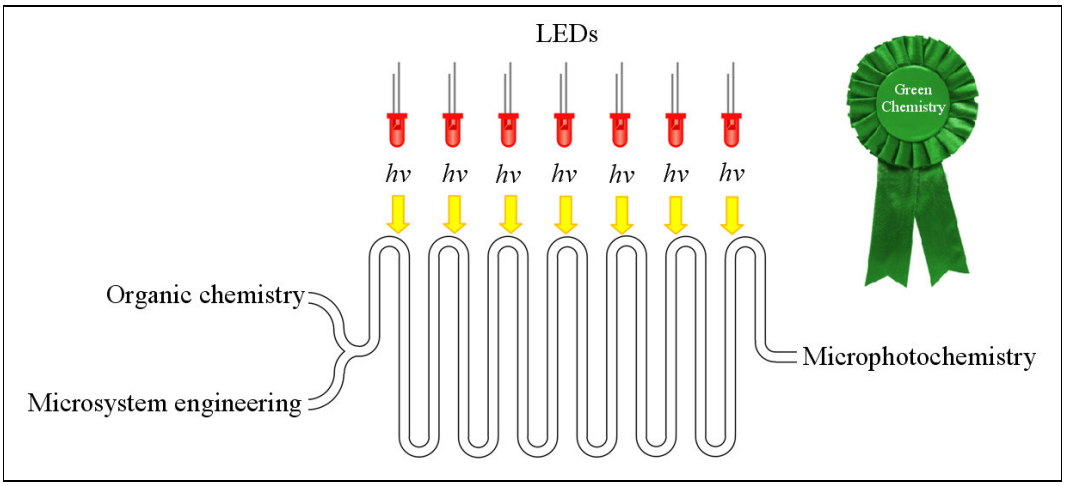


Figure 1: The concept of microphotochemistry – organic chemistry meets microsystem engineering

Microphotochemistry as a multidisciplinary subject is an important tool for some process sciences. It opens new resource- and energy-efficient approaches in synthetic chemistry. In the engineering of microreactors, photochemical processes are used as model reactions to optimise operational design. An important application of the LED-based micro-photoreactor technology is envisaged in modern R&D practice, in particular within the pharmaceutical industry. The device is small, resource-efficient,

easy to operate and should act in accordance with all cGMP-guidelines (current good manufacturing practice).

Recently, interdisciplinary research became more and more essential and photochemistry became a perfect example as a powerful bridge between chemistry, physics and biology, between material science, life science and synthesis.

1.3 Photochemistry

1.3.1 From photosynthesis in plant leaves to pilot plant production

The first photochemical reaction probably occurred billions of years ago, before life began on Earth. High-energy solar radiation evidently was an important factor in the development of large molecules, polymers and polypeptides from natural atmospheric resources such as methane, ammonia, and hydrogen. However, from a human perspective, the greatest photochemical breakthrough occurred when the first few quanta of light were absorbed by plant chlorophyll, resulting in the release of molecular oxygen to the atmosphere (Scheme 1), thus paving the way for all higher life:

$$n\mathrm{H_2O} + n\mathrm{CO_2} + \text{light absorber} \xrightarrow{h\nu} (\mathrm{CH_2O})n + n\mathrm{O_2}$$

Scheme 1: Simplified photosynthesis reaction[9]

Considering the importance of photochemistry in nature, it is surprising that it commenced "within laboratories" only in the eighteenth century. One of the first photochemical reactions noted in a laboratory was Scheele's observation of the blackening of silver halide salts in sunlight (in 1775). The other photochemical process discovered was bleaching of coloured materials. In 1834 Trommsdorf described other photochemical reactions. He observed that crystals of the compound α-santonin when exposed to sunlight turned yellow and burst. Isolated investigations of light effects on environmental processes continued within the eighteenth and nineteenth century.[10] The development of photochemistry laws and quantum theory in the early twentieth century increased the interest of chemists in photochemical transformations. This is demonstrated by the reported work of Ciacomo Ciamician,[11] Alexander Schönberg,[12] Günther Otto Schenck[13] and many others.[14]

The International Congress of Applied Chemistry in New York in 1912 was the starting point of official communication about photochemistry. At this congress Ciamician, who is considered as the father of photochemistry, realizing the enormous potential of photochemistry as a key component of future industry, predicted: *"On the arid lands*

there will spring up industrial colonies without smoke and without smokestacks; forests of glass tubes will extend over the plains, and glass buildings will rise everywhere; inside of these will take place the photochemical processes that hitherto have been the guarded secret of the plants, but that will have been mastered by human industry which will know how to make them even more abundant fruit than nature, for nature is not in a hurry and mankind is."[15]

At that time all photochemical reactions were carried out in sunlight. However, solar energy is not evenly distributed over the surface of the earth. That was the main limiting factor for a widespread use of this young research area consequently photochemical research was concentrated in privileged regions such as Italy, Egypt, Spain and Germany. As a result, interest in synthetic photochemistry decreased and studies on the subject remained rare for many years.

The first prosperity period in photochemistry was in the fifties and sixties of the 20th century. It is related to the development of the Woodward-Hoffmann rules and the reactivity potential of electronic excited states of molecules. Numerous light-induced reactions were discovered, modified and applied to synthetic problems. However up to 1995, only about 1% of the procedures and reactions in organic syntheses and in organic reactions dealt with photochemistry.[16]

A new revival of photochemistry occurred within the last twenty years due to the technological development of convenient and efficient high-intensity light sources. Consequently a reaction that fifty years ago might have taken weeks of illumination with sunlight to obtain a yield of product large enough to characterize could now be achieved in the laboratory in a few hours on a rainy day. Of equal importance in the burgeoning of this field has been the development of new reactors for photochemical reactions. A recent review by Hoffmann briefly summarizes the progress in synthetic organic photochemistry since the beginning of the 21st century.[17] This review, together with recently published books,[18–20] demonstrates that organic photochemistry is an evolving and lively topic, with much research into new biologically active compounds and reaction methodology.

A range of photochemical reactions have been carried out in microreactors and continuous flow devices to date.[21] This new principle – chemical synthesis in microreactors instead of round bottom flask – has promising opportunities for large-scale industrial syntheses as a more efficient, selective, controllable, adaptable and greener process.

Thus, microphotochemistry could be an important component of the future "industrial colonies" as predicted by Ciacomo Ciamician.

1.3.2 Principles of photochemistry

According to the IUPAC recommendations published in 1996,[22] photochemistry is "the branch of chemistry concerned with the chemical effects of light"; it studies chemical reactions, isomerisation and physical behaviour that may occur under the influence of electromagnetic radiation.

Two fundamental principles form the basis of understanding photochemical transformations:

- The first law of photochemistry, the Grotthuss-Draper law, states that light must be absorbed by a compound in order for a photochemical reaction to take place.
- The second law of photochemistry, the Stark-Einstein law or "photoequivalence law" states that for each photon of light absorbed by a chemical system, only one molecule is activated for subsequent reaction.

Normally a reaction occurs when a molecule gains the necessary activation energy to undergo changes. In the case of photochemical reactions light provides this energy. Max Planck theorized that energy was transferred in portions known as quanta and equal to *hv*. The interaction of a substrate molecule with light, where S_o is the ground state and S^* is the exited state of the molecule, can be seen below (Figure 2).

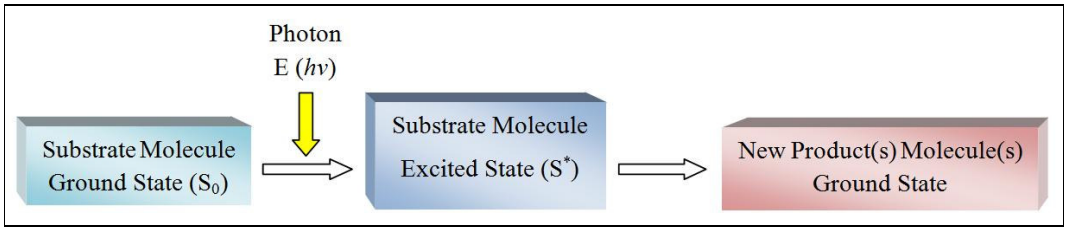


Figure 2: Electronic states in photochemical reactions

Absorption of visible and ultraviolet light (Figure 3) by a molecule introduces energy sufficient to break or reorganize covalent bonds. From the relationship $E = hc / \lambda$, it is clear that longer wavelength visible light (400 to 800 nm) is less energetic (293 to 167 kJ/mol) than light in the accessible shorter wavelength (200 to 400 nm) and near ultraviolet regions (628 to 293 kJ/mol). Consequently, ultraviolet light is most often used to induce photochemical changes.

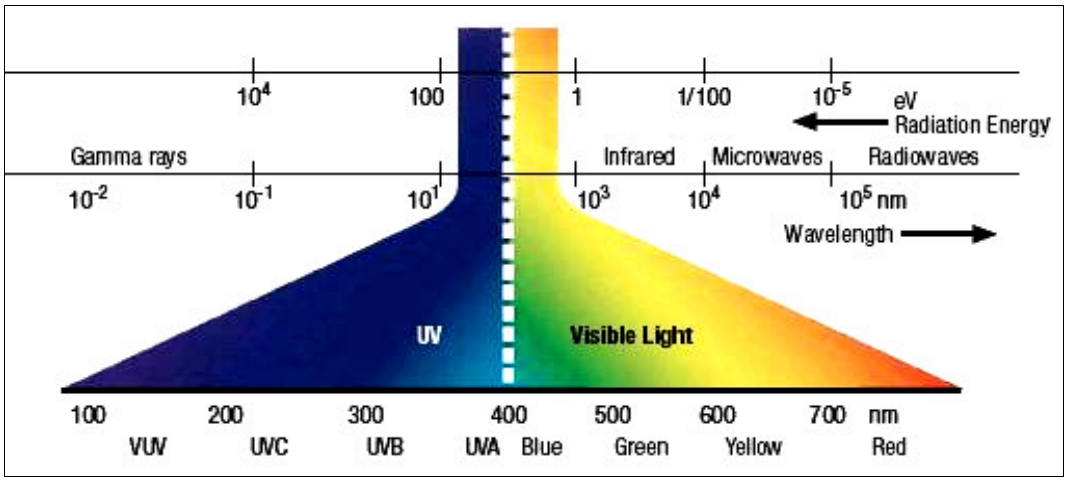


Figure 3: Electromagnetic spectrum[23]

A molecule is in its ground state (S_o, singlet state) before photon absorption. After photoexcitation the molecule is elevated to a state of higher energy, an excited singlet state (S_1), or after intersystem crossing (ISC) a triplet state (T_1), that is accompanied by electronic configuration changes. In the excited singlet state the electron spins are paired whereas in the triplet excited state it is parallel (Figure 4).

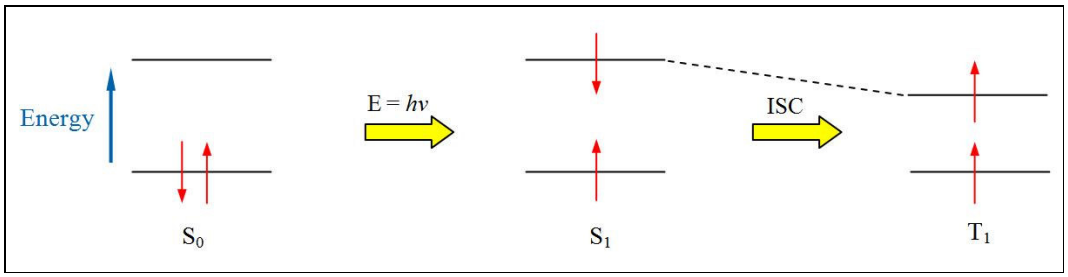


Figure 4: Singlet and triplet excited states

After excitation has occurred, there are a number of pathways which are important in the deactivation of the excited states.[24] The Jablonski diagram shown below (Figure 5) illustrates a few of these processes:

1. Emission of light and return to the ground state. If the photon emission occurs between states of the same spin state (*e.g.* $S_1 \rightarrow S_0$) this is called fluorescence. If the spin states of the initial and final energy levels are different (*e.g.* $T_1 \rightarrow S_0$), the emission is called phosphorescence. Phosphorescence occurs at a longer wavelength (lower energy). The lifetimes of fluorescent states are very short ($1 * 10^{-6}$ to 10^{-9} seconds), whereas those of phosphorescence are significantly longer ($1 * 10^{-3}$ seconds to minutes or even hours).

2. Nonradiative deactivation. There are three significant radiationless deactivation processes: Internal conversion (IC), Intersystem crossing (ISC) and vibrational relaxation. Internal conversion is a nonradiative transition between energy states of the same spin state (comparable with fluorescence as a radiative process). It takes place rapidly with loss of heat ($1*10^{-11}$ to 10^{-14} seconds). Intersystem crossing is a radiationless transition between different spin states (comparable to phosphorescence). It is slower than internal conversion ($1*10^{-6}$ to 10^{-11} seconds). Intersystem crossing allows the excited singlet state to reach the lower energy triplet state by spin inversion. Via this mechanism a triplet state can be populated indirectly. The lifetime of the triplet state is usually high as $T_1 \rightarrow S_0$ is forbidden.[25] Vibrational relaxation is the most common of the three nonradiative deactivation processes. It usually occurs very rapidly ($1 * 10^{-10}$ to 10^{-12} seconds) and brings the molecule into the new energy minimum structure for the excited state. Energy is released to the solvent.

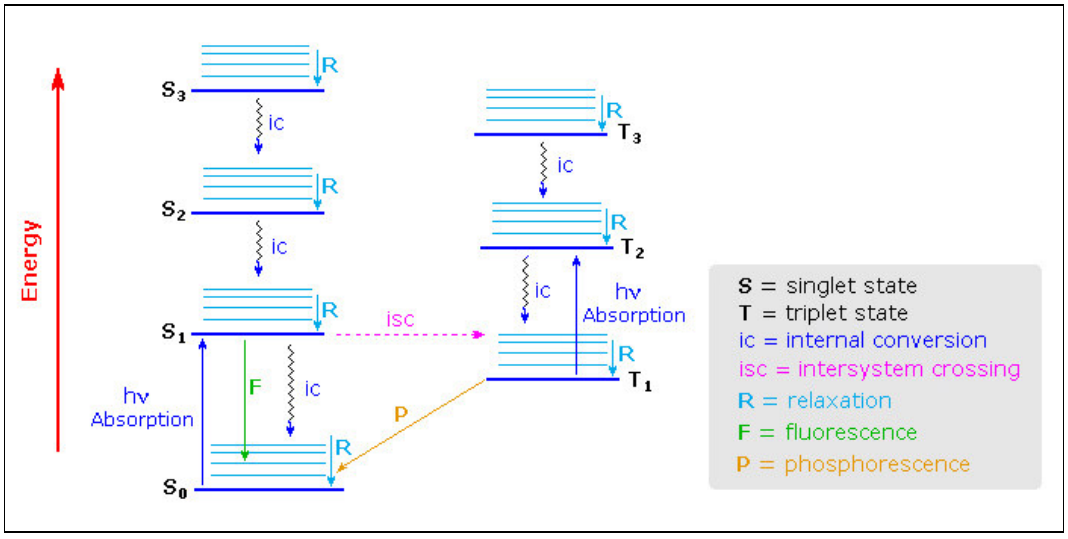


Figure 5: Simplified Jablonski Diagram

3. Quenching of the exited state. Energy is transferred to another molecule in the form of vibrations or rotations. This happens through collision of an excited molecule with another 'particle' in the reaction media. The main quenching component in liquid samples is solvent molecules. This effect could be reduced in photochemical transformations where acetone is used as both solvent and sensitizer. “Quenching” is a very important process for photochemical reactions when intersystem crossing of the substrate is inefficient. In this case the formation of the substrate triplet excited state is possible by energy transfer from a higher triplet excited state of a suitable sensitizer (catalyst) molecule. This collisional process is termed triplet sensitization and opens an

indirect route for $S_0 \rightarrow T_1$. The triplet energy of the sensitizer (donor) must be higher than that of the substrate (acceptor), i.e. E_T (Z) > E_T (M). Spin conservation requires that spin exchange take place during the collisional energy transfer. Thus, a sensitizer triplet (Z_T), generated from sensitizer molecule (Z_0), reacts with a ground state substrate molecule (M_0) as shown in Figure 6. The ideal sensitizer (Z) absorbs light preferentially with respect to the substrate (M), and undergoes efficient intersystem crossing to a triplet excited state (T_1). This energetic state then serves to activate a substrate molecule to a lower energy triplet state by collisional exothermic energy and spin exchange, returning the sensitizer to its ground state. A variety of useful sensitizers have been identified. A typical sensitizer used in this thesis, 4,4'-dimethoxybenzophenone (DMBP), has triplet energy 69.4 kcal/mol[26] and forms T_1 very efficiently with ISC of ~100%.

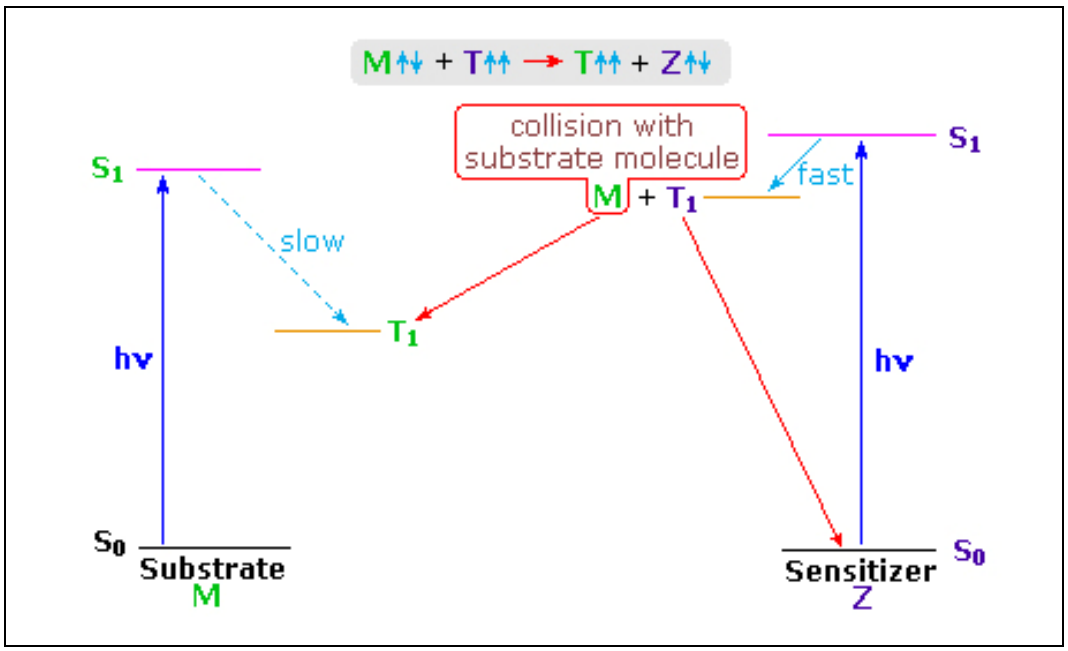


Figure 6: Triplet sensitisation process

1.3.3 Distinctive features of photochemical reactions

Absorption of a photon by an organic molecule yields an electronically excited state, which is a starting point for subsequent reaction steps. In this excited state one electron occupies a higher-energy orbital, rather than the lowest-energy orbital available to it, and the overall energy of the molecule is higher than in the ground state. The electronically excited state is a distinct species, with a given lifetime and with physical and chemical properties that differ from those of the ground state.[27]

Electronically excited states of organic molecules are essential for synthetic photochemistry. Furthermore, photoinduced electron transfer (PET) is capable of activating organic substrates by one-electron oxidation or reduction and thus, in optimal cases, singlet excited states are available to direct photon excitation, triplet states by triplet sensitization (or via rapid and efficient ISC from the corresponding excited singlet), radical anions by PET with an appropriate donor (e.g., an amine or thioether), and radical cations by PET with an appropriate acceptor (e.g., cyanoaromatics or pyrylium salts). Reactivity options are thus quintupled when compared to ground-state reactivity. Therefore, photochemistry means in many cases a multiplication of reactivity options, i.e. in addition to the ground state, the electronically excited singlets and triplets show different chemical behaviour and often differ so remarkably that they behave as completely new molecules. If not used, however, they simply disappear by radiative or non-radiative pathways in the dark (a key principle also of green chemistry).[16]

The attractive features of photochemical reactions are:

1. high atom economy;
2. relatively low cost, because no other reagents other than photons are needed;[28]
3. complex organic molecules can be produced from simple starting materials, in many cases without catalysts or additional reagents;
4. photochemically reacting organic compounds do not require any protecting groups;
5. using monochromatic light sources and chiral media or chiral sensitizer asymmetric syntheses (enantioselective catalysis) of organic molecules can be performed.[29] During the last decade highly chemo-, regio-, diastereo- as well as enantioselective reactions have been developed.[16,17]

1.4 Green chemistry

Green chemistry is the design philosophy of chemical research and engineering that aims to reduce or eliminate negative environmental impacts resulting from use and generation of hazardous substances. This concept is described in the 12 principles of Green Chemistry developed by Anastas and Warner.[30] As a chemical philosophy, green chemistry applies to organic chemistry, inorganic chemistry, biochemistry, analytical chemistry and physical chemistry. Photochemistry (chemical discipline) that uses a renewable and clean "reagent"- light, can serve as a chemical model in green chemistry.

Photochemical syntheses in microstructured devices[31] additionally matches the guideline set forth by the Institute for Green Chemistry and US Environmental Protection Agency within their capabilities (Table 1).

Table 1: Reaction and process parameters of photochemical synthesis in microstructured reactors match Green Chemistry principles

No	Green Chemistry principle	Environmental significances of Micro-photochemistry
1	Prevent waste	Less chemical and consequently waste volumes due to small scales; precise control minimizes off-spec production
2	Design safer chemicals and products	A photon is regarded as clean and traceless reagent; control with a "flick of a switch"
3	Design less hazardous chemical syntheses	Photooxidation reactions avoid the usage of hazardous and commonly toxic oxidants; photo-induced transformation often offers a greener pathway than their "dark" counterparts
4	Use renewable feedstock	Photochemical synthesis may involve renewable feedstock, e.g. α-terpinene or amino acids
5	Use catalysts, not stoichiometric reagents	Sensitised reactions use catalytic amounts of "photocatalyst" (sensitizer)
6	Avoid chemical derivatives	The course and thus selectivity can be controlled through the excited state of the chromophore, i.e. singlet vs. triplet state. The short residence time within the microchannel (flow through) avoid undesired side reactions or decompositions
7	Maximize atom economy	Most photochemical reactions show high atom economy
8	Use safer solvents and reaction conditions	Process parameters such as pressure, temperature, residence time, flow rate are more easily controlled in small volumes
9	Increase energy efficiency	Microreactors provide higher spatial illumination homogeneity and better light penetration through reaction media. Low energy LEDs may be employed as miniaturised light sources
10	Design chemicals and products to degrade after use	Excited states quickly deactivate in the dark
11	Analyze in real time to prevent pollution	The continuous flow design allows online UV- or IR-monitoring
12	Minimize the potential for accidents	Hazardous, toxic or potentially explosive products are kept in a confined space and on small scales

1.5 Photoreactor technologies

There are 2 main parts to a photochemical set-up: the reaction vessel or reactor and the light source.

1.5.1 Conventional photochemistry

In conventional photochemistry either immersion well reactors or Rayonet chamber reactors (Figure 7) are commonly used. Low-, medium- or high pressure mercury lamps are used as light sources in Immersion well reactors to provide sufficient energy for the reaction solution. In the Rayonet reactor 16 fluorescent lamps are used for this purpose. In the Rayonet reactor, reactions are carried out in test tubes or Schlenk flasks (made from Pyrex glass or Quartz) equipped with cooling finger (or cooler). The total volume of such reaction vessels is up to 1 L and is fixed.

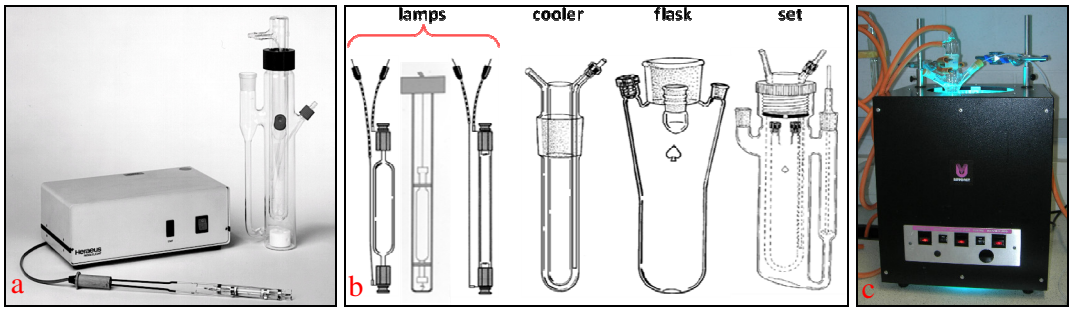


Figure 7: a) Immersion well reactor; b) Main parts of Immersion Well reactor; c) Rayonet reactor with Schlenck-flask

The traditional setups are examples of batch systems, and they have some undesired disadvantages:

- complete light absorption within a narrow layer of the reaction solution. High dilution of reactants is required to reduce this effect;
- limited application for large-scale photochemical synthesis. The photochemistry occurs most effectively in the places nearest to the light source and therefore, the amount of solution that can be effectively irradiated by the lamp is scale dependent.
- electrical losses due to the generation of heat. It is necessary to use water or air fans for cooling during reactor operation.
- emission of numerous wavelengths or broad emission (± 50 nm) at chosen wavelengths. Optical filters can be applied to overcome this effect, but this reduces energy efficiency further.

- limited lifetime of lamps (~2,000 h). As a consequent significant costs for installation are necessary.
- The photochemical process cannot be automated and follow-up reactions are possible. As an example formation of polymer films and iron deposits on/in immersion well.

1.5.2 Photochemistry in microreactors

The disadvantages of the above mentioned conventional reactors can be overcome by carrying out photochemical reactions in micro-reactors or microchips (Figure 8) equipped with high power LEDs as monochromatic miniaturised light sources. The advantages of photochemical synthesis in microdimensioned reaction vessels was first discussed by Porter and Volman.[32]

All devices presented in Figure 8 are commercially available. There are two main reactor types: serpentine channel reactors (Fig. 8: a, b, c, e) and falling film reactors (Fig. 8d). In those reactors the photochemical reaction takes place in tiny channels that ensure extensive penetration of light even for relatively concentrated solutions. The main feature of the serpentine reactor is its long path length, which may range from several centimetres to a meter or more. The longer path length can be used to increase residence time, and is therefore well suited to reactions in which a longer reaction time is needed. A multi-lane microreactor can be used for this purpose and also for scale-up assembly.

The falling film reactor is another commercially available design; where scale-up can be achieved as well using cylindrical reactor models (Fig. 8d) or larger channel plates. These devices are specifically designed for gas-liquid reactions. Over the last ten years oxidation,[33] chlorination,[34] fluorination,[35] and ozonolysis[36] reactions have been successfully performed in falling film microreactors. The central element of this microstructured reactor is the reaction plate on which parallel microchannels with widths from 100 up to 1200 µm and depths from 100 up to 600 µm are arranged. In those channels the liquid phase generates thin falling films that move by gravity force. The high interfacial area (up to 20 000 m^2/m^3) enables sufficient saturation of the film with reactant gas, that is moving over the liquid phase. This reactor type is thus more efficient than closed channel devices, which require presaturation of the reaction mixture with reagent gas.

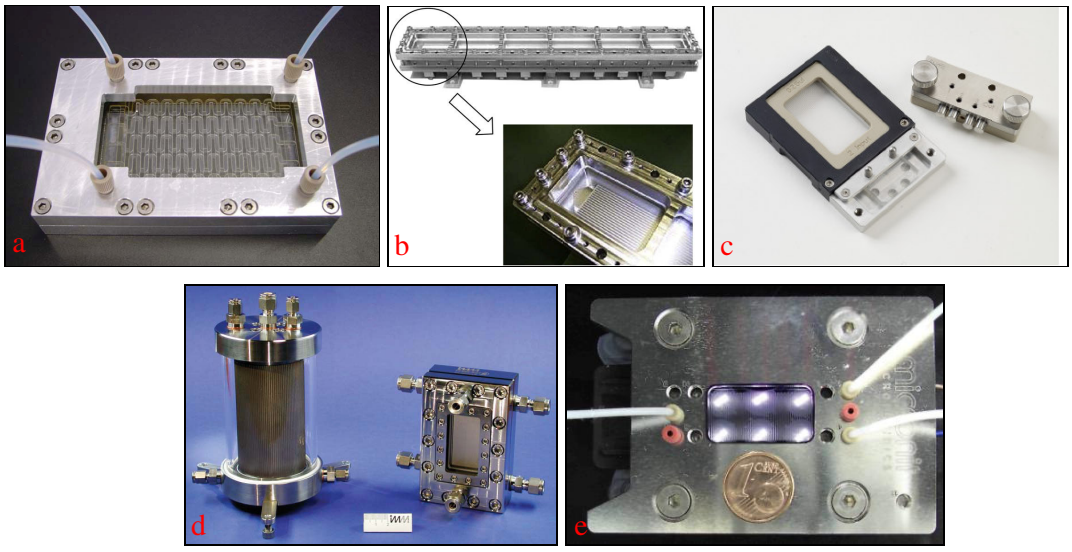


Figure 8: a) Dwell device (Mikroglas)[37]; b) Multi-lane microreactor (Dainippon Screen Mfg), Ryu *et al* [38]; c) Borosilicate 62.5 µl microreactor chip (Dolomite)[39]; d) Cylindrical falling film micro reactor (FFMR-cyl) for 10-fold scale-up and its standard version FFMR (IMM)[40]; e) Borosilicate microchip with 365 nm/ 75 mW UV-LED-array in stainless steel chip holder (Micronit)[41], Oelgemöller *et al.*[42]

Beside commercially available types of microreactors, many researchers continue to custom build their own reactors. This allows to optimise path length, channel depth and operating procedures. It also opens access to a broader variety of materials for solid supports, glass and light sources. An example of house-made microchip is shown in Figure 9.

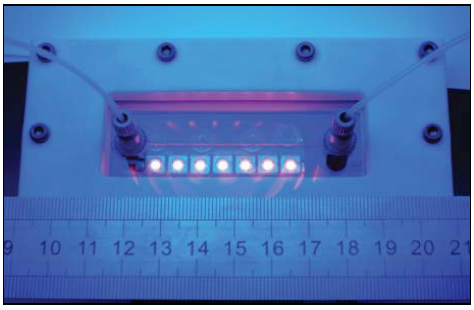


Figure 9: Quartz microchip design with 365 nm/ 500 mV UV-LED-array, Matsushita *et al.*[43]

1.5.2.1 Microstructured reactors (MR)

1.5.2.1.1 Definition and special properties of MR

Microstructured reactors are (generally, but not absolutely) reactors with three-dimensional structures, the inner parameters of which are under a millimetre in size, and more specifically between ten and a hundred micrometers.[44]

The significant promise of microreactors has already been demonstrated in the area of synthetic organic chemistry, as detailed in many review articles to date.[44–58] However, the application of microstructured reactors in organic photochemistry was summarised only in two review papers.[21,59]

Microstructured reactors have unique characteristics, which make them superior for photochemical processes:[51]

- the thin layers of microchannel plates (100-1000 μm) ensure extensive penetration of light within the reaction mixture, even for relatively concentrated solutions;
- the inner space of a microchannel is made up of an enormous area of walls (Figure 10). Therefore microstructured devices have a large surface area-to-volume ratio that provides fast heat and mass transfer. Specific surface areas of microstructures are between 10000 and 50000 m^2/m^3, while those of conventional reactors are generally about 100 m^2/m^3 and in rare cases may reach 1000 m^2/m^3. Since the heat-transfer coefficient is inversely proportional to the channel diameter, a value up to 10 kW/m^2K has been measured in micro heat-exchangers for liquid flows, which is significantly higher than for traditional exchangers. In addition large surface area ensures very efficient rates of light energy transfer;

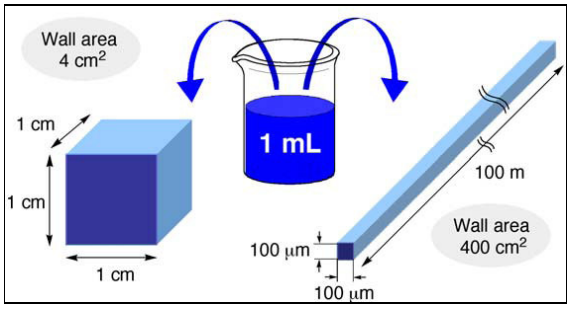


Figure 10: Surface area: macro- vs microspace [58]

- the microreactors are usually continuous flow devices with hydrodynamic flow, which is an important feature of microfluidics. The flows are mostly laminar,

directed and highly symmetric. This feature opens the possibility to simulate and design rational model system for microprocess engineering apparatus;

- the reaction reagents may be mixed directly in the reactor with two or more inlets in mixing channels preceding the reaction channel. The number of available micromixers can be easily utilized in the flow setup.[60] Also, the reagents can be introduced in a specific sequence to the reaction region using electrokinetic or hydrodynamic pumping.[51] Hence no pre-mixing is necessary in the microreactor system;
- the irradiation time of photochemical processes in a microreactor is easily changed, as it is directly proportional to the flow rate of the system. By changing the flow rate product formation can be precisely controlled and undesired side reactions or decompositions avoided;
- the small experimental scale reduces the total waste (green chemistry approach) and requires less amounts of solvents and chemicals;
- the microreactor design allows online UV-[61] or IR-monitoring[62] of the reaction;
- the small reactor size allows to employ miniaturised or compact energy saving light sources such as light-emitting diodes (LEDs) or black light.[38,43,63–70] LEDs have quasi-monochromatic emission spectra and are available in a range of wavelengths, they are small in size, robust and energy efficient. In addition, LEDs produce little or no heat, therefore no cooling is required;
- the processes in microreactors are safer to operate and can be automated.[38] The reactions proceeding in a small volume can be controlled much more easily with respect to pressure, temperature and residence time.[71] Thus, the risk of highly exothermic or explosive reactions can be reduced drastically;
- micro-reactors can be operated in series or in parallel clusters for scale-up or optimization studies.[38,72] The parallel network of microreactors offers a clear route to generating product volume on demand at the point of use, so reducing the need to store and transport hazardous or reactive chemicals. This is one more example, where microreactors make great contribution to the publics' perception of environmentally clean chemistry.

1.5.2.1.2 Microreactor technology (or Types of microreactors)

The majority of microreactors have a quite simple design that consists of a microchannel network often embedded in a solid base. Generally the reactor design depends on its applicability which is defined by several factors. The main issue in

reactor construction is made by the chemical and physical properties of the material used for reactor manufacturing and the type of reagent and solvent introduced to the system. Microreactors are produced from a range of materials, including glass, ceramics, polymers, stainless steel and silicon. The fabrication techniques, advantages and disadvantages of these different materials are presented in Table 2.[52,73]

Table 2: Fabrication and highlighted features of selected types of microreactors

Material	Fabrication techniques	Advantages	Disadvantages
Glass	Photolithography; powder blasting; wet etching; ultrasonic machining	High chemical resistance; direct visualization of reaction; photochemical reactions	Incompatible with strong aqueous bases at moderate temperature; only for temperatures above 0°C
Stainless steel	Lithography; electroplating and molding; stamping; micromachining	Operation at high pressure and temperature	Incompatible with acidic media and some organic solvents (acetone, THF, CH_2Cl_2, DMSO) except for expensive specialized steels
Plastic	Soft lithography; injection molding; hot embossing; phase-separation-micromolding	Fast fabrication; cheap development costs	Not stable to organic solvents; limited mechanical stability; not suitable for high temperatures and pressures
Silicon	Photolithography; wet and dry etching	Operation at high pressure and temperature; superior heat conductivity; high-aspect ratio designs	Incompatible with strong aqueous bases at moderate temperatures
Ceramic	Stereolithography; powder molding; electro- discharge machining; laser machining	Stable at high temperatures with low heat loss; chemically resistant	High development cost; shrinkage after sintering

1.5.2.1.2.1 Glass microreactors

Glass is the perfect material to work with in synthetic chemistry and especially in photochemistry. It offers the benefit for photochemistry such as light transparency. Additionally it allows visual control of the reaction progress and is chemically inert to most reagents and solvents. Different types of glass are used by reactor manufactures

and researchers in the laboratory. The choice of glass type depends mainly on the reaction conditions (absorption spectra of chromophore reagent) and emission spectra of the light source, because glass additionally plays the role of a cut-off filter. For example, various glass types have different light transparency: Quartz is transparent at $\lambda > 200$ nm (Figure 11), Vycor at $\lambda > 220$ nm, Foturan at $\lambda > 280$ nm, Pyrex at $\lambda > 280$-300 nm (Figure 11), Soda lime $\lambda > 320$ nm, Borosilicate at $\lambda > 350$ nm. However, Quartz and Pyrex are the two most common types of glass used in photochemistry.

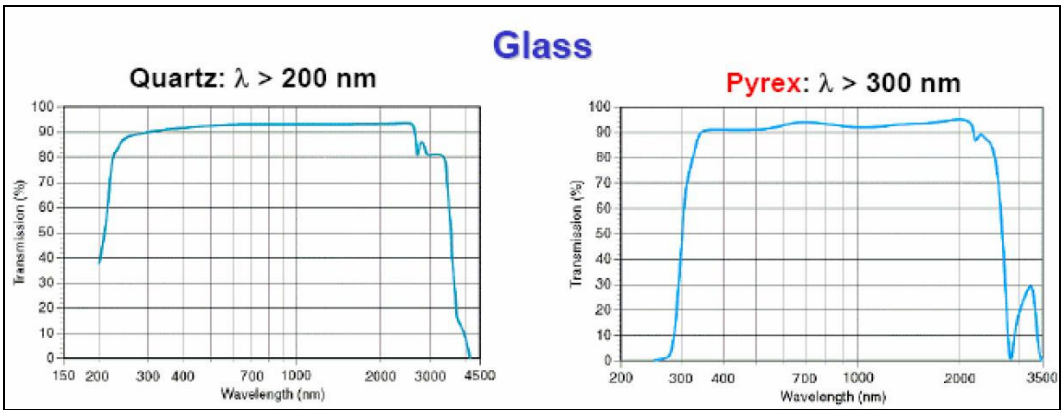


Figure 11: Transmission spectra of Quartz and Pyrex glass[74]

1.5.2.1.2.2 Stainless steel microreactors

Stainless steel is the material of choice for process chemistry. Therefore stainless steel microreactors or systems with microfabricated components have been developed. Metal is also the main material of manufactured holders for other reactor types. These reactors are primarily of interest for pilot-plant and fine chemical applications, but are rather expensive for academic synthesis laboratories. IMTEK[75] and IMM[40] provide a wide variety of stainless steel microreaction systems including micromixers, heat exchangers, reactor process plants, reactors for multiphase reactions and microreactors with incorporated viewing windows that could be suitable for photochemical reactions.

1.5.2.1.2.3 Polymer-based microreactors

Polymer-based microreactors, especially systems made of poly(dimethylsiloxane) (PDMS), poly(methylmethacrylate) (PMMA) and polystyrene (PS) are relatively inexpensive and easy to produce. However, the polymers are not stable to many solvents used for organic synthesis and show limited mechanical stability and low thermal conductivity. Thus the application of these reactors is mostly restricted to aqueous chemistry at atmospheric pressure and temperatures. However, PDMS

microfluidic systems are frequently used for biological purposes because they are biocompatible, non-toxic, optically transparent, highly gas permeable and moreover low-cost with the possibility of one time use to avoid cross-contamination.[76]

S. J. Haswell and D-P. Kim reported the creation of allylhydridopolycarbosilane (AHPCS) and polyvinylsilazane (PVSZ) polymer derived microreactors that are stable to ethanol, methanol, DMF, acetonilrile and THF. Moreover, the authors demonstrate the successful performance of model organic synthetic reactions in the novel polymer based microreactor. The obtained results showed higher reaction outputs in microsystems compared to batch conditions.[77]

The most common polymer material for applications in organic chemistry and particularly in photochemistry is fluorinated ethylene propylene (FEP). FEP is a molten copolymer of tetrafluoroethylene and perfluoropropylene (Figure 12) with a high-molecular, partly crystalline structure.

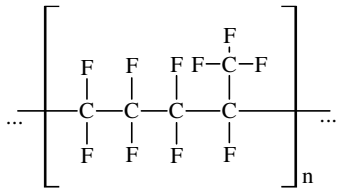


Figure 12: Chemical structure of FEP[78]

It has properties that are very important for application in synthetic photochemistry. FEP is resistant to irradiation and is UV transparent. The UV transparency of FEP tubing is 80.4% or 75.6% at 330 nm with a wall thickness of 250 µm and 300 µm, respectively.[79] Additionally it has almost universal chemical resistance, very good sliding and dielectric characteristics, non-adhesive surface, is non porous and free from extractable agents.[78]

FEP is not used directly in the manufacture of microreactors support, but FEP tubing and film are the main building blocks for the fabrication of home-made continuous flow photochemical reactors[79,80] and sophisticated multiple microcapillary thermal reactors,[81,82] where they functions as the reaction vessel. FEP tubing is flexible enough to wind tightly around lamps, glass cylinders or any other solid base. FEP is resistant at low and high temperatures (from -270°C to +205°C) and has a "burst pressure" up to 112 bar.[78] Moreover, it is commercially available in different diameters at relatively low prices.

1.5.2.1.2.4 Silicon microreactors

Silicon has also found applications in the construction of photomicroreactors[63] due to its glassy behaviour after oxidation and chemical resistance to most reagents and solvents. The main benefit of using silicon is excellent thermal conductivity. Therefore silicon microreactors have outstanding heat-transfer capabilities and are attractive for exothermal reactions and reactions that require very high or low temperatures. In addition, silicon-based microsensors can be readily incorporated in to the reactors.

1.5.2.1.2.5 Ceramic microreactors

Ceramic has been used in microsystem fabrication more rare than other materials, mainly as base in photocatalytic microreactors.[83–85] It is often difficult to microfabricate ceramic systems and they are typically limited to high temperature application.

1.5.2.1.3 Variety of reactor designs used in photochemistry and organic chemistry

Within the last decade many new reactors and microdevices have been designed utilising the above mentioned fabrication techniques and materials. The most advanced are the following models: spinning disc reactors,[86,87] microcapillary flow discs reactor,[81] Cambridge Disc Microreactor,[82] micromesh reactor,[88] continuous flow reactors (for macro-[80] and micro-scale[63,89] synthesis), excimer radiation systems,[90–92] thin film reactors,[93] solar parabolic trough reactors (e.g. the PROPHIS-plant),[94–96] microbatch reactors[97–99] and Fluidized Bed Photoreactor.[100]

1.5.3 Accessible light sources for photochemical reactions

Photochemical product formation results from the absorption of light and depends on the specific excited state species created during irradiation. Thus the properties of the light source often determine the photochemical product. There is a large variety of light sources used in batch- and micro-photochemistry.

Examples of artificial light sources used in laboratory experiments for continuous irradiation are:

- incandescent lamps;
- electrical discharge lamps such as mercury lamps (medium pressure and high pressure), xenon, antimony – xenon or mercury – xenon lamps;
- resonance lamps (low - pressure mercury lamps, lamps filled with pure vapour of other elements, e.g. Cd, Zn, Na, Kr, Xe);

- Rayonet lamps;
- excimer lamps;
- lasers;
- light emitting diodes (LEDs and OLEDs).

The characteristic emission spectra of main artificial light sources are presented on Figure 13.

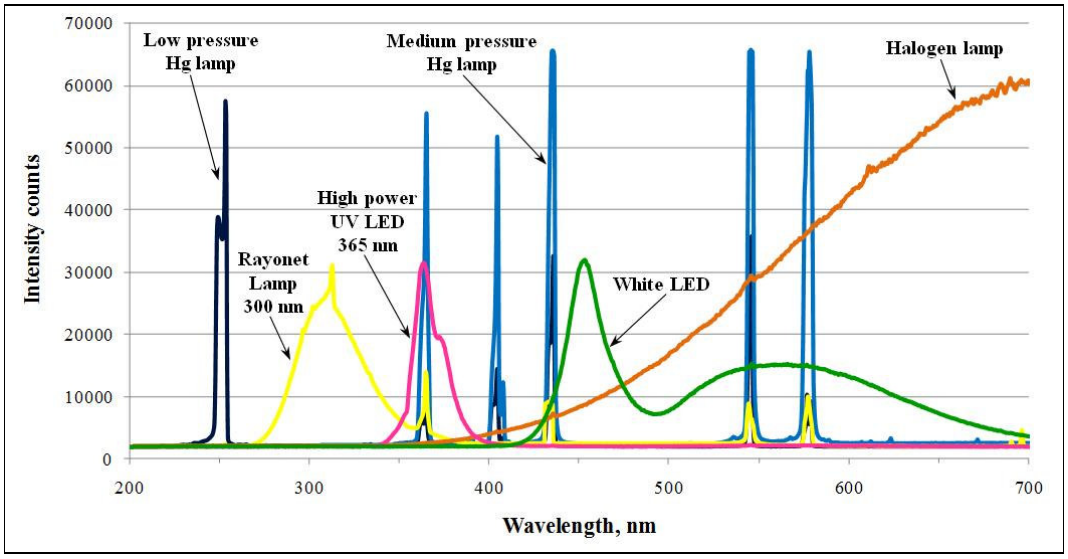


Figure 13: Spectra of common light sources

1.5.3.1 Incandescent lamps

The spectral characteristic of this light depends on the kind of the source. The incandescent lamps (a tungsten filament incandescent in an inert or halogen atmosphere) are used primarily as sources of polychromatic visible light characterized by a continuous spectrum. The working temperature of the lamps lies between 2200 and 3000 K – emitting a large quantity of infrared light (Figure 13). These lamps are utilized mainly for spectrophotometers and may be useful in the photoreactions of coloured chromophores, but due to heat generation and short life time their application in photochemistry is restricted.

1.5.3.2 Mercury and xenon based lamps

The most widely used sources of UV VIS light in laboratory experiments are xenon and mercury arc lamps. Their spectral irradiance is strongly dependent on the mercury vapour pressure. The medium-pressure mercury lamp (the vapour pressure of mercury is ~ 1 bar) produce a band or line spectra in the UVA, visible and near - IR regions,

whereas the low pressure mercury lamp (the vapour pressure of mercury is ~ 10^3 mbar) emits resonance radiation of atoms and can be used as a source of near monochromatic light, e.g. 184.9 nm and 253.7 nm (Figure 13). The common mercury-xenon lamps also produces significant mercury emission bands, especially in the UV region; the smoother xenon lamp spectrum finds application in environmental photochemistry experiments because of its resemblance to solar radiation. The most intense sources of UV radiation are the high-pressure (~100 bar) mercury arcs. The spectral lines are broadened due to the high pressure and temperature and they are superimposed on a continuous background of radiation. Depending on the transmittance of the quartz envelope, the short-wavelength line may be partially filtered out. These lamps are often utilized in Rayonet reactors. Rayonet lamps (fluorescent tubes) have specific wavelengths from secondary fluorescent emission of coated elements. Therefore they have rather broad emission spectra at specific wavelengths, e.g. 300 ± 25 nm, 350 ± 25 nm, 419 ± 25 nm (Figure 13).

The mercury based lamps play a dominant role among light sources used in photochemistry. However those lamps operate at high temperature and at high vapour pressure. The lamp envelope's temperature can reach 600°C and produces a considerable amount of infrared radiation. Therefore, cooling-water circulation or specific filters must be utilized during the lamps operation.

1.5.3.3 Excimer lamps

Excimer lamps are the most powerful supply of UV irradiation. High intensity ultraviolet (UV) and vacuum ultraviolet (VUV) radiation is generated from decaying excimer complexes through dielectric barrier discharge sources. Such sources provide a singular extremely narrow-band emission at various wavelengths between 126 – 354 nm. For example, the Ar_2 excimer lamp has a distinct emission peak at 126 nm, Kr_2 at 146 nm, Xe_2 at 172 nm, KrCl at 222 nm, XeBr at 282 nm, XeCl at 308 nm, XeF at 354 nm respectively. This enables its utilization for chemical reactions unattainable by a conventional lamp and allows acceleration of reaction rates.[90,101] Excimer lamps apart from exclusive radiation have high energy conversion efficiency from power to light and could be coupled in parallel for providing high photon fluxes over large areas. Therefore they can serve as alternatives to laser light sources for large scale industrial applications.

1.5.3.4 Lasers

Lasers are light sources of coherent radiation in the UV, visible or IR range. They produce electromagnetic radiation, using the process of optical amplification based on the stimulated emission of photons within a gain medium.[102] Depending on the active medium (lasing species) there are different kinds of lasers, e.g. argon, helium – neon, helium – cadmium, krypton, nitrogen, CO_2 , copper vapour, dye, semiconductor, neodymium laser, etc, that extend from wavelengths of less than 110 nm (VUV) to more than 100,000 nm (far-IR). Lasers have an immense impact in the field of photochemistry, spectroscopy and photophysics by providing scientists with an intense, polarized, and nearly monochromatic source of light.

Use of lasers in photochemical applications provides three main advantages[102] over conventional light sources such as discharge or arc lamps. Firstly, lasers are generally more powerful than conventional light sources. Secondly, laser light can be collimated into a beam with a very small divergence angle. The high degree of collimation of laser light permits efficient illumination at a chosen point within the sample, which could be far from the light source. Thirdly, laser light is exceptionally pure in colour.

Despite of the advantages of lasers, conventional light sources are still widely used in most photochemical investigations and commercial processes because of their simplicity and low cost. Laser systems are expensive and only restricted amounts of substrate can be irradiated in the focused laser beam.

1.5.3.5 LEDs

Light-emitting diodes (LEDs) are semiconductor light sources that found applications in photochemistry within the last decade. They are also the major irradiation source in micro-photochemistry due to their small size and sufficient output. An LED is often less than 1 mm^2 in area, and integrated optical components may be used to shape its radiation pattern. LEDs present many advantages over other light sources. Their main benefits are:

- lower energy consumption;
- longer lifetime;
- improved robustness;
- smaller size;
- faster switching;
- greater durability and reliability;
- mercury free and safe operation.

The lighting work of LEDs is based on electroluminescence. This mechanism involves charge carrier recombination in semiconductor materials forming an electron-hole pair (exciton). During recombination electrons release energy in the form of photons. The energy gap and the composition of semiconducting material determine the colour of the light. Nowadays LEDs are available across the visible, ultraviolet and infrared wavelengths, with very high brightness.

Successful utilization of LEDs and high power LEDs in photochemical transformations have been reported[38,43,63–70,99] including their applicability in micro-photochemistry.[38,43,64,65,99] It is expected that LEDs will emerge as major environmental and economic light source due to their large energy and thus cost savings.[66] The high power light emitting diodes with emission in the visible range are low cost, but UV-LEDs are currently still expensive and this limits their widespread employment. They also require more precise current and heat management than compact fluorescent lamp sources of comparable output. However, LEDs are increasingly used as light sources in photochemical equipment for preparative irradiation and for quantitative work such as quantum yield measurements.

2 Photochemical model reactions in microreactors

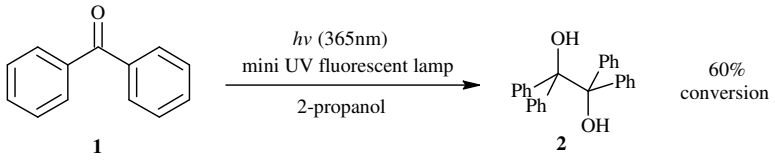
A number of examples concerning photochemical performances in microreactors already exist in the literature. The reactions carried out to date may be divided into three categories, based not on the reaction type, but rather on the conditions required:

- homogeneous reactions (the reagents are all in the same phase, i.e. in solution);
- heterogeneous reactions (reactions between liquid and gaseous reagents);
- catalytic reactions (reactions that involve heterogenic catalyst).

2.1 Homogeneous reactions

2.1.1 Photopinacolisation

This transformation is one of the earliest photochemical reactions that was investigated in microstructured reactors. Jensen and co-workers[61] studied the photopinacolisation of benzophenone **1** using isopropanol as solvent (Scheme 2). The reaction was carried out in two house-made microreactors. One reactor was fabricated by bonding a patterned silicon wafer to a Pyrex plate. The second reactor had a sandwich structure of a silicon wafer between two quartz wafers. The benefit of a quartz reactor design was possibility of parallel irradiation and UV detection in situ. Moreover in the quartz reactor lower wavelengths of light may be used for irradiation than allowed by Pyrex. In this investigation a mini fluorescent UV lamp was used as light source.



1 **2**

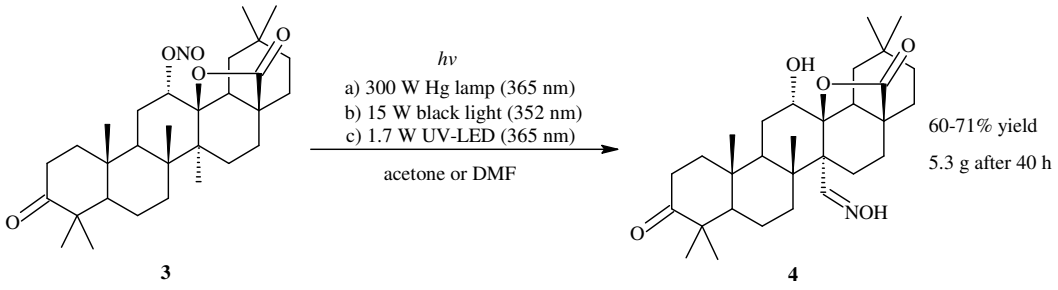
Scheme 2: Photopinacolisation of benzophenone

This reaction proceeds via a radical pathway and for greater conversion to benzopinacol **2** required longer residence time or lower flow rate. The authors reported that there was no detectable product formation for flow rates greater than 10 µl min^{-1}. With reduced flow rates, the conversion improved because the amount of absorbed light increases and the excited species has sufficient time to diffuse and react with benzophenone **1**. An adequate flow rate was established to be 4 µl min^{-1} and showed conversion of up to 60%. At flow rates lower than 3 µl min^{-1} product **2** precipitated in the microchannel and thus blocked the microreactor. The progress of the transformation was monitored *off-chip* using HPLC analysis and *on-line* using UV-spectroscopy. The concentration of

benzophenone was 0.5 M, which is relatively high for photochemical reactions. The use of these concentrated solutions effectively demonstrated the advantage of a microstructured reactor, as the shallow channel depth, only 500 µm, ensured complete irradiation of the reaction mixture which would not have been possible under conventional photochemical set-ups.

2.1.2 Barton reaction

The preparation of steroidal product **4**, from substrate **3** via the Barton reaction (Scheme 3) was selected as model reaction for microreactor testing by Sugimoto and co-workers.[38,103] This reaction is of importance because product **4** is a key intermediate for the synthesis of myriceric acid A (an endothelin receptor antagonist). The experiments were carried out in a glass-covered stainless-steel microreactor Type A or Type B (manufactured by Dainippon Screen Mfg). Microreactor Type A had one lane channel 1000 µm wide, 107 µm deep, 2.2 m long and a hold-up volume 0.2 ml. It was used for optimisation study. Microreactor Type B had 16 lanes with a channel 1000 µm wide, 500 µm deep, 0.5 m long and a hold-up volume 4 ml. This reactor type was used for multi-gram-scale production.



Scheme 3: Barton reaction

A short communication about reaction performance in those microreactors has been reported by the same authors in 2006.[103] Their initial work was concentrated on increasing reaction output through an optimised and energy saving experimental setup. Therefore the application of three different types of transparent glass covers (quartz, soda lime glass, Pyrex) and two light sources (high pressure 300 W Hg lamp and 15 W black light) were investigated. It was determined that Pyrex was most suited to the light source – a 15 W black light. In addition, the authors studied the temperature dependence (extensive degradation of the product at temperatures greater than 50°C) and the distance between microreactor and the light source, which was optimised at 7.5 cm. Following optimisation, a residence time of 12 minutes produced the desired product **4**

in 71% yield. In an extension of this study the same authors examined a UV-LEDs panel (48 pieces × 35 mW) as light source suitable in combination with microreactor Type A. After a residence time of 12 minutes the desired product **4** was isolated in a yield of 70 %. This result clearly demonstrated that UV-LEDs, despite the low intensity (compare to high pressure mercury lamp) have sufficient strength to activate the substrate. The authors also reported a gram scale synthesis of the target compound using two microstructured reactors Type B connected in series and coupled with 8 × 20 W black lights. After continuous operation for 20 h, the amount of isolated product **4** was 3.1g (60% yield). Encouraged by the successful gram-scale synthesis, Sugimoto and co-workers focused their forthcoming work on the development of practical and automated multi-gram-scale synthesis.[38] For this research they used an automated photo-microreactor system, DS-AMS-1 (manufactured by Dainippon Screen Mfg), Figure 14.



Figure 14: An automated photo-microreactor system DS-AMS-1[38]

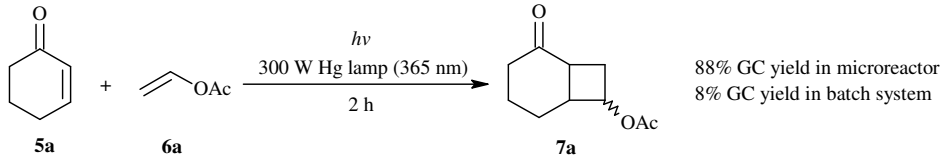
This system provided operation monitoring via PC-software and moreover had safety functions. It employed one set of a Type B microreactor and six small (15 W) black light lamps. After continuous operation for 40 h product **4** was obtained in an amount of 5.3 g (61% isolated yield). This clearly demonstrated the potential for numbering up of microstructured reactors and process optimization for the large scale production of chemicals.

2.1.3 Photocycloaddition reactions

2.1.3.1 Photochemical [2 + 2] cycloaddition of cyclohex-2-enone with vinyl acetate

The photochemical [2 + 2] cycloaddition reaction is one of the most powerful and versatile methods for the formation of four-membered rings, and has been extensively applied in organic synthesis. Fukuyama and co-workers[104] selected the photochemical

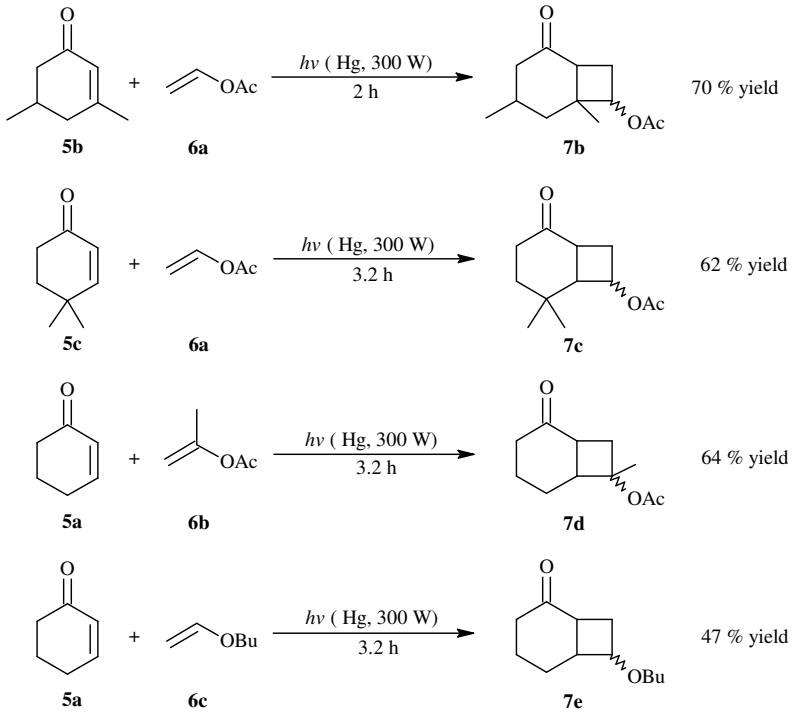
[2 + 2] cycloaddition of cyclohex-2-enone **5a** with vinyl acetate **6a** as a model reaction (Scheme 4) for testing in a commercially available microreactor dwell device (FOTURAN® glass, manufactured by Mikroglas). This reactor has a channel 500 µm deep, 1000 µm wide and 1.4 m long.



Scheme 4: Photochemical [2 + 2] cycloaddition of cyclohex-2-enone with vinyl acetate

A common high pressure mercury lamp (300 W) was used as a light source in this study. At a flow rate of 0.5 ml h^{-1}, which corresponds to a residence time of 2 h, a GC yield of desired product **7a** of 88% was achieved. This was compared to a batch reactor (10 ml Pyrex flask) irradiated using the same light source for 2 h, which yielded only 8% of **7a**. The same reaction was repeated with 2 microreactors in series at a flow rate of 1 ml h^{-1}, which resulted in a similar isolated yield of 85%. Thus, microstructured reactors can shorten irradiation times and increase yield at the same time.

The generality of the photochemical [2 + 2] cycloaddition in a microflow system have been verified by related reactions. Two additional cyclohexenones, **5b** and **5c**, and two additional alkenes, **6b** and **6c**, were examined (Scheme 5).



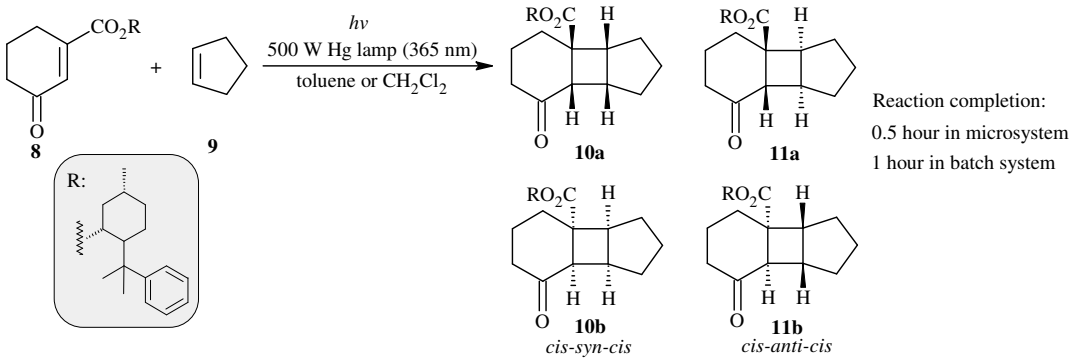
Scheme 5: Photochemical [2 + 2] cycloaddition of cyclohexenones with alkenes

In all cases examined, the corresponding cycloaddition products **7b**–**7e** were obtained in yields of 47–70% as regioisomeric mixtures.

Recently, the same authors reported an extended study of the [2 + 2] cycloaddition reactions and Paterno-Büchi reaction in several experimental microreactors.[105] The best results were achieved in a new photoreactor KeyChem-Lumino (YMC Co. Ltd.) with a single-lane stainless steel microchannel (1000 μm width, 200 μm depth and 56 cm length). The reactor was irradiated by an array of UV LEDs (6 × 250 mW; λ_{max} = 365 nm). In this microreactor an improved yield of **7a** of 91% and 95% was achieved after residence time of 15 min and 20 min, respectively.

2.1.3.2 Diastereoselective [2 + 2] photocycloaddition of a chiral cyclic enone with cyclopentene

Asymmetric photoreactions are of special importance due to the formation of potentially biologically active natural products and unique structural compounds. Hence Ryu and colleagues[106] explored the utility of a microflow system in photoinduced asymmetric reactions and compared the results with those obtained using a larger volume batch reactor. The model reaction examined was the reaction of the cyclo-hexenonecarboxylate derivative **8**, which includes a (–)-8-(phenyl)menthyl group as a chiral auxiliary, with cyclopentene **9** (Scheme 6).



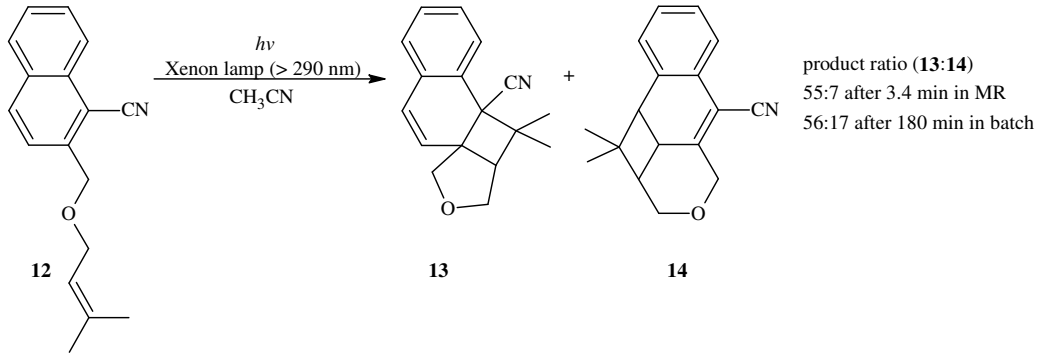
Scheme 6: Diastereoselective [2 + 2] cycloaddition of chiral cyclic enone and cyclopentene

The microreactor with one lane channel 1000 μm wide, 100 μm deep, 2.2 m long and hold-up volume 0.2 ml (manufactured by Dainippon Screen Mfg) was employed as microflow system. A simple Pyrex test tube with an ID of 13 mm was used for the batch test. Both systems were irradiated simultaneously by a common high pressure Hg lamp. The photoreaction in the microflow system reached completion in shorter residence

time, only 0.5 hour, which was two times faster than in the batch system (1 hour). However the ratios of stereoisomers **10** and **11** were almost identical in both systems. Additionally the authors investigated the effect of temperature on the diastereoselectivity. The highest diastereoisomeric excess values of **10** (82 %) and **11** (54 %) were observed in the microflow reaction at –40°C. This was explained by a more accurate temperature control in the microflow system associated with a very large surface area to volume ratio of the reaction chamber. In summary, this study has shown that a flow microreactor can be used for asymmetric photoreactions.

2.1.3.3 Intramolecular [2 + 2] photocycloaddition of a 1-cyanonaphthalene derivative

Microreactors providing continuous flow have found application in regioselectivity studies. The intramolecular [2π + 2π] photocycloaddition of 1-cyano-2-((3-methyl-2-butenyloxy)methyl)naphthalene **12** in acetonitrile (Scheme 7) has been reported by Maeda *et al.*[107] The authors compared the regioselectivity and efficiency for batch and microstructured reactor conditions.



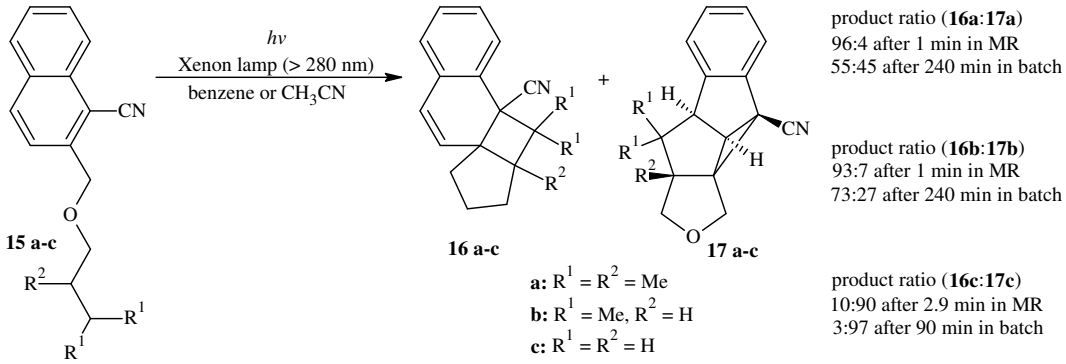
Scheme 7: Intramolecular [2π + 2π] – photocycloaddition of 1-cyano-2-((3-methyl-2-butenyloxy)methyl)naphthalene

The reaction was performed in custom-built reactors made from poly(dimethylsiloxane) with the channels 300 µm wide, 50 µm deep and 45 mm or 202 mm long. The reaction mixture was pumped through the microchannel with two flow rates 0.03 or 0.05 ml h^{-1} and was irradiated by a xenon lamp maintained with a UV-29 filter. The channel pathlength of 202 mm afforded prolonged reaction time and was found as optimal. After an irradiation time of 3.4 min the intramolecular photocycloadduct **13** at the 1,2-position of the naphthalene ring and a photocycloadduct **14** at the 3,4-position were detected in a ratio of 55:7 in the microreactor. In contrast, only 5% of photocycloadduct **13** and traces of photocycloadduct **14** were noticed under batch conditions after the

same reaction time. This reaction was also investigated in the batch system with a longer residence time of 180 min and photocycloadducts **13** and **14** were detected in a ratio of 56:17, respectively. The improved regioselectivity in the microreactor was explained by the rapid flow rate, the cycloadduct **13** initially formed is rapidly and continuously expelled from the system, thus reducing photocycloreversion back to the starting material **12**. Longer irradiation times (lower flow rates) gave increased yields of **14** since reversion to the starting material does not take place for this compound. The enantioselectivity was also evaluated using $Eu(hfc)_3$ and a small but significant enantiomeric excess of 2% (e.e.) was established.

2.1.3.4 Intramolecular [2 + 2] and [2 + 3] photocycloadditions of 2-(2-alkenyloxymethyl)-naphthalene-1-carbonitriles

In an extension of the above described work, Mizuno examined the intramolecular photocycloaddition of 2-(2-alkenyloxymethyl)-naphthalene-1-carbonitriles **15a–c** (Scheme 8).[108] The authors work included a comparison to a batch reaction (Pyrex tube, diameter 8 mm) and a study of the effects of substituents, solvent, residence time and flow rate and the dimensions of the microchannel.



Scheme 8: Intramolecular photocycloaddition of 2-(2-alkenyloxymethyl)-naphthalene-1-carbonitriles

For this investigation generally microreactor Type A was used, but also another reactor Type B was utilized for a comparison study of channel dimensions. The first (Type A) microreactor was commercially available (ICCDI05, Institute of Microchemical Technology), and was made from Pyrex glass with a channel 100 µm wide, 40 µm deep and 120 mm long. A second (Type B) microreactor was made in-house from Pyrex plates and had a channel width of 2.5 mm, a depth 50 µm and a length of 60 mm. The light source used was a xenon lamp (500 W). The results of this study showed, once

again, that microreactors facilitate improved regioselectivity and the initial photoproducts **16a–c** were selectively formed, while the undesirable photocycloreversion products **17a–c** were suppressed. A rapid flow rate ensured that the initial product is removed from the irradiation chamber before the secondary reaction may take place. Moreover, higher conversions of 69–75% were achieved in the microreactors after just 1 min, while the batch reactor showed a lower conversion of 74% after 3 h of irradiation. The increase in efficiency was explained by the better light penetration through the reaction medium in the microreactors compared to the batch system. It was also demonstrated that wider channels can significantly increase output while maintaining a shallow channel depth.

2.1.3.5 Intramolecular [2 + 2] Photocycloaddition of coumarin derivative

In Abbott Laboratories (US) a convenient flow-based photochemical microreactor LOPHTOR has been recently designed (Figure 15).[109] The unique aspect of this new tool was its integration with an auto-sampler that enabled a set of conditions to be programmed and executed without human intervention. The reaction microchannels of 1000 μm width, 250 μm depth and 3.93 m length were fabricated in stainless still that contains on the back side integrated cooling lines. The total volume of the serpentine flow cell channels was 0.98 ml and it was secured by a FEP membrane. This membrane also created the transparent front wall of the channel and was sealed by nitrogen during reactions (Figure 15c). A medium pressure mercury arc lamp (450 W) with a concentrator and cold integral mirror was used for irradiation. Additionally, the selective wavelength filtering could be provided by a set of uranium-doped quartz plates.

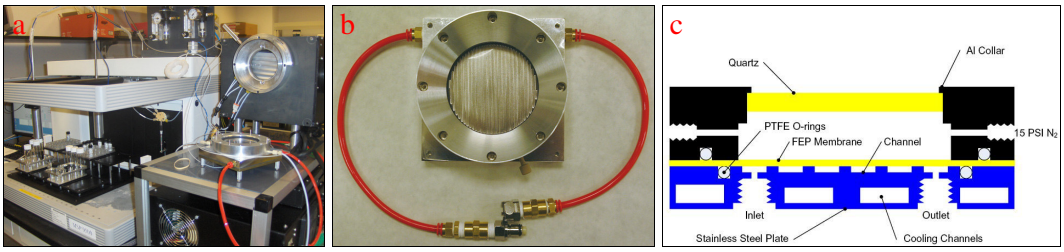
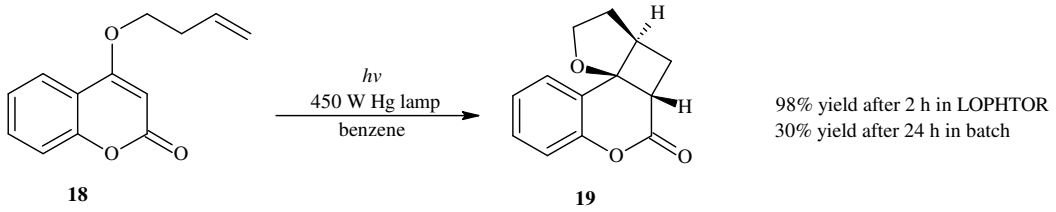


Figure 15: a) Fluidic system; b) Fully assembled microreactor; c) Cross-sectional view of microreactor.[109]

The utility of LOPHTOR for photochemical synthesis was evaluated by the authors using a known intramolecular [2 + 2] cycloaddition of a coumarin derivative (Scheme 9) as the model reaction. For comparison purposes, the same transformation was

attempted in a batch mode, i.e. in a round bottom flask fitted with a magnetic stirring bar and condenser.



Scheme 9: Intramolecular photocycloaddition of 4-(3-butenyloxy)-2*H*-chromenone-2

Initially, Vasudevan and co-workers investigated the dependency between product yields and residence time. The complete conversion of starting material **18** was achieved after 2 hours in the microreactor hereby the product **19** was isolated in yield of 98%. In contrast, a much lower yield of **19** (30%) was obtained in the batch system even after prolonged irradiation for 24 h. To prove better photoreaction efficiency in the microreactor compared to the batch system, the substrate scope has been expanded and the reaction procedure was applied to other coumarin derivatives. In all cases similar tendencies were observed. The product yields were significantly lower using conventional batch photochemical setups, despite longer reaction times, and were also characterised by extensive formation of side-products.

The effect of the reactant concentration on the conversion of **18** to **19** was also evaluated. Five different concentrations of **18** in the range from 0.085M to 0.425M were tested and no decrease in conversion rate was observed. This provides a convenient manner for scale-up of this process to generate 100's of milligrams of material that will ideally suit for early drug discovery applications.

In summary, a new flow-based microreactor has been designed. The option of reaction condition optimisation in an unattended manner coupled with the efficiency of generating larger amounts of material make this reactor a very attractive tool for photochemistry and drug discovery.

2.1.3.6 Photochemical [2 + 2] cycloaddition of maleimide with 1-hexyne and intramolecular [5 + 2] photocycloaddition of 3,4-dimethyl-1-pent-4-enylpyrrole-2,5-dione

An investigation into the use of laboratory constructed continuous flow reactor technology (Figure 16) to perform organic photochemistry on a large scale was carried out by Hook *et al.*[80,110] The main focus of this research was to show the superiority of a

continuous flow system over a batch reactor with respect to the product quality. This is one of the first research works in photochemistry where UV-transparent FEP tubing was used as the reaction vessel.

The authors described this system as a flow reactor rather than a microreactor. However, initially during the optimisation of the reactor design FEP tubing with an inner diameter 700 µm and outer diameter 1100 µm was used. Four different flow reactors were constructed with a total volume from 60 ml up to 280 ml, which was determined by the tubing length and dimensions. Being interested in multigram output, Hook and co-workers also considered a wider tubing with the dimensions 2700 µm ID x 3100 µm OD as optimal. One to five layers of this tubing was wrapped around a Pyrex or Vycor filter. A 400 W and 600 W medium pressure Hg lamps were used as light sources.

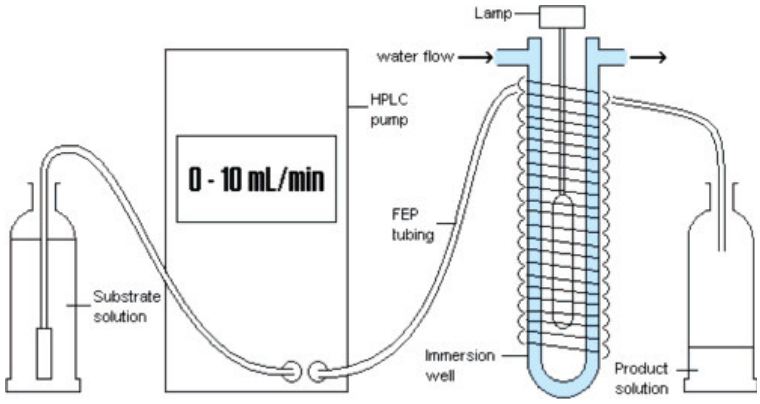
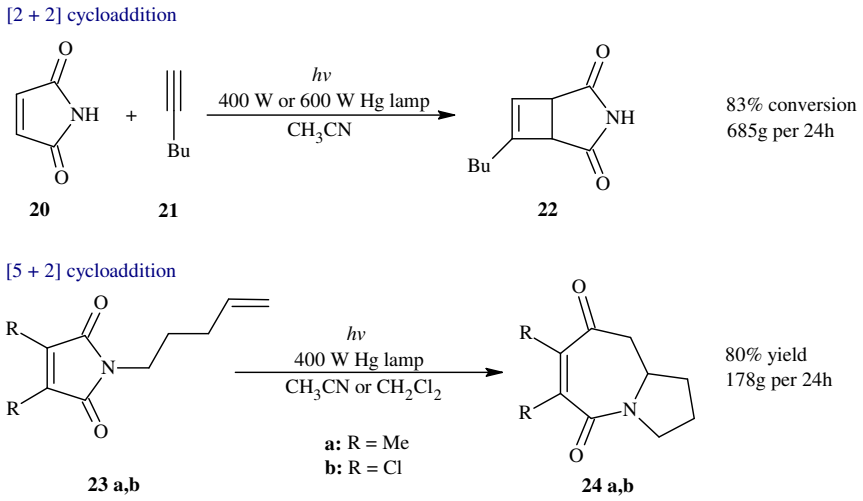


Figure 16: Schematic of FEP continuous flow reactor[80]

These reactors were assessed using the [2 + 2] photocycloaddition of malemide **20** with 1-hexyne **21** forming the cyclobutene product **22** and the intramolecular [5 + 2] photocycloaddition of 3,4-dimethyl-1-pent-4-enylpyrrole-2,5-dione **23a** to form the bicyclic azepine **24a** (Scheme 10), respectively. Using an optimized system with three layers of FEP tubing and Vycor filter these reactions were performed with outstanding results compared to other reactors. A 0.4 M solution of the malemide **20** underwent 83% conversion at 0.8 ml/min flow rate representing a projected yield of desired product cyclobutene **22** of over 685 g per 24 h. At the same flow rate a 0.1 M solution of initial compound **23a** was irradiated and bicyclic azepine **24a** was isolated in a yield of 80%, which represents a 24 h yield for **24a** of 178 g.

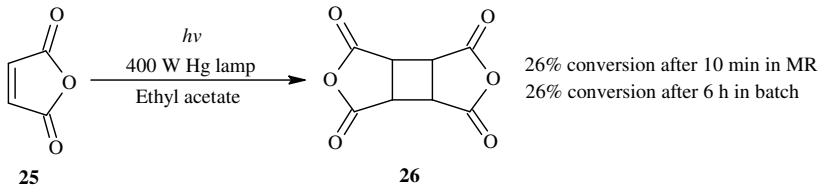


Scheme 10: [2 + 2] and [5 + 2] cycloaddition reactions of maleimide and its derivatives

Using a flow reactor, the residence time could be tuned by adjusting the volume of the reactor and the flow rate. This way, problematic photochemical reactions can be performed continuously, achieving the highest possible yield of product and limiting by-product formation. To demonstrate this principle, the authors selected the [5 + 2] intramolecular photocycloaddition reaction of 3,4-dichloro-1-pent-4-enyl-pyrrole-2,5-dione **23b** to form the bicyclic azepine **24b** and tested it in flow and batch setups. As expected, the desired azepine **24b** was obtained in significantly higher yield in the flow reactor (45 g) compared to the batch system (0.5-1 g).

2.1.4 Photodimerization of maleic anhydride

An important example of a problematic photochemical reaction is the photodimerisation of maleic anhydride (MA) **25** (Scheme 11). It is known that this reaction yields the insoluble cyclobutane tetracarboxylic dianhydride (CBTA) **26**, which is used as raw material of polyimide and of alignment films for liquid crystal displays.



Scheme 11: Photodimerisation of maleic anhydride

This reaction was selected by Yoshida and co-workers as a model reaction for a novel liquid/gas slug flow microreactor.[79] The main purpose of this approach in microreactor design (Figure 17a) was to show that the clogging problem within a photoreaction can

be overcome by the combination of two techniques such as slug flow and ultrasonication. Inert N_2 gas was introduced into the reaction solution as a "spacer" which swept through the reactor tube and transported precipitated products in the liquid segments (Figure 17b). Ultrasound vibrations inhibited the adhesion and sedimentation of precipitate in the reactor tube.

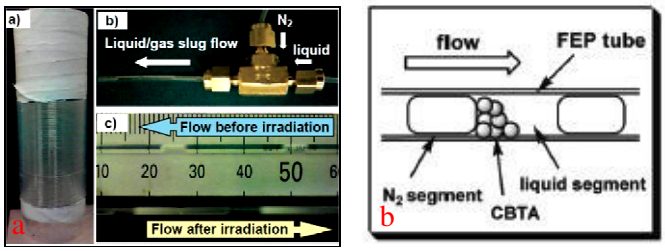


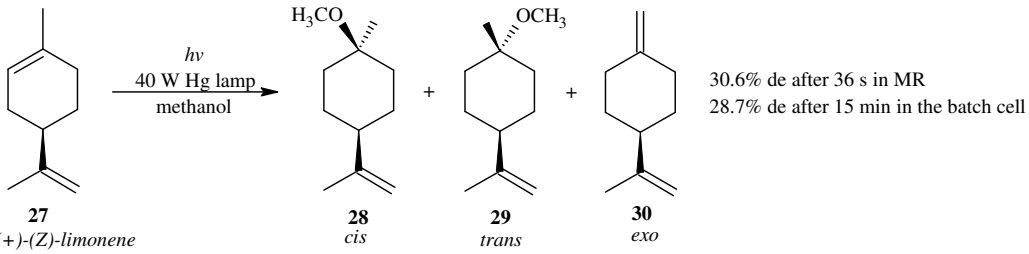
Figure 17: a) Slug flow microreactor: (a) FEP tube wrapped around the outside of a quartz beaker; (b) N_2 gas feed, via T-shaped connector; (c) liquid/gas slug flow before and after irradiation, b) continuous transportation of precipitate.[79]

Fluorinated ethylene propylene (FEP) tubes of various sizes were used as the reaction vessel and the impact of the tube dimensions on product conversion was examined. Additionally the effects of MA concentration and residence time were also investigated. As light source a 400 W high pressure Hg lamp was employed. The experimental results showed that a 10% solution of MA **25** underwent satisfactory conversion of 70 % after a residence time of 22 min in the FEP tube of 1.4 mm OD x 0.8 mm ID. The quality of the desired product CBTA **26** obtained in the microreactor was compared with that from the batch system (cylindrical glass vessel with ID 75 mm and height 300 mm) and was established to be more pure. Moreover, the unique design of the slug flow microreactor made it adaptable for continuous circulation and recycle operation to improve conversion and reduce MA waste. The slug flow microreactor could be operated for more than 16 h continuously without clogging. These findings effectively showed the ability to transfer microreactor technology to related reactions.

2.1.5 Diastereodifferentiating addition of methanol to (R)-(+)-(Z)-limonene

The other example of asymmetric synthesis performed in microreactors was toluene sensitized photoaddition of methanol to (R)-(+)-(Z)-limonene **27** (Scheme 12). This transformation was reported by Sakeda *et al.*[111] The authors demonstrated faster reactions proceeding and with higher diastereomeric excess (de) in microchannelled reactors compared to the microbatch cell. This transformation occurs with the formation

of three addition products: *cis*- and *trans*-4-isopropenyl-1-methoxy-1-methylcyclohexane (*cis* **28** and *trans* **29** isomers) and exocyclic isomer **30**.



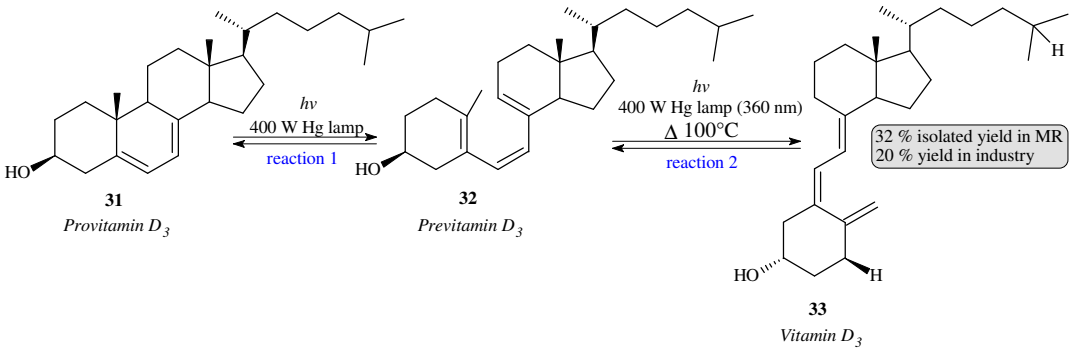
Scheme 12: Diastereodifferentiating photosensitized addition of methanol to (R)-(+)-(Z)-limonene

Three kinds of quartz microreactors (Shimadzu Co.) with channel sizes 500 µm × 300 µm × 60 mm, 400 µm × 40 µm × 100 mm and 200 µm × 20 µm × 100 mm (width × depth × length) and a quartz batch cell with a total volume of 1 ml (light pathlength 3 mm) were utilised for this study. A low-pressure mercury lamp (40 W, 253.7 nm) was used as light source. Irradiation time in microchannels was controlled by the injection rate of syringe pump. The yield of *cis* and *trans* isomers increased linearly during the examined irradiation period in the microreactors (135 s). While in the batch cell the yield increased linearly only for the initial time region of up to 20 min and reached a plateau. Furthermore, the diastereomeric excess value was 30.6% (36 s irradiation) in the microreactor while it was 28.7% (15 min irradiation) in the batch cell. The origin of the difference observed for the de value in the MR versus the batch cell was clarified by the estimated reaction constants for the *cis* and *trans* isomer formation. These constants were significantly higher for microchannels than for the batch chamber. In addition a comparison study of the effect of channel size on photon efficiency was carried out. Photon efficiency was shown to increase with the decreasing channel size and again was greater for microchannelled reactors (0.11-0.29) than batch conditions (0.06). In summary, the better reaction output in microchannelled reactors was explained by its benefits: excellent light penetration, spatial illumination homogeneity, short exposure time, fast and continuous product evacuation from the irradiated area and as a consequence suppression of side reactions.

2.1.6 Continuous-flow synthesis of vitamin D_3

The first impressive example regarding the simultaneous performing of both a photo- and thermal-reactions in a microreactor was described recently by Takahashi *et al.*[112]

As a model transformation the two step conversion of provitamin D_3 **31** to vitamin D_3 **33** via previtamin D_3 **32** was selected (Scheme 13).

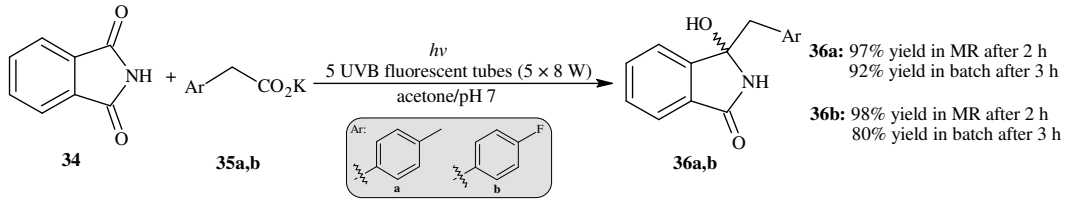


Scheme 13: Two-step conversion of provitamin D_3 to vitamin D_3

The first step of this transformation is photochemical and was carried out in a custom-made quartz microreactor with a channel 200 μm deep, 1 mm wide, 250 mm long and with a volume of 50 μL. For the second step the microreactor that enabled simultaneous photo- and thermal reactions was utilised. Its microchannel was 200 μm deep, 1 mm wide, 500 mm long and with an internal volume of 100 μL. Those two microreactors were connected together through PEEK tubing thus creating a distinct continuous-flow system with a joint light source. The first reactor was irradiated with 313–578 nm light (400 W high pressure mercury lamp with a Vycor filter). The second one was irradiated with 360 nm light (the same lamp with a Vicor and glass UV filters) and it was put on a hot oil bath (100°C). The optimization study of solvent, concentration and flow rate was carried out. Subsequently a concentrated 30 mM solution of provitamin D_3 in 1,4-dioxane was introduced by syringe pump to the combined system with a flow rate of 5 μL min^{-1}. The desired product vitamin D_3 **33** after chromatographic separation was obtained in a yield of 32% (HPLC-UV yield: 60%), which was significantly higher compared to the existing industrial preparation, where the yield of vitamin D_3 is less than 20%.[113] The parallel applying of photo- and thermal conditions within the second step of vitamin D_3 synthesis shifted the equilibrium for photo-isomerisation of the side product tachysterol to previtamin D_3 **32** thus producing it in higher amounts. Moreover, the generation of the other undesired product lumisterol was suppressed to less than 10%. In total this is the first micro-flow synthesis of vitamin D_3 that did not require the purification of intermediates or high dilution conditions, thereby reducing the waste.

2.1.7 Photodecarboxylative benzylations of phthalimide

Recently, the adaptability of the commercially available microreactor dwell device (Figure 8a, Microglas[37]) for the synthesis of new benzylated-hydroxyphthalimidines **36a** and **36b** via photoadditions of the corresponding phenylacetates **35a** or **35b** to phthalimide **34** (Scheme 14) have been announced by Oelgemöller *et al.*[114]

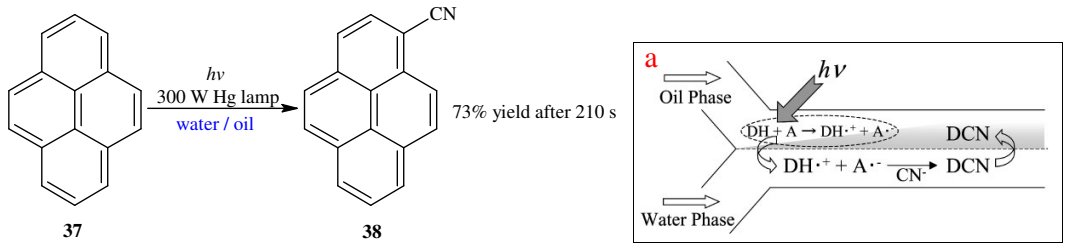


Scheme 14: Photoaddition of phenylacetates to phthalimide

The authors work was mainly focussed on the variety of synthetic transformations leading to the production of arylmethyleneisoindolin-1-ones and structurally related aristolactams, which represent an important class of pharmaceutically active compounds. Generally, photochemical transformations were performed in a Pyrex Schlenk tube (volume 100 ml) that was placed and irradiated on the Rayonet chamber reactor equipped with 16 UVB fluorescent lamps (8W each, $\lambda = 300 \pm 25$ nm). Only two reactions depicted in Scheme 14 were tested in the microreactor. The dwell-reactor is made out of Foturan^{TM} glass and consisted of a (bottom) serpentine reaction channel (0.5 mm depth, 2 mm width, 1.15 m length) and a second (top) heat-exchanging channel through which water was passed to control the reactor temperature. The microreactor was placed under a UV panel (Luzchem) fitted with the same five UVB lamps used in the Rayonet reactor. Using a residence time of 2 h, improved yields of 97% (**36a**) and 98% (**36b**) were achieved in the dwell device. In contrast, lower yields of 92% (**36a**) and 80% (**36b**) were obtained in the batch Rayonet reactor after an extended residence time of 3 h. The improved reaction progress in the microreactor was explained by better light penetration through the thin solution (concentration of phthalimide **34** was 15 mM) layer in the microchannelled plate.

2.1.8 Photocyanation of pyrene

The photocyanation of pyrene **37** (Scheme 15) across an oil/water interface has been described by Ueno and co-workers.[115]



Scheme 15: Photocyanation of pyrene; (a) photocyanation reaction in a microchannel

This transformation was performed in microchips made in-house from polystyrol substrate. Each chip consisted of a single serpentine microchannel with either 2 or 3 inlets, which made possible separate introduction of the oil and water phases. The channel was 100 µm wide, 20 µm deep and 350 mm long. Such microchip design ensured the formation of stable water/oil or water/oil/water interfaces at equal flow rates of both phases (Scheme 15a). The microchips were irradiated with light from a high-pressure mercury lamp (300 W) through a copper sulphate solution filter (>330 nm).
An aqueous solution of sodium cyanide (1 M) and a solution of pyrene **37** (20 mM) and 1,4-dicyanobenzene (DCB, 40 mM) in propylene carbonate were pumped through the reactors. During irradiation, photo-induced electron transfer (PET) occurs between pyrene (PyH) and 1,4-dicyanobenzene (DCB, electron acceptor, represented by A on Scheme 15a) and the resulting radical undergoes nucleophilic attack by CN- at the oil/water interface. The product, 1-cyanopyrene (DCN) **38**, concentrated in the oil layer. After a residence time of 210 s the photoproduct **38** was obtained in yields of 28% for the oil/water system and 73% for the water/oil/water system, respectively. A stable oil/water interface could not be obtained at a flow rate below 0.2 µl min^{-1} and this prevented further improvement of conversion rates and consequently yields.

2.2 Heterogeneous reactions

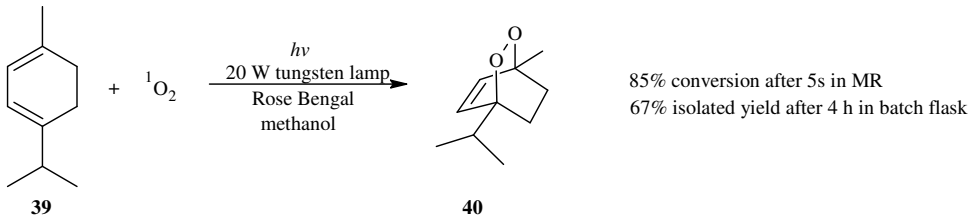
The heterogeneous reactions reported in microstructured reactors are described as interactions between liquid and gaseous reagents. It is necessary to provide a supply of gas to the reaction media continuously. The falling film type reactor is commercially available for this purpose, while other reactors have been adapted for use also.

2.2.1 Photooxygenation reactions

2.2.1.1 Photochemical generation and addition of singlet oxygen to α-terpinene

The first original study concerning safe synthesis of the potentially explosive compound ascaridole **40** in a microreactor was reported by Wootton *et al.*[116] The photochemical

synthesis of ascaridole **40** proceeds via addition of singlet oxygen to α-terpinene **39** in the presence of an organic dye as sensitizer (Scheme 16).



Scheme 16: Photoaddition of singlet oxygen to α-terpinene

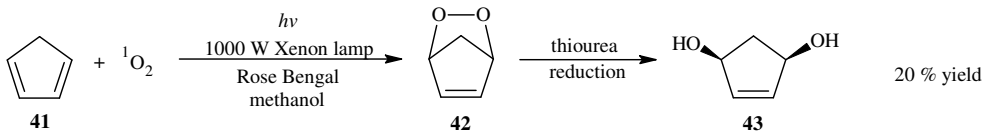
This reaction requires sufficient oxygen saturation and therefore large quantities of oxygenated organic liquids which can be explosive in nature. The authors proposed a new, safe and efficient, continuous-flow synthesis of ascaridole **40** from α-terpinene **39** in a microfabricated nanoreactor. The reactor was built in-house using a glass substrate and consisted of serpentine irradiation sector (of total length 50 mm) and an outlet channel. The channels had an average depth of 50 μm and an average width of 150 μm. The chip also had two individual inlets for reaction solution and oxygen. A methanol solution of α-terpinene with rose bengal was introduced via a divergent inlet channel with a flow rate of 1 μL/min and mixed with oxygen on-chip (flow rate of oxygen was 15 μL/min). In such reaction conditions no presaturation of the α-terpinene solution with oxygen was necessary. The singlet oxygen was generated in-situ (within the serpentine channel) when microreactor was irradiated by an unfiltered tungsten lamp (20 W, 6 V). The volume of aerated solvent in the system at any time was in the region of picolitres. Moreover nitrogen degassing of the product mixture was undertaken as soon as the solution was collected, hence also avoiding accumulation of oxygenated solvents.

The conversion of ascaridole **40** after workup was determined by GC and was 85% at a residence time of only 5 s. This work demonstrates clearly that microstructured reactors provide new and safer platforms for photooxygenation reactions.

2.2.1.2 Photochemical generation and addition of singlet oxygen to cyclopentadiene

A further example for the safe conduction of explosive reactions in commercially available microstructured reactor has been described by Jähnisch and Dingerdissen.[33] They showed that the falling-film microreactor (developed by Institute für Mikrotechnik) is also suitable for the continuous photochemical generation of singlet oxygen in the presence of dissolved rose bengal. The photo-oxygenation of

cyclopentadiene **41** by singlet oxygen, followed by the reduction to 2-cyclopenten-1,4-diol **43** has been chosen as a model reaction (Scheme 17).

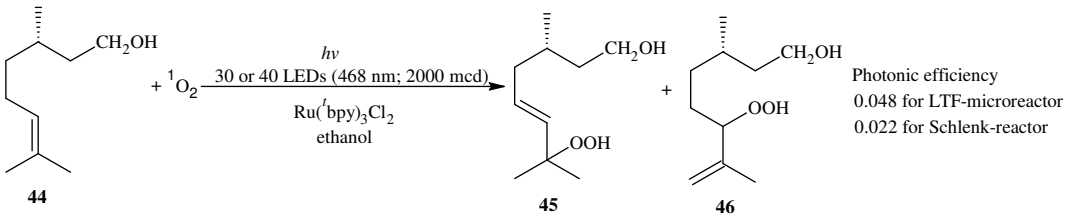


Scheme 17: Photoaddition of singlet oxygen to cyclopentadiene with further product reduction

The initially generated endoperoxide **42** is potentially explosive, which represents a safety concern for the large-scale conventional synthesis due to the pharmaceutical importance of its reduction product **43**. The photooxygenation step of this transformation took place on the reaction plate of a falling film microreactor, which has 32 parallel microchannels of 66 mm length, 600 µm width and 300 µm depth. A methanol solution of cyclopentadiene was pumped through the microreactor at a flow rate of 1 ml/min thus creating a very thin layer of liquid with a total volume that could be measured in microliters. Thus the concentration of the intermediate **42** remained low at all times. The reactor was furthermore cooled to 10–15 °C. The effluent containing the endoperoxide **42** was passed into a solution of thiourea in methanol at 10°C, which ensured immediate reduction of potentially explosive **42**. The above techniques and short holdup insured that the quantity of the present endoperoxide and oxygenated solution was always kept at a safe level. As a light source, the xenon lamp (1000 W) was used. The oxygen was fed to the reactor counter currently to the liquid with a flow rate of 15 L/h. Under non-optimised conditions, the desired product 2-cyclopenten-1,4-diol **43** was obtained in a yield of 20% (0.95 g). This study shows that a falling film microreactor is suitable for photooxygenation reactions on a preparative scale.

2.2.1.3 Photosensitized oxidation of citronellol

The photochemical oxidation of (*S*)-(–)-β-citronellol **44** is used to produce (–)-rose oxide as an elemental substance in the perfume industry. The first step of rose oxide synthesis is photochemical and represents the direct oxidation of (*S*)-(–)-β-citronellol **44** by singlet oxygen via a Schenck-ene reaction to give a mixture of peroxides **45** and **46** (Scheme 18). This transformation was selected by Meyer and co-workers as a model reaction for a comparison study of two different reactor types: microreactor and batch reactor in terms of space-time yield and photonic efficiency.[117]



Scheme 18: Dye-sensitized photooxygenation of (*S*)-(–)-β-citronellol

The microscale oxidation of (–)-citronellol was carried out in a commercially available microstructured reactor HT-residence glass (Little Things Factory GmbH) that consists of single half-round serpentine channel with a width of 1 mm, depth of 0.5 mm and total volume of 270 μL. The reaction mixture was saturated with compressed air in a double-wall storage container (outside the microreactor) and was continuously pumped through the microreactor in a loop where the illumination took place for about 60–70 h. As a light source an LED array (4 × 10 LEDs, λ_{max} = 468 nm) with a light intensity from 1 to 7.98 mW/cm^2 was utilised. The batch experiments were performed in the modified Schlenk-tube reactor with an illuminated volume 7.46 ml (total volume 40 ml). The light source LED-stick (2 × 15 LEDs, λ_{max} = 468 nm) with light intensity of 6.5 mW/cm^2 was placed in the middle of this reactor and an ethanol solution of (–)-β-citronellol was irradiated for 5-8 h. The reaction mixture before irradiation was also purged with compressed air for 20 min. The progress of the reaction was monitored by HPLC. The light intensity was measured with an electrical power meter. Based on the achieved results the photonic efficiency and space-time yields were calculated for both reactor types with regards to some experimental and mathematical presumptions. The photonic efficiency for the LTF-microreactor was 0.048, which was two times higher than the Schlenk-reactor. The highest STY has been detected for an initial concentration of citronellol 0.13 mol/L. However, on the direct comparison diagram the authors presented STYs of the microreactor at a citronellol start concentration of 0.06 mol/L and STYs of the batch reactor at a citronellol start concentration of 0.05 mol/L. At such conditions after a residence time of 20 min the STY was one order of magnitude higher in a microreactor than in a Schlenk-reactor.

It is also important to mention that Meyer and co-workers, in contrast to the commercial method, used a ruthenium polypyridyl complex (Ru(^{t}bpy)$_3$Cl$_2$ (tris(4,4'-*tert*-butyl-2,2'-dipyridyl)-ruthenium(II)-dichloride)) as photosensitizer for (–)-β-citronellol oxidation instead of conventional sensitizer rose bengal. They demonstrated that at higher citronellol/ruthenium complex ratio the photooxygenation of citronellol is faster. The ruthenium complex has higher photostability and quantum yields of singlet oxygen

formation compared with rose bengal. Nevertheless, the sensitizer comparison study completed by the authors with a 450 W xenon lamp (λ = 50–1600 nm) showed that rose bengal is about twice as efficient as the ruthenium complex.

In total this study demonstrated the superiority of the microreactor over the batch reactor in respect of photonic efficiency and STY. Also it showed the application of miniaturised light sources, *i.e.* LEDs arrays for photochemical reactions.

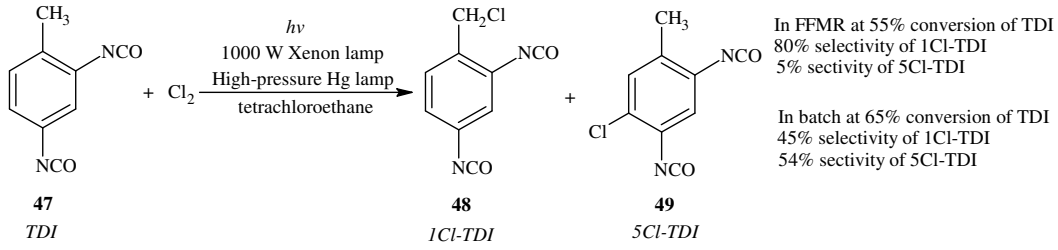
Recently, Seeberger and co-workers have studied the photooxygenation of alkenes, dienes, furan and thioether in a simple slug flow reactor.[118] The reactions were carried out in a fluorinated ethylene propylene tubing wrapped around a Schlenk photoreactor equipped with a 450 W medium pressure mercury lamp. Under optimal conditions, authors reported an unprecedented productivity of 2.5 mmol/min for photooxidation of citronellol.

The photosensitized oxygenations of α-terpinene, citronellol and allyl alcohols were also selected as a model transformations for the testing of a dual-channel microreactor[119] and triple-channel microreactor[120] by Kims' research group.

2.2.2 Photochlorination

2.2.2.1 Photochemical chlorination of alkylaromatics

The selective photochlorination of toluene-2,4-diisocyanate **47** (TDI, Scheme 19) was chosen by Jähnisch *et al.* as a model reaction to demonstrate the advantageous application of a falling film reactor over conventional reactors for photochemical heterogeneous reactions.[34] The selected transformation is of industrial interest due to the nature of its main product 1-chloromethyl-2,4-diisocyanatobenzene **48** (1Cl-TDI) which is used in the synthesis of polyurethanes.



Scheme 19: Photochlorination of toluene-2,4-diisocyanate

The experiments were carried out in a falling film microreactor (IMM) enclosed in a reaction plate with 32 parallel channels of width 600 μm, depth 300 μm and length 66 mm. The relatively concentrated solution of toluene-2,4-diisocyanate **47** (100 mmol in

30 ml of tetrachloroethane) was introduced to the reactor with flow rates ranging from 0.12 ml/min (defines residence time of 14 s) to 0.57 ml/min (defines residence time of 5 s) and was irradiated by an xenon lamp (1000 W, unfiltered) through a quartz reactor window. The backside of the reaction plate was maintained at a temperature of 130 °C to decrease side reactions (formation of a ring chlorinated undesired product toluene-5-chloro-2,4-diisocyanate (5Cl-TDI) **49**). It was revealed that the conversion of TDI **47** drastically increased from 30% to 81% with the increasing of residence time from 5s to 14s, while the selectivity of the target product 1Cl-TDI **48** decreased somewhat from 80% to 67% and this ensured enhancement of 1Cl-TDI **48** yield from 24% after 5s to 54% after 14s.

The effect of the reactor material on the reaction was investigated by using different reaction plates, one nickel and one iron. This study showed that the selectivity of the desired product **48** was affected notably by the plate material (50% for iron, 67% for nickel), which was attributed to the formation of $FeCl_3$ that acts as a Lewis acid. This led to increased formation of resin-like condensation products.

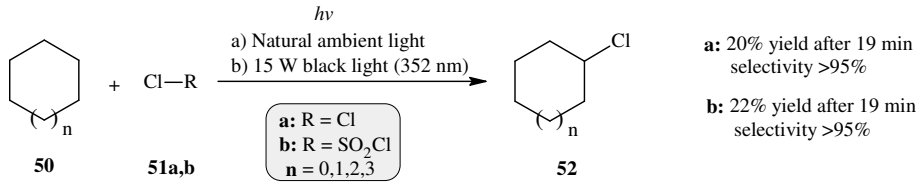
The microreactor results were compared to those obtained in a batch reactor and demonstrated that the use of the microstructured reactor led to increased product selectivity. The batch reactions were carried out in a glass flask with a high-pressure mercury lamp as light source. At similar conversion rates of toluene-2,4-diisocyanate **47** (55 % in FFMR, 65% in batch) the selectivity to the target product 1Cl-TDI **48** was 80% in the microreactor and only 45% in the conventional glass vessel. In addition the selectivity to the ring-chlorinated by-product (5Cl-TDI) **49** was significantly higher in the batch reactor (54%) compared to the FFMR (5%). The reactors efficiency was further characterised by the space-time yield of 1Cl-TDI **48**. The space-time yield of the desired product **48** achieved in the microstructured reactor (401 mol L^{-1} h^{-1}) was orders of magnitude higher compared to the conventional reactor (1.3 mol L^{-1} h^{-1}).

The advanced performance of the photochlorination reaction in the falling film microreactor was explained by the better penetration of photons and the higher mass-transfer rates in the thinner liquid films. Also, the chlorine radicals are located over the total film volume and high local concentration, which leads to recombination, are avoided. In a conventional reactor, the radical concentration near the light source is high, while at the centre of the reactor it is very low. As a result the selectivity of the desired side-chain chlorinated derivatives decreases and without photochemical induction chlorination prefers to take place at the aromatic core.

Based on the microreactor data, a former kinetic model for the TDI chlorination including by-product formation was suggested and used to predict product selectivity at full TDI conversion.

2.2.2.2 Photo-radical chlorination of cycloalkanes

Another example of selective synthesis of mono-chlorinated products **52** in flow microreactors with economic lighting was recently reported by Ryu *et al.*[121] This is the first example in microphotochemistry when ambient room light was used as a light source in microstructured reactors. The photo-radical chlorination of cycloalkanes (Scheme 20) was used as a model transformation for this study. It was investigated in two different microreactors and with two dissimilar light sources.



Scheme 20: Photo-radical chlorination of cycloalkanes

At the beginning the authors tested the chlorination of cyclohexane **50** (n = 1) with chlorine **51a** in a stainless steel microreactor (Dainippon Screen Mfg. Co., Ltd.) with a single channel 1000 μm wide, 300 μm deep and 2.35 m long (hold-up volume 0.7 mL). The reaction components were supplied to the microsystem separately (cyclohexane with flow rate 1.32 mL/h and Cl_2 with flow rate 7.68 mL/h) through a small T-shape micromixer (ID = 500 μm). In this micromixer molecular chlorine **51a** (1.1 mmol) was diffused in cyclohexane **50** (46 mmol) and uniform mixture entered into the reactor. The solution was flushed through microreactor while triggered by natural room light through Pyrex cover within 19 min. The eluted product was collected in a flask with 10% sodium sulphite and GC analysis showed that the desired monosubstituted chlorocyclohexane **52** was generated in a yield of 20% with selectivity >95%.

Next, authors investigated more gentle chlorination reagent sulfuryl chloride **51b**, which was at the same disperse phase as cyclohexane and did not require extra premixing. However, the back pressure regulator was connected to the reactor outlet to avoid slug flow formation during the process. Sulfuryl chloride **51b** needs UV light for the activation. Therefore, a 15 W single lamp with black light (λ = 352 nm) was employed as irradiation source and before described reactor was replaced for another one with additional cooling channel. This reactor was made of Foturan glass (Microglas Dwell

device) and had reaction channel of 1000 μm width, 500 μm depth, 1.9 m length and total hold-up volume 0.95 mL. In such conditions monosubstituted chlorocyclohexane **52** was again selectively formed in yield of 22% after irradiation for 19 min. Moreover, double increasing of molar ratio of cyclohexane **50** to 80 equiv. did not affect the product **52** yield (20%). As expected, higher product yields were achieved after prolonged residence time for 57 min (yield 35%) and duplication of light power to 30 W (yield 45%). The established procedure was applied to other cycloalkanes: cyclopentane, cycloheptane and cyclooctane. The achieved results clearly demonstrated that tested chlorination reactions yielded corresponding monochlorocycloalkanes with selectivity higher than 95% under irradiation by energy saving light sources or natural light.

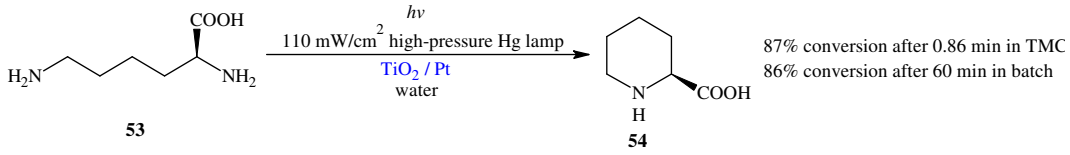
2.3 Catalytic reactions

Microreactors show potential for use in catalytic reactions due to their unique features. First of all they have large surface to volume ratio which is provided by microstructured channels. Therefore if a catalyst is immobilised on the walls of the channels it could be possible to increase the specific illuminated surface area of photocatalyst and consequently maximise interactions of catalyst with excitation light and reagents. The majority of the photocatalytic microreactors used in chemical investigations have been self-fabricated by researchers. Hence it has been widely accepted that the illuminated specific surface area of photocatalyst within a reactor is the most important design parameter of photocatalytic reactors. Secondly, a removal process for the catalyst immobilised on the channel walls is unnecessary in the reaction sequence. The product is separated from the catalyst by the flow, which can also improve the selectivity of the product. One of the most widely used photocatalyst is TiO_2.[122]

Microstructured catalytic photoreactors show potential for use in chemicals decomposition study,[123] hydrogen production,[124] treatment of waste water and exhaust air.[43,66,83,125–129] Only several examples of their application in synthetic chemistry have been documented in the literature to date and are depicted below.

2.3.1 Photocatalytic synthesis of L-pipecolinic acid

The first application of microsystem with integrated chemical functional units in organic synthesis have been reported by Takei *et al.*[130] The authors examined the photocatalytic redox-combined synthesis of L-pipecolinic acid **54** (L-PCA) from L-lysine **53** (Scheme 21) in a self-fabricated microchip.



Scheme 21: Photocatalytic synthesis of L-pipecolinic acid

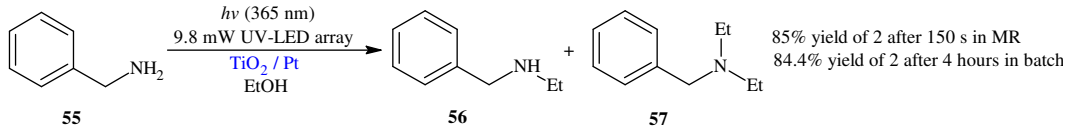
The titania-modified microchannel chip (TMC) used in this study was composed of two Pyrex glass substrates. One substrate with branched channels of 700 µm wide and 3.5 µm deep was fused to other substrate with a 300 nm thick coating of TiO_2. The TiO_2 coating film served as catalyser and was formed by TiO_2 particles with diameter 100 nm. Platinum was used as reducing agent at 0.2 wt% in the film. The microchip was irradiated using a high-pressure mercury lamp with a UV transmitting filter. A 2 mM aqueous solution of L-lysine was pumped through TMC with different flow rates thus determining the reaction time. The crude product mixture was collected from the reactor out-let and was analysed by HPLC. The reaction performance in TMC was compared to a batch set-up using a bulk-cuvette and TiO_2 particles (diameter 25 nm) in suspension. It is notable that the ratio of illuminated surface area to the solution volume was comparable in both setups (0.29 m^2/ml for TMC and 0.25 m^2/ml for suspended particles). The conversion of L-lysine **53** to L-pipecolinic acid **54** in the microchip reached 87% after a residence time less than 1 min (0.86 min). Whereas in the batch experiment the same conversion rate 86% was achieved only after 1 hour. The examination of selectivity and enantiomeric excess (ee) showed that these were independent of reaction time and were similar in micro- and bulk-setups (selectivity was 22% and ee was 50% and 47% respectively).

On the other hand, the productivity of L-PCA **54** i.e. amount moles produced per minute was much lower in microchip (2.8×10^{-10} mol/min) than that in the bulk system (1.9×10^{-8} mol/min). This was due to the larger volume capacity of batch cuvette (4 ml), but this disadvantage may be overcome through the formation of microreactor clusters in the future. An important advantage of the catalytic microreactor is the elimination of a separation step, as the photocatalyst remains in the microstructured reactor while the product is eluted. The authors also state other advantage of TMC the applicability to the potential-controlled photocatalytic reactions.

2.3.2 Photocatalytic *N*-alkylation of amines

A significant input in the photocatalytic synthesis performed in microstructured reactors has been done by Matsushita *et al.*[43,131] In their work they used not only miniaturised

reactors but also minimal space and low photon cost light source such as UV-LED array thus demonstrating the total miniaturisation of experimental setups. The adaptability of these setups for synthetic photoreactions was proved by successfully tested model reactions. Hence TiO_2 catalised *N*-ethylation of benzylamine **55** (Scheme 22) was chosen by authors as exemplary reaction.



55 **56** **57**

Scheme 22: *N*-ethylation of benzylamine

This reaction was studied in three house-made quarts microstructured reactors with specific illuminated surface area per unit of volume of 7.3×10^3, 6.0×10^3 and 4.0×10^3 m^2/m^3. Such huge areas were provided by reactor channels with width 500 µm, length 40 mm and depth 300, 500 or 1000 µm respectively. The channels sides and bottom were coated with catalyst TiO_2 (Pt-loaded and Pt-free). A 1 mM alcohol solution of benzylamine **55** was fed into the microreactors with a flow rate between 2 µl/min and 40 µl/min and was irradiated with the UV-LED array (λ_{max} = 365 nm) with total optical power output 9.8 mW. The reaction products were analysed by GC or HPLC methods. It was shown that benzylamine **55** could be converted to the main *N*-alkylated product **56** in yields of 43% after 90 s or 85% after 150 s.

The optimisation study of the reaction solvent was carried out and ethanol was found to be the most suitable solvent for this transformation due to the kinetic stability of its ethoxy radical. Therefore ethanol was applied for alkylation reactions of other amines. Aniline and butylamine were tested and gave corresponding *N*-ethylated products in yields of 11% and 36%, respectively after residence time of 180 s. An investigation of the effect of microchannel depth was performed in above mentioned reactors. It was revealed that the efficiency of *N*-alkylation was enhanced by decreasing depth, this was referred to the increased illuminated surface to volume ratio. Interestingly, this reaction was shown to proceed in the presence of titanium dioxide photocatalyst, even without co-catalyst platinum. Yields of up to 98% of *N*-alkylated product **56** were achieved after 90 s. In contrast to the data reported in other literature,[132] this reaction does not occur in batch conditions without the presence of platinum. In addition, no *N,N*-dialkylated product **57** was obtained when platinum was present or absent, as is usually the case in batch conditions. The absence of bis-alkylation was achieved by the continuous-flow mode and monochromatic irradiation, which prevents the undesired follow-up reaction.

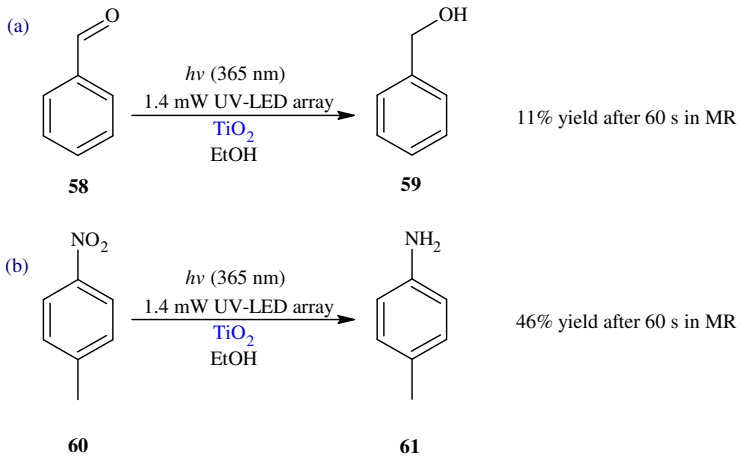
In an extension of this work authors further investigated the methodology of enhancement of reaction yield and selectivity by optimizing the irradiation and flow conditions.[133] For this study they developed new photocatalytic microreaction system with microchannels of 500 μm wide, 25 μm deep and 50 mm long. The remarkably high created surface area of TiO_2/Pt photocatalyst (4.0×10^3 m^2/m^3) was irradiated with more powerful LED array (total optical power output 490 mW). The alkylation of amines (benzylamine, aniline and piperidine) proceeded faster in this microsystem compare to previously described. For example *N*-ethylbenzylamine **56** was obtained in yield of 62% after 6 s, but next to that bis-alkylated product *N,N*-diethylbenzylamine **57** was also detected in 3.8% yield. The same trend was noticed for aniline. This phenomenon was described by authors as influence of excitation light intensity of UV-LEDs and residence time on product selectivity. Thus at shorter residence time (5 s) the formation of main product secondary amine **56** increased with the increasing of light intensity, but at prolonged residence time (60 s) the formation of consecutive product tertiary amine **57** enhanced with the increasing of light intensity. These results clearly demonstrate that two types of reaction products (secondary and tertiary amines) can be obtained selectively by precise control of the irradiation and flow conditions.

In total this study expressed the possibilities of catalytic microreaction systems for organic synthetic reactions.

2.3.3 Photocatalytic reduction in microreactors

Another example of synthetically useful transformation has been also reported by Matsushita *et al*.[134] The authors examined photocatalytic reduction of benzaldehyde **58** and nitrotoluene **60** (Scheme 23) as a model reactions in microreactors to prove their benefits for organic photocatalytic transformations.

For this study photocatalytic quartz microreactors with immobilized photocatalyst were fabricated by Matsushita and co-workers. These reactors have a microchannel of 500 μm width, 100 μm depth and 40 mm length with total specific illuminated surface area per unit of liquid of 1.4×10^4 m^2/m^3 (ca). The bottom and side walls of the microchannel were coated with a photocatalytic TiO_2 layer. An array of 365 nm UV-LEDs with optical power output 1.4 mW was employed for the excitation of a photocatalytic microrector.



Scheme 23: Photocatalytic reduction of (a) benzaldehyde and (b) nitrotoluene

Alcoholic solutions of benzaldehyde **58** (0.1 mM) saturated with nitrogen were used and ethanol was found to be the most efficient solvent. Under such conditions, benzyl alcohol **59** gave a yield of 11% after 60 s. Photoreduction of *p*-nitrotoluene **60** proceeded faster and *p*-toluidine **61** was obtained in a yield of 46% after 60 s. The assumed reactions mechanism was established and oxygen was revealed as quencher of TiO_2 catalyst. In general these unoptimised reactions demonstrated that microstructured reactor technology can be utilized for the efficient reduction of organic compounds.

2.4 Microphotochemistry in industry

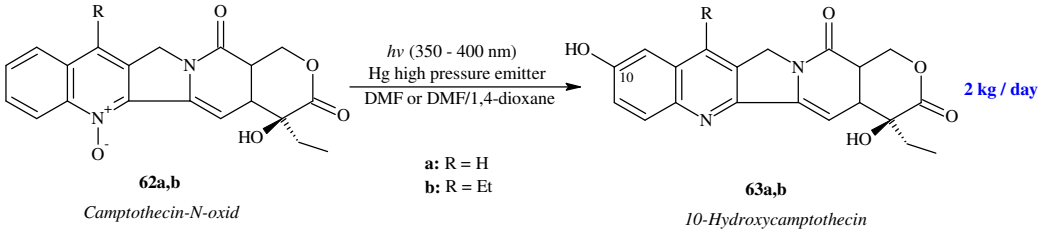
The above summarised photochemical transformations performed in microreactors have significant research interest and importance in academia, however the photochemical processes realised on industrial scale are still rare. There are several contributing factors for this:

- Specialised microreactors that are generally made from expensive materials, such as stainless steel or quartz-glass are required. Also the fabrication of reactor microchannels is costly and complicated itself.
- Light sources create a difficulty on an industrial scale. Despite the increased utilization of energy efficient LEDs as irradiating light sources for photochemical reactions, a medium and high pressure mercury lamps still have predominant position in this area. It is known that mercury lamps are costly to run, have a limited lifetime and additionally tend to generate a large amount of heat and therefore require additional cooling systems.
- Product synthesis in kilograms quantity. Microreactors 'numbering-up' generally involved further complex automation.

Nevertheless, the proved advantages of photochemical synthesis in microreactors overcame listed above difficulties and industrial scale syntheses of pharmaceutically important compounds in microreactor array have been declared recently.[72]

2.4.1 Synthesis of 10-hydroxycamptothecin and 7-alkyl-10-hydroxycamptothecin

The first sophisticated production of camptothecin derivatives in a microreactor plant (Figure 18) has been patented in 2009 by HERAEUS GmbH (Germany).[72] The synthesis of 10-hydroxycamptothecin **63a** and 7-ethyl-10-hydroxycamptothecin **63b** by irradiation of camptothecin N-oxide **62a** or 7-ethyl camptothecin N-oxide **62b,** respectively (Scheme 24), was performed. The camptothecin derivatives **63a** and **63b** are used in the synthesis of important pharmaceuticals for cancer treatment irinotecan and topotecan.



Scheme 24: Synthesis of camptothecin derivatives

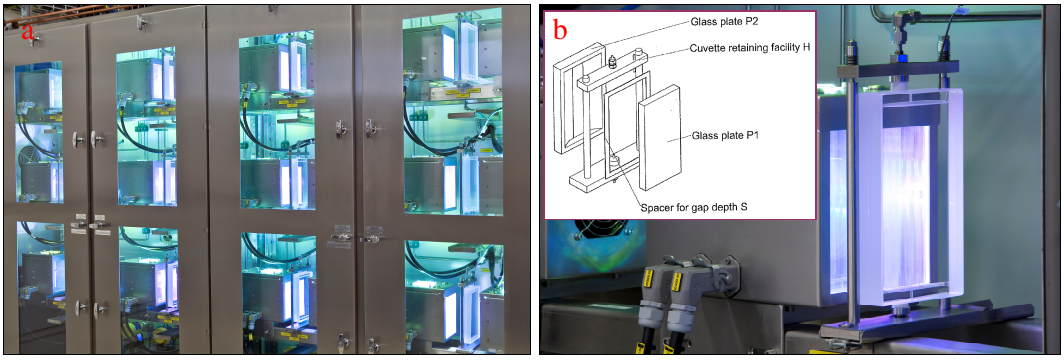


Figure 18: a) W. C. Heraeus: Photochemical production plant; b) quartz glass micro-photoreactor irradiated by Hg high pressure emitter (Heraeus Noblelight); inset shows a diagrammatic arrangement of microreactor

The developed microreactor plant consisted of twelve microreactors connected in parallel and irradiated by individual light sources (Figure 18a). The microreactors have a very simple design. They comprise of two transparent quartz glass plates arranged in parallel and connected in a firmly bonded manner with a spacer for the gap from 40 µm to 100 µm (Figure 18b, inset). Such a design provides a very thin layer of reaction liquid

for irradiation. As the light source is a mercury high pressure emitter (Heraeus Noblelight) with a UV emission wavelength range from 350 nm to 400 nm and optical power output of 250 W were used. These lamps were arranged in a spatially separated irradiation unit that also comprise spectral filters with a specific band pass and coating on both sides.

The productivity of the microreactor plant was estimated by the amount of 10-hydroxycamptothecin **63a** produced within 24 hours. It was established that at a conversion rate of 95% of camptothecin N-oxide **62a** to 10-hydroxycamptothecin **63a** the desired product **63a** was produced in 2 kg per day (yield 90%). In contrast, at the batch system the maximum reached conversion was only 85% with a product yield of 50%. Moreover, in the microreactor array the solution of camptothecin N-oxide was used at a concentration of 0.6% weight, which was six times more concentrated than in the batch (0.1% weight).

This is the first example of a photochemical process performed in a microreactor array, which is suitable for economic industrial production.

2.5 Concluding remarks

The examples presented in this chapter nicely demonstrate the potential of photochemical synthesis in microstructured reactors. A microphotochemistry is a promising and fast growing research area. Recently, the application of continuous flow reactors was further extended to synthesis of the anti-malaria drug artemisinin,[135] synthesis of enantiomerically pure *trans*-β-lactams,[136] organo-photocatalysis,[137–139] laser induced photochemical reduction of flavone,[140] preparation of *3H*-azepinones via photolysis of aryl azides,[141] synthesis of annelated cyclopentanone.[142] The microtechnology takes full advantage of the small dimensions and flow condition, which results in the reduction or complete elimination of side reactions, enhanced selectivity, improved mass transfer, increased photonic efficiency and reduction of hazards and wastes. The large area-to-volume ratio within the microchannels is especially advantageous for photocatalytic applications. Thus microphotochemistry has a good potential to emerge as an important future R&D tool, for example in modern lead development processes and production technology as have been recently demonstrated by Heraeus.

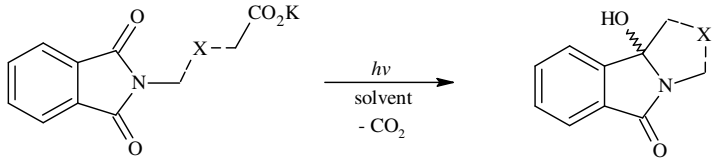
Thesis proposal

3. Thesis proposal

Microtechnology is currently an area of rapid growth in many fields of chemistry. For photochemical reactions, microreactors exhibit higher spatial illumination homogeneity, extensive light penetration, large surface-to-volume ratios and laminar flow, as described in the literature review chapter. Therefore, the main aim of this work was to develop a novel resource- and energy-efficient approach in synthetic photochemistry by combining techniques established in *organic photochemistry* and *microflow engineering* with both LED and fluorescent light technologies. To reach this aim the following plan of research work was suggested.

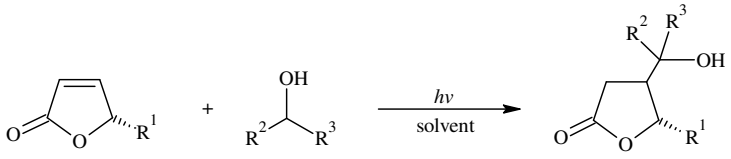
1. Determination of *homogeneous* and *heterogeneous* photochemical model reactions that are regarded as environmentally friendly alternatives to thermal reactions and have feasible industrial application. As an example:

– photodecarboxylative addition and cyclization reactions involving phthalimides, have been recently established as efficient alternatives to Grignard additions and SmI_2–catalyzed reactions (Scheme 25).[114,143–150]



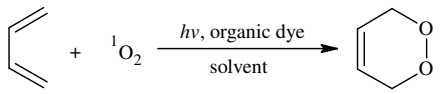
Scheme 25: Photodecarboxylative addition and cyclization

– the addition of photochemically generated radicals to α,β-unsaturated carbonyl and carboxyl compounds that represent an attractive alternative to the Michael addition (Scheme 26).[151]



Scheme 26: Photoalkylation

– photooxygenation reactions that were developed as a competent alternative to oxidations with metal oxides (Scheme 27).[152,153]



Scheme 27: Photooxygenation

2. The transfer and optimisation of selected model reactions from the conventional Rayonet reactor or Schlenk flasks to commercially available microreactors. The proposed homogeneous reactions will be transfer to the commercially available dwell device (mikroglas) and microchip (micronit) while heterogeneous reactions will be transferred to the falling film microreactor (IMM). Results obtained in the conventional reactor will be compared with the equivalent results achieved in the microflow conditions and any improvements or similarities will be determine and used for the assessment of reactor feasibility for photochemical synthesis.

3. Evaluation of feasibility of existing photoreactor set-ups for different type photochemical transformations. It is envisaged to investigate each model transformation in more than one experimental system and compare achieved results. All experimental setups will be evaluated in terms of products yield (conversion), energy efficiency and reactor efficiency.

4. Overcoming of exist disadvantages of commercially available photoreactors and development of a novel multicapillary reactor that represent an advance platform for future synthetic photochemistry and development of a new slug flow column reactor suitable for photooxygenation reactions.

5. Establishment of the most technically advanced and resource capable photochemical system.

Chapter 4

Intra- and intermolecular transformations involving phthalimides

4.1 Introduction

Phthalimides are an examples of heterocyclic aromatic imides. In organic photochemistry phthalimides can be used as protecting groups in peptide synthesis and for the formation of primary amines via Gabriel synthesis. [154] They have anti-fungal and herbicidal activities and are useful agrochemicals. Some phthalimides have pharmaceutical significance. For example bioactive compound AKS-186 possesses inhibitory activity for thromboxane A_2.[155]

Intra- and intermolecular transformations involving phthalimides have been selected as model reactions for a comparison study of batch vs. micro-photochemical reactor since they have a perfect atom economy, which means that all atoms from the starting materials appear in the final product. Also photochemistry of phthalimides has been studied in detail by the Oelgemöller research group in the last decade.[114,143–150]

In our work two experimental set-ups have been used: conventional Rayonet reactor and microflow dwell device. Both systems have been tested for the same model reactions and their efficiency was evaluated in terms of reaction conversion rates and space-time-yields.

4.2 Experimental set-ups

4.2.1 Batch system – Rayonet reactor

A conventional Rayonet chamber reactor RPR-200 (Southern New England, Figure 19) or RPR-100, equipped with 16 fluorescent tube lamps **5** was the main component of the batch setup. For UVB irradiation it was fitted with 16 RPR-3000Å lamps ($\lambda = 300 \pm 25$ nm) with total optical power output 128 W (16 × 8W). For UVA irradiation it was furnished with 16 RPR-3500Å lamps ($\lambda = 350 \pm 25$ nm) with the same total optical power output 128 W (16 × 8W). The prepared reaction mixture was filled into a Pyrex Schlenk flask **1** or Pyrex test tube ($\lambda \geq 280$–300 nm, transmission is about 30% at 300 nm), which was placed in the middle of the Rayonet reactor. The distance between flask and lamps was about 8.4–9.5 cm. The appropriate Schlenk flasks (32 mm inner ∅) for liquid volume 100 ml or 50 ml and Pyrex tubes (9 mm inner ∅) for liquid volume 15 ml were used as reaction vessels. To avoid overheating, the reaction mixture was cooled with water using a cold-finger **2** (24 mm outer ∅) inserted into the Schlenk flask **1** (cooling water demand 1–4 L min^{-1}) or using a general system fan. Thus the experimental temperature was kept constant and below 25 °C. The reaction mixture in the Schlenk flask was constantly flushed with a gentle stream of nitrogen **3** for

degassing (mainly remove O_2) and mixing purposes. The leaving gas stream was allowed to exit through a short Teflon tube **4** or syringe needle.

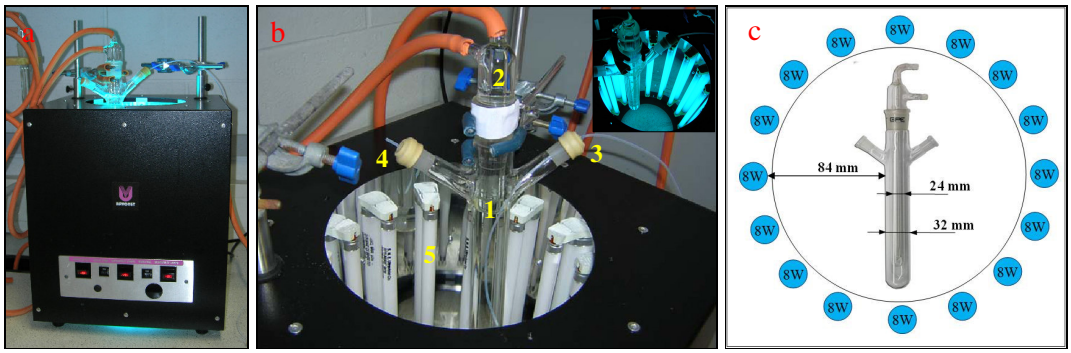


Figure 19: Rayonet photoreactor RPR-200 and experimental set-up (**a** and **b** actual set-up pictures; **c** – set-up arrangement): **1** – Pyrex Schlenk flask; **2** – cold finger; **3** – N_2 inlet; **4** – gas outlet; **5 –** 16 RPR-3000Å lamps

4.2.2 Continuous flow system – dwell device

The microsystem set-up consists of several individual components joined together thus creating a functional system (Figure 20). The major part of this set-up was the commercially available microreactor **1** (dwell device, mikroglas[37]) which was placed under a UV panel **2** (Luzchem) fitted with 5 fluorescent tube lamps (emissive area: 18 cm × 30 cm). For UVB irradiation 5 RPR-3000Å lamps ($\lambda = 300 \pm 25$ nm) with total optical power output 40 W (5 × 8W) were used. For UVA irradiation 5 RPR-3500Å lamps ($\lambda = 350 \pm 25$ nm) with the same total optical power output 40 W (5 × 8W) were utilised, respectively. The microreactor consists of a glass plate incorporated into a stainless steel frame (Figure 20a). The glass plate is made out of Foturan™ glass ($\lambda \geq 280$ nm, transmission is about 30% at 300 nm) and comprises two serpentine channelled glass layers (top and bottom) connected in a firmly bonded manner (Figure 21). The top glass layer has 5 short parallel heat-exchange channels through which water was passed to control the reactor temperature. The bottom layer has one serpentine reaction channel 2 mm wide, 0.5 mm deep, 1.15 m long (20 turns) with an internal volume of 1.68 ml where the reaction took place. The prepared reaction mixture was pumped through the reaction channel using a programmable syringe pump **3** while irradiated by Luzchem panel **2** via reactor aperture 118 mm × 73 mm. The distance between the lamps and reactor screen was 7.7 cm. The product mixture was collected in a round bottom flask **7** outside the irradiated area. To wash out the remaining reaction mixture from the reactor channel the syringe **4** was filled with pure solvent and loaded into the pump **3** with the

same flow rate as used during the experiment. The washed liquid was added to the previously collected product mixture. The used syringe **4** has a capacity of 10 ml (ID = 14.56 mm) and is made of borosilicatglass. The cooling water (200 ml) was re-circulated by a rotary pump **6** from a conical flask **8** placed in a beaker with ice, thus the experimental temperature was about 20°C. The ice bath was also placed on top of the Luzchem panel to prevent overheating of the lamps (not shown on the Figure 20). All set-up components, i.e. pumps, dwell reactor and flasks were connected by chemically resistant PTFE tubing. The PTFE shut-valve **5** was mounted between the syringe pump and microreactor to keep the liquid volume in the reactor constant and prevent its backward running during refilling of the syringe by solvent. All used connections were also made of PTFE.

The irradiation time was controlled via the pump flow rate and it simultaneous starts/stops with the Luzchem panel on/off switch.

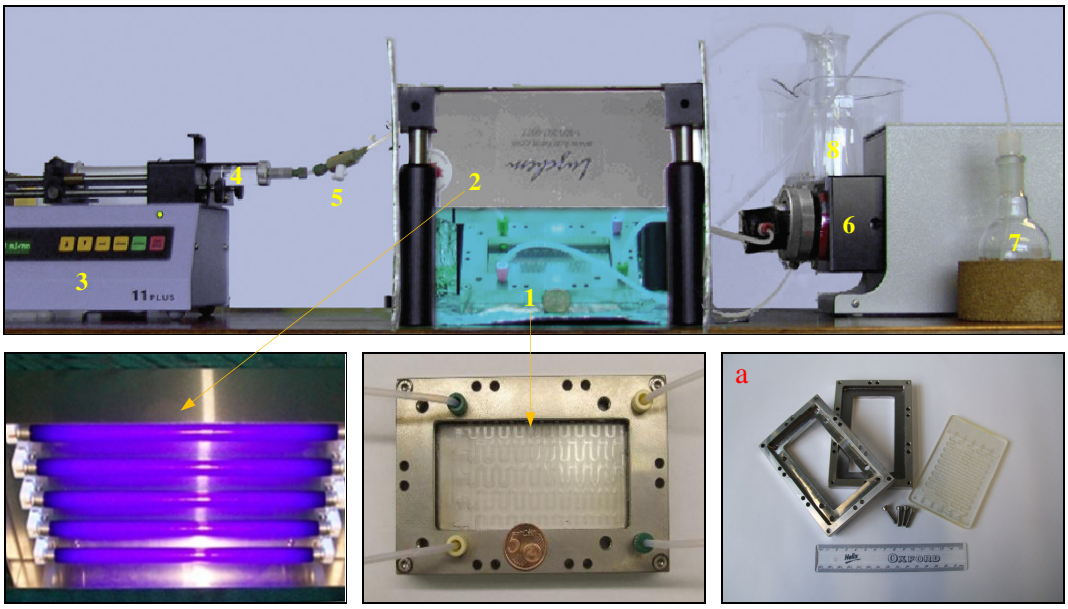


Figure 20: Dwell device setup: **1** – microreactor dwell device ((a) showed dissembled microreactor with its main part Foturan^{TM} glass plate); **2** – Luzchem panel with 5 RPR-3500Å lamps; **3** – programmable syringe pump; **4** – syringe for 10 ml; **5** – shut-valve; **6** – rotary pump; **7** – collection flask; **8 –** cooling system (conical flask with water in the ice beaker)

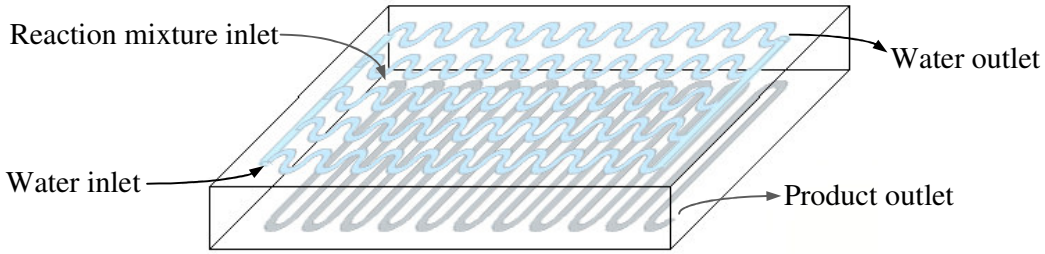
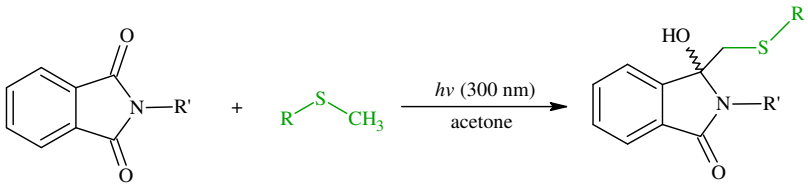


Figure 21: Schematic of the microreactor glass plate with the comprised two channelled layers: heat-exchange (shown in blue) and reaction (shown in grey)

4.3 Model reactions and experimental results

4.3.1 Intermolecular photoaddition of thioethers to N-methylphthalimide

This transformation was chosen as a model reaction for our study because upon UV irradiation, phthalimides react with thioethers via photoinduced electron transfer (PET) and yield only desired photoaddition products (Scheme 28). Additionally these reactions are sensitized by acetone ($\lambda_{max_{n\rightarrow\pi^*}}$ = 264 nm in H_2O), which also acts as solvent.



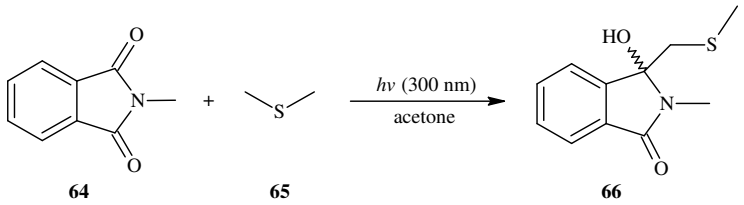
Scheme 28: Photoaddition of thioethers to phthalimides

This transformation was first described by Kanaoka and co-workers[156] but problems with the reproducibility of this reaction have since emerged. An additional drawback is the usage of large excess amounts of thioethers, typically 10 equivalents. Due to the volatility and the strong stench of most thioethers, however, working with them on a large scale is "problematic". For that reason the development of a microscale method could be a more favourable approach. Photoadditions involving the simple thioethers dimethyl sulphide **65** and ethyl methyl sulphide **67** to N-methylphthalimide (NMP) **64** were thus investigated.

4.3.1.1 The addition of dimethyl sulphide to N-methylphthalimide

The photochemical reaction shown in Scheme 29 was carried out in the Rayonet reactor (*experiments 1* and *2*) and simultaneously in the dwell device (*exp. 3*) and the conversions of NMP **64** were determined by ^{1}H-NMR spectroscopy of the crude

products. The signal integration for the NC$\underline{H}_3$ protons of **64** was compared to the signal integration for the NC$\underline{H}_3$ protons of **66**. It is important to indicate that the irradiated volume of the initial mixture in the batch system was 100 ml, whereas that in the microsystem was ten times smaller, only 10 ml. However the concentration of N-methylphthalimide solution was kept constant at 15 mM in all experiments.



64 **65** **66**

Scheme 29: Photoaddition of dimethyl sulphide to NMP

The results (Table 3) demonstrated that the Rayonet reactor outperformed the micro-dwell device. Even after careful optimization of some steps of the reaction procedure (dimethyl sulphide was added as last component and reaction mixture was further sonicated and degassed only for 5 min), the maximum conversion of NMP in the dwell device was low with just 8%, whereas the Rayonet reactor furnished conversions of 22% and 58%. Furthermore, all reactions were rather sluggish and the corresponding dehydration products, i.e. isomeric olefins, were commonly observed. Although dehydration is known to proceed in the presence of trace amounts of acids, the initial photoaddition products can be isolated from related photodecarboxylation reactions (described below). It is therefore believed that an unknown breakdown product of the thioether is causing this dehydration.

Table 3: The conversions of NMP in the photoaddition reactions with dimethyl sulphide

Experiment	Type of reactor	Residence time, [h]	Conversion, [%][a]
3	Dwell device	1	8
1	Rayonet	1	22
2	Rayonet	2	58

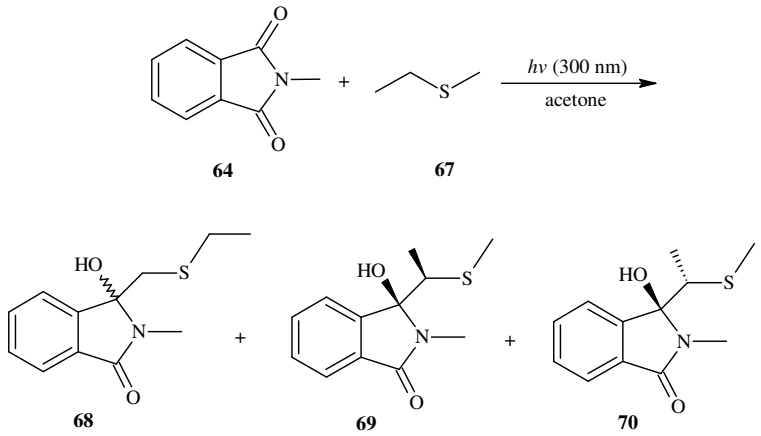
[a] Determined by ^{1}H-NMR spectroscopy

In the microsystem residence time is defined by the flow rate of syringe pump and was calculated according to the following equation *(1)*:

$$\text{time (min)} = \text{volume of microreactor (ml)} / \text{flow rate (ml/min)} \qquad (1)$$

4.3.1.2 The addition of ethylmethyl sulphide to N-methylphthalimide

The reaction of NMP **64** with ethylmethyl sulphide **67** (Scheme 30) was investigated in the Rayonet reactor only (*exp. 4*). The reaction showed low regioselectivity and gave a complex mixture of various isomeric products **68**, **69** and **70**. In contrast to the original procedure reported by Kanaoka and co-workers,[156] the reaction in the Rayonet reactor using a residence time of 2 hrs gave only a low conversion of 16%. A mixture of isomers was generated and the ratio of products was determined as 30:34:36 (**68:69:70**, respectively; Scheme 30). Given the poor performance of this reaction it was decided that it would not be suitable for transfer to the microreactor. The alternative addition reactions of sulphur containing carboxylates to NMP were chosen instead.



Scheme 30: Photoaddition of ethylmethyl sulphide to NMP

4.3.2 Intermolecular photodecarboxylative additions of carboxylates to NMP

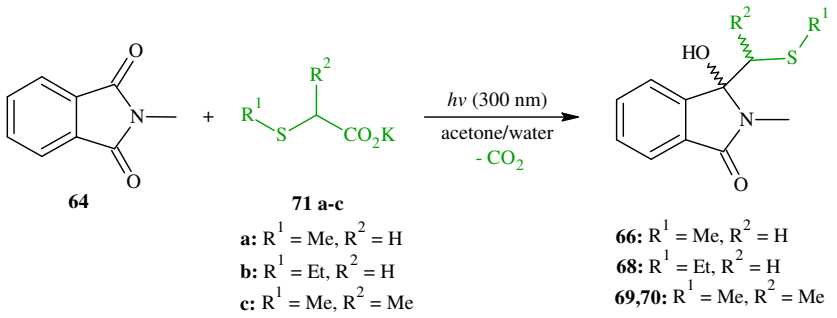
Photodecarboxylative (PDC) additions of carboxylates to phthalimides have been recently established as efficient alternatives to Grignard additions and SmI_2–catalyzed reactions.[114,143–150] Major advantages of the photodecarboxylation protocols are its simple procedure and the usage of carboxylates as alkylating agents. These starting materials are easily accessible in large quantities and with broad structural diversity, and are additionally stable and non-volatile. In contrast to other PET additions involving phthalimides,[157] loss of carbon dioxide proceeds irreversibly and regioselectively. Therefore photoadditions of alkyl carboxylates to NMP **64** furnished alkylphthalimidines as the only products. Also, these transformations have a generally high photon efficiency (Φ = 0.4-0.6) and are sensitized by acetone ($\lambda_{max_{n\rightarrow\pi^*}}$ = 264 nm in H_2O), which also acts as co-solvent. Direct excitation of NMP is also possible but may yield additional side products.

4.3.2.1 Intermolecular photodecarboxylative additions of sulphur-containing carboxylates to NMP

Sulphur-containing carboxylates are known to react with NMP via decarboxylation.[148,158] Compared to the corresponding thioethers, the sulphur-containing carboxylates are less volatile and consequently less unpleasant to work with. The regioselectivity of the reaction is furthermore dictated by the position of the carboxyl group. Addition exclusively occurs at the site of the leaving group carbon dioxide. In contrast, the thioether gives a mixture of regioisomers. Also irradiations involving α-thioalkyl-substituted carboxylates gave higher yields and conversions.
As sulphur containing carboxylates the potassium salts of the following carboxylic acids were utilised (Scheme 31):

- methylsulfanyl acetic acid (**71a**),
- ethylsulfanyl acetic acid (**71b**) and
- 2-methylthio propanoic acid (**71c**).

The ethylsulfanyl acetic acid **71b** was obtained from the commercial supplier *Fluka*. Two other acids, methylsulfanyl acetic acid **71a** and 2-methylthio propanoic acid **71c** were synthesised in the laboratorial conditions (*experiments 5 and 6*, respectively). The details of the acid synthesis are provided in the experimental part of this chapter.



Scheme 31: Intermolecular PDC additions of sulphur-containing carboxylates to NMP

4.3.2.1.1 Procedure optimization in the batch system

The initial study of photoaddition of sulphur containing carboxylates to NMP was done using a stoichiometric ratio of 1:10 of NMP to carboxylic acid (*exp. 7*). This ratio was the same as in the thioether photoaddition reactions. It was important to investigate the reaction output at lower acid concentration, as this would reduce the amount of chemicals used and consequently the amount of waste generated. The stoichiometry of

reagents was optimised using methylsulfanyl acetic acid **71a** (*exp. 8*). It was found that a ratio of 1:3 of NMP : methylsulfanyl acetic acid gave almost the same yields (86% vs. 88%) after the same residence time of 1 hour as compared to the ratio 1:10. Consequently, all further experiments were carried out using a 1:3 stoichiometric ratio. The results obtained in the *experiment 8* and the following *experiments 9* and *10* with the ethylsulfanyl acetic acid **71b** and 2-methylthio propanoic acid **71c,** respectively, are summarised in the Table 4. These results clearly demonstrate that the photoaddition of the carboxylates is indeed superior to the photoaddition of thioethers to NMP in respect of reaction rate, practicality (handling of starting materials), % conversion and isolated product yield.

Table 4: Comparison of the obtained yields in the photoaddition reactions of sulphur containing carboxylates and corresponding thioethers to NMP

Experiment	S-containing acid		Compound	Residence time, [h]	Yield, [%]
	R^1	R^2			
8	Me	H	**66**	2	86 (56[a])
9	Et	H	**68**	2	91 (6[b])
10	Me	Me	**69**,**70**	2	96 (6[b]) (45:55[c])

[a] Isolated yield of product **66** in the alternative reaction with thioether dimethyl sulphide; [b] isolated yield of products **68** and **69**, **70** (mixture of regioisomers) in the alternative reaction with ethylmethyl sulphide; [c] the ratio between diastereoisomers **69** and **70** respectively, determined by ^{1}H-NMR spectroscopy

4.3.2.1.2 Residence time optimisation study in the batch system (Rayonet) and microsystem (Dwell device)

The PDC addition of potassium 2-(methylthio) acetate **71a** to NMP **64** was selected as a model reaction for the investigation of the dependency between residence time and reaction efficiency. This transformation was studied in both systems: Rayonet and dwell device with four different residence times (*experiments 11–18*).

Residence time in the dwell device was adjusted to match the irradiation time in the Rayonet reactor. The obtained results are presented in Table 5 and they clearly demonstrate that this reaction underwent faster conversion in the microsystem compared to the batch reactor. Moreover, complete conversion was achieved in the dwell device after 1 hour and this residence time has been established as optimal. Whereas the Rayonet reactor gave incomplete conversion of 86% and required prolonged irradiation. The conversions of NMP **64** were determined by ^{1}H-NMR spectroscopy of the crude

products. The signal integration for the NC<u>H</u>$_3$ protons of **64** was compared to the signal integration for the NC<u>H</u>$_3$ protons of **66** (Figure 22).

Table 5: Conversion of NMP **64** to product **66** in dwell device vs. Rayonet reactor

Experiment	Flow rate, [ml/min]	Residence time, [min]	Conversion to 66, [%][a]	
			Dwell device[b]	Rayonet[c]
14[c], 18[b]	0.12	14	4	2
13[c], 17[b]	0.08	21	34	20
12[c], 16[b]	0.042	40	66	44
11[c], 15[b]	0.028	60	100	86

[a] Determined by ^{1}H-NMR spectroscopy; [b] number of corresponding experiment carried out in the dwell device; [c] number of corresponding experiment carried out in the Rayonet reactor

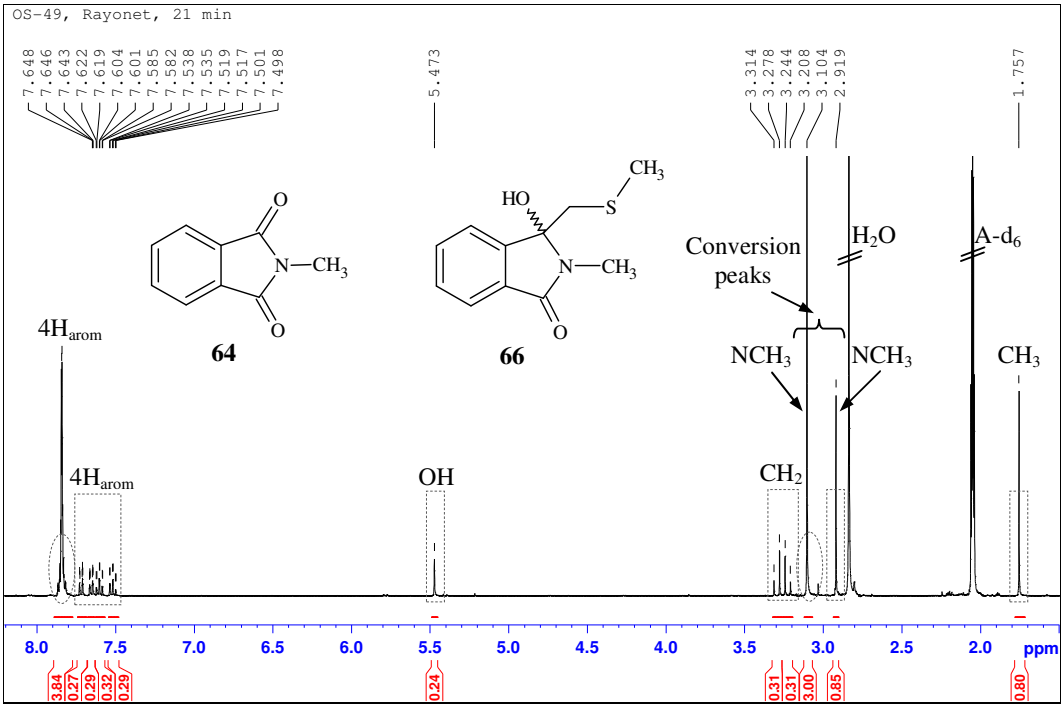


Figure 22: ^{1}H-NMR of the crude product obtained in the *experiment 13* after 21 min. Peaks marked by dashed square represent protons of the product **66**, peaks marked by dashed oval represent protons of N-methylphthalimide **64**

4.3.2.1.3 The efficiency of the addition reaction in Rayonet reactor operated with 5 lamps

The noteworthy difference between the Rayonet and dwell reactors was the number of lamps used for irradiation. The Rayonet reactor functioned with 16 UVB fluorescent tube lamps, where as the dwell device used only 5 lamps. To investigate energy savings

it was important to investigate the reaction efficiency in the Rayonet operated with the same number of lamps as the dwell device (*experiment 19*). The PDC addition of potassium 2-(methylthio) acetate **71a** to NMP **64** was used as a model reaction for this study. After 1 hour residence time, initial N-methylphthalimide underwent very weak conversion, only 17% in the Rayonet reactor equipped with 5 UVB lamps (Figure 23), that was 5 times lower than the result obtained in the Rayonet reactor operated with 16 lamps (86%) and 6 times lower when compared to the conversion obtained in the microsystem (100%). This achievement clearly demonstrates the superiority of dwell device compared to the batch system in respect to energy efficiency.

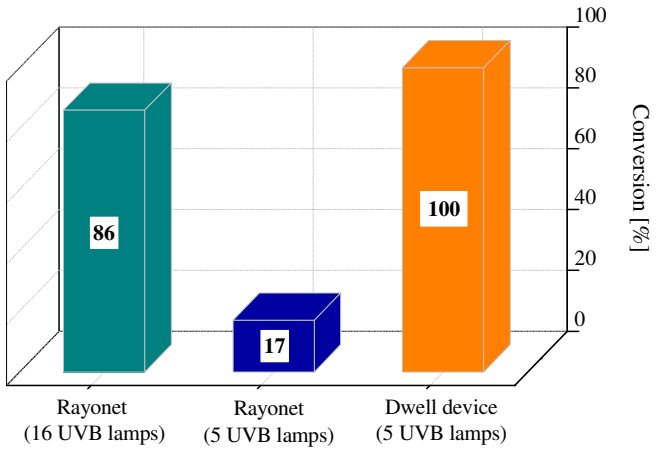


Figure 23: Conversion of NMP **64** to product **66** in Rayonet reactor operated with 5 and 16 UVB lamps vs. dwell device

4.3.2.1.4 Investigation of the effect of the sensitizer and irradiation wavelength on the reaction efficiency

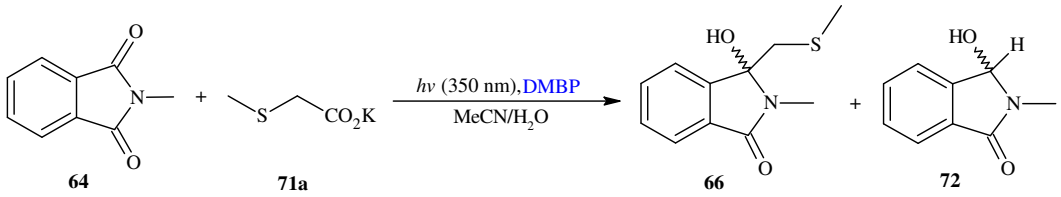
The above described experiments were carried out using UVB (300 nm) irradiation with acetone as the photo-sensitizer and solvent. To investigate the possibility of conducting PDC addition reactions at a more readily available and safer UVA (350 nm) irradiation, the optimised reaction procedures were further modified. The solvent acetone had been replaced by acetonitrile and two other sensitizers were used instead: 4-carboxybenzophenone (4-CBPH, *exp. 20*) and 4,4'-dimethoxybenzophenone (DMBP, *exp. 21*). These sensitisers have $n \rightarrow \pi^*$ absorption bands at approximately 350 nm and were used in a ratio of 0.1:1 to that of NMP. The PDC addition of potassium 2-(methylthio) acetate **71a** to NMP **64** was again used for this study. This reaction was initially investigated in the Rayonet reactor and the results are presented in Table 6.

Table 6: Optimisation study of the sensitizer type at chosen wavelength

Experiment	Sensitizer	Irradiation wavelength, [nm]	Residence time, [h]	Conversion to 66, [%][a]
20	4-CBPH	350	2	n.r.[b]
21	DMBP	350	1	100 (41[c])

[a] Determined by ^{1}H-NMR spectroscopy; [b] no reaction; [c] isolated yield of desired product **66**

As can be seen from the above table, N-methylphthalimide did not undergo any conversion under 4-carboxybenzophenone sensitisation and was reisolated even after a prolonged irradiation time of 2 hours. Whereas, in the reaction sensitised by DMBP complete conversion was achieved after 1 hour. However, the ^{1}H-NMR spectroscopy of the collected crude product showed that not only was the desired product **66** formed, but also the photoreduction product **72** of NMP (Scheme 32) and secondary products of sensitizer DMBP were detected.

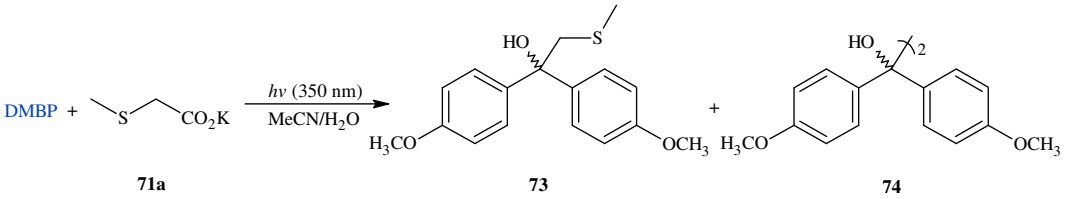


Scheme 32: DMBP sensitised PDC addition of methylsulfanyl acetate to NMP

The same experiment with DMBP as sensitizer was done in the dwell device (*exp. 22*). The crude product was collected after a residence time of 1 hour and was analysed by ^{1}H-NMR spectroscopy. 90% of initial NMP **64** converted to the desired product **66** and 10% of it remained unreactive. In contrast to the *experiment 21* in the batch system, the photoreduction product **72** of NMP and decomposition products of DMBP were not detected. The yields with DMBP sensitisation vary from those obtained in acetone (Table 4, *exp. 8*) and are slightly lower. However, these experiments clearly show that this reaction can be performed at 350 nm. The only disadvantage of DMBP is the necessity for its removal.

To investigate the reason why sensitizer DMBP did not survive under the batch conditions, the same reaction was repeated in the Rayonet reactor, but in the absence of N-methylphthalimide **64** (*exp. 23*). After 1 hour, DMBP was completely consumed and ^{1}H-NMR spectroscopy of crude product showed that the corresponding addition product **73** of DMBP and acid was formed next to the expected benzpinacol **74** (Scheme 33). In acetone-d_6, **73** gave singlets at 1.96 ppm for its –SCH_3 and at 3.41 ppm for its –CH_2S

group, respectively. These values were similar to those of the related benzophenone adduct.[159] The product ratio of **73/74** was determined to be 55:45. Based on this, it could be concluded that Rayonet reactor with its 16 lamps provided exhaustive irradiation which initiated side reactions of DMBP.



Scheme 33: PDC addition of potassium 2-(methylthio) acetate to DMBP

4.3.2.1.5 Study of the N-methylphthalimide reactivity under direct excitation

N-methylphthalimide has a weak absorption band at 300 nm and can be directly excited by UVB light. According to the data reported in the literature this is possible in the UVB transparent solvent such as acetonitrile.[157,160-162] Thus PDC addition of potassium 2-(methylthio) acetate **71a** to NMP **64** was further investigated under conditions of direct excitation in a batch system (*exp. 24*). The reaction mixture was irradiated for 1 hour and analysed by ^{1}H-NMR spectroscopy. The ^{1}H-NMR spectrum of the crude product showed that NMP underwent complete conversion 100% under direct sensitizing, that was 14% higher than under acetone activation (Table 4, *exp. 8*).

4.3.2.1.6 The affect of the N_2 stream rate on the reaction efficiency in the batch system

The general procedure of the described photochemical reactions included degassing of the reaction mixture with inert gas before or during irradiation. Nitrogen was used for this purpose in our experiments. Its main function was to displace oxygen. The removal of oxygen helps to avoid side reactions and triplet quenching. The additional function of nitrogen flow, especially in the batch system, was nonstop mixing of the reaction mixture to provide homogeneity of the reaction media and temperature. For this reason N_2 was used continuously during irradiation. Nitrogen could be supplied to the reaction mixture with different pressures. Therefore it was interesting to investigate its influence on the reaction efficiency in the batch system. The same model reaction PDC addition of **71a** to NMP **64** under direct excitation conditions was tested in the Rayonet reactor with slow (26.5 ml/min), vigorous (150.0 ml/min) and without N_2 bubbling (*experiments 25–27*, respectively). The achieved results are summarised in Table 7.

Table 7: Reaction efficiency vs. different flow rate of N_2

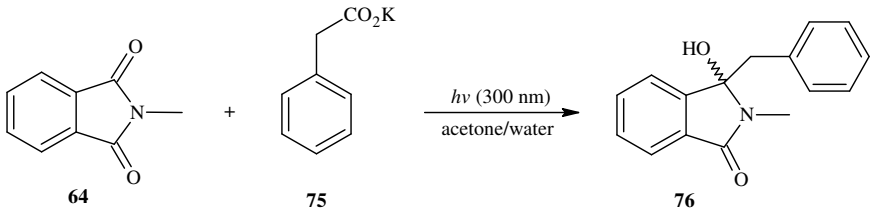
Experiment	N_2 flow rate, [ml/min]	Residence time, [h]	Conversion to 66, [%][a]
26	150.0	1	79
27	–[b]	1	96
25	26.5	1	100

[a] Determined by ^{1}H-NMR spectroscopy; [b] N_2 bubbling was not supplied during irradiation, the experimental mixture was degassed for 15 min before irradiation

The unexpected results of this study demonstrated that the rate of N_2 bubbling had a significant effect on the reaction efficiency. The conversion rate can vary from 79% at vigorous nitrogen bubbling to complete conversion at slow N_2 flow rate. Therefore, it was concluded that it is necessary to use a gentle stream of N_2 during irradiation in the batch system and this practice has been applied to all further experiments in the Rayonet reactor. Large nitrogen bubbles can cause considerable light scattering which leads to a lowering of direct light penetration, resulting in less efficient photochemical reactions.

4.3.2.2 Intermolecular photodecarboxylative addition of alkyl carboxylates to NMP

The potassium phenylacetate **75** was used as an example of alkyl carboxylates for this study. The photodecarboxylative benzylation of NMP **64** with phenylacetate **75** is known to proceed rapidly under acetone sensitisation (Scheme 34).[145]



Scheme 34: Intermolecular PDC addition of phenylacetate to NMP

4.3.2.2.1 Comparison study of the reaction performance in the batch system (Rayonet) and microsystem (Dwell device) at various residence times

The optimised procedures for PDC addition of sulphur-containing carboxylates to NMP in the Rayonet and dwell devices had been successfully transferred to the analogous photoaddition of phenylacetate **75** (alkyl carboxylate) to NMP **64** in the following *experiments 28–35* (Table 8). The desired product **76** was obtained in 83% and 97% after just 14 and 21 min, the complete conversion was reached after 40 min of irradiation in the dwell device. While in the larger Rayonet reactor entire conversion

was also achieved after 40 min, however, it was found that after shorter reaction time of 14 min the desired product **76** was made in almost half the yield compared to the microreactor. Moreover, the conversion dropped significantly to 29% when irradiation was performed for 1 hour with only 5 UVB lamps (*exp. 36*). The conversions of NMP were determined by ^{1}H-NMR spectroscopy of the crude products. The signal integration for the NC<u>H</u>$_3$ protons of **64** was compared to the signal integration for the NC<u>H</u>$_3$ protons of **76** (Figure 24). As can be seen from Table 8 the microreactor once again outperformed the Rayonet reactor regarding the conversion rate and energy efficiency.

Table 8: Conversion of NMP **64** to product **76** in dwell device vs. Rayonet reactor

Experiment	Flow rate, [ml/min]	Residence time, [min]	Conversion to 76, [%][a]	
			Dwell device[b]	Rayonet[c]
31[c], 35[b]	0.12	14	83	46
30[c], 34[b]	0.08	21	97	93
29[c], 33[b]	0.042	40	100	100
28[c], 32[b]	0.028	60	100	100 (29[d])

[a] Determined by ^{1}H-NMR spectroscopy; [b] number of corresponding experiment carried out in the dwell device; [c] number of corresponding experiment carried out in the Rayonet reactor; [d] with 5 UVB lamps

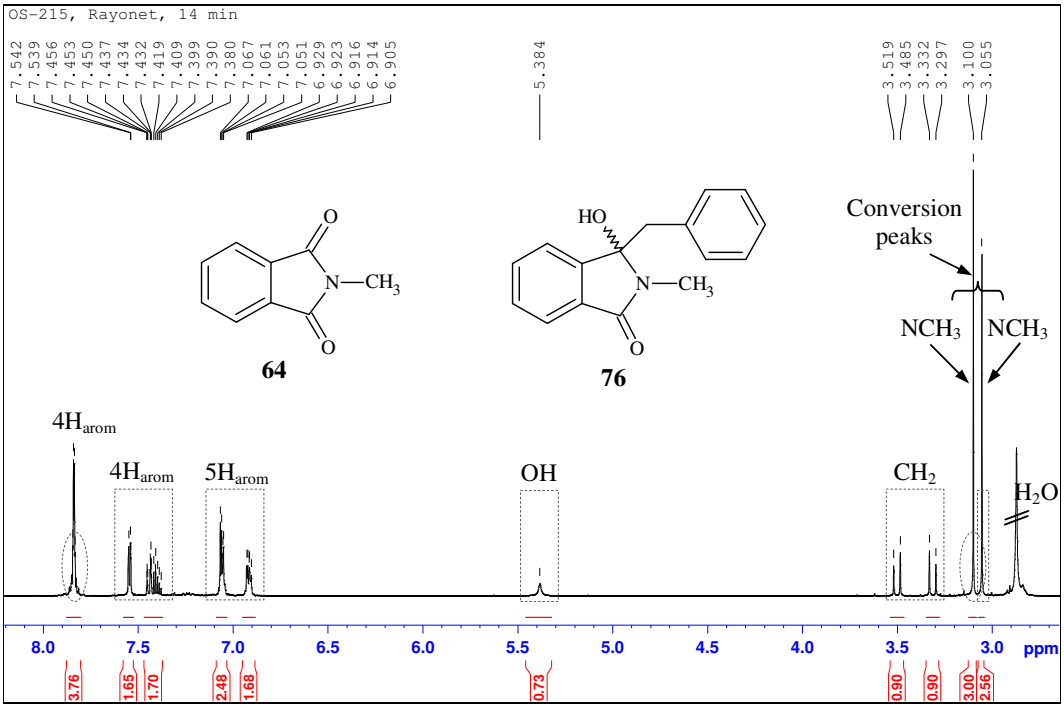


Figure 24: ^{1}H-NMR of the crude product obtained in the *experiment 31* after 14 min. Peaks marked by dashed square represent protons of the product **76**, peaks marked by dashed oval represent protons of N-methylphthalimide **64**

4.3.2.2.2 The effect of reagents concentration on the efficiency of addition

In acetone PDC addition of phenylacetate **75** to NMP **64** proceeds very fast, because the main reaction constituent that absorbs light was the solvent acetone and its concentration was very high (6.8 M) compared to the concentration of NMP (15 mM) and phenylacetate (45 mM). Therefore the effect of reagent concentration on reaction efficiency in micro- and batch systems was studied under conditions of direct NMP excitation, i.e. in photoinert solvent acetonitrile. The reaction time was furthermore set to 1 hour, while the concentrations of **64** and **75** were increased systematically (*exp. 37–44*). The results are summarised in Table 9. The microreactor gave complete conversion of NMP **64** at concentrations of 15 and 30 mmol/L, respectively. In contrast, the batch reactor reactions only showed total conversion at 15 mmol/L. At higher concentrations of N-methylphthalimide **64**, the conversions dropped gradually.

Table 9: Concentration study for PDC addition of phenylacetate to NMP in acetonitrile at constant residence time of 1 hour

Experiment	Concentrations, [mmol/L]		Conversion to 76, [%][a]	
	64	**75**	**Dwell device[b]**	**Rayonet[c]**
37[c], 41[b]	15	45	100	100
38[c], 42[b]	30	90	100	93
39[c], 43[b]	60	180	64	53
40[c], 44[b]	90	270	45	38

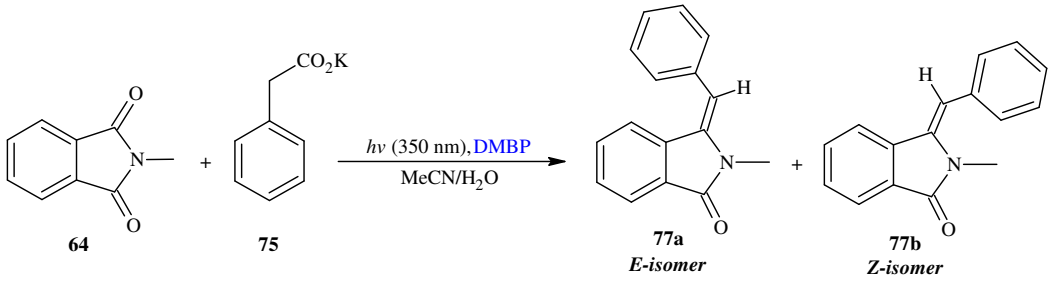
[a] Determined by ^{1}H-NMR spectroscopy; [b] number of corresponding experiment carried out in the dwell device; [c] number of corresponding experiment carried out in the Rayonet reactor

These experimental results demonstrate the superiority of photochemical reactions in microchannels over a Schlenk flask with respect to complete conversion of the starting material **64** to the desired product **76** even at two times higher solution concentration.

4.3.2.2.3 The DMBP sensitised PDC addition of phenylacetate to NMP

The DMBP sensitised addition of phenylacetate **75** to NMP **64** (Scheme 35) was investigated in a similar way to the DMBP sensitised addition of potassium 2-(methylthio) acetate **71a** (*exp. 45*). In contrast to the previous experiments a mixture of olefins **77a,b** were isolated instead of the photoaddition product **76**. It is known that olefins **77a,b** are formed after subsequent dehydration of the photoaddition product **76**. This can be caused by trace amounts of acid. Assignments of the two isomers (***E/Z***)

were consigned by comparison with known analogues reported in the literature.[114,145,163]



Scheme 35: DMBP sensitised PDC addition of phenylacetate to NMP

The crude product was analysed by ^{1}H-NMR spectroscopy. The spectrum showed that NMP **64** completely converted to the mixture of olefins **77a,b** after 1 hour of UVA irradiation in the Rayonet reactor. In this experiment the *E*-isomer was preferentially formed and only traces of the *Z*-isomer were detected by ^{1}H-NMR. The same product distribution was observed in the microreactor (*exp. 46*) after the identical residence time. Also it was noticed that DMBP slightly decomposed. Nevertheless, these experiments showed that this reaction can be efficiently performed at 350 nm and could be used for diastereoselective synthesis of the *E*-isomer.

4.3.2.2.4 Study of PDC addition of phenylacetate to NMP under direct excitation by UVA light

As have been demonstrated before, the N-methylphthalimide underwent very effective direct excitation under UVB irradiation. To check the effect of direct excitation by UVA light, PDC addition of phenylacetate **75** to NMP **64** was investigated without sensitizer DMBP (*exp. 47*). Acetonitrile was used as solvent and exposure time was set for 1 hour in Rayonet reactor. The collected crude product was analysed by ^{1}H-NMR spectroscopy and low conversion of 8% was determined for NMP **64**. Under the same experimental conditions in dwell device the conversion of NMP **64** was even lower and was just 4% (*exp. 48*). These results nicely proved that for the initiation of photoaddition reactions by UVA light the presence of sensitizer DMBP is essential.

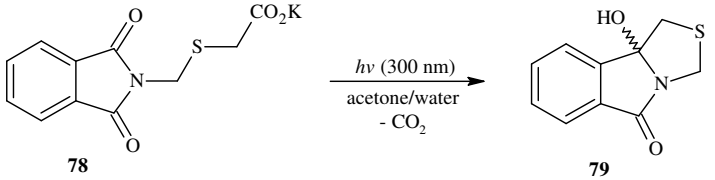
4.3.3 Intramolecular PDC-cyclizations of phthalimide derivatives

Intramolecular decarboxylative cyclizations of phthalimido-carboxylic acids are ideal model reactions since they show the impact of the heteroatom on the reaction rate and typically take less than one hour for completion. As a model transformation, the

cyclization of phthalimidomethylsulfanyl acetate was studied (Scheme 36) and compared to its related C_3-analogue, i.e. phthaloyl-γ-aminobutyrate (Scheme 38).

4.3.3.1 Intramolecular PDC cyclization of potassium phthalimidomethylsulfanyl acetate

Sulfur atoms in the α-position to a carboxylate group are known to accelerate photodecarboxylations of the phthalimido-carboxylic acids. The transformation of potassium phthalimidomethylsulfanyl acetate **78** to the thiazolidine derivative **79** was thus examined (Scheme 36). The relative initial phthalimidomethylsulfanylcarboxylic acid was prepared from the corresponding N-(bromomethyl)phthalimide and thioglycolic acid in the laboratorial conditions (*exp. 49*).[158,164,165]



Scheme 36: Intramolecular PDC cyclization of phthalimidomethylsulfanyl acetate

4.3.3.1.1 Reaction efficiency in the batch system (Rayonet) and microsystem (Dwell device) against to a range of residence time

Following the general procedure a solution of potassium phthalimidomethylsulfanyl acetate **78** was exposed to UVB irradiation in the Rayonet reactor and dwell device for a number of residence times (*experiments 50–56*). The dwell device again gave higher yields than the Rayonet reactor (Table 10). After exposure for 60 min, the isolated yields of **79** were 80% under flow-through (microreactor) and 72% (16 lamps) or 21% (5 lamps), respectively, under batch conditions (Rayonet).

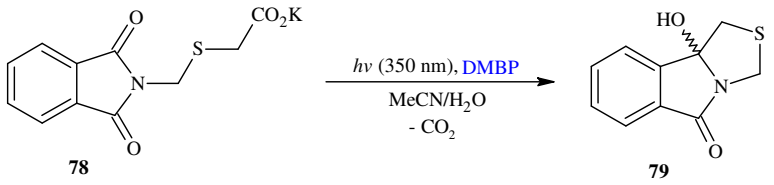
Table 10: Isolated yields of product **79** in dwell device vs. Rayonet reactor

Experiment	Flow rate, [ml/min]	Residence time, [min]	Yield of 79, [%][a]	
			Dwell device[b]	Rayonet[c]
52[c], 55[b]	0.08	21	39	36
51[c], 54[b]	0.042	40	70	59
50[c], 53[b]	0.028	60	80	72 (21[d])

[a] Determined by ^{1}H-NMR spectroscopy; [b] number of corresponding experiment carried out in the dwell device; [c] number of corresponding experiment carried out in the Rayonet reactor; [d] with 5 UVB lamps

4.3.3.1.2 Intramolecular PDC cyclization of phthalimidomethylsulfanyl acetate under DMBP sensitization

The PDC cyclization of compound **78** was also investigated in conditions using DMBP sensitization under UVA irradiation (Scheme 37). These experiments were carried out in the batch system and microreactor with a standard residence time of 1 hour (*exp. 57* and *58*). In both cases the desired product **79** was isolated in moderate yields of 57% and 56% respectively.

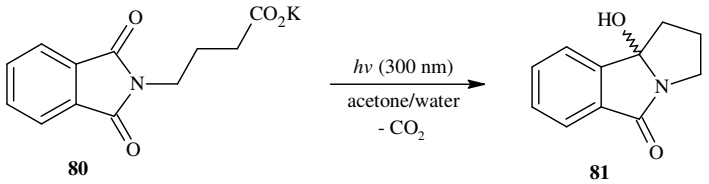


Scheme 37: DMBP sensitised PDC cyclization of phthalimidomethylsulfanyl acetate

It is important to note that in these experiments DMBP did not undergo any changes or decomposition and was reisolated by column chromatography. The fact that DMBP survived the cyclization conditions could be explained by the lower acidity and concentration of the initial phthalimidomethylsulfanyl acetic acid compared to the photoaddition experiments. Nevertheless these results clearly demonstrate that the above reaction can be performed at 350 nm irradiation.

4.3.3.2 Intramolecular PDC cyclization of potassium phthaloyl-γ-aminobutyrate

Photodecarboxylative cyclization of the potassium phthaloyl-γ-aminobutyrate **80** (Scheme 38) was studied for comparison to the corresponding S-containing analogue, i.e. phthalimidomethylsulfanyl acetate. It is known that this transformation proceeds rapidly and can reach completion after 1 hour.[166–168] Phthaloyl-γ-aminobutyric acid was prepared from phthalic anhydride and γ-aminobutyric acid in the laboratorial conditions (*experiment 59*).



Scheme 38: Intramolecular PDC cyclization of phthaloyl-γ-aminobutyrate

4.3.3.2.1 Assessment study of the reaction efficiency in the batch system (Rayonet) and microsystem (Dwell device) at a series of residence times

The PDC cyclization of potassium phthaloyl-γ-aminobutyrate **80** to the benzopyrrolizidine **81** was tested in the batch- and micro-systems with three different residence times in the following *experiments 60–66* (Table 11). Using the microreactor, the desired product **81** was isolated in a yield of 77% after 60 min of irradiation. In contrast, the yields from the Rayonet reactor were again lower with 69% (16 lamps) and 19% (5 lamps), respectively, after an identical irradiation time.

Table 11: Isolated yields of product **81** in dwell device vs. Rayonet reactor

Experiment	Flow rate, [ml/min]	Residence time, [min]	Yield of 81, [%][a]	
			Dwell device[b]	Rayonet[c]
62[c], 65[b]	0.08	21	33	46
61[c], 64[b]	0.042	40	69	53
60[c], 63[b]	0.028	60	77	69 (19[d])

[a] Determined by ^{1}H-NMR spectroscopy; [b] number of corresponding experiment carried out in the dwell device; [c] number of corresponding experiment carried out in the Rayonet reactor; [d] with 5 UVB lamps

4.3.3.2.2 Performance of the PDC cyclization of potassium phthaloyl-γ-aminobutyrate at UVA irradiation

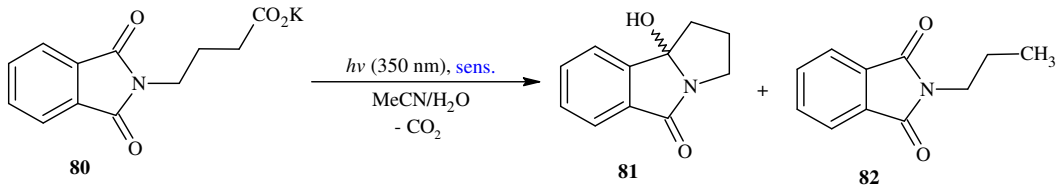
The results obtained for cyclization of potassium phthaloyl-γ-aminobutyrate **80** at 300 nm irradiation confirmed that this transformation proceeded quickly under acetone sensitisation. However, for LED application it would be ideal to use wavelengths in the region of 350 nm or greater since these UV LEDs are commercially available and cheaper. To determine if a light source with the emission of 350 nm could be used for this reaction, the PDC cyclization of **80** was investigated with two other sensitizers: 4-carboxybenzophenone (*exp. 67*) and 4,4'-dimethoxybenzophenone (*exp. 68*). Initially, these experiments were carried out in the Rayonet reactor with an optimal residence time of 1 hour and the results are presented in Table 12. In both cases the desired product benzopyrrolizidine **81** was isolated with similar yields of 31% and 29%, respectively.

Table 12: Reaction efficiency under different sensitisation at 350 nm irradiation

Experiment	Sensitizer	Irradiation wavelength, [nm]	Yield of 81, [%][a]	Conversion to 82, [%][b]
67	4-CBPH	350	31	9
68	DMBP	350	29	12

[a] Isolated yields; [b] determined by ^{1}H-NMR spectroscopy

As can be seen from Table 12, phthaloyl-γ-aminobutyrate **80** under 4-CBPH or DMBP sensitization was converted not only to the cyclical product **81** but also the decarboxylation product **82** (Scheme 39) was formed in a significant amount 9-12%. Moreover the desired product **81** was isolated in half the yield compared to the previous experiments under acetone sensitisation.



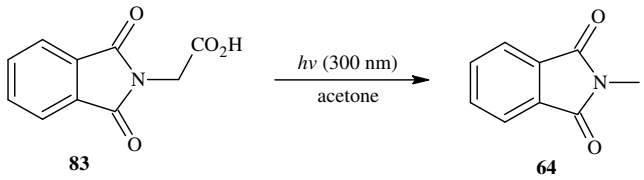
Scheme 39: PDC cyclization of potassium phthaloyl-γ-aminobutyrate under UVA irradiation

The same experiment with DMBP as sensitizer was also carried out in the microsystem dwell device (*exp. 69*). The results showed that this reaction has low selectivity under these conditions because the desired product **81** was yielded in 47% and simple decarboxylation product **82** in 19% (conversion). Therefore it was concluded that PDC cyclization of phthaloyl-γ-aminobutyrate will not be a suitable reaction for further investigation with UV-LEDs.

To check the necessity of sensitizer usage for the reaction progression under UVA irradiation the same experiments were repeated in both systems without any sensitizer (*exp. 70* and *71*). Acetonitrile was used as solvent. In the Rayonet reactor product **81** was isolated in the yield of 14.3% (*exp. 70*). In the dwell device the yield of cyclical product **81** was 8.4% (*exp. 71*). The conversion rate of simple decarboxylation product **82** was low and was just 1.3% in both cases. These results show that PDC cyclization of **80** has poor efficiency under direct excitation by UVA light.

4.3.4 Intramolecular PDC of phthaloyl glycine (Pht=Gly)

In an extension of this work intramolecular α-photodecarboxylation (-CO_2H/-H exchange) of phthaloyl glycine **83** (Scheme 40) was investigated. This transformation has been developed as an efficient access to α-deuterated primary amines.[169–172]



Scheme 40: α-Photodecarboxylation of phthaloyl glycine

4.3.4.1 Effect of the residence time on the reaction efficiency in both systems

The reaction protocol was applied to the batch Rayonet reactor and microreactor using the irradiation of phthaloyl glycine **83** in dry acetone (*experiments 72–82*). The effect of residence time on the decarboxylation efficiency (after a single run) was examined by alteration of the flow rate (Table 13). As would be expected, conversion rates improved for both reactor types with increasing reaction time (Figure 25), but the microreactor gave better results overall. For example, NMP **64** was formed in 92% next to 8% of unreacted starting material **83** after a residence time of 60 min. In contrast, the larger Rayonet reactor gave lower conversions of just 59% (16 lamps) and 22% (5 lamps), respectively, after the same irradiation time. The conversion rate was determined by ^{1}H-NMR spectroscopy of the crude product. The signal integration for the NC$\underline{H}_2$ protons of **83** was compared to the signal integration for the NC$\underline{H}_3$ protons of **64** (Figure 26).

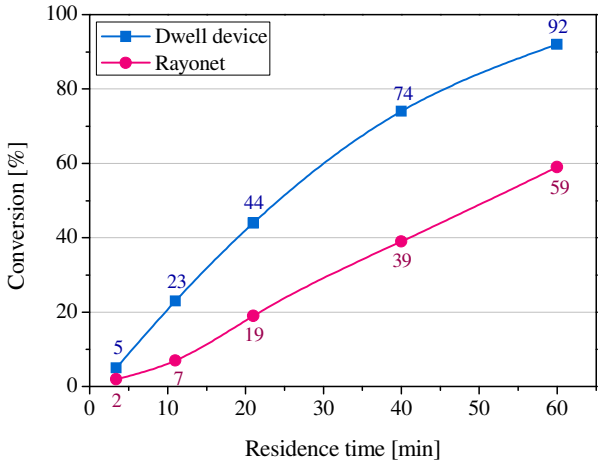


Figure 25: Conversion of phthaloyl glycine vs. residence time

Table 13: Conversions of Pht=Gly **83** to NMP **64** in dwell device vs. Rayonet reactor

Experiment	Flow rate, [ml/min]	Residence time, [min]	Conversion to 64, [%][a]	
			Dwell device[b]	Rayonet[c]
76[c], 81[b]	0.5	3.4	5	2
75[c], 80[b]	0.15	11	23	7
74[c], 79[b]	0.08	21	44	19
73[c], 78[b]	0.042	40	74	39
72[c], 77[b]	0.028	60	92	59 (22[d])

[a] Determined by ^{1}H-NMR spectroscopy; [b] number of corresponding experiment carried out in the dwell device; [c] number of corresponding experiment carried out in the Rayonet reactor; [d] with 5 UVB lamps

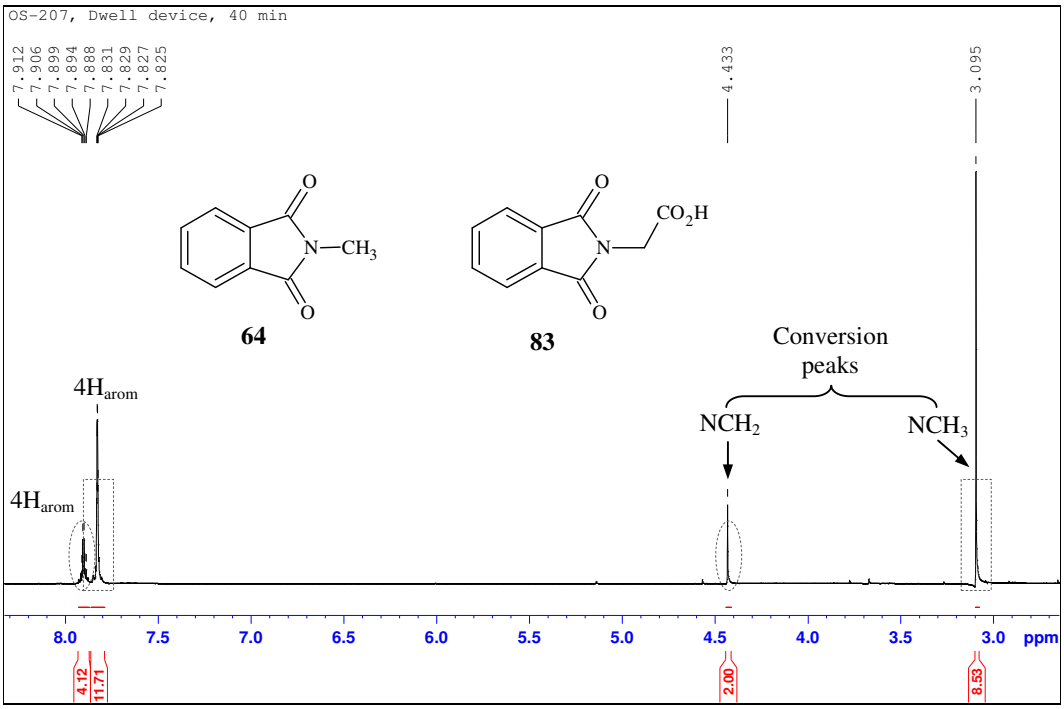
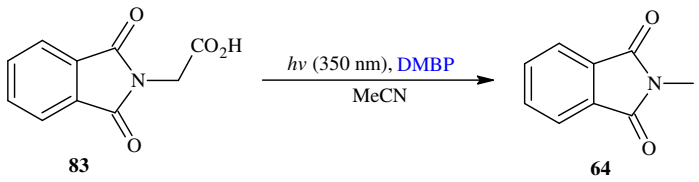


Figure 26: ^{1}H-NMR of the crude product obtained in the *experiment 78* after 40 min. Peaks marked by dashed square represent protons of phthaloyl glycine **83**, peaks marked by dashed oval represent protons of N-methylphthalimide **64**

4.3.4.2 Effect of the sensitizer and irradiation wavelength on the reaction efficiency

In completion of this study the α-photodecarboxylation of phthaloyl glycine **83** was investigated under DMBP sensitisation (Scheme 41). These experiments were carried out in the Rayonet reactor (*exp. 83*) and dwell device (*exp. 84*). In both cases, phthaloyl glycine **83** completely converted (100%) to the N-methylphthalimide **64** after an irradiation time of 1 hour. Moreover, DMBP survived in these experiments and its

decomposition or pinacolisation products were not observed. Thus it was concluded that this model reaction can be sensitized by DMBP and efficiently transferred to UVA irradiation.



83 **64**

Scheme 41: DMBP sensitised α-photodecarboxylation of phthaloyl glycine

The sensitivity of phthaloyl glycine **83** to direct excitation by UVA light was investigated in the next *experiments 85–86*. The acetonitrile solution of phthaloyl glycine **83** without any sensitizers was irradiated in the Rayonet reactor (*exp. 85*) and dwell device (*exp. 86*) for 1 hour. The ^{1}H-NMR spectroscopy analysis of collected crude products showed that conversion of phthaloyl glycine **83** to NMP **64** in the batch reactor was 10% while in the microsystem it was just 2%. These results demonstrated that α-photodecarboxylation of phthaloyl glycine **83** required presence of sensitizer DMBP under UVA irradiation.

4.4 Discussions

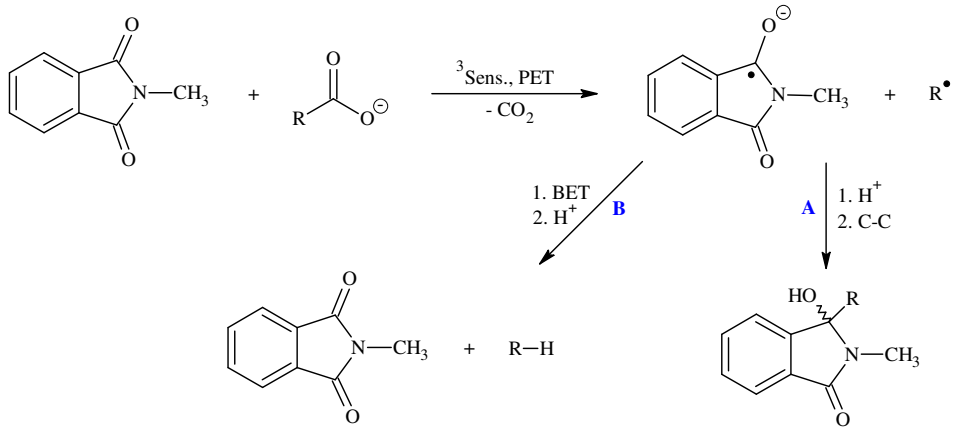
The range of intra- and intermolecular transformations involving phthalimides has been successfully studied in commercially available microreactor dwell device and batch reactor Rayonet. The achieved results clearly demonstrate the adaptability of novel engineering tools such as microreactors for photochemical synthesis.

4.4.1 Intra- and intermolecular reactions involving phthalimides

4.4.1.1 Intermolecular photoaddition reactions involving phthalimides

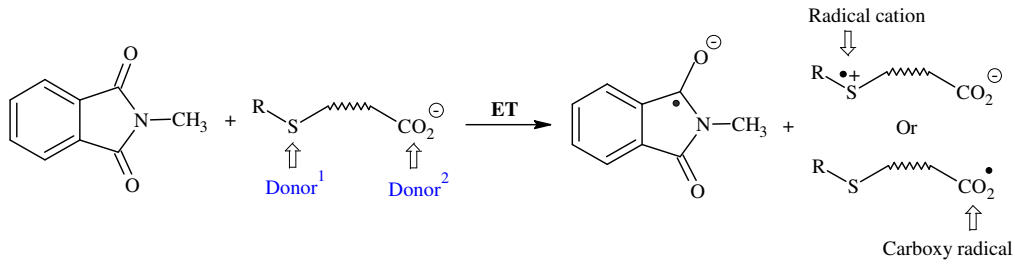
The studied photoadditions of thioethers, sulphur containing and alkyl carboxylates to N-methylphthalimide are reactions with high atom economy as they yielded single desired products (alkyl-phthalimidines). Moreover the photoadditions of carboxylates is accompanied by irreversible and regioselective loss of carbon dioxide and proceed via stable formed alkyl radicals.[173] The stability of the corresponding alkyl radicals control the rate of CO_2 loss and is estimated to be in the range of 10^9-10^{10} s^{-1} for simple alkyl acyloxy radicals.[173] The additions of alkyl radicals exclusively occur at the site of the leaving group carbon dioxide.

The benzylation of N-methylphthalimide was the most efficient reaction and the addition product **76** was selectively formed and isolated in high yield (96%) after short irradiation time 40 min in microreactor and batch experimental setups. The mechanism for the intermolecular photodecarboxylative addition of carboxylates to N-methylphthalimide is illustrated in Scheme 42.[174,175] PET plays a key role in this transformation where the carboxylate anion acts as electron donating group and the electronically excited imido group as electron acceptor. The reaction starts with the generation of triplet sensitised phthalimide, followed by a single electron transfer (SET) between phthalimide and the carboxylate. The relatively high oxidation potentials of carboxylates compared to other electron donor groups (e.g. acetate: E_{ox} = 1.54 V in MeCN, 2.65 V in H_2O vs. SCE[176]) made energetically feasible both intramolecular electron transfers: via the excited $^3\pi,\pi^*$ triplet state or the higher $^3n,\pi^*$ state. Subsequent decarboxylation of the carboxy radical yields the corresponding C-radical. Protonation of the phthalimide radical anion and C-C bond formation results in the desired photoaddition products (path A). In the alternative case (path B), back electron transfer (BET) takes place. The generated corresponding carbanions are protonated by water and simple decarboxylation products ($-CO_2H \leftrightarrow -H$) are formed. These products were not detected in our particular experiments.



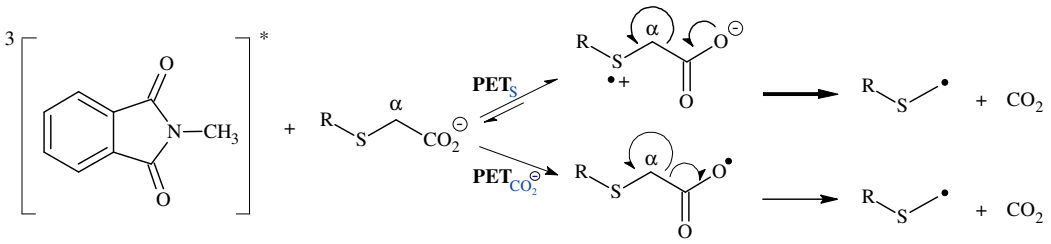
Scheme 42: Mechanism of photodecarboxylative addition of carboxylates to phthalimide

The incorporation of a heteroatom in the alkylcarboxylate molecule has a significant influence on the reaction mechanism. The photoadditions of sulphur-containing carboxylates involve an electron transfer from the neutral sulphur atom with the formation of its radical cation (Scheme 43)[177] or an electron transfer from the carboxylate.



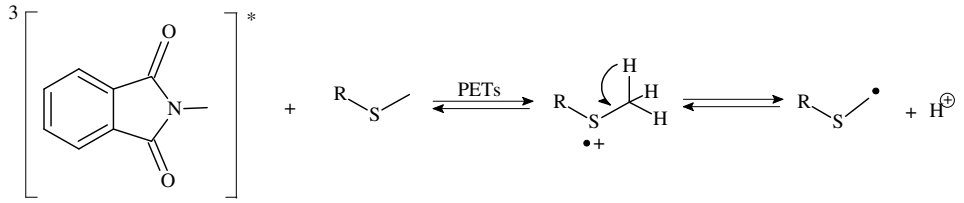
Scheme 43: Competitive scenario for sulphur-containing carboxylates

The feasibility of both pathways can be explained based on the oxidation properties of the competing donors ($E_{Ox.}$ S > $E_{Ox.}$ CO_2^-). Due to the favourable low oxidation potentials of thioethers (Me_2S: $E_{Ox.}$ = 1.25 V in MeCN vs. SCE[178]), the photoreactions involving sulphur-containing carboxylates are initiated by electron transfer from the heteroatom and not from the carboxylate. The resulting sulphur centred radical cation subsequently eliminates the carbon dioxide irreversibly from its α-position.[177] The formed terminal carbon-radical undergoes C-C bond formation to yield the photoaddition product (Scheme 44). An alternative electron transfer from the carboxylate would result in the same product, but is energetically disfavoured due to the high oxidation potential of the carboxylate group.



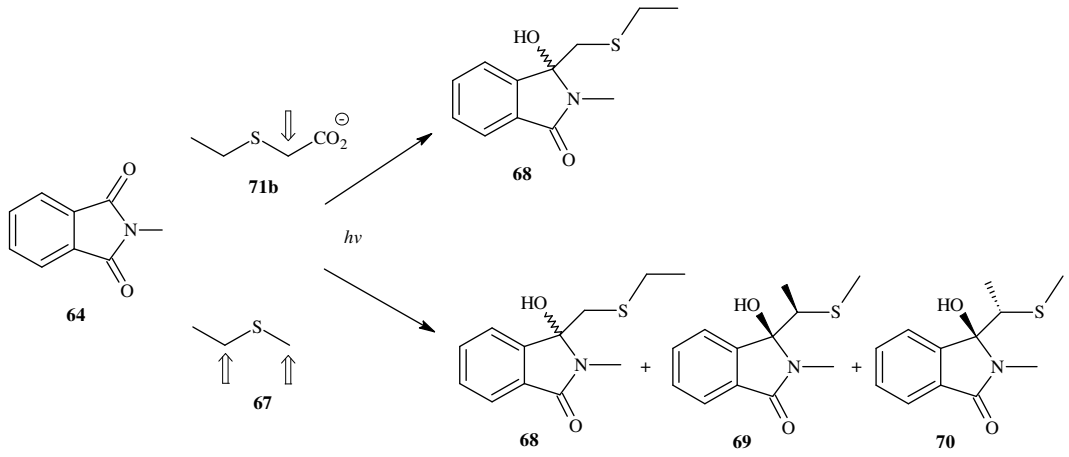
Scheme 44: Formation of sulphur centred radicals via α-decarboxylation

In contrast to the corresponding thioethers, photoadditions involving α-thioalkyl-substituted carboxylates gave higher yields and conversions. The efficiency of carboxylate additions can be explained by comparing the crucial departure of the leaving group. In case of thioethers (Scheme 45), both electron transfer and deprotonation are reversible and hence, prolonged irradiation times are required. While the α-thioalkyl-substituted carboxylates lose carbon dioxide irreversibly and thus significantly reduce the back electron transfer step and eventually increase the quantum efficiency.[179]



Scheme 45: Mechanistic key-steps for the addition of thioethers

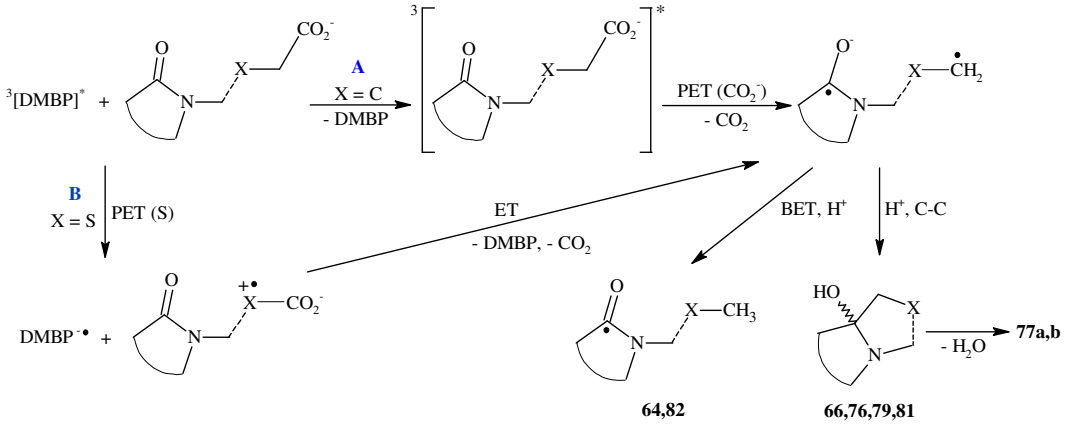
Another benefit of photoadditions involving carboxylates compared to the corresponding thioethers is the directing effect of the carboxylate group. Addition exclusively occurred at the position of the leaving group carbon dioxide. A nice example of such an effect is the photoaddition of ethylsulfanyl acetate **71b** and ethylmethyl sulphide **67** to N-methylphthalimide (Scheme 46). In the case of ethylsulfanyl acetate only one product **68** was selectively formed. In contrast, the ethylmethyl sulphide gave a mixture of regioisomers **68**, **69** and **70**.



Scheme 46: Directing effect of the carboxylate function

The ketone-sensitised photodecarboxylations involving phthalimides proceed via energy transfer or electron transfer processes.[180,181] The proposed mechanistic scenario for 4,4'-dimethoxybenzophenone (DMBP) sensitised PDC additions of carboxylates to NMP and PDC cyclizations of NMP derivatives are depicted in Scheme 47. Due to the comparable triplet energies of DMBP (T_1 = 69.4 kcal/mol or 290 kJ/mol[182]) and phthalimides (NMP: T_1 = 71 kcal/mol or 297 kJ/mol[183], energy transfer (Scheme 47, path A) is not very efficient but has been confirmed spectroscopically for a related N-phthalimidocarboxylate/benzophenone pair.[181] Subsequent electron transfer (ET) from the carboxylate anion to the triplet excited phthalimide furnishes an unstable carboxy radical, which undergoes rapid decarboxylation to the corresponding carbon radical. Protonation and C–C bond formation yields compounds **76** and **81**. Compound **76**

undergoes further dehydration to two isomers **77a,b**. Alternatively, back electron transfer (BET) and protonation generates the simple decarboxylation products **64** and **82**. Thus path A mirrors the above described mechanism for acetone sensitization. As have been mentioned earlier thioethers are more readily oxidized compared to carboxylates. Therefore, electron transfer to the triplet excited DMBP becomes energetically feasible[181] (Scheme 47, path B). Similar electron transfer processes have been established for photoreactions of N-methylphthalimide or benzophenone with either thioethers[156,184] or alkyl- and arylthioacetic acids[149,185], respectively. In case of phthalimidomethylsulfanyl acetate **78** or in the presence of N-methylphthalimide **64**, successive electron transfer generates the corresponding phthalimide radical anion. Subsequent decarboxylation, protonation and C–C bond formation furnish products **66** and **79**. In the absence of N-methylphthalimide **64** (*exp. 23*), protonation and C–C bond formation to **73** or photopinacolization to **74** operate instead (not shown on Scheme 47).



Scheme 47: Mechanism of DMBP sensitised intra- and intermolecular photodecarboxylations involving phthalimides

The absence of a sensitisation effect of 4-carboxybenzophenone compared to 4,4'-dimethoxybenzophenone (Table 6) could be explained by the presence of two electron rich centres in DMBP (Figure 27). The carboxylate group of 4-CBPH in its triplet sensitized state can compete with the carboxylate group of alkylcarboxylate **71a**.

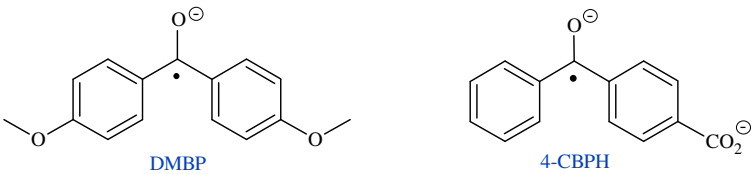


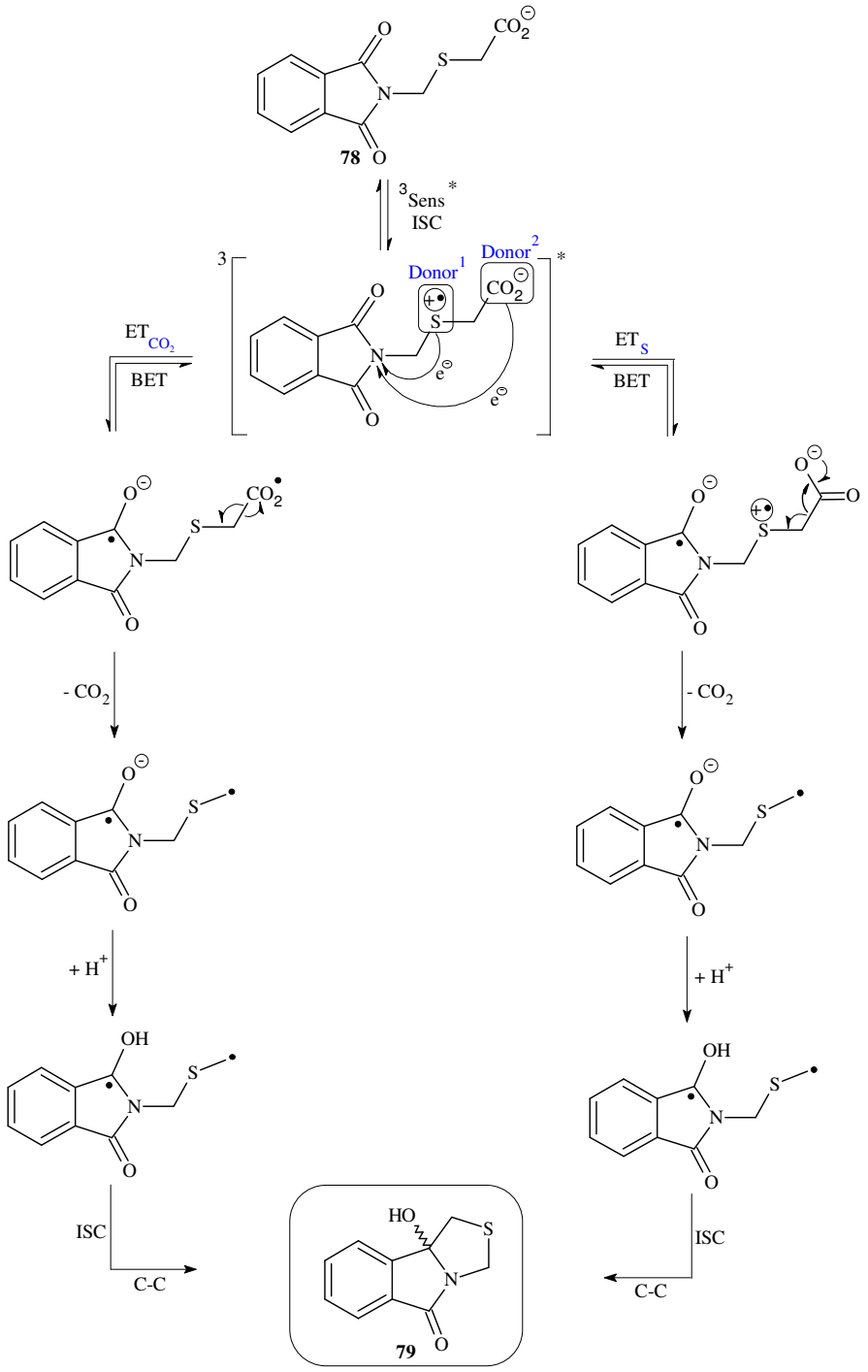
Figure 27: Triplet sensitized states of DMBP and 4-CBPH

4.4.1.2 Intramolecular PDC-cyclisation reactions involving phthalimide derivatives

The mechanism for the intramolecular cyclisation reactions is very similar to the related addition reactions due to the presence of the appropriate α-leaving group CO_2, which obviously enhances the chemical reactivity of the radical ion pair and suppresses the unproductive back electron transfer (BET) reaction.[174] The incorporation of a heteroatom into the phthalimide derivative alters the initial centre of electron transfer from carboxylate to sulphur.[158]

Thus, excellent cyclization efficiency of the phthalimidomethylsulfanyl acetate **78** can be explained mechanistically by a sulphur-assisted α-decarboxylation reaction (Scheme 48).[158] The intermolecular photoinduced electron transfer (PET) initiated by triplet excited acetone causes the oxidation of the thioether to a sulphur-centred radical cation, which further regioselectively eliminates carbon dioxide and generates an α-thio C radical. A second electron transfer from the acetone radical anion simultaneously produces the phthalimide radical anion, that after protonation and inter system crossing, combines with a terminal carbon radical and gives the tricyclic product **79**.

Likewise to the photoaddition reactions, the alternative electron transfer from carboxylate would result in the same product, but is energetically disfavoured. However, it is the main pathway in the intramolecular cyclisation of phthaloyl-γ-aminobutyrate **80** and leads to the formation of the desired cyclisation product **81**. Somewhat lower isolated yields of benzopyrrolizidine **81** compare to the thiazolidine derivative **79** could be explained by the weaker donor properties of the carboxylate anion in comparison to the thioether group and accordingly lower reaction efficiency.



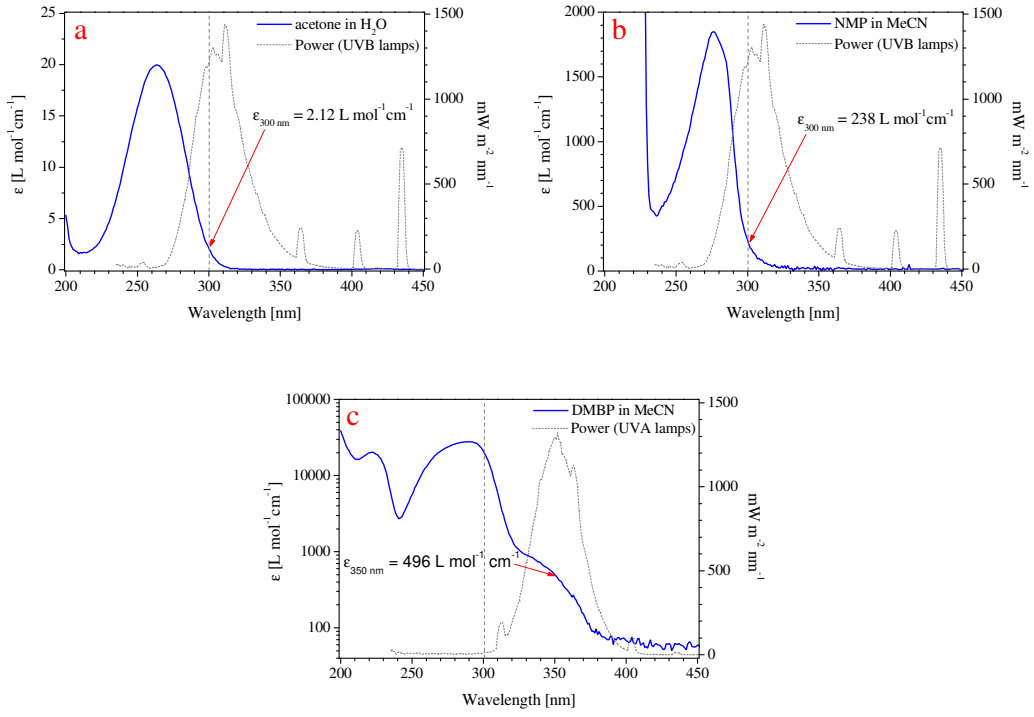
Scheme 48: Mechanistic scenario for phthalimidomethylsulfanyl acetate

Generally, almost all of the above expressed transformations involving phthalimides were investigated in two different experimental setups and obtained results were compared. As can be seen from the data presented in Tables 5, 8, 9, 10, 11 and 13, the chosen photochemical transformations proceeded more effectively in the microreactor than in the conventional Rayonet reactor. In order to understand the improved reaction performance in the microreactor subsequent aspects were established:

- light penetration profiles for the reaction vessels;
- energy efficiencies of the used light sources;
- reactors efficiency based on their geometry.

4.4.2 Wavelength matching and light penetration for experiments involving phthalimides

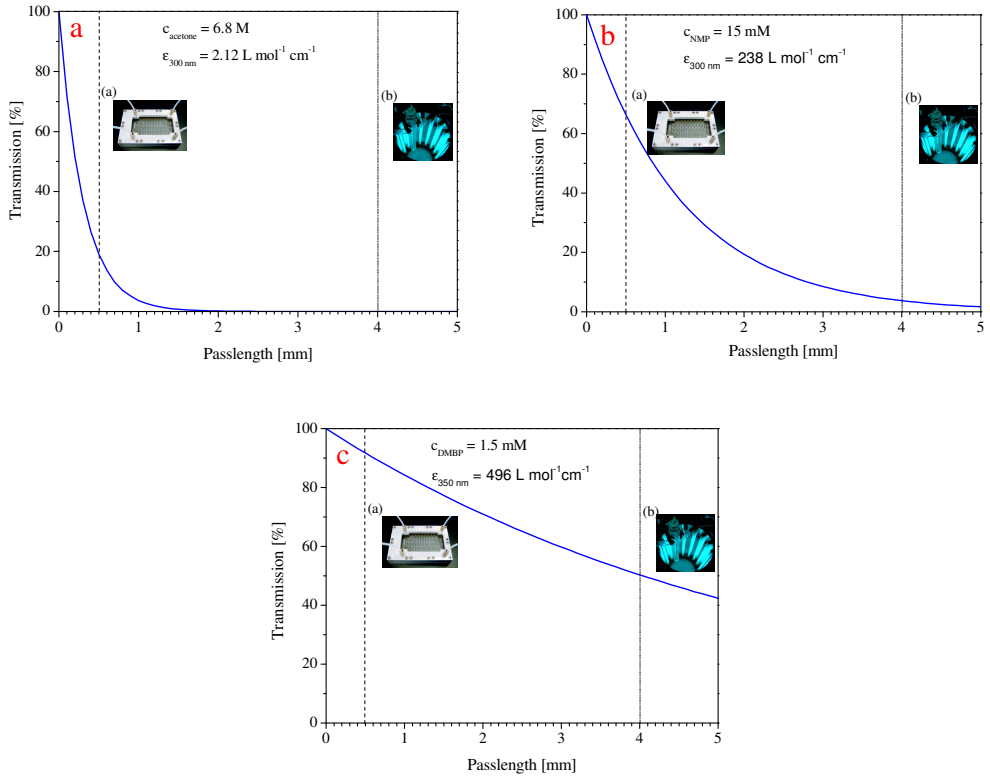
Initially, the UV spectra of all chromophoric materials were recorded. Likewise, the emission spectra of selected light sources were measured and matched with the absorption spectra of the chromophores (Figures 28). For acetone sensitization and direct NMP excitation, the cut-off of Pyrex and Foturan glass at 300 nm was taken into account. As can be seen on the Figure 28a, the absorption spectra of acetone and a UVB lamp have relatively poor overlap, however acetone functions as a sensitizer as well as co-solvent and is available in large excess amounts. The same UVB lamp emission spectrum also shows partial, but significant cover with the shoulder of $n \rightarrow \pi^*$ absorption band of NMP, which makes possible direct NMP excitation (Figure 28b). The UVA lamp shows a good overlap with the $n \rightarrow \pi^*$ absorption band of DMBP (Figure 28c) thus allowing to use sensitizer DMBP in relatively small amounts.



Figures 28: a) UV spectrum of acetone vs. emission spectrum of UVB lamp; b) UV spectrum of NMP vs. emission spectrum of UVB lamp; c) UV spectrum of DMBP vs. emission spectrum of UVA lamp. The dashed vertical line represents glass cut-off

Using the extinction coefficients and the concentrations used, light penetration plots were calculated using the Beer-Lambert's law. The results for acetone sensitized, DMBP sensitized and direct NMP excited experiments are depicted in Figures 29.

Comparison of the penetration profiles in acetone solution (Figure 29a) for the microchannel (dwell device) vs. the Schlenk flask (Rayonet) clearly reveals that the narrow depth of the microchannel (0.5 mm) allows extensive penetration of light, despite the high concentration of acetone (6.8 M). In contrast, complete absorption of light is achieved in the Schlenck flask with an average pathlength of about 4 mm (considering a circular arrangement of 16 lamps around the cylindrical vessel incorporated with a cold finger) within the first two millimeters. At the significantly lower concentrations of chromophore, like in case of the direct NMP excitation (15 mM, Figure 29b) or DMBP sensitization (1.5 mM, Figure 29c) the complete light penetration is achieved for the Schlenk flask but with much lower percent transmission.



Figures 29: a) Light penetration profile for a 6.8 M acetone solution at 300 nm; b) Light penetration profile for a 15 mM NMP solution at 300 nm; c) Light penetration profile for a 1.5 mM DMBP solution at 350 nm. The vertical broken line (a) represents the pathlength in the dwell device and the dotted line (b) the effective pathlength in the Schlenk flask

Beside the perfect light penetration, the microstructured channel of the dwell device has another important benefit; a large irradiation area (23 cm^2) over a small internal volume (1.68 ml). This parameter is very important for photochemical reactions as larger irradiated surfaces provide more light to the reaction media. Moreover, the microreactor channel is fabricated in the Foturan glass plate, which is UV transparent and additionally supplies light distribution around the channel. In contrast, the conventional Schlenk flask (for 100 ml and 50 ml liquid volume) has an irradiation surface of only 274.31 cm^2 and 85.41 cm^2, respectively, which is 5 and 8 times smaller than the microreactor channel (Table 14).

Not only does the geometry of the reaction vessel have a significant influence on reaction efficiency, but also the energy output of the light sources is significant. Thus 5 fluorescent tube lamps of the dwell device provides more light energy to the solution in a microchannel (1.74 W cm^{-2}) than the same 16 Rayonet lamps (0.47 or 1.50 W cm^{-2}) with the Schlenk flask (Table 14). The reasonably high lamp power per surface unit for the 50 ml Schlenk flask can partially compensate its lowest irradiated area to volume ratio (only 171 m^2 m^{-3} compare to 1369 m^2 m^{-3} in microreactor).

Table 14: Technical details of the dwell device and Rayonet reactor setups

Parameter	Rayonet reactor		Dwell device
	Schlenk flask for 100 ml	Schlenk flask for 50 ml	
Aperture, [cm^2]	274.31[a]	85.41[a]	86.14[b]
Irradiated area, [cm^2]	274.31	85.41	23.0[c]
Irradiated volume, [cm^3]	100	50	1.68
Irradiated area / volume ratio, [m^2 m^{-3}]	274	171	1369
Lamp power, [W]	16 × 8	16 × 8	5 × 8
Lamp power per aperture, [W cm^{-2}]	0.47 (0.15[d])	1.50 (0.47[d])	0.46
Lamp power per irradiated area, [W cm^{-2}]	0.47 (0.15[d])	1.50 (0.47[d])	1.74

[a] Assuming a cylindrical geometry, the liquid height in 100 ml Schlenk flask with inserted cold finger was 27.3 cm, in 50 ml Schlenk flask was 8.5 cm; [b] optical window; [c] micro channel; [d] Schlenk flask irradiated with 5 lamps

4.4.3 Energy efficiencies of the used light sources in the experiments involving phthalimides

The efficiency of the light set-up can be evaluated with respect to product yields per lamp power and irradiation time (% W^{-1} h^{-1}) and also with respect to product yields per lamp power and irradiated area (% W^{-1} h^{-1} cm^{-2}).[38] The results of such calculations for

five acetone sensitised model reactions are presented in Table 15. Experiments with incomplete conversions (residence time 21 min) were used to obtain values free of contributions from 'over-irradiation'. As can be seen from the results the microreactor setup has considerably higher energy efficiency compared to the batch system for all investigated cases.

Table 15: Energy efficiencies of the dwell device and Rayonet reactor setups

			Energy efficiencies, [% W^{-1} h^{-1}][b]				
Reactor	**Time, [min]**	**W h[a]**	Reaction				
			64 + 71a → 66	64 + 75 → 76	78 → 79	80 → 81	83 → 64
Rayonet	21	44.8	0.45	2.08	0.80	1.03	0.42
Dwell device	21	14.0	2.43	6.93	2.79	2.36	3.14
			Energy efficiencies, [% W^{-1} h^{-1} cm^{-2}][c]				
Rayonet	21	44.8	0.0016	0.0076	0.0094	0.0121	0.0015
Dwell device	21	14.0	0.106	0.301	0.121	0.103	0.137

[a] Lamp power × irradiation time; [b] product yield (conversion) / (lamp power × irradiation time); [c] product yield (conversion) / (lamp power × irradiation time × irradiated area)

4.4.4 Reactors efficiencies used in the experiments involving phthalimides

The efficiency of the microreactor and the batch reactor was further evaluated using space-time-yield (STY) calculations. STYs depended on the reactor geometry and were determined for the above mentioned acetone sensitised reactions (Table 16) using equation *(2)*:[117]

$$STY = n_R / (V_R \times t) \qquad (2)$$

where n_R is the amount of NMP or its derivative converted within the reactor volume, V_R is reactor volume and t is irradiation time.

The results achieved for experiments with incomplete conversion (residence time 21 min) are illustrated in Figure 30, the general results for all other residence times are summarised in Table 16. From direct comparison between the reactors it is apparent that STYs are comparable or higher in the microreactor than in the batch system. Among all studied transformations the photobenzylation to **76** furnished the highest STY of *ca.* 0.69 mmol L^{-1} min^{-1} after just 21 minutes.

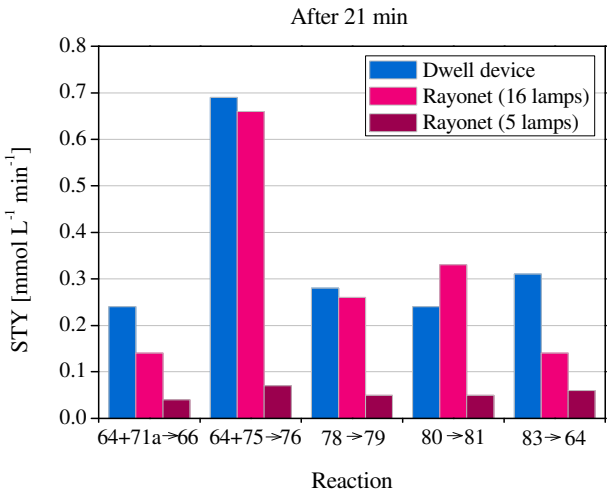


Figure 30: Space-time yields of five acetone-sensitized photodecarboxylation reactions (microreactor and Rayonet with 16 lamps, 21 min; Rayonet with 5 lamps, 60 min)

Table 16: Space-time yields for five acetone-sensitized photodecarboxylation reactions

		STY, [mmol L^{-1} min^{-1}]				
Reactor	**Time, [min]**	Reaction				
		64 + 71a → 66	64 + 75 → 76	78 → 79	80 → 81	83 → 64
Rayonet	21	0.14	0.66	0.26	0.33	0.14
Dwell device	21 (175[b])	0.24	0.69	0.28	0.24	0.31
Rayonet	40	0.17	0.38	0.22	0.20	0.15
Dwell device	40 (333[b])	0.25	0.38	0.26	0.26	0.28
Rayonet	60	0.22 (0.04[a])	0.25 (0.07[a])	0.18 (0.05[a])	0.17 (0.05[a])	0.15 (0.06[a])
Dwell device	60 (500[b])	0.25	0.25	0.20	0.19	0.23

[a] Rayonet with 5 lamps; [b] operation time including 'wash-out'

The essential drawback of the microreactor setup is the long experimental time required to pump the entire reaction mixture and additional solvent for 'wash-out' through the microchannel. Thus, nearly two hours (175 min) are needed to transfer 14 ml (reaction mixture 10 ml and solvent 4 ml) of liquid through the dwell device microchannel at a flow rate of 0.08 ml/min, which corresponds to a residence time of 21 min. For a prolonged irradiation time of 1 hour the experimental time is significantly extended to 8.5 hours. This fact could reasonably explain the problematic performance of dimethyl sulphide **65** photoaddition to NMP in the dwell device. It is known that dimethyl sulphide **65** is very volatile (boiling point 36°C) and quickly decompose in the presence of oxygen to sulphur dioxide.[186] Therefore an air tight reaction vessel is required. Such

conditions could be ensured in the batch Schlenk flask, but not in the microreactor, which operates in a flow through mode and is not a closed system.

However, the importance of continuous flow process was clearly demonstrated in the other experiments, i.e. DMBP sensitized photodecarboxylative additions. The exhaustive irradiation in a Rayonet reactor (transmission more than 50%, Figure 29c) caused DMBP to be involved in consecutive reactions, such as photoreduction and photopinacolisation.[187] Whereas in the microreactor, the surplus amount of triplet excited DMBP was continuously removed from the irradiated area. Consequently, photoreduction and photopinacolisation processes were significantly reduced and not observed in the equivalent microreactor experiments.

4.5 Summary

A series of intra and intermolecular photodecarboxylation transformations involving phthalimides had been studied in the conventional Rayonet reactor and successfully transferred to the microflow dwell device. Almost in all cases reactions proceeded more efficiently in the applied microreactor compared to the batch system at fixed residence time. Selected model reactions were studied with sensitizer 4,4'-dimethoxybenzophenone. Compared to the acetone-sensitized counterparts, the reactions were less selective and gave lower yields. Also DMBP had to be removed by column chromatography and underwent photoreduction processes in the batch system. However, the achieved results demonstrated the possibility to synthesise the same products under safer UVA irradiation.

The benefits of microflow reactor over the batch system have been discussed in terms of characteristic parameters of reaction vessel, energy efficiency of provided irradiation and reactors productivity as the space-time-yield of investigated reactions.

The small scales of the microreactions, up to 6 times reduced amounts of consumed chemicals and solvents and thus reduced amount of generated waste makes photochemical reactions in microscale advantageous for emerging area of Green Chemistry.

Chapter 5

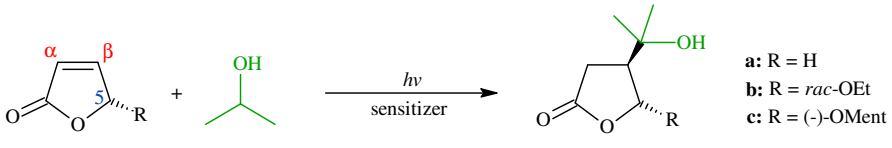
Highly efficient and stereoselective radical addition of secondary alcohols to electron-deficient alkenes in diverse manner experimental set-ups

5.1 Introduction

The addition of photochemically generated radicals to α,β-unsaturated carbonyl and carboxyl compounds is an attractive complement to the Michael addition.[188] The Michael addition is a well known synthetic transformation that represents an important method for stereoselective formation of C-C bonds. Following the original protocol, Michael reaction proceed via 1,4-addition of a stabilized carbon nucleophile (enolate) to an α,β-unsaturated carbonyl compound.[189] The important condition for the Michael addition to take place, are the presence of catalyst and protonation-deprotonation processes.[190] Frequently, Michael reactions are performed in chlorinated solvents and catalysts employed for the reaction have to be removed and recovered after the process, which is not an easy task.

In contrast to the C-C bond formation via typical Michael reactions the arrangement of the same bond type via photoaddition of radicals to α,β-unsaturated carbonyl compounds might represent a more environmentally friendly procedure. Thus the generation of corresponding radicals is entirely controlled by the "flick of a light switch" and some radicals could be generated directly from the applied solvent, for example from alcohols.[191] In addition, ordinary acetone could be used as a photocatalyst of such processes and could be further easily removed from the synthesised product.[192,193]

To demonstrate the suitability of photochemical procedures for synthetic processes directed for the stereoselective C-C bond formation under mild conditions, we selected several model reactions and applied them for our study. Initially, we explored photoinduced addition of isopropanol at the β-position of an α,β-unsaturated cyclic esters: unsubstituted 2(5*H*)-furanone and 5-alkoxy-2(5*H*)-furanones (Scheme 49).



84 a-c **85** **86 a-c**

Scheme 49: Photoaddition of isopropanol to furanones

The unsubstituted 2(5*H*)-furanone has been selected as substrate for this reaction because it is an attractive functionalized four carbon synthon that can be converted into a number of useful products.[194–196] 5-alkoxy-2(5*H*)-furanones are also multifunctional four carbon synthons, but with a stereocenter at C_5. Due to the possibility to obtain each of the enantiomers of the 5-alkoxy-2(5*H*)-furanone separately, by using different

methods, they are attractive starting materials in asymmetric synthesis. The most frequently used method so far is based on the preparation of (5*S*)- or (5*R*)-menthyloxy-2(5*H*)-furanone using *d*- or *l*-menthol, respectively, as a chiral auxiliary.[197]

A nice example of a practical application of the photoinduced addition of isopropanol to (5*R*)- and (5*S*)-5-substituted furan-2(5*H*)-ones has been reported by Mann and Wilson.[198] The authors applied this transformation for the synthesis of photoadducts that were used as intermediates in the synthesis of *cis*-chrysanthemic acids and novel nucleosides.

In our work the scope of the studied photoaddition reactions has been further extended by the handling of other secondary alcohols (3-pentanol and cyclopentanol) and common α,β-unsaturated esters: dimethyl fumarate and dimethyl maleate. The photoinduced additions of isopropanol and cyclopentanol to E/Z dimethyl esters of butenedioic acid are important transformations. Thus photoaddition of isopropanol to the esters leads to the formation of interesting methyl ester of terebic acid[187,199,200] and photoinduced addition of cyclopentanol to the esters represent a new promising route to spiro compounds.

Being interested not only in the introduction of greener procedures for synthetic chemistry, but also a competent and advance methodologies for most synthetic processes, we have investigated the above mentioned photochemical reactions not only in the conventional Rayonet photoreactor with traditional light sources but also in micro-photoreactors and microchips with current and energy saving UV-LEDs as the light source.

In our previous work that was done in the Rayonet reactor and Dwell device involving phthalimides we defined important deficiencies of the commercially available reactors, such as the set (by manufacture) pathlength and volume of a reaction vessel and single channel/vessel design.

To overcome such drawbacks of these experimental systems a newly made in-house dual-capillary reactor, where flexible PTFE capillary was utilised as reaction vessel, was developed. Furthermore practical examples of multi-parallel experiments performed simultaneously under the same conditions have not yet been reported. Therefore, the development of an optimised experimental system suitable not only for the individual synthesis, but also for the synthesis of small compound libraries has become a reasonable assignment. To address this task a novel multi-capillary reactor was designed and applied for multiple studies of photochemical processes.

Frequently, in the literature researchers reported comparison of batch operation mode vs. continuous flow mode.[21,201] However, the comparison of different microfluidic systems wasn't attempted so far in the literature. Such assessment could be very valuable because similar microfluidic systems differ significantly regarding the amount of synthesised material per time unit. "Micro" has to be as small as necessary and not more!

Hence our results achieved for the photoaddition of isopropanol to 2(5*H*)-furanones in different photoreactors were compared and applied for the establishment of the most reasonable operational system for photochemical synthesis.

5.2 Photoinduced addition of isopropanol to 2(5*H*)-furanones

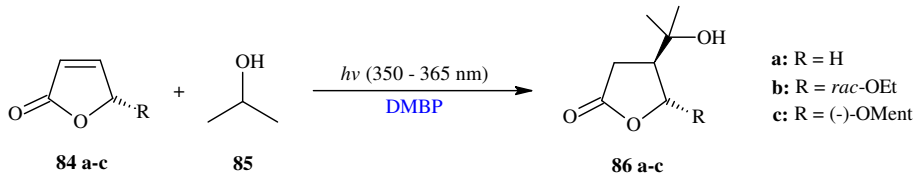
The photoaddition of isopropanol to 2(5*H*)-furanones is an example of a homogeneous model reaction. This transformation has a perfect atom economy, high chemical yields under conventional conditions and the solvent isopropanol additionally acts as an alkylation reagent. Moreover, the photoaddition of isopropanol to 5*R*-menthyloxy-2(5*H*)-furanone proceeds diastereoselectively.

The original protocol of this transformation used acetone as a sensitizer.[191,202] The ketyl or hydroxyisopropyl radicals resulting from acetone and isopropanol are identical which can lessen the formation of side products. However, the triplet energy of acetone is relatively high and required irradiation with lower wavelengths (UVB) for the n→π* transition may facilitate follow-up reactions.

Being interested in using the somewhat safer UVA irradiation instead of UVB irradiation which will allow for the use of energy efficient UV-LEDs, it was necessary to use an alternative sensitizer (the availability of UV-LEDs in the UVB range is limited and they are quite expensive).

4,4'-Dimethoxybenzophenone (DMBP), which has been used successfully for the related addition of amines to furanones,[203–205] was initially tested as a sensitiser and gave high conversion rates after short residence times and was thus chosen for this study. The n→π* absorption band of DMBP ($\lambda max_{n\rightarrow\pi^*} \approx 320$ nm in MeCN) showed a good overlap with the emission band of the UVA irradiation light sources. The only disadvantage of DMBP is the necessity for its removal by column chromatography for product purification. However, DMBP is generally needed in small amount and could be recovered in up to 90% yield.

Thus DMBP-sensitized isopropanol addition to three model furanones: unsubstituted 2(5*H*)-furanone, *rac*-2-ethoxy-2(5*H*)-furanone and (5*R*)-(-)-menthyloxy-2[5*H*]-furanone (Scheme 50) was investigated in different scale setups.



84 a-c **85** **86 a-c**

Scheme 50: DMBP-sensitized isopropanol addition to 2(5*H*)-furanones

5.2.1 Photoinduced addition of isopropanol to 2(5*H*)-furanones in the Rayonet reactor

Initially, in the *experiments 87-98*, photoinduced addition of isopropanol to 2(5*H*)-furanones was optimised in the batch Rayonet reactor (for experimental set-up description see § **4.2.1**). Experiments were carried out in the Pyrex test tubes (9 mm inner ∅) with both above mentioned sensitizers. The isopropanol solutions of furanones **84a–c** with catalytic amount of acetone were irradiated for 10 and 20 min by the fluorescent tubes with emission maximum in the UVB region (λ_{max} = 300±25 nm). After irradiation, solvent was evaporated and the conversions of furanones **84a–c** were determined by integration of baseline separated signals in the ^{1}H-NMR spectrum. Incomplete conversions were obtained for all experiments with acetone as sensitizer (*experiments 87-92*). The addition of isopropanol to 5-alkoxy-2(5*H*)-furanones **84b** and **84c** was stereospecific.[191,202] Crude products that were collected in the experiments with residence time of 20 min were purified by flash chromatography and photoadducts **86a–c** were isolated in yields between 75% and 81% (Table 17, entry 2). These values are close to the conversions indicating that the transformations proceeded highly selective.

The isopropanol solutions of furanones **84a–c** with a catalytic amount of DMBP were irradiated for 5 and 20 min by the fluorescent tubes with emission maxima in the UVA region (λ_{max} = 350±25 nm; *experiments 93-98*). The transformations occurred faster compared to acetone. After irradiation for just 5 min, high conversions of 87–90% were achieved. Prolonged irradiations for 20 min resulted in complete conversions and gave isolated yields of 87–94%, respectively (Table 17, entry 4).

Based on these results, it was concluded that DMBP is a worthy sensitizer for photoinduced addition of isopropanol to 2(5*H*)-furanones. Hence DMBP was used as sensitizer in our following experiments.

Table 17: Results obtained within the *experiments 87-98* in the Rayonet reactor

Entry	Residence time, [min]	Sensitizer	Conversion, [%][a]		
			R = H (86a)	R = OEt (86b)	R = OMent (86c)
1	10	Acetone	31	52	41
2	20	Acetone	80 (79[b])	94 (75[b])	82 (81[b])
3	5	DMBP	90	90	87
4	20	DMBP	100 (94[b])	100 (88[b])	100 (87[b])

[a] Determined by ^{1}H-NMR spectroscopy; [b] isolated yields

5.2.2 Photoinduced addition of isopropanol to 2(5*H*)-furanones in the Dwell device

The first microfluidic system that was employed for the testing of DMBP sensitised addition of isopropanol to 2(5*H*)-furanones was the commercially available microreactor dwell device. The detailed description of the dwell device experimental set-up was given in § **4.2.2**. The reactor comprised a reaction channel of 0.5 × 2 mm (D × W) with an internal volume of 1.68 ml.

In the next *experiments 99-104*, the isopropanol solutions of furanones **84a–c** with a catalytic amount of DMBP (6.67 mmol/L) were irradiated for 5 and 10 min with 5 UVA fluorescent tubes that have a maximum emission at 350 nm. The irradiation time was controlled by the flow rate of the syringe pump. The flow rate of 0.336 ml/min corresponded to a residence time of 5 min and flow rate of 0.168 ml/min corresponded to a residence time of 10 min, respectively. Results achieved in *experiments 99-104* are summarised in Table 18. The complete conversions of furanones **84a–c** to the corresponding photoadducts **86a–c** were achieved in all examined cases with the residence time of 10 min. After a shorter irradiation time of 5 min, the dwell device again gave almost complete conversions of 81% (**84a**), 99% (**84b**) and 98% (**84c**), respectively. To evaluate the efficiency of the microstructured system the results achieved in the dwell device after 5 min were compared with the same experimental results obtained in the batch Rayonet reactor (Table 17, entry 3, *exp. 93-95*). With the exception of the parent furanone **84a**, the microreactor gave higher conversion rates compared to the batch system after the identical reaction time of 5 min (Table 18, entry 1, *exp. 99-101*).

The conversions of unsubstituted furanone **84a** were determined by the comparison of signal integration for the protons attached to carbon 5 of the furanone ring of **84a** to the signal integration of the same protons of **86a** (Figure 31). The conversions of 5-alkoxy-

2(5*H*)-furanones **84b** and **84c** were determined by the comparison of signal integrations for the acetal proton (an example of such comparisons will be presented later).

Table 18: Results obtained within the *experiments 99-104* in the dwell device

Entry	Flow rate, [ml/min]	Residence time, [min]	Conversion, [%][a]		
			R = H (86a)	R = OEt (86b)	R = OMent (86c)
1	0.336	5	81 (90[b])	99 (90[b])	98 (87[b])
2	0.168	10	100	100	100

[a] Determined by ^{1}H-NMR spectroscopy; [b] conversions under batch conditions in the Rayonet reactor

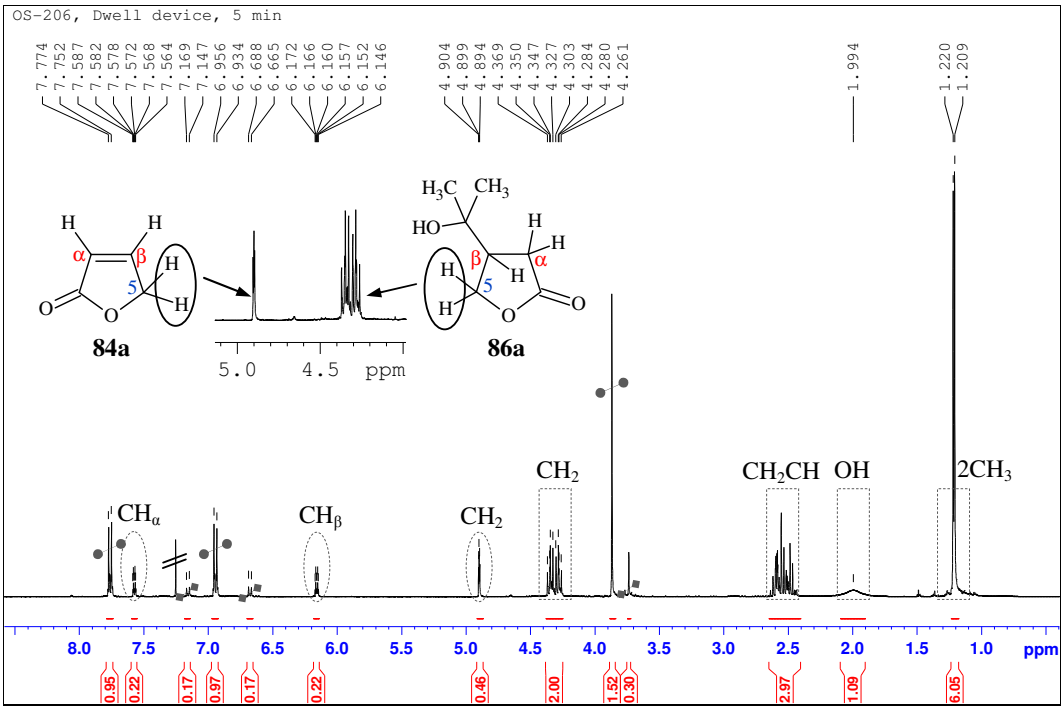


Figure 31: ^{1}H-NMR of the crude product obtained in the *experiment 99* after 5 min. Peaks marked by dashed square represent protons of the product **86a**, peaks marked by dashed oval represent protons of unsubstituted 2(5*H*)-furanone **84a**, peaks marked by "●-●" represent DMBP, peaks marked by "▪-▪" represent photoreduction product of DMBP

5.2.3 Photoinduced addition of isopropanol to 2(5*H*)-furanones in the microchip

Being interested to explore the dependency between further scale-down of the microfluidic system we assembled an LED-driven microchip. The volume of the microchip reaction vessel was just 13 µl. The microchip is also an example of a continuous-flow system. The key difference between the microchip set-up and the

previously used batch Rayonet and microsystem dwell device was the type of light source employed for irradiation. Thus, in the microchip system an array of 6 × 365 nm high-power LEDs was used, while in other set-ups the fluorescent tube lamps were utilized.

5.2.3.1 Microchip Micronit experimental set-up

The LED-driven microchip was the smallest experimental set-up used. The actual size of the employed microchip was comparable to a 1 cent coin (Figure 32a). The reaction channel was embedded inside of a glass plate with dimensions of 45 mm × 15 mm ×1.8 mm, length × width × thickness, respectively (Figure 32b).

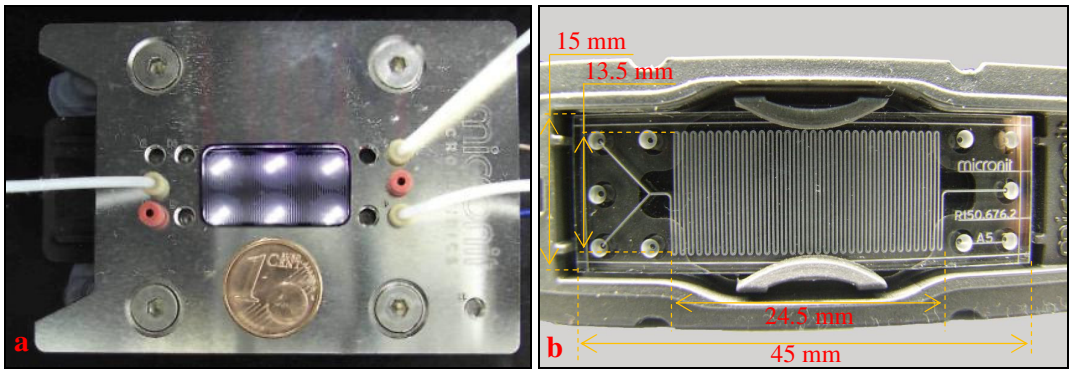


Figure 32: Microchip Micronit: a) compared to 1 cent coin; b) glass plate with embedded reaction channel

The LED-driven microchip set-up consisted of several devices (Figure 33). The main part was a microchip **1** (Micronit Microfluidics[41]) made of Borofloat® glass ($\lambda \geq 300$ nm, transmission is about 30% at 300 nm) in a stainless steel holder. The chip has a single reaction channel of 150 µm wide, 150 µm deep and 757 mm long (32 turns) with an internal volume of 13 µl (channel cross section: ⌓). The prepared reaction mixture was filled into a 1 ml glass syringe **3** (ID = 4.60 mm) and pumped by a programmable syringe pump **2** at various flow rates through the microchip via its two inlets using a T-piece **4**. To secure complete removal of air bubbles from the microsystem before the start of the experiment the reaction channel was always preliminary packed with the appropriate solvent through its single outlet. Air bubbles have a significant influence on the liquid flow rate within the channel and consequently on the residence time, therefore they have to be completely removed. The reaction mixture was irradiated while passing through the microchip and was collected in a small round bottom flask **7** (protected from light) outside the irradiation chamber. The remaining reaction mixture was washed

out from the microchannel by the appropriate solvent and was collected into the same flask **7**. Due to the small aperture of the chip viewing window (13.5 mm × 24.5 mm), an array of 6 × 75 mW high power UV-LEDs **5** (λ = 365 ± 5 nm) was used as a miniature light source. The house made LED array was positioned on the microchip base and irradiated the reaction microchannel from the bottom side at a distance of 1 mm. This positioning of the light source was preferred due to the thinner glass layer (700 μm) on the bottom side of the chip compared to the top side (1100 μm). The UV-LED current of 780 mA was provided and controlled by the power supply **6**. During irradiation, a small cooling fan **8** was mounted onto the LED-microchip and this setup was enclosed in a suitable light tight container **9** (container cover is omitted on the picture). The irradiation time was controlled by pump flow rate and a power supply current regulator.

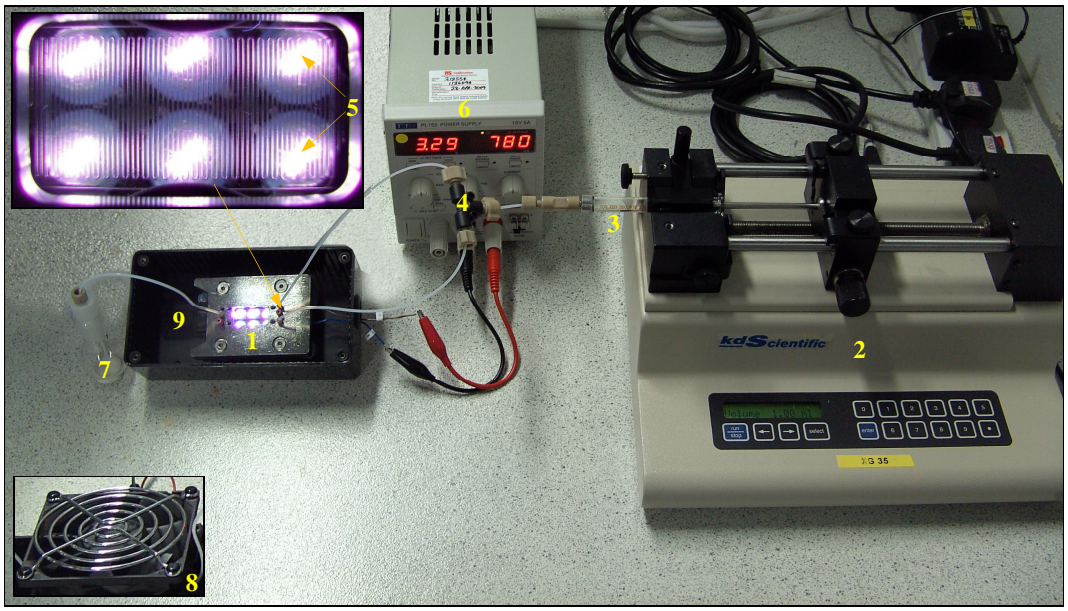


Figure 33: LED-driven microchip setup: **1** – microchip in a stainless steel holder with LEDs array on its bottom side (inset shows close-up of LED-microchip); **2** – programmable syringe pump; **3** – syringe for 1 ml; **4** – T-piece; **5** – 365 nm high power UV-LEDs; **6** – power supply; **7** – collection flask; **8 –** cooling fan; **9** – light tight container

5.2.3.2 Efficiency of photoinduced addition of isopropanol to 2(5*H*)-furanones in the microchip

The same three model reactions the photoaddition of isopropanol to furanones **84a–c** were tested in the next *experiments 105-114* that were carried out in the LED-driven microchip. Initially, residence time was set to 20 min and unsubstituted furanone **84a**

was investigated (*exp. 105*). The complete conversion of **84a** was achieved. In the following experiments the irradiation time was shortened to 5 min, 2.5 min and 1 min respectively. Complete conversions were again obtained, but after just 2.5 min in the case of 5-alkoxy-2(5*H*)-furanones **84b** and **84c** (Table 19, entry 2) and after 5 min in the case of unsubstituted 2(5*H*)-furanone **84a** (Table 19, entry 3).

In contrast, the equivalent experiments performed under batch conditions in the Rayonet chamber reactor and under continuous-flow conditions in the dwell device gave incomplete conversion rates for the same residence time of 5 min (Table 17, entry 3 and Table 18, entry 1, correspondingly).

Table 19: Results obtained within the *experiments 105-114* in the LED-driven microchip

Entry	Flow rate, [µl/min]	Residence time, [min]	Conversion, [%][a]		
			R = H (86a)	R = OEt (86b)	R = OMent (86c)
1	13	1	58	60	59
2	5.2	2.5	89	100	100
3	2.6	5	100 (90[b])	100 (90[b])	100 (87[b])
4	0.65	20	100	–[c]	–[c]

[a] Determined by ^{1}H-NMR spectroscopy; [b] conversions under batch conditions in the Rayonet reactor; [c] not determined

5.2.4 Photoinduced addition of isopropanol to 2(5*H*)-furanones in the in-house made dual-capillary microreactor

The above described experimental set-ups of the Rayonet reactor, dwell device and LED-driven microchip were based on commercially available systems. Thus the design and parameters of their reaction channels or vessels were fixed and preset by the manufacturer. Frequently, such parameters didn't match the requirements of the planned experiment. For example, the pathlength of the reaction channel was strictly confined by the size of the irradiation plate where the channel was embedded. Moreover, parallel experiments or experimental scale-up could only be achieved by increasing the number of employed microreactors, which is quite costly for an academia project. For example, the price of the Rayonet reactor is about 3,000 €, price of the dwell device is about 4,000 € and the price of the microchip is about 1,000 €.

To address this problem a new dual-capillary reactor was designed. This microreactor overcame the above mentioned disadvantages of the commercially available microreactors. Thus, instead of the single reaction channel, in the dual-capillary reactor

two individual polytetrafluoroethylene (PTFE) capillaries were used as reaction vessels and their pathlength was limited just by the length of the lamp employed for irradiation. Moreover, polytetrafluoroethylene capillaries are UV-transparent, chemically resistance, flexible and cheap, thus representing a suitable alternative to common silicate. The price for PTFE capillary is just 80 € for 100 meters and PTFE capillary is available in various diameters and wall thickness.

5.2.4.1 Dual-capillary microreactor experimental set-up

A dual microcapillary reactor (Figure 34) was designed in-house by Dr Alexander Yavorskyy. This photoreactor was constructed to demonstrate the potential of microstructured devices for product-scale and parallel synthesis.

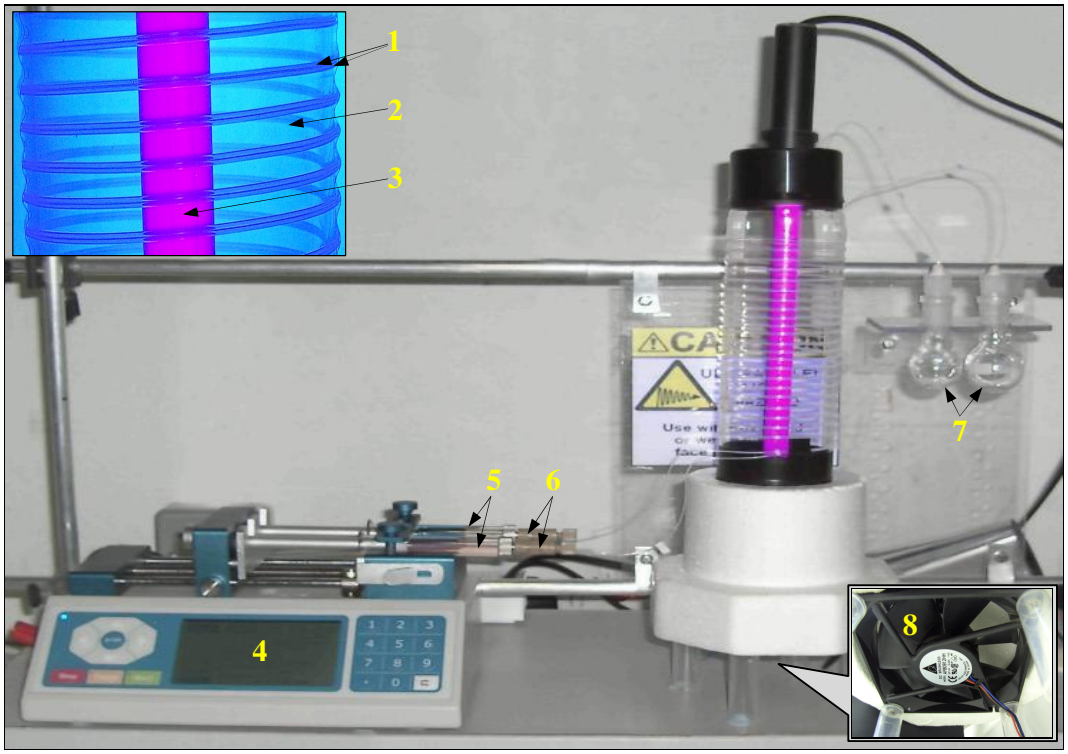


Figure 34: Dual capillary microreactor setup: **1** – two parallel PTFE capillaries; **2** – Pyrex glass cylinder; **3** – UVA lamp; **4** – programmable dual syringe pump; **5** – two syringes for 5 ml; **6** – two PTFE adaptors; **7** – collection flasks; **8 –** cooling fan

Two parallel PTFE capillaries **1** of 460 cm length each and 558 μm inner diameter (internal volume per capillary: 1.12 ml) were tightly wrapped around a Pyrex glass cylinder **2** ($\lambda \geq 280$–300 nm, transmission is about 30% at 300 nm) of 6.5 cm diameter and 20 cm height. Following this, 22 windings covering 14 cm of the glass body were achieved. The chosen set-up was used to conduct two different or two identical

experiments at the same time. A single RPR-3500Å lamp **3** (8 W, λ = 350±25 nm) was placed in the centre of the Pyrex cylinder **2** and provided sufficient UVA irradiation. Two capillaries were separately connected via PTFE adaptors **6** (Kinesis, P-627) to the 5 ml glass syringes **5** (ID = 10.29 mm) that were loaded into the programmable dual syringe pump **4**. The prepared reaction mixtures were transferred into the syringes and pumped through both microcapillaries at flow rates adjusted to the needed residence time. The irradiated products were collected into separate flasks **7**, which were protected from stray light. A small cooling fan **8** was mounted on the bottom of the glass cylinder to keep a constant experimental temperature. During irradiation, the cylinder and capillaries were covered by a foil shutter.

5.2.4.2 Efficiency of photoinduced addition of isopropanol to 2(5*H*)-furanones in the dual-capillary microreactor

The suitability of the dual-capillary microreactor for photochemical synthesis was evaluated using the above described model reactions of the photoaddition of isopropanol to furanones **84a–c**. Within the next *experiments 115-130* these model reactions were investigated at different residence times ranging from 2.5 min to 20 min. As usual, at the beginning of our study prolonged residence times of 15 min and 20 min were used and complete conversions were achieved in all cases (Table 20, entry 5 and 6). Afterwards, residence times were reduced up to 10 min, 7.5 min, 5 min and 2.5 min, respectively.

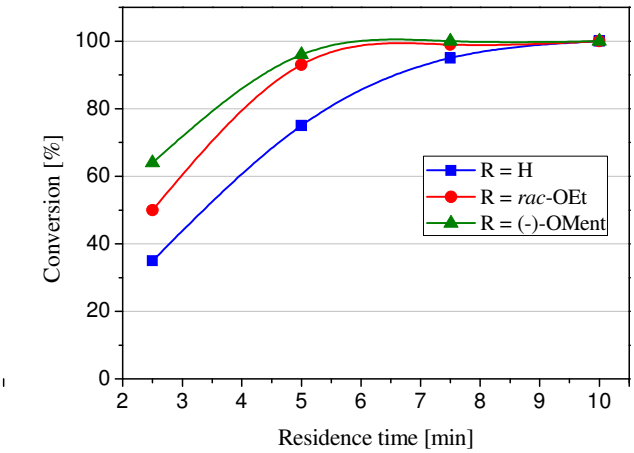


Figure 35: Conversion of furanones **84a–c** vs. residence time in the dual-capillary microreactor

As can be seen from the plots in Figure 35 and from the data summarised in Table 20, at shorter residence times the conversions were lower. However, unsubstituted 2(5*H*)-furanone **84a** and *rac*-2-ethoxy-2(5*H*)-furanone **84b** reached complete conversions after 10 min (entry 4) while (5*R*)-(-)-menthyloxy-2[5*H*]-furanone **84c** reached complete conversion after just 7.5 min (entry 3).

Table 20: Results obtained within the *experiments 115-130* in the dual-capillary microreactor

Entry	Flow rate, [µl/min]	Residence time, [min]	Conversion, [%][a]		
			R = H (86a)	R = OEt (86b)	R = OMent (86c)
1	460	2.5	35	50	64
2	230	5	75 (90[b])	96 (90[b])	99 (87[b])
3	153.3	7.5	95	99	100
4	115	10	100	100	100
5	76.7	15	100	–[c]	–[c]
6	57.5	20	100	100	100

[a] Determined by ^{1}H-NMR spectroscopy; [b] conversions under batch conditions in the Rayonet reactor; [c] not determined

The conversion rates of the three model furanones **84a-c** obtained in the dual capillary microreactor were compared to the results achieved in the batch setup using a fixed reaction time of 5 min (Table 20, entry 2). The microcapillary reactor gave conversion rates of 75% (**84a**), 96% (**84b**) and 99% (**84c**), respectively. Whereas the much larger Rayonet chamber reactor equipped with a set of 16 UVA lamps gave lower conversion rates of 90% (**84a**), 90% (**84b**) and 87% (**84c**). Again, with the exception of the parent furanone **84a**, the continuous-flow system gave higher conversion rates compared to the batch process.

As mentioned above, the conversion rates of unsubstituted furanone **84a** were determined by the comparison of the signal integration for the protons bound to carbon 5 of the furanone ring of **84a** with the signal integration of the same protons of **86a**. The conversions of 5-alkoxy-2(5*H*)-furanones **84b** and **84c** were determined by the comparison of signal integrations for the acetal protons. Representative ^{1}H-NMR spectra of the crude products obtained in the *experiments 129* and *130*, where *rac*-2-ethoxy-2(5*H*)-furanone **84b** and (5*R*)-(-)-menthyloxy-2[5*H*]-furanone **84c**, respectively, were irradiated for 2.5 min in the dual-capillary microreactor are presented on the Figures 36 and 37, respectively.

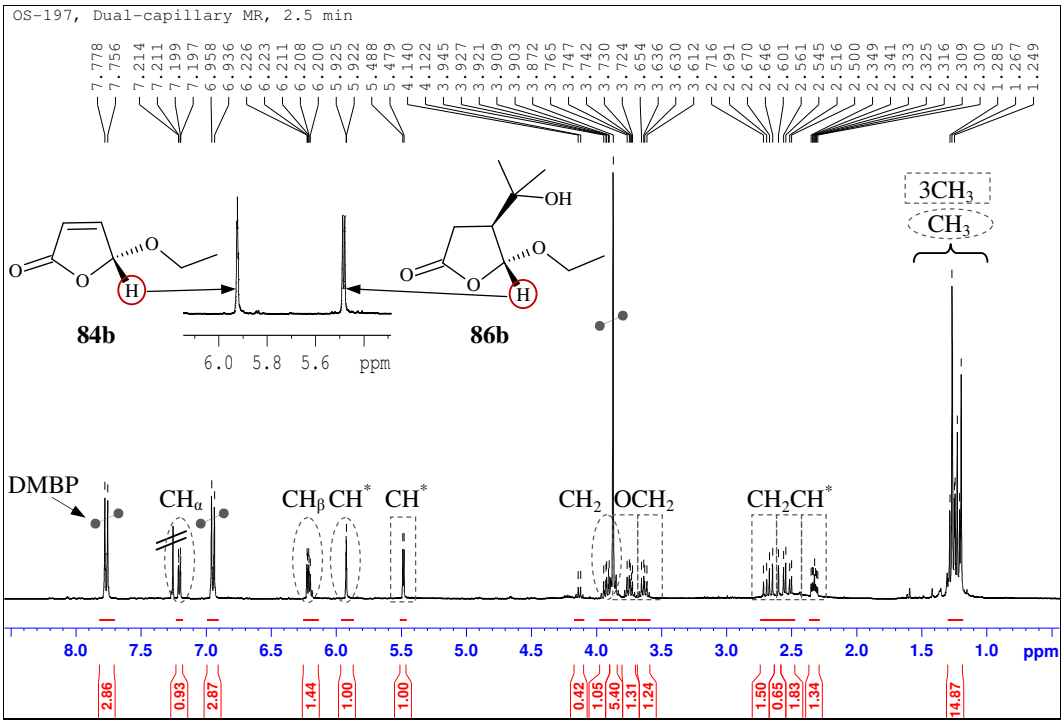


Figure 36: [1]H-NMR of the crude product obtained in the *experiment 129* after 2.5 min. Peaks marked by dashed square represent protons of the product **86b**, peaks marked by dashed oval represent protons of *rac*-2-ethoxy-2(5*H*)-furanone **84b**

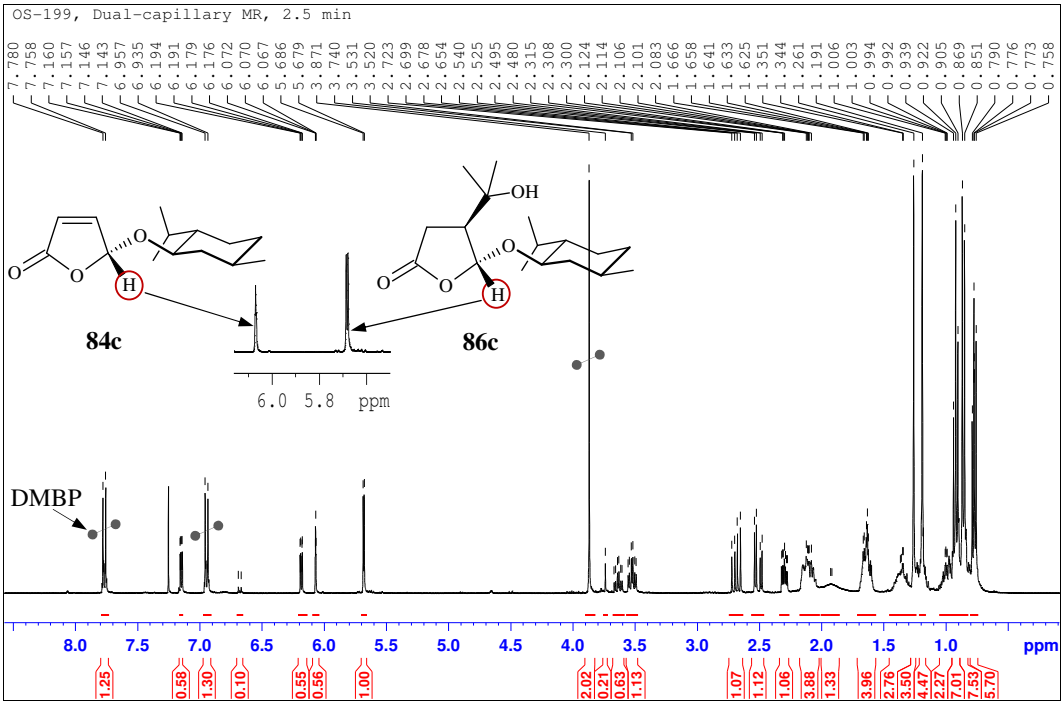


Figure 37: [1]H-NMR of the crude product obtained in the *experiment 130* after 2.5 min. Due to the considerable overlap of most product peaks with the peaks of initial furanone, only acetal protons of **84c** and **86c** are highlighted on the figure

5.2.5 Comparison of the efficiency of photoinduced addition of isopropanol to 2(5*H*)-furanones in the applied experimental set-ups

So far, the same three model reactions of the photoaddition of isopropanol to 2(5*H*)-furanones **84a–c** have been studied in four experimental set-ups, batch system Rayonet reactor, continuous flow dwell device, LED-driven microchip and dual-capillary reactor. Typically, the efficiency of reactions in the continuous flow systems was compared to the reaction efficiencies in the batch Rayonet reactor and in most cases higher conversion rates were achieved in the continuous flow system (Tables 18–20, entries 1, 3, 2, respectively, Figure 38).

However, the performance of various continuous flow systems itself hasn't been compared until now. Shown in Figure 38, are the comparisons of all reactors for a fixed residence time of 5 min. Only the microfluidic system LED-driven microchip gave 100% conversion. In the commercially available dwell device and the in-house made dual-capillary reactor, the reactions showed similar efficiency and almost complete conversions.

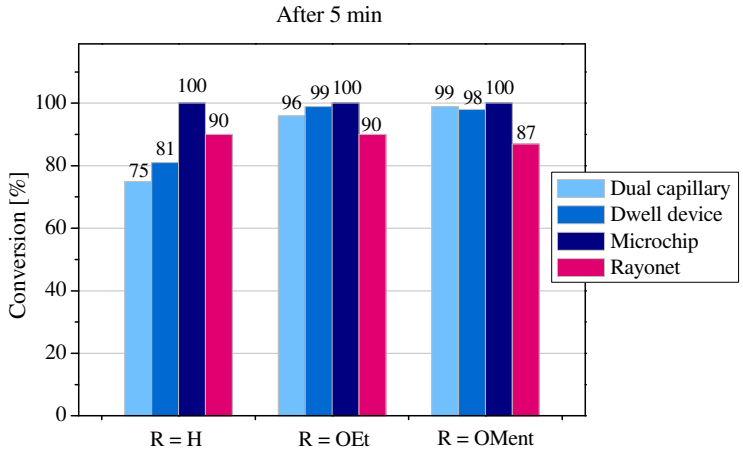


Figure 38: Comparison of 2(5*H*)-furanones **84a–c** conversion rates in different experimental set-ups at fixed residence time of 5 min

The highest efficiency of the studied photochemical reactions in the LED-driven microchip, its small size and reaction volume of just 13 µl, makes the LED-driven microchip an advantageous system for pharmaceutical research and development, where only small amounts of materials are required for biological screening.[53,206]

However, if the desired product needs to be produced in gram-scale it will be appropriate to come back to the microreactors, especially the in-house made dual-capillary reactor. As demonstrated above, the dual-capillary microreactor has excellent

potential for the realization of parallel experiments and is a promising set-up for product scale-up. Moreover, as seen from Figure 38, the dual-capillary reactor gave conversion rates equivalent to the conversion rates of the commercially available dwell device system. In addition, the dual-capillary reactor overcame an important drawback of the dwell device – fixed pathlength.

Based on the above described comparison, it could be concluded that the in-house made dual-capillary microreactor is an effective and competitive system for photochemical synthesis. A simple and 'easy-to-use' design makes it an attractive tool for users and a promising tool for future work.

5.3 Optimisation of photochemical processes in advanced and newly designed multi-microcapillary reactor

Being encouraged by the simplicity of the dual-capillary reactor design and its high efficiency, we decided to extend this work further.

As can be seen in Figure 34, the original design of the dual-capillary reactor was adequate, but some room for improvements could still be found. Firstly, the irradiated area of the glass cylinder wasn't optimally used because there was more than 5 mm of vacant area left between the subsequent rings of the capillaries. Due to the unused area, the pathlength of the capillaries were also limited. Secondly, the length of the utilised lamp for irradiation was just 26.5 cm and the length of the glass cylinder that was used as a reactor base wasn't optimal as well.

Considering the above mentioned potential of the dual capillary reactor, a novel multi-microcapillary tower design was realized and described in the next experimental set-up.

5.3.1 Multi-microcapillary tower experimental set-up

The multi-microcapillary tower experimental set-up (Figure 39) is quite similar to that of dual-capillary microreactor and was also designed by Dr Alexander Yavorskyy. The most significant differences are the number of used capillaries, their capacity and the length of lamp.

Instead of two PTFE capillaries, ten parallel FEP (fluorinated ethylene propylene) capillaries **1** were tightly wrapped around two Pyrex glass cylinders **2** ($\lambda \geq 280$–300 nm, transmission is about 30% at 300 nm), five capillaries per each cylinder. Both cylinders were of 60 cm height and 6 cm outer diameter, wall thickness was 2.2 mm. Each of ten FEP capillaries **1** was of 11.4 m total length including 10 m of capillary wrapped around the glass cylinder and 0.7 m on both sides for connections. Every 10 m of capillary

created 53 windings around the glass cylinder. So, in total each cylinder had 265 (53 × 5) windings covering 41 cm of the glass body. The internal diameter of each capillary was the same and was 800 μm. Following this, each of the 10 m of capillary had an internal volume of 5 ml. Thus the total volume of each tower was 25 ml and the entire volume of the whole system was 50 ml.

Two fluorescent lamps **3** (λ = 365±25 nm) with an optical power of 18 W each, were placed in the centre of the cylinders **2** and provided sufficient UVA irradiation. The length of fluorescent lamps was the same as the length of the cylinders and was 60 cm. To avoid cross-irradiation between the two lamps a black paper membrane **4** was placed in the middle.

Ten capillaries were separately connected via PTFE shut-valves **7** (Kinesis, P-732) to the individual 10 ml glass syringes **6** (ID = 14.56 mm) that can be prefilled with the different or the same experimental solutions. Syringes were loaded into the programmable syringe pump **5** equipped with special 10 channel infuse/withdraw holder. Solutions were pumped simultaneously through all capillaries at specific flow rates provided by the syringe pump **5** and adjusted to the necessary residence time. The irradiated products were collected into the individual round bottom flasks **8**.

The inlet and outlet of each capillary and positions of the syringes were labelled with the appropriate number from 1 to 10 to avoid any mix-up within the experiments (red and green tape labels on the capillaries and red labels on the syringes holder).

Glass cylinders were accommodated into styrofoam bases **10** and additionally fixed by plastic holders on the top. Each styrofoam base had a small cooling fan **9** encapsulated into its bottom part. Cooling fans were used to cool down the lamps inside of the glass cylinders and kept the experimental temperature stable.

During the experiment capillary towers were sheltered by a black fabric shutter **11** as shown in Figure 39b. The collection flasks were also protected from the ambient light by the black paper shields **12**. Syringes were covered by several layers of aluminium foil (not shown on the figure).

After the experiment was finished the capillaries can be cleaned with an appropriate solvent and then dried by nitrogen for 30 min. Nitrogen was supplied to the capillaries in a controllable and parallel manner using PTFE adaptors **13** (Kinesis, P-627), thus preventing damage of the capillaries.



Figure 39: a) Multi-microcapillary tower set-up: **1** – ten parallel FEP capillaries; **2** – two Pyrex glass cylinders wrapped with five FEP capillaries each (towers); **3** – two UVA fluorescent lamps; **4** – black paper membrane; **5** – programmable syringe pump; **6** – ten syringes for 10 ml each; **7** – ten PTFE shut-valves; **8** – ten collection flasks; **9** – two cooling fans; **10** – styrofoam base; **11** – black fabric shutter; **12** – black paper shields; **13** – five PTFE adaptors; b) multi-microcapillary reactor protected from ambient light during the experiment

5.3.2. Benefits of multi-microcapillary reactor

As can be seen in Figure 39 and from the description of the experimental set-up, multi-microcapillary reactor (m-CR) can be applied for:

1) the fast optimisation of any experimental procedure,
2) synthesis of small compounds library,
3) gram-scale production and
4) validation and standardization of photochemical processes.

The total volume of the multi-microcapillary reactor that could be irradiated per time unit was 50 ml, which is equivalent to the irradiation volume of a batch Schlenk flask. Moreover, the multi-microcapillary reactor is a continuous flow system and its capacity could be increased significantly. Furthermore, the multi-microcapillary reactor doesn't need cooling water and has low energy consumption.

No one of the above described experimental set-ups had such potential. Therefore, in the following paragraphs the benefits of multi-microcapillary reactor will be demonstrated and discussed based on the practical experiments and obtained results.

5.3.2.1 Reactions residence time optimisation study

The successful performance of DMBP sensitised photoadditions of isopropanol to 2(5*H*)-furanones **84a–c** in the commercially available micro-flow reactors and batch Rayonet reactor makes them suitable model transformations for further investigation in a novel multi-microcapillary reactor to estimate its efficiency. Each tower of the multi-microcapillary reactor was irradiated with a single UVA fluorescent lamp (λ = 365±35 nm) that was similar to the fluorescent tubes used in previous setups (λ = 350±25 nm).

The above established procedure of isopropanol additions to 2(5*H*)-furanones **84a–c** was used again and model transformations were investigated in multi-microcapillary reactor at different residence times from 1 min to 10 min (*experiments 131-135*). Residence times were defined by the flow rates of the syringe pump. As would be expected, conversion rates improved with the increasing of irradiation times (Figure 40) and reactions reached completion after just 7.5 min (**84c**) and 10 min (**84a** and **84b**).

Again, conversion rates achieved for the model reactions in the multi-microcapillary reactor were compared with that achieved in the batch reactor after a fixed residence time of 5 min (Table 21, entry 3). Somewhat lower or similar conversion rates were achieved in the tower system compared to the batch reactor. This somewhat unexpected finding might result from the considerably larger optical power of 128 W in the Rayonet

reactor provided by 16 fluorescent tubes. The optical power of the lamps used in multicapillary reactor was just 18 W.

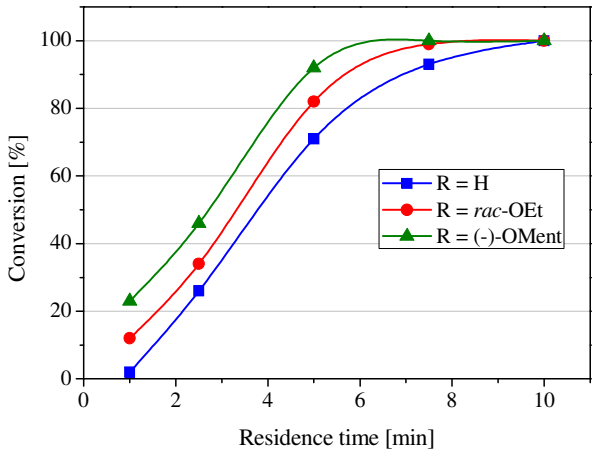


Figure 40: Conversion of furanones **84a–c** vs. residence time in the multi-microcapillary reactor

Table 21: Results obtained within the *experiments 131-135* in the multi-microcapillary reactor

Entry	Flow rate, [ml/min]	Residence time, [min]	Conversion, [%][a]		
			R = H (86a)	R = OEt (86b)	R = OMent (86c)
1	5	1	2	12	23
2	2	2.5	26	34	46
3	1	5	71 (90[b])	82 (90[b])	92 (87[b])
4	0.67	7.5	93	99	100
5	0.50	10	100	100	100

[a] Determined by ^{1}H-NMR spectroscopy; [b] conversions under batch conditions in the Rayonet reactor

5.3.2.2 Reproducibility study

One of the main purposes of the multi-microcapillary reactor was its application for parallel experiments. Therefore, it was important to show that both towers and all ten capillaries were working with the same efficiency. To realise this task, *experiment 136*, randomly selected DMBP sensitised photoaddition of isopropanol to unsubstituted 2(5*H*)-furanone **84a** was tested simultaneously in all capillaries at a flow rate of 1 ml/min which corresponded to a residence time of 5 min. Results achieved in this experiment were combined with two additional results obtained in the equivalent experiments (*exp. 133* and *141*) when studying the relationship between other

parameters. As can be seen from the data points presented in Figure 41, the conversion rates of **84a** were similar for all capillaries and were generally in the range of 67–73%. The standard deviation of conversion was just 3.2%. This achievement nicely demonstrates that the results obtained in the multi-capillary reactor are highly reproducible with a 4.5% RSD. Moreover, excellent reproducibility was not only achieved between the individual capillaries but also between the independent experiments.

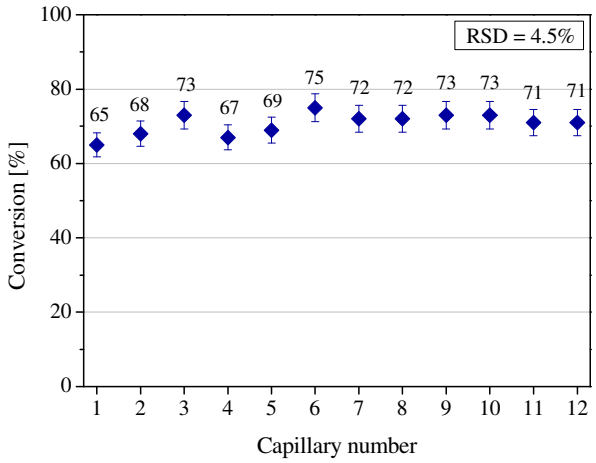


Figure 41: Reproducibility of the conversion of furanone **84a** within the individual capillaries of multi-capillary reactor

5.3.2.3 Scale-up product synthesis and energy efficiency of multi-microcapillary reactor

Other important assignment of multi-capillary reactor was scale-up synthesis of interested products. To explore the scale-up capacity of the multi-capillary reactor, *experiment 137*, DMBP sensitised photoaddition of isopropanol to unsubstituted 2(5*H*)-furanone **84a** was again tested in all capillaries, simultaneously, at a flow rate of 0.5 ml/min which corresponded to a residence time of 10 min. In contrast to the previous *experiment 136*, crude products from individual capillaries were collected not into separate round bottom flasks but into one common round bottom flask with a total volume of 250 ml. It has been established before (*exp. 131*) that at a residence time of 10 min the conversion of furanone **84a** to the product **86a** is complete and thus the pure product could be isolated in the maximum quantity. Therefore the crude product collected in the *experiment 137* was checked by ^{1}H-NMR and further purified by column chromatography. The desired product **86a** was isolated in the amount of 452 mg which corresponded to a reaction yield of 94%.

This result showed that a single output of the multi-capillary reactor could be equivalent to the batch Rayonet reactor with respect to the conversion rate and the actual amount of isolated product.

In order to evaluate the energy efficiency of the multi-capillary reactor and compare it to the Rayonet reactor, the energy consumption per hour of operation was measured using a commercially available domestic electricity meter. The Rayonet reactor with its' 16 lamps consumed 0.179 kW/h (Table 22, entry 1) which is almost three times larger than the sum of energy consumption of 0.063 kW/h of all devices involved in the multi-microcapillary set-up (Table 22, entry 2). However, it is important to mention that the total operation time of both systems for the production of the same amount of product was not equivalent. For example, in the multi-capillary reactor for the production of 451.7 mg of product **86a** the operation time was 40 min (residence time just 10 min) while in the Rayonet reactor residence time was always equivalent with the operation time and the same amount of product could be produced after 20 min. So to see if there is a real difference in energy consumption between the reactors, the quantity of energy used by each system to produce 1 kg of product was calculated. The obtained numbers show that in the multi-capillary reactor, despite its longer operation time, 1 kg of product could be produced with 30% of an electrical energy saving compared to the batch reactor (Table 22). Moreover, due to the significant generation of heat by the 16 lamps, the Rayonet reactor required continuous circulation of cooling water. The water consumption was subsequently determined to be 1-4 L/min. The fluorescent lamps of the multi-capillary reactor generated much less heat and were cooled down by simple cooling fans. Therefore no cooling water required.

Table 22: Comparison of energy consumption by the batch Rayonet reactor and continuous flow multi-capillary system

Entry	Appliance	Energy consumption, [kW/h]	Operation time, [h][a]	Total energy consumption, [kW][b]	
1	Rayonet reactor	0.179	737.9	132	
2	2 fluor. lamps	0.046	1475.9	67.9	93
	2 cooling fans	0.009		13.3	
	Syringe pump	0.008		11.8	

[a] Operation time to produce 1 kg of product; [b] total energy consumption to produce 1 kg of product

5.3.2.4 Effect of the sensitizer on the photoinduced addition of isopropanol to 2(5*H*)-furanone 84a

So far, the photoinduced addition of isopropanol to 2(5*H*)-furanones was investigated mainly with the sensitizer 4,4′-dimethoxybenzophenone and acetone. However, the number of available aromatic ketones that could be utilised for the generation of ketyl radicals from secondary alcohols in photoaddition reactions is much larger (Table 23).

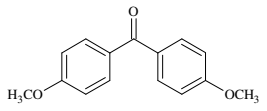
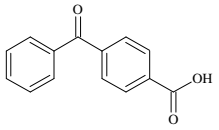
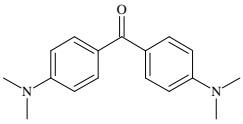
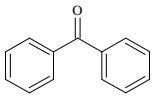
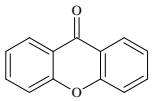
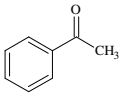
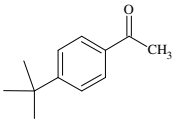
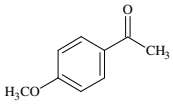
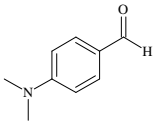
During our experimental work, it was observed that at prolonged residence time, DMBP frequently underwent photopinacolisation and photoreduction processes. Also DMBP had to be removed from the final product by column chromatography. Therefore, it was relevant to check other alternative sensitizers.

For example, as shown in our previous experience, 4-Benzoylbenzoic acid could be easily removed from the final product via extraction into water. However, attempts to isolate pure product **86a** in the corresponding experiment wasn't successful because product **86a** was also partially soluble in water and consequently isolated yields were quite low, just 16% (*exp. 139*).

Thus, in the next *experiment 138*, the photoinduced addition of isopropanol to unsubstituted 2(5*H*)-furanone **84a** was studied in the multi-capillary reactor with nine different sensitizers and without sensitizer at a residence time of 5 min. The concentration of the sensitizers was kept constant at 6.67 mmol/L. As can be seen from the results in *experiment 138* (Table 23), the initially selected sensitizer 4,4′-dimethoxybenzophenone gave the best conversion rate of 72%.

The test run without any sensitizer showed that unsubstituted 2(5*H*)-furanone **84a** was stable under the applied experimental conditions and did not undergo any side transformations.

Table 23: Effect of the sensitizer on the photoinduced addition of isopropanol to 2(5*H*)-furanone **84a**

Entry	Sensitizer		Triplet energy, [kcal mol^{-1}]	Conversion 86a, [%][a]
1	4,4′-Dimethoxy benzophenone		69.4[d]	72
2	4-Benzoylbenzoic acid		68.3[e]	37
3	4,4′-Bis(dimethylamino) benzophenone		62.0[e]	n.r.[c]
4	Benzophenone		69.2[e]	30
5	Xanthone		74.1[e]	47
6	Acetophenone		74.0[e]	4
7	4′-*tert*-Butylacetophenone		72.1[d]	n.r.
8	4′-Methoxyacetophenone		70.1[d]	n.r.
9	4-(Dimethylamino) benzaldehyde		70.0[e]	n.r.
10	n.s.[b]	–	–	n.r.

[a] Determined by ^{1}H-NMR spectroscopy; [b] no sensitizer; [c] no reaction; [d] ref. [26]; [e] ref. [207]

5.3.2.5 Effect of the sensitizer concentration on the photoinduced addition of isopropanol to 2(5*H*)-furanone 84a

All of the above experiments were performed at a constant concentration of sensitizer of 6.67 mmol/L. To see the influence of DMBP concentration on the reaction efficiency in *experiment 140* the concentration of sensitizer was increased from 1 mM to 14 mM. This study was carried out in the multi-capillary reactor at a fixed residence time of 5

min. Results obtained in *experiment 140* are summarised in Table 24 and presented in Figure 42.

As can be seen from Figure 42, the conversion of 2(5*H*)-furanone **84a** increased simultaneously with the increase of DMBP concentration until the point of 10 mmol/L was reached (Table 24, entries 1–10). At DMBP concentrations higher than 10 mmol/L the conversion of 2(5*H*)-furanone **84a** stopped increasing and dropped down to a rate of 71–73% and remained steady at that point (Table 24, entries 11-14).

It should be noted, that at DMBP concentrations higher than 10 mmol/L experimental solutions were not absolutely transparent and backward crystallisation of DMBP was observed inside of the syringes after 5-10 min of operation time. At concentrations of DMBP higher than the typical concentration of 6.67 mM, experimental solutions were transparent, but prolonged sonication and mixing for 30 min was required.

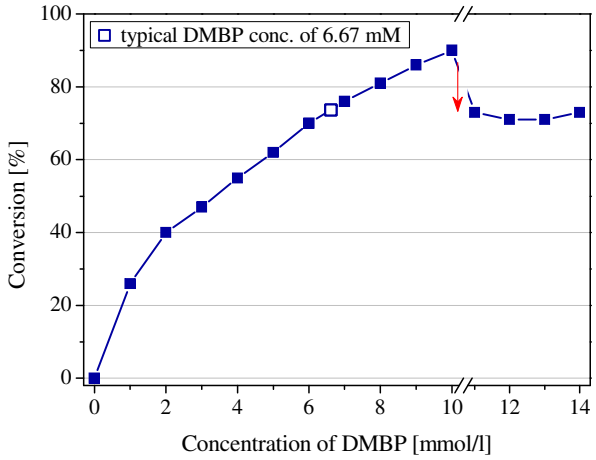


Figure 42: Conversion of furanone **84a** vs. DMBP concentration in m-CR

Table 24: Effect of DMBP concentration on the conversion of furanone **84a**

Entry	DMBP, [mmol/L]	Conversion 86a, [%][a]	Entry	DMBP, [mmol/L]	Conversion 86a, [%][a]
1	1	26	8	8	81
2	2	40	9	9	86
3	3	47	10	10	90
4	4	55	11	11	73
5	5	62	12	12	71
6	6	70	13	13	71
7	7	76	14	14	73

[a] Determined by ^{1}H-NMR spectroscopy

Based on the above reported results and observations it could be concluded that the previously used concentration of DMBP of 6.67 mmol/L is optimal, but a DMBP concentration of 10.0 mmol/L is the most efficient and maximum acceptable concentration.

5.3.2.6 Effect of the concentration of 2(5*H*)-furanone 84a on the reaction efficiency

The last parameter that was explored in the multi-capillary reactor was the concentration of the starting material 2(5*H*)-furanone **84a**. This investigation was done in *experiments 141-143*. The concentration of furanone **84a** was gradually increased from 33.3 mmol/L to 200 mmol/L, the concentration of DMBP was kept constant at 6.67 mmol/L (*exp. 141*), 8.33 mmol/L (*exp. 142*) and 10.0 mmol/L (*exp. 143*), respectively. Experimental residence times were fixed at 5 min.

Results obtained from these experiments show that with the increase of furanone concentration the reaction conversion proportionally decreased (Figure 43, Table 25). The concentration of DMBP didn't have any noticeable influence on the percentage of conversion.

In general, it is feasible to work with higher solution concentrations in the multi-capillary reactor. However, to obtain improved conversion rates the residence time must be increased beyond 5 minutes.

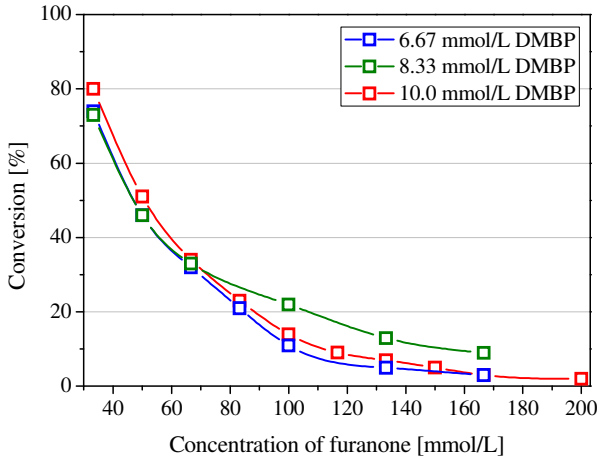


Figure 43: Conversion of furanone **84a** vs. its concentration in the multi-microcapillary reactor

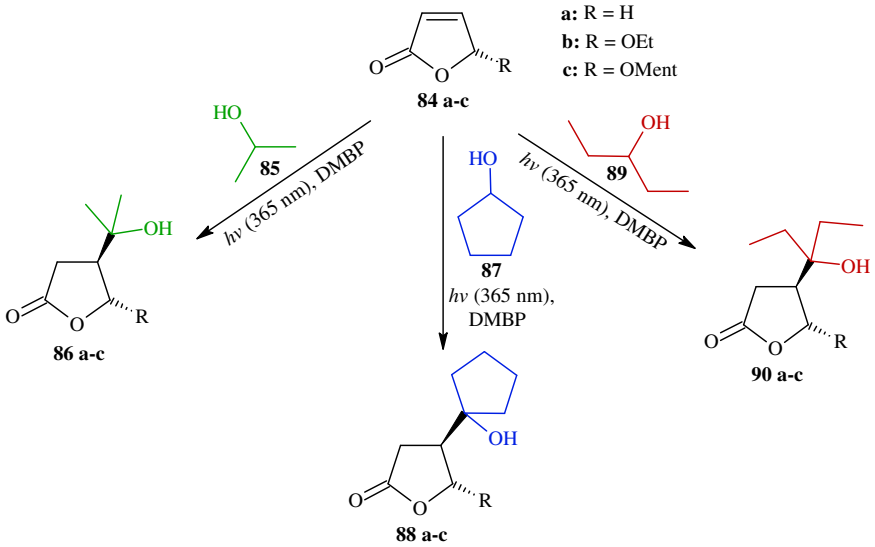
Table 25: Effect of furanone **84a** and DMBP concentrations on the conversion rate of reaction

Entry	84a, [mmol/L]	Conversion 86a, [%][a]		
		DMBP, [6.67 mmol/L]	DMBP, [8.33 mmol/L]	DMBP, [10.0 mmol/L]
1	33.3	74	73	80
2	50.0	46	46	51
3	66.7	32	33	34
4	83.3	21	–[b]	23
5	100.0	11	22	14
6	116.7	–[b]	–[b]	9
7	133.3	5	13	7
8	150.0	–[b]	–[b]	5
9	166.7	3	9	3
10	200.0	–[b]	–[b]	2

[a] Determined by ^{1}H-NMR spectroscopy; [b] not determined

5.3.2.7 Synthesis of small compound library

In *experiment 144* the synthesis of a small compound library was attempted. The same experimental procedure that was used for the photoaddition of isopropanol to furanones **84a-c** was applied for the photoaddition of cyclopentanol and 3-pentanol (Scheme 51).

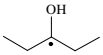
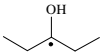
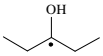


Scheme 51: Synthesis of 4-dihydrofuranone derivatives via DMBP sensitized photoaddition of secondary alcohols to furanones

Experimental residence time was preset to 10 min for isopropanol, and 20 min for cyclopentanol and 3-pentanol to make sure that conversion of the starting material was complete. At the end of the experiment all collected samples were purified and the desired products were isolated in good to excellent yields (Table 26).

The batch synthesis of products **86a-c**, **88c** and **90c** have been reported already in the literature.[191] However, the isolated products **88a,b** and **90a,b** are new compounds and their characteristic ^{1}H-NMR spectra are presented below (Figures 44–47). All proton peaks are appropriately labelled and described in more details in the experimental part of this chapter.

Table 26: Additions of photochemically generated radicals of secondary alcohols to furanones

Entry	Initial furanone	Alcohol radical	Residence time, [min]	Product	Isolated yield, [%][a]	^{13}C-NMR, [ppm],[b] C-OH
1	**84a**		10	**86a**	94	69.77
2	**84b**		10	**86b**	60	69.92
3	**84c**		10	**86c**	90	70.11
4	**84a**		20	**88a**	71	81.55
5	**84b**		20	**88b**	73	81.63
6	**84c**		20	**88c**	89	81.83
7	**84a**		20	**90a**	80	73.58
8	**84b**		20	**90b**	57	74.06
9	**84c**		20	**90c**	61	74.23

[a] Yield isolated after column chromatography; [b] in $CDCl_3$

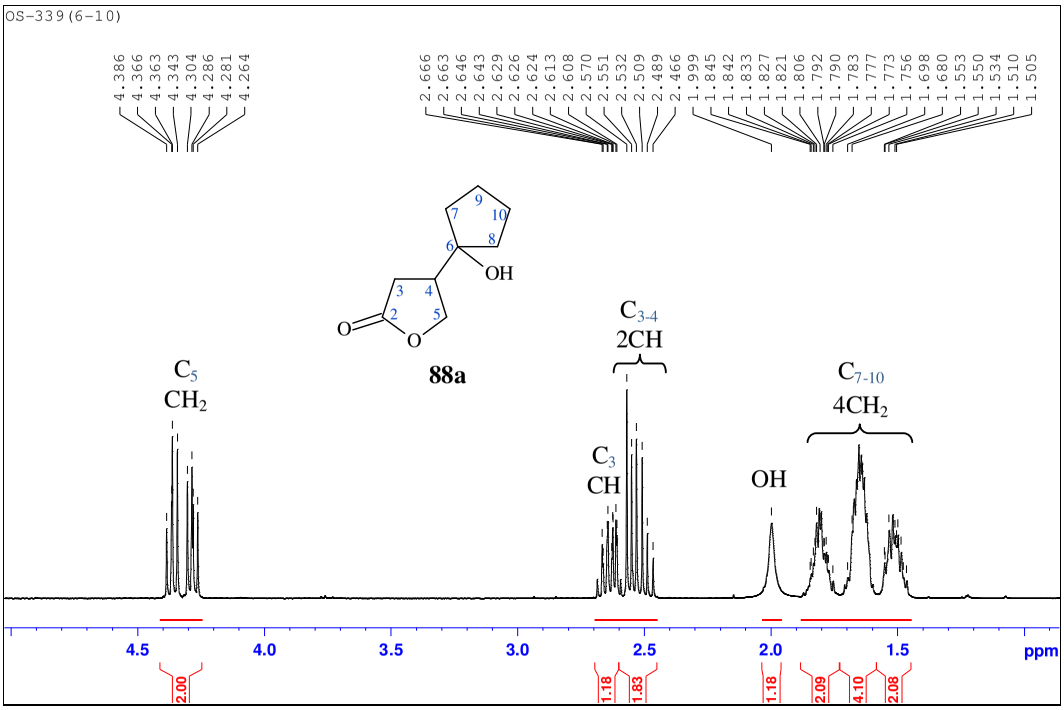


Figure 44: ^{1}H-NMR spectrum of **88a** in $CDCl_3$

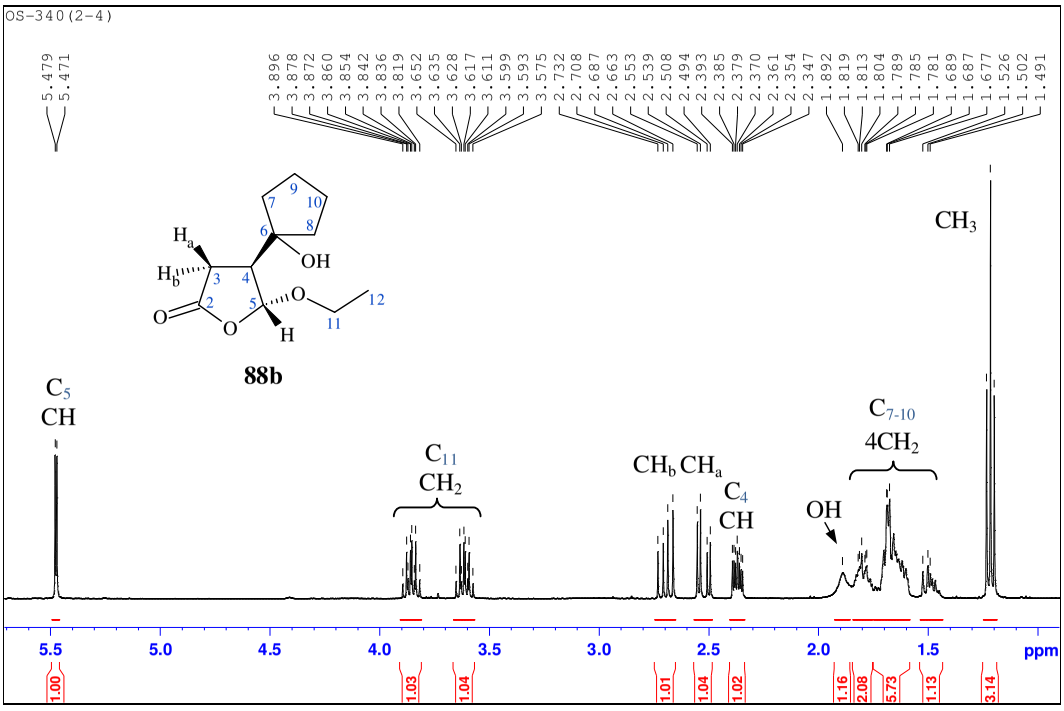


Figure 45: ^{1}H-NMR spectrum of **88b** in $CDCl_3$

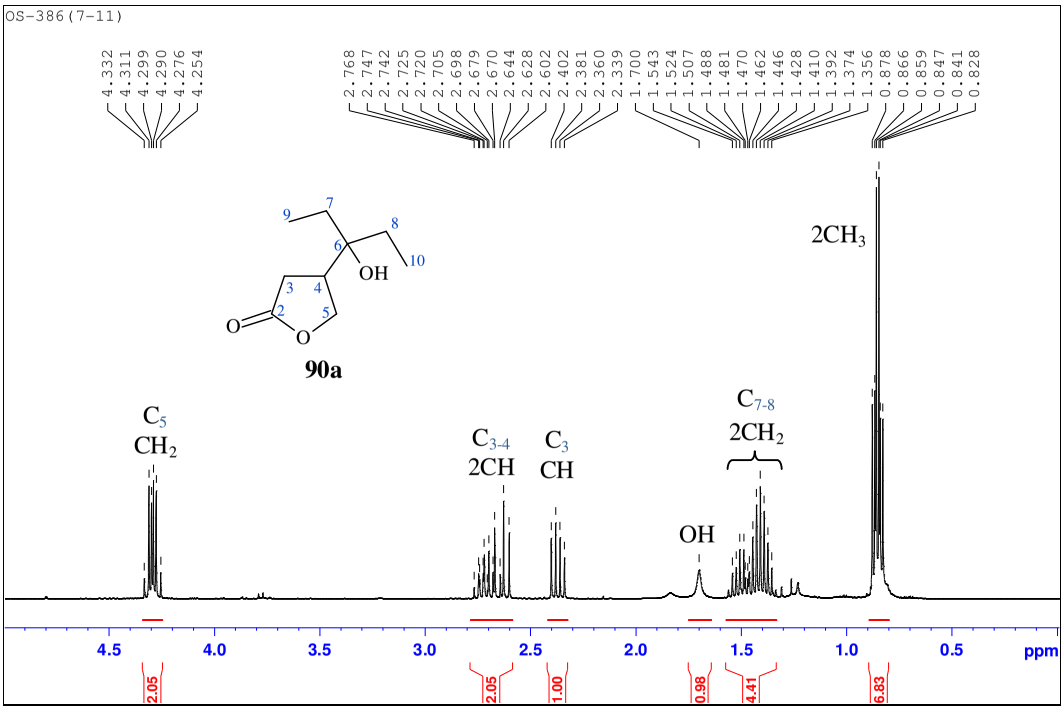


Figure 46: ^{1}H-NMR spectrum of **90a** in $CDCl_3$

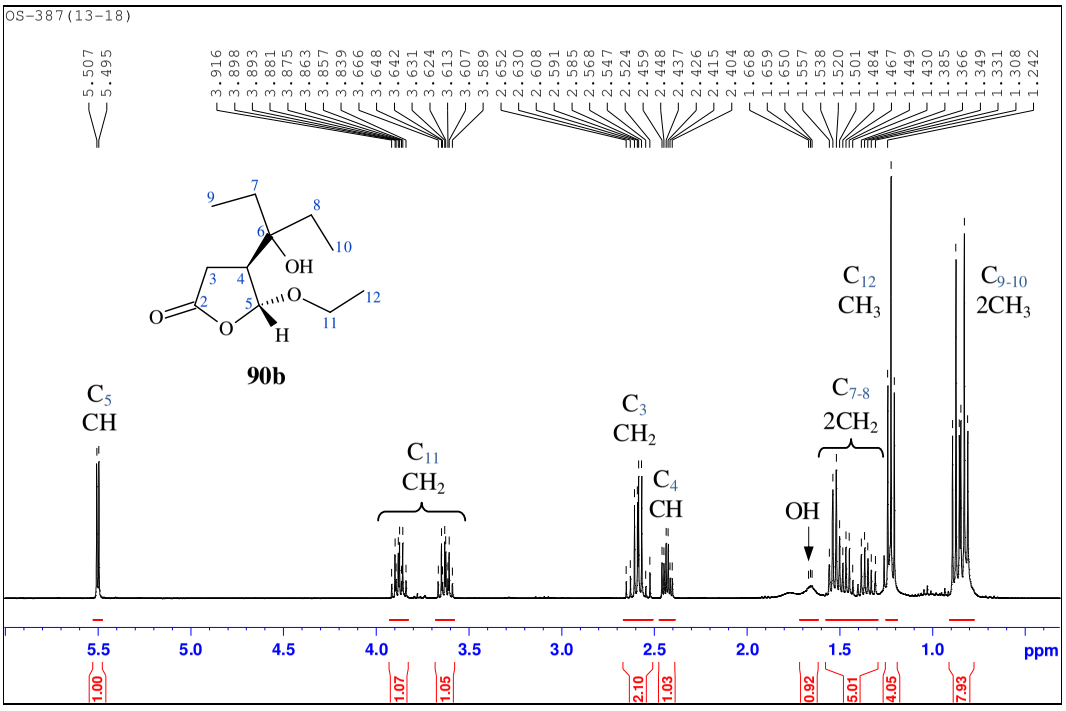
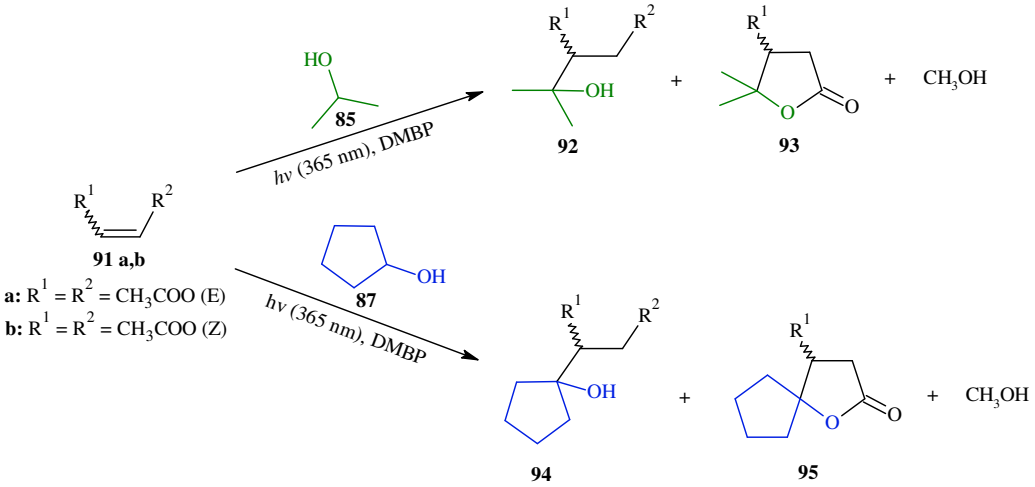


Figure 47: ^{1}H-NMR spectrum of **90b** in $CDCl_3$

On the final stage of our experimental study with the multi-capillary reactor, the procedure that was established for furanones was transferred to other α,β-unsaturated esters. In *experiments 145-146* photoinduced additions of isopropanol and cyclopentanol to dimethyl fumarate and dimethyl maleate were carried out (Scheme 52). In contrast to 2(5*H*)-furanones **84a-c**, reactions with dimethyl fumarate and dimethyl maleate proceeded in a less selective and slower rate. In all cases two main products were observed. Also prolonged residence times of 15 min or 1 hour were needed for reaction completion.



Scheme 52: Synthesis of methyl ester of terebic acid and spiro compound via DMBP sensitized photoaddition of secondary alcohols to E/Z dimethyl esters of butenedioic acid

The photoinduced addition of isopropanol to dimethyl fumarate **91a** and to dimethyl maleate **91b** proceeded very slowly compared to the above reported transformations. After irradiation of 15 min (*exp. 145*), only 21% and 27% of conversion were determined and mainly lactone **93** was formed (Table 27, entry 1 and 2). Unexpectedly, in the ^{1}H-NMR spectrum of the crude product obtained in the experiment with dimethyl fumarate, representative peaks of dimethyl maleate were also found. This result indicates that DMBP also sensitized the isomerisation of dimethyl fumarate to dimethyl maleate. This finding was later proved by the independent *experiment 147* where the equilibrium mixture of dimethyl fumarate and dimethyl maleate was irradiated in the presence of DMBP for 40 min. After irradiation, 95% of dimethyl maleate and only 5% of dimethyl fumarate were found in the mixture.

When the irradiation time of the photoaddition reactions was extended to 1 hour (*exp. 146*), complete conversions were reached in both cases. The collected crude products

were purified by column chromatography. In the case of dimethyl fumarate **91a**, two main fractions were collected. One fraction was the mixture of products **92** and **93** in a ratio of 9:1 and the second fraction was pure lactone **93**. Isolated yield of the pure lactone **93** was only 12%. In the case of dimethyl maleate **91b**, after column chromatography one main fraction was collected and it was the mixture of products **92** and **93** in ratio 4:1 (Table 27, entry 3 and 4, respectively). It is important to note that under such experimental conditions, the sensitizer DMBP remained unchanged at irradiation of 15 min, but after 1 hour DMBP was almost completely converted to its photoreduction product, which complicated the purification process.

The selective formation of lactone **93** could be achieved in the presence of an additional organic acid catalyst. For example, a 10 mg of *p*-toluenesulfonic acid induced selective formation of lactone **93** in the DMBP sensitised addition of isopropanol to dimethyl fumarate **91a** (*experiment 148*). However, the presence of acid introduced additional steps to the purification process.

The photoinduced addition of cyclopentanol to dimethyl fumarate **91a** and to dimethyl maleate **91b** progressed well and reactions were completed after 15 min (*exp. 145*). The collected crude products were also purified by column chromatography. In case of dimethyl fumarate **91a**, two main fractions were isolated. One fraction was the mixture of products **94** and **95** in ratio 3:1 and the second fraction was pure spiro compound **95**. Isolated yield of pure **95** was only 3%. In case of dimethyl maleate **91b**, after column chromatography two fractions were collected. One fraction was the mixture of products **94** and **95** in a ratio of 3:2 and the second fraction was pure spiro compound **95**. Isolated yield of pure **95** was 15%. In the experiments with cyclopentanol, the applied sensitizer DMBP did not undergo any secondary reactions and was recovered in 98% and 89% (Table 27, entry 5 and 6, respectively).

Table 27: Additions of photochemically generated radicals of secondary alcohols to dimethyl fumarate and dimethyl maleate

Entry	Initial ester	Alcohol radical	Residence time, [min]	Conversion, [%][a]	Product composition	Recovered DMBP, [%]
1	**91a**		15	21	**92:93** 1:4[b]	–[d]
2	**91b**		15	27	**92:93** 1:3[b]	–[d]
3	**91a**		60	100	**92:93** 9:1[c]	–[e]
4	**91b**		60	100	**92:93** 4:1[c]	–[e]
5	**91a**		15	100	**94:95** 3:1[c]	98
6	**91b**		15	100	**94:95** 3:2[c]	89

[a] Determined by ^{1}H-NMR spectroscopy; [b] determined by ^{1}H-NMR spectroscopy of the crude product mixture; [c] determined by ^{1}H-NMR spectroscopy of the purified product; [d] not determined; [e] DMBP was almost completely converted to its' dimer

The most interesting compound synthesised in the last experiments was the spiro compound **95**. This is a new compound and its' representative ^{1}H-NMR and ^{13}C-NMR spectra are presented in Figures 48 and 49. All proton and carbon peaks are appropriately labelled and described in more details in the experimental part.

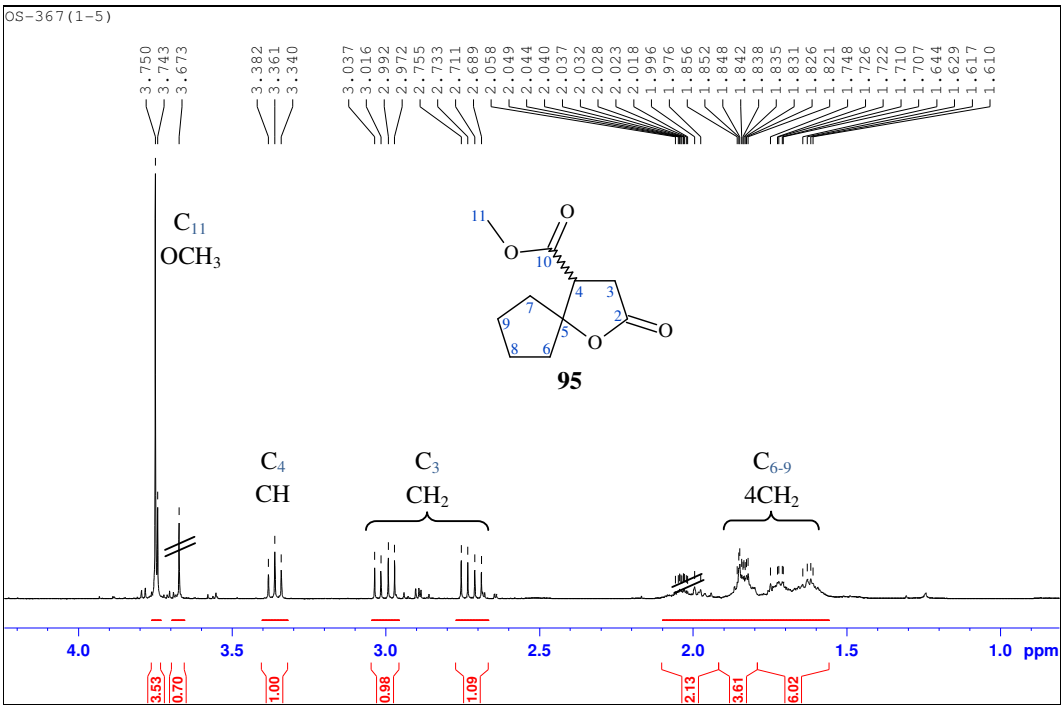


Figure 48: ^{1}H-NMR spectrum of **95** in $CDCl_3$

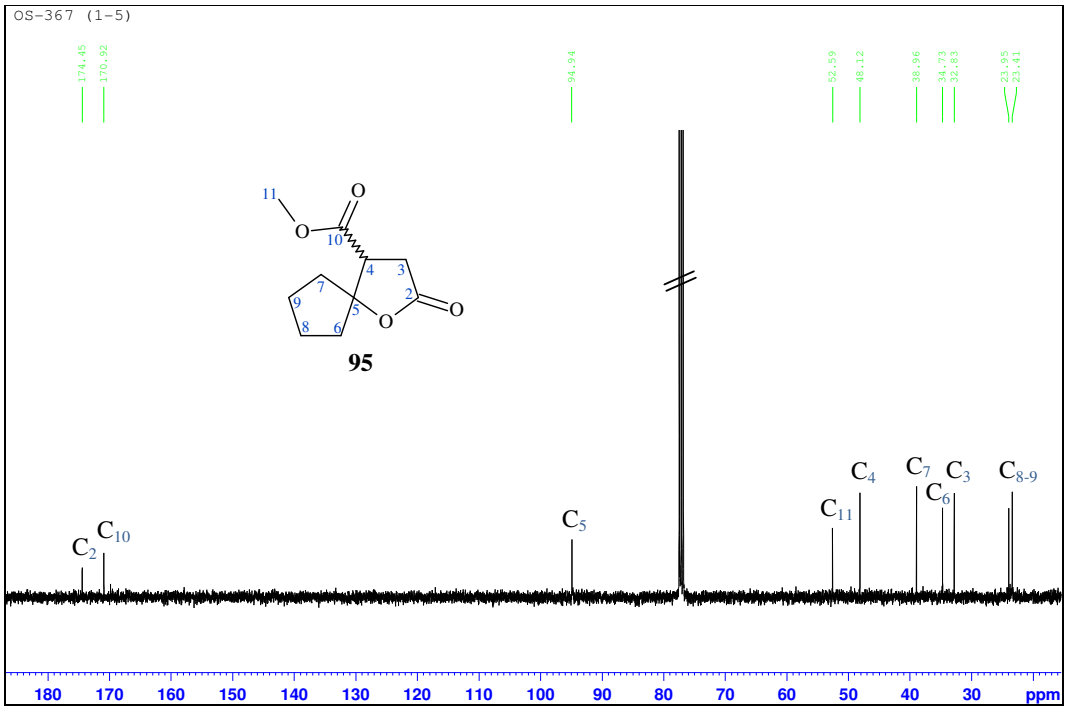


Figure 49: ^{13}C-NMR spectrum of **95** in $CDCl_3$

5.4 Discussions

5.4.1 Photosensitized addition of secondary alcohols to α,β-unsaturated esters

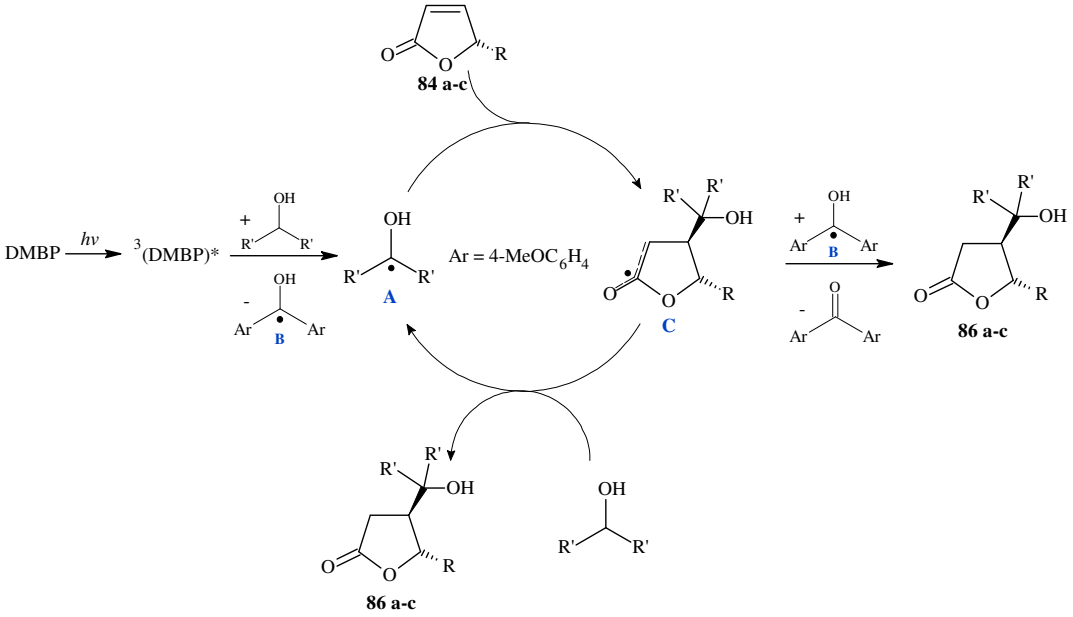
5.4.1.1 Photosensitized addition of secondary alcohols to furanones

Additions of photochemically generated radicals of secondary alcohols to furanones are an example of alkylation reactions that proceeded reasonably fast and gave good chemical yields.

The mechanistic scenario of the 4,4'-dimethoxybenzophenone sensitized additions of secondary alcohols to furanones is depicted in Scheme 53.[191] Hydrogen abstraction plays a key role in these transformations and initiates two feasible radical pathways: chain and non-chain. The reaction begins from hydrogen abstraction by the triplet excited DMBP, which generates the corresponding ketyl radicals **A** and **B**, respectively.[26,187,208] Regio- and diastereoselective addition of **A** to furanone furnishes the stabilized oxoallyl radical **C**. Hydrogen abstraction from a second alcohol molecule leads to the final product **86a–c**. The concomitantly generated ketyl radical **A** again adds to the furanone **84a–c** thus completing the radical chain process. Alternatively, hydrogen back-transfer from **B** yields the isolated products **86a–c**.[209,210] The competitive product resulting from the addition of radicals **B** to **84a–c** could not be detected in the crude product mixture. This side-reaction is often observed during

sensitization with acetone in the presence of other alcohols.[191] Upon exhaustive irradiation, DMBP is slowly consumed through photoreduction and photo pinacolisation processes.[187]

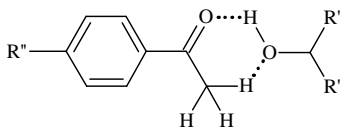
2(5H)-Furanone **84a** as a substrate in itself is not a chiral molecule, but the presence of alkoxy substituent at the C_5 of the ring (**84b** and **84c**) introduces a stereogenic centre into the molecule which can effect a stereoselective addition of the nucleophile radical to the double bond. The presence of the bulky substituent at C_5 can affect efficient π-face shielding of the rigid and near planar furanone ring and can force the radical to approach the double bond from the opposite and less hindered side. Such nucleophilic attack results, in most cases, in a stereospecific addition, giving only a *trans* 4,5-disubstituted furanone.[211,212]



Scheme 53: Mechanistic scenario for DMBP sensitized addition of secondary alcohols to furanones **84a-c**

A study that was carried out in *experiment 138* showed that among nine chosen sensitizers 4,4'-dimethoxybenzophenone had the best sensitisation effect on the photoaddition of isopropanol to 2(5H)-furanone **84a** (Table 23). The different reactivity of other benzophenone derived sensitizers (Table 23, entries 1-5) could be explained by the different steric and entropic effects of the substituents.[213] The absence of a sensitisation effect of 4,4′-Bis(dimethylamino)benzophenone (Michler's ketone) could be the consequence of its lowest triplet energy and poor solubility in isopropanol compared to other sensitizers. The acetophenone and its derivatives (Table 23, entries 6-

9) also showed very low or no influence on the photoaddition reaction. Such effect could be explained by the intermolecular forces and formation of intermolecular hydrogen bonds between sensitizer and alcohol molecules (Scheme 54).[214]



Scheme 54: The formation of intermolecular hydrogen bonds between the molecules of acetophenone derivatives and alcohol molecules

5.4.1.2 Photosensitized addition of secondary alcohols to E/Z dimethyl esters of butenedioic acid

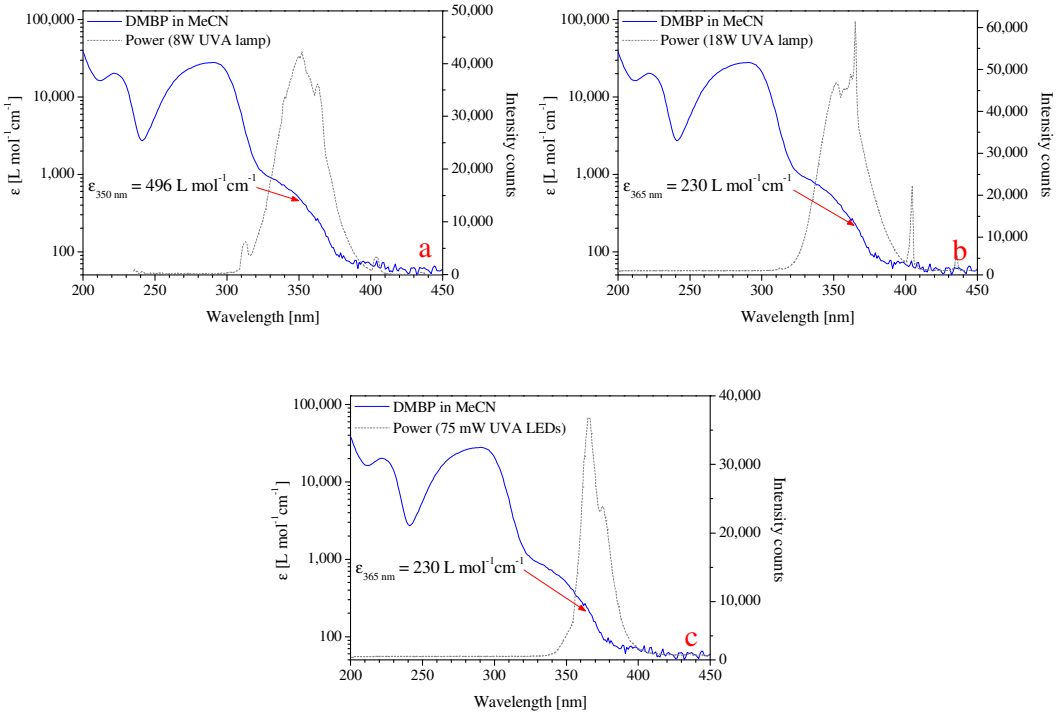
The 4,4'-dimethoxybenzophenone sensitized additions of secondary alcohols to dimethyl fumarate **91a** and to dimethyl maleate **91b** proceeded via a mechanistic scenario similar to that for furanones. The difference is that reactions didn't stop after the formation of photoaddition products **92** and **94**. The generated photoadducts **92** and **94** randomly underwent further intramolecular condensation and resulted in the formation of lactones **93** and **95**. The cyclisation process is accompanied by the elimination of a methanol molecule from the R_2 moiety of **92** and **94**.

5.4.2 Wavelength matching and light penetration for experiments involving furanones and E/Z dimethyl esters of butenedioic acid

The DMBP sensitized addition of isopropanol to furanones **84a-c** was tested in five experimental setups of different scales. In the batch Rayonet reactor and in four continuous flow systems: dwell device, dual-capillary and multi-capillary microreactors and LED-driven microchip. Three of these systems were operated with an appropriate number of identical UVA fluorescent tube lamps (λ_{max} = 350±25 nm) that had optical power of 8W each. Multi-capillary reactor was equipped with the similar UVA fluorescent tube lamps (λ_{max} = 365±25 nm) that had optical power of 18W each. The only system that was run with another light source was microchip. It was operated with an array of high power UV-LEDs (λ_{max} = 365 ± 5 nm, 6 × 75 mW).

The emission spectra of all light sources – both UVA lamps and LEDs were recorded and showed a good overlap with the n→π* absorption band of DMBP (Figures 50). The UVA lamp(s) with maximum emission at 350 nm showed a slightly better match (Figure 50a). The glass types of the reactors and the PTFE and FEP capillaries used

moreover provided the complete passage of UVA irradiation into the reaction media without any filter effects.



Figures 50: UV-spectrum of DMBP matched with the emission spectrum of: a) UVA fluorescence lamp (8W), b) UVA fluorescence lamp (18W), c) array of high power UV-LEDs (6 × 75 mW)

Based on the absorption of DMBP the penetration profiles of light were calculated at 350 nm and 365 nm and compared to the inner diameters of the Pyrex test tube, PTFE and FEP capillaries and microreactors channel depths (Figure 51). The microchip (150 µm) showed the best transmission of light at the given concentration of DMBP (6.67 mM), followed by the dwell device (500 µm), the PTFE microcapillary (558 µm) and the FEP microcapillary (800 µm). The batch irradiation was conducted in a Pyrex test tube (inner diameter 9 mm) with effective pathlength of 4.5 mm due to the circular arrangement of the lamps. Thus, complete penetration of light was achieved for the batch experiment although transmission was lowest.

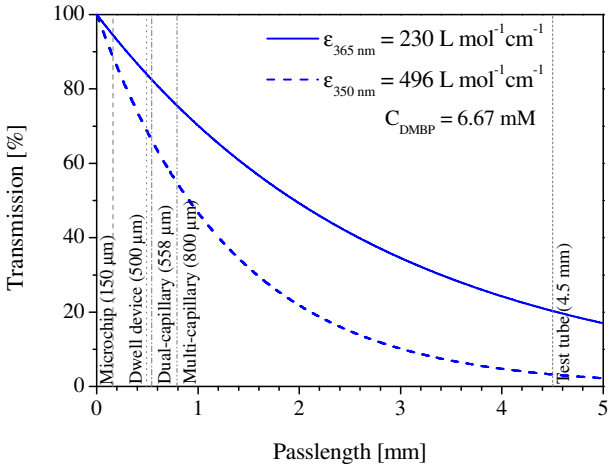


Figure 51: Light-penetration profiles for a 6.67 mM solution of DMBP at 350 and 365 nm. The vertical lines represent the pathlength of the microchip (--), the dwell device (···), the PTFE microcapillary (-·), the FEP microcapillary (-··) and the test tube (--)

Results obtained within the investigation of the dependency between DMBP concentration and reaction efficiency (*exp. 140*) showed that concentration of DMBP has a noticeable influence on the reaction efficiency. However the possibility to work with higher concentrations was limited by the solubility of sensitizer in isopropanol.

As can be seen from the graphs on Figure 52, the shallow depth or internal diameter of microchannels of continuous flow systems provided sufficient light penetration through the entire solution media even at the highest applied concentration of DMBP of 14 mM. Thus, it could be concluded that the main limitation factor of the work with high solution concentrations is the solubility of reagents in the appropriate solvent.

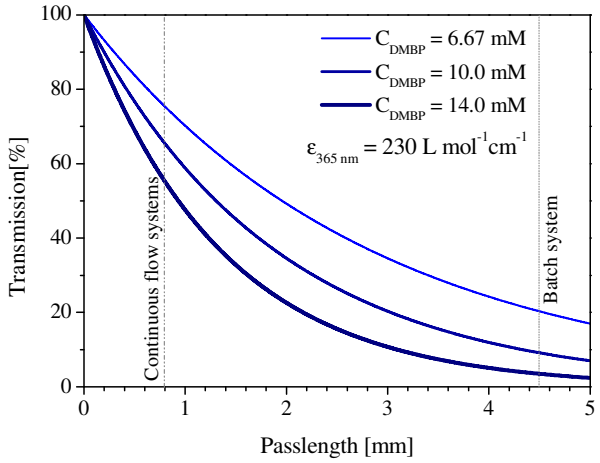


Figure 52: Light-penetration profiles for a 6.67 mM, 10.0 mM and 14.0 mM solutions of DMBP at 365 nm. The vertical lines represent the maximum pathlength of the continuous flow systems (-··) and batch system (--)

5.4.3 Irradiated area-to-volume ratio of experimental photoreactors

The microstructured reaction vessels in addition to the superior light penetration have also much larger irradiated area-to-volume (surface-to-volume) ratio compared to the conventional test tube (Figure 53). Thus the smallest microchip channel provides the largest irradiated area-to-volume ratio of 8735 m^2 m^{-3}, with a similar number for the dual-microcapillary reactor of 7169 m^2 m^{-3}. The multi-microcapillary reactor has an adequate value of 5000 m^2 m^{-3} (single capillary). The irradiated surface-to-volume ratio of the dwell device of 1369 m^2 m^{-3} is six times smaller compared to that of the microchip. A typical Rayonet test tube gives a ratio of 466 m^2 m^{-3} only.

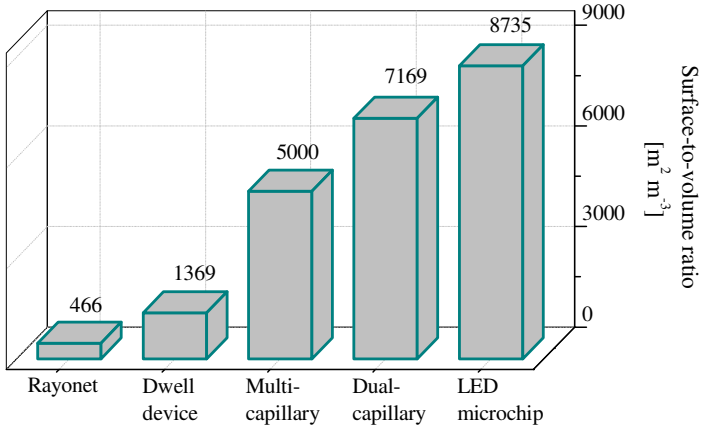


Figure 53: Surface-to-volume ratio of experimental photoreactors

The superior light penetration and huge irradiated surface-to-volume ratio of the microchip channel can partially explain the highest efficiency of furanones involved on photoaddition reactions in this setup. Hence the high or complete conversions of initial furanones **84a–c** were achieved after residence times of just 2.5 min (Table 19).

The evaluated photoreactor systems differed significantly and for a better understanding of the dependency between reaction performance and system design the key technical parameters for all setups are summarised in the Table 28. As can be seen from this table, the in-house made dual- and multi-capillary microreactors have the best parameters for the reaction vessel and irradiated area.

In addition to the different geometries of the reaction vessels, the applied photoreactors also varied in the power and type of light sources used. Assuming an even distribution of light, the lamp power-to-irradiated area ratios were established (Table 28). The large Rayonet chamber reactor with its 16 lamps naturally gave the highest value of 1.85 W

cm^{-2}. The lowest ratio of 0.029 W cm^{-2} was determined for the multi-microcapillary reactor and this is a result of using low power fluorescent lamps (18 W each). For the same reason a low ratio of 0.1 W cm^{-2} was found for the dual-capillary reactor. The microchip provided a value of 0.39 W cm^{-2} due to the low power of the LEDs in comparison with the UVA tubes (75 mW vs. 8 W). The dwell device gave a value of 1.74 W cm^{-2} that was similar to the batch setup. However, the chosen Luzchem irradiation panel with its emissive area of approximately 18 × 30 cm is about 6-times larger than the aperture of the dwell microreactor thus leaving a large unused irradiated area.

Table 28: Technical details of the experimental photoreactors

Parameter	Rayonet	Dwell device	Microchip	Dual-capillary	Multi-capillary
Aperture, [cm^2]	69.24[a]	86.14[b]	3.31[b]	285.74[c]	772.44[c] 1544.88[d]
Reaction vessel, [cm]	0.9 × 24.5 ID × H	0.2 × 0.05 × 115 W × D × L	0.015 × 0.015 × 75.7 W × D × L	0.056 × 460 ID × L	0.08 × 1000 ID × L
Irradiated area, [cm^2]	69.24	23.0[e]	1.14[e]	40.3[f,g] 80.6[f,h]	125.6[f,g] 628.0[f,i] 1256.0[f,j]
Irradiated volume, [cm^3]	15	1.68	0.013	1.12[g] 2.24[h]	5[g] 50[j]
Irradiated area / volume ratio, [m^2 m^{-3}]	466	1369	8735	7169	5000
Lamp power, [W]	16 × 8	5 × 8	6 × 0.075	1 × 8	2 × 18
Lamp power per aperture, [W cm^{-2}]	1.85	0.46	0.14	0.03	0.023[d]
Lamp power per irradiated area, [W cm^{-2}]	1.85	1.74	0.39	0.1	0.029[j]

[a] Assuming a cylindrical geometry, the liquid height in a 15 ml Pyrex test tube was 24.5 cm; [b] optical window; [c] glass cylinder; [d] two glass cylinders; [e] micro channel; [f] assuming that half of the capillary's surface is irradiated; [g] single capillary; [h] two capillaries; [i] one tower; [j] two towers

5.4.4 Energy efficiencies of the used light sources in the chosen experimental setups

The efficiency of irradiated energy in the utilised experimental setups could also be discussed with respect to calculated values of furanone conversions (yields) per light source power within an irradiation time (% W^{-1} h^{-1}) and conversions (yields) per light source power within irradiation time and irradiated area (% W^{-1} h^{-1} cm^{-2}).[38] The results of such estimations are presented in Table 29. Experiments with incomplete conversions (1 min or 5 min) were chosen to obtain values free of contributions from 'over-

irradiation'. Exhaustive irradiation may cause slow consumption of DMBP through photoreduction and photopinacolization processes.[187] The results clearly show that the energy efficiency of the LED-driven microchip is by far largest compared to the other systems. However, the main negative aspect of the microchip design is the long experimental time required to transfer the total volume of reaction mixture and 'wash-out' solvent (about 1.2 ml) through the microchannel with a holdup volume of just 13 µl. As an example, at a residence time of just 1 min the overall experimental time was 92 min. The energy efficiencies for the dual-capillary and multi-capillary reactors dropped significantly when the irradiated areas were taken into account. Nevertheless, the dual-capillary reactor gave better results than the technically more advanced dwell device.

In general, all continuous flow systems have noticeably better energy efficiencies compared to the batch set-up. The simple handling and reasonably short operation time of an in-house made multi-microcapillary reactor make it more practical compared to the commercial reactors with fixed parameters.

Table 29: Energy efficiency of chosen experimental setups

			Energy efficiencies					
			[% W^{-1} h^{-1}][b]			[% W^{-1} h^{-1} cm^{-2}][c]		
Reactor	**Time, [min]**	**W h[a]**	**84a**	**84b**	**84c**	**84a**	**84b**	**84c**
Rayonet	5	10.67	8.44	8.44	8.15	0.12	0.12	0.11
Dwell device	5 (42[d])	3.33	24.32	29.73	29.43	1.06	1.29	1.28
Microchip	1 (92[d])	0.0075	7733	8000	7867	6783	7018	6901
Dual-capillary[e]	5 (35[d])	0.67	111.94	143.28	147.76	2.78	3.56	3.67
Multi-capillary[e]	5 (20[d])	1.50	47.34	54.67	61.34	0.38	0.44	0.49

[a] Lamp power × irradiation time; [b] product conversion (yield) / (lamp power × irradiation time); [c] product conversion (yield) / (lamp power × irradiation time × irradiated area); [d] operation time including 'wash-out'; [e] single capillary

5.4.5 Efficiencies of reactors used in the furanone involved experiments

The effectiveness of tested experimental setups, specificly the reactors, could be further expressed in space-time-yield calculated numbers.[117] STYs are dependent on the reactor geometry and were calculated for reactions with incomplete conversions (1 min or 5 min; Table 30) using the above described equation *(2)*, where n_R is amount of **84a-c** converted within reactor volume. The microchip gave the highest STY values, whereas the dwell device, the dual-capillary and multi-

capillary reactors showed comparable STY numbers to the batch system.

Table 30: Space-time-yields of furanone involved photochemical reactions in different experimental set-ups

Reactor	Time, [min]	STY, [mmol L^{-1} min^{-1}][a]		
		84a	**84b**	**84c**
Rayonet	5	6.0	6.0	5.8
Dwell device	5	5.4	6.5	6.5
Microchip	1	19.1	19.8	19.5
Dual-capillary[b]	5	5.0	6.4	6.6
Multi-capillary[b]	5	4.7	5.5	6.1

[a] Calculated using equation 2; [b] single capillary

5.5 Summary

The outlined study of the photoinduced addition of secondary alcohols to electron deficient alkenes shows good potential for the stereoselective formation of carbon bonds via a greener pathway compared to thermal Michael additions. The established method used alcohol as both solvent and alkylating reagent and DMBP as photosensitizer.

The selected model transformations of the photoaddition of isopropanol to furanones **84a-c** have been investigated in different scale continuous flow systems and the obtained results were compared to the conventional techniques. In all cases higher or comparable conversion rates were achieved in the microflow devices. The smallest LED-driven microchip gave the best performance. The complete conversion of starting material **84b** and **84c** to the desired products **86b** and **86c**, respectively, have been recorded after just 2.5 min. Consequently, the LED-driven microchip has been considered as the most balanced system regarding the correlation of light source power to the size of irradiated area. Also, with respect to the small internal volume, the LED-driven microchip can serve as an advanced tool for the screening of small amounts of chemicals (leads in drug discovery). However, for the synthesis of lead compounds on the preparative scale other devices need to be used and the in-house made multi-capillary reactor represents a perfect alternative for the relevant task. Moreover, the unique design of a multi-capillary reactor overcame the important limitation of commercially available systems, such as fixed dimensions of reaction vessel. Following the comparison of the technical parameters of all experimental set-ups it was concluded that the multi-capillary reactor has the best parameters for reaction vessel and irradiated area.

Apart from that, the newly made multi-capillary reactor has other benefits that were demonstrated within our work. It has been successfully applied for the reproducibility study of photochemical reactions, optimisation study of experimental procedures and the synthesis of a small library of 4-dihydrofuranone derivatives.

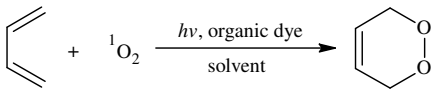
Hence, the multi-capillary reactor represents a perfect, practical tool that has adjustable technical parameters, satisfied efficiency and consequently could be represented as a new platform for future continuous-flow synthetic photochemistry. In addition, the multi-capillary reactor doesn’t require water for cooling.

Chapter 6

Rose bengal sensitised photooxygenation of α-terpinene – synthesis of ascaridole

6.1 Introduction

Photooxygenation of α-terpinene is an example of a heterogeneous dye-sensitised [4+2] cycloaddition of singlet oxygen to a diene resulting in the formation of endoperoxides (Scheme 55).[16] These reactions were developed as an efficient alternative to oxidations with metal oxides.[152,153] They simply require catalytic amounts of an organic dye as sensitizer and air as a safe and clean oxidant.[215–219] Due to the favourable absorption of most dyes within the visible spectrum photooxygenation reactions can also be performed solarchemically with sunlight and serve as an environmentally friendly model reaction.[94,220,221]



Scheme 55: General [4+2]-photooxygenation of diene to endoperoxide

Three organic dyes, namely rose bengal (λ_{max} = 548 nm in *i*-PrOH), methylene blue (λ_{max} = 648 nm in *i*-PrOH) and tetraphenylporphyrin (λ_{max} = 416 nm in *i*-PrOH) are generally used as sensitizers for photooxygenation reactions in academia and industry (Figure 54).

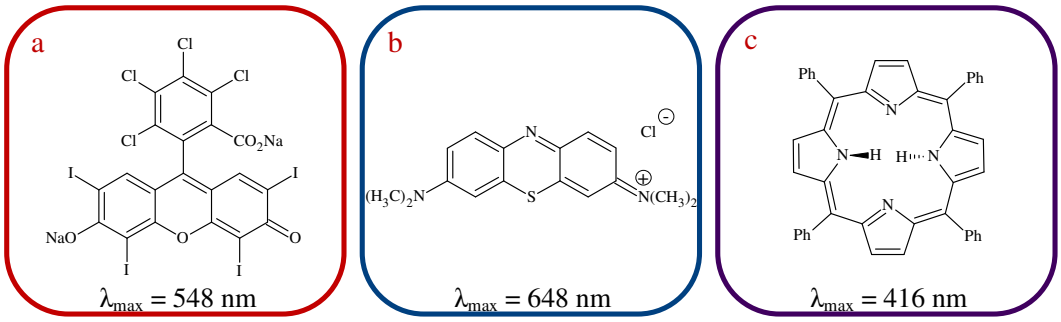


Figure 54: Sensitizers generally used for photooxygenation reactions: a) rose bengal, b) methylene blue, c) tetraphenylporphyrin

Ascaridole, the main constituent of chenopodium oil, is a natural bicyclic monoterpene that has an unusual bridging peroxide functional group.[222] Ascaridole is one of the best known anthelmintics. It also has antimalarial[223] and nematocidal[224] activities. Ascaridole derivatives are used in industry as radical initiators of polymerisation processes. Therefore, the synthesis of ascaridole has been the subject of research development in industry.[225–227]

The most common procedure of ascaridole synthesis comprises oxidation of α-terpinene by singlet oxygen. Generally, $^1O_2$ is formed photochemically (Figure 55) by irradiation

of molecular oxygen in the presence of a sensitizer (it can also be generated thermally with hydrogen peroxide[228] or ozone[229]). The generation of singlet oxygen via a photochemical pathway requires only trace amounts of organic dye and thus represents a greener process compared to the other methods where the presence of a transition metal based catalyst is a necessity. Singlet oxygen ($^1O_2$) is highly reactive with a very short lived species ($^1O_2$ lifetime in alcohols is 9.5–31 μs[230]). Its formation is literally controlled by a "flick of a switch". The atoms of molecular oxygen are completely incorporated into the product and are not wasted in the form of H_2O or CO_2. In addition, molecular oxygen is an environmentally friendly reagent due to its availability from air, low cost and negligible ecological impact.

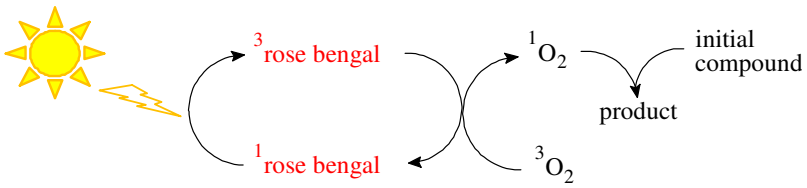
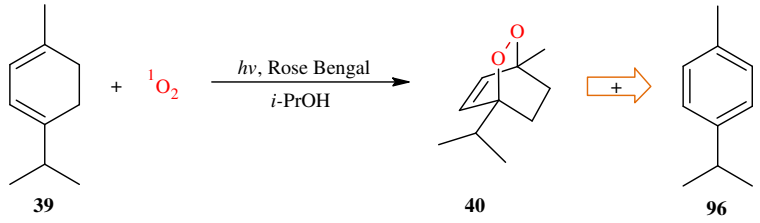


Figure 55: Simplified scheme of singlet oxygen formation via rose bengal sensitization

Up to date, photooxygenation of α-terpinene **39** to ascaridole **40** (Scheme 56) was investigated under different conditions, i.e with various sensitizers[231–233] including immobilized sensitizers,[234] with various solvents,[235,236] in continuous flow[116,118] and micro-capacitive systems.[99] However, the influence of reaction and setup parameters on product selectivity wasn't studied and discussed until now. Also the mechanism of formation of the side product *para*-cymene **96** remained unclear.



Scheme 56: Photooxygenation of α-terpinene

Para-cymene **96**, as a typical petrochemical, is a significant side product of the photooxygenation of α-terpinene. The reduction of ascaridole to *para*-cymene offers a promising route to *para*-cymene, from a renewable material.[237] However, the bulky scale production of ascaridole is limited due to the potentially explosive nature of endoperoxides and decreased photochemical efficiency with the increased concentration

of reagents. Therefore, the development of a safer, greener and industrially viable methodology is a relevant task.

To explore this assignment, a new approach for the preparation of endoperoxides in microflow systems has been established. A new experimental setup with commercially available and a continuous flow falling film microreactor has been constructed and adapted for photooxygenation of α-terpinene. In such conditions the volume of dangerous oxygenated solvent was only several microlitres and thus was simply kept under control within the operation time. Also the amount of produced endoperoxide was usually below 2.4 mmol (400 mg) after one single run.

6.2 Falling film microreactor experimental set-up

A falling film microreactor, developed by the Institut für Mikrotechnik (IMM, Mainz),[40] was specifically designed for heterogeneous model reactions (Figure 57, setup in the laboratory of Leibniz-Institut für Katalyse e.V., Rostock). The whole setup consists of several devices. The photochemical reaction takes place at the interface between liquid and gaseous components in the falling film microreactor **1**. This reactor consists of a bottom housing section with an integrated heat exchanger (microstructured cooling channels), a contact-zone mask, a top housing section with a gas chamber and the reaction plate (FFMR – 07029, 316 Ti), which has 32 parallel microchannels of 600 µm width, 200 µm depth and 78 mm length (Figure 56).

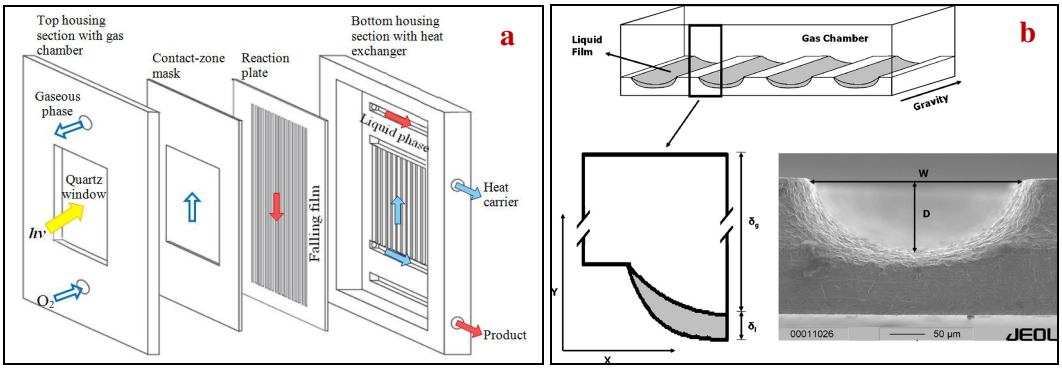


Figure 56: a) Construction of the falling film microreactor (source: IMM, Mainz[34,40]); b) Top: schematic view of the micro structured plate with the liquid volumes (grey) and the gas chamber; bottom left: enlarged view of the geometry part which is considered in the CFD model; bottom right: etched channel profile (exemplary).[238]

The reaction mixture (liquid phase) was transported to the reactor by the programmable syringe pump **3** at different flow rates. The pump was loaded by the glass syringe **4** with a PTFE plunger and total volume of 50 ml. The liquid phase was introduced into the

microreactor via a horizontal slot in the upper part of the bottom housing section and via another slit to the upper side of the reaction plate. The solution was then distributed to substreams, which enter the microchannels and flows downwards. A thin film of the liquid reactant was generated by the force of gravity. The gas phase was passed counter currently to the liquid phase through the reactor gas chamber and the chemical reaction took place at the interface between liquid and gaseous components. The gas was fed to the reactor with a constant flow rate of 10 ml/min through flow meter **8**. The reacted liquid was evacuated from the reactor by a small gear pump **5** with a slightly higher flow rate then supplied to the reactor. The gear pump flow rate was controlled via a rotameter **6**. The product was collected directly into a GC vial **7** and analysed instantly by CG-MS. The light source, domestic fluorescent lamp **2** with total optical power of 18 W, was placed in front of the falling film microreactor at a distance of 2 cm and the solution was irradiated through a Quartz window ($\lambda \geq 200$ nm). The viewing window itself is just 55 mm high and 28 mm wide thus covering parts of the reaction plate.

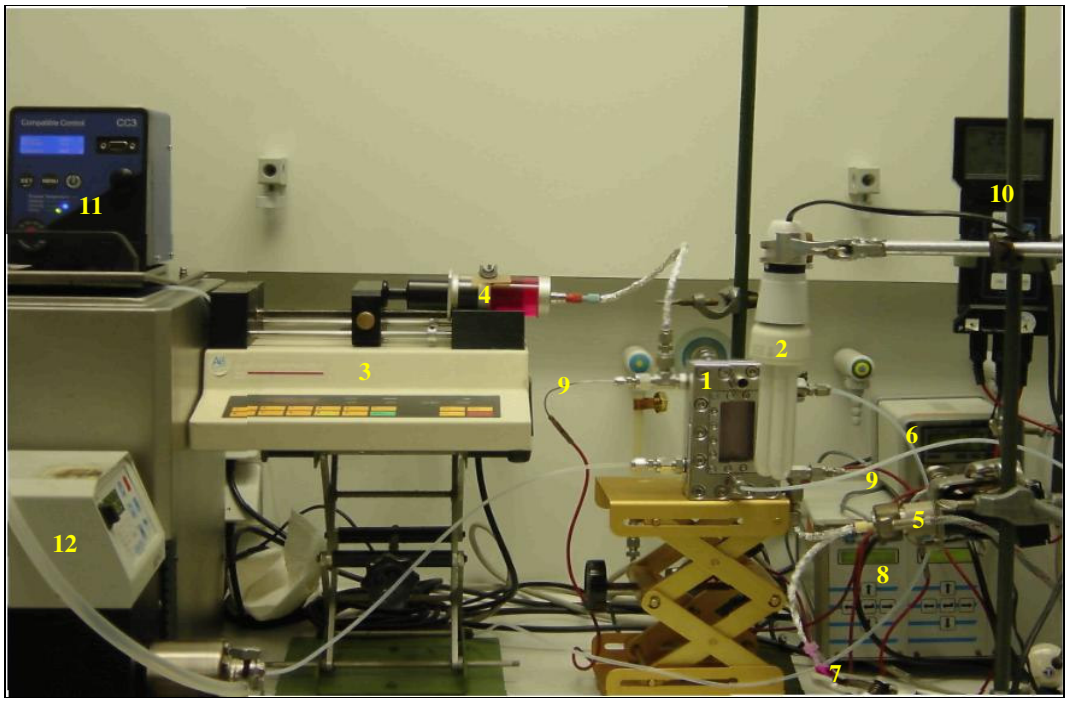


Figure 57: Falling film microreactor setup (in LIKAT): **1** – falling film microreactor; **2** – fluorescent lamp; **3** – programmable syringe pump; **4** – syringe for 50 ml with reaction mixture; **5** – gear pump; **6** – rotameter; **7** – GC vial; **8** – flow meter; **9 –** two thermocouples; **10** – thermo-recorder; **11** – cryostat; **12** – rotary pump

The fixed reaction temperature was provided by coolant that was constantly circulated through a cryostat **11** and heat exchanger located on the back side of the reaction plate

in FFMR. This circulation was maintained by a rotary pump **12**. To control the temperature of the reaction mixture inside the reactor, two thermocouples **9** were inserted into the microreactor inlet and outlet. The temperature was displayed by the thermo-recorder **10**. The syringe, GC vial and tubing used for the reaction mixture transportation were wrapped with aluminium foil during the experiment. All device connections and tubing were made of PTFE.

6.3 Investigation of ascaridole synthesis in the falling film microreactor

Initially the synthesis of ascaridole was realized in the falling film microreactor using the following procedure: a 10 mM solution of α-terpinene in isopropyl alcohol was irradiated with a 18 W domestic fluorescent lamp in the presence of 0.49 mmol/L of rose bengal as sensitizer while a gentle stream of oxygen (10 ml/min) was passed over the solution. To optimise this method and to demonstrate the influence of some procedure variables on the reaction efficiency the experiments described below were carried out.

6.3.1 Reaction residence time optimisation study

The irradiation time (τ) in the falling film microreactor is only several seconds and is defined by the liquid phase flow rate. In this microreactor the liquid phase is represented by a thin fluid film created by the gravity force inside of the microchannels. Therefore, the reaction volume was assigned as a volume of the generated film. The total internal volume of the microreactor plate was omitted and only thickness of the fluid film was taken into account and not the total channel depth of 200 μm. Thus reaction residence time was calculated according to the following equation *(3)*:[36]

$$\tau = \frac{V_{liq.film}}{\dot{V}_{liq}} \qquad (3)$$

where $V_{liq.film}$ = film volume, $\dot{V}_{liq}$ = liquid flow rate.

The volume of the liquid film was determined by the equation *(4)*:

$$V_{liq.film} = \delta \times l \times B \qquad (4)$$

where δ = film thickness, l = length of the channel irradiated zone, B = film width.

The film thickness (δ) inside the single microchannel was calculated based on the film theory according to the equation *(5)* (given by Perry[239,240]):

$$\delta = \left[\frac{3 \times \dot{V}_{liq} \times \eta_{liq}}{\rho_{liq} \times B \times g} \right]^{\frac{1}{3}} \quad (5)$$

where $\dot{V}_{liq}$ = liquid flow rate, η_{liq} = viscosity of the liquid, ρ_{liq} = density of the liquid, B = width of the film and g = acceleration due to gravity.

In *experiments 149-150* 25 and 50 mM solutions of α-terpinene were investigated with 6 main volumetric flow rates. The other experimental conditions were kept unchanged, the concentration of rose bengal was 0.49 mM, oxygen was used as the gas phase at a flow rate of 10 ml/min and a fluorescent lamp was used as the light source. After irradiation the samples were collected from the reactor outlet and instantly analysed by GC-MS. The obtained results are presented in Figure 58. As was expected, α-terpinene conversion increased with the increase of residence time. For 25 mM solution the conversion value went up from 16% at a residence time of only 6 sec to 94% at a residence time of 32 sec. For the 50 mM solution those numbers were lower and rose from 8% up to 57%, respectively. Thus, a residence time of 32 sec is considered as the best time when high conversion rates are needed. However, for the process modelling a shorter residence time of 6 sec, 10 sec and 13 sec will be recommended, as the total experimental time is then also shortened.

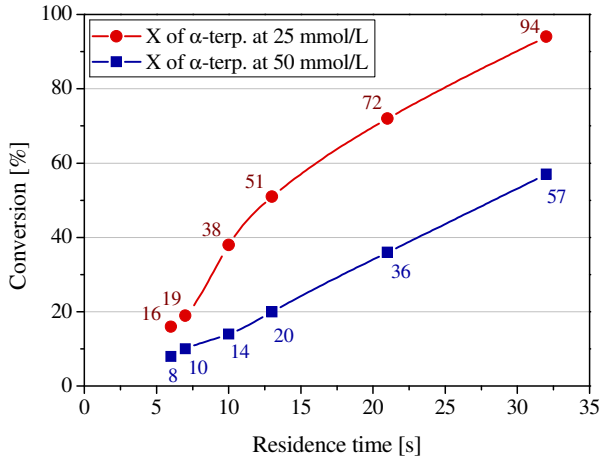


Figure 58: Effect of residence time on α-terpinene conversion

The calculated data for residence time, film thickness and film volume that corresponds to the tentative flow rates are presented in Table 31. All calculations were done for the experimental temperature of 20 °C. The lower flow rates gave extended residence times, thinner liquid film and smaller liquid volume and conversely for the higher flow rates.

Table 31: Calculated data of residence time, film thickness and film volume for the established flow rates at temperature of 20°C

Flow rate, [ml/min]	Film thickness, [µm][a]	Film volume, [µl][b]	Residence time, [s][c]
1	95	100	6
0.8	88	93	7
0.5	75	80	10
0.3	64	67	13
0.15	50	53	21
0.08	41	43	32

[a] calculated using equation 5; [b] calculated using equation 4; [c] calculated using equation 3

As mentioned above the photooxygenation of α-terpinene produced one main product ascaridole **40** and one side product *p*-cymene **96**. Therefore, it was important to determine the relative amount of α-terpinene that was converted directly to the desired endoperoxide ascaridole. This relative amount is also known as product selectivity. Within our study the conversion (X) of α-terpinene and the selectivity (S) of products (ascaridole, *p*-cymene) were calculated based on GC data and using the following equations *6* and *7*.[34–36,241] The ascaridole selectivity represents the amount of α-terpinene that was converted directly to the desired product ascaridole. The *p*-cymene selectivity represents the amount of α-terpinene that was converted directly to the secondary product *p*-cymene.

$$X_{\alpha-terpinene} = 1 - \frac{C^{outlet}_{\alpha-terpinene}}{C^{inlet}_{\alpha-terpinene}} \qquad (6)$$

$$S_i = \frac{C^{outlet}_{i}}{C^{inlet}_{\alpha-terpinene} - C^{outlet}_{\alpha-terpinene}} \qquad (7)$$

where i = ascaridole, *p*-cymene.

Other important parameters that have to be assessed for the synthetic processes in microreactors are yield and space time yield. These parameters are significant for the evaluation of microfluidic systems as a production tool. Product yield (Y) shows the amount of the desired product ascaridole formed from α-terpinene and was determined by the equation *8*.[34–36,241] Space time yield (STY) represents the number of moles of α-terpinene converted to ascaridole per volume and time unit. It was calculated using equation *9*:[34]

$$Y_{ascaridole} = \frac{C^{outlet}_{ascaridole}}{C^{inlet}_{\alpha-terpinene}} \quad (8)$$

$$STY = \frac{C^{inlet}_{\alpha-terpinene} \times X_{\alpha-terpinene} \times S_{ascaridole} \times \dot{V}_{liq}}{V_{liq.film}} \quad (9)$$

where $\dot{V}_{liq}$ = liquid flow rate.

The calculated data for product selectivity and space time yields for *experiments 149-150* is presented in Figure 59 and summarised in Table 32. As can be seen from Figure 59, selectivity of ascaridole showed the expected behaviour, it remained stable or slightly decreased with the increase of α-terpinene conversion. For example, at 25 mM solution the selectivity of ascaridole was in the range of 75–80% and was constant. At 50 mM solution concentration, ascaridole selectivity slightly decreased from 89% to 84%. In general, the dispersion of ascaridole selectivity was about 5% over the broad range of α-terpinene conversions (from 8% up to 94%). It is also important to notice that in these experimental conditions selectivity of side product *p*-cymene was stable and below 2%.

These experimental results clearly demonstrated the influence of two different concentrations of α-terpinene on the product selectivity over the complete range of α-terpinene conversions.

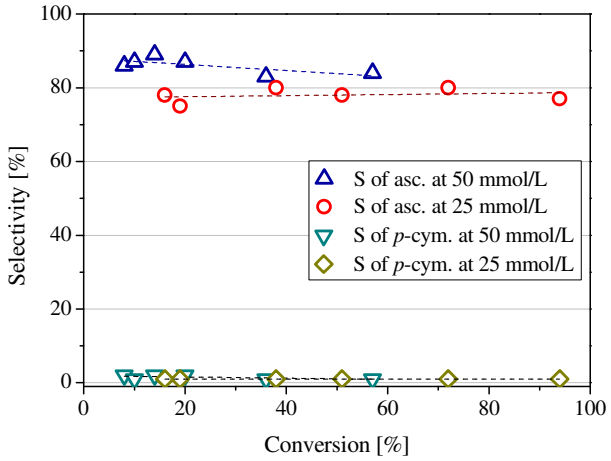


Figure 59: Selectivity of ascaridole and *p*-cymene vs. α-terpinene conversion

The highest space-time-yields of 2.6 mol L^{-1} h^{-1} and 2.5 mol L^{-1} h^{-1} were achieved for 25 mM solution at residence times of 10 sec and 13 sec which corresponded to flow rates of 0.5 ml/min and 0.3 ml/min, respectively. A comparable number of 2.4 mol L^{-1} h^{-1} was obtained for 50 mM solution after a residence time of 32 sec (flow rate 0.08 ml/min). In

general, there was only a small difference between numbers obtained for ascaridole space-time-yield, because a two times higher conversion of α-terpinene in 25 mM solution was balanced by the lower conversion but higher concentration in 50 mM solution.

Table 32: Reaction efficiency parameters vs. different residence times at 25 mM and 50 mM concentrations of α-terpinene

α-terpinene, [mmol/L]	**Residence time, [s]**	**$X_{\alpha\text{-terp}}$, [%][a,b]**	**S_{asc}, [%][a,c]**	**$S_{p\text{-cym}}$, [%][a,c]**	**Y_{asc}, [%][a,d]**	**STY, [mol L^{-1} h^{-1}][e]**
25	6	16	78	1	12	1.7
25	7	19	75	1	14	1.7
25	10	38	80	1	31	2.6
25	13	51	78	1	40	2.5
25	21	72	80	1	58	2.2
25	32	94	77	1	72	1.9
50	6	8	86	2	7	1.9
50	7	10	87	1	8	2.1
50	10	14	89	2	12	2.1
50	13	20	87	2	17	2.1
50	21	36	83	1	30	2.3
50	32	57	84	1	48	2.4

[a] Determined by GC area analysis; [b] calculated using equation 6; [c] calculated using equation 7; [d] calculated using equation 8; [e] calculated using equation 9

6.3.2 Reproducibility study

The remarkable initial results achieved in the falling film microreactor encouraged further investigation. However, before doing other experiments it was important to ensure that the obtained results are reproducible. Therefore *experiment 150* was repeated twice (*experiments 151* and *152*). The average data points of α-terpinene conversion and product selectivity for these three experiments are presented in Figures 60 and 61. As can be seen from Figure 60 the conversion of α-terpinene showed very good reproducibility with standard deviation of 1.5% and 6.2% RSD. Excellent reproducibility demonstrated also selectivity of ascaridole with a standard deviation of 2.5% and 2.9% RSD. Selectivity of *p*-cymene was consistent at 1–2% (Figure 61, Table 33).

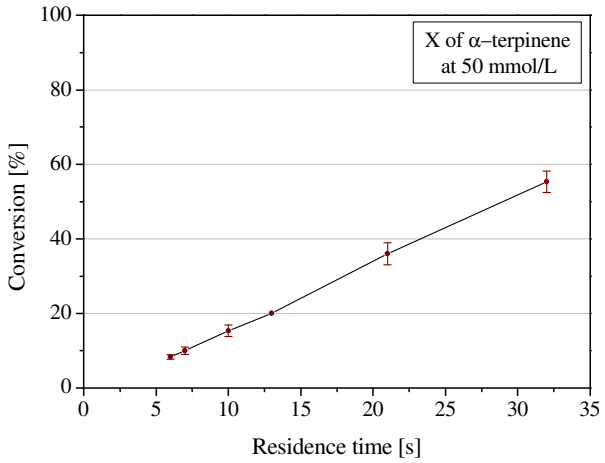


Figure 60: Average data points of α-terpinene conversion vs. the range of residence times in the identical *experiments 150*, *151* and *152*

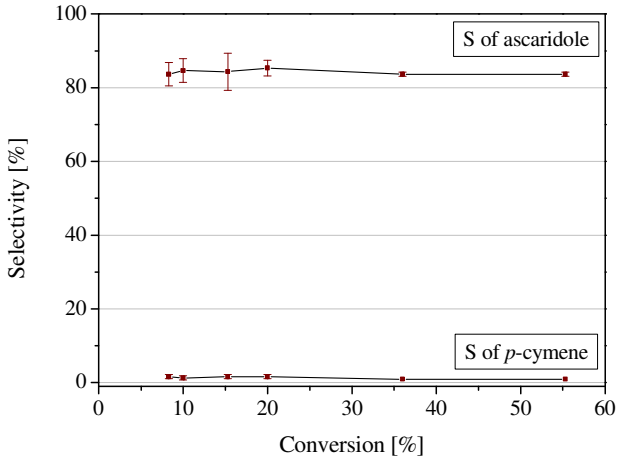


Figure 61: Average data points of ascaridole and *p*-cymene selectivity vs. α-terpinene conversion in the identical *experiments 150*, *151* and *152*

For *experiments 150*, *151* and *152*, the ascaridole yields and space time yields were also determined (Table 33). The ascaridole yield had a standard deviation of 1.4% with 5.6% RSD, while the space time yield had a standard deviation of just 0.1% with 4.9% RSD, which is within accepted limits of industrial processes.

Table 33: Reaction efficiency parameters established for the identical *experiments 150*, *151* and *152*

Residence time, [s]	$X_{\alpha\text{-terp}}$, [%][a,b]			S_{asc}, [%][a,c]			$S_{p\text{-cym}}$, [%][a,c]			Y_{asc}, [%][a,d]			STY, [mol L^{-1} h^{-1}][e]		
	1[f]	2[f]	3[f]	1	2	3	1	2	3	1	2	3	1	2	3
6	8	9	8	86	80	85	2	1	2	7	7	7	1.9	2.0	1.9
7	10	11	9	87	81	86	1	1	2	8	8	8	2.1	2.2	1.8
10	14	15	17	89	79	85	2	1	2	12	12	15	2.1	2.1	2.5
13	20	20	20	87	83	86	2	1	2	17	17	16	2.1	2.1	2.1
21	36	39	33	83	84	84	1	1	1	30	33	27	2.3	2.6	2.2
32	57	57	52	84	84	83	1	1	1	48	49	43	2.4	2.5	2.2

[a] Determined by GC area analysis; [b] calculated using equation 6; [c] calculated using equation 7; [d] calculated using equation 8; [e] calculated using equation 9; [f] results obtained in the appropriate experiments: 1 – *exp. 150*, 2 – *exp. 151*, 3 – *exp. 152*

6.3.3 Effect of oxygen concentration on the ascaridole synthesis

Pure oxygen or air could be used as the source of singlet oxygen for the photooxygenation reaction. According to the literature the rate of oxygenation reactions significantly increases when pure oxygen is used. However, air is cheaper, safer and an environmentally favourable reagent. Therefore, synthesis of ascaridole was investigated in a falling film microreactor with both gases. Previously described *experiment 150* where pure oxygen (99.5% of O_2) was used as a gas phase was compared with the *experiment 153* where air (21% of O_2) was applied. All other experimental parameters were kept constant: concentration of α-terpinene was 50 mM, concentration of RB was 0.49 mM, isopropanol was used as solvent and a fluorescent lamp was used as light source, gas flow rate was 10 ml/min. The obtained results showed that the concentration of oxygen has a noticeable influence on the reaction efficiency only at the prolonged residence times when interaction between liquid phase and gas phase is also extended. At residence times shorter than 21 sec the concentration of oxygen in the gas phase has an insignificant effect (Figure 62, Table 34). Also, the results showed that α-terpinene conversion below 40% could be reached either with pure oxygen or air, however for higher conversions it will be preferable to use pure oxygen. Almost no difference was observed for product selectivity when different concentrations of oxygen were used (Figure 63, Table 34). The ascaridole yields and space time yields were also within comparable ranges (Table 34).

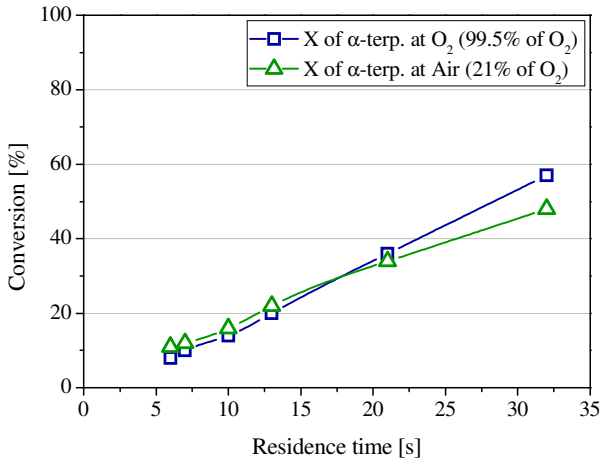


Figure 62: Conversion of α-terpinene vs. residence time at different concentration of O_2

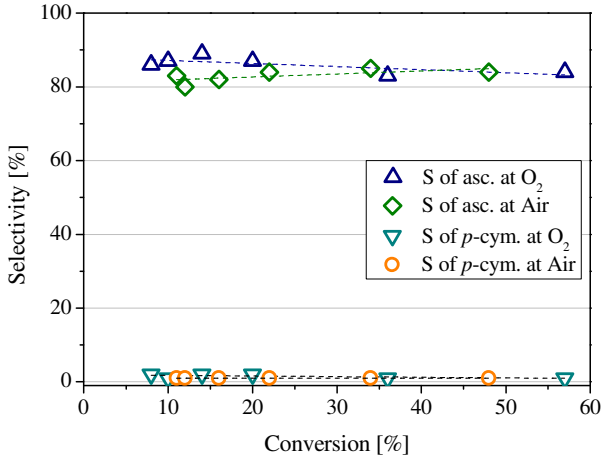


Figure 63: Selectivity of ascaridole and *p*-cymene vs. α-terpinene conversion at different concentration of O_2

Table 34: Reaction efficiency parameters established at different concentration of O_2

Residence time, [s]	$X_{\alpha\text{-terp}}$, [%][a,b]		S_{asc}, [%][a,c]		$S_{p\text{-cym}}$, [%][a,c]		Y_{asc}, [%][a,d]		STY, [mol L^{-1} h^{-1}][e]	
	O_2	Air	O_2	Air	O_2	Air	O_2	Air	O_2	Air
6	8	10	86	83	2	1	7	8	1.9	2.3
7	10	12	87	80	1	1	8	9	2.1	2.3
10	14	16	89	82	2	1	12	13	2.1	2.3
13	20	22	87	84	2	1	17	18	2.1	2.3
21	36	34	83	84	1	1	30	29	2.3	2.2
32	57	47	84	84	1	1	48	40	2.4	2.0

[a] Determined by GC area analysis; [b] calculated using equation 6; [c] calculated using equation 7; [d] calculated using equation 8; [e] calculated using equation 9

6.3.4 Effect of solvent on the ascaridole synthesis

In the above described experiments isopropanol was used as solvent. The utilised sensitizer rose bengal has poor solubility in isopropanol. As a result the prepared reaction mixture had a low transparency. Addition of 10 Vol-% of water as a co-solvent noticeably improved the solubility of rose bengal and a fully transparent solution was obtained. The influence of isopropanol/water (90:10) mixture on the reaction efficiency was studied in *experiment 154* and the results obtained were compared with the results achieved in *experiment 150*, where isopropanol was used as solvent. Other reaction parameters were kept unchanged. The addition of 10% water to isopropanol had little effect on α-terpinene conversion at residence times above 21 sec (Figure 64).

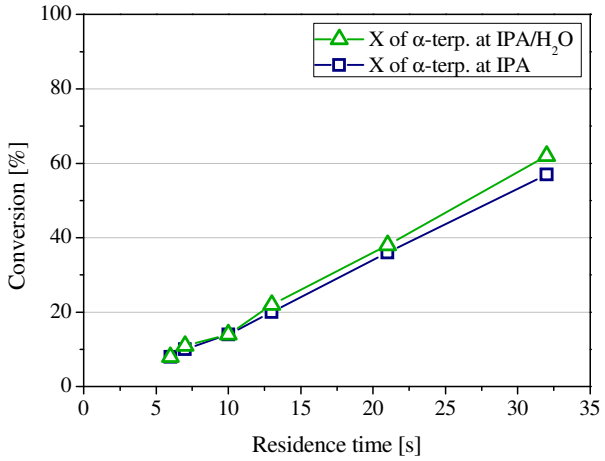


Figure 64: Conversion of α-terpinene vs. residence time in isopropanol and isopropanol/water mixture (9:1)

As can be seen in Figure 65 the presence of 10% water had no effect on product selectivity. The selectivity for ascaridole was 79–83% which is slightly lower than 83–89% in the experiment without water, and the selectivityof the by-product *p*-cymene remained stable and below 2%.

Ascaridole yields and space time yields were equivalent within *experiments 154* and *150*. Somewhat lower ascaridole selectivity was compensated by the higher α-terpinene conversion which caused almost equivalent yields (Table 35).

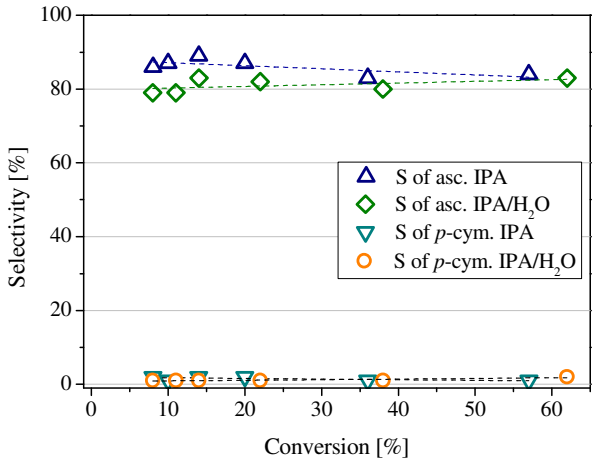


Figure 65: Selectivity of ascaridole and *p*-cymene vs. α-terpinene conversion in isopropanol and isopropanol/water mixture (9:1)

Table 35: Reaction efficiency parameters established for the experiments when blank isopropanol and isopropanol/water mixture (9:1) where used as solvent

Residence time, [s]	$X_{\alpha\text{-terp}}$, [%][a,b]		S_{asc}, [%][a,c]		$S_{p\text{-cym}}$, [%][a,c]		Y_{asc}, [%][a,d]		STY, [mol L^{-1} h^{-1}][e]	
	IPA	IPA_{H2O}	IPA	IPA_{H2O}	IPA	IPA_{H2O}	IPA	IPA_{H2O}	IPA	IPA_{H2O}
6	8	8	86	79	2	1	7	7	1.9	1.8
7	10	11	87	79	1	1	8	8	2.1	2.1
10	14	14	89	83	2	1	12	12	2.1	2.0
13	20	22	87	82	2	1	17	17	2.1	2.2
21	36	38	83	80	1	1	30	30	2.3	2.4
32	57	62	84	83	1	2	48	50	2.4	2.6

[a] Determined by GC area analysis; [b] calculated using equation 6; [c] calculated using equation 7; [d] calculated using equation 8; [e] calculated using equation 9; IPA – blank isopropanol; IPA_{H2O} – isopropanol/water mixture in ratio 9:1

6.3.5 Effect of α-terpinene concentration on the ascaridole synthesis

The above described *experiments 150-154* were carried out at constant α-terpinene concentration of 50 mM. At this solution concentration the reaction did not reach completion after the extended residence time of 32 sec. Results obtained in *experiment 149* also showed that at a concentration of 25 mM the conversion of α-terpinene nearly doubled to 94% but still, the reaction was incomplete after a residence time of 32 sec. Therefore, the conversion of α-terpinene and thus the reaction efficiency could be further improved by increasing residence time or by decreasing reagent concentration.

Residence time in the falling film microreactor is inversely proportional to the liquid phase flow rate. Prolonged residence time could be achieved at fluid flow rates below 0.08 ml/min. However, such low fluid flow rates generate very small volumes of liquid phase inside of the reactor microchannels. For example, the total volume of the microchannels is 211.2 µl while the volume of liquid is below 43 µl at flow rates lower than 0.08 ml/min. This means that only one fifth of the microchannel volume is filled by the liquid phase and the rest is gas phase (gas phase is continuously blown over the liquid phase). Therefore, the evaporation of solution has to be prevented by using an adequate fluid flow rate that cannot be below 0.08 ml/min. Consequently, the lowest optimal flow rate established for the liquid phase was 0.08 ml/min.

Regarding the solution concentration it is important to notice that the efficiency of photochemical reactions is directly dependent on reagent concentration and especially the concentration of the light absorbing component. However, the solution concentration should not be too low, because the reaction output with respect to the quantity of product will be insignificant. Hence, the next step investigated the effect of α-terpinene concentration at 10 mM, 75 mM and 100 mM. In the *experiment 155*, at a concentration of 10 mM, the reaction reached 100% conversion after 32 sec. At that point, selectivity of ascaridole was somewhat lower than normally and was 72%.

Experiments 156 and *157* were set-up with solution concentrations 75 mM and 100 mM, respectively (other reaction parameters were kept unchanged). The experimental residence times were preset to 6 sec, 13 sec and 32 sec.

Results obtained from these experiments were combined with the appropriate results obtained in the *experiments 149* and *150* and are summarised in Table 36 and presented in Figures 66 and 67. As can be seen in Figure 66 the conversion of α-terpinene to ascaridole consistently decreased with the increase of α-terpinene concentration. At a fixed residence time of 32 seconds conversion dropped down from 100% at 10 mM solution to 32% at 100 mM solution. These results adequately show that conversion of α-terpinene declined only three times for a 10 times more concentrated solution. At shorter residence times of 6 sec and 13 sec the achieved results were less satisfactory. Thus at an irradiation time of 13 sec the conversion declined from 82% to 12% and at 6 sec the conversion declined from 40% (10 mM solution) to 5% (100 mM solution), respectively. However, for 75 mM and 100 mM solutions the conversions varied within only 2–5%.

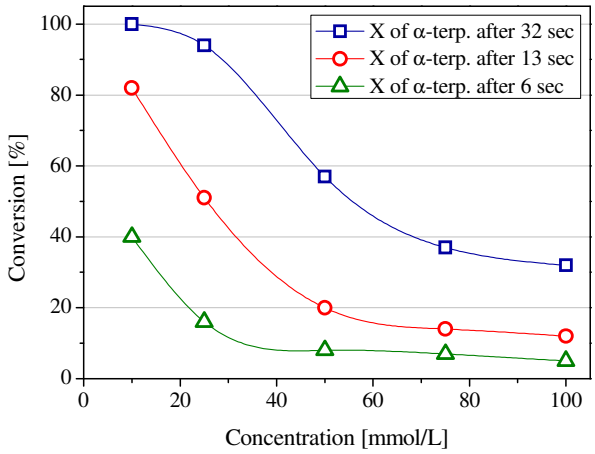


Figure 66: Conversion of α-terpinene vs. concentration of α-terpinene at fixed residence times of 6 sec, 13 sec and 32 sec

The selectivity of the main product ascaridole was up to 20% higher at 50 mM and 75 mM solution concentrations compared to the 10 mM and 100 mM solutions. In general, except for the last point, the selectivity of ascaridole increased with increasing α-terpinene concentration. The selectivity of the side product *p*-cymene remained at 3% for all experiments (Figure 67, Table 36).

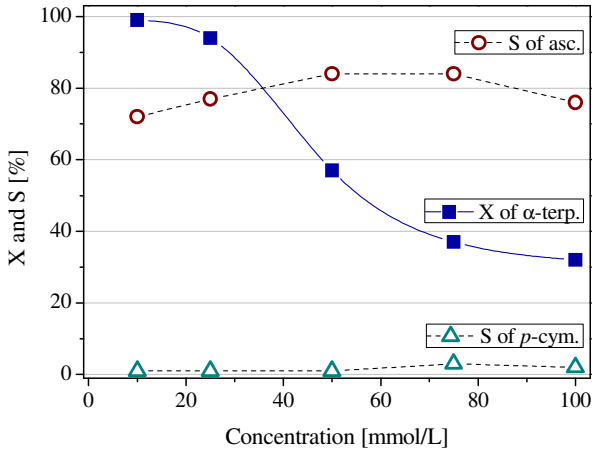


Figure 67: Conversion of α-terpinene and selectivity of ascaridole and *p*-cymene vs. concentration of α-terpinene

In parallel with the increase of α-terpinene concentration the ascaridole space time yield slightly increased. The highest space time yields of 2.4–2.5 mol L^{-1} h^{-1} were established for concentrations higher than 25 mM at residence times of 13 sec and 32 sec, respectively (Table 36).

Table 36: Reaction efficiency parameters established for the experiments with different α-terpinene concentration

α-terp., [mmol/L]	$X_{\alpha\text{-terp}}$, [%][a,b]			S_{asc}, [%][a,c]			$S_{p\text{-cym}}$, [%][a,c]			Y_{asc}, [%][a,d]			STY, [mol L^{-1} h^{-1}][e]		
	6[f]	13[f]	32[f]	6	13	32	6	13	32	6	13	32	6	13	32
10	40	82	100	67	70	72	1	1	1	26	57	71	1.5	1.4	0.7
25	16	51	94	78	78	77	1	1	1	12	40	72	1.7	2.5	1.9
50	8	20	57	86	87	84	2	2	1	7	17	48	1.9	2.1	2.4
75	7	14	37	69	78	84	3	2	3	5	11	31	2.0	2.0	2.4
100	5	12	32	66	69	76	3	2	2	3	8	24	1.8	2.0	2.5

[a] Determined by GC area analysis; [b] calculated using equation 6; [c] calculated using equation 7; [d] calculated using equation 8; [e] calculated using equation 9; [f] residence time

6.3.6 Effect of rose bengal concentration on the ascaridole synthesis

The concentration of rose bengal might have a significant impact on the reaction output. In the above described *experiments 149-157* the concentration of rose bengal was constant at 0.49 mM. Hence, in the following *experiment 158* the effect of double concentration of rose bengal (0.98 mM) on the reaction efficiency was studied for the broad range of α-terpinene concentration from 10 mM to 100 mM. In *experiment 159* the effect of half the concentration of rose bengal (0.25 mM) on the reaction efficiency was studied for the α-terpinene concentration from 10 mM to 50 mM only. Reaction residence time was set to either 6 sec or 13 sec. Other reaction parameters were the same as before.

Initially, isopropanol was used as solvent in *experiments 158* and *159*. During the experimental work-up the crystallisation of rose bengal occurred inside the reactor microchannels and clogged them. This caused the disruption of the homogeneous distribution of the solution within the channels and inhibited the continuous flow. To solve this problem 10 Vol-% of water was added as co-solvent which improved the solubility of rose bengal. Moreover water helped to keep rose bengal in the dissolved state when its concentration was increased or reduced. Therefore in *experiments 158* and *159* isopropanol with 10 Vol-% of water was used as solvent.

Results obtained in *experiment 158* with double the concentration of RB were compared with the appropriate results obtained in *experiments 149, 150, 155, 156* and *157*. The results achieved at residence times of 6 and 13 sec are summarised in Table 37 and presented in Figures 68 and 69. Figure 68 demonstrates the dependency between α-terpinene conversion and α-terpinene concentration at 0.49 mM and 0.98 mM of rose

bengal and residence times of 6 sec and 13 sec. As can be seen from Figure 68 doubling the concentration of rose bengal induced a steady increase of about 10% of α-terpinene conversion over the entire range of α-terpinene concentration at a residence time of 13 sec. At a residence time of 6 sec and an α-terpinene concentration of 10 mM the conversion improved by the largest number of 26% while at α-terpinene concentrations above 50 mM the conversion improved by 5% only.

The determined data for ascaridole and *p*-cymene selectivity showed that higher concentrations of rose bengal did not affect product selectivity (Figure 69, Table 37). These results were very important for further process optimisation.

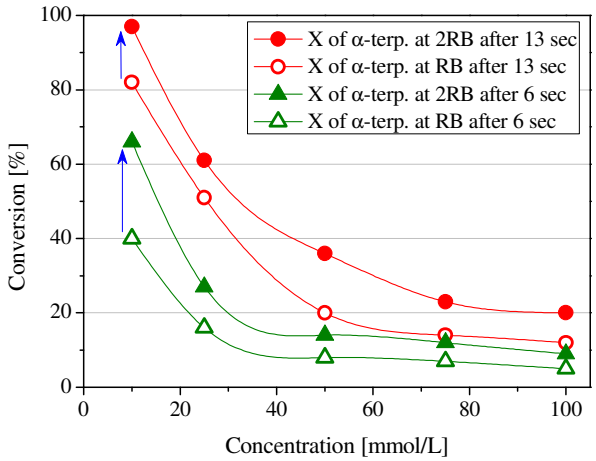


Figure 68: Conversion of α-terpinene vs. concentration of α-terpinene at 0.49 mM and 0.98 mM concentration of rose bengal and at fixed residence times of 6 sec and 13 sec

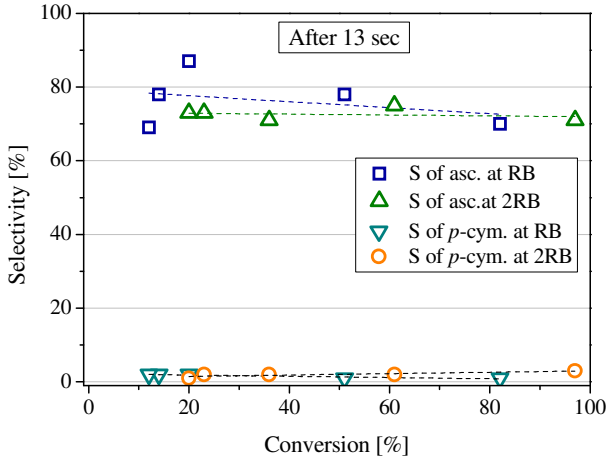


Figure 69: Selectivity of ascaridole and *p*-cymene vs. concentration of α-terpinene at 0.49 mM and 0.98 mM concentration of rose bengal and fixed residence time of 13 sec

The increase of α-terpinene conversion in concert with the stable and high ascaridole selectivity resulted in approximately 3–8% higher yields of ascaridole at 0.98 mM concentration of rose bengal. Somewhat higher ascaridole yields of 47% and 69% were observed for 10 mM concentration of α-terpinene. At sensitizer concentration of 0.98 mM the ascaridole space time yields were also about 1 mol L^{-1} h^{-1} higher compared to the results obtained at 0.49 mM concentration of rose bengal. So far, the highest space time yield of ascaridole synthesis of 3.6 mol L^{-1} h^{-1} was determined for the α-terpinene solutions with the concentration of 75 mM and 100 mM at residence times of 6 sec and 13 sec, respectively, and at a sensitizer concentration of 0.98 mM (Table 37).

Table 37: Reaction efficiency parameters established for the experiments with 0.49 mM and 0.98 mM concentrations of rose bengal at different α-terpinene concentrations and fixed residence times of 6 sec and 13 sec

α-terp., [mmol/L]	**$X_{α\text{-terp}}$, [%][a,b]**		**S_{asc}, [%][a,c]**		**$S_{p\text{-cym}}$, [%][a,c]**		**Y_{asc}, [%][a,d]**		**STY, [mol L^{-1} h^{-1}][e]**	
	RB[f]	**2RB[f]**	**RB**	**2RB**	**RB**	**2RB**	**RB**	**2RB**	**RB**	**2RB**
At residence time of 6 sec										
10	40	66	67	73	1	2	26	47	1.5	2.7
25	16	27	78	66	1	2	12	18	1.7	2.5
50	8	14	86	66	2	1	7	9	1.9	2.5
75	7	12	69	74	3	2	5	8	2.0	3.6
100	5	9	66	68	3	2	3	6	1.8	3.4
At residence time of 13 sec										
10	82	97	70	71	1	3	57	69	1.4	1.7
25	51	61	78	75	1	2	40	45	2.5	2.8
50	20	36	87	71	2	2	17	25	2.1	3.2
75	14	23	78	73	2	2	11	17	2.0	3.1
100	12	20	69	73	2	1	8	15	2.0	3.6

[a] Determined by GC area analysis; [b] calculated using equation 6; [c] calculated using equation 7; [d] calculated using equation 8; [e] calculated using equation 9; [f] RB – concentration of rose bengal 0.49 mM; 2RB – concentration of rose bengal 0.98 mM

In *experiment 159*, at a concentration for rose bengal of 0.25 mM, the observed tendency of the reaction efficiency was opposite to that observed in *experiment 158* with twice the sensitizer concentration (0.98 mM). At an irradiation time of 13 sec the conversion of α-terpinene decreased by 27%, 13% or 4% at α-terpinene concentrations of 10 mM, 25 mM and 50 mM, respectively. At the shorter residence time of 6 sec the conversion of α-terpinene also decreased, but less markedly (up to 8%) and at an α-

terpinene concentration above 25 mM the conversion of α-terpinene did not decline further and remained the same as in *experiments 149* and *150* (Figure 70).

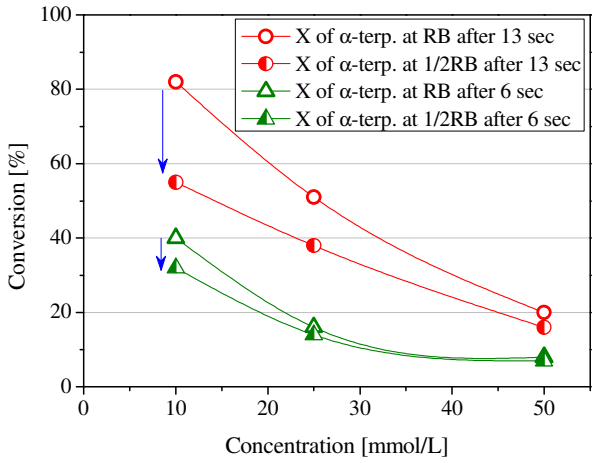


Figure 70: Conversion of α-terpinene vs. concentration of α-terpinene at 0.49 mM and 0.25 mM concentration of rose bengal and at fixed residence times of 6 sec and 13 sec

The selectivity of ascaridole was somewhat lower (62–74%) at a sensitizer concentration of 0.25 mM compared to the ascaridole selectivity (67–87%) at rose bengal concentration of 0.49 mM. As before the selectivity of *p*-cymene was not affected by the change of sensitizer concentration (Table 38).

Table 38: Reaction efficiency parameters established for the experiments with 0.49 mM and 0.25 mM concentrations of rose bengal at different α-terpinene concentrations and fixed residence times of 6 sec and 13 sec

α-terp., [mmol/L]	**$X_{\alpha\text{-terp}}$, [%][a,b]**		**S_{asc}, [%][a,c]**		**$S_{p\text{-cym}}$, [%][a,c]**		**Y_{asc}, [%][a,d]**		**STY, [mol L^{-1} h^{-1}][e]**	
	RB[f]	**½RB[f]**	**RB**	**½RB**	**RB**	**½RB**	**RB**	**½RB**	**RB**	**½RB**
At residence time of 6 sec										
10	40	32	67	62	1	1	26	20	1.5	1.1
25	16	14	78	69	1	2	12	9	1.7	1.3
50	8	7	86	68	2	1	7	5	1.9	1.3
At residence time of 13 sec										
10	82	55	70	69	1	2	57	38	1.4	0.9
25	51	38	78	74	1	2	40	28	2.5	1.7
50	20	16	87	67	2	2	17	11	2.1	1.3

[a] Determined by GC area analysis; [b] calculated using equation 6; [c] calculated using equation 7; [d] calculated using equation 8; [e] calculated using equation 9; [f] RB – concentration of rose bengal 0.49 mM; ½RB – concentration of rose bengal 0.25 mM

Owing to the decrease of α-terpinene conversion and ascaridole selectivity the ascaridole yields and space time yields also declined (Table 38). The largest decrease of the ascaridole yield by 19% was recorded for α-terpinene concentration of 10 mM at residence time of 13 sec. The ascaridole space time yields decreased by 0.4–0.6 mol L^{-1} h^{-1} at residence time of 6 sec and decreased by 0.5–0.8 mol L^{-1} h^{-1} at residence time of 13 sec.

During the test runs that have been performed before each above described *experiment 149-159* a low conversion of α-terpinene was observed. The test runs were carried out at the same conditions as other runs within the experiment. The only difference of the test runs was that the solution in the microreactor was not irradiated by any light source. A flow rate for the liquid phase was 1 ml/min.

In the test run of *experiment 155* with a solution concentration of 10 mM a conversion of α-terpinene of 15% was recorded. At higher solution concentrations the conversions were noticeably smaller. Thus for 25 mM (*exp. 149*), 50 mM (*exp. 150*), 75 mM (*exp. 156*) and 100 mM (*exp. 157*) solution concentrations the α-terpinene conversions of 5%, 2%, 2% and 1% were observed, respectively. These results demonstrated that photooxygenation of α-terpinene is very sensitive to the presence of oxygen and to the momentary exposure of ambient light.

Afterwards, it was suggested that α-terpinene might undergo self-sensitisation. The corresponding experiment without sensitizer rose bengal was carried out (*experiment 160*). In this experiment 10 mM solution of α-terpinene was investigated at three flow rates of 1 ml/min, 0.5 ml/min and 0.08 ml/min that corresponded residence time of 6 sec, 10 sec and 32 sec, respectively. Other reaction parameters were kept unchanged. The achieved results showed that α-terpinene didn't undergo any self-sensitisation and was additionally stable under the applied conditions. The detected conversion of α-terpinene was below 4%. However, the GC-MS analysis of crude products showed that neither ascaridole nor any other oxidation products were formed and were found. These results clearly demonstrated that ascaridole synthesis via photooxygenation of α-terpinene requires the presence of sensitizer rose bengal.

To find the reason of detected conversion of α-terpinene of 4% the following *experiment 161* was done. In this experiment 10 mM solution of α-terpinene was investigated without rose bengal and without light at flow rates of 0.5 ml/min and 0.08 ml/min. Oxygen was used as gas phase at a flow rate of 10 ml/min. The collected products were analysed by GC-MS and conversion of α-terpinene below 4% was detected again. Ascaridole or any other products were not found. Therefore it could be

suggested that 4% conversion of α-terpinene was established due to the loss of α-terpinene via its volatilization by the continuous flow of gas phase.

6.3.7 Effect of oxygen flow rate on the ascaridole synthesis

Ascaridole synthesis via photooxygenation of α-terpinene is an example of a heterogeneous reaction. Therefore sufficient saturation of the solution film with oxygen is an important factor for reaction efficiency. The influence of oxygen flow rate on the reaction output was studied in *experiment 162*. In this experiment 75 mM and 100 mM solutions of α-terpinene were investigated with higher oxygen flow rates of 20 ml/min and 50 ml/min. The achieved results were compared with the results obtained in *experiments 156* and *157* when a general oxygen flow rate of 10 ml/min was used. In *experiment 162* other reaction parameters were unchanged. The residence time was set to 10 sec and 13 sec. The experimental results are summarised in Table 39. As can be seen from the obtained results the increase of oxygen flow rate had no influence on the α-terpinene conversion, product selectivity, product yields and thus on the general reaction efficiency.

Table 39: Reaction efficiency parameters established for the experiments with different oxygen flow rates

Residence time, [s]	$X_{\alpha\text{-terp}}$, [%][a,b]			S_{asc}, [%][a,c]			$S_{p\text{-cym}}$, [%][a,c]			Y_{asc}, [%][a,d]			STY, [mol L^{-1} h^{-1}][e]		
	10[f]	20[f]	50[f]	10	20	50	10	20	50	10	20	50	10	20	50
At α-terpinene conc. of 75 mM															
13	14	16	–[g]	78	71	–	2	3	–	11	11	–	2.0	2.1	–
10	–	10	11	–	78	81	–	2	3	–	8	9	–	2.0	2.3
At α-terpinene conc. of 100 mM															
13	12	12	–	69	69	–	2	3	–	8	8	–	2.0	2.0	–
10	–	9	9	–	65	78	–	3	3	–	6	7	–	2.0	2.4

[a] Determined by GC area analysis; [b] calculated using equation 6; [c] calculated using equation 7; [d] calculated using equation 8; [e] calculated using equation 9; [f] flow rate of oxygen expressed in ml/min; [g] was not investigated

The results achieved in *experiment 162* were quite unexpected. It is obvious that the amount of generated singlet oxygen depends on the concentration of molecular oxygen in solution and from the concentration of the sensitizer rose bengal. Therefore the lack of impact of oxygen flow rate on the reaction efficiency could be caused by the insufficient concentration of sensitizer rose bengal. As shown previously, a larger

concentration of rose bengal (0.98 mM) alone had a significant effect on the reaction efficiency. Therefore, in *experiment 163* the influence of oxygen flow rate of 50 ml/min on the reaction efficiency was investigated at a sensitizer concentration of 0.98 mM. The applied concentration of α-terpinene was 50 mM and the residence time was set to 10 sec, 13 sec and 32 sec.

Results achieved in *experiment 163* were compared with the appropriate results obtained in *experiment 150* and are summarised in Table 40. As can be seen from Figure 71 conversion of α-terpinene significantly increased when larger concentrations of rose bengal and an oxygen flow rate of 50 ml/min were applied. The highest conversion of α-terpinene, 87%, was reached at a residence time of 32 sec.

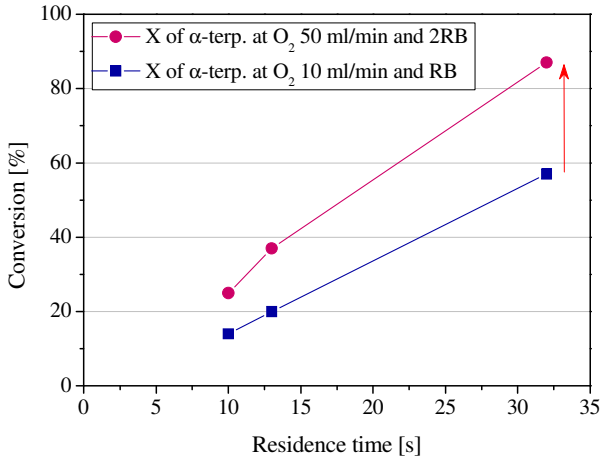


Figure 71: Conversion of α-terpinene vs. residence time at 0.49 mM sensitizer concentration and oxygen flow rate of 10 ml/min and at 0.98 mM sensitizer concentration and oxygen flow rate of 50 ml/min

Due to the significant increase of α-terpinene conversion the selectivity of the main product ascaridole decreased by 14% and the selectivity of the by-product *p*-cymene was steady but higher at 4% (Figure 72).

The considerable increase of α-terpinene conversion enhanced ascaridole yields and space time yields especially at the residence time of 32 sec. A high ascaridole space time yield of 3.2–3.4 mol L^{-1} h^{-1} were achieved for all residence times under the experimental conditions established for the *experiment 163*.

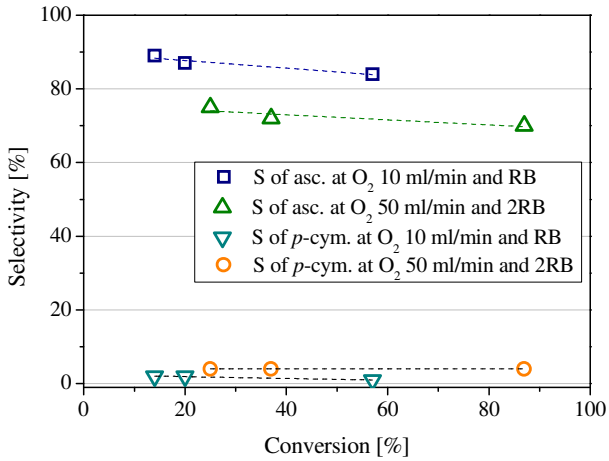


Figure 72: Selectivity of ascaridole and *p*-cymene vs. α-terpinene conversion at 0.49 mM sensitizer concentration and oxygen flow rate of 10 ml/min and at 0.98 mM sensitizer concentration and oxygen flow rate of 50 ml/min

Table 40: Reaction efficiency parameters established at 0.49 mM sensitizer concentration and oxygen flow rate of 10 ml/min and at 0.98 mM sensitizer concentration and oxygen flow rate of 50 ml/min

Residence time, [s]	$X_{\alpha\text{-terp}}$, [%][a,b]		S_{asc}, [%][a,c]		$S_{p\text{-cym}}$, [%][a,c]		Y_{asc}, [%][a,d]		STY, [mol L^{-1} h^{-1}][e]	
	150[f]	163[f]	150	163	150	163	150	163	150	163
10	14	25	89	75	2	4	12	20	2.1	3.3
13	20	37	87	72	2	4	17	27	2.1	3.4
32	57	87	84	70	1	4	48	60	2.4	3.2

[a] Determined by GC area analysis; [b] calculated using equation 6; [c] calculated using equation 7; [d] calculated using equation 8; [e] calculated using equation 9; [f] experiment number

6.3.8 Effect of temperature on ascaridole synthesis

The above described *experiments 149-163* were performed at constant room temperature at 20°C. Temperature was precisely controlled by the thermocouples positioned on the inlet and outlet of the microreactor. Moreover, the cooling water was continuously circulated via the reactors' cooling channels and cryostat. The increase of temperature has two different effects on the reaction: (a) solubility of oxygen inside the liquid phase decreases with the increase of temperature,[242] (b) the rates of non-photochemical steps increase with the increase of temperature.

It is also important to notice that film thickness and film volume of the liquid phase in the falling film microreactor are temperature dependent and decrease with the increase

of temperature (Table 41). In the applied experimental conditions the main variables that have significant influence on the film thickness and film volume are volumetric flow rate of the fluid phase and viscosity and density of solvent (isopropanol). An example of the calculated film thickness, film volume and residence time over the broad temperature range at a constant fluid flow rate of 0.5 ml/min is presented in Table 41.

Table 41: Calculated data of film thickness, film volume and residence time for different temperatures at constant fluid flow rate of 0.5 ml/min

t, [°C]	$\rho_{i\text{-PrOH}}$, [g cm^{-3}]	$\eta_{i\text{-PrOH}}$, [g cm^{-1} s^{-1}]	Flow rate, [ml/min]	Film thickness, [µm][a]	Film volume, [µl][b]	Residence time, [s][c]
0	0.804	4.621	0.5	91	97	12
3	0.801	4.223	0.5	89	94	11
5	0.799	3.977	0.5	87	92	11
8	0.797	3.635	0.5	85	89	11
18	0.788	2.693	0.5	77	81	10
20	0.786	2.536	0.5	75	80	10
29	0.778	1.936	0.5	69	73	9
40	0.768	1.392	0.5	62	66	8

[a] calculated using equation 5; [b] calculated using equation 4; [c] calculated using equation 3

The dependency between different fluid flow rates and film thickness and film volume has been shown before at a temperature of 20°C (Table 31). At this temperature the density and viscosity of isopropanol are 0.786 g cm^{-3} and 2.536 g cm^{-1}s^{-1}, respectively. At a temperature of 0°C the density and viscosity of isopropanol are noticeably larger 0.804 g cm^{-3} and 4.621 g cm^{-1} s^{-1}.[239] Therefore, higher isopropanol density and viscosity at a temperature of 0°C induced the enlargement of the film thickness and film volume for the same fluid flow rate. In the falling film microreactor the estimated residence time is also dependent from the viscosity and density of solvent. Therefore residence time is longer at a temperature of 0°C compared to the residence time at temperature of 20°C. The calculated data of film thickness, film volume and residence time that corresponds to the experimental flow rates at a temperature of 0°C is presented in the Table 42.

Table 42: Calculated data of residence time, film thickness and film volume for the experimental flow rates at temperature of 0°C

Flow rate, [ml/min]	Film thickness, [µm][a]	Film volume, [µl][b]	Residence time, [s][c]
1	115	122	7
0.8	107	113	8
0.5	91	97	12
0.3	77	81	16
0.15	61	65	26
0.08	50	52	39

[a] calculated using equation 5; [b] calculated using equation 4; [c] calculated using equation 3

The photooxygenation of α-terpinene yielded one main product ascaridole and one by-product *p*-cymene. At 20°C the selectivity of ascaridole varied within a broad range from 62% up to 89%, but the selectivity of *p*-cymene was stable and below 4% in all examined cases. Hence, it was essential to investigate the conversion of α-terpinene and selectivity of the products at different temperatures. This study was done in *experiment 164*.

In this experiment 25 mM solution of α-terpinene was investigated at several temperatures in the range from –3.0°C to +41.0°C. At temperatures below –3.0°C experiments were not carried out because the internal standard hexadecane crystallised on the reaction plate. The experiments were not carried out also at temperatures higher than +41.0°C because isopropanol and α-terpinene began to evaporate at these temperatures. In *experiment 164* all reaction parameters were as previous with a flow rate preset to 0.5 ml/min and was kept constant within the experiment. Temperature of the reaction was defined by the temperature of the coolant and was adjusted via the cryostat. Ethanol was utilized as the cooling liquid instead of water in this experiment. Ethanol was continuously circulated through the heat exchanger positioned on the back side of the reaction plate thus providing the uniform temperature distribution.

Results achieved in *experiment 164* showed that the temperature change from –3.0°C to +41.0°C did not affect the efficiency of the reaction (Table 43). The conversion of α-terpinene was in the narrow range of 32–36% at all examined temperatures. Ascaridole yields and space time yields were also the same. Selectivity of the side product *p*-cymene was stable and was 4%. The only parameter that was affected by temperature was ascaridole selectivity. Somewhat higher ascaridole selectivity of 75–77% was established for temperatures from 10°C to 20°C. At temperatures below 9°C and above 22°C ascaridole selectivity was lower and was 66–69% (Figure 73).

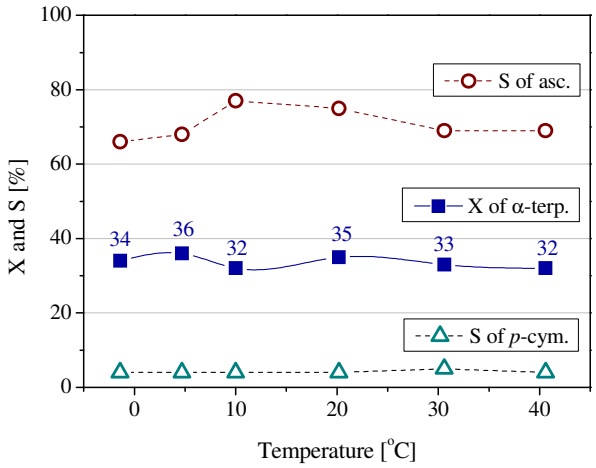


Figure 73: Conversion of α-terpinene and selectivity of ascaridole and *p*-cymene vs. different temperatures

Table 43: Reaction efficiency parameters vs. different temperatures

Inlet t, [°C]	Outlet t, [°C]	$X_{\alpha\text{-terp}}$, [%][a,b]	S_{asc}, [%][a,c]	$S_{p\text{-cym}}$, [%][a,c]	Y_{asc}, [%][a,d]	STY, [mol L^{-1} h^{-1}][e]
–2.4	+0.3	34	66	4	22	1.7
+3.7	+5.7	36	68	4	25	1.9
+9.3	+10.6	32	77	4	25	2.0
+19.6	+20.7	35	75	4	26	2.4
+30.7	+30.4	33	69	5	23	2.3
+41.0	+40.1	32	69	4	22	2.4

[a] Determined by GC area analysis; [b] calculated using equation 6; [c] calculated using equation 7; [d] calculated using equation 8; [e] calculated using equation 9

In *experiment 165* the impact of temperature on ascaridole synthesis was further studied. A 25 mM solution of α-terpinene was investigated with different flow rates at 0°C. Results achieved in *experiment 165* were compared with the results achieved in *experiment 149* (Table 44). In *experiment 165* all reaction parameters except temperature were the same as in *experiment 149*. As can be seen in Figure 74 the conversion of α-terpinene again was not affected by temperature and gradually decreased with the increase of flow rate. In contrast to the graphs presented in Figures 58, 60, 62, 64 and 71 the graphs in Figure 74 represents the dependency between α-terpinene conversion and solution flow rate instead of residence time, because the same solution flow rate corresponds for different residence times at different temperatures.

At a temperature of 0°C selectivity of ascaridole was about 10% lower compared to the ascaridole selectivity at a temperature of 20°C. Selectivity of *p*-cymene showed the opposite tendency. At a temperature of 0°C it was higher and was 4% while at a temperature of 20°C selectivity of *p*-cymene was only 1% (Figure 75, Table 44). Significantly lower ascaridole selectivity at a temperature of 0°C caused lower ascaridole yields and space time yields. For example, ascaridole space time yields were about 1 mol L^{-1} h^{-1} lower at flow rates of 0.5 ml/min and 0.3 ml/min and temperature at 0°C compared to the ascaridole space time yields at the same flow rates at 20°C (Table 44).

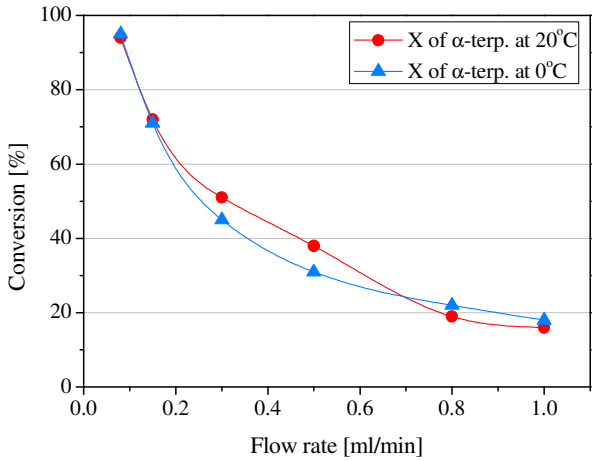


Figure 74: Conversion of α-terpinene vs. flow rate at temperature of 0°C and 20°C

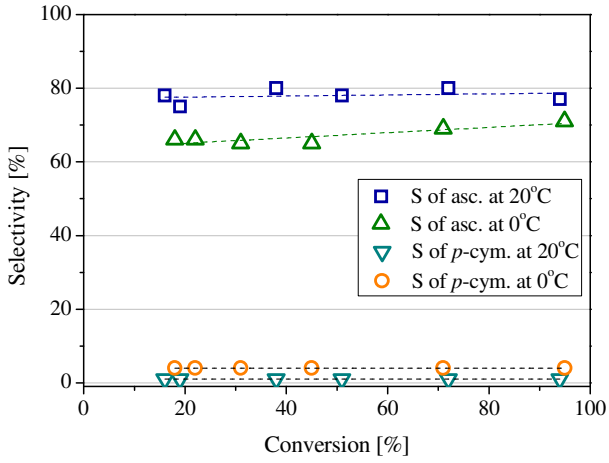


Figure 75: Selectivity of ascaridole and *p*-cymene vs. α-terpinene conversion at temperature of 0°C and 20°C

Table 44: Reaction efficiency parameters established for the experiments carried out at temperature of 0°C and 20°C

Flow rate [ml/min]	$X_{\alpha\text{-terp}}$, [%][a,b]		S_{asc}, [%][a,c]		$S_{p\text{-cym}}$, [%][a,c]		Y_{asc}, [%][a,d]		STY, [mol L^{-1} h^{-1}][e]	
	0°C	20°C	0°C	20°C	0°C	20°C	0°C	20°C	0°C	20°C
1	18	16	66	78	4	1	12	12	1.4	1.7
0.8	22	19	66	75	4	1	13	14	1.4	1.7
0.5	31	38	65	80	4	1	20	31	1.5	2.6
0.3	45	51	65	78	4	1	28	40	1.5	2.5
0.15	71	72	69	80	4	1	49	58	1.6	2.2
0.08	95	94	71	77	4	1	69	72	1.4	1.9

[a] Determined by GC area analysis; [b] calculated using equation 6; [c] calculated using equation 7; [d] calculated using equation 8; [e] calculated using equation 9

6.3.9 Effect of the light source on the ascaridole synthesis

The domestic fluorescent lamp with a total optical power of 18 W was used for the irradiation in the above described *experiments 149-165*. Hence in *experiment 166* the influence of another energy saving light source on the reaction efficiency was studied. An array of 60 white LEDs with a total optical power of 3 W was used for the irradiation in *experiment 166*. Other reaction parameters were the same as in *experiment 150.* Residence time was set to 7 sec, 13 sec and 32 sec. Results achieved in *experiment 166* were compared with the appropriate results obtained in *experiment 150* and are presented in Figures 76–77 and summarised in Table 45.

As can be observed from Figure 76 the conversion of α-terpinene was larger when a fluorescent lamp was used for irradiation compared to the conversion of α-terpinene when an array of white LEDs was used. The conversion of α-terpinene was larger by 3% at a residence time of 7 sec, by 8% at a residence time of 13 sec and by 24% at a residence time of 32 sec, respectively (Table 45). Selectivity of the main product ascaridole of 64–72% was essentially lower when white LEDs were used compared to the ascaridole selectivity of 84–87% when a fluorescent lamp was applied for irradiation. Selectivity of *p*-cymene was not affected by the type of light source.

Noticeably lower α-terpinene conversion and ascaridole selectivity induced lower ascaridole yields and ascaridole space time yields in the experiment with white LEDs. Thus ascaridole yields were two times lower and ascaridole space time yields were about 1 mol L^{-1} h^{-1} lower in this experiment compared to the previous test with fluorescent lamp (Table 45).

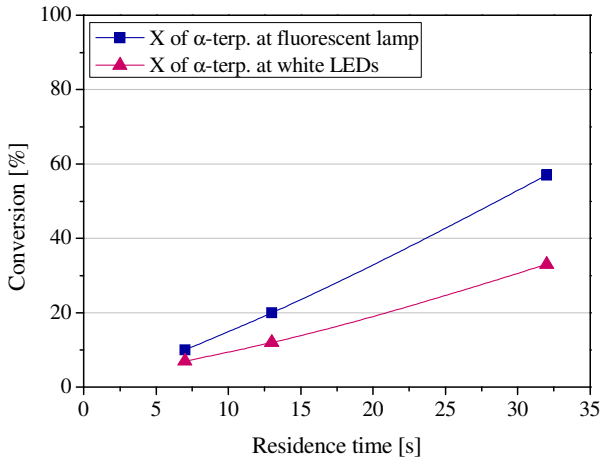


Figure 76: Conversion of α-terpinene vs. residence time at different light sources

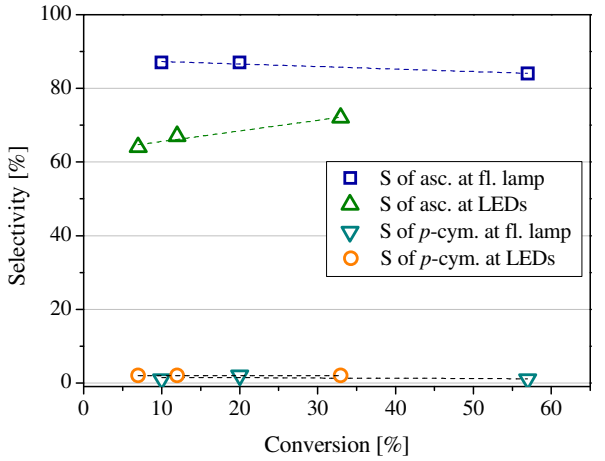


Figure 77: Selectivity of ascaridole and *p*-cymene vs. α-terpinene conversion at different light sources

Table 45: Reaction efficiency parameters established for the experiments carried out with different light sources

Residence time, [s]	$X_{\alpha\text{-terp}}$, [%][a,b]		S_{asc}, [%][a,c]		$S_{p\text{-cym}}$, [%][a,c]		Y_{asc}, [%][a,d]		STY, [mol L^{-1} h^{-1}][e]	
	FL[f]	LED	FL	LED	FL	LED	FL	LED	FL	LED
7	10	7	87	64	1	2	8	4	2.1	1.1
13	20	12	87	67	2	2	17	8	2.1	1.0
32	57	33	84	72	1	2	48	24	2.4	1.2

[a] Determined by GC area analysis; [b] calculated using equation 6; [c] calculated using equation 7; [d] calculated using equation 8; [e] calculated using equation 9; [f] fluorescent lamp

6.3.10 Stability study of the synthesised ascaridole

Due to the endoperoxide nature of ascaridole it was important to check its stability with time. This test was done in *experiment 167*. Three samples of collected products were randomly selected and left on the working desk for 10 days. Samples were affected only by ambient light and room temperature. After 10 days these samples were checked by GC-MS and the obtained results were compared with the results obtained directly after the experiment (Table 46).

Sample 1 was the product collected at residence time of 32 sec in *experiment 155*.

Sample 2 was the product collected at residence time of 32 sec in *experiment 149*.

Sample 3 was the product collected at residence time of 13 sec and α-terpinene concentration of 10 mM in *experiment 158*.

Table 46: Comparison of the experimental results obtained directly after the experiment and results reviewed 10 days later

Sample	Time period	$X_{\alpha\text{-terp}}$, [%][a,b]	S_{asc}, [%][a,c]	$S_{p\text{-cym}}$, [%][a,c]	Y_{asc}, [%][a,d]
1	After exp.	100	72	1	71
	After 10 days	100	70	4	69
2	After exp.	94	77	1	72
	After 10 days	100	70	4	69
3	After exp.	97	71	3	70
	After 10 days	100	62	6	61

[a] Determined by GC area analysis; [b] calculated using equation 6; [c] calculated using equation 7; [d] calculated using equation 8

Results presented in Table 46 clearly show that α-terpinene and ascaridole are quite sensitive to ambient light. In samples 2 and 3 α-terpinene conversion was incomplete after the experiment, but the reaction continued to progress when samples were exposed to ambient light and complete conversion of α-terpinene of 100% was observed in the samples after 10 days. However despite the complete conversion of α-terpinene the interested product ascaridole underwent some changes after 10 days. Thus ascaridole selectivity and consequently ascaridole yield decreased by 2–9% after it was exposed to ambient light for 10 days. At the same time selectivity of the by-product *p*-cymene increased by 3% within 10 days. Consequently, it could be suggested that *p*-cymene is a photodecomposition product of ascaridole as no other secondary products were detected by the applied GC-MS method.

6.3.11 Optimised experimental procedure for ascaridole synthesis in the falling film microreactor

Based on the above reported results, the following experimental conditions could be considered as the most favourable: concentration of α-terpinene of 50 mM (685 mg per 100 ml), concentration of sensitizer rose bengal of 0.98 mM, oxygen (or air) a gas phase flow rate of 10 or 50 ml/min, isopropanol with 10 Vol-% of water as solvent, solution flow rate of 0.08 ml/min which corresponded to a residence time of 32 sec, domestic fluorescent lamp as a light source and an experimental temperature from 10°C to 20°C. Under such experimental conditions ascaridole was synthesised in the amount of 478 mg (2.84 mmol) after one single run and the product space time yield of 3.2 mol L^{-1} h^{-1} was established.

6.4 Investigation of ascaridole synthesis in the batch system

The falling film microreactor is an example of a microfluidic system with continuous flow process. However in conventional photochemistry the batch reactors are generally used. To demonstrate the difference of efficiency of ascaridole synthesis in both systems we assembled a simple batch set-up and applied it for the same reaction procedure as the falling film microreactor.

6.4.1 Experimental batch set-up

The main parts of our batch set-up were Quartz Schlenk flask **1** ($\lambda \geq 200$ nm) and the same domestic fluorescent lamp **3** (Figure 78). Schlenk flask (30 mm inner ∅) with the total volume of 50 ml was used as the reaction vessel. Pyrex cold finger (24 mm outer ∅) was inserted into the Schlenk flask to create a "thinner" solution layer of 6 mm instead of 30 mm for better light penetration. Another role of the cold finger was to keep the experimental temperature constant. Cold water was continuously circulated through the cold finger and provided smooth temperature distribution. Reaction mixture was placed into the Schlenk flask and was irradiated by fluorescent lamp with total optical power of 18 W. The solution was constantly saturated with oxygen through a PTFE tubing **4**. The continuous bubbling of oxygen also ensured solution mixing. Schlenk flask wasn't a closed system due to the heterogeneous nature of ascaridole synthesis. To prevent any losses of solvent or possible volatile products one open side-neck of the flask was connected to the condenser **6** and the condenser was additionally placed into the beaker with crushed ice **7**. Second open side-neck of the flask was

tightly covered with parafilm. After certain time periods the samples of irradiated solution were taken for GC-MS analysis using 2 ml sampling syringe **8**. During the experiment the Schlenk flask together with the fluorescent lamp were protected from the surroundings by an aluminium shield (not shown on the Figure 78).

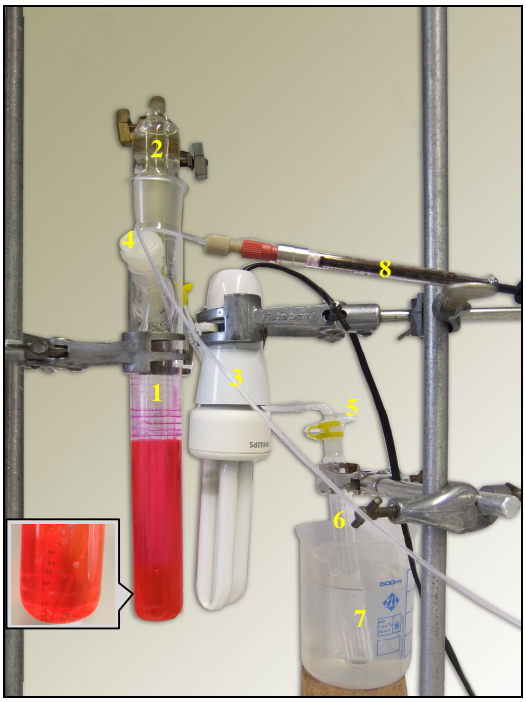


Figure 78: Batch set-up for photooxygenation reactions: **1** – Quartz Schlenk flask; **2** – Pyrex cold finger; **3** – fluorescent lamp; **4** – oxygen inlet; **5** – gas outlet; **6** – condenser; **7** – beaker with crushed ice; **8** – syringe for sampling

6.4.2 Efficiency of ascaridole synthesis in the batch set-up

Ascaridole synthesis in the Quartz Schlenk flask was studied in *experiment 168*. For this experiment a 25 mM solution of α-terpinene with 0.49 mM concentration of rose bengal was prepared. 50 ml of this solution were placed into the Schlenk flask and were irradiated by the fluorescent lamp for 2 hours. During the irradiation time the experimental solution was continuously purged with pure oxygen at a flow rate of 10 ml/min. The progress of the reaction was controlled by CG-MS and solution samples were taken for analysis every 15 min within the first hour and every half an hour during the second hour. Results obtained in *experiment 168* showed that photooxygenation of α-terpinene proceeded relatively fast and high conversion of α-terpinene of 79% was achieved after 15 min and the reaction was completed after 30 min (Table 47). Further irradiation of the solution for up to 2 hours had no influence on the reaction output. Selectivity of the desired product ascaridole was comparatively high and was about 78–

80% (Table 47). It is important to note that selectivity of ascaridole was not affected by the irradiation time. Selectivity of the by-product *p*-cymene was generally low and less than 2%. Due to the high ascaridole selectivity its yield remained high at about 79% at a prolonged residence time of over 30 min. The ascaridole space time yield was 0.9 mol L^{-1} h^{-1} at an irradiation time of 15 min and 1.2 mol L^{-1} h^{-1} at irradiation time of 30 min and longer (Table 47).

Table 47: Reaction efficiency parameters established for the experiments in the batch set-up

Residence time, [min]	$X_{\alpha\text{-terp}}$, [%][a,b]	S_{asc}, [%][a,c]	$S_{p\text{-cym}}$, [%][a,c]	Y_{asc}, [%][a,d]	STY, [mol L^{-1} h^{-1}][e]
15	79	78	2	62	0.9
30	100	80	2	79	1.2
45–120	100	78–80	2	77–79	1.2

[a] Determined by GC area analysis; [b] calculated using equation 6; [c] calculated using equation 7; [d] calculated using equation 8; [e] calculated using equation 9 and assuming flow rate of the liquid of 50 ml/min

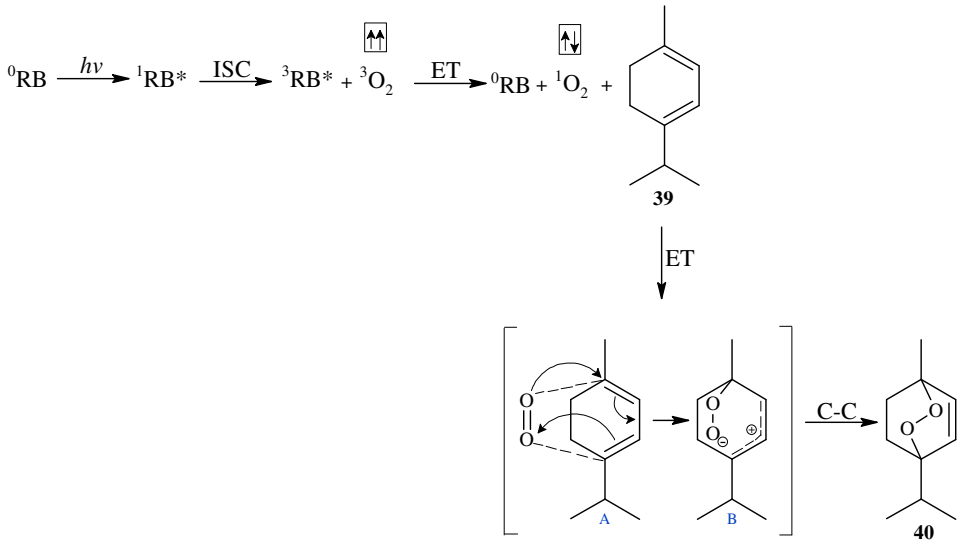
When compared to the results obtained in the batch system (*experiment 168*) with the results obtained for the same experimental solution in the falling film microreactor (*experiment 150*) it can be observed that photooxygenation of α-terpinene proceeded more efficiently under microflow conditions. Thus, 94% conversion of α-terpinene was achieved in the falling film microreactor at a residence time of only 32 sec while in the batch Schlenk flask the conversion of α-terpinene was 79% and was reached only after irradiation for 15 min. Moreover, ascaridole synthesis with the product space time yield of 1.7–2.7 mol L^{-1} h^{-1} was twice as productive in the falling film microreactor compared to the batch system where ascaridole space time yield was 0.9–1.2 mol L^{-1} h^{-1}. Selectivity of the products was not affected by the type of experimental system and remained reasonably high of 75–80% in both cases.

6.5 Discussions

6.5.1 Rose bengal sensitised photooxygenation of α-terpinene (synthesis of ascaridole)

Photooxidation of α-terpinene is an example of a photo-Diels-Alder reaction, where singlet oxygen acts as a dienophile. This reaction proceeds via [4 + 2] cycloaddition of singlet oxygen to α-terpinene **39** (Scheme 57) and generates stable endoperoxide

ascaridole **40** as a main product. In the falling film microreactor ascaridole was produced with very high selectivity of up to 89% at residence time of several seconds. The start point of this reaction is formation of singlet oxygen by electron transfer from triplet exited photosensitizer rose bengal. Singlet oxygen is one of the most reactive species of oxygen, it is relatively stable and has lifetime of 22 seconds in the isopropyl alcohol.[230,243] Singlet oxygen interacts with α-terpinene via an intermediate exciplex *A* and zwitterionic species *B*, which further results a C-C bond arrangement and ascaridole formation.

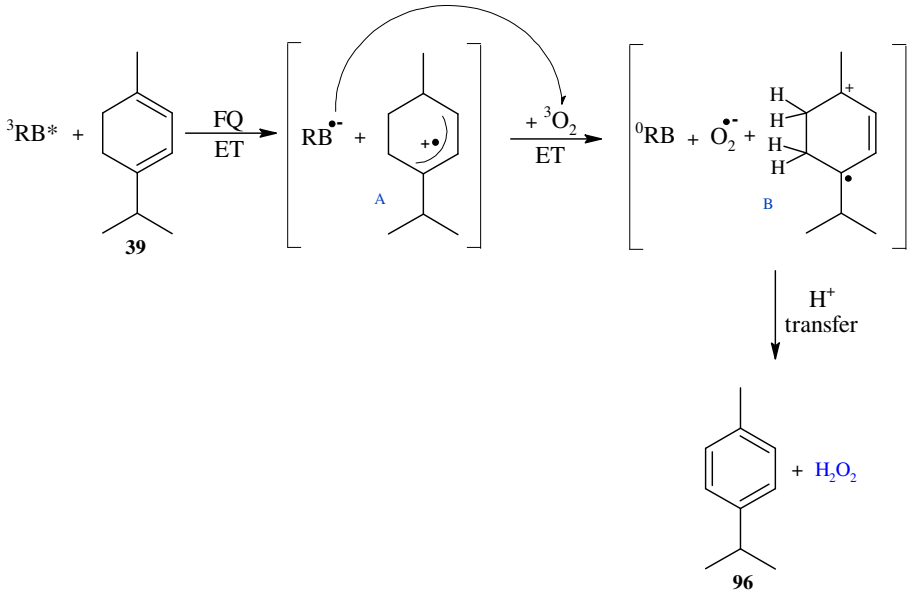


Scheme 57: Mechanism of rose bengal sensitised photooxygenation of α-terpinene (synthesis of ascaridole)

In all examined cases, despite the high ascaridole selectivity the formation of undesired side product *p*-cymene **96** was also observed. The rate of its formation was low (1–4%) and steady, but essential. *Para*-cymene is an aromatic hydrocarbon and the mechanistic scenario for its formation differs from that for ascaridole. It could be proposed that formation of *p*-cymene proceeds via a radical pathway (Scheme 58), which was detailed by Chen[231] (for perylene diimide sensitised photooxygenation of α-terpinene) and by Karapire[232] (for 5,6-benzocoumarin sensitised photooxygenation of α-terpinene).

The initial step in this mechanism might be a fluorescence quenching of rose bengal by α-terpinene, since it had been shown several years ago that conjugated dienes such as α-terpinene quench the fluorescence of aromatic hydrocarbons by an "exciplex" mechanism.[244] The fluorescence quenching should produce an exciplex or a contact radical ion-pair *A*, which are further attacked by triplet oxygen. Following electron transfer creates superoxide or hydroperoxyl radical that after proton transfer within the

exciplex *B* producing hydrogen peroxide and concomitantly *p*-cymene **96** is formed (Scheme 58). However, the rate of this radical pathway is very low due to rapid decay of the exciplex complexes, which mainly results in regeneration of the ground states of sensitizer and α-terpinene.



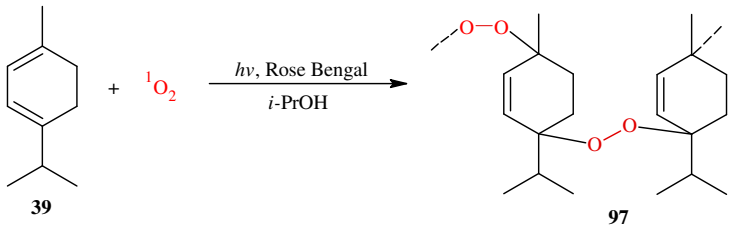
Scheme 58: Mechanism of *p*-cymene formation within α-terpinene photooxygenation

The stable and low selectivity of *p*-cymene formation within the photooxygenation of α-terpinene (selectivity-conversion plots on figures 59, 61, 63, 65, 67, 69, 72, 73, 75 and 77) along with the feasibility of *p*-cymene formation via a radical pathway might indicate that the formation of *p*-cymene is a parallel reaction and not involved in the ascaridole synthesis.

It has also been suggested in the literature that the origin of *p*-cymene results as a decomposition product of ascaridole.[229] Our results from the stability study of ascaridole (Table 46) supports this hypothesis.

It is also important to mention that despite the high ascaridole selectivity and notable *p*-cymene selectivity within the photooxygenation of α-terpinene the absolute conversion of α-terpinene exclusively to the determined products wasn't observed. The difference between the amount of reacted α-terpinene and the sum of products detected by GC was about from 10% to 20% (sum of ascaridole and p-cymene selectivity was always below 100%). This difference could be partially explained by the loss of α-terpinene through the continuous gas flow. However, in *experiment 161* it has been shown that the rate of such loss is only 4%. Therefore, suggested by Günther and co-workers [245] formation of polymeric peroxides within the photooxygenation of α-terpinene (Scheme 59) might be

a plausible explanation. Nevertheless, this concept required additional verification because the GC method used for product analysis was inappropriate to detect formation of polymers.

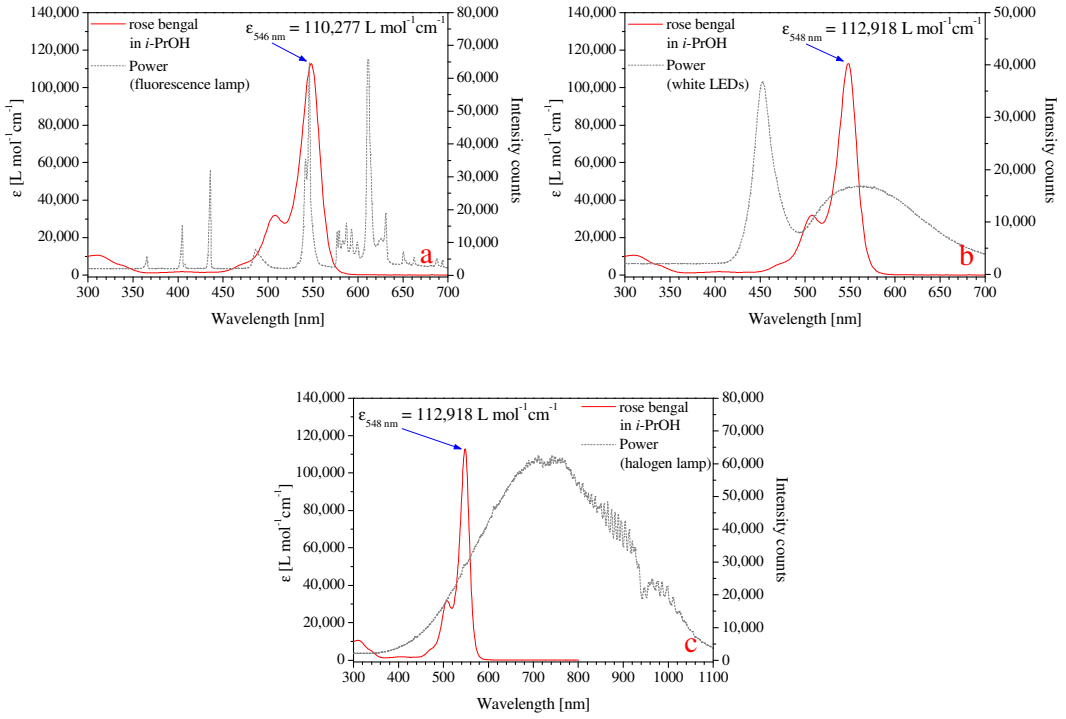


39 **97**

Scheme 59: Formation of polymeric peroxides within the photooxygenation of α-terpinene

6.5.2 Wavelength matching and light penetration for the experiments of ascaridole synthesis

In first time in the record of ascaridole synthesis the domestic fluorescent lamp was used as a light source for the activation of the photosensitizer rose bengal.



Figures 79: Absorption spectrum of rose bengal matched with the emission spectrum of: a) fluorescence lamp (18W), b) white LED panel (3 W), c) halogen lamp (550 W)

The emission spectrum of a fluorescent lamp perfectly matches the main absorption band of rose bengal (λ_{max} = 548 nm, Figure 79a). The white LED panel and frequently used in the batch experiments halogen lamp (Schlenk flasks) showed a broader coverage but their main emission did not match that well with the absorption maxima of the sensitizer (Figures 79b and 79c).

As has been mentioned above the sensitizer rose bengal has a very strong absorption of visible light. The extinction coefficient of rose bengal in isopropanol was 112918 L $mol^{-1}cm^{-1}$ at 548 nm and 110277 L $mol^{-1}cm^{-1}$ at 546 nm. Subsequently the light penetration profiles were calculated for the applied concentrations of rose bengal of 0.49 mM, 0.98 mM and 0.25 mM at 546 nm. The generated graphs of light penetration were compared with the pathlength of the created falling film, the used reactor microchannel and the Schlenk tube (Figure 80). Due to the inserted cold finger and continuous solution mixing by the gas bubble flow the effective pathlength of the Schlenk flask was reduced to 3 mm. The established results showed that relatively low concentrations of rose bengal (0.49 mM) caused the complete attenuation of light within just 0.8 mm of the solution layer. At twice this concentration of rose bengal (0.98 mM) resulted in entire light attenuation within 0.4 mm and at a rose bengal concentration of 0.25 mM caused light attenuation within 1.6 mm of the solution layer, respectively. Thus, for all used concentrations of rose bengal, the optimal light transmission was ensured only by the falling film of solution inside of the reactor microchannels.

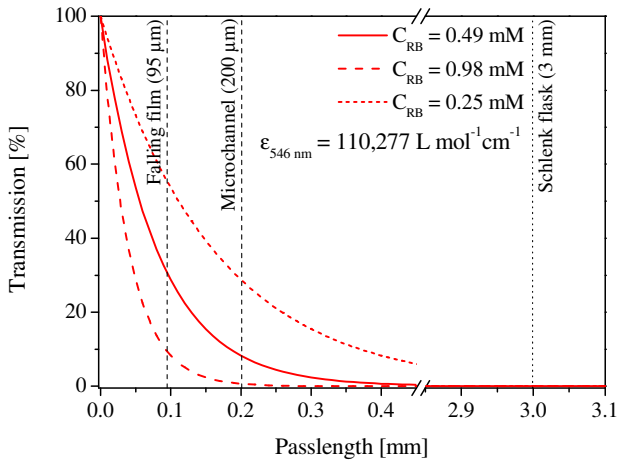


Figure 80: Light-penetration profiles for 0.49 mM, 0.98 mM and 0.25 mM solutions of rose bengal at 546 nm. The vertical lines represent the pathlength of the thickest liquid film at flow rate of 1 ml/min (--), the depth of falling film reactor microchannel (--) and effective pathlength of the Schlenk flask (⋯)

6.5.3 Irradiated area-to-volume ratio of experimental set-ups involved in ascaridole synthesis

The superior performance of ascaridole synthesis in the falling film microreactor was partially explained by the effective light penetration through the created fluid film. The other important benefit provided by the microreactor is the large irradiated surface-to-volume ratio. In the falling film microreactor, 32 parallel microchannels of 600 μm wide and 55 mm long formed surface of 10.56 cm^2 and less than 100 μl of solution were generally spread over this area creating a surface-to-volume ratio of several thousands (10560–24558 m^2 m^{-3}) which is considerably larger than just several hundreds for the irradiated surface-to-volume ratio of a conventional Schlenk flask (330 m^2 m^{-3}). The calculated numbers of irradiated surface-to-volume ratio and other technical details of both experimental set-ups are presented in Table 48.

Table 48: Technical details of the falling film microreactor and Quartz Schlenk flask

Parameter	Falling film MR	Schlenk flask
Aperture, [cm^2]	15.40[a]	164.85[b]
Irradiated area, [cm^2]	10.56[c]	164.85
Irradiated volume, [cm^3]	0.043 – 0.1	50
Irradiated area / volume ratio, [m^2 m^{-3}]	24558 – 10560	330
Lamp power, [W]	18	18
Lamp power per aperture, [W cm^{-2}]	1.17	0.11
Lamp power per irradiated area, [W cm^{-2}]	1.70	0.11

[a] Viewing window; [b] Assuming a cylindrical geometry, the liquid height in Quartz Schlenk flask with inserted cold finger was 17.5 cm; [c] 32 microchannels

In the falling film microreactor 1.17 W and 1.70 W of lamp power were provided per every square centimetre of irradiated area, while in the Schlenk flask every square centimetre of irradiated area received only 0.11 W of lamp power (Table 48). These results show that the Schlenk flask solution didn't received sufficient irradiation energy and consequently our batch system didn't have a balance between the scale of the reaction vessel and the applied light source.

However, in this our work we were mainly concentrated to establish the dependency between products selectivity and parameters of experimental procedure rather than to compare two different systems. Therefore the work done in the Schlenk flask still represents valuable results.

6.5.4 Energy efficiencies of the light sources used for ascaridole synthesis in the falling film microreactor

In the falling film microreactor ascaridole synthesis was carried out mainly with the fluorescent bulb and one experiment was done with the white LED panel. Achieved results showed that with the fluorescent bulb ascaridole synthesis proceeded more efficiently in respect of α-terpinene conversion, products selectivity and ascaridole yield. However, the calculated data of energy efficiency for the identical experiments just with different light sources showed that irradiation provided by the white LED panel was three times more efficiently utilized for the ascaridole synthesis compared to the fluorescent bulb (Table 49). Energy efficiency of LED array was 889 % W^{-1} h^{-1} and concerning to the irradiated area energy efficiency was 84.2 % W^{-1} h^{-1} cm^{-2}. These somewhat unexpected numbers could be explained by the relatively high ascaridole yield of 24% granted by the comparatively weak optical power of LED panel (3W). Thus six times more powerful fluorescent bulb ensured only two times higher ascaridole yield of 48% under identical conditions.

Table 49: Energy efficiencies of the falling film microreactor irradiated by the fluorescent lamp and LED panel

Light source power, [W]	Residence time, [s]	$Y_{asc,}$ [%][a,b]	W h[c]	Energy efficiencies	
				[% W^{-1} h^{-1}][d]	[% W^{-1} h^{-1} cm^{-2}][e]
18 (fl. lamp)	32	48	0.160	300	28.4
3 (LEDs)	32	24	0.027	889	84.2

[a] Determined by GC area analysis; [b] calculated using equation 8; [c] lamp power × irradiation time; [d] ascaridole yield / (lamp power × irradiation time); [e] ascaridole yield / (lamp power × irradiation time × irradiated area)

6.5.5 Interfacial area of experimental set-ups involved in ascaridole synthesis

The efficiency of heterogeneous reactions activated by light depends not only from the scale of solution area exposed to the light but also from the size of gas-liquid contact area. The falling film microreactor has an interfacial area of 10530–24438 m^2 m^{-3} (Table 50). Such huge area was created by 32 channels with microdimensions (600 μm width and 55 mm length) and was calculated according to the following equation *(10)*:

$$\alpha = \frac{A}{V_{liq.film}} \qquad (10)$$

where A = surface area of film, $V_{liq.film}$ = film volume.

As can be seen from the Table 50 the scale of interfacial area is dependent of the liquid phase flow rate and increase when fluid flow rate decrease. Consequently, the lowest fluid flow rate of 0.08 ml/min corresponds not only for the prolonged residence time of 32 seconds but also for the largest interfacial area of 24438 $m^2 m^{-3}$. Respectively, at the highest fluid flow rate of 1 ml/min interfacial area is the smallest (10530 m^2 m^{-3}). Therefore the reasonably high α-terpinene conversions of 32–100% (Table 36) achieved in the falling film microreactor after residence time of just 32 seconds could be additionally explained by the contributed influence of huge interfacial area. The decline of ascaridole selectivity and enlarged formation of *p*-cymene at temperature about 0°C (Table 44) could be also fairly referred to the decrease of interfacial area at temperature about 0°C. However, at the decrease of temperature residence time shows opposite tendency. The same fluid flow rate defines shorted residence time at temperature about 20°C and longer residence time at temperature about 0°C (Table 50). Based on that it might be indicated that at temperature about 20°C other to photochemical processes such as mass transfer and diffusion (flow processes) also take place.

Table 50: Interfacial areas and residence times vs. fluid flow rates at temperature of 20°C and 0°C

Flow rate, [ml/min]	Residence time at 20°C, [s][a]	Interfacial area at 20°C, [m^2/m^3][b]	Residence time at 0°C, [s][a]	Interfacial area at 0°C, [m^2/m^3][b]
1	6	10530	7	8685
0.8	7	11343	8	9356
0.5	10	13267	12	10943
0.3	13	15730	16	12974
0.15	21	19818	26	16346
0.08	32	24438	39	20157

[a] Calculated using equation 3; [b] calculated using equation 10

An example of established dependency between temperature, residence time and interfacial area for the constant fluid flow rate of 0.5 ml/min is provided in the Table 51. The change of temperature is in the same range as was in the *experiment 164*. As can be seen from the presented data, at gradual temperature change from 0°C to 40°C the interfacial area steady increased from 10943 $m^2 m^{-3}$ to 14464 $m^2 m^{-3}$. The residence time was less responsive for the temperature change and decreased only by 1 second per every 10°C. This notion can somewhat explain the weak influence of temperature on the α-terpinene conversion (Table 43). At lower temperatures the gas-liquid contact area was smaller but interaction proceeded for longer time and conversely for higher

temperatures. Such statement can also clarify somewhat higher ascaridole selectivity of 75–77% at temperatures between 10°C and 20°C, because this temperature range has optimal value of both parameters, i.e. optimal residence time and optimal interfacial area.

Table 51: Interfacial areas and residence times vs. experimental temperatures at constant fluid flow rate of 0.5 ml/min

Temperature, [°C]	Flow rate, [ml/min]	Residence time, [s][a]	Interfacial area, [m^2/m^3][b]
0	0.5	12	10943
3	0.5	11	11263
5	0.5	11	11482
8	0.5	11	11819
18	0.5	10	13012
20	0.5	10	13265
29	0.5	9	14464
40	0.5	8	16077

[a] Calculated using equation 3; [b] calculated using equation 10

6.6 Summary

The rose bengal sensitized photooxygenation of α-terpinene in the falling film microreactor represents a new approach for the preparative scale synthesis of ascaridole. The established productivity of ascaridole synthesis in the falling film microreactor was about 2.5–3.2 mol L^{-1} h^{-1} which can worthily compete with existing techniques.

For the first time in the study of ascaridole synthesis the relationship between ascaridole selectivity and experimental parameters, such as α-terpinene concentration, rose bengal concentration, oxygen concentration, oxygen flow rate, residence time, temperature and light source have been established and discussed. The expressed dependencies represent a new valuable tool about the efficiency of photooxygenation processes. It has been determined that selectivity of ascaridole synthesis in the falling film microreactor was relatively high at 89% and was notably affected by the temperatures below 9°C and above 22°C and higher oxygen flow rate of 50 ml/min. Application of a white LED panel instead of a fluorescent lamp as light source also resulted in loss of ascaridole selectivity.

The potential efficiency of ascaridole synthesis in the falling film microreactor has been additionally described by the unique technical features of the microreactor itself. These distinctive characteristics included large interfacial area, huge irradiated surface-to-volume ratio of about 20000 m^2 m^{-3} and very efficient light penetration through the created thin film of solution. Owing to these technical features it has been shown that in the falling film microreactor it is possible to work with up to 10 times higher solution concentrations and up to two times higher concentration of chromophoric reagent.

In general, the reported study of dye sensitized photooxygenation of α-terpinene clearly demonstrates that ascaridole synthesis in the falling film microreactor can serve as a powerful and highly selective alternative to the existing batch processes and thermal oxidation with metal oxides. Moreover, the oxygenation processes in microreactor are considerably safer and most environmentally friendly as the formation and storage of large volumes of oxygenated solvent is entirely avoided. The volume of oxygenated solvent inside the microreactor was below 150 microlitres.

Chapter 7

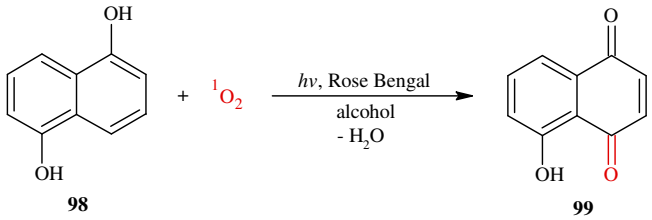
Dye sensitised photooxygenation of 1,5-dihydroxynaphthalene – synthesis of Juglone

7.1 Introduction

The superb results obtained for ascaridole synthesis via rose bengal sensitised photooxygenation of α-terpinene in a falling film microreactor induced our further investigation in this area. The synthesis of Juglone via dye sensitised photooxygenation of 1,5-dihydroxynaphthalene became a new subject of our study.[246,247] Juglone is a natural product which serves as a useful intermediate to quinonoid bioactive compounds.[248–254] Juglone is most commonly synthesized through Jones oxidation with chromic acid but this procedure gives low yields (<10%) and suffers from poor reproducibility and hazardous reaction conditions.[152,153,255] The dye-sensitized photooxygenation represents an alternative pathway and gives the desired product in good to high yields.[256,257] In addition, photooxygenation reactions can be carried out with sunlight which makes this transformations especially attractive for the growing field of environmentally friendly chemistry.[94,220,221]

At the beginning of our study, the literature established experimental procedures of Juglone synthesis[256,257] were transferred to the continuous flow system falling film microreactor. Unexpectedly, it was found that falling film microreactor is not suitable for the photooxygenation of 1,5-dihydroxynaphthalene because this reaction required prolonged residence times of more than 1 hour (compared to max 32 sec in the FFMR) and the generated product Juglone interacted with the metal material of microreactor base and connections.

Accordingly to the all previous discussions about the weaknesses of batch systems and benefits of microflow system, in case of Juglone synthesis a new challenge arose. To address this difficulty a new slug flow column reactor was designed. This reactor implements generation of microfilm in the narrow glass tube. To demonstrate the suitability of bubble column reactor for photooxygenation reactions it was applied for a series of tests using Juglone synthesis as model reaction (Scheme 60).



Scheme 60: Synthesis of Juglone via photooxygenation of 1,5-dihydroxynaphthalene

7.2 Synthesis of Juglone in the falling film microreactor using fluorescent lamp

7.2.1 Experimental set-up

Similar to the experimental set-up established at the Leibniz-Institut of Catalysis (Rostock), the falling film microreactor set-up was constructed in our laboratory at Dublin City University (Figure 81).

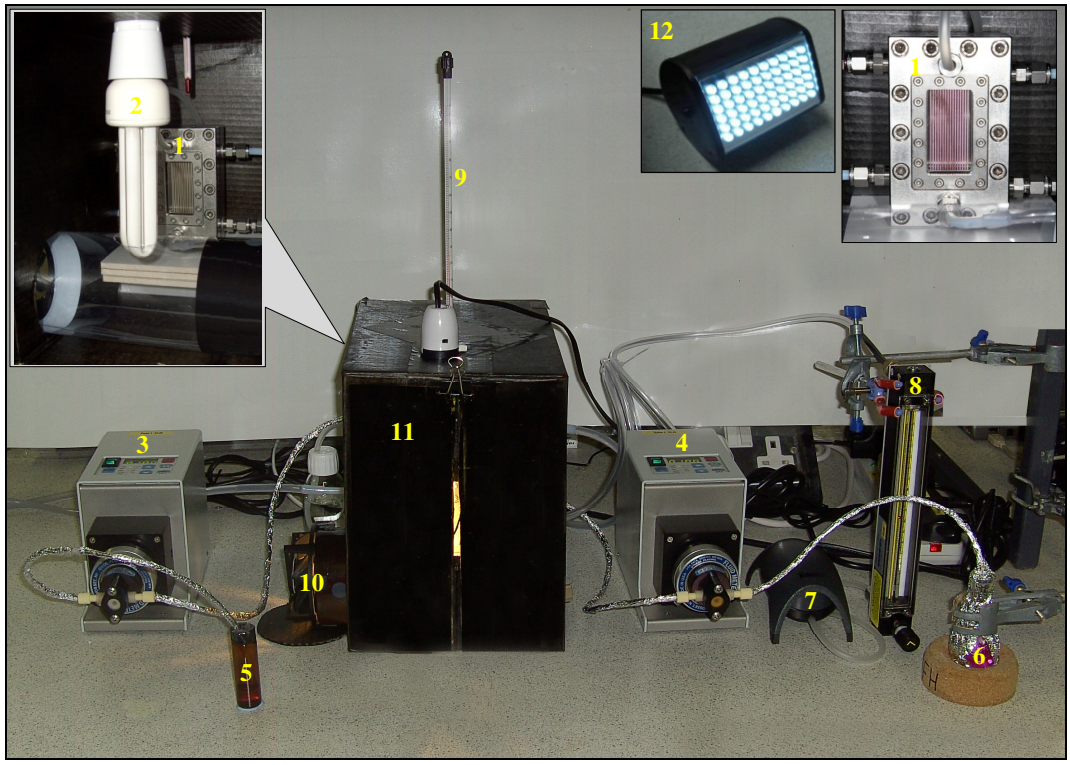


Figure 81: Falling film microreactor setup (in DCU): **1** – falling film microreactor; **2** – fluorescent lamp; **3** – programmable rotary pump; **4** – programmable rotary pump; **5** – amber vial; **6** – covered round bottom flask; **7** – air pump; **8 –** flow-meter; **9** – thermometer; **10** – cooling fan; **11** – protected box; **12** – white LEDs array

The main parts of this setup were placed in a black box **11** to avoid any interference from laboratory light. In addition, all tubing was wrapped with aluminium foil. The box hosts the actual falling film reactor **1** (the same model as used in the Rostock setup) together with the light source **2**. The front window of the falling film reactor (55 × 28 mm, H × W) is made of quartz glass ($\lambda \geq 200$ nm) and the reaction plate (FFMR – 07029, 316 Ti) consists of 16 parallel channels with the dimensions 1200 µm width, 400 µm depth and 78 mm length. A fluorescence lamp **2** (Philips, 18 W) was placed in front of the falling film reactor at a distance of 10 cm from the window and was cooled using a small fan **10** and air tube. Alternatively, an array of 60 white LEDs **12** (total optical

power 3 W) was used. The reaction temperature inside the box was monitored using a standard thermometer **9**. The reaction mixture was drawn from an amber vial **5** by a programmable rotary pump **3**. A second programmable rotary pump **4** empties the reactor chamber and pumps the product mixture into a covered round bottom flask **6**. In the experiments, where recirculation was necessary, a short PTFE tube on the pump outlet side was replaced by a longer one, which was connected to the inlet of pump **3** and outlet of pump **4**. This technique created a closed circle allowing the reaction mixture to move in a loop until the necessary residence time was reached. Air flow was supplied using a simple electrical air pump **7** in combination with a flow-meter **8**.

7.2.2 Efficiency of Juglone synthesis in the falling film microreactor

In the falling film microreactor the photooxygenation of 1,5-dihydroxynaphthalene was investigated with two main fluid flow rates of 0.08 ml/min and 0.16 ml/min which corresponded residence time of 32 sec and 20 sec, respectively (Table 52). From the literature it is known that this transformation required prolonged residence time. A 32 sec was the maximum feasible residence time in the falling film microreactor after a single run. Therefore, to reach reasonable conversion rate, the reaction mixture was five or ten times recycled through the reactor microchannels while was additionally exposed to the light.

Table 52: Calculated data of residence time, film thickness, film volume and interfacial area for the applied flow rates

Flow rate, [ml/min]	Residence time, [s][a]	Film thickness, [µm][b]	Film volume, [µl][c]	Interfacial area, [m^2/m^3][d]
0.08	32	41	43	24438
0.16	20	52	54	19396

[a] calculated using equation 3; [b] calculated using equation 5; [c] calculated using equation 4; [d] calculated using equation 10

At the beginning, the synthesis of Juglone was carried out in the falling film microreactor using isopropanol as solvent and an energy-saving fluorescent lamp as light source (Table 53, *experiment 169*). The solution was recycled through the microreactor five times and total exposure time of 160 sec was reached. The poor conversion of diol **98** of 10% was achieved. Doubling the concentration of rose bengal gave two times higher conversion of **98** of 21% (*experiment 170*), but the sensitizer remained partially undissolved and threatened to crystallised inside of the microchannels and clog them. When the concentration of diol **98** and rose bengal was

halved, an 18% conversion of 1,5-dihydroxynaphthalene **98** to Juglone **99** were determined (*experiment 171*). Similar to our previous experience, the prepared experimental solutions had low transparency due to the poor solubility of rose bengal in the isopropanol. Therefore 10 vol-% of water was used as co-solvent again and fully transparent solution was obtained. On the next step, *experiment 169* was repeated, but with the aqueous isopropanol as solvent and the highest conversion of diol **98** of 31% was achieved (*experiment 172*). When the fluorescence lamp was replaced by an array of white LEDs the conversion of diol **98** dropped to 9% (*experiment 173*). This result could be explained by the lower power output of white LEDs (3 W vs. 18 W for the fluorescence lamp). In the final *experiment 174* flow rate of solution and number of cycles were doubled and prolonged residence time of 200 sec was offered. However, the efficiency of reaction was even lower. The conversion of diol **98** was just 8%. Such low reaction output at higher solution flow rate might be explained by the decrease of interfacial area (Table 52). In all above described experiments, air was used as source of oxygen and was supplied to the reaction chamber with a constant flow rate of 26.5 ml/min. All reactions proceeded with high selectivity and no other products could be detected by NMR analysis.

Table 53: Efficiency of Juglone synthesis in the falling film microreactor

Exp.	Solvent	Light source	1,5-DHN, [mmol/L]	RB, [mmol/L]	Flow rate, [ml/min]	Residence time, [s]	Conversion of 98, [%][a]
169	*i*-PrOH	Fluor. bulb	10	0.49	0.08	32×5^{b} (160^{c})	10
170	*i*-PrOH	Fluor. bulb	10	0.98	0.08	32×5^{b} (160^{c})	21
171	*i*-PrOH	Fluor. bulb	5	0.25	0.08	32×5^{b} (160^{c})	18
172	*i*-PrOH/H_2O (9:1)	Fluor. bulb	10	0.49	0.08	32×5^{b} (160^{c})	31
173	*i*-PrOH/H_2O (9:1)	LEDs	10	0.49	0.08	32×5^{b} (160^{c})	9
174	*i*-PrOH/H_2O (9:1)	LEDs	10	0.49	0.16	20×10^{b} (200^{c})	8

[a] Determined by ^{1}H-NMR spectroscopy; [b] number of cycles; [c] total residence time

The conversions of 1,5-dihydroxynaphthalene **98** to Juglone **99** were determined by ^{1}H-NMR spectroscopy of the crude products. The signal integration for the quinonoid protons of Juglone (2 doublets with an integration of 2) was compared to the signal integration for the two protons of 1,5-dihydroxynaphthalene represented by the most upfield doublet (integration of 2).

It is important to notice that the formation of a thin brownish coating on the reaction plate had been observed during the experiments. Therefore additional cleaning steps including reactor dissembling were necessary. The coating was analysed by ^{1}H-NMR-spectroscopy, but only solvent picks were detected. Thus it could be suggested that the coating was formed by the undetected impurities present in 1,5-dihydroxynaphthalene which was used in technical grade or by the decomposition products of sensitizer rose bengal.

The total experimental time in the falling film microreactor was relatively long, it took 80 min to pump 6 ml of the solution containing 10 mg (0.06 mmol) of 1,5-dihydroxynaphthalene through the microreactor with a flow rate of 0.08 ml/min. Based on this it was concluded that the falling film microreactor is not appropriate experimental system for the photooxygenation of 1,5-dihydroxynaphthalene. However, the reasonable conversion of diol of 31% still could be achieved at the exposure time of just 160 sec and this could be further improved by the usage of more powerful light source.

7.3 Synthesis of Juglone in the in-house made slug flow column reactor

Since, the typical batch system and selected continuous flow falling film microreactor were not ideal systems for the photooxygenation of 1,5-dihydroxynaphthalene **98**, a new in-house made glass column reactor with a unique slug flow was designed and introduced for photooxygenation processes.

7.3.1 Experimental set-up

A slug flow column reactor (Figure 82) was constructed by Dr Alexander Yavorskyy from cheap and generally used laboratorial equipment. The unique feature of this setup was the combination of a microstructured reactor (generation of thin liquid layer and huge interfacial area) with the generality of a batch system.

As can be seen on Figure 82 – the slug flow column reactor consists of several devices. The main component of this set-up was a glass tube **1** placed between two fluorescent lamps **2**. The glass tube of 1.5 m long with an inner diameter of 4.5 mm and outer diameter of 6.0 mm was used as the reaction vessel. It was always filled with 10 ml of the reaction mixture using an HPLC pump **3**. The level of pressure (vacuum) was controlled by the manometer **4** before it entered the system. To secure precise filling of the glass tube with liquid, several valves were maintained between the preparation flask and the pump. The first valve **5** was used for pump pressure control; second valve **6**

served to protect the HPLC pump from incidental reaction mixture or solvent splashing and generally was kept open; the third valve **7** was used for the changing of feeding nozzles.

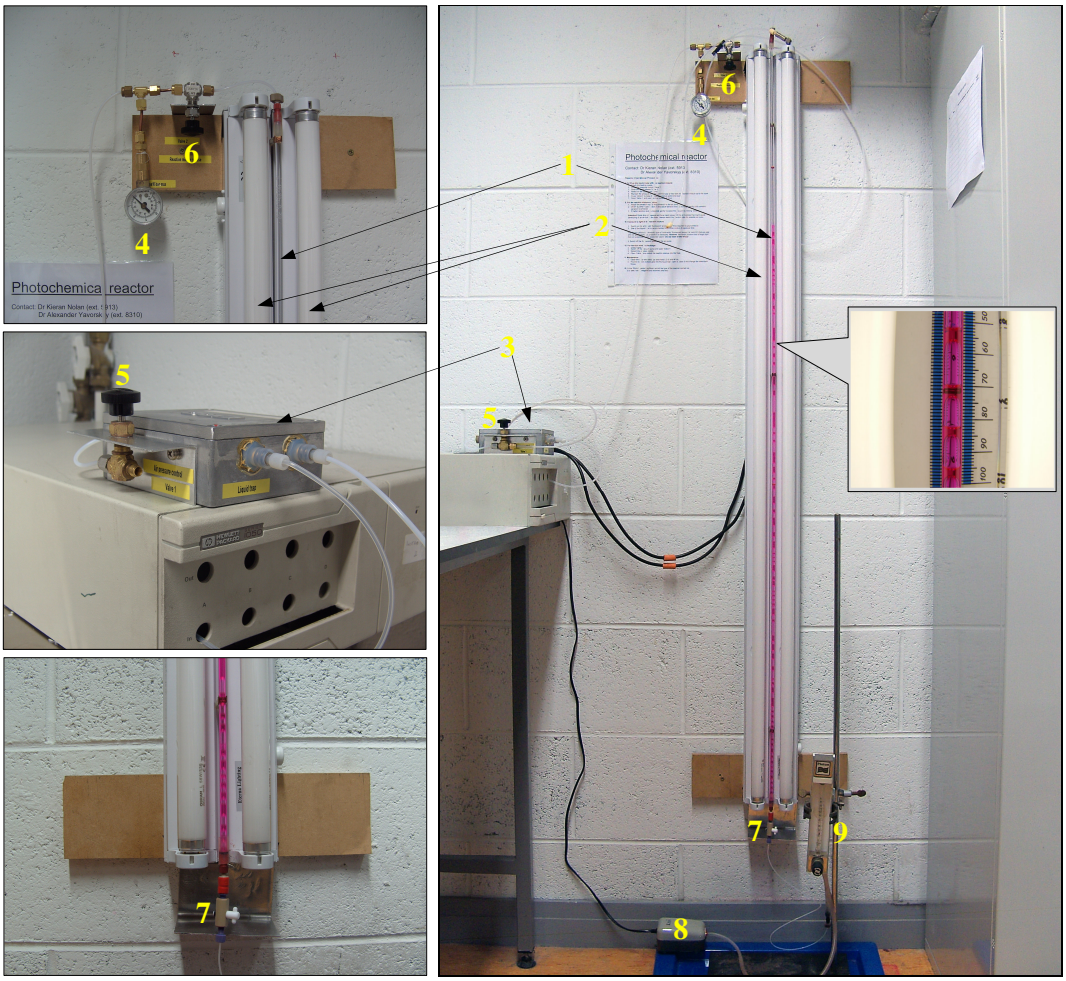


Figure 82: Slug flow column reactor setup: **1** – glass tube; **2** – two fluorescent lamps; **3** – HPLC pump; **4** – manometer; **5** – valve for pump pressure control; **6** – safety valve; **7** – valve for changing of feeding nozzles; **8 –** air pump; **9** – flow meter

The filling of the glass tube with the reaction mixture started from the connection of the capillary feeding nozzle with ID of 0.8 mm to the valve **7**. The other capillary end was placed into the flask with the prepared reaction mixture. The pressure control valve **5** was closed and the HPLC pump switched on. The pressure was applied up to 10 bars until the tube was filled with the reaction mixture (the height of the liquid in the tube was 60 cm). Afterwards, valves **6** and **7** were closed and the pump was switched off immediately. The capillary feeding nozzle was changed to the aeration nozzle (with appropriate ID) and was connected through the flow meter **9** to the air pump **8**. Next, valves **6** and **7** were slowly opened, the air pump switched on in parallel with the lamps

and the solution was exposed to light for the desired time period. The irradiation was provided by two domestic type fluorescent lamps with total optical power of 60 W that emit light in the visible spectra region (λ = 400 – 700 nm). The lamps were positioned alongside the glass tube at a distance of 1.5 cm. Moreover the lamps' length entirely covers the length of the glass tube. The air (bubbles) flow was controlled by the flow rate meter **9**.

After reaction completion the fluorescent lamps were switched off, valve **7** was closed and the air pump was disconnected straight away. The aeration nozzle was replaced for the feeding nozzle, valve **7** was open and the reaction mixture was released from the glass tube into the collection flask. After that the glass tube was rinsed with the appropriate solvent (the same mechanistic steps as for the reaction mixture).

7.3.2 Flow patterns in the in-house made glass column reactor

The general principle of photooxygenation processes in the glass column reactor was similar to that one used in the batch systems. Experimental solutions were saturated with air by the continuous flow of air (7-10 cm^3/min). Air was provided to the solution through the capillary nozzle with an internal diameter of 100 μm. In this manner, an even bubble flow with bubbles of approximately 100-150 μm in diameter was achieved (Figure 83).

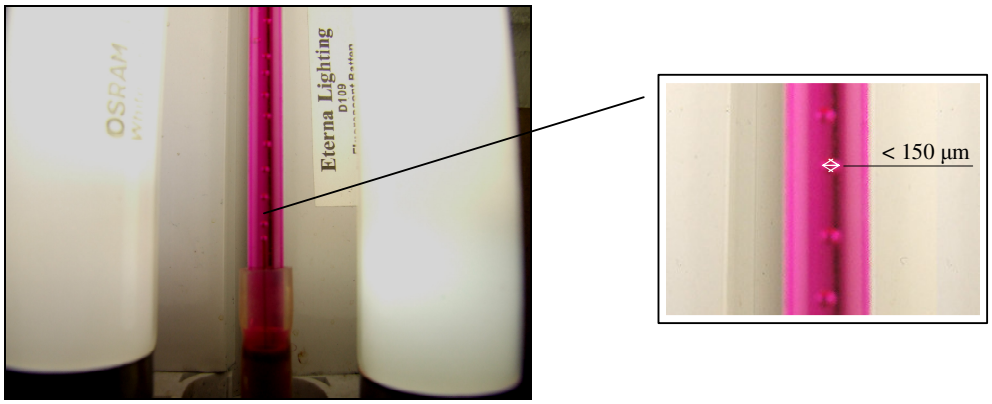


Figure 83: Solution aeration via 100 μm capillary

When a capillary with larger internal diameter of 500 μm was utilised as the aeration nozzle, a completely different shape and size of air bubble was observed. The bubbles had a bullet shape and the diameter was similar to that of the glass tube (Figure 84). Surprisingly, between the air bubbles and the wall of the glass tube a thin solution layer was observed. This finding was very important because it is the first time that a thin solution film was created in such a way. It was also observed that large air bubbles

facilitate a smooth distribution of solution within the entire tube length and created movement of liquid similar to a laminar flow. In contrast, small air bubbles did not have a noticeable influence on the distribution of solution within the glass tube and the height of the liquid column was almost the same as without aeration. The generated small air bubbles mostly provided mixing of the solution.

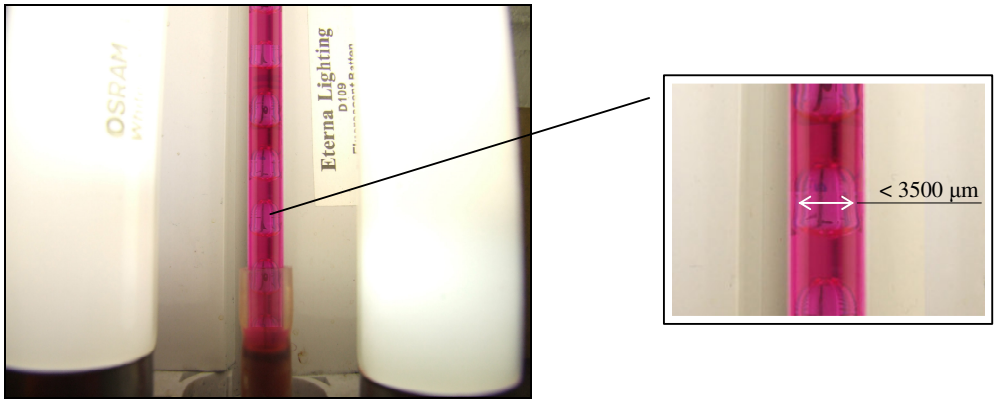
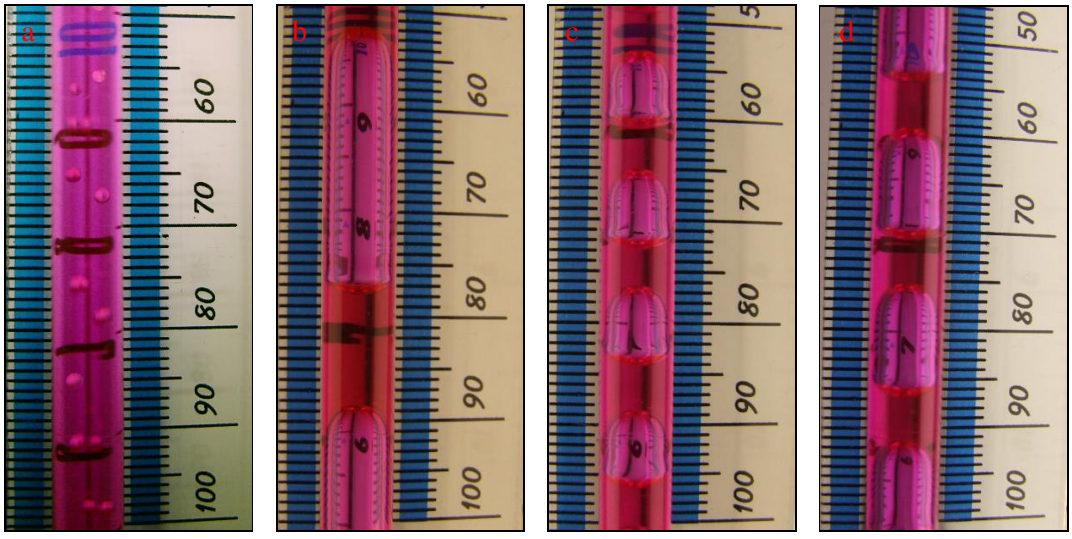


Figure 84: Solution aeration via 500 µm capillary

Based on the above described observations it was decided to outline two main flow patterns in the glass column reactor. A *bubble flow pattern* with small air bubbles (Figure 85a) and a *slug flow pattern* with large air bubbles (Figures 85b-d).



Figures 85: Images of the flow pattern formed inside the glass tube in different solvents (air flow rate: 10 cm^3/min; taken at a height of approximately 30 cm): a) bubble flow in isopropanol/water (100 µm capillary); b) slug flow in methanol/water (500 µm capillary); c) slug flow in isopropanol/water (500 µm capillary); d) slug flow in *tert*-amyl alcohol/water (500 µm capillary)

A similar slug flow pattern has been recently reported by Lévesque and Seeberger for photooxygenations in a micro-capillary under flow conditions.[118] Under a *slug flow pattern* with constant air flow rate, the average length of the bubbles depended on the solvent and its physicochemical properties. The largest air bubbles (Figure 85b) were obtained in aqueous methanol (10 vol-% of water, 90 vol-% of methanol).

7.3.3 Assessment of the glass column reactor suitability for photooxygenation processes

7.3.3.1 Effect of solvent on the photooxygenation of 1,5-dihydroxynaphthalene

For this study different alcohols were utilised as environmentally benign solvents. Primarily, *experiments 175–184* were carried out in a glass column reactor under a *bubble flow pattern* (100 µm aeration capillary). The concentration of starting materials was kept the same as in the previous batch and microreactor experiments (1,5-DHN: 10 mM; RB: 0.49 mM). The investigated volume of prepared mixture was 10 ml for one test. The flow rate of air was constant and was 7-10 cm^3/min. The results obtained within these experiments are summarised in the Table 54.

Table 54: The efficiency of 1,5-dihydroxynaphthalene oxygenation in different alcohols

Experiment	Solvent	Residence time, [h]	Conversion of 98, [%][a]
175	*i*-PrOH	0.5	37
176	*i*-PrOH	1	52
177	*i*-PrOH	3	100
178	*i*-PrOH/H_2O (9:1)	0.5	55
179	*i*-PrOH/H_2O (9:1)	1.5	82
180	*i*-PrOH/H_2O (9:1)	2	91
181	*i*-PrOH/H_2O (9:1)	2.5	100
182	*t*-AmOH/H_2O (9:1)	2	91
183	EtOH/H_2O (9:1)	2	88
184	MeOH/H_2O (9:1)	2	75

[a] Determined by ^{1}H-NMR spectroscopy

As demonstrated before and realised again for isopropanol (*exp. 175–181*), the addition of 10 vol-% of water gave higher conversions due to the improved transparency of the reaction mixture. For example, in aqueous isopropanol the conversion of **98** of 55% was

achieved after 30 min of irradiation (*exp. 178*), while in the pure isopropanol a similar value of 52% was reached only after 1 hour (*exp. 176*). The complete conversions were observed after 2.5 and 3 hours, respectively (*exp. 177* and *181*), which was more efficient if compared to reactions performed in conventional Schlenk flasks. The photooxygenation proceeded faster in aqueous isopropyl and *tert*-amyl alcohol than in ethanol or methanol (*exp. 180* and *182* vs. *exp. 183* and *184*). This is supported by the prolonged life time of singlet oxygen in these solvents (31 μs in *t*-BuOH [shown for comparison]; 22 μs in *i*-PrOH; 9.7-15.3 μs in EtOH; 9.5-10.4 μs in MeOH).[230,243]

7.3.3.2 Effect of flow patterns on the photooxygenation of 1,5-dihydroxynaphthalene

The photooxygenation of 1,5-dihydroxynaphthalene has a heterogeneous nature due to the presence of two phases: gas phase (air) and liquid phase (alcohol solution of 1,5-dihydroxynaphthalene and sensitizer). Therefore it was important to investigate the influence of both, bubble size and distribution, on the reaction efficiency. For this purpose air was delivered to the solution through a capillary with different inner diameters and consequently *bubble flow* and *slug flow patterns* were generated.

As can be seen from the data presented in Table 55, the air flow pattern had a significant influence on the photooxygenation reaction. Bubble flow conditions required prolonged irradiation times in order to reach high conversions of diol **98** (*exp. 185–187*). In contrast, high to complete conversion values were achieved after just 1 hour under slug flow conditions (*exp. 188–189*).

Table 55: The efficiency of 1,5-dihydroxynaphthalene oxygenation under *bubble flow* and *slug flow patterns*

Experiment	Solvent	Residence time, [h]	Air flow, [cm^3/min]	ID of capillary, [μm] (pattern)	Conversion of 98, [%][a]
185	*i*-PrOH/H_2O (9:1)	3	10	50 (bubble)	49
186	*i*-PrOH/H_2O (9:1)	1.5	10	100 (bubble)	82
187	*i*-PrOH/H_2O (9:1)	3	10	100 (bubble)	100
188	*i*-PrOH/H_2O (9:1)	1	20	500 (flow)	91
189	*t*-AmOH/H_2O (9:1)	1	20	500 (flow)	100

[a] Determined by ^{1}H-NMR spectroscopy

7.3.3.3 Effect of sensitizer and its concentration on the photooxygenation of 1,5-dihydroxynaphthalene

Another factor that could have an influence on the photooxygenation reaction is the sensitizer and its concentration. These parameters were investigated in the following *experiments 190–197* under *bubble flow* (air flow rate: 10 cm^3/min) and *slug flow* conditions (air flow rate: 20 cm^3/min) using aqueous isopropyl or *tert*- amyl alcohol as a solvent. The concentration of rose bengal was doubled or halved and methylene blue was tested as an alternative sensitizer (Table 56). The increase or reduction in rose bengal concentration had almost no impact on the reaction efficiency under the applied conditions. In case of the *bubble flow pattern*, Juglone **99** was formed in similar amounts of 88–92% after irradiation for 2 hours (*exp. 190–192*). Under *slug flow* conditions similar conversion rates of 83% and 87% were obtained after irradiation for just 30 min (*exp. 193–194*). Based on these results, it was concluded that previously used concentration of rose bengal of 0.49 mM is optimal for photooxygenation processes in the glass column reactor. Within this study the concentration of diol **98** was kept the same and was 10 mM.

Table 56: The efficiency of 1,5-dihydroxynaphthalene oxygenation under different sensitization conditions

Experiment	Solvent	Residence time, [h]	Rose bengal, [mmol/L]	ID of capillary, [µm]	Conversion of 98, [%][a]
190	*i*-PrOH/H_2O (9:1)	2	0.49	100	91
191	*i*-PrOH/H_2O (9:1)	2	0.98	100	88
192	*i*-PrOH/H_2O (9:1)	2	0.25	100	92
193	*t*-AmOH/H_2O (9:1)	0.5	0.49	500	87
194	*t*-AmOH/H_2O (9:1)	0.5	0.25	500	83
195	*t*-AmOH/H_2O (9:1)	0.5	0.25[b]	500	56
196	*t*-AmOH/H_2O (9:1)	0.5	–[c]	500	8
197	*t*-AmOH/H_2O (9:1)	1	–[c]	500	35

[a] Determined by ^{1}H-NMR spectroscopy; [b] concentration of methylene blue; [c] no sensitizer

The photooxygenation experiment with methylene blue as sensitizer gave a much lower value of 56% under identical *slug flow* conditions (*exp. 195*). This could be a result of

the poor solubility of MB in *tert*-amyl alcohol and its lower quantum yield for singlet oxygen formation (Φ^1O_2 = 0.52 for MB; Φ^1O_2 = 0.68 for RB).[258]

It is known that 1,5-dihydroxynaphthalenes are good self-sensitizers.[259] They undergo self-sensitisation to Juglone **99** under UV or visible light.[247,260] Consequently, irradiation of diol **98** under *slug flow* conditions in the absence of any sensitizer resulted in a low conversion to **99** of 8% after 30 min and 35% after 1 hour (*exp. 196–197*).

7.3.3.4 Effect of the irradiation time and the air flow rate on the photooxygenation of 1,5-dihydroxynaphthalene

The influence of the irradiation time and the air flow rate was furthermore investigated in aqueous *tert*-amyl alcohol under slug flow conditions (500 µm aeration capillary) and with rose bengal as sensitizer (*exp. 198–206*). The results obtained in this study are summarised in Table 57. As was expected, the amount of formed Juglone **99** steadily improved with increasing residence time (Figure 86, *exp. 198–202*). More than half of diol **98** (64%) was converted after just 15 min and complete conversion to **99** was achieved after 1 hour (*exp. 199* and *201*). The experiment, with residence time of 1 hour was done twice and identical results, *i.e.* complete conversions were achieved (*exp. 201–202*).

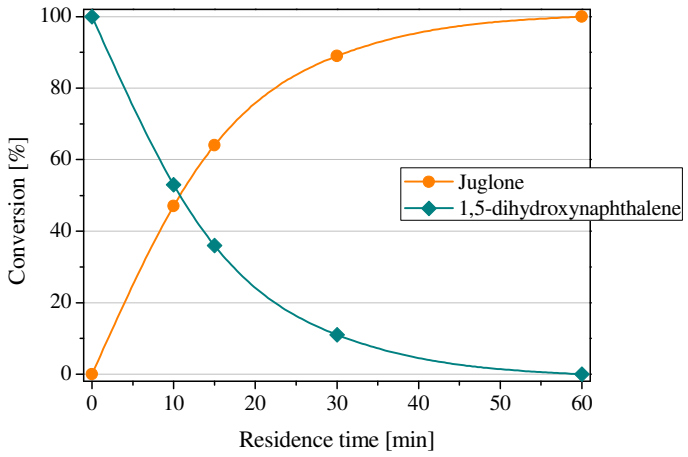


Figure 86: The changing composition of 1,5-dihydroxynaphthalene and Juglone vs. residence time

As could be seen from the results presented in Table 57, the air flow rate had no influence on the reaction efficiency. For example, irradiations for 30 min at air flows of 20 and 90 cm^3/min gave almost identical conversion values of 87% and 89% (*exp. 204* and *200*), respectively.

Table 57: The efficiency of 1,5-dihydroxynaphthalene oxygenation at different air flow rates and different residence times

Experiment	Solvent	Residence time, [h]	Air flow, [cm^3/min]	Conversion of 98, [%][a]
198	*t*-AmOH/H_2O (9:1)	0.17	90	47
199	*t*-AmOH/H_2O (9:1)	0.25	90	64
200	*t*-AmOH/H_2O (9:1)	0.5	90	89
201	*t*-AmOH/H_2O (9:1)	1	90	100
202	*t*-AmOH/H_2O (9:1)	1	90	100
203	*t*-AmOH/H_2O (9:1)	0.17	20	46
204	*t*-AmOH/H_2O (9:1)	0.5	20	87
205	*t*-AmOH/H_2O (9:1)	1	10	100
206	*t*-AmOH/H_2O (9:1)	1.5	10	100

[a] Determined by ^{1}H-NMR spectroscopy

7.3.3.5 Optimised condition of Juglone synthesis and experimental scale-up

Based on the above reported results of Juglone synthesis in the glass column reactor the following experimental conditions could be admitted as optimal at a concentration of 1,5-dihydroxynaphthalene of 10 mM: air flow rate 10 or 20 cm^3/min, residence time 1 hour, solvent 10% aqueous *tert*-amyl or isopropyl alcohol, rose bengal as sensitizer at a concentration of 0.49 mM, aeration capillary with an inner diameter of 500 μm.

During the optimisation of the experimental conditions in the glass column reactor, the percent conversion of 1,5-dihydroxynaphthalene **98** has been used as an assessment indicator of reaction efficiency and isolation of Juglone **99** was not attempted due to the small reaction scales of 100 μmol of **98**. Therefore, to verify our results, the photooxygenation of 1,5-dihydroxynaphthalene **98** was conducted on a three-fold scale (30 ml) and purified Juglone was isolated after column chromatography (Table 58). The excellent reproducibility of the reaction justified the isolation of the photoproduct **99** by combining three reaction mixtures obtained under identical conditions. Using an optimised experimental procedure, the reaction performed in aqueous isopropanol showed a conversion of 91% and gave an isolated yield of Juglone **99** of 54% (*exp. 207*). Irradiation in aqueous *tert*-amyl alcohol furnished complete conversion and gave a higher isolated yield of 70% (*exp. 208*). These results are superior compared to the experiments reported in the literature, where 38% of Juglone **99** was obtained after 5 hours of irradiation using a 150 W medium-pressure mercury lamp, 55% after 10 hours of irradiation using 2×500 W halogen lamps, 39% after 3.5 hours of irradiation with

non- concentrated sunlight and 71% of irradiation with moderately concentrated sunlight, respectively.[256]

Table 58: Isolated yields of Juglone under optimised reaction conditions

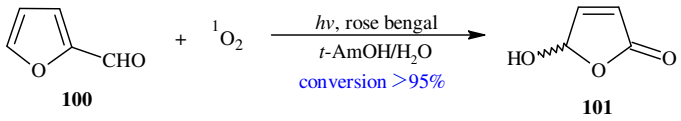
Experiment	Solvent	Residence time, [h]	Conversion of 98, [%][a]	Yield of 99, [%]
207	*i*-PrOH/H_2O (9:1)	1	91	54
208	*t*-AmOH/H_2O (9:1)	1	100	70

[a] Determined by ^{1}H-NMR spectroscopy

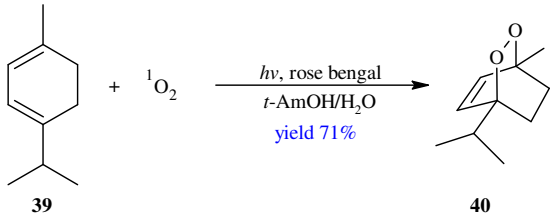
7.3.3.6 Suitability of slug flow column reactor for other photooxygenation reactions

The optimized irradiation conditions in the column reactor were transferred to other photooxygenation reactions (*exp. 209–211*). The interaction of furfural **100** with singlet oxygen gave 5-hydroxyfuranone **101** in a conversion of >95% without any pseudo-ester (Scheme 61).[261,262] The well known, [4+2]-cycloaddition of α-terpinene **39** gave ascaridole **40** in a yield of 71%. In contrast to the falling film microreactor, no trace of the by-product *p*-cymene **96** was detected in the crude product (Scheme 62). The Schenck-*ene*-reaction of citronellol **44** is an important key-step in the industrially valuable synthesis of the fragrance rose oxide (Scheme 63).[263,264] After irradiation for 1 hour in the slug flow column reactor, complete conversion of **44** to a 1.1:1 mixture of the regioisomeric hydroperoxides **45** and **46** (the latter in a 1:1 mixture of diastereoisomers) was achieved.

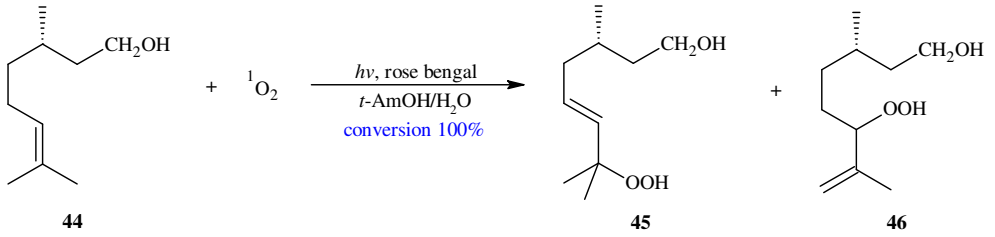
These examples clearly show the general suitability of the column reactor for photooxygenation reactions on the preparative scale.



Scheme 61: Photooxygenation of furfural



Scheme 62: Photooxygenation of α-terpinene

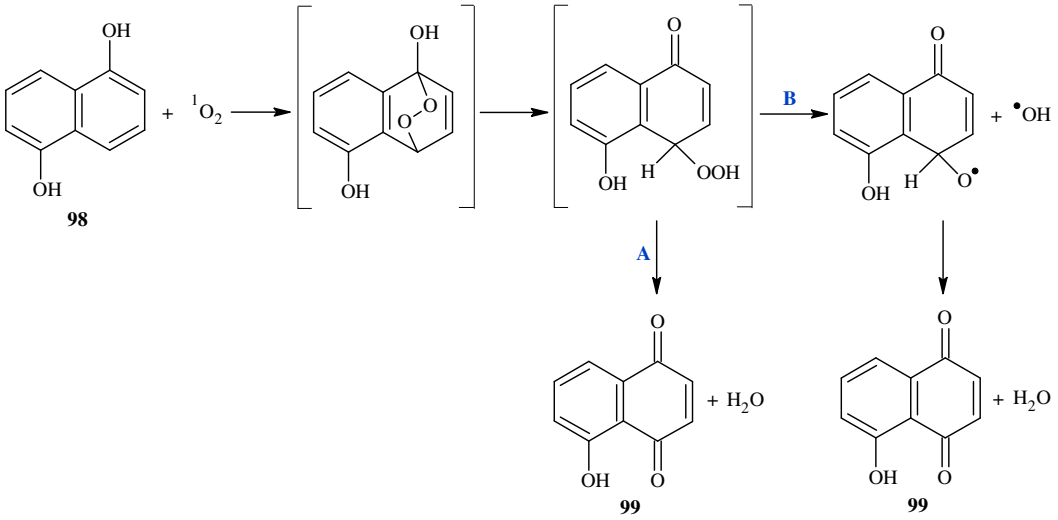


Scheme 63: Photooxygenation of (*S*)-(–)-β-citronellol

7.4 Discussions

7.4.1 Dye-sensitised photooxygenation of 1,5-dihydroxynaphthalene (synthesis of Juglone)

The oxidation of 1,5-dihydroxynaphthalene by singlet oxygen, created through dye-sensitised photochemical pathway, is an environmentally friendly procedure for the synthesis of Juglone. This reaction is an example of a photo-Diels Alder reaction ([4+2]-cycloaddition), in which 1,5-dihydroxynaphthalene functions as a diene and singlet oxygen as a dienophile. The photo-Diels Alder reaction produces an endoperoxide, which subsequently undergoes the loss of water to yield 1,4-naphthoquinone. The mechanism of this reaction is depicted on Scheme 64.[246,247] It is believed that the conversion of the endoperoxide to the naphthoquinone is spontaneous due to the instability of the endoperoxide.[247] It has been proposed in the literature that an intramolecular acid catalysis occurs causing conversion of the endoperoxide to the hydroperoxide. The hydroperoxide is subsequently converted to the naphthoquinone either via heterolytic (A) or homolytic pathways (B).[246]

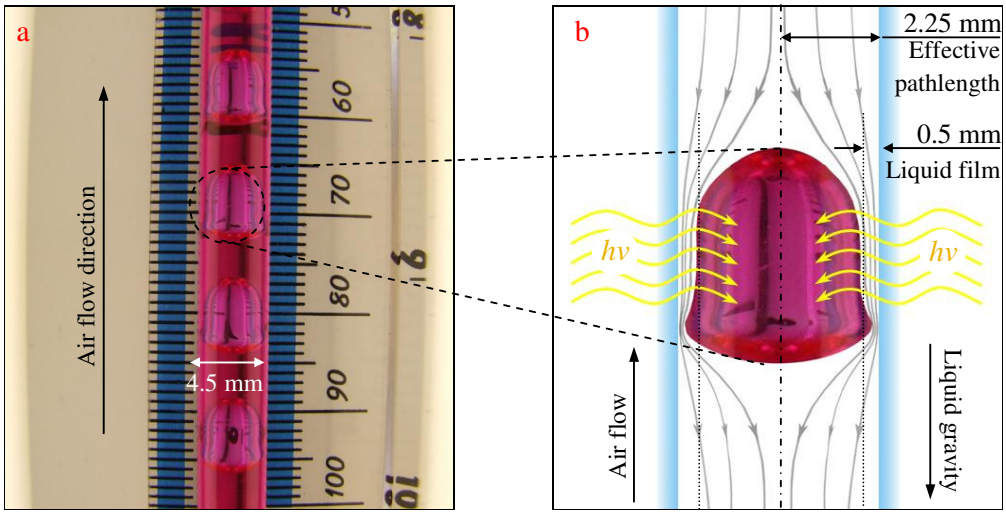


Scheme 64: Mechanism of Juglone synthesis

7.4.2 Benefits of slug flow pattern for photooxygenation reactions

The best performance for the photooxygenation of 1,5-dihydroxynaphthalene have been achieved in the glass column reactor under slug flow conditions. The Juglone was isolated in a yield of 70% that was obtained after a residence time of just 1 hour.

Under slug flow conditions the generated large air bubbles allows for the formation of a thin liquid film (<0.5 mm) along the bubble sides (Figures 87). Consequently, the interfacial area of the liquid phase is increased significantly, which subsequently results in an improved mass transfer. In addition, this thin film of solution allowed for a superior light penetration. The additional effect of the air stream in the slug flow manner is to allow minor mixing of the reaction mixture to occur during irradiation.



Figures 87: a) Image of the slug flow pattern formed inside the glass tube in methanol/water (9:1) mixture at air flow rate of 10 cm^3/min; b) representation of the vertical slug flow pattern and important dimensions

7.4.3 Wavelength matching and light penetration for the experiments in glass column reactor

The white fluorescent lamps used are the safest artificial light source. The emission spectra of these lamps showed a sufficient overlap with the main absorption band of rose bengal (Figure 88).

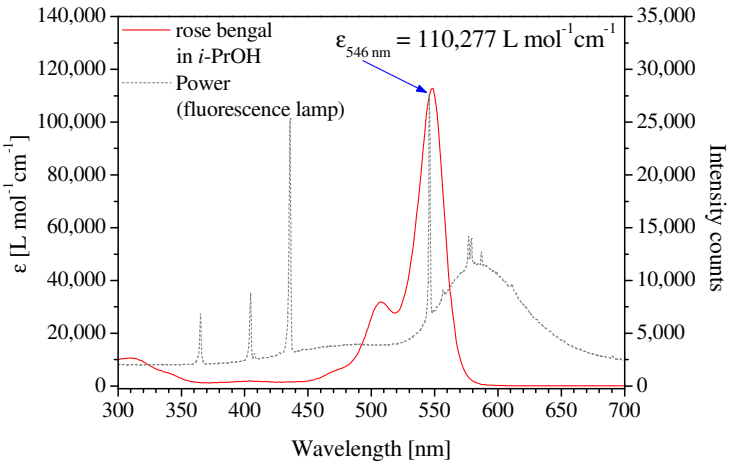


Figure 88: UV-spectrum of rose bengal vs. emission spectrum of the 60W fluorescent lamps

Based on the absorption of the sensitizer the penetration profile of light was calculated at 546 nm and was compared to the pathlength of the film and the glass tube (Figure 89). Due to the allocation of the lamps at both sides of the glass tube (4.5 mm inner ∅) its effective pathlength was reduced to 2.25 mm. The generated thin liquid film (<0.5 mm) provided complete transmission of light at the given concentration of rose bengal.

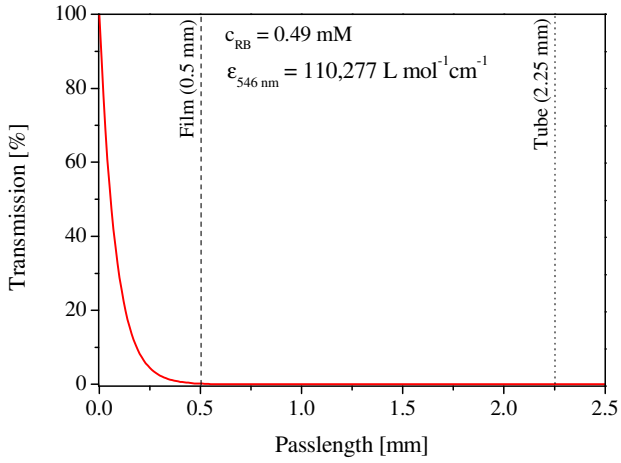


Figure 89: Light-penetration profile for a 0.49 mM solution of rose bengal at 546 nm. The vertical lines represent the maximum pathlength of the film (--) and the effective pathlength of the reactor tube (⋯)

7.4.4 Technical parameters of glass column reactor and its efficiency

The used fluorescent lamps have a total optical power of 120 W. The light from these lamps covered the entire surface of glass tube of 211.95 cm^2. Such technical parameters

of the reactor design provided an adequate irradiated area to volume ratio of 2119.5 m^2 m^{-3} and a lamp power per irradiated area of 0.57 W cm^{-2}. The efficiency of the reactor was further evaluated using space-time-yield (STY) calculations. STYs were calculated using the previously described equation *(2)*, where n_R is the amount of isolated Juglone. For the preparative irradiation performed in aqueous *tert*-amyl alcohol (*exp. 208*), a STY of 0.12 mmol L^{-1} min^{-1} was achieved. In the experiment with aqueous isopropanol (*exp. 207*), a somewhat lower STY of 0.09 mmol L^{-1} min^{-1} was observed and this resulted in a poorer isolated yield of Juglone. Following the literature, isopropanol might promote photodegradation of Juglone via hydrogen abstraction and subsequently result in a lower yield.[265,266] In *tert*-amyl alcohol this degradation process is prevented or significantly reduced.

7.6 Summary

A new glass column reactor equipped with two domestic fluorescent lamps has been designed and successfully adopted for the photooxygenation reactions. The obtained results clearly demonstrate that this system is an efficient and reliable tool for photooxygenation processes.

Both *bubble flow* and *slug flow patterns* were easily created using an aeration capillary with appropriate internal diameter. The photooxygenation of 1,5-dihydroxynaphthalene has been studied under both flow patterns and significantly higher conversion rates were achieved under the slug flow conditions. This outcome was supported by the enlarged interfacial area, improved mass transfer and better light penetration with the slug flow.

The desired product Juglone was isolated in an improved yield of 70% after irradiation for just 1 hour under slug flow conditions. This achievement is significantly better compared to the results obtained in the glass column reactor under bubble flow conditions and in the conventional Schlenk flask. This newly established glass column reactor with a slug flow pattern can serve as a valuable alternative to the existing techniques. Moreover, general fluorescent lamps were found to be a suitable and safe light source for rose bengal sensitised photooxygenation reactions.

Thesis conclusions

8. Thesis conclusions

The outlined above research work thoroughly describes micro-photochemistry as a new environmentally friendly and resource efficient technology for synthetic chemistry. It also demonstrates the practical application of recent techniques of microflow engineering and light technology in the synthetic photochemistry. The feasibility of micro-photochemistry concept has been evaluated using versatile *homogeneous* and *heterogeneous* photochemical model reactions and diverse manner experimental set-ups.

Phthalimide chemistry:

Phthalimide chemistry was in details discussed in Chapter 4. A series of acetone- and DMBP-mediated photodecarboxylation reactions involving phthalimides, which are an efficient alternatives to thermal Grignard and SmI_2-mediated reactions, were successfully studied in a commercially available microreactor dwell device and batch Rayonet chamber reactor. In almost all cases examined, reactions tested in dwell device gave superior results in terms of conversions or isolated yields, especially if considering results achieved in experiments with the same amount of light, 40W, in both systems. Under such conditions, the microreactor set-up gave between 3.5- and 6-times higher yields or conversions, respectively. In addition, the products formed in the microreactor appeared cleaner and less purification was required. Compared to the acetone-sensitized reactions, the DMBP-mediated reactions were less selective and DMBP had to be removed by column chromatography. The higher reaction efficiency in the microreactor was explained by special microchannel geometry. Under the applied experimental conditions, the shallow depth of created solution layer in the microchannel (0.5 mm) provided extensive light penetration through whole media, while in the batch Schlenk flask light was completely absorbed by the solution within the first 1.5 mm (effective pathlength 4 mm), consequently most of the solution remained without activation energy. Also, the microstructured channel has significantly larger surface to volume ratio compared to the batch flask. These factors ultimately result in higher space-time yields (STYs) for all studied photodecarboxylation reactions and open the possibility to work with two times higher solution concentration in dwell device without losing process efficiency.

Furanone and alkene chemistry:

In Chapter 5, the stereoselective additions of photochemically generated radicals of secondary alcohols to furanones and electron-deficient alkenes have been studied in different commercially available and in-house made microflow devices. The efficiencies of reaction progress in microfluidic systems were compared to that achieved in the conventional batch system and were discussed in terms of light penetration, geometry of reaction vessel, energy efficiency, reactor efficiency and irradiated area-to-volume ratio. In most cases, the microflow devices outperformed conventional Rayonet reactor or gave comparable results. The LED-driven microchip showed the best overall performance, which was supported by its superior geometric features and energy efficiency. The studied photoaddition reactions reached completion after just 2.5 or 5 min, while in all other systems for the same time period incomplete conversion rates of 75-99% were observed. Due to very small internal volume of the microchip channel, only 13 µl, and its resourceful potency it can serve as a source and energy efficient R&D tool. However, for the operational processes that required a gram-amount of material the microreactors represent more feasible devices. Nevertheless, the commercially available microreactors have important limitations such as fixed length of the reaction channel, the single-channel design and significant cost investment for numbering-up. Therefore, flexible FEP capillaries were found as cost-efficient alternatives and were used as reaction chamber in the new in-house made capillary reactors. Hence, a simple continuous microflow *dual-capillary reactor* and its optimised version *multi-microcapillary tower* were developed. The coiled design allowed simple and cheap gram-scale synthesis of interested product. The tower design enabled parallel operation of 10 experiments and thus fast optimisation of experimental procedure and synthesis of small library of 4-dihydrofuranone derivatives. Consequently, multi-capillary reactor represents a capable device not just for synthetic photochemistry but also for other applied areas of continuous flow. In addition multi-capillary reactor can be used as a reliable tool for the standardisation and validation of photochemical processes, parallel testing of biologically active compounds, process modelling, in situ analysis and combinatorial chemistry.

Ascaridole chemistry:

In Chapter 6, the rose bengal initiated synthesis of ascaridole was investigated in a commercially available falling film microreactor which was irradiated by a single fluorescent lamp. The main importance of this study was the development of a safer

technology for the preparative scale synthesis of potentially explosive endoperoxide ascaridole. In the microreactor the volume of oxygenated solution was precisely controlled and constantly kept below 150 microlitres which minimised the risk of explosion. Also, the unique reactor parameters such as huge interfacial area, big irradiated surface-to-volume ratio of about 20000 m^2 m^{-3} and efficient light penetration facilitated adequate output of ascaridole synthesis of 2.5–3.2 mol L^{-1} h^{-1}.

In addition, a GC procedure for the off-line process monitoring was developed and the general experimental procedure was optimised. During an optimisation study the relation between products selectivity and experimental parameters, such as α-terpinene concentration, rose bengal concentration, oxygen concentration, oxygen flow rate, residence time, temperature and light source nature have been established and discussed first time. It was found that the selectivity of ascaridole synthesis in the falling film microreactor was steady and relatively high of up to 89% in most cases. The only factors that had noticeable influence on the ascaridole selectivity were temperatures below 9°C and above 22°C and oxygen flow rates above 50 ml/min. The established experimental set-up could be further applied for the study of the reaction kinetic.

Juglone chemistry:

The research work reported in Chapter 7 was focused on the development of new slug flow column reactor suitable for the Juglone synthesis in the laboratorial conditions. For the first time, the domestic fluorescent lamps were proposed as artificial light source suitable for the rose bengal sensitised photooxygenation of 1,5-dihydroxynaphthalene. In contrast to the traditional halogen lamps the used fluorescent lamps gave important advantages such as longer life time, minor heat generation and necessary activation energy for photochemical processes. During the experimental set-up optimisation study a *bubble flow* and *slug flow* patterns have been observed and discusses. It was found that *slug flow* pattern has features similar to that of microfluidic film. These features are huge interfacial area and thin solution layer which ensured a necessary saturation of solution with oxygen and sufficient light penetration. Under slug flow conditions the interested product Juglone was isolated in the improved yield of 70% after irradiation time of just 1 hour. The extended study of photooxygenation of α-terpinene, furfural and citronellol also gave advances results and confirmed adaptability of new slug flow column reactor.

In general, the above reported research work nicely proved the superiority of microflow-photochemistry concept.

Chapter 9

Experimental

General methods

Spectroscopic methods

Nuclear magnetic resonance spectroscopy (NMR): NMR spectra were recorded on a *Bruker 400 Ultrashield*^{TM} instrument (400 MHz for ^{1}H; 100 MHz for ^{13}C) using the *Bruker Topspin 2.0* software. Chemical shift values are referred to solvent residual resonances: $CDCl_3$ (7.26/77.16 ppm) and acetone-d_6 (2.05/29.84 and 206.26 ppm). Chemical shifts δ are given in ppm, coupling constants J in Hz.

UV-Visible spectroscopy: UV-Vis spectra were recorded using a Varian Cary 50 scan UV-Vis spectrophotometer.

Emission measurement: Light sources emission spectra were recorded using Ocean Optics spectrophotometer Maya 2000 Pro with calibrated light source LSCJ 705 and optical fibre AL 0220 (ID 50 μm).

Chromatography methods

Gas chromatography–mass spectrometry (GC-MS): GC spectra were recorded using a Agilent GC System 6890 with flame ionization detector (FID) and HP-5 5% Phenyl Methyl Siloxan column: Agilent 19091J-413.

Column chromatography: Column chromatography was carried out using Merck silica gel 60 (particle size 0.063-0.200 nm for column chromatography) 70-230 mesh ASTM.

Thin Layer Chromatography (TLC): Analytical thin-layer chromatography was performed on aluminium sheets coated with 0.20 mm of Fluka silica gel ITCL-cards with fluorescent indicator 254 nm, layer thickness: 0.2 mm. Visualisation was carried out under UV-lamp (245 nm and 366 nm) or using phosphomolybdic acid solution in case of furanones, dimethyl fumarate and dimethyl maleate.

9.1 Chapter 2: Intra- and intermolecular transformations involving phthalimides

Conventional photolysis. Batch set-up

Glassware: Photoreactions were performed in 50 ml and 100 ml *Pyrex Schlenk flasks* equipped with a *Pyrex cold finger*.

Conventional reactor: Photochemical reactions were performed in a *RPR–200 Rayonet photochemical chamber reactor* (Southern New England Ultraviolet Company).

Irradiation source: *Rayonet reactor* was equipped with 16 RPR-3000Å (for UVB irradiation, λ_{max} = 300 ± 25 nm) or 16 RPR-3500Å (for UVA irradiation, λ_{max} = 350 ± 25 nm) fluorescent tube lamps (8 W each).

Micro photolysis. Dwell device set-up

Microreactor: Microreactions were performed in a *dwell-device* (*Mikroglas*), made of Foturan™ glass and consisted of a bottom serpentine reaction channel (0.5 mm depth, 2 mm width, 1.15 m length, 1.68 ml internal volume) and a top heat-exchanging channel. Microreactor irradiation aperture was 118 mm × 73 mm.

Irradiation source: The *dwell device* was placed under a Luzchem UV-panel equipped with 5 RPR-3000Å (for UVB irradiation, λ_{max} = 300 ± 25 nm) or 5 RPR-3500Å (for UVA irradiation, λ_{max} = 350 ± 25 nm) fluorescent tube lamps (8 W each).

Pumps: Programmable syringe pump (Harvard apparatus 11 plus, serial No. B – 43281) was used to pump a reaction mixture through the reaction channel of the microreactor. A rotary pump ISMATEC® (serial No. 313412) was used for the circulation of cooling water.

Syringe: A 10 ml glass syringe (ID = 14.56 mm) made of Borosilicatglass (Duran®, ILS, Germany) with a PTFE plunger was used for the loading of reaction mixtures into the syringe pump.

Solvents and reagents

All solvents and starting materials were obtained from commercial suppliers (*Sigma-Aldrich* and *Fluka*) and were used without further purification.

9.1.1 General procedure (GP-1) for the photoaddition of thioethers to N-methylphthalimide under batch conditions (Rayonet):

N-Methylphthalimide (1.5 mmol) was placed in a Pyrex Schlenk flask and was dissolved in 50 ml of acetone. To this solution a corresponding thioether (15 mmol) and 50 ml of acetone were added to make up 100 ml of total volume. This solution was sonicated for 15 min using an ultrasound bath and degassed with a slow stream of N_2 for 5 minutes. The reaction mixture was then placed in the photoreactor and irradiated at 300±25nm (Rayonet RPR-200, equipped with 16 × RPR-3000Å lamps, 16 × 8 W). After evaporation of the solvent, the conversion rate was determined by ^{1}H-NMR spectroscopy of the crude product. The signal integration for the NC$\underline{H}_3$ protons of NMP was compared to the signal integration for the NC$\underline{H}_3$ protons of the product. Pure products were isolated by column chromatography on silica gel with suitable mobile phase and further characterized by ^{1}H-NMR and ^{13}C-NMR spectroscopy.

Experiment 1

The addition of dimethyl sulphide to NMP (OS-44)

General procedure (GP-1) was followed using NMP (242 mg; 1.5 mmol) and dimethyl sulphide (1.1 ml; 15 mmol). After irradiation for 1 hr the reaction was stopped, acetone was evaporated by rotary evaporation and the crude product was analysed by ^{1}H-NMR spectroscopy. The composition of NMP to product **66** was calculated from the ^{1}H-NMR integration to be 78:22.

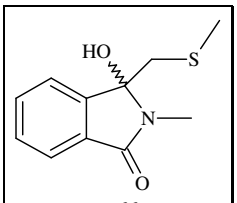
For ^{1}H-NMR data of product **66** see experiment 2.

Experiment 2

The addition of dimethyl sulphide to NMP (OS-41)

General procedure (GP-1) was followed using NMP (242 mg; 1.5 mmol) and dimethyl sulphide (1.1 ml; 15 mmol). After irradiation for 2 hrs the reaction was stopped, acetone was evaporated by rotary evaporation and the crude product was analysed by ^{1}H-NMR spectroscopy. The composition of NMP to product **66** was calculated from the ^{1}H-NMR integration to be 42:58. The collected crude product was further purified by column chromatography using ethyl acetate:n-hexane (1:3) as eluent. The isolated yield of **66** was found to be 188 mg (0.84 mmol, 56%). The product was confirmed by both ^{1}H-NMR and ^{13}C-NMR.

Analytical data of *3-hydroxy-2-methyl-3-(methylthiomethyl) isoindolin-1-one* (66)



66

$C_{11}H_{13}NSO_2$

Mol. Wt.: 223.3 g/mol

TLC: *Rf* = 0.26 (ethyl acetate/n-hexane 1:1)

Melting point (colourless solid)**:** 110-114ºC (Lit.[156]: 114-116ºC)

^{1}H–NMR: (400 MHz, Acetone-d_6)

δ (ppm) = 1.76 (s, 3 H, SCH_3), 2.92 (s, 3 H, NCH_3), 3.20 (d, ^2J = 14.0 Hz, 1 H, CH_2), 3.27 (d, ^2J = 14.0 Hz, 1 H, CH_2), 5.47 (s, 1 H, OH), 7.50 (ddd, ^3J = 7.6, ^3J = 7.6, ^4J = 1.2 Hz, 1 H, H_{arom}), 7.58 (ddd, ^3J = 7.6, ^3J = 7.6, ^4J = 1.2 Hz, 1 H, H_{arom}), 7.64 (dd, ^3J = 7.6, ^4J = 1.2 Hz, 1 H, H_{arom}), 7.71 (dd, ^3J = 7.6, ^4J = 1.2 Hz, 1 H, H_{arom}).

^{13}C–NMR: (100 MHz, Acetone-d_6)

δ (ppm) = 16.7 (s, 1 C, SCH_3), 23.5 (s, 1 C, NCH_3), 40.8 (s, 1 C, CH_2S), 90.9 (s, 1 C, COH), 123.1 (d, 1 C, CH_{arom}), 123.3 (d, 1 C, CH_{arom}), 130.2 (s, 1 C, CH_{arom}), 132.5 (s, 1 C, CH_{arom}), 133.1 (s, 1 C, Cq_{arom}), 147.8 (s, 1 C, Cq_{arom}), 167.1 (s, 1 C, CON).

9.1.2 General procedure (GP-2) for photoaddition of thioethers to N-methylphthalimide in the dwell-microreactor:

N-Methylphthalimide (0.225 mmol) was placed in a Pyrex test tube and was dissolved in 10 ml of acetone. To this solution a corresponding thioether (2.25 mmol) and 5 ml of acetone were added to make up 15 ml of total solution. This solution was sonicated for 15 min using an ultrasound bath and degassed with a slow stream of N_2 for 5 minutes. The microreactor was prepared by pumping the pre-sonicated acetone through the reaction channel until all air bubbles had been removed. Then 10 ml of prepared reaction mixture was transferred into a 10 ml glass syringe, any air bubbles were expelled and the syringe was loaded into a syringe pump. The flow rate was set and the solution was pumped through a micro-reactor (mikroglas dwell device) while irradiated at 300±25 nm (Luzchem UV exposure panel equipped with 5 × RPR-3000Å lamps, 5 × 8 W). During the reaction, the reactor was kept cool by pumping cold water through the cooling channel. When the syringe was empty, the syringe pump and the lamps were switched off simultaneously. The syringe was refilled with acetone and loaded into a

syringe pump again. The syringe pump was then turned on simultaneously with the lamps. When the reaction was complete, acetone was removed by rotary evaporation and the conversion rate for the reaction was determined by ^{1}H-NMR spectroscopy of the crude product. The signal integration for the NC$\underline{H}_3$ protons of NMP was compared to the signal integration for the NC$\underline{H}_3$ protons of the product. Pure products were not isolated in these experiments.

Experiment 3

The addition of dimethyl sulphide to NMP (OS-72)

General procedure (GP-2) was followed using NMP (36 mg; 0.225 mmol) and dimethyl sulphide (170 µl; 2.25 mmol). The flow rate used was 0.028 ml/min; residence time: 1 hr. The composition of NMP to product **66** was calculated from the ^{1}H-NMR integration to be 92:8.

For ^{1}H-NMR data of product **66** see experiment 2.

Experiment 4

The addition of ethylmethyl sulphide to NMP (OS-42)

General procedure (GP-1) was followed using NMP (242 mg; 1.5 mmol) and ethylmethyl sulphide (1.39 ml; 15 mmol). After irradiation for 2 hrs the reaction was stopped and acetone was evaporated by rotary evaporation. The ^{1}H-NMR analysis of the crude product showed the presence of isomers **68**, **69** and **70** and a high percentage of unreacted NMP was also found. The composition of NMP to the mixture of isomers was calculated from the ^{1}H-NMR integration to be 84:16. The collected crude product was further purified by column chromatography using acetone:n-hexane (1:5) as eluent. The isolated yield of the isomer mixture was found to be 21 mg (0.09 mmol, 6%). The ratio of isomers was determined as 30:34:36 (**68:69:70**), respectively. Assignments of the three isomers (**68:69:70**) were consigned by comparison with known analogues reported in the literature.[149]

For ^{1}H-NMR data of product **68** see experiment 9.
For ^{1}H-NMR data of isomers **69** and **70** see experiment 10.

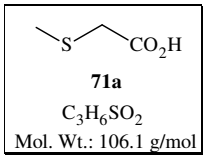
Experiment 5

Synthesis of methylsulfanyl acetic acid (OS-2)

7 ml (100.68 mmol) of thioglycolic acid was dissolved in 200 ml 1N NaOH and to this solution 10 ml (160.63 mmol) of iodomethane (MeI) was added and the reaction mixture was left to stir at room temperature for 3 days. This solution was washed with diethyl ether (2 × 100 ml), then conc. H_2SO_4 was added until the solution acidity was pH = 1, at this stage the solution colour turned from colourless to yellow orange after addition of sulphuric acid.

This solution was extracted with diethyl ether (5 × 50 ml) and the organic layer was washed with saturated NaCl and dried over $MgSO_4$ and filtered by vacuum filtration. The filtrate was evaporated by rotary evaporator to give 6.10 g (57.47 mmol; 57%) of **71a** as a liquid.

Analytical data of *methylsulfanyl acetic acid* (71a)



71a

$C_3H_6SO_2$

Mol. Wt.: 106.1 g/mol

^{1}H–NMR: (400 MHz, $CDCl_3$)

δ (ppm) = 2.19 (s, 3 H, CH_3), 3.19 (s, 2 H, CH_2), 9.27 (s, 1 H, OH).

^{13}C–NMR: (100 MHz, $CDCl_3$)

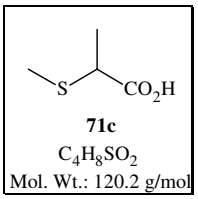
δ (ppm) = 16.6 (s, 1 C, CH_3), 35.9 (s, 1 C, CH_2), 176.6 (s, 1 C, C=O).

Experiment 6

Synthesis of 2-(methylsulfanyl)propanoic acid (OS-14)

9.0 ml (101.5 mmol) of thiolactic acid was dissolved in 200 ml 1 N NaOH and to this solution 10 ml (160.63 mmol) of iodomethane (MeI) was added and the reaction mixture was left to stir at room temperature for 3 days. This solution was washed once with diethyl ether (1 × 100 ml) to remove unreacted starting material. The aqueous layer was acidified with conc. H_2SO_4 (pH = 1) and extracted 3-times with diethyl ether (3 × 50 ml). The combined organic layer was washed with saturated NaCl and was dried over $MgSO_4$ and filtered by vacuum filtration. The filtrate was evaporated by rotary evaporator to give 7.45 g (62 mmol, 61%) of **71c** as a colourless liquid.

Analytical data of *2-(methylsulfanyl)propanoic acid* (71c)



71c
$C_4H_8SO_2$
Mol. Wt.: 120.2 g/mol

^{1}H–NMR: (400 MHz, $CDCl_3$)

δ (ppm) = 1.41 (d, ^3J = 7.2 Hz, 3 H, CH_3), 2.16 (s, 3 H, SCH_3), 3.30 (q, ^3J = 7.2 Hz, 1 H, $CHCO_2$), 11.89 (br. s, 1 H, CO_2H).

^{13}C–NMR: (100 MHz, $CDCl_3$)

δ (ppm) = 14.1 (q, 1 C, CH_3), 16.1 (q, 1C, SCH_3), 41.7 (d, 1 C, $\underline{C}HCO_2$), 179.3 (s, 1 C, CO_2).

9.1.3 General procedure (GP-3) for photodecarboxylative additions of sulphur containing and alkyl carboxylates to N-methylphthalimide under batch conditions (Rayonet):

N-Methylphthalimide (1.5 mmol) was dissolved in 10 ml of acetone. The corresponding carboxylic acid (4.5 mmol or 15 mmol) and K_2CO_3 (2.25 mmol or 7.5 mmol) were dissolved in 20 ml of 25% acetone/H_2O and sonicated using an ultrasound bath until the formation of CO_2 had ceased. The two solutions were poured into a Pyrex Schlenk flask, which was filled up to 100 ml with a 1:1 Vol-% mixture of acetone and H_2O. The solution was further sonicated for 10 minutes and was irradiated at 300±25 nm (Rayonet RPR-200, equipped with 16 × RPR-3000Å lamps, 16 × 8 W) while a gentle stream of nitrogen was flushed through the solution. After irradiation most of the acetone was removed by rotary evaporation and the crude product mixture was extracted with CH_2Cl_2 (3 × 50 ml). The combined organic layers were washed with saturated $NaHCO_3$ (2 × 50 ml), brine (2 × 50 ml) and dried over $MgSO_4$, filtered and evaporated. The conversion rate was determined by ^{1}H-NMR spectroscopy of the crude product. The signal integration for the $NC\underline{H}_3$ protons of NMP was compared to the signal integration for the $NC\underline{H}_3$ protons of the product. Pure products were isolated by column chromatography on silica gel with suitable mobile phase and further characterized by ^{1}H-NMR and ^{13}C-NMR spectroscopy.

Experiment 7

The addition of potassium 2-(methylthio) acetate to NMP (OS-3)

General procedure (GP-3) was followed using NMP (242 mg; 1.5 mmol), methylsulfanyl acetic acid (1.59 g; 15 mmol) and K_2CO_3 (1.04g; 7.5 mmol). After irradiation for 2 hrs the reaction was worked up and the crude product was analysed by ^{1}H-NMR spectroscopy. The conversion was found to be 100% and the yield for isolated product was found to be 295 mg (1.32 mmol, 88%). The product was confirmed by both ^{1}H-NMR and ^{13}C-NMR.

For ^{1}H-NMR data of product **66** see experiment 2.

Experiment 8

The addition of potassium 2-(methylthio) acetate to NMP (OS-51)

General procedure (GP-3) was followed using NMP (242 mg; 1.5 mmol), methylsulfanyl acetic acid (478 mg; 4.5 mmol) and K_2CO_3 (311 mg; 2.25 mmol). After irradiation for 2 hrs the reaction was worked up and the crude product was analysed by ^{1}H-NMR spectroscopy. The conversion was found to be 100% and the yield for the isolated product was found to be 288 mg (1.29 mmol, 86%). The product was confirmed by both ^{1}H-NMR and ^{13}C-NMR.

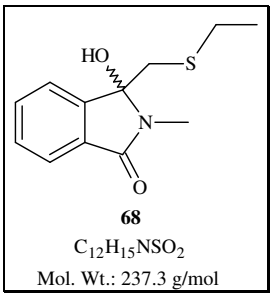
For ^{1}H-NMR data of product **66** see experiment 2.

Experiment 9

The addition of potassium ethylsulfanyl acetate to NMP (OS-65)

General procedure (GP-3) was followed using NMP (242 mg; 1.5 mmol), ethylsulfanyl acetic acid (541 mg; 4.5 mmol) and K_2CO_3 (311 mg; 2.25 mmol). After irradiation for 2 hrs the reaction was worked up and achieved crude product was analysed by ^{1}H-NMR spectroscopy. The conversion was found to be 100% and the yield for the isolated product was found to be 326 mg (1.37 mmol, 91%). The product **68** was confirmed by both ^{1}H-NMR and ^{13}C-NMR.

Analytical data of *3-hydroxy-2-methyl-3-(ethylthiomethyl) isoindolin-1-one* (68)



68

$C_{12}H_{15}NSO_2$

Mol. Wt.: 237.3 g/mol

TLC: *Rf* = 0.21 (ethyl acetate/n-hexane 1:1)

Melting point (colourless solid)**:** 117-119ºC (Lit.[156]: 120-121ºC)

^{1}H–NMR: (400 MHz, Acetone-d_6)

δ (ppm) = 1.01 (t, ^{3}J = 7.2 Hz, 3 H, $CH_2C\underline{H}_3$), 2.18 (q, ^{3}J = 7.2 Hz, 2 H, $C\underline{H}_2CH_3$), 2.92 (s, 3 H, NCH_3), 3.21 (d, ^{2}J = 13.6 Hz, 1 H, CH_2), 3.33 (d, ^{2}J = 14.0 Hz, 1 H, CH_2), 5.48 (s, 1 H, OH), 7.49 (ddd, ^{3}J = 7.6, ^{4}J = 1.2, ^{5}J = 1.2 Hz, 1 H, H_{arom}), 7.58 (ddd, ^{3}J = 7.6, ^{4}J = 1.2, ^{5}J = 1.2 Hz, 1 H, H_{arom}), 7.63 (ddd, ^{3}J = 7.2, ^{4}J = 1.6, ^{5}J = 0.8 Hz, 1 H, H_{arom}), 7.71 (ddd, ^{3}J = 7.2, ^{4}J = 2.0, ^{5}J = 0.8 Hz, 1 H, H_{arom}).

^{13}C–NMR: (100 MHz, Acetone-d_6)

δ (ppm) = 15.0 (s, 1 C, $CH_2\underline{C}H_3$), 23.4 (s, 1 C, NCH_3), 27.1 (s, 1 C, $\underline{C}H_2CH_3$), 38.1 (s, 1 C, CH_2S), 90.7 (s, 1 C, COH), 122.9 (d, 1 C, CH_{arom}), 123.1 (d, 1 C, CH_{arom}), 130.1 (s, 1 C, CH_{arom}), 132.4 (s, 1 C, CH_{arom}), 133.4 (s, 1 C, Cq_{arom}), 147.6 (s, 1 C, Cq_{arom}), 167.0 (s, 1 C, CON).

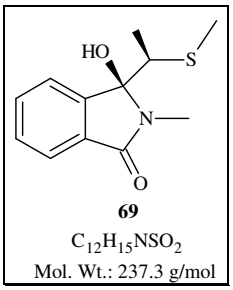
Experiment 10

The addition of potassium 2-methylthio propanoate to NMP (OS-64)

General procedure (GP-3) was followed using NMP (242 mg; 1.5 mmol), 2-methylthio propanoic acid (541 mg; 4.5 mmol) and K_2CO_3 (311 mg; 2.25 mmol). After irradiation for 2 hrs the reaction was worked up and the crude product was analysed by ^{1}H-NMR spectroscopy. The conversion was found to be 100% and the yield of the two isomers **69** and **70** was found to be 341 mg (1.44 mmol, 96%). The ratio of isomers was determined as 45:55 (**69:70**), respectively by ^{1}H-NMR. The signal integration for the $NC\underline{H}_3$ protons of isomer **69** was compared to the signal integration for the $NC\underline{H}_3$ protons of isomer **70**. Assignments of the isomers (**69** and **70**) were consigned by comparison with known analogues reported in the literature.[149]

Analytical data of *3-hydroxy-2-methyl-3-(1-(methylthio)ethyl) isoindolin-1-one* (diastereoisomers 69 and 70)

***Unlike*-3-hydroxy-2-methyl-3-(1-(methylthio)ethyl)isoindolin-1-one (69)**



69

$C_{12}H_{15}NSO_2$

Mol. Wt.: 237.3 g/mol

TLC: *Rf* = 0.19 (ethyl acetate/n-hexane 1:1)

Melting point (colourless solid)**:** 129-131ºC (Lit.[156]: 132-134ºC)

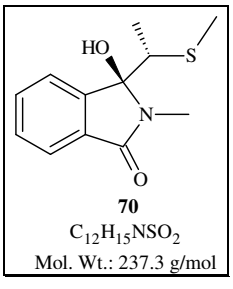
^{1}H–NMR: (400 MHz, Acetone-d_6)

δ (ppm) = 0.83 (d, ^{3}J = 7.2 Hz, 3 H, CH_3), 2.29 (s, 3H, SCH_3), 2.95 (s, 3 H, NCH_3), 3.42 (q, ^{3}J = 7.2 Hz, 1 H, CHS), 5.46 (s, 1 H, OH), 7.50 (ddd, ^{3}J = 7.6 Hz, 1 H, H_{arom}), 7.63 (m, 2 H, H_{arom}), 8.06 (d, ^{3}J = 7.5 Hz, 1 H, H_{arom}).

^{13}C–NMR: (100 MHz, Acetone-d_6)

δ (ppm) = 16.5 (q, 1 C, SCH3), 17.4 (q, 1 C, CH_3), 23.6 (q, 1 C, NCH_3), 47.6 (d, 1 C, CHS), 93.4 (s, 1 C, COH), 123.1 (d, 1 C, CH_{arom}), 124.9 (d, 1 C, CH_{arom}), 130.1 (d, 1 C, CH_{arom}), 132.1 (s, 1 C, CH_{arom}), 133.5 (d, 1 C, Cq_{arom}), 146.5 (s, 1 C, Cq_{arom}), 166.9 (s, 1 C, CON).

***Like*-3-hydroxy-2-methyl-3-(1-(methylthio)ethyl)isoindolin-1-one (70)**



70

$C_{12}H_{15}NSO_2$

Mol. Wt.: 237.3 g/mol

TLC: *Rf* = 0.31 (ethyl acetate/n-hexane 1:1)

Melting point (colourless solid)**:** 133-135ºC (Lit.[156]: 136-138ºC)

^{1}H–NMR: (400 MHz, Acetone-d_6)

δ (ppm) = 1.48 (d, ^{3}J = 7.0 Hz, 3 H, CH_3), 1.88 (s, 3H, SCH_3), 2.97 (s, 3 H, NCH_3), 3.43 (q, ^{3}J = 7.0 Hz, 1 H, CHS), 5.50 (s, 1 H, OH), 7.56 (m, 1 H, H_{arom}), 7.65 (m, 2 H, H_{arom}), 7.67 (d, ^{3}J = 7.5 Hz, 1 H, H_{arom}).

^{13}C–NMR: (100 MHz, Acetone-d_6)

δ (ppm) = 14.3 (q, 1 C, SCH3), 16.6 (q, 1 C, CH_3), 24.1 (q, 1 C, NCH_3), 48.2 (d, 1 C, CHS), 92.6 (s, 1 C, COH), 122.9 (d, 1 C, CH_{arom}), 123.9 (d, 1 C, CH_{arom}), 130.2 (d, 1 C, CH_{arom}), 132.1 (s, 1 C, CH_{arom}), 133.8 (d, 1 C, Cq_{arom}), 146.6 (s, 1 C, Cq_{arom}), 167.0 (s, 1 C, CON).

Experiment 11

The addition of potassium 2-(methylthio) acetate to NMP (OS-11)

General procedure (GP-3) was followed using NMP (242 mg; 1.5 mmol), methylsulfanyl acetic acid (478 mg; 4.5 mmol) and K_2CO_3 (311 mg; 2.25 mmol). After irradiation for 1 hr the reaction was stopped and worked up. The obtained crude product was analysed by ^{1}H-NMR spectroscopy and the composition of NMP to product **66** was calculated from the ^{1}H-NMR integration to be 14:86.

For ^{1}H-NMR data of product **66** see experiment 2.

Experiment 12

The addition of potassium 2-(methylthio) acetate to NMP (OS-54)

General procedure (GP-3) was followed using NMP (242 mg; 1.5 mmol), methylsulfanyl acetic acid (478 mg; 4.5 mmol) and K_2CO_3 (311 mg; 2.25 mmol). After irradiation for 40 min the reaction was stopped and worked up. The obtained crude product was analysed by ^{1}H-NMR spectroscopy and the composition of NMP to product **66** was calculated from the ^{1}H-NMR integration to be 56:44.

For ^{1}H-NMR data of product **66** see experiment 2.

Experiment 13

The addition of potassium 2-(methylthio) acetate to NMP (OS-49)

General procedure (GP-3) was followed using NMP (242 mg; 1.5 mmol), methylsulfanyl acetic acid (478 mg; 4.5 mmol) and K_2CO_3 (311 mg; 2.25 mmol). After irradiation for 21 min the reaction was stopped and worked up. The obtained crude product was analysed by ^{1}H-NMR spectroscopy and the composition of NMP to product **66** was calculated from the ^{1}H-NMR integration to be 80:20.

For ^{1}H-NMR data of product **66** see experiment 2.

Experiment 14

The addition of potassium 2-(methylthio) acetate to NMP (OS-218)

General procedure (GP-3) was followed using NMP (242 mg; 1.5 mmol), methylsulfanyl acetic acid (478 mg; 4.5 mmol) and K_2CO_3 (311 mg; 2.25 mmol). After irradiation for 14 min the reaction was stopped and worked up. The obtained crude product was analysed by ^{1}H-NMR spectroscopy and the composition of NMP to product **66** was calculated from the ^{1}H-NMR integration to be 98:2.

For ^{1}H-NMR data of product **66** see experiment 2.

9.1.4 General procedure (GP-4) for photodecarboxylative additions of potassium 2-(methylthio) acetate or phenylacetate to N-methylphthalimide in the dwell-microreactor:

N-Methylphthalimide (0.225 mmol) was dissolved in 1.5 ml of acetone. The corresponding carboxylic acid (0.675 mmol) and K_2CO_3 (0.338 mmol) were dissolved in 2 ml of H_2O and 0.5 ml of acetone and were sonicated using an ultrasound bath until the formation of CO_2 had ceased. The solutions were poured into a Pyrex test tube, which was filled up to 15 ml with a 1:1 Vol% mixture of acetone and H_2O. This solution was further sonicated for 15 min using an ultrasound bath and degassed with a slow stream of N_2 for 15 minutes. The microreactor was prepared by pumping the pre-sonicated acetone/water mixture (1:1) through the reaction channel until all air bubbles had been removed. Then 10 ml of prepared reaction mixture was transferred into a 10 ml glass syringe, any air bubbles were expelled and the syringe was loaded into a syringe pump. The flow rate was set and the solution was pumped through a micro-reactor (mikroglas dwell device) while irradiated at 300±25 nm (Luzchem UV exposure panel equipped with 5 × RPR-3000Å lamps, 5 × 8 W). During the reaction, the reactor was kept cool by pumping cold water through the cooling channel. When the syringe was empty, the syringe pump and the lamps were switched off simultaneously. The syringe was refilled with acetone/water mixture and loaded into a syringe pump again. The syringe pump was then turned on simultaneously with the lamps. After irradiation most of the acetone was removed by rotary evaporation and the remaining solution was extracted with CH_2Cl_2 (3 × 10 ml). The combined organic layer was washed with sat. $NaHCO_3$ (2 × 10 ml), brine (2 × 10 ml), dried over $MgSO_4$, filtered and removed by rotary evaporation. The conversion rate was determined by ^{1}H-NMR spectroscopy of

the crude product. The signal integration for the NCH_3 protons of NMP was compared to the signal integration for the NCH_3 protons of the product.

Experiment 15

The addition of potassium 2-(methylthio) acetate to NMP (OS-21)

General procedure (GP-4) was followed using NMP (36 mg; 0.225 mmol), methylsulfanyl acetic acid (72 mg; 0.675 mmol) and K_2CO_3 (47 mg; 0.338 mmol). The flow rate used was 0.028 ml/min; residence time: 1 hr. The conversion was found to be 100% and the yield was found to be 29 mg (0.13 mmol, 88%). Both the ^{1}H-NMR and ^{13}C-NMR confirmed the product to be pure product **66**.

For ^{1}H-NMR data of product **66** see experiment 2.

Experiment 16

The addition of potassium 2-(methylthio) acetate to NMP (OS-17)

General procedure (GP-4) was followed using NMP (36 mg; 0.225 mmol), methylsulfanyl acetic acid (72 mg; 0.675 mmol) and K_2CO_3 (47 mg; 0.338 mmol). The flow rate used was 0.042 ml/min; residence time: 40 min. The composition of NMP to product **66** was calculated from the ^{1}H-NMR integration to be 34:66.

For ^{1}H-NMR data of product **66** see experiment 2.

Experiment 17

The addition of potassium 2-(methylthio) acetate to NMP (OS-8)

General procedure (GP-4) was followed using NMP (36 mg; 0.225 mmol), methylsulfanyl acetic acid (72 mg; 0.675 mmol) and K_2CO_3 (47 mg; 0.338 mmol). The flow rate used was 0.08 ml/min; residence time: 21 min. The composition of NMP to product **66** was calculated from the ^{1}H-NMR integration to be 66:34.

For ^{1}H-NMR data of product **66** see experiment 2.

Experiment 18

The addition of potassium 2-(methylthio) acetate to NMP (OS-219)

General procedure (GP-4) was followed using NMP (36 mg; 0.225 mmol), methylsulfanyl acetic acid (72 mg; 0.675 mmol) and K_2CO_3 (47 mg; 0.338 mmol). The

flow rate used was 0.12 ml/min; residence time: 14 min. The composition of NMP to product **66** was calculated from the ^{1}H-NMR integration to be 96:4.

For ^{1}H-NMR data of product **66** see experiment 2.

Experiment 19

The addition of potassium 2-(methylthio) acetate to NMP (OS-213)

General procedure (GP-3) was followed, with one variation, using NMP (242 mg; 1.5 mmol), methylsulfanyl acetic acid (478 mg; 4.5 mmol) and K_2CO_3 (311 mg; 2.25 mmol). In this experiment the Rayonet reactor was equipped with 5 × RPR-3000Å lamps (5 × 8 W, λ_{max} = 300±25 nm) and 11 cool white lamps F8T5/CW (11 × 8 W, λ = 400–700 nm) instead of 16 × RPR-3000Å lamps. After irradiation for 1 hr the reaction was stopped and worked up. The obtained crude product was analysed by ^{1}H-NMR spectroscopy and the composition of NMP to product **66** was calculated from the ^{1}H-NMR integration to be 83:17.

For ^{1}H-NMR data of product **66** see experiment 2.

9.1.5 General procedure (GP-5) for photodecarboxylative addition of potassium 2-(methylthio) acetate or phenylacetate to N-methylphthalimide under DMBP or 4-CBPH sensitisation in the batch system (Rayonet):

N-Methylphthalimide (1.5 mmol) and the sensitizer (4,4'-dimethoxybenzophenone or 4-carboxybenzophenone; 0.15 mmol) were dissolved in 10 ml of acetonitrile. The corresponding carboxylic acid (4.5 mmol) and K_2CO_3 (311 mg; 2.25 mmol) were dissolved in 20 ml of 25% acetonitrile/H_2O and then sonicated using an ultrasound bath until the formation of CO_2 had ceased. The solutions were poured into a Pyrex Schlenk flask, which was filled up to 100 ml with a 1:1 Vol% mixture of acetonitrile and H_2O. The solution was further sonicated for 10 minutes and was irradiated at 350±25 nm (Rayonet RPR-200, equipped with 16 × RPR-3500Å lamps, 16 × 8 W) while a gentle stream of nitrogen was flushed through the solution. After irradiation most of the acetonitrile was evaporated and the crude product mixture was extracted with CH_2Cl_2 (3 × 50 ml). The combined organic layer was washed with saturated $NaHCO_3$ (2 × 50 ml), brine (2 × 50 ml), dried over $MgSO_4$, filtered and evaporated. The conversion rate was determined by ^{1}H-NMR integration of the crude product. The signal integration for the $NC\underline{H}_3$ protons of NMP was compared to the signal integration for the $NC\underline{H}_3$ protons of

the product. Pure products were isolated by column chromatography on silica gel with suitable mobile phase and further characterized by ^{1}H-NMR and ^{13}C-NMR spectroscopy.

Experiment 20

The addition of potassium 2-(methylthio) acetate to NMP under 4-Carboxybenzophenone sensitization (OS-24)

General procedure (GP-5) was followed using NMP (242 mg; 1.5 mmol), 4-carboxybenzophenone (34 mg; 0.15 mmol), methylsulfanyl acetic acid (478 mg; 4.5 mmol) and K_2CO_3 (311 mg; 2.25 mmol). After irradiation for 2 hr the reaction was stopped and worked up. The obtained crude product was analysed by ^{1}H-NMR spectroscopy and result showed that NMP did not undergo any conversion and was recovered in 82% (198 mg; 1.2 mmol).

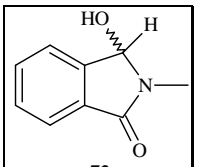
Experiment 21

The addition of potassium 2-(methylthio) acetate to NMP under 4,4'-Dimethoxybenzophenone sensitization (OS-28)

General procedure (GP-5) was followed using NMP (242 mg; 1.5 mmol), 4,4'-dimethoxybenzophenone (36 mg; 0.15 mmol), methylsulfanyl acetic acid (478 mg; 4.5 mmol) and K_2CO_3 (311 mg; 2.25 mmol). After irradiation for 1 hr the reaction was stopped and worked up. The obtained crude product was analysed by ^{1}H-NMR and the conversion was found to be 100%. A mixture of desired product **66**, photoreduction product **72** and secondary products of the sensitizer DMBP were also obtained. The crude product was further purified by column chromatography using ethyl acetate/n-hexane (1:1). The isolated yield of **66** was found to be 68 mg (0.31 mmol, 41%) and the isolated yield of the photoreduction product **72** was found to be 11 mg (0.07 mmol, 9%).

For ^{1}H-NMR data of product **66** see experiment 2.

Analytical data of *3–Hydroxy–2–methyl–2,3–dihydroisoindol–1–on* (72)



72

$C_9H_9NO_2$

Mol. Wt.: 163.2 g/mol

TLC: *Rf* = 0.16 (ethyl acetate/n-hexane 1:1)

Melting point (colorless solid)**:** 127-129ºC (Lit.[267]: 128-129ºC)

^{1}H–NMR: (400 MHz, Acetone-d_6)

δ (ppm) = 3.04 (s, 3 H, NCH_3), 5.40 (d, ^3J = 9.6 Hz, 1 H, OH), 5.78 (d, ^3J = 9.6 Hz, 1 H, CHN), 7.50 (m, 1 H, H_{arom}), 7.60 (m, 2 H, H_{arom}), 7.65 (d, ^3J = 7.6 Hz, 1 H, H_{arom}).

^{13}C–NMR: (100 MHz, $CDCl_3$)

δ (ppm) = 26.0 (q, 1 C, NCH_3), 83.5 (d, 1 C, CHN), 122.8 (d, 1 C, CH_{arom}), 123.1 (d, 1 C, CH_{arom}), 131.2 (s, 1 C, Cq_{arom}), 132.0 (d, 1 C, CH_{arom}), 133.8 (d, 1 C, CH_{arom}), 143.8 (s, 1 C, Cq_{arom}), 167.6 (s, 1 C, CON).

9.1.6 General procedure (GP-6) for photodecarboxylative addition of potassium 2-(methylthio) acetate or phenylacetate to N-methylphthalimide under DMBP sensitisation in the dwell-microreactor:

N-Methylphthalimide (0.225 mmol) and sensitizer 4,4'-dimethoxybenzophenone (22.5 µmol) were dissolved in 1.5 ml of acetonitrile. The corresponding carboxylic acid (0.675 mmol) and K_2CO_3 (0.338 mmol) were dissolved in 2 ml of H_2O and 0.5 ml of acetonitrile and were sonicated using an ultrasound bath until the formation of CO_2 ceased. The solutions were poured into a Pyrex test tube, which was filled up to 15 ml with a 1:1 Vol% mixture of acetonitrile and H_2O. This solution was further sonicated for 15 min using an ultrasound bath and degassed with a slow stream of N_2 for 15 minutes. The microreactor was prepared by pumping the pre-sonicated acetonitrile/water mixture (1:1) through the reaction channel until all air bubbles had been removed. Then 10 ml of prepared reaction mixture was transferred into a 10 ml glass syringe, any air bubbles were expelled and the syringe was loaded into a syringe pump. The flow rate was set and the solution was pumped through a micro-reactor (mikroglas dwell device) while irradiated at 350±25 nm (Luzchem UV exposure panel equipped with 5 × RPR-3500Å lamps, 5 × 8 W). During the reaction, the reactor was kept cool by pumping cold water through the cooling channel. When the syringe was

empty, the syringe pump and the lamps were switched off simultaneously. The syringe was refilled with an acetonitrile/water mixture and loaded into a syringe pump again. The syringe pump was then turned on simultaneously with the lamps. After irradiation most of the acetonitrile was evaporated and the crude product mixture was extracted with CH_2Cl_2 (3 × 10 ml). The combined organic layers were washed with sat. $NaHCO_3$ (2 × 10 ml), brine (2 × 10 ml), dried over $MgSO_4$, filtered and evaporated. The conversion rate was determined by ^{1}H-NMR of the crude product. The signal integration for the NC$\underline{H}_3$ protons of NMP was compared to the signal integration for the NC$\underline{H}_3$ protons of the product. Pure products were isolated by column chromatography on silica gel with suitable mobile phase and further characterized by ^{1}H-NMR and ^{13}C-NMR spectroscopy.

Experiment 22

The addition of potassium 2-(methylthio) acetate to NMP under 4,4'-Dimethoxybenzophenone sensitization (OS-92)

General procedure (GP-6) was followed using NMP (36 mg; 0.225 mmol), 4,4'-dimethoxybenzophenone (5.5 mg; 22.5 µmol), methylsulfanyl acetic acid (72 mg; 0.675 mmol) and K_2CO_3 (47 mg; 0.338 mmol). The flow rate used was 0.028 ml/min; residence time: 1 hr. The composition of NMP to product **66** was calculated from the ^{1}H-NMR integration to be 10:90. The photoreduction product **72** of NMP and decomposition products of DMBP were not detected.

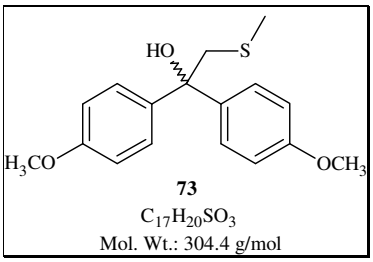
For ^{1}H-NMR data of product **66** see experiment 2.

Experiment 23

The addition of potassium 2-(methylthio) acetate to 4,4'-Dimethoxybenzophenone (OS-66)

General procedure (GP-5) was followed, with two variations, using 4,4'-dimethoxybenzophenone (18 mg; 0.075 mmol), methylsulfanyl acetic acid (239 mg; 2.25 mmol) and K_2CO_3 (156 mg; 1.13 mmol). This experiment was carried out without NMP and the total volume of prepared solution was 50 ml. After irradiation for 1 hr the reaction was stopped and worked up. The obtained crude product was analysed by ^{1}H-NMR and the conversion was found to be 100%. The addition product **73** and benzpinacol **74** were formed in the ratio of 55:45 (**73**:**74**), respectively. The ratio of **73**:**74** was calculated by comparing the signal integrations for the C$\underline{H}_{arom}$ protons.

Analytical data of *1,1-Bis(4-methoxyphenyl)-2-(methylthio)ethanol* (73)



73

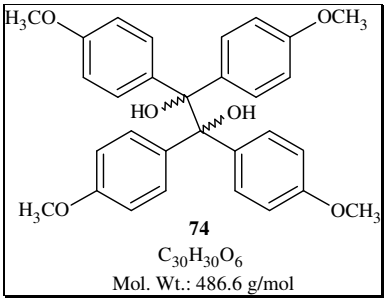
$C_{17}H_{20}SO_3$

Mol. Wt.: 304.4 g/mol

^{1}H–NMR: (400 MHz, Acetone-d_6)

δ (ppm) = 1.96 (s, 3 H, SCH_3), 3.41 (s, 2 H, CH_2S), 3.76 (s, 6 H, OCH_3), 4.38 (s, 1 H, OH), 6.84 (d, ^3J = 9.2 Hz, 4 H, H_{arom}), 7.39 (d, ^3J = 9.2 Hz, 4 H, H_{arom}).

Analytical data of *1,1,2,2-Tetrakis(4-methoxyphenyl)ethane-1,2-diol* (74)



74

$C_{30}H_{30}O_6$

Mol. Wt.: 486.6 g/mol

^{1}H–NMR: (400 MHz, Acetone-d_6)

δ (ppm) = 3.72 (s, 12 H, OCH_3), 4.47 (s, 2 H, OH), 6.65 (d, ^3J = 9.2 Hz, 8 H, H_{arom}), 7.31 (d, ^3J = 9.2 Hz, 8 H, H_{arom}).

Experiment 24

The addition of potassium 2-(methylthio) acetate to NMP under direct excitation (OS-125)

General procedure (GP-3) was followed, with one variation, using NMP (242 mg; 1.5 mmol), methylsulfanyl acetic acid (478 mg; 4.5 mmol) and K_2CO_3 (311 mg; 2.25 mmol). In this experiment the solvent acetone was replaced with acetonitrile. After irradiation for 1 hr the reaction was worked up and the crude product was analysed by ^{1}H-NMR. The conversion was found to be 100% and ^{1}H-NMR confirmed that this was product **66**.

For ^{1}H-NMR data of product **66** see experiment 2.

Experiment 25

The addition of potassium 2-(methylthio) acetate to NMP under direct excitation (OS-135)

General procedure (GP-3) was followed, with two variations, using NMP (242 mg; 1.5 mmol), methylsulfanyl acetic acid (478 mg; 4.5 mmol) and K_2CO_3 (311 mg; 2.25 mmol). In this experiment the solvent acetone was replaced with acetonitrile and a stream of N_2 was precisely controlled during irradiation at a flow rate of 26.5 ml/min. After irradiation for 1 hr the reaction was worked up and the crude product was analysed by ^{1}H-NMR. The conversion was found to be 100% and ^{1}H-NMR confirmed that this was product **66**.

For ^{1}H-NMR data of product **66** see experiment 2.

Experiment 26

The addition of potassium 2-(methylthio) acetate to NMP under direct excitation (OS-119)

General procedure (GP-3) was followed, with two variations, using NMP (242 mg; 1.5 mmol), methylsulfanyl acetic acid (478 mg; 4.5 mmol) and K_2CO_3 (311 mg; 2.25 mmol). In this experiment acetone was replaced with acetonitrile and a stream of N_2 was precisely controlled during irradiation at a flow rate of 150.0 ml/min. After irradiation for 1 hr the reaction was worked up and the crude product was analysed by ^{1}H-NMR. The composition of NMP to product **66** was calculated from the ^{1}H-NMR integration to be 21:79.

For ^{1}H-NMR data of product **66** see experiment 2.

Experiment 27

The addition of potassium 2-(methylthio) acetate to NMP under direct excitation (OS-134)

General procedure (GP-3) was followed, with two variations, using NMP (242 mg; 1.5 mmol), methylsulfanyl acetic acid (478 mg; 4.5 mmol) and K_2CO_3 (311 mg; 2.25 mmol). In this experiment acetone was replaced with acetonitrile and the solution was degassed with a slow stream of N_2 for 15 minutes before irradiation. After irradiation

for 1 hr the reaction was worked up and the crude product was analysed by ^{1}H-NMR. The composition of NMP to product **66** was calculated to be 4:96.

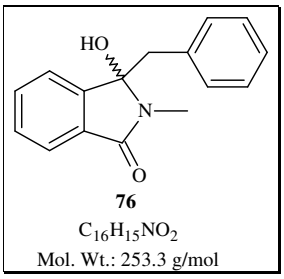
For ^{1}H-NMR data of product **66** see experiment 2.

Experiment 28

The addition of phenylacetate to NMP (OS-103)

General procedure (GP-3) was followed using NMP (242 mg; 1.5 mmol), phenylacetic acid (613 mg, 4.5 mmol) and K_2CO_3 (311 mg; 2.25 mmol). After irradiation for 1 hr the reaction was stopped and worked up. The conversion was found to be 100% and the isolated yield was 372 mg (1.47 mmol, 98%). The ^{1}H-NMR and ^{13}C-NMR spectroscopy confirmed the product to be **76**.

Analytical data of *3-benzyl-3-hydroxy-2-methylisoindolin-1-one* (76)



76

$C_{16}H_{15}NO_2$

Mol. Wt.: 253.3 g/mol

TLC: ***Rf*** = 0.29 (ethyl acetate/n-hexane 1:1)

Melting point (colourless solid)**:** 164-168ºC (Lit.[268]: 165-168ºC)

^{1}H–NMR: (400 MHz, Acetone-d_6)

δ (ppm) = 3.05 (s, 3 H, NCH_3), 3.30 (d, ^{2}J = 13.6 Hz, 1 H, CH_2Ph), 3.48 (d, ^{2}J = 13.6 Hz, 1 H, CH_2Ph), 5.38 (s, 1 H, OH), 6.90 (m, 2 H, H_{arom}), 7.05 (m, 3 H, H_{arom}), 7.38–7.45 (m, 2 H, H_{arom}), 7.54 (m, 2 H, H_{arom}).

^{13}C–NMR: (100 MHz, Acetone-d_6)

δ (ppm) = 24.0 (s, 1 C, NCH_3), 42.9 (s, 1 C, CH_2Ph), 91.2 (s, 1 C, COH), 122.9 (d, 1 C, CH_{arom}), 123.7 (d, 1 C, CH_{arom}), 127.3 (d, 1 C, CH_{arom}), 128.5 (d, 2 C, CH_{arom}), 129.8 (d, 1 C, CH_{arom}), 130.8 (d, 2 C, CH_{arom}), 132.1 (d, 1 C, CH_{arom}), 133.0 (s, 1 C, Cq_{arom}), 136.3 (s, 1 C, Cq_{arom}), 147.9 (s, 1 C, Cq_{arom}), 166.8 (s, 1 C, CON).

Experiment 29

The addition of phenylacetate to NMP (OS-216)

General procedure (GP-3) was followed using NMP (242 mg; 1.5 mmol), phenylacetic acid (613 mg, 4.5 mmol) and K_2CO_3 (311 mg; 2.25 mmol). After irradiation for 40 min the reaction was stopped and worked up. The conversion was found to be 100% and the isolated yield was 375 mg (1.47 mmol, 98%). The structure of **76** was confirmed by both ^{1}H-NMR and ^{13}C-NMR.

For ^{1}H-NMR data of product **76** see experiment 28.

Experiment 30

The addition of phenylacetate to NMP (OS-217)

General procedure (GP-3) was followed using NMP (242 mg; 1.5 mmol), phenylacetic acid (613 mg, 4.5 mmol) and K_2CO_3 (311 mg; 2.25 mmol). After irradiation for 21 min the reaction was stopped and worked up. The obtained crude product was analysed by ^{1}H-NMR and the composition of NMP to product **76** was calculated from the ^{1}H-NMR integration to be 7:93.

For ^{1}H-NMR data of product **76** see experiment 28.

Experiment 31

The addition of phenylacetate to NMP (OS-215)

General procedure (GP-3) was followed using NMP (242 mg; 1.5 mmol), phenylacetic acid (613 mg, 4.5 mmol) and K_2CO_3 (311 mg; 2.25 mmol). After irradiation for 14 min the reaction was stopped and worked up. The obtained crude product was analysed by ^{1}H-NMR and the composition of NMP to product **76** was calculated from the ^{1}H-NMR integration to be 54:46.

For ^{1}H-NMR data of product **76** see experiment 28.

Experiment 32

The addition of phenylacetate to NMP (OS-104)

General procedure (GP-4) was followed using NMP (36 mg; 0.225 mmol), phenylacetic acid (92 mg; 0.675 mmol) and K_2CO_3 (47 mg; 0.338 mmol). The flow rate used was

0.028 ml/min; residence time: 1 hr. The conversion was found to be 100% and the isolated yield was found to be 38 mg (0.15 mmol, 100%). The structure of **76** was confirmed by both ^{1}H-NMR and ^{13}C-NMR.

For ^{1}H-NMR data of product **76** see experiment 28.

Experiment 33

The addition of phenylacetate to NMP (SG-194)

General procedure (GP-4) was followed using NMP (36 mg; 0.225 mmol), phenylacetic acid (92 mg; 0.675 mmol) and K_2CO_3 (47 mg; 0.338 mmol). The flow rate used was 0.042 ml/min; residence time: 40 min. The conversion was found to be 100% and the yield of the isolated product was 39 mg (0.15 mmol, 100%). The structure of **76** was confirmed by both ^{1}H-NMR and ^{13}C-NMR.

For ^{1}H-NMR data of product **76** see experiment 28.

Experiment 34

The addition of phenylacetate to NMP (SG-205)

General procedure (GP-4) was followed using NMP (36 mg; 0.225 mmol), phenylacetic acid (92 mg; 0.675 mmol) and K_2CO_3 (47 mg; 0.338 mmol). The flow rate used was 0.08 ml/min; residence time: 21 min. The composition of NMP to product **76** was calculated from the ^{1}H-NMR integration to be 3:97.

For ^{1}H-NMR data of product **76** see experiment 28.

Experiment 35

The addition of phenylacetate to NMP (SG-204)

General procedure (GP-4) was followed using NMP (36 mg; 0.225 mmol), phenylacetic acid (92 mg; 0.675 mmol) and K_2CO_3 (47 mg; 0.338 mmol). The flow rate used was 0.12 ml/min; residence time: 14 min. The composition of NMP to product **76** was calculated from the ^{1}H-NMR integration to be 17:83.

For ^{1}H-NMR data of product **76** see experiment 28.

Experiment 36

The addition of phenylacetate to NMP (OS-102)

General procedure (GP-3) was followed, with one variation, using NMP (242 mg; 1.5 mmol), phenylacetic acid (613 mg, 4.5 mmol) and K_2CO_3 (311 mg; 2.25 mmol). In this experiment the Rayonet reactor was equipped with 5 × RPR-3000Å lamps (5 × 8 W, λ_{max} = 300±25 nm) and 11 cool white lamps F8T5/CW (11 × 8 W, λ = 400–700 nm) instead of 16 × RPR-3000Å lamps. After irradiation for 1 hr the reaction was stopped and worked up. The obtained crude product was analysed by ^{1}H-NMR and the composition of NMP to product **76** was calculated from the ^{1}H-NMR integration to be 71:29.

For ^{1}H-NMR data of product **76** see experiment 28.

Experiment 37

The addition of phenylacetate to NMP (OS-152)

General procedure (GP-3) was followed, with the variation of using acetonitrile as the solvent instead of acetone and using NMP (242 mg; 1.5 mmol), phenylacetic acid (613 mg, 4.5 mmol) and K_2CO_3 (311 mg; 2.25 mmol). After irradiation for 1 hr the reaction was stopped and worked up. The conversion was found to be 100% and the yield of isolated product was 336 mg (1.33 mmol, 89%). The structure of **76** was confirmed by both ^{1}H-NMR and ^{13}C-NMR.

For ^{1}H-NMR data of product **76** see experiment 28.

Experiment 38

The addition of phenylacetate to NMP (OS-153)

General procedure (GP-3) was followed, with the variation of using acetonitrile as the solvent instead of acetone and using NMP (484 mg; 3.0 mmol), phenylacetic acid (1.23 g, 9.0 mmol) and K_2CO_3 (622 mg; 4.5 mmol). After irradiation for 1 hr the reaction was stopped and worked up. The obtained crude product was analysed by ^{1}H-NMR and the composition of NMP to product **76** was calculated from the ^{1}H-NMR integration to be 7:93.

For ^{1}H-NMR data of product **76** see experiment 28.

Experiment 39

The addition of phenylacetate to NMP (OS-178)

General procedure (GP-3) was followed, with the variation of using acetonitrile as the solvent instead of acetone and using NMP (968 mg; 6.0 mmol), phenylacetic acid (2.45 g, 18.0 mmol) and K_2CO_3 (1.24 mg; 9.0 mmol). After irradiation for 1 hr the reaction was stopped and worked up. The obtained crude product was analysed by ^{1}H-NMR and the composition of NMP to product **76** was calculated from the ^{1}H-NMR integration to be 47:53.

For ^{1}H-NMR data of product **76** see experiment 28.

Experiment 40

The addition of phenylacetate to NMP (OS-179)

General procedure (GP-3) was followed, with the variation of using acetonitrile as the solvent instead of acetone and using NMP (1.45 g; 9.0 mmol), phenylacetic acid (3.68 g, 27.0 mmol) and K_2CO_3 (1.87 mg; 13.5 mmol). After irradiation for 1 hr the reaction was stopped and worked up. The obtained crude product was analysed by ^{1}H-NMR and the composition of NMP to product **76** was calculated from the ^{1}H-NMR integration to be 62:38.

For ^{1}H-NMR data of product **76** see experiment 28.

Experiment 41

The addition of phenylacetate to NMP (OS-162)

General procedure (GP-4) was followed, with the variation of using acetonitrile as the solvent instead of acetone and using NMP (36 mg; 0.225 mmol), phenylacetic acid (92 mg, 0.675 mmol) and K_2CO_3 (47 mg; 0.338 mmol). The flow rate used was 0.028 ml/min; residence time: 1 hr. The conversion was found to be 100% and the yield of isolated product was 35 mg (0.14 mmol, 93%). The structure of **76** was confirmed by both ^{1}H-NMR and ^{13}C-NMR.

For ^{1}H-NMR data of product **76** see experiment 28.

Experiment 42

The addition of phenylacetate to NMP (OS-163)

General procedure (GP-4) was followed, with the variation of using acetonitrile as the solvent instead of acetone and using NMP (73 mg; 0.46 mmol), phenylacetic acid (184 mg, 1.35 mmol) and K_2CO_3 (93 mg; 0.673 mmol). The flow rate used was 0.028 ml/min; residence time: 1 hr. The conversion was found to be 100% and the yield of isolated product was 71 mg (0.28 mmol, 91%). The structure of **76** was confirmed by both ^{1}H-NMR and ^{13}C-NMR.

For ^{1}H-NMR data of product **76** see experiment 28.

Experiment 43

The addition of phenylacetate to NMP (OS-175)

General procedure (GP-4) was followed, with the variation of using acetonitrile as the solvent instead of acetone and using NMP (145 mg; 0.91 mmol), phenylacetic acid (368 mg, 2.7 mmol) and K_2CO_3 (187 mg; 1.35 mmol). The flow rate used was 0.028 ml/min; residence time: 1 hr. The composition of NMP to product **76** was calculated from the ^{1}H-NMR integration to be 36:64.

For ^{1}H-NMR data of product **76** see experiment 28.

Experiment 44

The addition of phenylacetate to NMP (OS-190)

General procedure (GP-4) was followed, with the variation of using acetonitrile as the solvent instead of acetone and using NMP (218 mg; 1.36 mmol), phenylacetic acid (551 mg, 4.05 mmol) and K_2CO_3 (280 mg; 2.03 mmol). The flow rate used was 0.028 ml/min; residence time: 1 hr. The composition of NMP to product **76** was calculated from the ^{1}H-NMR integration to be 55:45.

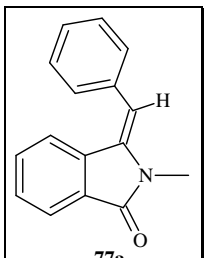
For ^{1}H-NMR data of product **76** see experiment 28.

Experiment 45

The addition of phenylacetate to NMP under 4,4'-Dimethoxybenzophenone sensitization (OS-96)

General procedure (GP-5) was followed using NMP (242 mg; 1.5 mmol), 4,4'-dimethoxybenzophenone (36 mg; 0.15 mmol), phenylacetic acid (613 mg, 4.5 mmol) and K_2CO_3 (311 mg; 2.25 mmol). After irradiation for 1 hr the reaction was stopped and worked up. The obtained crude product was analysed by ^{1}H-NMR and the conversion was found to be 100%. A mixture of olefins **77a,b** were isolated instead of the photoaddition product **76**. The *E*-isomer was preferentially formed and only traces of the *Z*-isomer were detected by ^{1}H-NMR. Assignments of the two isomers (***E/Z***) were consigned by comparison with known analogues reported in the literature.[114,145,163]

Analytical data of *(3E)–3–benzylidene–2–methylisoindolin–1–one* (77a)



77a
E-isomer
$C_{16}H_{13}NO$
Mol. Wt.: 235.3 g/mol

TLC: ***Rf*** = 0.55 (ethyl acetate/n-hexane 1:1)

^{1}H–NMR: (400 MHz, Acetone-d_6)

δ (ppm) = 3.36 (s, 3 H, NCH_3), 6.69 (s, 1 H, H_{olef}), 7.35 (d, ^3J = 7.6 Hz, 1 H, H_{arom}), 7.41 (m, 2 H, H_{arom}), 7.48 (m, 5 H, H_{arom}), 7.75 (d, ^3J = 7.6 Hz, 1 H, H_{arom}).

^{13}C–NMR: (100 MHz, $CDCl_3$)

δ (ppm) = 26.3, 110.4, 123.1, 127.9, 128.8, 129.3, 129.7, 130.8, 131.6, 134.0, 135.0, 135.4, 137.6, 166.7.

Experiment 46

The addition of phenylacetate to NMP under 4,4'-Dimethoxybenzophenone sensitization (OS-97)

General procedure (GP-6) was followed using NMP (36 mg; 0.225 mmol), 4,4'-dimethoxybenzophenone (5.5 mg; 22.5 µmol), phenylacetic acid (92 mg, 0.675 mmol)

and K_2CO_3 (47 mg; 0.338 mmol). The flow rate used was 0.028 ml/min; residence time: 1 hr. The obtained crude product was analysed by ^{1}H-NMR and the conversion was found to be 100%. A mixture of olefins **77a,b** were isolated instead of the photoaddition product **76**. The *E*-isomer was preferentially formed and only traces of the *Z*-isomer were detected by ^{1}H-NMR.

For ^{1}H-NMR data of product **77a** see experiment 45.

Experiment 47

The addition of phenylacetate to NMP under direct excitation (OS-372)

General procedure (GP-5) was followed, with two variations, using NMP (121 mg; 0.75 mmol), phenylacetic acid (306 mg, 2.25 mmol) and K_2CO_3 (156 mg; 1.13 mmol). In this experiment the sensitizer was not added to the experimental solution and the total volume of prepared solution was 50 ml. After irradiation for 1 hr the reaction was worked up and the crude product was analysed by ^{1}H-NMR. The composition of NMP to product **76** was calculated from the ^{1}H-NMR integration to be 92:8.

For ^{1}H-NMR data of product **76** see experiment 28.

Experiment 48

The addition of phenylacetate to NMP under direct excitation (OS-380)

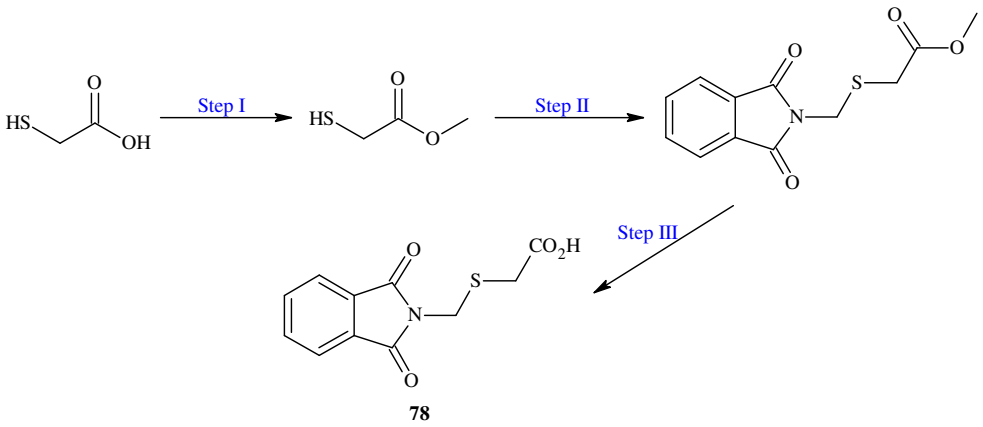
General procedure (GP-6) was followed, with one variation, using NMP (36 mg; 0.225 mmol), phenylacetic acid (92 mg, 0.675 mmol) and K_2CO_3 (47 mg; 0.338 mmol). In this experiment the sensitizer was not added to the experimental solution. The flow rate used was 0.028 ml/min; residence time: 1 hr. The composition of NMP to product **76** was calculated from the ^{1}H-NMR integration to be 96:4.

For ^{1}H-NMR data of product **76** see experiment 28.

Experiment 49

Synthesis of (phthalimidomethylsulfanyl)acetic acid (OS-4)

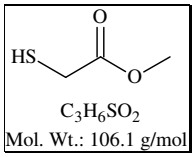
This experimental procedure includes three steps (Scheme 65).



Scheme 65: Synthesis of (phthalimidomethylsulfanyl)acetic acid **78**

Step I: In a round bottom flask, 30.0 ml (412 mmol) of thioglycolic acid and 6.0 g (32 mmol) of *p*-toluenesulfonic acid monohydrate were dissolved in 250 ml of methanol and refluxed for 2 days. After cooling down to room temperature, the solvent was removed by evaporation and the oily residue was diluted with 50 ml of water. The pH was adjusted to pH 9 by the addition of 15% aqueous NaOH solution. The solution was extracted 5-times with ethyl acetate (5 × 30 ml). The combined organic extracts were washed with saturated NaCl-solution and dried over $MgSO_4$. Filtration, followed by evaporation under reduced pressure gave 31.5 g (297 mmol, 72%) of methyl sulfanylacetate as a colorless liquid.

Analytical data of *methyl sulfanylacetate*



^{1}H–NMR: (400 MHz, $CDCl_3$)

δ (ppm) = 1.98 (t, ^{3}J = 8.2 Hz, 1 H, SH), 3.24 (d, ^{3}J = 8.2 Hz, 2 H, CH_2), 3.73 (s, 3 H, OCH_3).

^{13}C–NMR: (100 MHz, $CDCl_3$)

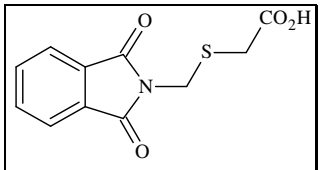
δ (ppm) = 26.3 (t, 1 C, CH_2), 52.7 (q, 1 C, OCH_3), 171.3 (s, 1 C, CO_2).

Step II: In a round-bottom flask, 1.96 g (10.0 mmol) N–(Bromomethyl)phthalimide, 1.0 ml (11.0 mmol) methyl sulfanylacetate and 2.0 g (14.5 mmol) anhydrous K_2CO_3 were dissolved in 50 ml of DMF. The mixture was stirred for 24 h at room temperature. 50 ml of water was added to the solution. The reaction mixture was extracted 5-times with

ethyl acetate (5 × 30 ml). The combined organic extracts were washed with saturated NaCl-solution and dried over $MgSO_4$. Filtration, evaporation and drying under vacuum gave 2.36 g (8.9 mmol, 89%) of methyl(phthalimidomethylsulfanyl)acetate (Pht=$NCH_2SCH_2CO_2CH_3$) as a yellowish solid.

Step III: 2.36 g (8.88 mmol) of methyl(phthalimidomethylsulfanyl)acetate were placed in a round-bottom flask. 40 ml of acetone, 28 ml of water and 12 ml of conc. HCl were added. The reaction mixture was refluxed for 2–5 h until TLC indicated complete disappearance of the starting material. The acetone was removed under reduced pressure and the remaining solution was diluted with 50 ml of water. The reaction mixture was extracted 5-times with ethyl acetate (5 × 30 ml). The combined organic extracts were washed with saturated NaCl-solution and dried over $MgSO_4$. Filtration, evaporation and drying under vacuum gave 1.61 g (6.4 mmol, 72%) of (phthalimidomethylsulfanyl)-acetic acid **78** (Pht=$NCH_2SCH_2CO_2H$) as a colorless solid.

Analytical data of *(phthalimidomethylsulfanyl)acetic acid* (78)



78

$C_{11}H_9NSO_4$

Mol. Wt.: 251.3 g/mol

^{1}H–NMR: (400 MHz, $CDCl_3$, 10% CF_3CO_2H)

δ (ppm) = 3.61 (s, 2 H, CH_2CO_2), 4.95 (s, 2 H, NCH_2), 7.80 (dd, ^3J = 5.6, ^4J = 3.2 Hz, 2 H, H_{arom}), 7.91 (dd, ^3J = 5.6, ^4J = 3.2 Hz, 2 H, H_{arom}), 9.32 (br. s, 1 H, CO_2H).

^{13}C–NMR: (100 MHz, $CDCl_3$, 10% CF_3CO_2H)

δ (ppm) = 33.9 (t, 1 C, $\underline{C}H_2CO_2$), 39.6 (t, 1 C, NCH_2), 123.7 (d, 2 C, CH_{arom}), 131.9 (s, 2 C, CH_{arom}), 134.4 (d, 2 C, CH_{arom}), 167.6 (s, 2 C, CON), 175.8 (s, 1 C, CO_2).

9.1.7 General procedure (GP-7) for photodecarboxylative cyclizations of phthalimidomethylsulfanyl acetate and phthaloyl-γ-aminobutyrate under batch conditions (Rayonet):

The phthalimidomethylsulfanylcarboxylic acid or phthaloyl-γ-aminobutyric acid (0.75 mmol) was placed into a Pyrex Schlenk flask and was dissolved in 10 ml of acetone. K_2CO_3 (0.375 mmol) was dissolved in 10 ml of distilled water. The two solutions were sonicated separately for 15 min before being mixed together. The solution of K_2CO_3

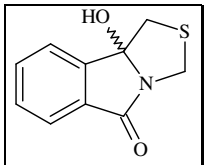
was added into a Pyrex Schlenk flask, which was brought up to 50 ml with a 1:1 Vol% mixture of acetone and H_2O. The solution was further sonicated using an ultrasound bath until the formation of CO_2 had ceased and the mixture was irradiated at 300±25 nm (Rayonet RPR-200, equipped with 16 × RPR-3000Å lamps, 16 × 8 W) while a gentle stream of nitrogen was flushed through the solution. After irradiation most of the acetone was removed under reduced pressure and the crude product mixture was extracted with CH_2Cl_2 (3 × 30 ml). The combined organic layers were washed with saturated $NaHCO_3$ (2 × 30 ml), brine (2 × 30 ml) and dried over $MgSO_4$. Filtration and evaporation gave pure product **79** or **81**, respectively.

Experiment 50

The PDC cyclization of phthalimidomethylsulfanyl acetate (OS-10)

General procedure (GP-7) was followed using phthalimidomethylsulfanylcarboxylic acid (189 mg; 0.75 mmol) and K_2CO_3 (52 mg; 0.375 mmol). After irradiation for 1 hr the reaction was stopped and worked up. The yield of isolated product was 112 mg (0.54 mmol, 72%). The structure of **79** was confirmed by both ^{1}H-NMR and ^{13}C-NMR.

Analytical data of *9b-hydroxy-1,9b-dihydrothiazolo[4,3-a]isoindol-5-one* (79)



79
$C_{10}H_9NSO_2$
Mol. Wt.: 207.3 g/mol

TLC: ***Rf*** = 0.31 (ethyl acetate/n-hexane 1:1)
Melting point (colorless solid)**:** 121-122ºC (Lit.[156]: 124-125ºC)
^{1}H–NMR: (400 MHz, Acetone-d_6)
δ (ppm) = 2.97 (d, ^{2}J = 11.2 Hz, 1 H, CH_2S), 3.39 (d, ^{2}J = 11.2 Hz, 1 H, CH_2S), 4.36 (d, ^{2}J = 8.8 Hz, 1 H, NCH_2S), 4.93 (d, ^{2}J = 8.8 Hz, 1 H, NCH_2S), 5.83 (s , 1 H, OH), 7.57 (m, 1 H, H_{arom}), 7.64 (dd, ^{3}J = 7.6 Hz, ^{4}J = 1.2 Hz, 1 H, H_{arom}), 7.71 (m, 2 H, H_{arom}).
^{13}C–NMR: (100 MHz, Acetone-d_6)
δ (ppm) = 40.2 (s, 1 C, S<u>C</u>H_2C), 42.7 (s, 1 C, NCH_2S), 98.4 (s, 1 C, COH), 123.4 (d, 1 C, CH_{arom}), 123.9 (d, 1 C, CH_{arom}), 130.8 (s, 1 C, CH_{arom}), 131.3 (s, 1 C, CH_{arom}), 134.1 (s, 1 C, Cq_{arom}), 147.6 (s, 1 C, Cq_{arom}), 167.9 (s, 1 C, CON).

Experiment 51

The PDC cyclization of phthalimidomethylsulfanyl acetate (OS-47)

General procedure (GP-7) was followed using phthalimidomethylsulfanylcarboxylic acid (189 mg; 0.75 mmol) and K_2CO_3 (52 mg; 0.375 mmol). After irradiation for 40 min the reaction was stopped and worked up. The yield of isolated product was 91 mg (0.44 mmol, 59%). The structure of **79** was confirmed by both ^{1}H-NMR and ^{13}C-NMR.

For ^{1}H-NMR data of product **79** see experiment 50.

Experiment 52

The PDC cyclization of phthalimidomethylsulfanyl acetate (OS-45)

General procedure (GP-7) was followed using phthalimidomethylsulfanylcarboxylic acid (189 mg; 0.75 mmol) and K_2CO_3 (52 mg; 0.375 mmol). After irradiation for 21 min the reaction was stopped and worked up. The yield of isolated product was 56 mg (0.27 mmol, 36%). The structure of **79** was confirmed by both ^{1}H-NMR and ^{13}C-NMR.

For ^{1}H-NMR data of product **79** see experiment 50.

9.1.8 General procedure (GP-8) for photodecarboxylative cyclizations of phthalimidomethylsulfanyl acetate and phthaloyl-γ-aminobutyrate in the dwell-microreactor:

Phthalimidomethylsulfanylcarboxylic acid or phthaloyl-γ-aminobutyric acid (0.225 mmol) was placed into a Pyrex test tube and was dissolved in 2 ml of acetone. Potassium carbonate (0.113 mmol) was dissolved in 2 ml of distilled water. The two solutions were then sonicated separately for 15 min before being mixed together. The solution of K_2CO_3 was added into a Pyrex test tube, which was filled up to 15 ml with a 1:1 Vol% mixture of acetone and H_2O. This solution was further sonicated using an ultrasound bath until the formation of CO_2 had ceased and was degassed with a slow stream of N_2 for 15 minutes. The microreactor was prepared by pumping the pre-sonicated acetone/water mixture (1:1) through the reaction channel until all air bubbles had been removed. Then 10 ml of the prepared reaction mixture was transferred into a 10 ml glass syringe, any air bubbles were expelled and the syringe was loaded into a syringe pump. The flow rate was set and the solution was pumped through a micro-reactor (mikroglas dwell device) while irradiated at 300±25 nm (Luzchem UV exposure panel equipped with 5 × RPR-3000Å lamps, 5 × 8 W). During the reaction, the reactor

was kept cool by pumping cold water through the cooling channel. When the syringe was empty, the syringe pump and the lamps were switched off simultaneously. The syringe was refilled with an acetone/water mixture and loaded into a syringe pump again. The syringe pump was then turned on simultaneously with the lamps. After irradiation most of the acetone was removed by rotary evaporation and the remaining solution was extracted with CH_2Cl_2 (3 × 10 ml). The combined organic layer was washed with sat. $NaHCO_3$ (2 × 10 ml), brine (2 × 10 ml) and dried over $MgSO_4$. Filtration and evaporation gave pure product **79** or **81**, respectively.

Experiment 53

The PDC cyclization of phthalimidomethylsulfanyl acetate (OS-20)

General procedure (GP-8) was followed using phthalimidomethylsulfanylcarboxylic acid (57 mg; 0.225 mmol) and K_2CO_3 (16 mg; 0.113 mmol). The flow rate used was 0.028 ml/min; residence time: 1 hr. The yield of isolated product was 25 mg (0.12 mmol, 80%). Both ^{1}H-NMR and ^{13}C-NMR spectroscopy confirmed the product to be **79**.

For ^{1}H-NMR data of product **79** see experiment 50.

Experiment 54

The PDC cyclization of phthalimidomethylsulfanyl acetate (OS-15)

General procedure (GP-8) was followed using phthalimidomethylsulfanylcarboxylic acid (57 mg; 0.225 mmol) and K_2CO_3 (16 mg; 0.113 mmol). The flow rate used was 0.042 ml/min; residence time: 40 min. The yield of isolated product was 22 mg (0.11 mmol, 70%). Both ^{1}H-NMR and ^{13}C-NMR spectroscopy confirmed the product to be **79**.

For ^{1}H-NMR data of product **79** see experiment 50.

Experiment 55

The PDC cyclization of phthalimidomethylsulfanyl acetate (OS-9)

General procedure (GP-8) was followed using phthalimidomethylsulfanylcarboxylic acid (57 mg; 0.225 mmol) and K_2CO_3 (16 mg; 0.113 mmol). The flow rate used was 0.08 ml/min; residence time: 21 min. The yield of isolated product was 12 mg (0.06

mmol, 39%). Both ^{1}H-NMR and ^{13}C-NMR spectroscopy confirmed the product to be **79**.

For ^{1}H-NMR data of product **79** see experiment 50.

Experiment 56

The PDC cyclization of phthalimidomethylsulfanyl acetate (OS-60)

General procedure (GP-7) was followed, with one variation, using phthalimidomethylsulfanylcarboxylic acid (189 mg; 0.75 mmol) and K_2CO_3 (52 mg; 0.375 mmol). In this experiment a Rayonet reactor was equipped with 5 × RPR-3000Å lamps (5 × 8 W, λ_{max} = 300±25 nm) and 11 cool white lamps F8T5/CW (11 × 8 W, λ = 400–700 nm) instead of 16 × RPR-3000Å lamps. After irradiation for 1 hr the reaction was stopped and worked up. The yield of isolated product was 33 mg (0.16 mmol, 21%). Both ^{1}H-NMR and ^{13}C-NMR spectroscopy confirmed the product to be **79**.

For ^{1}H-NMR data of product **79** see experiment 50.

9.1.9 General procedure (GP-9) for photodecarboxylative cyclizations of phthalimidomethylsulfanyl acetate and phthaloyl-γ-aminobutyrate under DMBP or 4-CBPH sensitisation in the batch system (Rayonet):

The phthalimidomethylsulfanylcarboxylic acid or phthaloyl-γ-aminobutyric acid (0.75 mmol) and sensitizer (4,4'-Dimethoxybenzophenone or 4-Carboxybenzophenone, 75 µmol) were placed into a Pyrex Schlenk flask and were dissolved in 10 ml of acetonitrile. Potassium carbonate (0.375 mmol) was dissolved in 10 ml of distilled water. The two solutions were sonicated separately for 15 min before being mixed together. The solution of K_2CO_3 was added into a Pyrex Schlenk flask, which was filled up to 50 ml with a 1:1 Vol% mixture of acetonitrile and H_2O. The solution was further sonicated using an ultrasound bath until the formation of CO_2 had ceased and then was irradiated at 350±25 nm (Rayonet RPR-200, equipped with 16 × RPR-3500Å lamps, 16 × 8 W) while a gentle stream of nitrogen was flushed through the solution. After irradiation most of the acetonitrile was evaporated and the crude product mixture was extracted with CH_2Cl_2 (3 × 30 ml). The combined organic layers were washed with saturated $NaHCO_3$ (2 × 30 ml), brine (2 × 30 ml), dried over $MgSO_4$, filtered and evaporated. The obtained crude product was analysed by ^{1}H-NMR spectroscopy. Pure

products were isolated by column chromatography on silica gel with suitable mobile phase and further characterized by ^{1}H-NMR and ^{13}C-NMR spectroscopy.

Experiment 57

The PDC cyclization of phthalimidomethylsulfanyl acetate under DMBP sensitization (OS-29)

General procedure (GP-9) was followed using phthalimidomethylsulfanylcarboxylic acid (189 mg; 0.75 mmol), 4,4'-dimethoxybenzophenone (18 mg; 75 µmol) and K_2CO_3 (52 mg; 0.375 mmol). After irradiation for 1 hr the reaction was stopped and worked up. The ^{1}H-NMR analysis of the crude product showed that a mixture of desired product **79** and sensitiser (DMBP) were obtained after extraction. The crude product was further purified by column chromatography using ethyl acetate:n-hexane (1:1) as eluent. The isolated yield of **79** was found to be 89 mg (0.43 mmol, 57%). The structure of **79** was confirmed by both ^{1}H-NMR and ^{13}C-NMR.

For ^{1}H-NMR data of product **79** see experiment 50.

9.1.10 General procedure (GP-10) for photodecarboxylative cyclizations of phthalimidomethylsulfanyl acetate and phthaloyl-γ-aminobutyrate under DMBP sensitisation in the dwell-microreactor:

The phthalimidomethylsulfanylcarboxylic acid or phthaloyl-γ-aminobutyric acid (0.225 mmol) and 4,4'-dimethoxybenzophenone (6 mg; 22.5 µmol) were placed into a Pyrex test tube and were dissolved in 2 ml of acetonitrile. Potassium carbonate (16 mg; 0.113 mmol) was dissolved in 2 ml of distilled water. Those solutions were sonicated separately for 15 min before being mixed together. The solution of K_2CO_3 was added into a Pyrex test tube, which was filled up to 15 ml with a 1:1 Vol% mixture of acetonitrile and H_2O. This solution was further sonicated using an ultrasound bath until the formation of CO_2 had ceased and was degassed with a slow stream of N_2 for 15 minutes. The microreactor was prepared by pumping the pre-sonicated acetonitrile/water mixture (1:1) through the reaction channel until all air bubbles had been removed. Then 10 ml of prepared reaction mixture was transferred into a 10 ml glass syringe, any air bubbles were expelled and the syringe was loaded into a syringe pump. The flow rate was set and the solution was pumped through a micro-reactor (mikroglas dwell device) while irradiated at 350±25 nm (Luzchem UV exposure panel equipped with 5 × RPR-3500Å lamps, 5 × 8 W). During the reaction, the reactor was

kept cool by pumping cold water through the cooling channel. When the syringe was empty, the syringe pump and the lamps were switched off simultaneously. The syringe was refilled with an acetonitrile/water mixture and loaded into a syringe pump again. The syringe pump was then turned on simultaneously with the lamps. After irradiation most of the acetonitrile was removed under reduced pressure and the crude product mixture was extracted with CH_2Cl_2 (3 × 10 ml). The combined organic layers were washed with sat. $NaHCO_3$ (2 × 10 ml), brine (2 × 10 ml), dried over $MgSO_4$, filtered and evaporated. The obtained crude product was analysed by ^{1}H-NMR spectroscopy. Pure products were isolated by column chromatography on silica gel with suitable mobile phase and further characterized by ^{1}H-NMR and ^{13}C-NMR spectroscopy.

Experiment 58

The PDC cyclization of phthalimidomethylsulfanyl acetate under DMBP sensitization (OS-57)

General procedure (GP-10) was followed using phthalimidomethylsulfanylcarboxylic acid (57 mg; 0.225 mmol), 4,4'-dimethoxybenzophenone (6 mg; 22.5 µmol) and K_2CO_3 (16 mg; 0.113 mmol). The flow rate used was 0.028 ml/min; residence time: 1 hr. The ^{1}H-NMR analysis of the crude product showed that a mixture of desired product **79** and sensitiser (DMBP) was obtained after extraction. The crude product was further purified by column chromatography using ethyl acetate:n-hexane (1:1) as eluent. The isolated yield of **79** was found to be 18 mg (0.09 mmol, 56%). The structure of **79** was confirmed by both ^{1}H-NMR and ^{13}C-NMR.

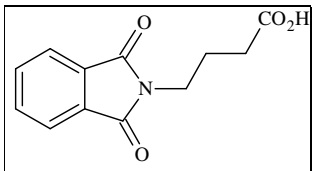
For ^{1}H-NMR data of product **79** see experiment 50.

Experiment 59

Synthesis of phthaloyl-γ-aminobutyric acid (OS-374)

10.5 g (71 mmol) of phthalic anhydride were mixed with 7.3 g (71 mmol) of gamma-aminobutyric acid in an open conical flask, to this mixture 5 ml of DMF were added and the solution was heated in an oil bath at 160°C for 1 hour (clear melt was formed). The flask was removed and 10 ml of acetone was added. This solution was transferred into a beaker with crushed ice and the product instantly precipitated as a colourless solid. Filtration and drying using an oil-pump gave 9.43 g (40 mmol, 57%) of phthaloyl-γ-aminobutyric acid **80** (Pht=$NCH_2CH_2CH_2CO_2H$) as a colourless solid.

Analytical data of *phthaloyl-γ-aminobutyric acid* (80)



80
$C_{12}H_{11}NO_4$
Mol. Wt.: 233.1 g/mol

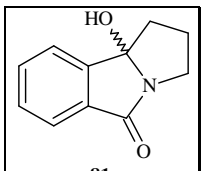
^{1}H–NMR: (400 MHz, $CDCl_3$, 10% CF_3CO_2H)
δ (ppm) = 2.03 (m, ^{3}J = 7.3, 6.8 Hz, 2 H, CH_2), 2.50 (t, ^{3}J = 7.3 Hz, 2 H, CH_2CO_2), 3.79 (t, ^{3}J = 6.8 Hz, 2 H, NCH_2), 7.72 (dd, ^{3}J = 5.5, ^{4}J = 3.0 Hz, 2 H, H_{arom}), 7.86 (dd, ^{3}J = 5.5, ^{4}J = 3.0 Hz, 2 H, H_{arom}).
^{13}C–NMR: (100 MHz, $CDCl_3$, 10% CF_3CO_2H)
δ (ppm) = 23.2 (t, 1 C, CH_2), 31.0 (t, 1 C, $\underline{C}H_2CO_2$), 37.1 (t, 1 C, NCH_2), 123.8 (d, 2 C, CH_{arom}), 131.4 (s, 2 C, Cq_{arom}), 134.7 (d, 2 C, CH_{arom}), 168.4 (s, 2 C, CON), 178.3 (s, 1 C, CO_2).

Experiment 60

The PDC cyclization of phthaloyl-γ-aminobutyrate (OS-6)

General procedure (GP-7) was followed using phthaloyl-γ-aminobutyric acid (175 mg; 0.75 mmol) and K_2CO_3 (52 mg; 0.375 mmol). After irradiation for 1 hr the reaction was stopped and worked up. The yield of isolated product was 98 mg (0.52 mmol, 69%). Both ^{1}H-NMR and ^{13}C-NMR spectroscopy confirmed the product to be **81**.

Analytical data of *9b-hydroxy-1,2,3,9b-tetrahydro-5H-pyrrolo[2,1-a]isoindol-5-one* (81)



81
$C_{11}H_{11}NO_2$
Mol. Wt.: 189.2 g/mol

TLC: *Rf* = 0.30 (ethyl acetate/n-hexane 1:1)
Melting point (colorless solid): 125-127ºC (Lit.[269]: 123-125ºC)

^{1}H–NMR: (400 MHz, Acetone-d_6)

δ (ppm) = 1.50 (m, 1 H, CH_2), 2.24 (m, 2 H, CH_2), 2.53 (m, 1 H, CH_2), 3.32 (m, 1 H, NCH_2), 3.57 (m, 1 H, NCH_2), 5.22 (s, 1 H, OH), 7.48 (m, 1 H, H_{arom}), 7.57 (m, 3 H, H_{arom}).

^{13}C–NMR: (100 MHz, Acetone-d_6)

δ (ppm) = 28.3 (s, 1 C, C$\underline{C}H_2$C), 36.0 (s, 1 C, C$\underline{C}H_2$C), 42.1 (s, 1 C, C$\underline{C}H_2$N), 96.9 (s, 1 C, COH), 123.5 (d, 1 C, CH_{arom}), 123.7 (d, 1 C, CH_{arom}), 130.1 (s, 1 C, CH_{arom}), 133.0 (s, 1 C, CH_{arom}), 133.2 (s, 1 C, Cq_{arom}), 149.2 (s, 1 C, Cq_{arom}), 170.1 (s, 1 C, CON).

Experiment 61

The PDC cyclization of phthaloyl-γ-aminobutyrate (OS-48)

General procedure (GP-7) was followed using phthaloyl-γ-aminobutyric acid (175 mg; 0.75 mmol) and K_2CO_3 (52 mg; 0.375 mmol). After irradiation for 40 min the reaction was stopped and worked up. The yield of isolated product was 75 mg (0.40 mmol, 53%). Both ^{1}H-NMR and ^{13}C-NMR spectroscopy confirmed the product to be **81**.

For ^{1}H-NMR data of product **81** see experiment 60.

Experiment 62

The PDC cyclization of phthaloyl-γ-aminobutyrate (OS-46)

General procedure (GP-7) was followed using phthaloyl-γ-aminobutyric acid (175 mg; 0.75 mmol) and K_2CO_3 (52 mg; 0.375 mmol). After irradiation for 21 min the reaction was stopped and worked up. The yield of isolated product was 66 mg (0.35 mmol, 46%). Both ^{1}H-NMR and ^{13}C-NMR spectroscopy confirmed the product to be **81**.

For ^{1}H-NMR data of product **81** see experiment 60.

Experiment 63

The PDC cyclization of phthaloyl-γ-aminobutyrate (OS-22)

General procedure (GP-8) was followed using phthaloyl-γ-aminobutyric acid (53 mg; 0.225 mmol) and K_2CO_3 (16 mg; 0.113 mmol). The flow rate used was 0.028 ml/min; residence time: 1 hr. The yield of isolated product was 22 mg (0.12 mmol, 77%). Both ^{1}H-NMR and ^{13}C-NMR spectroscopy confirmed the product to be **81**.

For ^{1}H-NMR data of product **81** see experiment 60.

Experiment 64

The PDC cyclization of phthaloyl-γ-aminobutyrate (OS-16)

General procedure (GP-8) was followed using phthaloyl-γ-aminobutyric acid (53 mg; 0.225 mmol) and K_2CO_3 (16 mg; 0.113 mmol). The flow rate used was 0.042 ml/min; residence time: 40 min. The yield of isolated product was 19 mg (0.10 mmol, 69%). Both ^{1}H-NMR and ^{13}C-NMR spectroscopy confirmed the product to be **81**.

For ^{1}H-NMR data of product **81** see experiment 60.

Experiment 65

The PDC cyclization of phthaloyl-γ-aminobutyrate (OS-18)

General procedure (GP-8) was followed using phthaloyl-γ-aminobutyric acid (53 mg; 0.225 mmol) and K_2CO_3 (16 mg; 0.113 mmol). The flow rate used was 0.08 ml/min; residence time: 21 min. The yield of isolated product was 9 mg (0.05 mmol, 33%). Both ^{1}H-NMR and ^{13}C-NMR spectroscopy confirmed the product to be **81**.

For ^{1}H-NMR data of product **81** see experiment 60.

Experiment 66

The PDC cyclization of phthaloyl-γ-aminobutyrate (OS-59)

General procedure (GP-7) was followed, with one variation, using phthaloyl-γ-aminobutyric acid (175 mg; 0.75 mmol) and K_2CO_3 (52 mg; 0.375 mmol). In this experiment a Rayonet reactor was equipped with 5 × RPR-3000Å lamps (5 × 8 W, λ_{max} = 300±25 nm) and 11 cool white lamps F8T5/CW (11 × 8 W, λ = 400–700 nm) instead of 16 × RPR-3000Å lamps. After irradiation for 1 hr the reaction was stopped and worked up. The yield of isolated product was 26 mg (0.14 mmol, 19%). Both ^{1}H-NMR and ^{13}C-NMR spectroscopy confirmed the product to be **81**.

For ^{1}H-NMR data of product **81** see experiment 60.

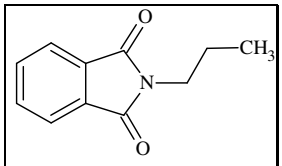
Experiment 67

The PDC cyclization of phthaloyl-γ-aminobutyrate under 4-CBPH sensitisation (OS-67)

General procedure (GP-9) was followed using phthaloyl-γ-aminobutyric acid (175 mg; 0.75 mmol), 4-Carboxybenzophenone (17 mg; 75 µmol) and K_2CO_3 (52 mg; 0.375 mmol). After irradiation for 1 hr the reaction was stopped and worked up. The ^{1}H-NMR analysis of the crude product showed that a mixture of the desired cyclic product **81** and the decarboxylation product **82** were obtained after extraction. The conversion rate of **80** to **82** was determined by ^{1}H-NMR spectroscopy of the crude product. The signal integration for the $NC\underline{H}_2$ protons of **81** was compared to the signal integration for the $C\underline{H}_3$ protons of **82**. The composition of product **81** to product **82** was calculated to be 91:9. The crude product was further purified by column chromatography using ethyl acetate:n-hexane (1:1) as eluent. The isolated yield of **81** was found to be 44 mg (0.23 mmol, 31%). Both ^{1}H-NMR and ^{13}C-NMR confirmed the product to be **81**.

For ^{1}H-NMR data of product **81** see experiment 60.

Analytical data of *2-propyl-1H-isoindole-1,3(2H)-dione* (82)



82

$C_{11}H_{11}NO_2$

Mol. Wt.: 189.2 g/mol

TLC: ***Rf*** = 0.68 (ethyl acetate/n-hexane 1:1)

^{1}H–NMR: (400 MHz, Acetone-d_6)

δ (ppm) = 0.90 (t, ^{3}J = 7.4 Hz, 3 H, CH_3), 1.65 (q, ^{3}J = 7.4 Hz, 2 H, CH_2), 3.59 (t, ^{3}J = 7.4 Hz, 2 H, NCH_2), 7.84 (m, 4 H, H_{arom}).

Experiment 68

The PDC cyclization of phthaloyl-γ-aminobutyrate under DMBP sensitisation (OS-30)

General procedure (GP-9) was followed using phthaloyl-γ-aminobutyric acid (175 mg; 0.75 mmol), 4,4'-dimethoxybenzophenone (18 mg; 75 µmol) and K_2CO_3 (52 mg; 0.375

mmol). After irradiation for 1 hr the reaction was stopped and worked up. The ^{1}H-NMR analysis of the crude product showed that a mixture of the desired cyclic product **81**, the decarboxylation product **82** and DMBP were obtained after extraction. The conversion rate of **80** to **82** was determined by ^{1}H-NMR spectroscopy of the crude product. The signal integration for the NC$\underline{H}_2$ protons of **81** was compared to the signal integration for the C$\underline{H}_3$ protons of **82**. The composition of product **81** to product **82** was calculated to be 88:12. The crude product was further purified by column chromatography using ethyl acetate:n-hexane (1:1) as eluent. The isolated yield of **81** was found to be 41 mg (0.22 mmol, 29%). Both ^{1}H-NMR and ^{13}C-NMR spectroscopy confirmed the product to be **81**.

For ^{1}H-NMR data of product **81** see experiment 60.
For ^{1}H-NMR data of product **82** see experiment 67.

Experiment 69

The PDC cyclization of phthaloyl-γ-aminobutyrate under DMBP sensitisation (OS-100)

General procedure (GP-10) was followed using phthaloyl-γ-aminobutyric acid (53 mg; 0.225 mmol), 4,4'-dimethoxybenzophenone (6 mg; 22.5 μmol) and K_2CO_3 (16 mg; 0.113 mmol). The flow rate used was 0.028 ml/min; residence time: 1 hr. The ^{1}H-NMR analysis of the crude product showed that a mixture of the desired cyclic product **81**, the decarboxylation product **82** and DMBP were obtained after extraction. The conversion rate of **80** to **82** was determined by ^{1}H-NMR spectroscopy of the crude product. The signal integration for the NC$\underline{H}_2$ protons of **81** was compared to the signal integration for the C$\underline{H}_3$ protons of **82**. The composition of product **81** to product **82** was calculated to be 81:19. The crude product was further purified by column chromatography using ethyl acetate:n-hexane (1:1) as eluent. The isolated yield of **81** was found to be 13 mg (0.07 mmol, 47%). Both ^{1}H-NMR and ^{13}C-NMR spectroscopy confirmed the product to be **81**.

For ^{1}H-NMR data of product **81** see experiment 60.
For ^{1}H-NMR data of product **82** see experiment 67.

Experiment 70

The PDC cyclization of phthaloyl-γ-aminobutyrate under direct excitation (OS-375)

General procedure (GP-9) was followed, with one variation, using phthaloyl-γ-aminobutyric acid (175 mg; 0.75 mmol) and K_2CO_3 (52 mg; 0.375 mmol). In this experiment the sensitizer was not added to the experimental solution. After irradiation for 1 hr the reaction was stopped and worked up. The isolated yield of **81** was 20 mg (0.11 mmol, 14%). The conversion to decarboxylation product **82** was calculated from the ^{1}H-NMR integration to be 1.3%.

For ^{1}H-NMR data of product **81** see experiment 60.
For ^{1}H-NMR data of product **82** see experiment 67.

Experiment 71

The PDC cyclization of phthaloyl-γ-aminobutyrate under direct excitation (OS-379)

General procedure (GP-10) was followed, with one variation, using phthaloyl-γ-aminobutyric acid (53 mg; 0.225 mmol) and K_2CO_3 (16 mg; 0.113 mmol). In this experiment the sensitizer was not added to the experimental solution. The flow rate used was 0.028 ml/min; residence time: 1 hr. The isolated yield of **81** was 3 mg (0.02 mmol, 8%). The conversion to decarboxylation product **82** was calculated from the ^{1}H-NMR integration to be 1.3%.

For ^{1}H-NMR data of product **81** see experiment 60.
For ^{1}H-NMR data of product **82** see experiment 67.

9.1.11 General procedure (GP-11) for α-photodecarboxylation of phthaloyl glycine under batch conditions (Rayonet):

Phthaloyl glycine (1.5 mmol) was placed into a Pyrex Schlenk flask and was dissolved in 100 ml of acetone. The solution was sonicated for 15 min using an ultrasound bath and was irradiated at 300±25nm (Rayonet RPR-200, equipped with 16 × RPR-3000Å lamps, 16 × 8 W) while a gentle stream of nitrogen was flushed through the solution. After evaporation of the solvent under reduced pressure, the conversion rate was determined by ^{1}H-NMR spectroscopy of the crude product. The signal integration for

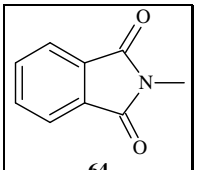
the NC<u>H</u>$_2$ protons of **83** was compared to the signal integration for the NC<u>H</u>$_3$ protons of **64**. For characterization purposes, **64** was purified by column chromatography on silica gel (SiO_2; ethyl acetate/n-hexane 1:1).

Experiment 72

The α-photodecarboxylation of phthaloyl glycine (OS-50)

General procedure (GP-11) was followed using phthaloyl glycine (308 mg; 1.5 mmol). The irradiation time was 1 hr. The composition of **83** to **64** was calculated from the ^{1}H-NMR integration to be 41:59. For characterization of **64**, the crude product was purified by column chromatography on silica gel (SiO_2; ethyl acetate/n-hexane 1:1).

Analytical data of *N-Methylphthalimide* (64)



64
$C_9H_7NO_2$
Mol. Wt.: 161.2 g/mol

TLC: ***Rf*** = 0.62 (ethyl acetate/n-hexane 1:1)
Melting point (colourless needles)**:** 133-134ºC (Lit.[270]: 135ºC)
^{1}H–NMR: (400 MHz, Acetone-d_6)
δ (ppm) = 3.11 (s, 3 H, NCH_3), 7.83 (m, ^3J = 2.4 Hz, 4 H, H_{arom}).
^{13}C–NMR: (100 MHz, Acetone-d_6)
δ (ppm) = 23.9 (s, 1 C, NCH_3), 123.6 (s, 2 C, CH_{arom}), 133.3 (s, 2 C, Cq_{arom}), 134.8 (s, 2 C, CH_{arom}), 168.8 (s, 2 C, C=O).

Experiment 73

The α-photodecarboxylation of phthaloyl glycine (OS-55)

General procedure (GP-11) was followed using phthaloyl glycine (308 mg; 1.5 mmol). The irradiation time was 40 min. The composition of **83** to **64** was calculated from the ^{1}H-NMR integration to be 61:39.

For ^{1}H-NMR data of **64** see experiment 72.

Experiment 74

The α-photodecarboxylation of phthaloyl glycine (OS-56)

General procedure (GP-11) was followed using phthaloyl glycine (308 mg; 1.5 mmol). The irradiation time was 21 min. The composition of **83** to **64** was calculated from the ^{1}H-NMR integration to be 81:19.

For ^{1}H-NMR data of **64** see experiment 72.

Experiment 75

The α-photodecarboxylation of phthaloyl glycine (OS-80)

General procedure (GP-11) was followed using phthaloyl glycine (308 mg; 1.5 mmol). The irradiation time was 11 min. The composition of **83** to **64** was calculated from the ^{1}H-NMR integration to be 93:7.

For ^{1}H-NMR data of **64** see experiment 72.

Experiment 76

The α-photodecarboxylation of phthaloyl glycine (OS-79)

General procedure (GP-11) was followed using phthaloyl glycine (308 mg; 1.5 mmol). The irradiation time was 3.4 min. The composition of **83** to **64** was calculated from the ^{1}H-NMR integration to be 98:2.

For ^{1}H-NMR data of **64** see experiment 72.

9.1.12 General procedure (GP-12) for α-photodecarboxylation of phthaloyl glycine in the dwell-microreactor:

Phthaloyl glycine (0.225 mmol) was placed into a Pyrex test tube and was dissolved in 15 ml of acetone. The solution was sonicated for 15 min using an ultrasound bath and degassed with a slow stream of N_2 for 15 minutes. The microreactor was prepared by pumping the pre-sonicated acetone through the reaction channel until all air bubbles had been removed. Then 10 ml of prepared reaction mixture was transferred into a 10 ml glass syringe, any air bubbles were expelled and the syringe was loaded into a syringe pump. The flow rate was set and the solution was pumped through a micro-reactor (mikroglas dwell device) while irradiated at 300±25 nm (Luzchem UV exposure panel equipped with 5 × RPR-3000Å lamps, 5 × 8 W). During the reaction, the reactor was

kept cool by pumping cold water through the cooling channel. When the syringe was empty, the syringe pump and the lamps were switched off simultaneously. The syringe was refilled with acetone and loaded into a syringe pump again. The syringe pump was then turned on simultaneously with the lamps. After evaporation of the solvent under reduced pressure, the conversion rate was determined by ^{1}H-NMR spectroscopy of the crude product. The signal integration for the NC$\underline{H}_2$ protons of **83** was compared to the signal integration for the NC$\underline{H}_3$ protons of **64**.

Experiment 77

The α-photodecarboxylation of phthaloyl glycine (OS-208)

General procedure (GP-12) was followed using phthaloyl glycine (46 mg; 0.225 mmol). The flow rate used was 0.028 ml/min; residence time: 1 hr. The composition of **83** to **64** was calculated from the ^{1}H-NMR integration to be 8:92.

For ^{1}H-NMR data of **64** see experiment 72.

Experiment 78

The α-photodecarboxylation of phthaloyl glycine (OS-207)

General procedure (GP-12) was followed using phthaloyl glycine (46 mg; 0.225 mmol). The flow rate used was 0.042 ml/min; residence time: 40 min. The composition of **83** to **64** was calculated from the ^{1}H-NMR integration to be 26:74.

For ^{1}H-NMR data of **64** see experiment 72.

Experiment 79

The α-photodecarboxylation of phthaloyl glycine (OS-189)

General procedure (GP-12) was followed using phthaloyl glycine (46 mg; 0.225 mmol). The flow rate used was 0.08 ml/min; residence time: 21 min. The composition of **83** to **64** was calculated from the ^{1}H-NMR integration to be 56:44.

For ^{1}H-NMR data of **64** see experiment 72.

Experiment 80

The α-photodecarboxylation of phthaloyl glycine (OS-214)

General procedure (GP-12) was followed using phthaloyl glycine (46 mg; 0.225 mmol). The flow rate used was 0.15 ml/min; residence time: 11 min. The composition of **83** to **64** was calculated from the ^{1}H-NMR integration to be 77:23.

For ^{1}H-NMR data of **64** see experiment 72.

Experiment 81

The α-photodecarboxylation of phthaloyl glycine (OS-212)

General procedure (GP-12) was followed using phthaloyl glycine (46 mg; 0.225 mmol). The flow rate used was 0.5 ml/min; residence time: 3.4 min. The composition of **83** to **64** was calculated from the ^{1}H-NMR integration to be 95:5.

For ^{1}H-NMR data of **64** see experiment 72.

Experiment 82

The α-photodecarboxylation of phthaloyl glycine (OS-71)

General procedure (GP-11) was followed, with one variation, using phthaloyl glycine (308 mg; 1.5 mmol). In this experiment a Rayonet reactor was equipped with 5 × RPR-3000Å lamps (5 × 8 W, λ_{max} = 300±25 nm) and 11 cool white lamps F8T5/CW (11 × 8 W, λ = 400–700 nm) instead of 16 × RPR-3000Å lamps. The irradiation time was 1 hr. The composition of **83** to **64** was calculated from the ^{1}H-NMR integration to be 78:22.

For ^{1}H-NMR data of **64** see experiment 72.

Experiment 83

The α-photodecarboxylation of phthaloyl glycine under DMBP sensitisation (OS-93)

General procedure (GP-11) was followed, with three variations, using phthaloyl glycine (308 mg; 1.5 mmol). In this experiment the sensitizer DMBP (36 mg, 0.15 mmol) was added to the experimental solution, acetonitrile was used as solvent instead of acetone and a Rayonet reactor was equipped with 16 × RPR-3500Å lamps, (λ = 350±25 nm, 16 × 8 W) instead of 16 × RPR-3000Å lamps. The irradiation time was 1 hr. The obtained

crude product was analysed by ^{1}H-NMR spectroscopy and the conversion was found to be 100%.

For ^{1}H-NMR data of **64** see experiment 72.

Experiment 84

The α-photodecarboxylation of phthaloyl glycine under DMBP sensitisation (OS-91)

General procedure (GP-12) was followed, with three variations, using phthaloyl glycine (46 mg; 0.225 mmol). In this experiment the sensitizer DMBP (5.5 mg, 22.5 μmol) was added to the experimental solution, acetonitrile was used as solvent instead of acetone. A Luzchem panel equipped with 5 × RPR-3500Å lamps, (λ = 350±25 nm, 5 × 8 W) instead of 5 × RPR-3000Å lamps was used. The flow rate used was 0.028 ml/min; residence time: 1 hr. The obtained crude product was analysed by ^{1}H-NMR spectroscopy and the conversion was found to be 100%.

For ^{1}H-NMR data of **64** see experiment 72.

Experiment 85

The α-photodecarboxylation of phthaloyl glycine under direct excitation (OS-373)

General procedure (GP-11) was followed, with two variations, using phthaloyl glycine (308 mg; 1.5 mmol). In this experiment, acetonitrile was used as solvent instead of acetone and a Rayonet reactor equipped with 16 × RPR-3500Å lamps, (λ = 350±25 nm, 16 × 8 W) instead of 16 × RPR-3000Å lamps was used. The irradiation time was 1 hr. The composition of **83** to **64** was calculated from the ^{1}H-NMR integration to be 90:10.

For ^{1}H-NMR data of **64** see experiment 72.

Experiment 86

The α-photodecarboxylation of phthaloyl glycine under direct excitation (OS-378)

General procedure (GP-12) was followed, with two variations, using phthaloyl glycine (46 mg; 0.225 mmol). In this experiment, acetonitrile was used as solvent instead of acetone and a Luzchem panel equipped with 5 × RPR-3500Å lamps, (λ = 350±25 nm, 5 × 8 W) instead of 5 × RPR-3000Å lamps was used. The flow rate used was 0.028

ml/min; residence time: 1 hr. The composition of **83** to **64** was calculated from the ^{1}H-NMR integration to be 98:2.

For ^{1}H-NMR data of **64** see experiment 72.

9.2 Chapter 3: Highly efficient and stereoselective radical addition of secondary alcohols to electron-deficient alkenes in diverse manner experimental set-ups

Conventional photolysis. Batch set-up

Glassware: Photoreactions were performed in 15 ml *Pyrex test tubes* (9 mm inner ∅).

Conventional reactor: Photochemical reactions were performed in a *RPR–100 Rayonet photochemical chamber reactor* (Southern New England Ultraviolet Company).

Irradiation source: *Rayonet reactor* was equipped with 16 RPR-3000Å (for UVB irradiation, λ_{max} = 300±25 nm) or 16 RPR-3500Å (for UVA irradiation, λ_{max} = 350±25 nm) fluorescent tube lamps (8 W each).

Micro photolysis:

- **Dwell device set-up**

Microreactor: Microreactions were performed in a *dwell-device* (*mikroglas*), made of Foturan™ glass and consisted of a bottom serpentine reaction channel (0.5 mm depth, 2 mm width, 1.15 m length, 1.68 ml internal volume) and a top heat-exchanging channel. Microreactor irradiation aperture was 118 mm × 73 mm.

Irradiation source: The *dwell device* was placed under a Luzchem UV-panel equipped with 5 RPR-3500Å (λ_{max} = 350±25 nm) fluorescent tube lamps (8 W each).

Pumps: Programmable syringe pump (Harvard apparatus 11 plus, serial No. B – 43281) was used to pump a reaction mixture through the reaction channel of microreactor. A rotary pump ISMATEC® (serial No. 313412) was used for the circulation of cooling water.

Syringe: A 10 ml glass syringe (ID = 14.56 mm) made of Borosilicatglass (Duran®, ILS, Germany) with a PTFE plunger was used for the loading of reaction mixture into the syringe pump.

- **Microchip set-up**

Microchip: Microreactions were performed in a *microchip* (*Micronit Microfluidics* FC_R150.676.2), made of Borofloat® glass and consisted of a single reaction channel of 150 μm wide, 150 μm deep and 757 mm long (32 turns) with an internal volume of 13 μl. Microchip irradiation aperture was 13.5 mm × 24.5 mm.

Irradiation source: The *microchip* was irradiated by an array of 6 × 75 mW high power UV-LEDs (λ_{max} = 365±5 nm, Seoul Optodevice, P8D236). The UV-LED current of 780 mA was provided and controlled by the power supply (TT*i* PL 155, serial No. 312554). During operation, the UV-LEDs array was cooled by a small air fan (Intel®, DTC–AAL03).

Pump: Programmable syringe pump (kdScientific, serial No. 111396) was used to pump a reaction mixture through the reaction channel of microchip.

Syringe: A 1 ml glass syringe (ID = 4.60 mm) made of Borosilicatglass (Duran®, ILS, Germany) with a PTFE plunger was used for the loading of reaction mixture into the syringe pump.

- **Dual-capillary microreactor set-up**

Dual-capillary reactor: Microreactions were performed in two parallel *PTFE capillaries* of 460 cm length each and 558 μm inner diameter (internal volume per capillary: 1.12 ml). These capillaries were tightly wrapped around a Pyrex glass cylinder of 6.5 cm diameter and 20 cm height.

Irradiation source: A single RPR-3500Å lamp (8 W, λ_{max} = 350±25 nm) was placed in the centre of the Pyrex cylinder. During operation, the lamp was cooled by a small air fan (model AFB0912HH, DC Brushless).

Pump: Programmable dual syringe pump (Fusion 200, Chemyx inc., serial No. 210628) was used to pump reaction mixtures through the parallel PTFE capillaries.

Syringes: Two glass syringes with the capacity of 5 ml each (ID = 10.29 mm, made of Borosilicatglass, Duran®, ILS, Germany) were used for the loading of reaction mixtures into the syringe pump.

- **Multi-capillary microreactor set-up**

Multi-capillary reactor: Microreactions were performed in ten parallel *FEP capillaries* of 11.4 m length and 800 μm inner diameter (internal volume per capillary: 5 ml). These capillaries were tightly wrapped around two Pyrex glass cylinders of 6 cm diameter and 60 cm height.

Irradiation source: Two blacklight fluorescent lamps (Skytronic, 18W/350, T8 Tube, λ_{max} = 365±25 nm) with optical power of 18 W each, were placed in the centre of the

Pyrex cylinders. During operation, the lamps were cooled by small air fans (model AFB0912HH, DC Brushless).

Pump: Programmable syringe pump equipped with special 10-channel rack (Fusion 200, Chemyx inc., serial No. 210828) was used to pump reaction mixtures through the parallel FEP capillaries.

Syringes: Ten glass syringes with the capacity of 10 ml each (ID = 14.56 mm, made of Borosilicatglass, Duran®, ILS, Germany) were used for the loading of reaction mixtures into the syringe pump.

Solvents and reagents

All solvents and starting materials were obtained from commercial suppliers (*Sigma-Aldrich* and *Fluka*) and were used without purification. The synthesis of compounds **84a-c**[191,271] have been done by the research group of Prof. Norbert Hoffmann (CNRS-University of Reims) and compounds were used without further purification or modification.

9.2.1 General procedure (GP-13) for photosensitized addition of isopropanol to furanones 84a-c under batch conditions (Rayonet):

A solution of the corresponding furanone (0.5 mmol) and sensitizer (acetone or DMBP; 0.1 mmol) in isopropanol (15 ml) was filled in a Pyrex glass test tube and was sonicated for 15 min using an ultrasound bath and was further degassed with a slow stream of argon for 15 min. The tube was stoppered and the reaction mixture was irradiated at 350±25 nm (Rayonet RPR-100, equipped with 16 × RPR-3500Å lamps, 16 × 8 W). After irradiation, the solvent was removed by rotary evaporation and the conversion rate was determined by ^{1}H-NMR of the crude product. The signal integration for the proton(s) bound to carbon 5 of the furanone ring of **84a-c** was compared to the signal integration of the same protons of **86a-c**. Pure products were isolated by column chromatography on silica gel with suitable mobile phase and further characterized by ^{1}H-NMR and ^{13}C-NMR spectroscopy.

Experiment 87

The addition of isopropanol to 2(5*H*)-furanone (CNRS-University of Reims)

General procedure (GP-13) was followed using furan-2(*5H*)-one (42 mg; 0.5 mmol) and acetone (1 ml; 14 mmol). After irradiation for 10 min the reaction was stopped, isopropanol was evaporated under reduced pressure and the crude product was analysed by ^{1}H-NMR. The composition of **84a** to product **86a** was calculated from the ^{1}H-NMR integration to be 69:31.

For ^{1}H-NMR data of product **86a** see experiment 90.

Experiment 88

The addition of isopropanol to *rac*-2-ethoxy-2(5*H*)-furanone (CNRS-University of Reims)

General procedure (GP-13) was followed using 5-ethoxyfuran-2(*5H*)-one (64 mg; 0.5 mmol) and acetone (1 ml; 14 mmol). After irradiation for 10 min the reaction was stopped, isopropanol was evaporated under reduced pressure and the crude product was analysed by ^{1}H-NMR. The composition of **84b** to product **86b** was calculated from the ^{1}H-NMR integration to be 48:52.

For ^{1}H-NMR data of product **86b** see experiment 91.

Experiment 89

The addition of isopropanol to (5*R*)-(-)-menthyloxy-2[5*H*]-furanone (CNRS-University of Reims)

General procedure (GP-13) was followed using (5*R*)-(-)-menthyloxy-2[5*H*]-furanone (119 mg; 0.5 mmol) and acetone (1 ml; 14 mmol). After irradiation for 10 min the reaction was stopped, isopropanol was evaporated under reduced pressure and the crude product was analysed by ^{1}H-NMR. The composition of **84c** to product **86c** was calculated from the ^{1}H-NMR integration to be 59:41.

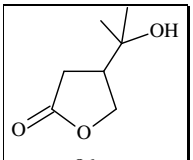
For ^{1}H-NMR data of product **86c** see experiment 92.

Experiment 90

The addition of isopropanol to 2(5*H*)-furanone (CNRS-University of Reims)

General procedure (GP-13) was followed using furan-2(*5H*)-one (42 mg; 0.5 mmol) and acetone (1 ml; 14 mmol). After irradiation for 20 min the reaction was stopped, isopropanol was evaporated under reduced pressure and the crude product was analysed by ^{1}H-NMR. The composition of **84a** to product **86a** was calculated from the ^{1}H-NMR integration to be 20:80. The crude product was further purified by column chromatography using ethyl acetate:petroleum ether (1:3) as eluent. The isolated yield of **86a** was found to be 57 mg (0.40 mmol, 79%). The product was confirmed by both ^{1}H-NMR and ^{13}C-NMR.

Analytical data of *4-(2-Hydroxypropan-2-yl)-dihydrofuran-2(3H)-one* (86a)



86a
$C_7H_{12}O_3$
Mol. Wt.: 144.2 g/mol

TLC: *Rf* = 0.32 (ethyl acetate/petroleum ether 1:3), yellow liquid

^{1}H–NMR: (400 MHz, $CDCl_3$)

δ (ppm) = 4.31 (dd, ^{3}J = 9.2, ^{4}J = 7.6 Hz, 1 H, OCH_2), 4.24 (dd, ^{3}J = 8.8, ^{4}J = 8.0 Hz, 1 H, OCH_2), 2.44-2.58 (m, 4 H, CH_2CH, OH), 1.17 (d, ^{2}J = 4.4 Hz, 6 H, $2CH_3$).

^{13}C–NMR: (100 MHz, $CDCl_3$)

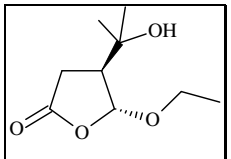
δ (ppm) = 177.8 (s, 1 C, C=O), 69.8 (s, 1 C, COH), 69.4 (s, 1 C, OCH_2), 45.7 (s, 1 C, CH), 29.8 (s, 1 C, CH_2), 28.0 (s, 1 C, CH_3), 27.7 (s, 1 C, CH_3).

Experiment 91

The addition of isopropanol to *rac*-2-ethoxy-2(5*H*)-furanone (CNRS-University of Reims)

General procedure (GP-13) was followed using 5-ethoxyfuran-2(*5H*)-one (64 mg; 0.5 mmol) and acetone (1 ml; 14 mmol). After irradiation for 20 min the reaction was stopped, isopropanol was evaporated under reduced pressure and the crude product was analysed by ^{1}H-NMR. The composition of **84b** to product **86b** was calculated from the ^{1}H-NMR integration to be 6:94. The crude product was further purified by column chromatography using ethyl acetate:n-hexane (1:3) as eluent. The isolated yield of **86b** was found to be 71 mg (0.38 mmol, 75%). The product was confirmed by both ^{1}H-NMR and ^{13}C-NMR.

Analytical data of *(4S,5R)-5-ethoxy-4-(2-hydroxypropan-2-yl)-dihydrofuran-2(3H)-one* (86b)



86b

$C_9H_{16}O_4$

Mol. Wt.: 188.2 g/mol

TLC: ***Rf*** = 0.43 (ethyl acetate/petroleum ether 7:3), yellow liquid

^{1}H–NMR: (400 MHz, $CDCl_3$)

δ (ppm) = 5.48 (d, ^{2}J = 3.6 Hz, 1 H, OCHO), 3.83 (dq, ^{3}J = 14.0, ^{4}J = 7.2 Hz, 1 H, C$\underline{H}_2$CH$_3$), 3.59 (dq, ^{3}J = 14.0, ^{4}J = 7.2 Hz, 1 H, C$\underline{H}_2$CH$_3$), 2.64 (dd, ^{3}J = 18.0, ^{4}J = 9.6 Hz, 1 H, C$\underline{H}_2$), 2.50 (dd, ^{3}J = 18.0, ^{4}J = 6.4 Hz, 1 H, C$\underline{H}_2$), 2.29-2.34 (m, 1 H, CH), 1.83 (br. s, 1 H, OH), 1.26 (s, 3 H, CH_3), 1.23 (t, ^{3}J = 7.2 Hz, 3 H, CH_3), 1.19 (s, 3 H, CH_3).

^{13}C–NMR: (100 MHz, $CDCl_3$)

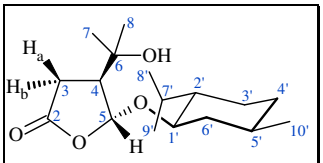
δ (ppm) = 176.1 (s, 1 C, C=O), 105.8 (s, 1 C, OCHO), 69.9 (s, 1 C, COH), 65.7 (s, 1 C, $\underline{C}H_2CH_3$), 51.9 (s, 1 C, CH), 30.0 (s, 1 C, CH_2), 28.1 (d, 1 C, CH_3), 27.9 (d, 1 C, CH_3), 15.1 (s, 1 C, $CH_2\underline{C}H_3$).

Experiment 92

The addition of isopropanol to (5*R*)-(-)-menthyloxy-2[5*H*]-furanone (CNRS-University of Reims)

General procedure (GP-13) was followed using (5*R*)-(-)-menthyloxy-2[5*H*]-furanone (119 mg; 0.5 mmol) and acetone (1 ml; 14 mmol). After irradiation for 20 min the reaction was stopped, isopropanol was evaporated under reduced pressure and the crude product was analysed by ^{1}H-NMR spectroscopy. The composition of **84c** to product **86c** was calculated from the ^{1}H-NMR integration to be 18:82. The crude product was further purified by column chromatography using ethyl acetate:n-hexane (1:4) as eluent. The isolated yield of **86c** was found to be 121 mg (0.41 mmol, 81%). The product was confirmed by both ^{1}H-NMR and ^{13}C-NMR.

Analytical data of *(4S,5R)-4-(2-hydroxypropan-2-yl)-5-((-)-menthyloxy)-dihydrofuran-2(3H)-one* (86c)



86c

$C_{17}H_{30}O_4$

Mol. Wt.: 298.4 g/mol

TLC: *Rf* = 0.48 (ethyl acetate/petroleum ether 15:85), colourless crystals

^{1}H–NMR: (400 MHz, $CDCl_3$)

δ (ppm) = 5.67 (d, J = 3.2 Hz, 1 H, C_5-H), 3.48 (dt, J = 10.8, 4.0 Hz, 1 H, $C_{1'}$-H), 2.64 (dd, J = 18.0, 9.6 Hz, 1 H, C_3-H_b), 2.48 (dd, J = 18.4, 6.0 Hz, 1 H, C_3-H_a), 2.26-2.31 (m, 1 H, C_4-H), 2.06-2.15 (m, 2 H, $C_{6'}$-H, $C_{7'}$-H), 1.86 (br.s, 1 H, C_6-O<u>H</u>), 1.58-1.63 (m, 2 H, $C_{3'}$-H, $C_{4'}$-H), 1.29-1.41 (m, 1 H, $C_{5'}$-H), 1.25 (s, 3 H, $C_{7,8}$-3H), 1.20-1.24 (m, 1 H, $C_{2'}$-H), 1.18 (s, 3 H, $C_{7,8}$-3H), 0.88 (d, J = 6 Hz, 3 H, C_{10}-3H), 0.83 (d, J = 6.8 Hz, 3 H, $C_{8',9'}$-3H), 0.75 (d, J = 6.8 Hz, 3 H, $C_{8',9'}$-3H), 0.78-1.03 (m, 3 H, $C_{3'}$-H, $C_{4'}$-H, $C_{6'}$-H).

^{13}C–NMR: (100 MHz, $CDCl_3$)

δ (ppm) = 176.22 (s, 1 C, C_2), 102.16 (s, 1 C, C_5), 77.32 (s, 1 C, $C_{1'}$), 70.11 (s, 1 C, C_6), 51.85 (s, 1 C, C_4), 47.86 (s, 1 C, $C_{2'}$), 39.87 (s, 1 C, $C_{6'}$), 34.35 (s, 1 C, $C_{4'}$), 31.43 (s, 1 C, $C_{5'}$), 30.18 (s, 1 C, C_3), 28.00 (d, 1 C, $C_{7,8}$), 27.75 (d, 1 C, $C_{7,8}$), 25.42 (s, 1 C, $C_{7'}$), 23.11 (s, 1 C, $C_{3'}$), 22.34 (s, 1 C, $C_{10'}$), 20.98 (s, 1 C, $C_{8',9'}$), 15.71 (s, 1 C, $C_{8',9'}$).

Experiment 93

The addition of isopropanol to 2(5*H*)-furanone (CNRS-University of Reims)

General procedure (GP-13) was followed using furan-2(*5H*)-one (42 mg; 0.5 mmol) and DMBP (24 mg; 0.1 mmol). After irradiation for 5 min the reaction was stopped, isopropanol was evaporated under reduced pressure and the crude product was analysed by ^{1}H-NMR. The composition of **84a** to product **86a** was calculated from the ^{1}H-NMR integration to be 10:90.

For ^{1}H-NMR data of product **86a** see experiment 90.

Experiment 94

The addition of isopropanol to *rac*-2-ethoxy-2(5*H*)-furanone (CNRS-University of Reims)

General procedure (GP-13) was followed using 5-ethoxyfuran-2(*5H*)-one (64 mg; 0.5 mmol) and DMBP (24 mg; 0.1 mmol). After irradiation for 5 min the reaction was stopped, isopropanol was evaporated under reduced pressure and the crude product was analysed by ^{1}H-NMR. The composition of **84b** to product **86b** was calculated from the ^{1}H-NMR integration to be 10:90.

For ^{1}H-NMR data of product **86b** see experiment 91.

Experiment 95

The addition of isopropanol to (5*R*)-(-)-menthyloxy-2[5*H*]-furanone (CNRS-University of Reims)

General procedure (GP-13) was followed using (5*R*)-(-)-menthyloxy-2[5*H*]-furanone (119 mg; 0.5 mmol) and DMBP (24 mg; 0.1 mmol). After irradiation for 5 min the reaction was stopped, isopropanol was evaporated under reduced pressure and the crude product was analysed by ^{1}H-NMR. The composition of **84c** to product **86c** was calculated from the ^{1}H-NMR integration to be 13:87.

For ^{1}H-NMR data of product **86c** see experiment 92.

Experiment 96

The addition of isopropanol to 2(5*H*)-furanone (CNRS-University of Reims)

General procedure (GP-13) was followed using furan-2(*5H*)-one (42 mg; 0.5 mmol) and DMBP (24 mg; 0.1 mmol). After irradiation for 20 min the reaction was stopped, isopropanol was evaporated under reduced pressure and the crude product was analysed by ^{1}H-NMR. The conversion was found to be 100% and the isolated yield was found to be 68 mg (0.47 mmol, 94%). Both ^{1}H-NMR and ^{13}C-NMR spectroscopy confirmed the product to be **86a**.

For ^{1}H-NMR data of product **86a** see experiment 90.

Experiment 97

The addition of isopropanol to *rac*-2-ethoxy-2(5*H*)-furanone (CNRS-University of Reims)

General procedure (GP-13) was followed using 5-ethoxyfuran-2(*5H*)-one (64 mg; 0.5 mmol) and DMBP (24 mg; 0.1 mmol). After irradiation for 20 min the reaction was stopped, isopropanol was evaporated under reduced pressure and the crude product was analysed by ^{1}H-NMR. The conversion was found to be 100% and the isolated yield was found to be 83 mg (0.44 mmol, 88%). Both ^{1}H-NMR and ^{13}C-NMR spectroscopy confirmed the product to be **86b**.

For ^{1}H-NMR data of product **86b** see experiment 91.

Experiment 98

The addition of isopropanol to (5*R*)-(-)-menthyloxy-2[5*H*]-furanone (CNRS-University of Reims)

General procedure (GP-13) was followed using (5*R*)-(-)-menthyloxy-2[5*H*]-furanone (119 mg; 0.5 mmol) and DMBP (24 mg; 0.1 mmol). After irradiation for 20 min the reaction was stopped, isopropanol was evaporated under reduced pressure and the crude product was analysed by ^{1}H-NMR. The conversion was found to be 100% and the isolated yield was found to be 130 mg (0.44 mmol, 87 %). Both ^{1}H-NMR and ^{13}C-NMR spectroscopy confirmed the product to be **86c**.

For ^{1}H-NMR data of product **86c** see experiment 92.

9.2.2 General procedure (GP-14) for photosensitized addition of isopropanol to furanones 84a-c in the dwell-microreactor:

A solution of the corresponding furanone (0.5 mmol) and sensitizer DMBP (0.1 mmol) in isopropanol (15 ml) was sonicated for 15 min using an ultrasound bath and degassed with a slow stream of N_2 for 15 minutes. The microreactor was prepared by pumping the pre-sonicated isopropanol through the reaction channel until all air bubbles had been removed. Then 10 ml of prepared solution was transferred into a 10 ml glass syringe, any air bubbles were expelled and the syringe was loaded into a syringe pump. The flow rate was set and solution was pumped through a micro-reactor (mikroglas dwell device) while irradiated at 350±25 nm (Luzchem UV exposure panel equipped with 5 × RPR-3500Å lamps, 5 × 8 W). During the reaction, the reactor was kept cool by pumping cold water through the cooling channel. When the syringe was empty, the syringe pump and the lamps were switched off simultaneously. The syringe was refilled with isopropanol and loaded into a syringe pump again. The syringe pump was then turned on simultaneously with the lamps. When the reaction was complete, isopropanol was removed by rotary evaporation and the conversion rate of reaction was determined by ^{1}H-NMR analysis of the crude product. The signal integration for the proton(s) bound to carbon 5 of the furanone ring of **84a-c** was compared to the signal integration of the same protons of **86a-c**. Pure products were not isolated in these experiments.

Experiment 99

The addition of isopropanol to 2(5*H*)-furanone (OS-206)

General procedure (GP-14) was followed using furan-2(*5H*)-one (42 mg; 0.5 mmol) and DMBP (24 mg; 0.1 mmol). The flow rate used was 0.336 ml/min; residence time: 5 min. The composition of **84a** to product **86a** was calculated from the ^{1}H-NMR integration to be 19:81.

For ^{1}H-NMR data of product **86a** see experiment 90.

Experiment 100

The addition of isopropanol to *rac*-2-ethoxy-2(5*H*)-furanone (OS-202)

General procedure (GP-14) was followed using 5-ethoxyfuran-2(*5H*)-one (64 mg; 0.5 mmol) and DMBP (24 mg; 0.1 mmol). The flow rate used was 0.336 ml/min; residence

time: 5 min. The composition of **84b** to product **86b** was calculated from the ^{1}H-NMR integration to be 1:99.

For ^{1}H-NMR data of product **86b** see experiment 91.

Experiment 101

The addition of isopropanol to (5*R*)-(-)-menthyloxy-2[5*H*]-furanone (OS-200)

General procedure (GP-14) was followed using (5*R*)-(-)-menthyloxy-2[5*H*]-furanone (119 mg; 0.5 mmol) and DMBP (24 mg; 0.1 mmol). The flow rate used was 0.336 ml/min; residence time: 5 min. The composition of **84c** to product **86c** was calculated from the ^{1}H-NMR integration to be 2:98.

For ^{1}H-NMR data of product **86c** see experiment 92.

Experiment 102

The addition of isopropanol to 2(5*H*)-furanone (OS-205)

General procedure (GP-14) was followed using furan-2(*5H*)-one (42 mg; 0.5 mmol) and DMBP (24 mg; 0.1 mmol). The flow rate used was 0.168 ml/min; residence time: 10 min. The conversion was found to be 100%.

For ^{1}H-NMR data of product **86a** see experiment 90.

Experiment 103

The addition of isopropanol to *rac*-2-ethoxy-2(5*H*)-furanone (OS-203)

General procedure (GP-14) was followed using 5-ethoxyfuran-2(*5H*)-one (64 mg; 0.5 mmol) and DMBP (24 mg; 0.1 mmol). The flow rate used was 0.168 ml/min; residence time: 10 min. The conversion was found to be 100%.

For ^{1}H-NMR data of product **86b** see experiment 91.

Experiment 104

The addition of isopropanol to (5*R*)-(-)-menthyloxy-2[5*H*]-furanone (OS-212)

General procedure (GP-14) was followed using (5*R*)-(-)-menthyloxy-2[5*H*]-furanone (119 mg; 0.5 mmol) and DMBP (24 mg; 0.1 mmol). The flow rate used was 0.168 ml/min; residence time: 10 min. The conversion was found to be 100%.

For ^{1}H-NMR data of product **86c** see experiment 92.

9.2.3 General procedure (GP-15) for photosensitized addition of isopropanol to furanones 84a-c in the LED-microchip:

The corresponding furanone (0.1 mmol) and sensitizer DMBP (20 μmol) were dissolved in isopropanol (3 ml) and the solution was sonicated for 15 min using an ultrasound bath and degassed with a slow stream of N_2 for 5 minutes. The microchip was prepared by pumping the pre-sonicated isopropanol through the reaction channel until all air bubbles had been removed. Then 1 ml of prepared solution was transferred into a 1 ml glass syringe, any air bubbles were expelled and the syringe was loaded into a syringe pump. The flow rate was set and the solution was pumped through a microchip (Micronit) while irradiated by 6 × 365 nm high power LEDs (6 × 75 mW). When the syringe was empty, the syringe pump and the LEDs were switched off simultaneously. The syringe was refilled with isopropanol and loaded into a syringe pump again. The syringe pump was then turned on simultaneously with the LEDs. When the reaction was complete, isopropanol was removed by rotary evaporation and the conversion rate of the reaction was determined by ^{1}H-NMR analysis of the crude product. The signal integration for the proton(s) bound to carbon 5 of the furanone ring of **84a-c** was compared to the signal integration of the same protons of **86a-c**. Pure products were not isolated in these experiments.

Experiment 105

The addition of isopropanol to 2(5*H*)-furanone (OS-166)

General procedure (GP-15) was followed using furan-2(*5H*)-one (8 mg; 0.1 mmol) and DMBP (5 mg; 20 μmol). The flow rate used was 0.65 μl/min; residence time: 20 min. The conversion was found to be 100%.

For ^{1}H-NMR data of product **86a** see experiment 90.

Experiment 106

The addition of isopropanol to 2(5*H*)-furanone (OS-171)

General procedure (GP-15) was followed using furan-2(*5H*)-one (8 mg; 0.1 mmol) and DMBP (5 mg; 20 μmol). The flow rate used was 2.6 μl/min; residence time: 5 min. The conversion was found to be 100%.

For ^{1}H-NMR data of product **86a** see experiment 90.

Experiment 107

The addition of isopropanol to *rac*-2-ethoxy-2(5*H*)-furanone (OS-198)

General procedure (GP-15) was followed using 5-ethoxyfuran-2(*5H*)-one (13 mg; 0.1 mmol) and DMBP (5 mg; 20 μmol). The flow rate used was 2.6 μl/min; residence time: 5 min. The conversion was found to be 100%.

For ^{1}H-NMR data of product **86b** see experiment 91.

Experiment 108

The addition of isopropanol to (5*R*)-(-)-menthyloxy-2[5*H*]-furanone (OS-183)

General procedure (GP-15) was followed using (5*R*)-(-)-menthyloxy-2[5*H*]-furanone (24 mg; 0.1 mmol) and DMBP (5 mg; 20 μmol). The flow rate used was 2.6 μl/min; residence time: 5 min. The conversion was found to be 100%.

For ^{1}H-NMR data of product **86c** see experiment 92.

Experiment 109

The addition of isopropanol to 2(5*H*)-furanone (OS-209)

General procedure (GP-15) was followed using furan-2(*5H*)-one (8 mg; 0.1 mmol) and DMBP (5 mg; 20 μmol). The flow rate used was 5.2 μl/min; residence time: 2.5 min. The composition of **84a** to product **86a** was calculated from the ^{1}H-NMR integration to be 11:89.

For ^{1}H-NMR data of product **86a** see experiment 90.

Experiment 110

The addition of isopropanol to *rac*-2-ethoxy-2(5*H*)-furanone (OS-210)

General procedure (GP-15) was followed using 5-ethoxyfuran-2(*5H*)-one (13 mg; 0.1 mmol) and DMBP (5 mg; 20 μmol). The flow rate used was 5.2 μl/min; residence time: 2.5 min. The conversion was found to be 100%.

For ^{1}H-NMR data of product **86b** see experiment 91.

Experiment 111

The addition of isopropanol to (5*R*)-(-)-menthyloxy-2[5*H*]-furanone (OS-211)

General procedure (GP-15) was followed using (5*R*)-(-)-menthyloxy-2[5*H*]-furanone (24 mg; 0.1 mmol) and DMBP (5 mg; 20 μmol). The flow rate used was 5.2 μl/min; residence time: 2.5 min. The conversion was found to be 100%.

For ^{1}H-NMR data of product **86c** see experiment 92.

Experiment 112

The addition of isopropanol to 2(5*H*)-furanone (OS-192)

General procedure (GP-15) was followed using furan-2(*5H*)-one (8 mg; 0.1 mmol) and DMBP (5 mg; 20 μmol). The flow rate used was 13 μl/min; residence time: 1 min. The composition of **84a** to product **86a** was calculated from the ^{1}H-NMR integration to be 42:58.

For ^{1}H-NMR data of product **86a** see experiment 90.

Experiment 113

The addition of isopropanol to *rac*-2-ethoxy-2(5*H*)-furanone (OS-204)

General procedure (GP-15) was followed using 5-ethoxyfuran-2(*5H*)-one (13 mg; 0.1 mmol) and DMBP (5 mg; 20 μmol). The flow rate used was 13 μl/min; residence time: 1 min. The composition of **84b** to product **86b** was calculated from the ^{1}H-NMR integration to be 40:60.

For ^{1}H-NMR data of product **86b** see experiment 91.

Experiment 114

The addition of isopropanol to (5*R*)-(-)-menthyloxy-2[5*H*]-furanone (OS-201)

General procedure (GP-15) was followed using (5*R*)-(-)-menthyloxy-2[5*H*]-furanone (24 mg; 0.1 mmol) and DMBP (5 mg; 20 μmol). The flow rate used was 13 μl/min; residence time: 1 min. The composition of **84c** to product **86c** was calculated from the ^{1}H-NMR integration to be 41:59.

For ^{1}H-NMR data of product **86c** see experiment 92.

9.2.4 General procedure (GP-16) for photosensitized addition of isopropanol to furanones 84a-c in the dual-capillary microreactor:

The corresponding furanone (0.5 mmol) and sensitizer DMBP (0.1 mmol) were dissolved in isopropanol (15 ml) and the solution was sonicated for 15 min using an ultrasound bath and degassed with a slow stream of N_2 for 15 minutes. Then this reaction mixture was distributed over two syringes (5 ml each), any air bubbles were expelled and syringes were loaded into a dual syringe pump. The flow rate was set and the solution was pumped through the microcapillaries while being irradiated by a single UVA lamp (RPR-3500Å, 8 W). When the syringes were empty, the dual syringe pump and the UVA lamp were switched off simultaneously. The syringes were refilled with isopropanol and loaded into a dual syringe pump again. The syringe pump was then turned on simultaneously with the UVA lamp. When the reaction was complete, the reaction mixtures from both capillaries were combined and isopropanol was removed by rotary evaporation. The crude product was analyzed by ^{1}H-NMR to determine the conversion. The signal integration for the proton(s) bound to carbon 5 of the furanone ring of **84a-c** was compared to the signal integration of the same protons of **86a-c**. Pure products were not isolated in these experiments.

Experiment 115

The addition of isopropanol to 2(5*H*)-furanone (OS-164)

General procedure (GP-16) was followed using furan-2(*5H*)-one (42 mg; 0.5 mmol) and DMBP (24 mg; 0.1 mmol). The flow rate used was 57.5 µl/min; residence time: 20 min. The conversion was found to be 100%.

For ^{1}H-NMR data of product **86a** see experiment 90.

Experiment 116

The addition of isopropanol to *rac*-2-ethoxy-2(5*H*)-furanone (OS-167)

General procedure (GP-16) was followed using 5-ethoxyfuran-2(*5H*)-one (64 mg; 0.5 mmol) and DMBP (24 mg; 0.1 mmol). The flow rate used was 57.5 µl/min; residence time: 20 min. The conversion was found to be 100%.

For ^{1}H-NMR data of product **86b** see experiment 91.

Experiment 117

The addition of isopropanol to (5*R*)-(-)-menthyloxy-2[5*H*]-furanone (OS-168)

General procedure (GP-16) was followed using (5*R*)-(-)-menthyloxy-2[5*H*]-furanone (119 mg; 0.5 mmol) and DMBP (24 mg; 0.1 mmol). The flow rate used was 57.5 µl/min; residence time: 20 min. The conversion was found to be 100%.

For ^{1}H-NMR data of product **86c** see experiment 92.

Experiment 118

The addition of isopropanol to 2(5*H*)-furanone (OS-173)

General procedure (GP-16) was followed using furan-2(*5H*)-one (42 mg; 0.5 mmol) and DMBP (24 mg; 0.1 mmol). The flow rate used was 76.7 µl/min; residence time: 15 min. The conversion was found to be 100%.

For ^{1}H-NMR data of product **86a** see experiment 90.

Experiment 119

The addition of isopropanol to 2(5*H*)-furanone (OS-180)

General procedure (GP-16) was followed using furan-2(*5H*)-one (42 mg; 0.5 mmol) and DMBP (24 mg; 0.1 mmol). The flow rate used was 115 µl/min; residence time: 10 min. The conversion was found to be 100%.

For ^{1}H-NMR data of product **86a** see experiment 90.

Experiment 120

The addition of isopropanol to *rac*-2-ethoxy-2(5*H*)-furanone (OS-181, OS-184)

General procedure (GP-16) was followed using 5-ethoxyfuran-2(*5H*)-one (64 mg; 0.5 mmol) and DMBP (24 mg; 0.1 mmol). The flow rate used was 115 µl/min; residence time: 10 min. The conversion was found to be 100%.

For ^{1}H-NMR data of product **86b** see experiment 91.

Experiment 121

The addition of isopropanol to (5*R*)-(-)-menthyloxy-2[5*H*]-furanone (OS-185)

General procedure (GP-16) was followed using (5*R*)-(-)-menthyloxy-2[5*H*]-furanone (119 mg; 0.5 mmol) and DMBP (24 mg; 0.1 mmol). The flow rate used was 115 µl/min; residence time: 10 min. The conversion was found to be 100%.

For ^{1}H-NMR data of product **86c** see experiment 92.

Experiment 122

The addition of isopropanol to 2(5*H*)-furanone (OS-191)

General procedure (GP-16) was followed using furan-2(*5H*)-one (42 mg; 0.5 mmol) and DMBP (24 mg; 0.1 mmol). The flow rate used was 153.3 µl/min; residence time: 7.5 min. The composition of **84a** to product **86a** was calculated from the ^{1}H-NMR integration to be 5:95.

For ^{1}H-NMR data of product **86a** see experiment 90.

Experiment 123

The addition of isopropanol to *rac*-2-ethoxy-2(5*H*)-furanone (OS-186)

General procedure (GP-16) was followed using 5-ethoxyfuran-2(*5H*)-one (64 mg; 0.5 mmol) and DMBP (24 mg; 0.1 mmol). The flow rate used was 153.3 µl/min; residence time: 7.5 min. The composition of **84b** to product **86b** was calculated from the ^{1}H-NMR integration to be 1:99.

For ^{1}H-NMR data of product **86b** see experiment 91.

Experiment 124

The addition of isopropanol to (5*R*)-(-)-menthyloxy-2[5*H*]-furanone (OS-187)

General procedure (GP-16) was followed using (5*R*)-(-)-menthyloxy-2[5*H*]-furanone (119 mg; 0.5 mmol) and DMBP (24 mg; 0.1 mmol). The flow rate used was 153.3 µl/min; residence time: 7.5 min. The conversion was found to be 100%.

For ^{1}H-NMR data of product **86c** see experiment 92.

Experiment 125

The addition of isopropanol to 2(5*H*)-furanone (OS-182)

General procedure (GP-16) was followed using furan-2(*5H*)-one (42 mg; 0.5 mmol) and DMBP (24 mg; 0.1 mmol). The flow rate used was 230 µl/min; residence time: 5 min. The composition of **84a** to product **86a** was calculated from the ^{1}H-NMR integration to be 25:75.

For ^{1}H-NMR data of product **86a** see experiment 90.

Experiment 126

The addition of isopropanol to *rac*-2-ethoxy-2(5*H*)-furanone (OS-169)

General procedure (GP-16) was followed using 5-ethoxyfuran-2(*5H*)-one (64 mg; 0.5 mmol) and DMBP (24 mg; 0.1 mmol). The flow rate used was 230 µl/min; residence time: 5 min. The composition of **84b** to product **86b** was calculated from the ^{1}H-NMR integration to be 4:96.

For ^{1}H-NMR data of product **86b** see experiment 91.

Experiment 127

The addition of isopropanol to (5*R*)-(-)-menthyloxy-2[5*H*]-furanone (OS-170)

General procedure (GP-16) was followed using (5*R*)-(-)-menthyloxy-2[5*H*]-furanone (119 mg; 0.5 mmol) and DMBP (24 mg; 0.1 mmol). The flow rate used was 230 µl/min; residence time: 5 min. The composition of **84c** to product **86c** was calculated from the ^{1}H-NMR integration to be 1:99.

For ^{1}H-NMR data of product **86c** see experiment 92.

Experiment 128

The addition of isopropanol to 2(5*H*)-furanone (OS-196)

General procedure (GP-16) was followed using furan-2(*5H*)-one (42 mg; 0.5 mmol) and DMBP (24 mg; 0.1 mmol). The flow rate used was 460 µl/min; residence time: 2.5 min. The composition of **84a** to product **86a** was calculated from the ^{1}H-NMR integration to be 65:35.

For ^{1}H-NMR data of product **86a** see experiment 90.

Experiment 129

The addition of isopropanol to *rac*-2-ethoxy-2(5*H*)-furanone (OS-197)

General procedure (GP-16) was followed using 5-ethoxyfuran-2(*5H*)-one (64 mg; 0.5 mmol) and DMBP (24 mg; 0.1 mmol). The flow rate used was 460 µl/min; residence time: 2.5 min. The composition of **84b** to product **86b** was calculated from the ^{1}H-NMR integration to be 50:50.

For ^{1}H-NMR data of product **86b** see experiment 91.

Experiment 130

The addition of isopropanol to (5*R*)-(-)-menthyloxy-2[5*H*]-furanone (OS-199)

General procedure (GP-16) was followed using (5*R*)-(-)-menthyloxy-2[5*H*]-furanone (119 mg; 0.5 mmol) and DMBP (24 mg; 0.1 mmol). The flow rate used was 460 µl/min; residence time: 2.5 min. The composition of **84c** to product **86c** was calculated from the ^{1}H-NMR integration to be 36:64.

For ^{1}H-NMR data of product **86c** see experiment 92.

9.2.5 General procedure (GP-17) for photosensitized addition of secondary alcohols to furanones 84a-c and α,β-unsaturated esters 91a,b in the multi-capillary reactor:

Ten individual alcohol solutions of the corresponding furanone (mg; mmol) or α,β-unsaturated ester (mg; mmol) and sensitizer (mg; mmol) were prepared in separate glass vials with a total volume of 15 ml each. The prepared solutions were simultaneously sonicated for 15 min using an ultrasound bath and further degassed with a slow stream of N_2 for 15 minutes. Then these solutions (11 ml of each) were transferred into 10 individual glass syringes (for 10 ml each) and every syringe was appropriately labelled. Any air bubbles were expelled and the syringes were loaded into a syringe pump with a special 10 channel infuse/withdraw holder. The syringes were equipped with shut valves and initially were not connected to the capillaries. The flow rate of liquid was set to 1 ml/min and the pump was started. After a few seconds, the pump was stopped when the first drops of solution were flushed out of all of the syringes. The shut valves were closed and each syringe was connected to the individual capillary. The liquid flow rate was changed to the required flow (adjusted to the residence time) and the syringe pump was preset to pump exactly 10 ml of solution through each capillary. Afterwards, the

shut valves were opened and solutions were pumped through the microcapillaries while being irradiated by a single UVA fluorescent lamp (λ_{max} = 365±25 nm, 18 W each). When the syringe pump stopped automatically, the fluorescent lamps were switched off manually and all syringes were refilled with the appropriate solvent (secondary alcohol) and loaded into the syringe pump again. The syringe pump was then turned on simultaneously with the fluorescent lamps. The experimental solutions from each capillary were collected into individual round bottom flasks and solvent was removed by rotary evaporation. The crude products were analyzed by ^{1}H-NMR to determine the conversion. In the case of furanones **84a-c**, the signal integration for the proton(s) bound to carbon 5 of the furanone ring of the initial furanone was compared to the signal integration of the same protons of the furanone product. In the case of α,β-unsaturated esters **91a,b** the signal integration for the C<u>H</u> protons of the initial ester was compared to the signal integration of the C<u>H$_3$</u> protons of the photoaddition product(s). Pure products were isolated by column chromatography on silica gel with suitable mobile phase and further characterized by ^{1}H-NMR and ^{13}C-NMR spectroscopy.

Experiment 131

Effect of residence time on the reactions efficiency

General procedure (GP-17) was followed with the slight variation of preparing three experimental solutions and employing only three parallel capillaries instead of ten for a single run. The flow rate used was 0.5 ml/min; residence time: 10 min.

<u>Solution 1</u> (OS-228): was prepared using furan-2(*5H*)-one (42 mg; 0.5 mmol), DMBP (24 mg; 0.1 mmol) and isopropanol as solvent. The conversion was found to be 100%. For ^{1}H-NMR data of product **86a** see experiment 90.

<u>Solution 2</u> (OS-331): was prepared using 5-ethoxyfuran-2(*5H*)-one (64 mg; 0.5 mmol), DMBP (24 mg; 0.1 mmol) and isopropanol as solvent. The conversion was found to be 100%. For ^{1}H-NMR data of product **86b** see experiment 91.

<u>Solution 3</u> (OS-332): was prepared using (5*R*)-(-)-menthyloxy-2[5*H*]-furanone (119 mg; 0.5 mmol), DMBP (24 mg; 0.1 mmol) and isopropanol as solvent. The conversion was found to be 100%. For ^{1}H-NMR data of product **86c** see experiment 92.

Experiment 132

Effect of residence time on the reactions efficiency

General procedure (GP-17) was followed with the slight variation of preparing three experimental solutions and employing only three parallel capillaries instead of ten for a single run. The flow rate used was 0.67 ml/min; residence time: 7.5 min.

Solution 1 (OS-361): was prepared using furan-2(*5H*)-one (42 mg; 0.5 mmol), DMBP (24 mg; 0.1 mmol) and isopropanol as solvent. The composition of **84a** to product **86a** was calculated from the ^{1}H-NMR integration to be 7:93. For ^{1}H-NMR data of product **86a** see experiment 90.

Solution 2 (OS-333): was prepared using 5-ethoxyfuran-2(*5H*)-one (64 mg; 0.5 mmol), DMBP (24 mg; 0.1 mmol) and isopropanol as solvent. The composition of **84b** to product **86b** was calculated from the ^{1}H-NMR integration to be 1:99. For ^{1}H-NMR data of product **86b** see experiment 91.

Solution 3 (OS-334): was prepared using (5*R*)-(-)-menthyloxy-2[5*H*]-furanone (119 mg; 0.5 mmol), DMBP (24 mg; 0.1 mmol) and isopropanol as solvent. The conversion was found to be 100%. For ^{1}H-NMR data of product **86c** see experiment 92.

Experiment 133

Effect of residence time on the reactions efficiency

General procedure (GP-17) was followed with the slight variation of preparing three experimental solutions and employing only three parallel capillaries instead of ten for a single run. The flow rate used was 1.0 ml/min; residence time: 5 min.

Solution 1 (OS-237): was prepared using furan-2(*5H*)-one (42 mg; 0.5 mmol), DMBP (24 mg; 0.1 mmol) and isopropanol as solvent. The composition of **84a** to product **86a** was calculated from the ^{1}H-NMR integration to be 29:71. For ^{1}H-NMR data of product **86a** see experiment 90.

Solution 2 (OS-337): was prepared using 5-ethoxyfuran-2(*5H*)-one (64 mg; 0.5 mmol), DMBP (24 mg; 0.1 mmol) and isopropanol as solvent. The composition of **84b** to product **86b** was calculated from the ^{1}H-NMR integration to be 18:82. For ^{1}H-NMR data of product **86b** see experiment 91.

Solution 3 (OS-338): was prepared using (5*R*)-(-)-menthyloxy-2[5*H*]-furanone (119 mg; 0.5 mmol), DMBP (24 mg; 0.1 mmol) and isopropanol as solvent. The composition of **84c** to product **86c** was calculated from the ^{1}H-NMR integration to be 8:92. For ^{1}H-NMR data of product **86c** see experiment 92.

Experiment 134

Effect of residence time on the reactions efficiency

General procedure (GP-17) was followed with the slight variation of preparing three experimental solutions and employing only three parallel capillaries instead of ten for a single run. The flow rate used was 2.0 ml/min; residence time: 2.5 min.

Solution 1 (OS-360): was prepared using furan-2(*5H*)-one (42 mg; 0.5 mmol), DMBP (24 mg; 0.1 mmol) and isopropanol as solvent. The composition of **84a** to product **86a** was calculated from the ^{1}H-NMR integration to be 74:26. For ^{1}H-NMR data of product **86a** see experiment 90.

Solution 2 (OS-335): was prepared using 5-ethoxyfuran-2(*5H*)-one (64 mg; 0.5 mmol), DMBP (24 mg; 0.1 mmol) and isopropanol as solvent. The composition of **84b** to product **86b** was calculated from the ^{1}H-NMR integration to be 66:34. For ^{1}H-NMR data of product **86b** see experiment 91.

Solution 3 (OS-336): was prepared using (5*R*)-(-)-menthyloxy-2[5*H*]-furanone (119 mg; 0.5 mmol), DMBP (24 mg; 0.1 mmol) and isopropanol as solvent. The composition of **84c** to product **86c** was calculated from the ^{1}H-NMR integration to be 54:46. For ^{1}H-NMR data of product **86c** see experiment 92.

Experiment 135

Effect of residence time on the reactions efficiency

General procedure (GP-17) was followed with the slight variation of preparing three experimental solutions and employing only three parallel capillaries instead of ten for a single run. The flow rate used was 5.0 ml/min; residence time: 1 min.

Solution 1 (OS-359): was prepared using furan-2(*5H*)-one (42 mg; 0.5 mmol), DMBP (24 mg; 0.1 mmol) and isopropanol as solvent. The composition of **84a** to product **86a** was calculated from the ^{1}H-NMR integration to be 98:2. For ^{1}H-NMR data of product **86a** see experiment 90.

Solution 2 (OS-329): was prepared using 5-ethoxyfuran-2(*5H*)-one (64 mg; 0.5 mmol), DMBP (24 mg; 0.1 mmol) and isopropanol as solvent. The composition of **84b** to product **86b** was calculated from the ^{1}H-NMR integration to be 88:12. For ^{1}H-NMR data of product **86b** see experiment 91.

Solution 3 (OS-330): was prepared using (5*R*)-(-)-menthyloxy-2[5*H*]-furanone (119 mg; 0.5 mmol), DMBP (24 mg; 0.1 mmol) and isopropanol as solvent. The composition of

84c to product **86c** was calculated from the ^{1}H-NMR integration to be 77:23. For ^{1}H-NMR data of product **86c** see experiment 92.

Experiment 136

Reproducibility study

General procedure (GP-17) was followed and ten identical experimental solutions were prepared and tested within a single run. The flow rate used was 1.0 ml/min; residence time: 5 min.

Solution 1 (OS-266): was prepared using furan-2(*5H*)-one (43 mg; 0.5 mmol), DMBP (24 mg; 0.1 mmol) and isopropanol as solvent. The composition of **84a** to product **86a** was calculated from the ^{1}H-NMR integration to be 35:65.

Solution 2 (OS-267): was prepared using furan-2(*5H*)-one (43 mg; 0.5 mmol), DMBP (24 mg; 0.1 mmol) and isopropanol as solvent. The composition of **84a** to product **86a** was calculated from the ^{1}H-NMR integration to be 32:68.

Solution 3 (OS-268): was prepared using furan-2(*5H*)-one (42 mg; 0.5 mmol), DMBP (24 mg; 0.1 mmol) and isopropanol as solvent. The composition of **84a** to product **86a** was calculated from the ^{1}H-NMR integration to be 27:73.

Solution 4 (OS-269): was prepared using furan-2(*5H*)-one (43 mg; 0.5 mmol), DMBP (24 mg; 0.1 mmol) and isopropanol as solvent. The composition of **84a** to product **86a** was calculated from the ^{1}H-NMR integration to be 33:67.

Solution 5 (OS-270): was prepared using furan-2(*5H*)-one (43 mg; 0.5 mmol), DMBP (24 mg; 0.1 mmol) and isopropanol as solvent. The composition of **84a** to product **86a** was calculated from the ^{1}H-NMR integration to be 31:69.

Solution 6 (OS-271): was prepared using furan-2(*5H*)-one (43 mg; 0.5 mmol), DMBP (24 mg; 0.1 mmol) and isopropanol as solvent. The composition of **84a** to product **86a** was calculated from the ^{1}H-NMR integration to be 25:75.

Solution 7 (OS-272): was prepared using furan-2(*5H*)-one (43 mg; 0.5 mmol), DMBP (24 mg; 0.1 mmol) and isopropanol as solvent. The composition of **84a** to product **86a** was calculated from the ^{1}H-NMR integration to be 28:72.

Solution 8 (OS-273): was prepared using furan-2(*5H*)-one (42 mg; 0.5 mmol), DMBP (24 mg; 0.1 mmol) and isopropanol as solvent. The composition of **84a** to product **86a** was calculated from the ^{1}H-NMR integration to be 28:72.

Solution 9 (OS-274): was prepared using furan-2(*5H*)-one (43 mg; 0.5 mmol), DMBP (25 mg; 0.1 mmol) and isopropanol as solvent. The composition of **84a** to product **86a** was calculated from the ^{1}H-NMR integration to be 27:73.

Solution 10 (OS-275): was prepared using furan-2(*5H*)-one (43 mg; 0.5 mmol), DMBP (24 mg; 0.1 mmol) and isopropanol as solvent. The composition of **84a** to product **86a** was calculated from the ^{1}H-NMR integration to be 27:73.

For ^{1}H-NMR data of product **86a** see experiment 90.

Experiment 137

Scale-up synthesis of *4-(2-Hydroxypropan-2-yl)-dihydrofuran-2(3H)-one* 86a (OS-328)

General procedure (GP-17) was followed with the variation of preparing a 135 ml of a single experimental solution and divided into 10 syringes. The experimental solution was prepared using furan-2(*5H*)-one (371 mg; 4.5 mmol), DMBP (218 mg; 0.9 mmol) and isopropanol as solvent (135 ml). The flow rate used was 0.5 ml/min; residence time: 10 min. The products from individual capillaries were collected into a single round bottom flask with a total volume of 250 ml. After evaporation of isopropanol under reduced pressure the crude product was analysed by ^{1}H-NMR. The conversion was found to be 100%. The crude product was further purified by column chromatography using ethyl acetate:petroleum ether (1:3) as eluent. The isolated yield of **86a** was found to be 452 mg (3.1 mmol, 94%). Both ^{1}H-NMR and ^{13}C-NMR spectroscopy confirmed the product to be **86a**.

For ^{1}H-NMR data of product **86a** see experiment 90.

Experiment 138

Effect of the sensitizer on the addition of isopropanol to 2(5*H*)-furanone 84a

General procedure (GP-17) was followed and ten experimental solutions with different sensitizers were prepared and tested within a single run. The flow rate used was 1.0 ml/min; residence time: 5 min.

Solution 1 (OS-306): was prepared using furan-2(*5H*)-one (42 mg; 0.5 mmol), 4,4′-dimethoxy benzophenone (24 mg; 0.1 mmol) and isopropanol as solvent. The composition of **84a** to product **86a** was calculated from the ^{1}H-NMR integration to be 28:72.

Solution 2 (OS-307): was prepared using furan-2(*5H*)-one (43 mg; 0.5 mmol), 4-benzoylbenzoic acid (23 mg; 0.1 mmol) and isopropanol as solvent. The composition of **84a** to product **86a** was calculated from the ^{1}H-NMR integration to be 63:37.

Solution 3 (OS-308): was prepared using furan-2(*5H*)-one (42 mg; 0.5 mmol), 4,4′-bis(dimethylamino)benzophenone (27 mg; 0.1 mmol) and isopropanol as solvent. The ^{1}H-NMR analysis of the crude product showed that **84a** did not undergo any conversion.

Solution 4 (OS-309): was prepared using furan-2(*5H*)-one (43 mg; 0.5 mmol), benzophenone (18 mg; 0.1 mmol) and isopropanol as solvent. The composition of **84a** to product **86a** was calculated from the ^{1}H-NMR integration to be 70:30.

Solution 5 (OS-313): was prepared using furan-2(*5H*)-one (42 mg; 0.5 mmol), xanthone (19 mg; 0.1 mmol) and isopropanol as solvent. The composition of **84a** to product **86a** was calculated from the ^{1}H-NMR integration to be 53:47.

Solution 6 (OS-310): was prepared using furan-2(*5H*)-one (43 mg; 0.5 mmol), acetophenone (13 mg; 0.1 mmol) and isopropanol as solvent. The composition of **84a** to product **86a** was calculated from the ^{1}H-NMR integration to be 96:4.

Solution 7 (OS-311): was prepared using furan-2(*5H*)-one (48 mg; 0.5 mmol), 4′-*tert*-butylacetophenone (18 mg; 0.1 mmol) and isopropanol as solvent. The ^{1}H-NMR analysis of the crude product showed that **84a** did not undergo any conversion.

Solution 8 (OS-312): was prepared using furan-2(*5H*)-one (42 mg; 0.5 mmol), 4′-methoxyacetophenone (15 mg; 0.1 mmol) and isopropanol as solvent. The ^{1}H-NMR analysis of the crude product showed that **84a** did not undergo any conversion.

Solution 9 (OS-314): was prepared using furan-2(*5H*)-one (43 mg; 0.5 mmol), 4-(dimethylamino)benzaldehyde (15 mg; 0.1 mmol) and isopropanol as solvent. The ^{1}H-NMR analysis of the crude product showed that **84a** did not undergo any conversion.

Solution 10 (OS-381): was prepared using only furan-2(*5H*)-one (42 mg; 0.5 mmol) and isopropanol as solvent. The sensitizer was not added to the solution. The ^{1}H-NMR analysis of the crude product showed that **84a** did not undergo any conversion.

For ^{1}H-NMR data of product **86a** see experiment 90.

Experiment 139

The addition of isopropanol to 2(5*H*)-furanone under 4-carboxybenzophenone sensitization (OS-348)

General procedure (GP-17) was followed with the slight variation of preparing one experimental solution and employing only one capillary instead of ten for a single run. The flow rate used was 0.083 ml/min; residence time: 1 hour. The experimental solution was prepared using furan-2(*5H*)-one (44 mg; 0.5 mmol), 4-benzoylbenzoic acid (23 mg;

0.1 mmol) and isopropanol as solvent. After irradiation the isopropanol was removed by rotary evaporation and the remaining residue was dissolved in 10 ml of dichloromethane. The solution was washed with sat. $NaHCO_3$ (3 × 10 ml), brine (2 × 10 ml), dried over $MgSO_4$, filtered and evaporated. During the washing step the solution of $NaHCO_3$ changed from clear to yellow, which might indicate partial solubility of the product in water. The isolated yield of **86a** was found to be 12 mg (0.08 mmol, 16%). Both ^{1}H-NMR and ^{13}C-NMR spectroscopy confirmed the product to be **86a**.

For ^{1}H-NMR data of product **86a** see experiment 4.

Experiment 140

Effect of the sensitizer concentration on the addition of isopropanol to 2(5*H*)-furanone 84a

General procedure (GP-17) was followed with the slight variation of preparing fourteen experimental solutions and employing ten parallel capillaries for the first run (Solutions 1-10) and four parallel capillaries for the second run (Solutions 11-14). The flow rate used was 1.0 ml/min; residence time: 5 min.

Solution 1 (OS-393): was prepared using furan-2(*5H*)-one (42 mg; 0.5 mmol), DMBP (4 mg; 0.015 mmol) and isopropanol as solvent. The composition of **84a** to product **86a** was calculated from the ^{1}H-NMR integration to be 74:26.

Solution 2 (OS-394): was prepared using furan-2(*5H*)-one (42 mg; 0.5 mmol), DMBP (7 mg; 0.03 mmol) and isopropanol as solvent. The composition of **84a** to product **86a** was calculated from the ^{1}H-NMR integration to be 60:40.

Solution 3 (OS-395): was prepared using furan-2(*5H*)-one (43 mg; 0.5 mmol), DMBP (11 mg; 0.046 mmol) and isopropanol as solvent. The composition of **84a** to product **86a** was calculated from the ^{1}H-NMR integration to be 53:47.

Solution 4 (OS-396): was prepared using furan-2(*5H*)-one (44 mg; 0.5 mmol), DMBP (15 mg; 0.062 mmol) and isopropanol as solvent. The composition of **84a** to product **86a** was calculated from the ^{1}H-NMR integration to be 45:55.

Solution 5 (OS-397): was prepared using furan-2(*5H*)-one (43 mg; 0.5 mmol), DMBP (19 mg; 0.078 mmol) and isopropanol as solvent. The composition of **84a** to product **86a** was calculated from the ^{1}H-NMR integration to be 38:62.

Solution 6 (OS-398): was prepared using furan-2(*5H*)-one (42 mg; 0.5 mmol), DMBP (22 mg; 0.09 mmol) and isopropanol as solvent. The composition of **84a** to product **86a** was calculated from the ^{1}H-NMR integration to be 30:70.

Solution 7 (OS-399): was prepared using furan-2(*5H*)-one (43 mg; 0.5 mmol), DMBP (26 mg; 0.11 mmol) and isopropanol as solvent. The composition of **84a** to product **86a** was calculated from the ^{1}H-NMR integration to be 24:76.

Solution 8 (OS-400): was prepared using furan-2(*5H*)-one (43 mg; 0.5 mmol), DMBP (29 mg; 0.12 mmol) and isopropanol as solvent. The composition of **84a** to product **86a** was calculated from the ^{1}H-NMR integration to be 19:81.

Solution 9 (OS-401): was prepared using furan-2(*5H*)-one (43 mg; 0.5 mmol), DMBP (33 mg; 0.14 mmol) and isopropanol as solvent. The composition of **84a** to product **86a** was calculated from the ^{1}H-NMR integration to be 14:86.

Solution 10 (OS-402): was prepared using furan-2(*5H*)-one (42 mg; 0.5 mmol), DMBP (36 mg; 0.15 mmol) and isopropanol as solvent. The composition of **84a** to product **86a** was calculated from the ^{1}H-NMR integration to be 10:90.

Solution 11 (OS-403): was prepared using furan-2(*5H*)-one (42 mg; 0.5 mmol), DMBP (40 mg; 0.17 mmol) and isopropanol as solvent. The composition of **84a** to product **86a** was calculated from the ^{1}H-NMR integration to be 27:73.

Solution 12 (OS-404): was prepared using furan-2(*5H*)-one (43 mg; 0.5 mmol), DMBP (44 mg; 0.18 mmol) and isopropanol as solvent. The composition of **84a** to product **86a** was calculated from the ^{1}H-NMR integration to be 29:71.

Solution 13 (OS-405): was prepared using furan-2(*5H*)-one (43 mg; 0.5 mmol), DMBP (47 mg; 0.19 mmol) and isopropanol as solvent. The composition of **84a** to product **86a** was calculated from the ^{1}H-NMR integration to be 29:71.

Solution 14 (OS-406): was prepared using furan-2(*5H*)-one (44 mg; 0.5 mmol), DMBP (50 mg; 0.21 mmol) and isopropanol as solvent. The composition of **84a** to product **86a** was calculated from the ^{1}H-NMR integration to be 27:73.

For ^{1}H-NMR data of product **86a** see experiment 90.

Experiment 141

Effect of the concentration of 2(5*H*)-furanone 84a on the addition of isopropanol to 2(5*H*)-furanone 84a

General procedure (GP-17) was followed with the slight variation of preparing seven experimental solutions and employing seven parallel capillaries instead of ten for a single run. The flow rate used was 1.0 ml/min; residence time: 5 min.

Solution 1 (OS-276): was prepared using furan-2(*5H*)-one (43 mg; 0.5 mmol), DMBP (25 mg; 0.1 mmol) and isopropanol as solvent. The composition of **84a** to product **86a** was calculated from the ^{1}H-NMR integration to be 26:74.

Solution 2 (OS-305): was prepared using furan-2(*5H*)-one (63 mg; 0.75 mmol), DMBP (25 mg; 0.1 mmol) and isopropanol as solvent. The composition of **84a** to product **86a** was calculated from the ^{1}H-NMR integration to be 54:46.

Solution 3 (OS-277): was prepared using furan-2(*5H*)-one (85 mg; 1.0 mmol), DMBP (24 mg; 0.1 mmol) and isopropanol as solvent. The composition of **84a** to product **86a** was calculated from the ^{1}H-NMR integration to be 68:32.

Solution 4 (OS-304): was prepared using furan-2(*5H*)-one (106 mg; 1.25 mmol), DMBP (25 mg; 0.1 mmol) and isopropanol as solvent. The composition of **84a** to product **86a** was calculated from the ^{1}H-NMR integration to be 79:21.

Solution 5 (OS-278): was prepared using furan-2(*5H*)-one (126 mg; 1.5 mmol), DMBP (25 mg; 0.1 mmol) and isopropanol as solvent. The composition of **84a** to product **86a** was calculated from the ^{1}H-NMR integration to be 89:11.

Solution 6 (OS-279): was prepared using furan-2(*5H*)-one (169 mg; 2.0 mmol), DMBP (24 mg; 0.1 mmol) and isopropanol as solvent. The composition of **84a** to product **86a** was calculated from the ^{1}H-NMR integration to be 95:5.

Solution 7 (OS-280): was prepared using furan-2(*5H*)-one (210 mg; 2.5 mmol), DMBP (25 mg; 0.1 mmol) and isopropanol as solvent. The composition of **84a** to product **86a** was calculated from the ^{1}H-NMR integration to be 97:3.

For ^{1}H-NMR data of product **86a** see experiment 90.

Experiment 142

Effect of the concentration of 2(5*H*)-furanone 84a on the addition of isopropanol to 2(5*H*)-furanone 84a

General procedure (GP-17) was followed with the slight variation of preparing six experimental solutions and employing six parallel capillaries instead of ten for a single run. The flow rate used was 1.0 ml/min; residence time: 5 min.

Solution 1 (OS-298): was prepared using furan-2(*5H*)-one (43 mg; 0.5 mmol), DMBP (31 mg; 0.125 mmol) and isopropanol as solvent. The composition of **84a** to product **86a** was calculated from the ^{1}H-NMR integration to be 27:73.

Solution 2 (OS-299): was prepared using furan-2(*5H*)-one (63 mg; 0.75 mmol), DMBP (31 mg; 0.125 mmol) and isopropanol as solvent. The composition of **84a** to product **86a** was calculated from the ^{1}H-NMR integration to be 54:46.
Solution 3 (OS-300): was prepared using furan-2(*5H*)-one (85 mg; 1.0 mmol), DMBP (31 mg; 0.125 mmol) and isopropanol as solvent. The composition of **84a** to product **86a** was calculated from the ^{1}H-NMR integration to be 67:33.
Solution 4 (OS-301): was prepared using furan-2(*5H*)-one (127 mg; 1.5 mmol), DMBP (31 mg; 0.125 mmol) and isopropanol as solvent. The composition of **84a** to product **86a** was calculated from the ^{1}H-NMR integration to be 78:22.
Solution 5 (OS-302): was prepared using furan-2(*5H*)-one (168 mg; 2.0 mmol), DMBP (31 mg; 0.125 mmol) and isopropanol as solvent. The composition of **84a** to product **86a** was calculated from the ^{1}H-NMR integration to be 87:13.
Solution 6 (OS-303): was prepared using furan-2(*5H*)-one (210 mg; 2.5 mmol), DMBP (31 mg; 0.125 mmol) and isopropanol as solvent. The composition of **84a** to product **86a** was calculated from the ^{1}H-NMR integration to be 91:9.

For ^{1}H-NMR data of product **86a** see experiment 90.

Experiment 143

Effect of the concentration of 2(5*H*)-furanone 84a on the addition of isopropanol to 2(5*H*)-furanone 84a

General procedure (GP-17) was followed and ten experimental solutions with different concentrations of 2(5*H*)-furanone **84a** were prepared and tested within a single run. The flow rate used was 1.0 ml/min; residence time: 5 min.
Solution 1 (OS-296): was prepared using furan-2(*5H*)-one (42 mg; 0.5 mmol), DMBP (37 mg; 0.15 mmol) and isopropanol as solvent. The composition of **84a** to product **86a** was calculated from the ^{1}H-NMR integration to be 20:80.
Solution 2 (OS-287): was prepared using furan-2(*5H*)-one (63 mg; 0.75 mmol), DMBP (36 mg; 0.15 mmol) and isopropanol as solvent. The composition of **84a** to product **86a** was calculated from the ^{1}H-NMR integration to be 49:51.
Solution 3 (OS-284): was prepared using furan-2(*5H*)-one (84 mg; 1.0 mmol), DMBP (37 mg; 0.15 mmol) and isopropanol as solvent. The composition of **84a** to product **86a** was calculated from the ^{1}H-NMR integration to be 66:34.

Solution 4 (OS-297): was prepared using furan-2(*5H*)-one (106 mg; 1.25 mmol), DMBP (37 mg; 0.15 mmol) and isopropanol as solvent. The composition of **84a** to product **86a** was calculated from the ^{1}H-NMR integration to be 77:23.

Solution 5 (OS-290): was prepared using furan-2(*5H*)-one (126 mg; 1.5 mmol), DMBP (36 mg; 0.15 mmol) and isopropanol as solvent. The composition of **84a** to product **86a** was calculated from the ^{1}H-NMR integration to be 86:14.

Solution 6 (OS-291): was prepared using furan-2(*5H*)-one (147 mg; 1.75 mmol), DMBP (36 mg; 0.15 mmol) and isopropanol as solvent. The composition of **84a** to product **86a** was calculated from the ^{1}H-NMR integration to be 91:9.

Solution 7 (OS-292): was prepared using furan-2(*5H*)-one (168 mg; 2.0 mmol), DMBP (36 mg; 0.15 mmol) and isopropanol as solvent. The composition of **84a** to product **86a** was calculated from the ^{1}H-NMR integration to be 93:7.

Solution 8 (OS-293): was prepared using furan-2(*5H*)-one (189 mg; 2.25 mmol), DMBP (36 mg; 0.15 mmol) and isopropanol as solvent. The composition of **84a** to product **86a** was calculated from the ^{1}H-NMR integration to be 95:5.

Solution 9 (OS-294): was prepared using furan-2(*5H*)-one (211 mg; 2.5 mmol), DMBP (36 mg; 0.15 mmol) and isopropanol as solvent. The composition of **84a** to product **86a** was calculated from the ^{1}H-NMR integration to be 97:3.

Solution 10 (OS-295): was prepared using furan-2(*5H*)-one (252 mg; 3.0 mmol), DMBP (37 mg; 0.15 mmol) and isopropanol as solvent. The composition of **84a** to product **86a** was calculated from the ^{1}H-NMR integration to be 98:2.

For ^{1}H-NMR data of product **86a** see experiment 90.

Experiment 144

Synthesis of small compound library

General procedure (GP-17) was followed with the slight variation of preparing nine experimental solutions and employing three parallel capillaries for the first run (Solutions 1-3) at flow rate of 0.5 ml/min (residence time: 10 min) and employing six parallel capillaries for the second run (Solutions 4-9) at flow rate of 0.25 ml/min (residence time: 20 min).

Solution 1 (OS-371): was prepared using furan-2(*5H*)-one (42 mg; 0.5 mmol), DMBP (24 mg; 0.1 mmol) and isopropanol as solvent. After evaporation of isopropanol the crude product was analysed by ^{1}H-NMR. The conversion was found to be 100%. The crude product was further purified by column chromatography using a solvent mixture

of ethyl acetate:petroleum ether (1:3). The isolated yield of **86a** was found to be 45 mg (0.31 mmol, 94%). Both ^{1}H-NMR and ^{13}C-NMR spectroscopy confirmed the product to be **86a**.

For ^{1}H-NMR data of product **86a** see experiment 90.

Solution 2 (OS-369): was prepared using 5-ethoxyfuran-2(*5H*)-one (65 mg; 0.5 mmol), DMBP (24 mg; 0.1 mmol) and isopropanol as solvent. After evaporation of isopropanol the crude product was analysed by ^{1}H-NMR spectroscopy. The conversion was found to be 100%. The crude product was further purified by column chromatography using a solvent mixture of ethyl acetate:hexane (1:3). The isolated yield of **86b** was found to be 38 mg (0.20 mmol, 60%). Both ^{1}H-NMR and ^{13}C-NMR spectroscopy confirmed the product to be **86b**.

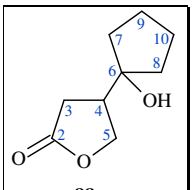
For ^{1}H-NMR data of product **86b** see experiment 91.

Solution 3 (OS-370): was prepared using (5*R*)-(-)-menthyloxy-2[5*H*]-furanone (119 mg; 0.5 mmol), DMBP (25 mg; 0.1 mmol) and isopropanol as solvent. After evaporation of isopropanol the crude product was analysed by ^{1}H-NMR. The conversion was found to be 100%. The crude product was further purified by column chromatography using a solvent mixture of ethyl acetate:hexane (1:4). The isolated yield of **86c** was found to be 90 mg (0.30 mmol, 90%). Both ^{1}H-NMR and ^{13}C-NMR spectroscopy confirmed the product to be **86c**.

For ^{1}H-NMR data of product **86c** see experiment 92.

Solution 4 (OS-339): was prepared using furan-2(*5H*)-one (44 mg; 0.5 mmol), DMBP (25 mg; 0.1 mmol) and cyclopentanol as solvent. After evaporation of cyclopentanol by nitrogen flow, the crude product was analysed by ^{1}H-NMR. The conversion was found to be 100%. The crude product was further purified by column chromatography using a solvent mixture of ethyl acetate:hexane (1:2), the concentration of ethyl acetate was increased to 3:0.5 for the end (gradient). The isolated yield of **88a** was found to be 40 mg (0.24 mmol, 71%). Both ^{1}H-NMR and ^{13}C-NMR spectroscopy confirmed the product to be **88a**.

Analytical data of *4-(1-Hydroxycyclopentyl)dihydrofuran-2(3H)-one* (88a)



88a
$C_9H_{14}O_3$
Mol. Wt.: 170.2 g/mol

TLC: *Rf* = 0.19 (ethyl acetate/hexane 1:2), yellow liquid

^{1}H–NMR: (400 MHz, $CDCl_3$)

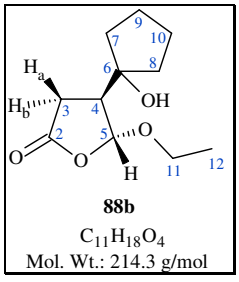
δ (ppm) = 4.26 (dt, J = 15.6, 8.0 Hz, 2 H, C_5-2H), 2.61-2.67 (m, 1 H, C_3-H), 2.47-2.57 (m, 2 H, C_3-H, C_4-H), 2.0 (br.s, 1 H, C_6-OH), 1.76-1.85 (m, 2 H, $C_{7\text{-}10}$-2H), 1.59-1.72 (m, 4 H, $C_{7\text{-}10}$-4H), 1.46-1.57 (m, 2 H, $C_{7\text{-}10}$-2H).

^{13}C–NMR: (100 MHz, $CDCl_3$)

δ (ppm) = 178.1 (s, 1 C, C_2), 81.6 (s, 1 C, C_6), 70.0 (s, 1 C, C_5), 44.6 (s, 1 C, C_4), 38.8 (s, 1 C, $C_{7,8}$), 38.3 (s, 1 C, $C_{7,8}$), 30.4 (s, 1 C, C_3), 23.8 (s, 1 C, $C_{9,10}$), 23.6 (s 1 C, $C_{9,10}$).

Solution 5 (OS-340): was prepared using 5-ethoxyfuran-2(*5H*)-one (68 mg; 0.5 mmol), DMBP (24 mg; 0.1 mmol) and cyclopentanol as solvent. After evaporation of cyclopentanol by nitrogen flow, the crude product was analysed by ^{1}H-NMR. The conversion was found to be 100%. The crude product was further purified by column chromatography using a solvent mixture of ethyl acetate:hexane (1:2). The concentration of ethyl acetate was increased to 3:0.5 for the end (gradient), the isolated yield of **88b** was found to be 52 mg (0.24 mmol, 73%). Both ^{1}H-NMR and ^{13}C-NMR spectroscopy confirmed the product to be **88b**.

Analytical data of *(4S,5R)-5-ethoxy-4-(1-hydroxycyclopentyl)dihydrofuran-2(3H)-one* (88b)



88b
$C_{11}H_{18}O_4$
Mol. Wt.: 214.3 g/mol

TLC: *Rf* = 0.24 (ethyl acetate/hexane 1:2), yellow liquid

^{1}H–NMR: (400 MHz, $CDCl_3$)

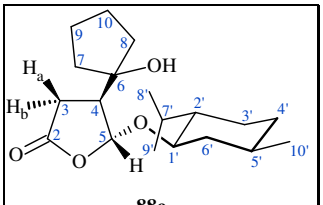
δ (ppm) = 5.47 (d, ^{2}J = 3.2 Hz, 1 H, C_5-H), 3.82 (dq, ^{3}J = 6.8, ^{4}J = 2.4 Hz, 1 H, C_{11}-H), 3.58 (dq, ^{3}J = 7.2, ^{4}J = 2.4 Hz, 1 H, C_{11}-H), 2.66 (dd, ^{3}J = 18.0, ^{4}J = 9.6 Hz, 1 H, C_3-H_b), 2.49 (dd, ^{3}J = 18.0, ^{4}J = 5.6 Hz, 1 H, C_3-H_a), 2.35-2.39 (m, 1 H, C_4-H), 1.89 (br.s, 1 H, C_6-O<u>H</u>), 1.77-1.85 (m, 2 H, $C_{7\text{-}10}$-2H), 1.59-1.72 (m, 5 H, $C_{7\text{-}10}$-5H), 1.46-1.53 (m, 1 H, $C_{7\text{-}10}$-1H), 1.22 (t, ^{3}J = 7.2 Hz, 3 H, C_{12}-3H).

^{13}C–NMR: (100 MHz, $CDCl_3$)

δ (ppm) = 176.1 (s, 1 C, C_2), 106.1 (s, 1 C, C_5), 81.6 (s, 1 C, C_6), 65.7 (s, 1 C, C_{11}), 50.7 (s, 1 C, C_4), 38.8 (s, 1 C, $C_{7,8}$), 38.4 (s, 1 C, $C_{7,8}$), 30.4 (s, 1 C, C_3), 23.8 (s, 1 C, $C_{9,10}$), 23.5 (s, 1 C, $C_{9,10}$), 15.1 (s, 1 C, C_{12}).

<u>Solution 6</u> (OS-341): was prepared using (5*R*)-(-)-menthyloxy-2[5*H*]-furanone (119 mg; 0.5 mmol), DMBP (25 mg; 0.1 mmol) and cyclopentanol as solvent. After evaporation of cyclopentanol by nitrogen flow, the crude product was analysed by ^{1}H-NMR. The conversion was found to be 100%. The crude product was further purified by column chromatography using a solvent mixture of ethyl acetate:hexane (1:2), the concentration of ethyl acetate was increased to 1:1 for the end (gradient). The isolated yield of **88c** was found to be 96 mg (0.30 mmol, 89%). Both ^{1}H-NMR and ^{13}C-NMR spectroscopy confirmed the product to be **88c**.

Analytical data of *(4S,5R)-4-(1-hydroxycyclopentyl)-5-((-)-menthyloxy)-dihydrofuran-2(3H)-one* (88c)



88c

$C_{19}H_{32}O_4$

Mol. Wt.: 324.5 g/mol

TLC: ***Rf*** = 0.59 (ethyl acetate/hexane 1:2), light-green crystals

^{1}H–NMR: (400 MHz, $CDCl_3$)

δ (ppm) = 5.68 (d, J = 2.8 Hz, 1 H, C_5-H), 3.50 (dt, J = 10.8, 4.4 Hz, 1 H, $C_{1'}$-H), 2.69 (dd, J = 18.0, 9.6 Hz, 1 H, C_3-H_b), 2.49 (dd, J = 18.0, 5.6 Hz, 1 H, C_3-H_a), 2.34-2.39 (m, 1 H, C_4-H), 2.07-2.13 (m, 2 H, $C_{6'}$-H, $C_{7'}$-H), 1.59-1.89 (m, 6 H, C_7-2H, C_8-2H, $C_{3'}$-H, $C_{4'}$-H), 1.58 (s, 1 H, C_6-O<u>H</u>), 1.45-1.56 (m, 4 H, C_9-2H, C_{10}-2H), 1.35-1.40 (m, 1 H, $C_{2'}$-

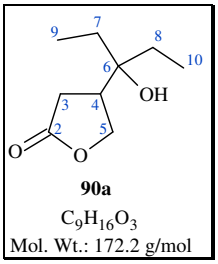
H), 1.16-1.23 (m, 1 H, $C_{5'}$-H), 0.92 (d, J = 6.4 Hz, 3 H, $C_{8',9'}$-3H), 0.86 (d, J = 7.2 Hz, 3 H, $C_{10'}$-3H), 0.77 (d, J = 7.2 Hz, 3 H, $C_{8',9'}$-3H), 0.80-1.06 (m, 3 H, $C_{3'}$-H, $C_{4'}$-H, $C_{6'}$-H).

^{13}C–NMR: (100 MHz, $CDCl_3$)

δ (ppm) = 176.27 (s, 1 C, C_2), 102.65 (s, 1 C, C_5), 81.83 (s, 1 C, C_6), 77.32 (s, 1 C, $C_{1'}$), 50.79 (s, 1 C, C_4), 47.94 (s, 1 C, $C_{2'}$), 39.98 (s, 1 C, $C_{6'}$), 38.89 (s, 1 C, $C_{7,8}$), 38.50 (s, 1 C, $C_{7,8}$), 34.41 (s, 1 C, $C_{4'}$), 31.48 (s, 1 C, $C_{5'}$), 30.61 (s, 1 C, C_3), 25.50 (s, 1 C, $C_{7'}$), 23.88 (t, 1 C, $C_{9,10}$), 23.52 (t, 1 C, $C_{9,10}$), 23.16 (t, 1 C, $C_{3'}$), 22.41 (s, 1 C, $C_{10'}$), 21.03 (s, 1 C, $C_{8',9'}$), 15.77 (s, 1 C, $C_{8',9'}$).

Solution 7 (OS-386): was prepared using furan-2(*5H*)-one (42 mg; 0.5 mmol), DMBP (25 mg; 0.1 mmol) and 3-pentanol as solvent. After evaporation of 3-pentanol by nitrogen flow, the crude product was analysed by ^{1}H-NMR. The conversion was found to be 100%. The crude product was further purified by column chromatography using a solvent mixture of ethyl acetate:hexane (1:2). The isolated yield of **90a** was found to be 46 mg (0.27 mmol, 80%). Both ^{1}H-NMR and ^{13}C-NMR spectroscopy confirmed the product to be **90a**.

Analytical data of *4-(3-Hydroxypentan-3-yl)dihydrofuran-2(3H)-one* (90a)



90a

$C_9H_{16}O_3$

Mol. Wt.: 172.2 g/mol

TLC: ***Rf*** = 0.27 (ethyl acetate/hexane 1:2), yellow liquid

^{1}H–NMR: (400 MHz, $CDCl_3$)

δ (ppm) = 4.25 (sex, ^{2}J = 8.8, ^{3}J = 5.6, ^{4}J = 3.6 Hz, 2 H, C_5-2H), 2.60-2.77 (m, 2 H, C_3-H, C_4-H), 2.34 (q, J = 8.4 Hz, 1 H, C_3-H), 1.70 (br.s, 1 H, C_6-OH), 1.36-1.54 (m, 4 H, C_7-2H, C_8-2H), 0.83 (sex, ^{2}J = 5.2, ^{3}J = 4.8, ^{4}J = 2.4 Hz, 6 H, C_9-3H, C_{10}-3H).

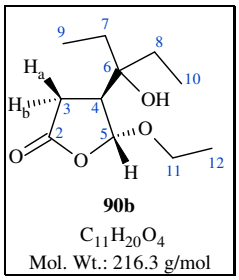
^{13}C–NMR: (100 MHz, $CDCl_3$)

δ (ppm) = 177.8 (s, 1 C, C_2), 73.6 (s, 1 C, C_6), 68.8 (s, 1 C, C_5), 42.4 (s, 1 C, C_4), 29.6 (s, 1 C, C_7), 28.9 (s, 1 C, C_3), 28.5 (s, 1 C, C_8), 7.8 (d, 1 C, $C_{9,10}$), 7.7 (d, 1 C, $C_{9,10}$).

Solution 8 (OS-387): was prepared using 5-ethoxyfuran-2(*5H*)-one (66 mg; 0.5 mmol), DMBP (25 mg; 0.1 mmol) and 3-pentanol as solvent. After evaporation of 3-pentanol by nitrogen flow, the crude product was analysed by ^{1}H-NMR. The conversion was

found to be 100%. The crude product was further purified by column chromatography using a solvent mixture of ethyl acetate:hexane (1:2). The isolated yield of **90b** was found to be 41 mg (0.19 mmol, 57%). %). Both ^{1}H-NMR and ^{13}C-NMR spectroscopy confirmed the product to be **90b**.

Analytical data of *(4S,5R)-5-ethoxy-4-(3-hydroxypentan-3-yl)dihydrofuran-2(3H)-one* (90b)



90b

$C_{11}H_{20}O_4$

Mol. Wt.: 216.3 g/mol

TLC: ***Rf*** = 0.33 (ethyl acetate/hexane 1:2), yellow liquid

^{1}H–NMR: (400 MHz, $CDCl_3$)

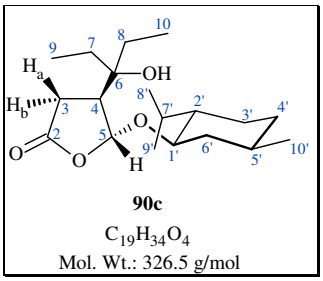
δ (ppm) = 5.50 (d, ^{2}J = 4.8 Hz, 1 H, C_5-H), 3.84 (dq, ^{3}J = 7.2, ^{4}J = 2.4 Hz, 1 H, C_{11}-H), 3.59 (dq, ^{3}J = 7.2, ^{4}J = 2.4 Hz, 1 H, C_{11}-H), 2.52-2.65 (m, 2 H, C_3-2H), 2.40 (td, ^{3}J = 4.4 Hz, 1 H, C_4-H), 1.65 (br.s, 1 H, C_6-O<u>H</u>), 1.43-1.56 (m, 2 H, $C_{7,8}$-2H), 1.31-1.39 (m, 2 H, $C_{7,8}$-2H), 1.22 (t, ^{3}J = 7.2 Hz, 3 H, C_{12}-3H), 0.80 (dt, ^{3}J = 17.6, ^{4}J = 7.2 Hz, 6 H, C_9-3H, C_{10}-3H).

^{13}C–NMR: (100 MHz, $CDCl_3$)

δ (ppm) = 175.8 (s, 1 C, C_2), 105.8 (s, 1 C, C_5), 74.1 (s, 1 C, C_6), 66.0 (s, 1 C, C_{11}), 48.3 (s, 1 C, C_4), 29.6 (s, 1 C, C_7), 29.2 (s, 1 C, C_8), 28.4 (s, 1 C, C_3), 15.2 (s, 1 C, C_{12}), 7.7 (d, 1 C, $C_{9,10}$), 7.7 (d, 1 C, $C_{9,10}$).

<u>Solution 9</u> (OS-388): was prepared using (5*R*)-(-)-menthyloxy-2[5*H*]-furanone (120 mg; 0.5 mmol), DMBP (25 mg; 0.1 mmol) and 3-pentanol as solvent. After evaporation of 3-pentanol by nitrogen flow, the crude product was analysed by ^{1}H-NMR. The conversion was found to be 100%. The crude product was further purified by column chromatography using a solvent mixture of ethyl acetate:hexane (1:9). The isolated yield of **90c** was found to be 66 mg (0.20 mmol, 61%). Both ^{1}H-NMR and ^{13}C-NMR spectroscopy confirmed the product to be **90c**.

Analytical data of *(4S,5R)-4-(3-hydroxypentan-3-yl)-5-((-)-menthyloxy)-dihydrofuran-2(3H)-one* (90c)



90c

$C_{19}H_{34}O_4$

Mol. Wt.: 326.5 g/mol

TLC: ***Rf*** = 0.50 (ethyl acetate/hexane 1:2), light-green liquid

^{1}H–NMR: (400 MHz, $CDCl_3$)

δ (ppm) = 5.70 (d, J = 3.6 Hz, 1 H, C_5-H), 3.50 (dt, J = 10.4, 6.4 Hz, 1 H, $C_{1'}$-H), 2.58 (d, J = 8.4 Hz, 2 H, C_3-H_b, C_3-H_a), 2.37 (dt, J = 8.0, 4.0 Hz, 1 H, C_4-H), 2.10-2.16 (m, 2 H, $C_{6'}$-H, $C_{7'}$-H), 1.70 (br.s, 1 H, C_6-O<u>H</u>), 1.59-1.66 (m, 2 H, C_7-H, C_8-H), 1.52-1.58 (dd, J = 7.6, 2.0 Hz, 2 H, C_7-H, C_8-H), 1.44-1.50 (m, 1 H, $C_{2'}$-H), 1.33-1.38 (m, 2 H, $C_{3'}$-H, $C_{4'}$-H), 1.15-1.25 (m, 1 H, $C_{5'}$-H), 0.91 (d, J = 6.4 Hz, 3 H, $C_{8',9'}$-3H) 0.81-0.88 (m, 9 H, C_9-3H, C_{10}-3H, $C_{10'}$-3H), 0.76 (d, J = 6.8 Hz, 3 H, $C_{8',9'}$-3H), 0.81-1.00 (m, 3 H, $C_{3'}$-H, $C_{4'}$-H, $C_{6'}$-H).

^{13}C–NMR: (100 MHz, $CDCl_3$)

δ (ppm) = 176.06 (s, 1 C, C_2), 101.92 (s, 1 C, C_5), 77.30 (s, 1 C, $C_{1'}$), 74.23 (s, 1 C, C_6), 48.11 (d, 1 C, C_4), 47.94 (d, 1 C, $C_{2'}$), 39.72 (s, 1 C, $C_{6'}$), 34.38 (s, 1 C, $C_{4'}$), 31.44 (s, 1 C, $C_{5'}$), 29.70 (s, 1 C, C_3), 28.99 (s, 1 C, $C_{7,8}$), 28.34 (s, 1 C, $C_{7,8}$), 25.41 (s, 1 C, $C_{7'}$), 23.12 (s, 1 C, $C_{3'}$), 22.38 (s, 1 C, $C_{10'}$), 21.02 (s, 1 C, $C_{8',9'}$), 15.76 (s, 1 C, $C_{8',9'}$), 7.77 (d, 1 C, $C_{9,10}$), 7.59 (d, 1 C, $C_{9,10}$).

Experiment 145

Synthesis of small compound library

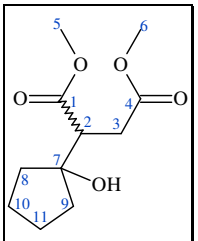
General procedure (GP-17) was followed with the slight variation of preparing four experimental solutions and employing only four parallel capillaries instead of ten for a single run. The flow rate used was 0.33 ml/min; residence time: 15 min.

<u>Solution 1</u> (OS-363): was prepared using dimethyl fumarate (72 mg; 0.5 mmol), DMBP (24 mg; 0.1 mmol) and isopropanol as solvent. The conversion of **91a** to products **92** and **93** was calculated from the ^{1}H-NMR integration to be 21%. The products **92** and **93** were formed in a ratio of 1:4. For ^{1}H-NMR data of products **92** and **93** see experiment 146.

Solution 2 (OS-364): was prepared using dimethyl maleate (73 mg; 0.5 mmol), DMBP (24 mg; 0.1 mmol) and isopropanol as solvent. The conversion of **91b** to products **92** and **93** was calculated from the ^{1}H-NMR integration to be 27%. The products **92** and **93** were formed in a ratio of 1:3. For ^{1}H-NMR data of products **92** and **93** see experiment 146.

Solution 3 (OS-366): was prepared using dimethyl fumarate (73 mg; 0.5 mmol), DMBP (24 mg; 0.1 mmol) and cyclopentanol as solvent. After evaporation of cyclopentanol by nitrogen flow, the crude product was analysed by ^{1}H-NMR. The conversion was found to be 100%. The crude product was further purified by column chromatography using a solvent mixture of ethyl acetate:hexane (1:4) and three main fractions were isolated. One fraction was DMBP recovered in the amount of 15.7 mg (0.07 mmol, 98%). Second fraction was collected in the amount of 15 mg and it was the mixture of products **94** and **95** in a ratio 3:1. The ratio between products **94** and **95** was determined by ^{1}H-NMR spectroscopy, the signal integration for the CH proton of **94** was compared to the signal integration of CH proton of **95**. Third fraction was a pure spiro compound **95**. The isolated yield of **95** was found to be 2 mg (0.01 mmol, 3%). Both ^{1}H-NMR and ^{13}C-NMR spectroscopy confirmed the product to be **95**.

Analytical data of *Dimethyl-2-(1-hydroxycyclopentyl)butanedioate* (94)



94

$C_{11}H_{18}O_5$

Mol. Wt.: 230.3 g/mol

TLC: ***Rf*** = 0.34 (ethyl acetate/petroleum ether 1:3), yellow liquid

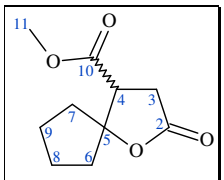
^{1}H–NMR: (400 MHz, $CDCl_3$)

δ (ppm) = 3.74 (s, 3 H, $C_{5,6}$-3H), 3.67 (s, 3 H, $C_{5,6}$-3H), 2.86 (m, 2 H, C_3-2H), 2.64 (dd, ^{3}J = 12.8, ^{4}J = 2.4 Hz, 1 H, C_2-H), 2.52 (br.s, 1 H, C_7-OH), 1.77-1.85 (m, 2 H, $C_{8\text{-}11}$-2H), 1.53-1.72 (m, 5 H, $C_{8\text{-}11}$-5H), 1.41-1.51 (m, 1 H, $C_{8\text{-}11}$-H).

^{13}C–NMR: (100 MHz, $CDCl_3$)

δ (ppm) = 175.5 (s, 1 C, C_4), 173.2 (s, 1 C, C_1), 82.1 (s, 1 C, C_7), 52.2 (s, 1 C, $C_{5,6}$), 52.1 (s, 1 C, $C_{5,6}$), 51.0 (s, 1 C, C_2), 39.6 (s, 1 C, $C_{8,9}$), 37.9 (s, 1 C, $C_{8,9}$), 33.4 (s, 1 C, C_3), 23.8 (d, 1 C, $C_{10,11}$), 23.7 (d, 1 C, $C_{10,11}$).

Analytical data of *Methyl-2-oxo-1-oxaspiro[4.4]nonane-4-carboxylate* (95)



95

$C_{10}H_{14}O_4$

Mol. Wt.: 198.2 g/mol

TLC: ***Rf*** = 0.41 (ethyl acetate/petroleum ether 1:3), yellow liquid

^{1}H–NMR: (400 MHz, $CDCl_3$)

δ (ppm) = 3.75 (s, 3 H, C_{11}-3H), 3.36 (t, ^3J = 8.4 Hz, 1 H, C_4-H), 2.97 (q, J = 9.6 Hz, 1 H, C_3-H), 2.69 (q, J = 8.8 Hz, 1 H, C_3-H), 1.82-1.86 (m, 3 H, $C_{6\text{-}9}$-3H), 1.60-1.75 (m, 5 H, $C_{6\text{-}9}$-5H).

^{13}C–NMR: (100 MHz, $CDCl_3$)

δ (ppm) = 174.5 (s, 1 C, C_2), 170.9 (s, 1 C, C_{10}), 94.9 (s, 1 C, C_5), 52.6 (s, 1 C, C_{11}), 48.1 (s, 1 C, C_4), 39.0 (s, 1 C, C_7), 34.7 (s, 1 C, C_6), 32.8 (s, 1 C, C_3), 24.0 (s, 1 C, $C_{8,9}$), 23.4 (s, 1 C, $C_{8,9}$).

Solution 4 (OS-367): was prepared using dimethyl maleate (72 mg; 0.5 mmol), DMBP (25 mg; 0.1 mmol) and cyclopentanol as solvent. After evaporation of cyclopentanol by nitrogen flow, the crude product was analysed by ^{1}H-NMR. The conversion was found to be 100%. The crude product was further purified by column chromatography using a solvent mixture of ethyl acetate:hexane (1:4) and three main fractions were isolated. One fraction was DMBP recovered in the amount of 14.4 mg (0.06 mmol, 89%). Second fraction was collected in the amount of 10 mg and it was the mixture of products **94** and **95** in a ratio 3:2. The ratio between products **94** and **95** was determined by ^{1}H-NMR spectroscopy, the signal integration for the CH proton of **94** was compared to the signal integration of CH proton of **95**. Third fraction was a pure spiro compound **95**. The isolated yield of **95** was found to be 10 mg (0.05 mmol, 15%). Both ^{1}H-NMR and ^{13}C-NMR spectroscopy confirmed the product to be **95**.

For ^{1}H-NMR data of products **94** and **95** see above Solution 3.

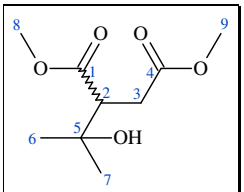
Experiment 146

Synthesis of small compound library

General procedure (GP-17) was followed with the slight variation of preparing two experimental solutions and employing only two parallel capillaries instead of ten for a single run. The flow rate used was 0.083 ml/min; residence time: 1 hour.

Solution 1 (OS-345): was prepared using dimethyl fumarate (74 mg; 0.5 mmol), DMBP (25 mg; 0.1 mmol) and isopropanol as solvent. After irradiation, the isopropanol was removed by rotary evaporation and the crude product was analysed by ^{1}H-NMR. The conversion was found to be 100%. The crude product was further purified by column chromatography using a solvent mixture of ethyl acetate:hexane (1:3) and the two main fractions were isolated. One fraction was collected in the amount of 39 mg and it was the mixture of products **92** and **93** in a ratio 9:1. The ratio between products **92** and **93** was determined by ^{1}H-NMR spectroscopy, the signal integration for the 2C$\underline{H}_3$ protons of **92** was compared to the signal integration of 2C$\underline{H}_3$ protons of **93**. Second fraction was a pure lactone **93**. The isolated yield of **93** was found to be 7 mg (0.04 mmol, 12%). Both ^{1}H-NMR and ^{13}C-NMR spectroscopy confirmed the product to be **93**.

Analytical data of *Dimethyl-2-(2-hydroxypropan-2-yl)-butanedioate* (92)



92

$C_9H_{16}O_5$

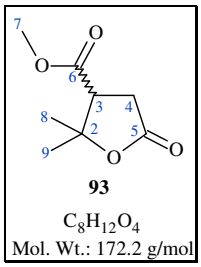
Mol. Wt.: 204.2 g/mol

TLC: ***Rf*** = 0.28 (ethyl acetate/hexane 1:2), yellow liquid

^{1}H–NMR: (400 MHz, $CDCl_3$)

δ (ppm) = 3.75 (s, 3 H, $C_{8,9}$-3H), 3.68 (s, 3 H, $C_{8,9}$-3H), 2.90 (dd, ^{3}J = 6.4, ^{4}J = 4.0 Hz, 1 H, C_3-H), 2.79 (dd, ^{3}J = 10.4, ^{4}J = 6.4 Hz, 1 H, C_2-H), 2.64 (dd, ^{3}J = 12.8, ^{4}J = 4.0 Hz, 1 H, C_3-H), 2.58 (br.s, 1 H, C_5-O$\underline{H}$), 1.23 (d, ^{2}J = 6.4 Hz, 6 H, C_6-3H, C_7-3H).

Analytical data of *Methyl-2,2-dimethyl-5-oxotetrahydrofuran-3-carboxylate* (93)



93

$C_8H_{12}O_4$

Mol. Wt.: 172.2 g/mol

TLC: ***Rf*** = 0.40 (ethyl acetate/hexane 1:2), brownish liquid

^{1}H–NMR: (400 MHz, $CDCl_3$)

δ (ppm) = 3.76 (s, 3 H, C_7-3H), 3.18 (t, ^3J = 8.8 Hz, 1 H, C_4-H), 3.06 (dd, ^3J = 9.6, ^4J = 8.0 Hz, 1 H, C_3-H), 2.67 (q, J = 8.8 Hz, 1 H, C_4-H), 1.60 (s, 3 H, C_2-3H), 1.31 (s, 3 H, C_2-3H).

^{13}C–NMR: (100 MHz, $CDCl_3$)

δ (ppm) = 170.2 (s, 1 C, C_5), 167.5 (s, 1 C, C_6), 85.1 (s, 1 C, C_2), 52.6 (s, 1 C, C_7), 50.5 (s, 1 C, C_3), 31.9 (s, 1 C, C_4), 28.6 (s, 1 C, $C_{8,9}$), 23.5 (s, 1 C, $C_{8,9}$).

Solution 2 (OS-346): was prepared using dimethyl maleate (74 mg; 0.5 mmol), DMBP (25 mg; 0.1 mmol) and isopropanol as solvent. After irradiation, the isopropanol was removed by rotary evaporation and the crude product was analysed by ^{1}H-NMR. The conversion was found to be 100%. The crude product was further purified by column chromatography using a solvent mixture of ethyl acetate:hexane (1:3) and only one product fraction was isolated. This fraction was collected in the amount of 38 mg and it was the mixture of products **92** and **93** in a ratio 4:1. The ratio between products **92** and **93** was determined by ^{1}H-NMR spectroscopy, the signal integration for the 2C$\underline{H}_3$ protons of **92** was compared to the signal integration of 2C$\underline{H}_3$ protons of **93**.

For ^{1}H-NMR data of products **92** and **93** see above Solution 1.

Experiment 147

The DMBP sensitized isomerisation of dimethyl fumarate to dimethyl maleate (OS-392)

General procedure (GP-17) was followed with the slight variation of preparing one experimental solution and employing only one capillary instead of ten for a single run. The flow rate used was 0.125 ml/min; residence time: 40 min. The experimental solution was prepared using dimethyl fumarate (37 mg; 0.25 mM), dimethyl maleate

(36 mg; 0.25 mM), DMBP (25 mg; 0.1 mmol) and acetonitrile (15 ml) as solvent. After irradiation, the acetonitrile was removed by rotary evaporation and the obtained crude product was analysed by ^{1}H-NMR. The composition of **91a** to **91b** was calculated from the ^{1}H-NMR to be 5:95. The ratio between **91a** and **91b** was determined by the comparison of the signal integration for the C<u>H</u> proton of **91a** to the signal integration of the C<u>H</u> proton of **91b**.

Experiment 148

The DMBP sensitized addition of isopropanol to dimethyl fumarate in the presence of *p*-toluenesulfonic acid (OS-391)

General procedure (GP-17) was followed with the slight variation of preparing one experimental solution and employing only one capillary instead of ten for a single run. The flow rate used was 0.125 ml/min; residence time: 40 min. The experimental solution was prepared using dimethyl fumarate (73 mg; 0.5 mM), DMBP (25 mg; 0.1 mmol), *p*-toluenesulfonic acid (10 mg) and isopropanol (15 ml) as solvent. After irradiation, the isopropanol was removed by rotary evaporation and the crude product was analysed by ^{1}H-NMR. The conversion was found to be 100% and lactone **93** was selectively formed. The attempt to isolate pure product wasn't made in this experiment.

For ^{1}H-NMR data of product **93** see experiment 146.

9.3 Chapter 4: Rose bengal sensitised photooxygenation of α-terpinene – synthesis of ascaridole

Conventional photolysis. Batch set-up

Glassware: Photoreactions were performed in 50 ml *Quartz Schlenk flask* equipped with a *Pyrex cold finger*.

Irradiation source: A single 18 W domestic fluorescent lamp Phillips GENIE Warm White was used as light source.

Micro photolysis. Falling film microreactor set-up

Microreactor: Photoreactions were performed in a stainless steel *falling film microreactor* (IMM) with Quartz viewing window. Microreactor was equipped with a FFMR – 07029, 316 Ti reaction plate that has 32 parallel microchannels of 600 µm width, 200 µm depth and 78 mm length.

Irradiation source: A single 18 W domestic fluorescent lamp Phillips GENIE Warm White or an array of 60 white LEDs (Powerfix®, 3 W total) were used as light sources.

Pumps: Programmable syringe pump Harvard apparatus 22 (serial No. B - 03720) was used to deliver the reaction mixture to the microreactor. A gear pump mzr® - 2905 HNP Microsysteme GmbH (serial No. 3564K024B C) was employed to evacuate the reacted liquid from the microreactor. The gear pump flow rate was controlled by a rotameter + hourmeter mzr® - S05 HNP Microsysteme GmbH (serial No. 874–1145 BMBF). A rotary pump ISMATEC® MCP–Z (type ISM405A, serial No. 03444–00365) was used for the circulation of coolant.

Syringe: A 50 ml glass syringe made of Pyrex glass with a PTFE plunger was used for the loading of reaction mixture into the syringe pump.

Flow meter: Mass flow meter/controller EL–FLOW® BRONKHORST HI–TEC (serial No. 99201016 B) was utilised for the control of gas flow rate.

Cryostat: Cryostat CC3 Huber® (serial No. 69630/07) was used to keep temperature of coolant constant.

Thermocouples and thermo-recorder: Two thermocouples series P 600 inserted into the microreactor inlet and outlet (serial No. 60505100322; couple inlet serial No. 000383, couple outlet serial No. 00385) were employed to control temperature of the

reaction mixture inside the reactor. The temperature was displayed on the screen of thermo-recorder P 505 (serial No. 48777).

Solvents and reagents

All solvents and starting materials were obtained from commercial suppliers (*Sigma-Aldrich* and *Fluka*) and were used without purification. α-terpinene (CAS No. 99-86-5) was acquired from *Sigma Aldrich* with special certificate of analysis that certified its purity of 93.1%.

9.3.1 General procedure (GP-18) for rose bengal sensitised photooxygenation of α-terpinene 39 (synthesis of ascaridole 40) in the falling film microreactor

α-Terpinene (mg; 1-10 mmol), hexadecane as internal standard (mg; 0.5-6 mmol) and rose bengal (50 mg; 49 μmol) were dissolved in 100 ml of isopropanol that was preliminary degassed with argon for 15 min. The prepared reaction mixture was sonicated for 15 min and transferred into a 50 ml glass syringe (total volume 50 ml). Any air bubbles were expelled and syringe was loaded into the programmable syringe pump. The solution was supplied to the falling film microreactor with definite volumetric flow rate preset by the pump. The solution was then distributed to substreams, which created a thin fluid film inside the microchannels. The gas phase – oxygen was fed into the reactor chamber with constant flow rate of 10 ml/min and moved counter currently to the liquid flow. A single fluorescent lamp (18 W) was used for irradiation. The reaction solution was continually evacuated from the falling film microreactor by the gear pump and directly collected into a GC vial and instantly analysed by CG-MS. During the reaction, the reactor was kept at a single temperature by pumping coolant (mainly water) through the heat exchanger positioned on the back side of the reaction plate. The experimental temperature was continually controlled by two thermocouples inserted into the microreactor inlet and outlet. The temperature was recorded by a thermo-recorder. When the syringe was empty, the syringe pump and fluorescent lamp were switched off simultaneously. The syringe was refilled with the experimental stock solution or solvent used for the reaction and placed again on the syringe pump which was turned on simultaneously with the lamp if the experiment was continued or without the lamp for reactor cleaning. When the experiment was complete, the entire system was cleaned with the pure methanol.

Practical details of the ascaridole synthesis experiments

The experimental stock solutions were always prepared in 100 ml volumetric flasks that were covered by several layers of aluminium foil. The syringe, microreactor and light source, GC vial and tubing used for the reaction mixture transport/storage were also wrapped with several layers of aluminium foil during the experiment. The GC vials with the collected products were always closed under an argon atmosphere.

All product samples were injected into the GC column twice and than average numbers were generated. The standard deviations of the obtained results were generally below 0.5%.

The falling film microreactor was constantly checked for two test runs before any experiment to make sure that the setup worked well. One test run was without light and with argon and a second test run was without light and with oxygen. Flow rate of the solution was 1 ml/min during test runs. The GC results obtained for the test runs were compared with the GC results obtained for the experimental stock solution from the volumetric flask. If the fallibility of achieved data was ± 5% the system was considered as smoothly running and suitable for further experimental usage.

Most of the experiments in the falling film microreactor were carried out at six main volumetric flow rates (syringe pump): 1 ml/min, 0.8 ml/min, 0.5 ml/min, 0.3 ml/min, 0.15 ml/min and 0.08 ml/min which corresponded residence times of 6 sec, 7 sec, 10 sec, 13 sec, 21 sec and 32 sec, respectively. The falling film microreactor setup was continuously operated during the experiment, therefore the flow rate of the syringe pump was gradually changed from highest, *e.i.* 1 ml/min to lowest, *e.i.* 0.08 ml/min after certain time intervals and product samples were collected at the end of each time interval (Table 59). After the flow rate of the syringe pump was changed (two to three minutes) the rotations of gear pump on the reactor suck side were also altered. Thus the work of both pumps, on the reactor supplied and vacuum sides, were synchronised so that the microreactor was not overloaded by liquid phase and the gas phase was not "sucked" into the collected products.

Table 59: Adjusted flow rates of syringe pump and rotations of gear pump next to the time periods when they were changed and products were collected

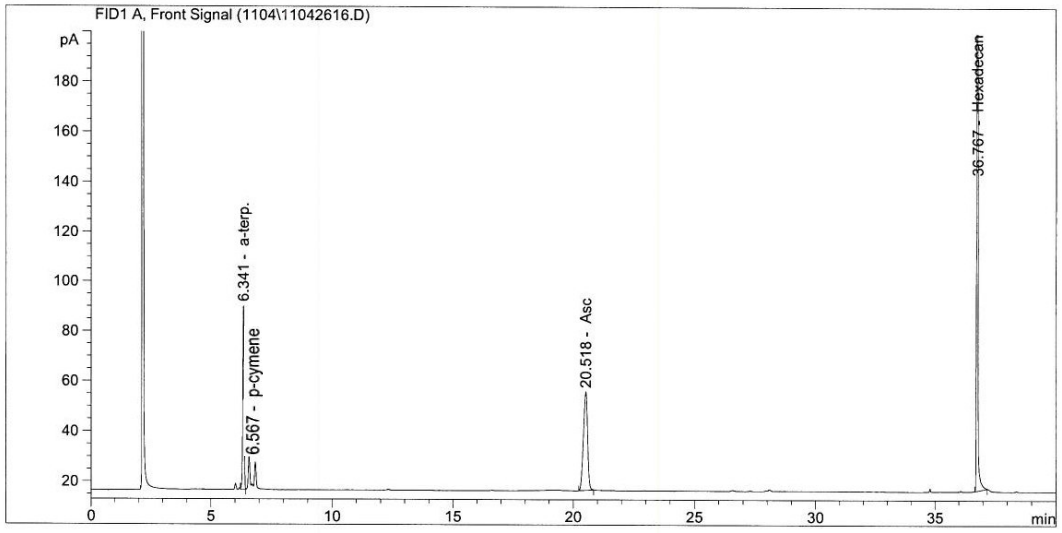
Flow rate of syringe pump, [ml/min]	Residence time, [s]	Rotations of gear pump, [rpm]	Time interval, [min][a]
1.0	6	3220	12
0.8	7	2600	15
0.5	10	1630	22
0.3	13	960	35
0.15	21	480	70
0.08	32	250	130

[a] time intervals when the products were collected since the pumps flow rates were changed

9.3.1.1 Details of the GC analytical method for products analysis of ascaridole synthesis

Column: HP-5 5% Phenyl Methyl Siloxan, 325°C: 30 m × 250 µm × 0.25 µm;
Oven Program: 90°C for 25 min (initial temperature), then 8°C/min to 260°C (rate).
Inlet temperature: 160°C
FID: 300°C
Run time: 42 min
Split Ratio: 50:1
Argon carrier gas flow rate: 1ml/min
Hexadecane was used as internal standard.

Retention times of α-terpinene – 6.341 min;
p-cymene – 6.567 min;
ascaridole – 20.518 min;
hexadecane – 36.767 min (Figure 90).



RetTime [min]	Type	ISTD used	Area [pA*s]	Amt/Area ratio	Amount [mg]	Grp	Name
6.576	VV	1	62.98730	1.01667	1.81724		p-cymene
6.341	VV	1	309.46848	1.13468	9.96477		a-terp.
20.518	BB	1	473.58646	1.40844	18.92851		Asc
36.767	BB	I 1	1218.31152	1.00000	34.57300		Hexadecan

Figure 90: Example of the GC chromatogram of the crude product (product OS-8y)

The amount of formed ascaridole and *p*-cymene and the amount of unconverted α-terpinene were calculated based on the GC area analysis for each experiment. Therefore, the calibration graphs for α-terpinene, ascaridole and *p*-cymene were established prior

to the synthetic experiments. Calibration graphs for α-terpinene and ascaridole were generated using GC data of eight calibration solutions. These solutions were prepared with exact mass-concentrations of α-terpinene and ascaridole (from 1.0 mg to 40.0 mg, which ensured that the whole range of later studied concentrations was covered). Concentration of internal standard hexane was kept the same in all calibration solutions and was 13.866 mg per 10 ml. The calibration graph of *p*-cymene was made using only three calibration solutions due to the very low concentration of *p*-cymene (from 1.0 mg to 3.0 mg). The established calibration graphs showed linear dependency between the area and amount ratios, $R^2 > 0.99$ (Figures 91–93).

For the calibration graphs commercially available α-terpinene (CAS No. 99-86-5, purity 93.1%), *p*-cymene (CAS No. 99-87-6, purity 99%) and hexadecane (CAS No. 544-76-3, analytical standard) were used. Ascaridole was prepared in the laboratory order using the general Schlenk flask as a reaction vessel and xenon lamp as light source. After irradiation time of one hour crude product was excluded and further purified by column chromatography, mobile phase ethyl acetate/cyclohexane 1:3. Ascaridole was isolated as yellow liquid and its identity and purity were confirmed by ^{1}H-NMR, ^{13}C-NMR and GC-MS (data provided in paragraph 9.3.1.2).

The commercially available α-terpinene was also checked by GC-MS. The results confirmed its purity of 93.1% and showed that the other 6.9% impurities are composed of *p*-cymene (retention time 6.567 min), *o*-cymene and *m*-cymene (retention time 7.071 min), α-phellandrene and 1-methyl-4-(propan-2-yl)-7-oxabicyclo[2.2.1]heptane (retention time 6.121 min). The retention time of all impurities lies in the region very close to the retention time of α-terpinene. However the GC-MS monitoring of the impurities peaks showed that their area, except the *p*-cymene peak, remained constant during the experiments and thus had no influence on the final results. There was found to be about 2% of *p*-cymene in the original α-terpinene solution. Therefore the final amount of *p*-cymene in the crude product was always lowered by this percent.

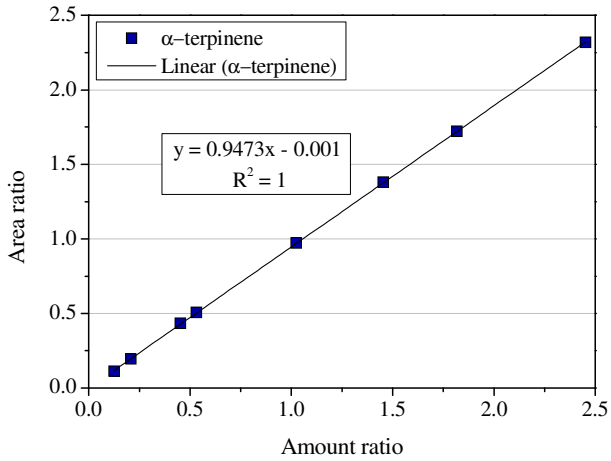


Figure 91: Calibration graph of α-terpinene (ref. GC data OS-1k – OS-8k)

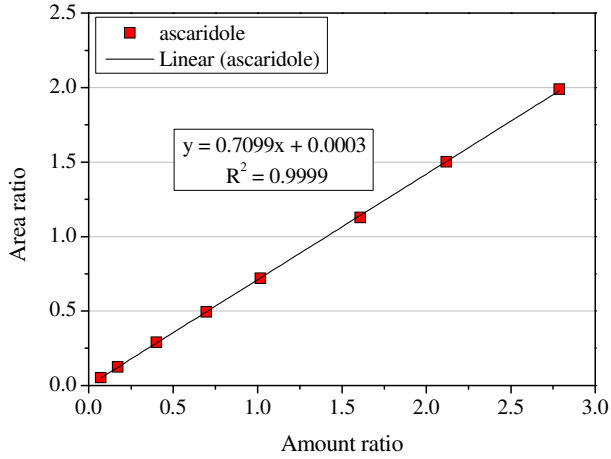


Figure 92: Calibration graph of ascaridole (ref. GC data OS-1k – OS-8k)

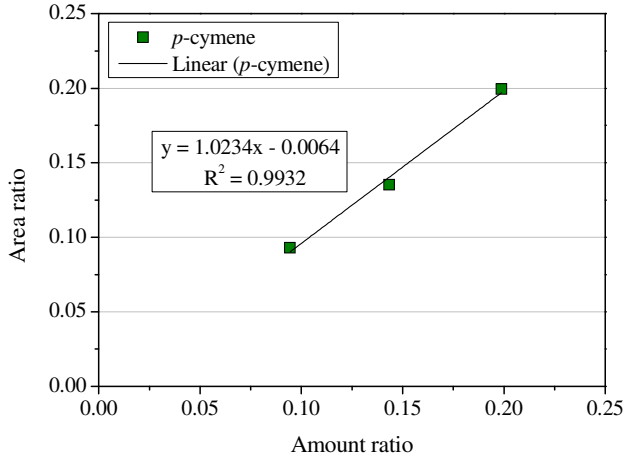
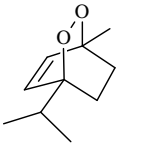


Figure 93: Calibration graph of *p*-cymene (ref. GC data OS-9k – OS-11k)

9.3.1.2 Analytical data of *1-methyl-4-(propan-2-yl)-2,3-dioxabicyclo[2.2.2]oct-5-ene* (ascaridole 40)



40

$C_{10}H_{16}O_2$

Mol. Wt.: 168.23 g/mol

TLC: ***Rf*** = 0.52 (ethyl acetate/cyclohexane 1:3), yellow liquid

^{1}H–NMR: (400 MHz, $CDCl_3$)

δ (ppm) = 0.95 (d, ^{2}J = 6.8 Hz, 6 H, C<u>H</u>$_3$CHC<u>H</u>$_3$), 1.36 (s, 3 H, CH_3), 1.48-1.54 (m, 2 H, CH_2), 1.82 (quin, ^{3}J = 0.8 Hz, 1 H, CH), 1.98-2.02 (m, 2 H, CH_2), 6.41 (d, ^{2}J = 8.2 Hz, 1 H), 6.49 (d, ^{2}J = 8.2 Hz, 1 H).

^{13}C–NMR: (100 MHz, $CDCl_3$)

δ (ppm) = 17.2 (d, 1 C, CH<u>C</u>H$_3$), 17.3 (d, 1 C, CH<u>C</u>H$_3$), 21.4 (s, 1 C, CH_3), 25.6 (s, 1 C, CH_2), 29.5 (s, 1 C, CH_2), 32.2 (s, 1 C, CH$_3$<u>C</u>HCH$_3$), 74.4 (s, 1 C, <u>C</u>-O-O-C), 79.8 (s, 1 C, C-O-O-<u>C</u>), 133.1 (s, 1 C, CH), 136.4 (s, 1 C, CH).

Experiment 149

Effect of residence time on the ascaridole synthesis at 25 mM concentration of α-terpinene (OS-7, LIKAT)

General procedure (GP-18) was followed using α-terpinene (341 mg; 2.5 mmol), hexadecane (340 mg; 1.5 mmol) and rose bengal (51 mg; 50 μmol). Experimental temperature was kept at 20°C. The prepared reaction mixture was investigated with six main volumetric flow rates of syringe pump: 1 ml/min, 0.8 ml/min, 0.5 ml/min, 0.3 ml/min, 0.15 ml/min and 0.08 ml/min which corresponded residence times of 6 sec, 7 sec, 10 sec, 13 sec, 21 sec and 32 sec, respectively. The collected crude products were analysed by GC-MS. The results determined by GC area analysis are presented in the Table 60.

Table 60: Data determined by GC area analysis within the *experiment 149*

Ref. GC data	Residence time, [s]	α-terp., [mg]	α-terp., [mmol]	Asc., [mg]	Asc., [mmol]	*p*-cym., [mg]	*p*-cym., [mmol]
OS-1g[a]	0	312	2.29	0	0	8	0.06
OS-2g[b]	0	312	2.29	0	0	8	0.06
OS-3g[c]	0	297	2.18	3	0.02	8	0.06
OS-4g	6	262	1.92	49	0.29	8	0.06
OS-5g	7	252	1.85	55	0.33	9	0.07
OS-6g	10	193	1.41	118	0.70	9	0.07
OS-7g	13	153	1.12	153	0.91	10	0.08
OS-8g	21	87	0.64	223	1.32	10	0.08
OS-9g	32	19	0.14	280	1.66	11	0.08

[a] GC results determined for the stock solution OS-7 in the flask; [b] GC results determined for the sample collected from the microreactor outlet after first test run; [c] GC results determined for the sample collected from the microreactor outlet after second test run

Experiment 150

Effect of residence time on the ascaridole synthesis at 50 mM concentration of α-terpinene (OS-5, LIKAT)

General procedure (GP-18) was followed using α-terpinene (683 mg; 5.0 mmol), hexadecane (691 mg; 3.1 mmol) and rose bengal (50 mg; 49 μmol). Experimental temperature was kept at 20°C. The prepared reaction mixture was investigated with six main volumetric flow rates of syringe pump: 1 ml/min, 0.8 ml/min, 0.5 ml/min, 0.3 ml/min, 0.15 ml/min and 0.08 ml/min which corresponded residence times of 6 sec, 7 sec, 10 sec, 13 sec, 21 sec and 32 sec, respectively. The collected crude products were analysed by GC-MS. The results determined by GC area analysis are presented in the Table 61.

Table 61: Data determined by GC area analysis within the *experiment 150*

Ref. GC data	Residence time, [s]	α-terp., [mg]	α-terp., [mmol]	Asc., [mg]	Asc., [mmol]	*p*-cym., [mg]	*p*-cym., [mmol]
OS-1e[a]	0	623	4.57	0	0	15	0.11
OS-2e[b]	0	623	4.57	0	0	16	0.12
OS-3e[c]	0	610	4.48	6	0.04	15	0.11
OS-4e	6	572	4.20	53	0.32	16	0.12
OS-5e	7	563	4.13	64	0.38	16	0.12
OS-6e	10	539	3.94	94	0.56	16	0.12
OS-7e	13	504	3.66	131	0.78	17	0.13
OS-8e	21	397	2.94	227	1.35	18	0.14
OS-9e	32	262	1.95	370	2.20	19	0.15

[a] GC results determined for the stock solution OS-5 in the flask; [b] GC results determined for the sample collected from the microreactor outlet after first test run; [c] GC results determined for the sample collected from the microreactor outlet after second test run

Experiment 151

Reproducibility of the *experiment 2* (OS-1, LIKAT)

General procedure (GP-18) was followed using α-terpinene (688 mg; 5.1 mmol), hexadecane (690 mg; 3.1 mmol) and rose bengal (51 mg; 50 μmol). Experimental temperature was kept at 20°C. The prepared reaction mixture was investigated with six main volumetric flow rates of syringe pump: 1 ml/min, 0.8 ml/min, 0.5 ml/min, 0.3 ml/min, 0.15 ml/min and 0.08 ml/min which corresponded residence times of 6 sec, 7 sec, 10 sec, 13 sec, 21 sec and 32 sec, respectively. The collected crude products were analysed by GC-MS. The results determined by GC area analysis are presented in the Table 62.

Table 62: Data determined by GC area analysis within the *experiment 151*

Ref. GC data	Residence time, [s]	α-terp., [mg]	α-terp., [mmol]	Asc., [mg]	Asc., [mmol]	*p*-cym., [mg]	*p*-cym., [mmol]
OS-1a[a]	0	638	4.68	0	0	14	0.11
OS-2a[b]	0	638	4.69	0	0	14	0.11
OS-3a[c]	0	635	4.66	6	0.04	14	0.11
OS-4a	6	584	4.29	52	0.31	15	0.11
OS-5a	7	571	4.19	66	0.39	15	0.11
OS-6a	10	544	3.99	93	0.55	15	0.12
OS-7a	13	511	3.75	131	0.78	16	0.12
OS-8a	21	389	2.86	257	1.53	17	0.13
OS-9a	32	270	2.00	382	2.27	18	0.13

[a] GC results determined for the stock solution OS-1 in the flask; [b] GC results determined for the sample collected from the microreactor outlet after first test run; [c] GC results determined for the sample collected from the microreactor outlet after second test run

Experiment 152

Reproducibility of the *experiment 2* (OS-3, LIKAT)

General procedure (GP-18) was followed using α-terpinene (685 mg; 5.0 mmol), hexadecane (692 mg; 3.1 mmol) and rose bengal (51 mg; 50 μmol). Experimental temperature was kept at 20°C. The prepared reaction mixture was investigated with six main volumetric flow rates of syringe pump: 1 ml/min, 0.8 ml/min, 0.5 ml/min, 0.3 ml/min, 0.15 ml/min and 0.08 ml/min which corresponded residence times of 6 sec, 7 sec, 10 sec, 13 sec, 21 sec and 32 sec, respectively. The collected crude products were analysed by GC-MS. The results determined by GC area analysis are presented in the Table 63.

Table 63: Data determined by GC area analysis within the *experiment 152*

Ref. GC data	Residence time, [s]	α-terp., [mg]	α-terp., [mmol]	Asc., [mg]	Asc., [mmol]	*p*-cym., [mg]	*p*-cym., [mmol]
OS-1c[a]	0	625	4.58	0	0	14	0.11
OS-2c[b]	0	625	4.58	0	0	14	0.11
OS-3c[c]	0	620	4.55	7	0.04	14	0.11
OS-4c	6	573	4.20	54	0.32	15	0.11
OS-5c	7	566	4.16	61	0.36	15	0.11
OS-6c	10	516	3.79	113	0.67	16	0.12
OS-7c	13	502	3.68	129	0.77	16	0.12
OS-8c	21	416	3.05	214	1.27	17	0.13
OS-9c	32	297	2.18	335	1.99	18	0.14

[a] GC results determined for the stock solution OS-3 in the flask; [b] GC results determined for the sample collected from the microreactor outlet after first test run; [c] GC results determined for the sample collected from the microreactor outlet after second test run

Experiment 153

Effect of oxygen concentration on the ascaridole synthesis (OS-2, LIKAT)

General procedure (GP-18) was followed, with one variation, using α-terpinene (687 mg; 5.0 mmol), hexadecane (683 mg; 3.0 mmol) and rose bengal (51 mg; 50 μmol). In this experiment air was used as gas phase instead of pure oxygen. Flow rate of air was the same as oxygen of 10 ml/min. Experimental temperature was kept at 20°C. The prepared reaction mixture was investigated with six main volumetric flow rates of syringe pump: 1 ml/min, 0.8 ml/min, 0.5 ml/min, 0.3 ml/min, 0.15 ml/min and 0.08 ml/min which corresponded residence times of 6 sec, 7 sec, 10 sec, 13 sec, 21 sec and 32 sec, respectively. The collected crude products were analysed by GC-MS. The results determined by GC area analysis are presented in the Table 64.

Table 64: Data determined by GC area analysis within the *experiment 153*

Ref. GC data	Residence time, [s]	α-terp., [mg]	α-terp., [mmol]	Asc., [mg]	Asc., [mmol]	*p*-cym., [mg]	*p*-cym., [mmol]
OS-1b[a]	0	627	4.60	0	0	14	0.11
OS-2b[b]	0	614	4.51	17	0.1	14	0.11
OS-3b[c]	0	613	4.50	17	0.1	14	0.11
OS-4b	6	567	4.16	62	0.37	15	0.11
OS-5b	7	550	4.04	76	0.45	15	0.11
OS-6b	10	525	3.85	103	0.61	16	0.12
OS-7b	13	490	3.60	141	0.84	16	0.12
OS-8b	21	413	3.03	219	1.30	17	0.13
OS-9b	32	331	2.43	306	1.82	18	0.13

[a] GC results determined for the stock solution OS-2 in the flask; [b] GC results determined for the sample collected from the microreactor outlet after first test run; [c] GC results determined for the sample collected from the microreactor outlet after second test run

Experiment 154

Effect of solvent on the ascaridole synthesis (OS-4, LIKAT)

General procedure (GP-18) was followed, with one variation, using α-terpinene (689 mg; 5.1 mmol), hexadecane (682 mg; 3.0 mmol) and rose bengal (51 mg; 50 μmol). In this experiment isopropanol/water mixture in the ratio 9:1 (90 ml of *i*-PrOH and 10 ml of H_2O) was used as solvent instead of blank isopropanol. Experimental temperature was kept at 20°C. The prepared reaction mixture was investigated with six main volumetric flow rates of syringe pump: 1 ml/min, 0.8 ml/min, 0.5 ml/min, 0.3 ml/min, 0.15 ml/min and 0.08 ml/min which corresponded residence times of 6 sec, 7 sec, 10 sec, 13 sec, 21 sec and 32 sec, respectively. The collected crude products were analysed by GC-MS. The results determined by GC area analysis are presented in the Table 65.

Table 65: Data determined by GC area analysis within the *experiment 154*

Ref. GC data	Residence time, [s]	α-terp., [mg]	α-terp., [mmol]	Asc., [mg]	Asc., [mmol]	*p*-cym., [mg]	*p*-cym., [mmol]
OS-1d[a]	0	628	4.61	0	0	14	0.11
OS-2d[b]	0	623	4.57	7	0.04	14	0.11
OS-3d[c]	0	622	4.57	7	0.04	14	0.11
OS-4d	6	575	4.22	52	0.31	15	0.11
OS-5d	7	560	4.11	66	0.39	15	0.11
OS-6d	10	539	3.96	91	0.54	15	0.11
OS-7d	13	492	3.61	138	0.82	16	0.12
OS-8d	21	391	2.87	234	1.39	17	0.13
OS-9d	32	245	1.80	392	2.33	20	0.15

[a] GC results determined for the stock solution OS-4 in the flask; [b] GC results determined for the sample collected from the microreactor outlet after first test run; [c] GC results determined for the sample collected from the microreactor outlet after second test run

Experiment 155

Effect of residence time on the ascaridole synthesis at 10 mM concentration of α-terpinene (OS-6, LIKAT)

General procedure (GP-18) was followed using α-terpinene (136 mg; 1.0 mmol), hexadecane (136 mg; 0.6 mmol) and rose bengal (50 mg; 49 μmol). Experimental temperature was kept at 20°C. The prepared reaction mixture was investigated with three volumetric flow rates of syringe pump: 1 ml/min, 0.3 ml/min and 0.08 ml/min which corresponded residence times of 6 sec, 13 sec and 32 sec, respectively. The collected crude products were analysed by GC-MS. The results determined by GC area analysis are presented in the Table 66.

Table 66: Data determined by GC area analysis within the *experiment 155*

Ref. GC data	Residence time, [s]	α-terp., [mg]	α-terp., [mmol]	Asc., [mg]	Asc., [mmol]	*p*-cym., [mg]	*p*-cym., [mmol]
OS-1f[a]	0	121	0.89	3	0.02	3	0.02
OS-2f[b]	0	113	0.83	5	0.03	3	0.02
OS-3f[c]	0	106	0.78	7	0.04	3	0.02
OS-4v	6	75	0.55	40	0.24	6	0.04
OS-4f	13	22	0.16	88	0.52	4	0.03
OS-6f	32	0	0.00	109	0.65	5	0.04

[a] GC results determined for the stock solution OS-6 in the flask; [b] GC results determined for the sample collected from the microreactor outlet after first test run; [c] GC results determined for the sample collected from the microreactor outlet after second test run

Experiment 156

Effect of residence time on the ascaridole synthesis at 75 mM concentration of α-terpinene (OS-13, LIKAT)

General procedure (GP-18) was followed using α-terpinene (1.02 g; 7.5 mmol), hexadecane (1.02 g; 4.5 mmol) and rose bengal (50 mg; 50 μmol). Experimental temperature was kept at 20°C. The prepared reaction mixture was investigated with three volumetric flow rates of syringe pump: 1 ml/min, 0.3 ml/min and 0.08 ml/min which corresponded residence times of 6 sec, 13 sec and 32 sec, respectively. The collected crude products were analysed by GC-MS. The results determined by GC area analysis are presented in the Table 67.

Table 67: Data determined by GC area analysis within the *experiment 156*

Ref. GC data	Residence time, [s]	α-terp., [mg]	α-terp., [mmol]	Asc., [mg]	Asc., [mmol]	*p*-cym., [mg]	*p*-cym., [mmol]
OS-1r[a]	0	932	6.84	0	0	24	0.18
OS-2r[b]	0	926	6.80	5	0.03	26	0.19
OS-3r[c]	0	920	6.75	7	0.04	26	0.19
OS-4r	6	867	6.36	56	0.33	26	0.19
OS-5r	13	798	5.86	126	0.75	27	0.20
OS-7r	32	589	4.32	360	2.14	35	0.26

[a] GC results determined for the stock solution OS-13 in the flask; [b] GC results determined for the sample collected from the microreactor outlet after first test run; [c] GC results determined for the sample collected from the microreactor outlet after second test run

Experiment 157

Effect of residence time on the ascaridole synthesis at 100 mM concentration of α-terpinene (OS-14, LIKAT)

General procedure (GP-18) was followed using α-terpinene (1.37 g; 10.0 mmol), hexadecane (1.36 g; 6.0 mmol) and rose bengal (50 mg; 50 μmol). Experimental temperature was kept at 20°C. The prepared reaction mixture was investigated with three volumetric flow rates of syringe pump: 1 ml/min, 0.3 ml/min and 0.08 ml/min which corresponded residence times of 6 sec, 13 sec and 32 sec, respectively. The collected crude products were analysed by GC-MS. The results determined by GC area analysis are presented in the Table 68.

Table 68: Data determined by GC area analysis within the *experiment 157*

Ref. GC data	Residence time, [s]	α-terp., [g]	α-terp., [mmol]	Asc., [mg]	Asc., [mmol]	*p*-cym., [mg]	*p*-cym., [mmol]
OS-1s[a]	0	1.25	9.15	0	0	35	0.26
OS-2s[b]	0	1.23	9.06	2	0.01	35	0.26
OS-3s[c]	0	1.23	9.05	7	0.04	35	0.26
OS-4s	6	1.18	8.68	52	0.31	38	0.28
OS-5s	13	1.09	8.04	128	0.76	39	0.29
OS-6s	32	0.85	6.22	373	2.22	44	0.33

[a] GC results determined for the stock solution OS-14 in the flask; [b] GC results determined for the sample collected from the microreactor outlet after first test run; [c] GC results determined for the sample collected from the microreactor outlet after second test run

9.3.2 General procedure (GP-19) for rose bengal sensitised photooxygenation of α-terpinene 39 (synthesis of ascaridole 40) in the falling film microreactor

Five experimental solutions (solutions 1-5) with the concentration of rose bengal of 0.98 mM and α-terpinene concentration of 10 mM, 25 mM, 50 mM, 75 mM and 100 mM, respectively have been prepared. Concentration of internal standard hexadecane was adjusted accordingly to the concentration of α-terpinene. Solutions were prepared in the 100 ml volumetric flasks. Isopropanol/water mixture in the ratio of 9:1 was used as solvent. Solvent was degassed with argon for 15 min before the usage. The prepared solutions were sonicated for 15 min and then solution 1 was transferred into a 50 ml glass syringe. Any air bubbles were expelled and syringe was loaded into the programmable syringe pump. Solution 1 was investigated with two volumetric flow rates of syringe pump: 1 ml/min and 0.3 ml/min which corresponded residence times of 6 sec and 13 sec, respectively. As gas phase pure oxygen at flow rate of 10 ml/min was used. A single fluorescent lamp (18 W) was employed for irradiation. The product samples were collected from the reactor outlet and instantly analysed by the GC-MS. When the experiment with solution 1 was finished, the syringe pump and fluorescent lamp were switched off simultaneously. The syringe was refilled with the experimental solution 2 and loaded into the syringe pump again. Prior to the beginning of the testing of solution 2, falling film microreactor has been treated with this solution for 10 min at volumetric flow rate of 1 ml/min and without light. Afterwards solution 2 was investigated with the same volumetric flow rates of 1 ml/min and 0.3 ml/min as solution 1. After the test with solution 2 was finished the same procedure was applied to the solutions 3, 4 and 5.

During the experiment, the microreactor was kept at temperature of 20°C by the continuous circulation of water (20±2°C) through the reactor heat exchanger positioned on the back side of the reaction plate. The experimental temperature was continually controlled by two thermocouples positioned on the microreactor inlet and outlet. The temperature was recorded by thermo-recorder. When the experiment was complete, whole system was cleaned with the pure methanol.

Experiment 158

Effect of double concentration of rose bengal of 0.98 mM on the ascaridole synthesis (OS-9, LIKAT)

General procedure (GP-19) was followed and five experimental solutions were prepared:

Solution 1 (OS-9a) with α-terpinene (137 mg; 1.0 mmol), hexadecane (137 mg; 0.6 mmol) and rose bengal (101 mg; 100 μmol);

Solution 2 (OS-9b) with α-terpinene (345 mg; 2.5 mmol), hexadecane (348 mg; 1.5 mmol) and rose bengal (101 mg; 99 μmol);

Solution 3 (OS-9c) with α-terpinene (684 mg; 5.0 mmol), hexadecane (683 mg; 3.0 mmol) and rose bengal (101 mg; 99 μmol);

Solution 4 (OS-9d) with α-terpinene (1.02 g; 7.5 mmol), hexadecane (1.02 g; 4.5 mmol) and rose bengal (101 mg; 99 μmol);

Solution 5 (OS-9e) with α-terpinene (1.37 g; 10.1 mmol), hexadecane (1.36 g; 6.0 mmol) and rose bengal (100 mg; 98 μmol).

The collected crude products were analysed by GC-MS. The results determined by GC area analysis are presented in the Table 69.

Table 69: Data determined by GC area analysis within the *experiment 158*

Ref. GC data	Residence time, [s]	α-terp., [mg]	α-terp., [mmol]	Asc., [mg]	Asc., [mmol]	*p*-cym., [mg]	*p*-cym., [mmol]
OS-1i[a]	0	124	0.91	3	0.02	3	0.02
OS-2i	6	44	0.32	74	0.44	4	0.03
OS-3i	13	4	0.03	108	0.64	7	0.05
OS-1j[b]	0	315	2.31	0	0	8	0.06
OS-2j	6	230	1.69	69	0.41	9	0.07
OS-3j	13	123	0.90	175	1.04	11	0.08
OS-1k[c]	0	624	4.58	0	0	14	0.11
OS-2k	6	535	3.93	72	0.43	15	0.11
OS-3k	13	400	2.93	195	1.16	17	0.13
OS-1l[d]	0	933	6.85	0	0	23	0.17
OS-2l	6	819	6.01	104	0.62	25	0.19
OS-3l	13	716	5.25	197	1.17	28	0.21
OS-1m[e]	0	1252	9.19	0	0	32	0.24
OS-2m	6	1135	8.33	99	0.59	35	0.26
OS-3m	13	990	7.27	237	1.41	34	0.25

[a] GC results determined for the stock solution OS-9a in the flask; [b] GC results determined for the stock solution OS-9b in the flask; [c] GC results determined for the stock solution OS-9c in the flask; [d] GC results determined for the stock solution OS-9d in the flask; [e] GC results determined for the stock solution OS-9e in the flask

Experiment 159

Effect of halved concentration of rose bengal of 0.25 mM on the ascaridole synthesis (OS-11, LIKAT)

General procedure (GP-19) was followed, with one variation, instead of five experimental solutions only three solutions (solutions 1-3) were prepared and studied:
Solution 1 (OS-11a) with α-terpinene (135 mg; 1.0 mmol), hexadecane (139 mg; 0.6 mmol) and rose bengal (26 mg; 25 μmol);
Solution 2 (OS-11b) with α-terpinene (342 mg; 2.5 mmol), hexadecane (340 mg; 1.5 mmol) and rose bengal (26 mg; 25 μmol);
Solution 3 (OS-11c) with α-terpinene (686 mg; 5.0 mmol), hexadecane (682 mg; 3.0 mmol) and rose bengal (26 mg; 25 μmol).
The collected crude products were analysed by GC-MS. The results determined by GC area analysis are presented in the Table 70.

Table 70: Data determined by GC area analysis within the *experiment 159*

Ref. GC data	Residence time, [s]	α-terp., [mg]	α-terp., [mmol]	Asc., [mg]	Asc., [mmol]	*p*-cym., [mg]	*p*-cym., [mmol]
OS-1h[a]	0	123	0.90	3	0.02	3	0.02
OS-2h	6	86	0.63	30	0.18	3	0.02
OS-3h	13	56	0.41	59	0.35	4	0.03
OS-1o[b]	0	311	2.28	0	0	8	0.06
OS-2o	6	268	1.97	35	0.21	9	0.07
OS-3o	13	192	1.41	108	0.64	11	0.08
OS-1p[c]	0	625	4.59	0	0	16	0.12
OS-2p	6	578	4.24	40	0.24	16	0.12
OS-3p	13	523	3.84	84	0.50	18	0.14

[a] GC results determined for the stock solution OS-11a in the flask; [b] GC results determined for the stock solution OS-11b in the flask; [c] GC results determined for the stock solution OS-11c in the flask

Experiment 160

Verification of α-terpinene self-sensitisation (OS-20, LIKAT)

General procedure (GP-18) was followed, with one variation, the experimental solution was prepared without rose bengal just using α-terpinene (138 mg; 1.0 mmol) and hexadecane (132 mg; 0.6 mmol). Experimental temperature was kept at 20°C. The prepared reaction mixture was investigated with three volumetric flow rates of syringe

pump: 1 ml/min, 0.5 ml/min and 0.08 ml/min which corresponded residence times of 6 sec, 10 sec and 32 sec, respectively. The collected crude products were analysed by GC-MS. The results determined by GC area analysis are presented in the Table 71.

Table 71: Data determined by GC area analysis within the *experiment 160*

Ref. GC data	Residence time, [s]	α-terp., [mg]	α-terp., [mmol]	Asc., [mg]	Asc., [mmol]	*p*-cym., [mg]	*p*-cym., [mmol]
OS-1z[a]	0	128	0.94	w.d.[d]	w.d.	3	0.02
OS-2z[b]	0	126	0.93	w.d.	w.d.	3	0.02
OS-3z[c]	0	126	0.93	w.d.	w.d.	3	0.02
OS-4z	6	126	0.92	w.d.	w.d.	3	0.02
OS-5z	10	123	0.90	w.d.	w.d.	3	0.02
OS-6z	32	122	0.90	w.d.	w.d.	3	0.02

[a] GC results determined for the stock solution OS-20 in the flask; [b] GC results determined for the sample collected from the microreactor outlet after first test run; [c] GC results determined for the sample collected from the microreactor outlet after second test run; [d] wasn't detected

Experiment 161

Investigation of the loss of α-terpinene during the experiment (OS-16, LIKAT)

General procedure (GP-18) was followed, with two variations, the experimental solution was prepared without rose bengal just using α-terpinene (135 mg; 1.0 mmol) and hexadecane (135 mg; 0.6 mmol). The experimental solution wasn't irradiated by any light source and viewing window of the reactor was additionally covered with several layers of aluminium foil. Experimental temperature was kept at 20°C. The prepared reaction mixture was investigated with two volumetric flow rates of syringe pump: 0.5 ml/min and 0.08 ml/min which corresponded residence times of 10 sec and 32 sec, respectively. The collected crude products were analysed by GC-MS. The results determined by GC area analysis are presented in the Table 72.

Table 72: Data determined by GC area analysis within the *experiment 161*

Ref. GC data	Residence time, [s]	α-terp., [mg]	α-terp., [mmol]	Asc., [mg]	Asc., [mmol]	*p*-cym., [mg]	*p*-cym., [mmol]
OS-1u[a]	0	125	0.92	w.d.[b]	w.d.	3	0.02
OS-2u	10	123	0.90	w.d.	w.d.	3	0.02
OS-3u	32	120	0.88	w.d.	w.d.	3	0.02

[a] GC results determined for the stock solution OS-16 in the flask; [b] wasn't detected

Experiment 162

Effect of oxygen flow rate on the ascaridole synthesis (OS-13 and OS-14, LIKAT)

The same stock solutions OS-13 and OS-14 that have been prepared within the *experiments 8* and *9* were further investigated in this experiment with the changed flow rates of gas phase – pure oxygen. A single fluorescent lamp (18 W) was used for irradiation.

Primarily, a 50 ml glass syringe was filled up with the solution OS-13 and was loaded into the syringe pump. Syringe pump was set to volumetric flow rate of 0.3 ml/min which corresponded residence time of 13 sec. Oxygen was fed into the reactor chamber with flow rate of 20 ml/min and moved counter currently to the liquid flow. Solution OS-13 was tested under such conditions and product collected from microreactor outlet was instantly analysed by GC-MS (ref. GC data OS-6r). Afterwards flow rate of syringe pump was changed to 0.5 ml/min (residence time 10 sec), but flow rate of oxygen was kept the same of 20 ml/min and next product sample was collected (ref. GC data OS-8r). At last, flow rate of syringe pump was kept the same of 0.5 ml/min, but flow rate of oxygen was enlarged to 50 ml/min and final product sample was collected (ref. GC data OS-9r). When the testing of solution OS-13 was finished, the syringe was refilled with the experimental solution OS-14 and loaded into the syringe pump again. Prior to the beginning of the testing of solution OS-14, falling film microreactor has been treated with this solution for 10 min at volumetric flow rate of 1 ml/min and without light. Afterwards solution OS-14 was investigated under the same conditions as above described for the solution OS-13 and three product samples were collected (ref. GC data OS-7s, OS-8s and OS-9s, correspondingly). The results determined by GC area analysis are presented in the Table 73.

During the experiment, the microreactor was kept at temperature of 20°C by the continuous circulation of water (20±2°C) through the reactor heat exchanger positioned on the back side of the reaction plate. The experimental temperature was continually controlled by two thermocouples positioned on the microreactor inlet and outlet. The temperature was recorded by thermo-recorder. When the experiment was complete, whole system was cleaned with the pure methanol.

Table 73: Data determined by GC area analysis within the *experiment 162*

Ref. GC data	Residence time, [s]	α-terp., [g]	α-terp., [mmol]	Asc., [mg]	Asc., [mmol]	*p*-cym., [mg]	*p*-cym., [mmol]
OS-6r	13	0.78	5.74	130	0.77	28	0.21
OS-8r	10	0.84	6.16	90	0.53	27	0.20
OS-9r	10	0.83	6.07	104	0.62	28	0.21
OS-7s	13	1.09	8.03	130	0.77	40	0.30
OS-8s	10	1.14	8.35	88	0.52	39	0.29
OS-9s	10	1.13	8.32	109	0.65	39	0.29

Experiment 163

Effect of double concentration of rose bengal of 0.98 mM on the ascaridole synthesis at oxygen flow rate of 50 ml/min (OS-17, LIKAT)

General procedure (GP-18) was followed with three variations. The concentration of rose bengal was two times higher and was 0.98 mM, isopropanol/water mixture in the ratio 9:1 (90 ml of *i*-PrOH and 10 ml of H_2O) was used as solvent and flow rate of oxygen was five times larger and was 50 ml/min. The experimental solution OS-17 was prepared using α-terpinene (689 mg; 5.1 mmol), hexadecane (688 mg; 3.0 mmol) and rose bengal (101 mg; 99 μmol). Experimental temperature was kept at 20°C. The prepared reaction mixture was investigated with three volumetric flow rates of syringe pump: 0.5 ml/min, 0.3 ml/min, 0.15 ml/min and 0.08 ml/min which corresponded residence times of 10 sec, 13 sec, and 32 sec, respectively. The collected crude products were analysed by GC-MS. The results determined by GC area analysis are presented in the Table 74.

Table 74: Data determined by GC area analysis within the *experiment 163*

Ref. GC data	Residence time, [s]	α-terp., [mg]	α-terp., [mmol]	Asc., [mg]	Asc., [mmol]	*p*-cym., [mg]	*p*-cym., [mmol]
OS-1w[a]	0	641	4.70	0	0	19	0.14
OS-2w[b]	0	629	4.62	0	0	19	0.14
OS-3w[c]	0	629	4.62	2	0.01	19	0.14
OS-4w	10	471	3.46	157	0.93	26	0.19
OS-5w	13	398	2.92	217	1.29	28	0.21
OS-6w	32	85	0.62	478	2.84	40	0.30

[a] GC results determined for the stock solution OS-17 in the flask; [b] GC results determined for the sample collected from the microreactor outlet after first test run; [c] GC results determined for the sample collected from the microreactor outlet after second test run

Experiment 164

Effect of different temperatures on the ascaridole synthesis (OS-18, LIKAT)

General procedure (GP-18) was followed using α-terpinene (353 mg; 2.6 mmol), hexadecane (346 mg; 1.5 mmol) and rose bengal (50 mg; 49 μmol). The prepared reaction mixture was investigated at different temperatures in the range from –3.0°C to +41.0°C. The experimental temperature was gradually increased from sub-zero temperature to temperature plus 41.0°C. The exact increment of temperature is showed in the Table 75. Flow rate of syringe pump was set to 0.5 ml/min and was kept constant within the experiment.

Initially, the experimental temperature was set below 0°C by continuous circulation of ethanol through the cryostat and reactor heat exchanger positioned on the back side of the reaction plate. The experimental temperature was constantly controlled by two thermocouples positioned on the microreactor inlet and outlet. Temperature was recorded by thermo-recorder and is presented in the Table 75. The temperature of cryostat was set few degrees Celsius lower (–4.0°C) than temperature required for microreactor due to the loss of power by the circulation through connecting tubing. To reduce the loss of temperature power, all connecting tubes and microreactor were covered with thick layer of fibreglass. Generally it took up to 30 minutes to get even-tempered distribution of temperature within the system. The experimental solution was continually circulated through microreactor channels at flow rate of 0.5 ml/min without irradiation until the appropriate steady temperature was reached. When the required

temperature was achieved, the solution was irradiated by the fluorescent lamp and product sample was collected. Next, temperature of cryostat was changed to slightly higher of +2.5°C and above described practice was repeated. In total, the same procedure has been repeated every time after the incensement of temperature as showed in the Table 75. When the experiment was complete and last product sample was collected whole system was cleaned with the pure methanol. The collected crude products were analysed by GC-MS. The results determined by GC area analysis are presented in the Table 75.

Table 75: Data determined by GC area analysis within the *experiment 164*

Ref. GC data	Cryostat t, [°C]	Inlet t, [°C]	Outlet t, [°C]	α-terp., [mg]	α-terp., [mmol]	Asc., [mg]	Asc., [mmol]	*p*-cym., [mg]	*p*-cym., [mmol]
OS-1x[a]	–	–	–	328	2.41	0	0	11	0.08
OS-2x[b]	–4.0	–2.4	+0.1	327	2.39	0	0	11	0.08
OS-3x[c]	–4.0	–2.4	–0.1	313	2.30	5	0.03	11	0.08
OS-4x	–4.0	–2.4	+0.3	217	1.59	91	0.54	15	0.11
OS-5x	+2.5	+3.7	+5.7	210	1.54	99	0.59	15	0.11
OS-6x	+8.5	+9.3	+10.6	223	1.64	99	0.59	15	0.11
OS-7x	+18.0	+19.6	+20.7	214	1.57	106	0.63	15	0.11
OS-8x	+31.0	+30.7	+30.4	219	1.61	93	0.55	16	0.12
OS-9x	+42.0	+41.0	+40.1	223	1.64	89	0.53	15	0.11

[a] GC results determined for the stock solution OS-18 in the flask; [b] GC results determined for the sample collected from the microreactor outlet after first test run; [c] GC results determined for the sample collected from the microreactor outlet after second test run

Experiment 165

Effect of residence time on the ascaridole synthesis at 25 mM concentration of α-terpinene and temperature about 0°C (OS-19, LIKAT)

General procedure (GP-18) was followed using α-terpinene (356 mg; 2.6 mmol), hexadecane (346 mg; 1.5 mmol) and rose bengal (50 mg; 49 μmol). Experimental temperature was set about 0°C and was kept unchanged by continuous circulation of ethanol through the cryostat and reactor heat exchanger positioned on the back side of the reaction plate. The temperature of cryostat (–4.0±0.5°C) was set few degrees Celsius lower than temperature required for experiment due to the loss of ethanol temperature power by the circulation through connecting tubing. To reduce the loss of temperature

power, all connecting tubes and microreactor were covered with thick layer of fibreglass. The prepared reaction mixture was investigated with six main volumetric flow rates of syringe pump: 1 ml/min, 0.8 ml/min, 0.5 ml/min, 0.3 ml/min, 0.15 ml/min and 0.08 ml/min which corresponded residence times of 7 sec, 8 sec, 12 sec, 16 sec, 26 sec and 39 sec, respectively. The collected crude products were analysed by GC-MS. The results determined by GC area analysis are presented in the Table 76.

Table 76: Data determined by GC area analysis within the *experiment 165*

Ref. GC data	Residence time, [s]	α-terp., [mg]	α-terp., [mmol]	Asc., [mg]	Asc., [mmol]	*p*-cym., [mg]	*p*-cym., [mmol]
OS-1y[a]	0	316	2.32	0	0	11	0.08
OS-2y[b]	0	313	2.30	0	0	11	0.08
OS-3y[c]	0	307	2.25	2	0.01	11	0.08
OS-4y	7	259	1.90	45	0.27	13	0.10
OS-5y	8	248	1.82	56	0.33	13	0.10
OS-6y	12	219	1.61	77	0.46	15	0.11
OS-7y	16	176	1.29	111	0.66	16	0.12
OS-8y	26	93	0.68	190	1.13	19	0.14
OS-9y	39	16	0.12	268	1.59	22	0.16

[a] GC results determined for the stock solution OS-19 in the flask; [b] GC results determined for the sample collected from the microreactor outlet after first test run; [c] GC results determined for the sample collected from the microreactor outlet after second test run

Experiment 166

Effect of the light source on the ascaridole synthesis (OS-15, LIKAT)

General procedure (GP-18) was followed, with one variation, using α-terpinene (680 mg; 5.0 mmol), hexadecane (684 mg; 3.0 mmol) and rose bengal (51 mg; 50 μmol). In this experiment an array of 60 white LEDs with total optical power of 3 W was used for irradiation instead of single fluorescent lamp. Experimental temperature was kept at 20°C. The prepared reaction mixture was investigated with three volumetric flow rates of syringe pump: 0.8 ml/min, 0.3 ml/min and 0.08 ml/min which corresponded residence times of 7 sec, 13 sec and 32 sec, respectively. The collected crude products were analysed by GC-MS. The results determined by GC area analysis are presented in the Table 77.

Table 77: Data determined by GC area analysis within the *experiment 166*

Ref. GC data	Residence time, [s]	α-terp., [mg]	α-terp., [mmol]	Asc., [mg]	Asc., [mmol]	*p*-cym., [mg]	*p*-cym., [mmol]
OS-1t[a]	0	621	4.56	0	0	19	0.14
OS-2t[b]	0	609	4.47	0	0	19	0.14
OS-3t[c]	0	608	4.46	3	0.02	19	0.14
OS-7t	7	578	4.24	34	0.20	20	0.15
OS-8t	13	544	3.99	64	0.38	20	0.15
OS-9t	32	417	3.06	180	1.07	23	0.17

[a] GC results determined for the stock solution OS-15 in the flask; [b] GC results determined for the sample collected from the microreactor outlet after first test run; [c] GC results determined for the sample collected from the microreactor outlet after second test run

Experiment 167

Stability study of the synthesised ascaridole

Three samples of previously collected products were randomly selected and left on the working desk for 10 days. Sample 1 – ref. GC data OS-6f, sample 2 – ref. GC data OS-9g, sample 3 – ref. GC data OS-3i. Samples were affected by the ambient light and room temperature. After 10 days these samples were checked by the GC-MS and results determined by GC area analysis are presented in the Table 78.

Table 78: Data determined by GC area analysis within the *experiment 167*

Ref. GC data	Sample	α-terp., [mg]	α-terp., [mmol]	Asc., [mg]	Asc., [mmol]	*p*-cym., [mg]	*p*-cym., [mmol]
OS-6ff	1	0	0.00	104	0.62	8	0.06
OS-9gg	2	0	0.00	266	1.58	20	0.15
OS-3ii	3	0	0.00	94	0.56	9	0.07

9.3.3 General procedure (GP-20) for rose bengal sensitised photooxygenation of α-terpinene 39 (synthesis of ascaridole 40) in the conventional Schlenk flask

α-terpinene (mg; 1-10 mmol), hexadecane as internal standard (mg; 0.5-6 mmol) and rose bengal (50 mg; 49 μmol) were dissolved in 100 ml of isopropanol that was preliminary degassed with argon for 15 min. The prepared reaction mixture was sonicated for 15 min and transferred into a 50 ml Quartz Schlenk flask. A Pyrex cold

finger and PTFE tubing for oxygenation were inserted into the flask and flask was fixed on the lab stand. Experimental solution in the flask was irradiated for 2 hours by the single fluorescent lamp (18 W) while a gentle stream of oxygen at flow rate of 10 ml/min was flushed through the solution. During the reaction, temperature of solution was kept stable at 20°C by continuous circulation of chilly water through the cold finger. The product samples of solution were taken for analysis every 15 min within first hour and every half an hour during the second hour. A 2 ml glass syringe was used for sampling. The taken product samples were instantly analysed by CG-MS.

Experiment 168

Effect of residence time on the ascaridole synthesis in the batch set-up (OS-12, LIKAT)

General procedure (GP-20) was followed using α-terpinene (343 mg; 2.5 mmol), hexadecane (345 mg; 1.5 mmol) and rose bengal (50 mg; 49 μmol). The taken crude products were analysed by GC-MS. The results determined by GC area analysis are presented in the Table 79.

Table 79: Data determined by GC area analysis within the *experiment 168*

Ref. GC data	Residence time, [min]	α-terp., [mg]	α-terp., [mmol]	Asc., [mg]	Asc., [mmol]	*p*-cym., [mg]	*p*-cym., [mmol]
OS-1q[a]	0	319	2.34	0	0	8	0.06
OS-2q	15	67	0.49	244	1.45	12	0.09
OS-3q	30	0	0.00	313	1.86	12	0.09
OS-4q	45	0	0.00	315	1.87	13	0.10
OS-5q	60	0	0.00	313	1.86	13	0.10
OS-6q	90	0	0.00	306	1.82	13	0.10
OS-7q	120	0	0.00	305	1.81	13	0.10

[a] GC results determined for the stock solution OS-12 in the flask

9.4 Chapter 5: Dye sensitised photooxygenation of 1,5-dihydroxynaphthalene – synthesis of Juglone

Micro photolysis. Falling film microreactor set-up

Microreactor: Photoreactions were performed in a stainless steel *falling film microreactor* (IMM) with Quartz viewing window. Microreactor was equipped with a FFMR – 07029, 316 Ti reaction plate that has 16 parallel microchannels of 1200 µm width, 400 µm depth and 78 mm length.

Irradiation source: A single 18 W domestic fluorescent lamp Phillips GENIE Warm White or an array of 60 white LEDs Powerfix® (3 W total) were used as light sources. During operation, the fluorescent lamp was cooled by a small air fan (Intel®, DTC–AAL03).

Pumps: A programmable rotary pump ISMATEC® (serial No. 313412) was used to deliver the reaction mixture from the amber vial to the microreactor. A second programmable rotary pump ISMATEC® (serial No. 486994) was employed to empty the reactor chamber and to pump the product mixture into the collection flask.

Air pump: A simple electrical air pump Tetratec® (serial No. 351629) was used to supply the air (oxygen) into the reaction mixture.

Flow meter: The flow-meter Supelco® (serial No. 234995-5) was utilised for the control of gas flow rate.

Meso photolysis. Slug flow column reactor set-up

Glassware: Photoreactions were performed in a *Pyrex glass tube* that was 1.5 m long and 4.5 mm wide.

Irradiation source: Two domestic type 60 W fluorescent lamps (OSRAM, L 58W/535, T8 Tube) that emit light in the visible spectra region (λ = 400 – 700 nm) were used as light source.

Pump: A HPLC pump Hewlett Packard 1050 (series No 3418J02081) was used to fill the glass tube with the reaction mixture.

Manometer: The manometer Ashcroft® (series No 0708) was employed to control the level of the pressure (vacuum).

Air pump: A simple electrical air pump STELLAR (series No 285077) was used to supply the air (oxygen) into the reaction mixture.

Flow meter: The flow-meter Platon® (C1D 384PC) was utilised for the control of gas flow rate.

Capillaries: A flexible fused silica capillaries TSP050150 with ID of 50±3 μm and TSP100200 with ID of 100±4 μm or PTFE capillary with ID of 500±5 μm were used as aeration nozzle.

Solvents and reagents

All solvents and starting materials were obtained from commercial suppliers (*Sigma-Aldrich* and *Fluka*) and were used without purification. A 1,5-dihydroxynaphthalene (CAS No. 83-56-7) was purchased from Aldrich Chemical Co with a technical grade and was also used without further purification.

9.4.1 General procedure (GP-21) for rose bengal sensitised photooxygenation of 1,5-dihydroxynaphthalene 98 (synthesis of Juglone 99) in the falling film microreactor:

1,5-dihydroxynaphthalene (mg; 60 μmol) and rose bengal (mg; 3 μmol) were dissolved in 6 ml of isopropanol or isopropanol/water mixture (9:1). The solvent was preliminary degassed with nitrogen for 15 min. The reaction mixture was prepared in the amber vial and was sonicated for 30 min. The experimental solution was pumped directly from the amber vial to the falling film microreactor by the programmable rotary pump. The volumetric flow rate of liquid phase was preset by the pump. The solution was then distributed to substreams, which created a thin fluid film inside the microchannels. The gas phase – air was fed into the reactor chamber with constant flow rate of 26.5 ml/min and moved counter currently to the liquid flow. A single fluorescent lamp (18 W) was used for irradiation. The reaction solution was continually evacuated from the falling film microreactor into a collection round bottom flask or was transported to the first rotary pump and recirculated through the microreactor again until the necessary residence time was reached. During the reaction, the reactor was kept at a single temperature by driving cold tap water through the heat exchanger positioned on the back side of the reaction plate. When the experiment was completed, the whole system was cleaned with pure methanol. The solvent from the collected product was removed by rotary evaporation. The obtained residue was analyzed by ^{1}H-NMR spectroscopy to determine the conversion. The signal integration for the quinonoid protons of Juglone (2 doublets with an integration of 2) was compared to the signal integration for the two protons of 1,5-dihydroxynaphthalene represented by the most upfield doublet (integration of 2). The pure products were not isolated in these experiments.

Experiment 169

Effect of rose bengal concentration of 0.49 mM on the Juglone synthesis (OS-81)

General procedure (GP-21) was followed using 1,5-dihydroxynaphthalene (10 mg; 60 μmol), rose bengal (3 mg; 3 μmol) and isopropanol (6 ml) as solvent. The prepared reaction mixture was recirculated through the falling film microreactor 5 times at a volumetric flow rate of (rotary pump) 0.08 ml/min which corresponded to a single residence time of 32 sec and gave a total residence time of 160 sec. The obtained crude product was analysed by ^{1}H-NMR. The composition of **98** to product **99** was calculated from the ^{1}H-NMR integration to be 90:10.

For ^{1}H-NMR data of product **99** see experiment 207.

Experiment 170

Effect of double concentration of rose bengal of 0.98 mM on the Juglone synthesis (OS-82)

General procedure (GP-21) was followed using 1,5-dihydroxynaphthalene (10 mg; 60 μmol), rose bengal (6 mg; 6 μmol) and isopropanol (6 ml) as solvent. The prepared reaction mixture was recirculated through the falling film microreactor 5 times at a volumetric flow rate of (rotary pump) 0.08 ml/min which corresponded to a single residence time of 32 sec and gave a total residence time of 160 sec. The obtained crude product was analysed by ^{1}H-NMR. The composition of **98** to product **99** was calculated from the ^{1}H-NMR integration to be 79:21.

For ^{1}H-NMR data of product **99** see experiment 207.

Experiment 171

Effect of halved concentration of rose bengal of 0.25 mM on the Juglone synthesis (OS-83)

General procedure (GP-21) was followed using 1,5-dihydroxynaphthalene (5 mg; 30 μmol), rose bengal (1.5 mg; 1.5 μmol) and isopropanol (6 ml) as solvent. The prepared reaction mixture was recirculated through the falling film microreactor 5 times at a volumetric flow rate of (rotary pump) 0.08 ml/min which corresponded to a single residence time of 32 sec and gave a total residence time of 160 sec. The obtained crude product was analysed by ^{1}H-NMR. The composition of **98** to product **99** was calculated from the ^{1}H-NMR integration to be 82:18.

For ^{1}H-NMR data of product **99** see experiment 207.

Experiment 172

Effect of solvent on the Juglone synthesis (OS-84)

General procedure (GP-21) was followed using 1,5-dihydroxynaphthalene (10 mg; 60 μmol), rose bengal (3 mg; 3 μmol) and isopropanol/water mixture (9:1) as solvent. The prepared reaction mixture was recirculated through the falling film microreactor 5 times at volumetric flow rate of (rotary pump) 0.08 ml/min which corresponded to a single residence time of 32 sec and gave a total residence time of 160 sec. The obtained crude

product was analysed by ^{1}H-NMR. The composition of **98** to product **99** was calculated from the ^{1}H-NMR integration to be 69:31.

For ^{1}H-NMR data of product **99** see experiment 207.

Experiment 173

Effect of the light source on the Juglone synthesis (OS-87)

General procedure (GP-21) was followed, with one variation, using 1,5-dihydroxynaphthalene (10 mg; 60 μmol), rose bengal (3 mg; 3 μmol) and isopropanol/water mixture (9:1) as solvent. In this experiment an array of 60 white LEDs with a total optical power of 3 W was used for irradiation instead of a single fluorescent lamp. The prepared reaction mixture was recirculated through the falling film microreactor 5 times at a volumetric flow rate of (rotary pump) 0.08 ml/min which corresponded to a single residence time of 32 sec and gave a total residence time of 160 sec. The obtained crude product was analysed by ^{1}H-NMR. The composition of **98** to product **99** was calculated from the ^{1}H-NMR integration to be 91:9.

For ^{1}H-NMR data of product **99** see experiment 207.

Experiment 174

Effect of residence time on the Juglone synthesis (OS-88)

General procedure (GP-21) was followed, with one variation, using 1,5-dihydroxynaphthalene (10 mg; 60 μmol), rose bengal (3 mg; 3 μmol) and isopropanol/water mixture (9:1) as solvent. In this experiment an array of 60 white LEDs with a total optical power of 3 W was used for irradiation instead of a single fluorescent lamp. The prepared reaction mixture was recirculated through the falling film microreactor 10 times at a volumetric flow rate of (rotary pump) 0.16 ml/min which corresponded to a single residence time of 20 sec and gave a total residence time of 200 sec. The obtained crude product was analysed by ^{1}H-NMR. The composition of **98** to product **99** was calculated from the ^{1}H-NMR integration to be 92:8.

For ^{1}H-NMR data of product **99** see experiment 207.

9.4.2 General procedure (GP-22) for rose bengal sensitised photooxygenation of 1,5-dihydroxynaphthalene 98 (synthesis of Juglone 99) in the slug flow column reactor:

1,5-dihydroxynaphthalene (mg; 100 µmol) and rose bengal (mg; 5 µmol) were dissolved in a preliminary degassed 10 ml of the corresponding alcohol or alcohol/water mixture (9:1) and sonicated for 30 min. The prepared reaction mixture was filled into the glass tube by vacuum (filling height: approx. 60 cm) and was continuously purged with air bubbles and irradiated by two fluorescent lamps (60 W each). The air was fed into the glass tube at certain flow rates via the appropriate capillary aeration nozzle attached to the bottom orifice of the tube. The air increased the solution level to approx. 145 cm. After a set irradiation time, the reaction mixture was collected into a round bottom flask, solvent was evaporated and the resulting residue was analysed by ^{1}H-NMR to determine the conversion rate. The signal integration for the quinonoid protons of Juglone (2 doublets with an integration of 2) was compared to the signal integration for the two protons of 1,5-dihydroxynaphthalene represented by the most upfield doublet (integration of 2). In some experiments the pure products were isolated by column chromatography on silica gel with suitable mobile phase.

Experiment 175

Effect of solvent on the photooxygenation of 1,5-dihydroxynaphthalene (OS-115)

General procedure (GP-22) was followed using 1,5-dihydroxynaphthalene (16 mg; 100 µmol), rose bengal (5 mg; 5 µmol) and isopropanol as solvent. A fused silica capillary TSP100200 with ID of 100 µm was used as aeration nozzle. The flow rate of air was 7-10 cm^{3}/min, residence time was 30 min. The obtained crude product was analysed by ^{1}H-NMR. The composition of **98** to product **99** was calculated from the ^{1}H-NMR integration to be 63:37.

For ^{1}H-NMR data of product **99** see experiment 207.

Experiment 176

Effect of solvent on the photooxygenation of 1,5-dihydroxynaphthalene (OS-116)

General procedure (GP-22) was followed using 1,5-dihydroxynaphthalene (16 mg; 100 µmol), rose bengal (5 mg; 5 µmol) and isopropanol as solvent. A fused silica capillary TSP100200 with ID of 100 µm was used as aeration nozzle. The flow rate of air was 7-

10 cm^3/min, residence time was 1 hour. The obtained crude product was analysed by ^{1}H-NMR. The composition of **98** to product **99** was calculated from the ^{1}H-NMR integration to be 48:52.

For ^{1}H-NMR data of product **99** see experiment 207.

Experiment 177

Effect of solvent on the photooxygenation of 1,5-dihydroxynaphthalene (OS-123)

General procedure (GP-22) was followed using 1,5-dihydroxynaphthalene (16 mg; 100 μmol), rose bengal (5 mg; 5 μmol) and isopropanol as solvent. A fused silica capillary TSP100200 with ID of 100 μm was used as aeration nozzle. The flow rate of air was 7-10 cm^3/min, residence time was 3 hours. The obtained crude product was analysed by ^{1}H-NMR. The conversion was found to be 100%.

For ^{1}H-NMR data of product **99** see experiment 207.

Experiment 178

Effect of solvent on the photooxygenation of 1,5-dihydroxynaphthalene (OS-133)

General procedure (GP-22) was followed using 1,5-dihydroxynaphthalene (16 mg; 100 μmol), rose bengal (5 mg; 5 μmol) and isopropanol/water mixture (9:1) as solvent. A fused silica capillary TSP100200 with ID of 100 μm was used as aeration nozzle. The flow rate of air was 7-10 cm^3/min, residence time was 30 min. The obtained crude product was analysed by ^{1}H-NMR. The composition of **98** to product **99** was calculated from the ^{1}H-NMR integration to be 45:55.

For ^{1}H-NMR data of product **99** see experiment 207.

Experiment 179

Effect of solvent on the photooxygenation of 1,5-dihydroxynaphthalene (OS-129)

General procedure (GP-22) was followed using 1,5-dihydroxynaphthalene (16 mg; 100 μmol), rose bengal (5 mg; 5 μmol) and isopropanol/water mixture (9:1) as solvent. A fused silica capillary TSP100200 with ID of 100 μm was used as aeration nozzle. The flow rate of air was 7-10 cm^3/min, residence time was 1.5 hour. The obtained crude product was analysed by ^{1}H-NMR. The composition of **98** to product **99** was calculated from the ^{1}H-NMR integration to be 18:82.

For ^{1}H-NMR data of product **99** see experiment 207.

Experiment 180

Effect of solvent on the photooxygenation of 1,5-dihydroxynaphthalene (OS-128)

General procedure (GP-22) was followed using 1,5-dihydroxynaphthalene (16 mg; 100 μmol), rose bengal (5 mg; 5 μmol) and isopropanol/water mixture (9:1) as solvent. A fused silica capillary TSP100200 with ID of 100 μm was used as aeration nozzle. The flow rate of air was 7-10 cm^3/min, residence time was 2 hours. The obtained crude product was analysed by ^{1}H-NMR. The composition of **98** to product **99** was calculated from the ^{1}H-NMR integration to be 9:91.

For ^{1}H-NMR data of product **99** see experiment 207.

Experiment 181

Effect of solvent on the photooxygenation of 1,5-dihydroxynaphthalene (OS-130)

General procedure (GP-22) was followed using 1,5-dihydroxynaphthalene (16 mg; 100 μmol), rose bengal (5 mg; 5 μmol) and isopropanol/water mixture (9:1) as solvent. A fused silica capillary TSP100200 with ID of 100 μm was used as aeration nozzle. The flow rate of air was 7-10 cm^3/min, residence time was 2.5 hours. The obtained crude product was analysed by ^{1}H-NMR. The conversion was found to be 100%.

For ^{1}H-NMR data of product **99** see experiment 207.

Experiment 182

Effect of solvent on the photooxygenation of 1,5-dihydroxynaphthalene (OS-139)

General procedure (GP-22) was followed using 1,5-dihydroxynaphthalene (16 mg; 100 μmol), rose bengal (5 mg; 5 μmol) and *tert*-amyl alcohol/water mixture (9:1) as solvent. A fused silica capillary TSP100200 with ID of 100 μm was used as aeration nozzle. The flow rate of air was 7-10 cm^3/min, residence time was 2 hours. The obtained crude product was analysed by ^{1}H-NMR. The composition of **98** to product **99** was calculated from the ^{1}H-NMR integration to be 9:91.

For ^{1}H-NMR data of product **99** see experiment 207.

Experiment 183

Effect of solvent on the photooxygenation of 1,5-dihydroxynaphthalene (OS-140)

General procedure (GP-22) was followed using 1,5-dihydroxynaphthalene (16 mg; 100 μmol), rose bengal (5 mg; 5 μmol) and ethanol/water mixture (9:1) as solvent. A fused silica capillary TSP100200 with ID of 100 μm was used as aeration nozzle. The flow rate of air was 7-10 cm^3/min, residence time was 2 hours. The obtained crude product was analysed by ^{1}H-NMR. The composition of **98** to product **99** was calculated from the ^{1}H-NMR integration to be 12:88.

For ^{1}H-NMR data of product **99** see experiment 207.

Experiment 184

Effect of solvent on the photooxygenation of 1,5-dihydroxynaphthalene (OS-141)

General procedure (GP-22) was followed using 1,5-dihydroxynaphthalene (16 mg; 100 μmol), rose bengal (5 mg; 5 μmol) and methanol/water mixture (9:1) as solvent. A fused silica capillary TSP100200 with ID of 100 μm was used as aeration nozzle. The flow rate of air was 7-10 cm^3/min, residence time was 2 hours. The obtained crude product was analysed by ^{1}H-NMR. The composition of **98** to product **99** was calculated from the ^{1}H-NMR integration to be 25:75.

For ^{1}H-NMR data of product **99** see experiment 207.

Experiment 185

Effect of bubble flow pattern on the photooxygenation of 1,5-dihydroxynaphthalene (OS-407)

General procedure (GP-22) was followed using 1,5-dihydroxynaphthalene (16 mg; 100 μmol), rose bengal (5 mg; 5 μmol) and isopropanol/water mixture (9:1) as solvent. A fused silica capillary TSP050150 with ID of 50 μm was used as aeration nozzle. The flow rate of air was 10 cm^3/min, residence time was 3 hours. The obtained crude product was analysed by ^{1}H-NMR. The composition of **98** to product **99** was calculated from the ^{1}H-NMR integration to be 51:49.

For ^{1}H-NMR data of product **99** see experiment 207.

Experiment 186

Effect of bubble flow pattern on the photooxygenation of 1,5-dihydroxynaphthalene (OS-132)

The same as *experiment 179* (OS-129).

Experiment 187

Effect of bubble flow pattern on the photooxygenation of 1,5-dihydroxynaphthalene (OS-409)

General procedure (GP-22) was followed using 1,5-dihydroxynaphthalene (16 mg; 100 μmol), rose bengal (5 mg; 5 μmol) and isopropanol/water mixture (9:1) as solvent. A fused silica capillary TSP100200 with ID of 100 μm was used as aeration nozzle. The flow rate of air was 10 cm^3/min, residence time was 3 hours. The obtained crude product was analysed by ^{1}H-NMR. The conversion was found to be 100%.

For ^{1}H-NMR data of product **99** see experiment 207.

Experiment 188

Effect of slug flow pattern on the photooxygenation of 1,5-dihydroxynaphthalene (OS-224)

General procedure (GP-22) was followed using 1,5-dihydroxynaphthalene (16 mg; 100 μmol), rose bengal (5 mg; 5 μmol) and isopropanol/water mixture (9:1) as solvent. A PTFE capillary with ID of 500 μm was used as aeration nozzle. The flow rate of air was 20 cm^3/min, residence time was 1 hour. The obtained crude product was analysed by ^{1}H-NMR. The composition of **98** to product **99** was calculated from the ^{1}H-NMR integration to be 9:91.

For ^{1}H-NMR data of product **99** see experiment 207.

Experiment 189

Effect of slug flow pattern on the photooxygenation of 1,5-dihydroxynaphthalene (OS-147)

General procedure (GP-22) was followed using 1,5-dihydroxynaphthalene (16 mg; 100 μmol), rose bengal (5 mg; 5 μmol) and *tert*-amyl alcohol/water mixture (9:1) as solvent. A PTFE capillary with ID of 500 μm was used as aeration nozzle. The flow rate of air

was 20 cm^3/min, residence time was 1 hour. The obtained crude product was analysed by ^{1}H-NMR. The conversion was found to be 100%.

For ^{1}H-NMR data of product **99** see experiment 207.

Experiment 190

Effect of rose bengal concentration of 0.49 mM on the photooxygenation of 1,5-dihydroxynaphthalene (OS-131)

The same as *experiment 180* (OS-128).

Experiment 191

Effect of double concentration of rose bengal of 0.98 mM on the photooxygenation of 1,5-dihydroxynaphthalene (OS-137)

General procedure (GP-22) was followed using 1,5-dihydroxynaphthalene (16 mg; 100 μmol), rose bengal (10 mg; 10 μmol) and isopropanol/water mixture (9:1) as solvent. A fused silica capillary TSP100200 with ID of 100 μm was used as aeration nozzle. The flow rate of air was 10 cm^3/min, residence time was 2 hours. The obtained crude product was analysed by ^{1}H-NMR. The composition of **98** to product **99** was calculated from the ^{1}H-NMR integration to be 12:88.

For ^{1}H-NMR data of product **99** see experiment 207.

Experiment 192

Effect of halved concentration of rose bengal of 0.25 mM on the photooxygenation of 1,5-dihydroxynaphthalene (OS-138)

General procedure (GP-22) was followed using 1,5-dihydroxynaphthalene (16 mg; 100 μmol), rose bengal (3 mg; 2.5 μmol) and isopropanol/water mixture (9:1) as solvent. A fused silica capillary TSP100200 with ID of 100 μm was used as aeration nozzle. The flow rate of air was 10 cm^3/min, residence time was 2 hours. The obtained crude product was analysed by ^{1}H-NMR. The composition of **98** to product **99** was calculated from the ^{1}H-NMR integration to be 8:92.

For ^{1}H-NMR data of product **99** see experiment 207.

Experiment 193

Effect of rose bengal concentration of 0.49 mM on the photooxygenation of 1,5-dihydroxynaphthalene (OS-143)

General procedure (GP-22) was followed using 1,5-dihydroxynaphthalene (16 mg; 100 μmol), rose bengal (5 mg; 5 μmol) and *tert*-amyl alcohol/water mixture (9:1) as solvent. A PTFE capillary with ID of 500 μm was used as aeration nozzle. The flow rate of air was 20 cm^3/min, residence time was 30 min. The obtained crude product was analysed by ^{1}H-NMR. The composition of **98** to product **99** was calculated from the ^{1}H-NMR integration to be 13:87.

For ^{1}H-NMR data of product **99** see experiment 207.

Experiment 194

Effect of halved concentration of rose bengal of 0.25 mM on the photooxygenation of 1,5-dihydroxynaphthalene (OS-177)

General procedure (GP-22) was followed using 1,5-dihydroxynaphthalene (16 mg; 100 μmol), rose bengal (3 mg; 2.5 μmol) and *tert*-amyl alcohol/water mixture (9:1) as solvent. A PTFE capillary with ID of 500 μm was used as aeration nozzle. The flow rate of air was 20 cm^3/min, residence time was 30 min. The obtained crude product was analysed by ^{1}H-NMR. The composition of **98** to product **99** was calculated from the ^{1}H-NMR integration to be 17:83.

For ^{1}H-NMR data of product **99** see experiment 207.

Experiment 195

Effect of methylene blue concentration of 0.25 mM on the photooxygenation of 1,5-dihydroxynaphthalene (OS-176)

General procedure (GP-22) was followed using 1,5-dihydroxynaphthalene (16 mg; 100 μmol), methylene blue (1 mg; 2.5 μmol) and *tert*-amyl alcohol/water mixture (9:1) as solvent. A PTFE capillary with ID of 500 μm was used as aeration nozzle. The flow rate of air was 20 cm^3/min, residence time was 30 min. The obtained crude product was analysed by ^{1}H-NMR. The composition of **98** to product **99** was calculated from the ^{1}H-NMR integration to be 44:56.

For ^{1}H-NMR data of product **99** see experiment 207.

Experiment 196

The photooxygenation of 1,5-dihydroxynaphthalene under direct excitation (OS-408)

General procedure (GP-22) was followed with one variation, using 1,5-dihydroxynaphthalene (16 mg; 100 μmol) and *tert*-amyl alcohol/water mixture (9:1) as solvent. In this experiment the rose bengal or any other sensitizers were not added to the experimental solution. A PTFE capillary with ID of 500 μm was used as aeration nozzle. The flow rate of air was 20 cm^3/min, residence time was 30 min. The obtained crude product was analysed by ^{1}H-NMR. The composition of **98** to product **99** was calculated from the ^{1}H-NMR integration to be 92:8.

For ^{1}H-NMR data of product **99** see experiment 207.

Experiment 197

The photooxygenation of 1,5-dihydroxynaphthalene under direct excitation (OS-160)

General procedure (GP-22) was followed with one variation, using 1,5-dihydroxynaphthalene (16 mg; 100 μmol) and *tert*-amyl alcohol/water mixture (9:1) as solvent. In this experiment the rose bengal or any other sensitizers were not added to the experimental solution. A PTFE capillary with ID of 500 μm was used as aeration nozzle. The flow rate of air was 20 cm^3/min, residence time was 1 hour. The obtained crude product was analysed by ^{1}H-NMR. The composition of **98** to product **99** was calculated from the ^{1}H-NMR integration to be 65:35.

For ^{1}H-NMR data of product **99** see experiment 207.

Experiment 198

Effect of the irradiation time on the photooxygenation of 1,5-dihydroxynaphthalene (OS-151)

General procedure (GP-22) was followed using 1,5-dihydroxynaphthalene (16 mg; 100 μmol), rose bengal (5 mg; 5 μmol) and *tert*-amyl alcohol/water mixture (9:1) as solvent. A PTFE capillary with ID of 500 μm was used as aeration nozzle. The flow rate of air was 90 cm^3/min, residence time was 10 min. The obtained crude product was analysed

by ^{1}H-NMR. The composition of **98** to product **99** was calculated from the ^{1}H-NMR integration to be 53:47.

For ^{1}H-NMR data of product **99** see experiment 207.

Experiment 199

Effect of the irradiation time on the photooxygenation of 1,5-dihydroxynaphthalene (OS-158)

General procedure (GP-22) was followed using 1,5-dihydroxynaphthalene (16 mg; 100 μmol), rose bengal (5 mg; 5 μmol) and *tert*-amyl alcohol/water mixture (9:1) as solvent. A PTFE capillary with ID of 500 μm was used as aeration nozzle. The flow rate of air was 90 cm^{3}/min, residence time was 15 min. The obtained crude product was analysed by ^{1}H-NMR. The composition of **98** to product **99** was calculated from the ^{1}H-NMR integration to be 36:64.

For ^{1}H-NMR data of product **99** see experiment 207.

Experiment 200

Effect of the irradiation time on the photooxygenation of 1,5-dihydroxynaphthalene (OS-157)

General procedure (GP-22) was followed using 1,5-dihydroxynaphthalene (16 mg; 100 μmol), rose bengal (5 mg; 5 μmol) and *tert*-amyl alcohol/water mixture (9:1) as solvent. A PTFE capillary with ID of 500 μm was used as aeration nozzle. The flow rate of air was 90 cm^{3}/min, residence time was 30 min. The obtained crude product was analysed by ^{1}H-NMR. The composition of **98** to product **99** was calculated from the ^{1}H-NMR integration to be 11:89.

For ^{1}H-NMR data of product **99** see experiment 207.

Experiment 201

Effect of the irradiation time on the photooxygenation of 1,5-dihydroxynaphthalene (OS-159)

General procedure (GP-22) was followed using 1,5-dihydroxynaphthalene (16 mg; 100 μmol), rose bengal (5 mg; 5 μmol) and *tert*-amyl alcohol/water mixture (9:1) as solvent. A PTFE capillary with ID of 500 μm was used as aeration nozzle. The flow rate of air

was 90 cm^3/min, residence time was 1 hour. The obtained crude product was analysed by ^{1}H-NMR. The conversion was found to be 100%.

For ^{1}H-NMR data of product **99** see experiment 207.

Experiment 202

Effect of the irradiation time on the photooxygenation of 1,5-dihydroxynaphthalene (OS-161)

The same as *experiment 201* (OS-159).

Experiment 203

Effect of the irradiation time on the photooxygenation of 1,5-dihydroxynaphthalene (OS-150)

General procedure (GP-22) was followed using 1,5-dihydroxynaphthalene (16 mg; 100 μmol), rose bengal (5 mg; 5 μmol) and *tert*-amyl alcohol/water mixture (9:1) as solvent. A PTFE capillary with ID of 500 μm was used as aeration nozzle. The flow rate of air was 20 cm^3/min, residence time was 10 min. The obtained crude product was analysed by ^{1}H-NMR. The composition of **98** to product **99** was calculated from the ^{1}H-NMR integration to be 54:46.

For ^{1}H-NMR data of product **99** see experiment 207.

Experiment 204

Effect of the irradiation time on the photooxygenation of 1,5-dihydroxynaphthalene (OS-149)

The same as *experiment 193* (OS-143).

Experiment 205

Effect of the irradiation time on the photooxygenation of 1,5-dihydroxynaphthalene (OS-145)

General procedure (GP-22) was followed using 1,5-dihydroxynaphthalene (16 mg; 100 μmol), rose bengal (5 mg; 5 μmol) and *tert*-amyl alcohol/water mixture (9:1) as solvent. A PTFE capillary with ID of 500 μm was used as aeration nozzle. The flow rate of air

was 10 cm^3/min, residence time was 1 hour. The obtained crude product was analysed by ^{1}H-NMR. The conversion was found to be 100%.

For ^{1}H-NMR data of product **99** see experiment 207.

Experiment 206

Effect of the irradiation time on the photooxygenation of 1,5-dihydroxynaphthalene (OS-146)

General procedure (GP-22) was followed using 1,5-dihydroxynaphthalene (16 mg; 100 μmol), rose bengal (5 mg; 5 μmol) and *tert*-amyl alcohol/water mixture (9:1) as solvent. A PTFE capillary with ID of 500 μm was used as aeration nozzle. The flow rate of air was 10 cm^3/min, residence time was 1.5 hour. The obtained crude product was analysed by ^{1}H-NMR. The conversion was found to be 100%.

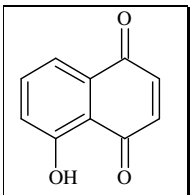
For ^{1}H-NMR data of product **99** see experiment 207.

Experiment 207

Scale-up synthesis of Juglone 99 (OS-224)

General procedure (GP-22) was followed with the variation of preparing a 30 ml experimental solution and performing three individual irradiations under identical conditions (10 ml each). The experimental solution was prepared using 1,5-dihydroxynaphthalene (48 mg; 300 μmol), rose bengal (15 mg; 15 μmol) and isopropanol/water mixture (9:1) as solvent (30 ml). A PTFE capillary with ID of 500 μm was used as the aeration nozzle. The flow rate of air was 10 cm^3/min, residence time was 1 hour for each irradiation and total experimental time was 3 hours. The collected crude products were combined and the solvent was removed by rotary evaporation. The obtained crude product was analysed by ^{1}H-NMR. The conversion was found to be 91%. The crude product was further purified by column chromatography using chloroform as a mobile phase. The isolated yield of **99** was found to be 28 mg (0.16 mmol, 54%). Both ^{1}H-NMR and ^{13}C-NMR confirmed this was the pure product.

Analytical data of *5-hydroxynaphthalene-1,4-dione* (99)



99

$C_{10}H_6O_3$
Mol. Wt.: 174.2 g/mol

TLC: *Rf* = 0.74 (chloroform)

Melting point (orange needle crystals)**:** 152°C (Lit.[260]: 151-154 °C)

^{1}H–NMR: (400 MHz, Acetone-d_6)

δ (ppm) = 7.04 (d, ^{3}J = 10.4 Hz, 1 H, H_{quin}), 7.08 (d, ^{3}J = 10.4 Hz, 1 H, H_{quin}), 7.33 (d, ^{3}J = 8.4 Hz, ^{4}J = 1.2 Hz, 1 H, $H_{arom.}$), 7.58 (d, ^{3}J = 7.6 Hz, ^{4}J = 1.2 Hz, 1 H, $H_{arom.}$), 7.78 (dd, ^{3}J = 7.6 Hz, 8.4 Hz, 1 H, $H_{arom.}$), 11.92 (br. s, 1 H, OH).

^{13}C–NMR: (100 MHz, Acetone-d_6)

δ (ppm) = 114.0 (s, 1 C, Cq_{arom}), 118.1 (s, 1 C, CH_{arom}), 123.5 (s, 1 C, CH_{arom}), 130.8 (s, 1 C, Cq_{arom}), 135.5 (s, 1 C, CH_{arom}), 137.6 (s, 1 C, CH_{quin}), 138.6 (s, 1 C, CH_{quin}), 160.6 (s, 1 C, COH), 183.2 (s, 1 C, C=O), 189.3 (s, 1 C, C=O).

Experiment 208

Scale-up synthesis of Juglone 99 (OS-194)

General procedure (GP-22) was followed with the variation of preparing a 30 ml experimental solution and performing three individual irradiations under identical conditions (10 ml each). The experimental solution was prepared using 1,5-dihydroxynaphthalene (48 mg; 300 µmol), rose bengal (15 mg; 15 µmol) and *tert*-amyl alcohol/water mixture (9:1) as solvent (30 ml). A PTFE capillary with ID of 500 µm was used as the aeration nozzle. The flow rate of air was 10 cm^3/min, residence time was 1 hour for each irradiation and total experimental time was 3 hours. The collected crude products were combined and the solvent was removed by rotary evaporation. The obtained crude product was analysed by ^{1}H-NMR. The conversion was found to be 100%. The crude product was further purified by column chromatography using chloroform as a mobile phase. The isolated yield of **99** was found to be 37 mg (0.21 mmol, 70%). Both ^{1}H-NMR and ^{13}C-NMR confirmed this was the pure product.

For ^{1}H-NMR data of product **99** see experiment 207.

Experiment 209

Photooxygenation of 2-furaldehyde 100 (OS-227)

General procedure (GP-22) was followed using 2-furaldehyde (10 mg; 100 μmol), rose bengal (5 mg; 5 μmol) and *tert*-amyl alcohol/water mixture (9:1) as solvent. A PTFE capillary with ID of 500 μm was used as aeration nozzle. The flow rate of air was 10 cm^3/min, residence time was 1 hour. The obtained crude product was analysed by ^{1}H-NMR. The conversion was found to be 100%. No peaks of 2-furaldehyde were found however small peaks of unidentified impurities (below 5%) were detected. The attempt to isolate pure product wasn't made in this experiment. The ^{1}H-NMR of crude 5-hydroxy-*5H*-furan-2-one **101** was identical with those reported in literature.[261,272]

Experiment 210

Photooxygenation of α-terpinene 39 (OS-225)

General procedure (GP-22) was followed using α-terpinene (14 mg; 100 μmol), rose bengal (5 mg; 5 μmol) and *tert*-amyl alcohol/water mixture (9:1) as solvent. A PTFE capillary with ID of 500 μm was used as aeration nozzle. The flow rate of air was 10 cm^3/min, residence time was 1 hour. The obtained crude product was analysed by ^{1}H-NMR. The conversion was found to be 100%. The crude product was further purified by column chromatography using a solvent mixture of ethyl acetate:n-hexane (1:3). The isolated yield of **40** was found to be 12 mg (0.07 mmol, 71%). Both ^{1}H-NMR and ^{13}C-NMR confirmed this was the pure product.

For ^{1}H-NMR data of product **40** see paragraph 9.3.1.2.

Experiment 211

Photooxygenation of (*S*)-(–)-β-citronellol 44 (OS-195)

General procedure (GP-22) was followed using (*S*)-(–)-β-citronellol (16 mg; 100 μmol), rose bengal (5 mg; 5 μmol) and *tert*-amyl alcohol/water mixture (9:1) as solvent. A PTFE capillary with ID of 500 μm was used as aeration nozzle. The flow rate of air was 10 cm^3/min, residence time was 1 hour. The obtained crude product was analysed by ^{1}H-NMR. The conversion was found to be 100% and a mixture of the regioisomeric hydroperoxides **45** and **46** in a ratio 1.1:1 was isolated. The ratio between diastereoisomers **46** was determined to be 1:1. The signal integration for the hydroperoxide proton of **45** (singlet at 8.30 ppm) was compared to the signal integration

for the two hydroperoxide protons of diastereoisomers **46** (singlet at 8.66 and singlet at 8.78). The attempt to isolate pure isomers wasn't made in this experiment. The ^{1}H-NMR of crude mixture of 7-hydroperoxy-3,7-dimethyloct-5-en-1-ol and 6-hydroperoxy-3,7-dimethyloct-7-en-1-ol matched the ^{1}H-NMR of these pure isomers reported in the literature.[117,273]

References

10. References

[1] P. J. Dunn, S. Galvin, K. Hettenbach, The development of an environmentally benign synthesis of sildenafil citrate (Viagra™) and its assessment by Green Chemistry metrics, *Green Chem*., **2004**, 6, 43–48.

[2] J. Dewulf, G. Van der Vorst, W. Aelterman, B. De Witte, H. Vanbaelen, H. Van Langenhove, Integral resource management by exergy analysis for the selection of a separation process in the pharmaceutical industry, *Green Chem.*, **2007**, 9, 785–791.

[3] D. Y. Wu, B. Chen, X. G. Fu, L. Z. Wu, L. P. Zhang and C. H. Tung, Nanosized particles of organically modified silica as microreactors to enhance the regioselectivity in the photocycloaddition of 9-substituted anthracenes, *Org. Lett.*, **2003**, 5, 1075–1077.

[4] E. L. Clennan, W. H. Zhou and J. Chan, Mechanistic organic chemistry in a microreactor. Zeolite-controlled photooxidations of organic sulfides, *J. Org. Chem.*, **2002**, 67, 9368–9378.

[5] Z. Yuan, S. Zheng, Y. Zeng, J. Chen, Y. Han, Y. Li and Y. Li, Photosensitized oxidation of alkenes with dendrimers as microreactors: controllable selectivity between energy and electron transfer pathway, *New J. Chem*., **2010**, 34, 718–722.

[6] D. G. Shchukin, E. Ustinovich, D. V. Sviridov, Y. M. Lvov and G. B. Sukhorukov, Photocatalytic microreactors based on TiO_2-modified polyelectrolyte multilayer capsules, *Photochem. Photobiol. Sci.*, **2003**, 2, 975–977.

[7] S. S. Lee, A. M. Rideau and L. B. McGown, Toward building a better microreactor: Increasing microenvironmental diversity in AOT reversed micelles using a bile salt cosurfactant, *J. Phys. Chem.*, **1996**, 100, 5880–5887.

[8] E. Verpoorte, Microfluidic chips for clinical and forensic analysis, *Electrophoresis*, **2002**, 23 (5), 677–712.

[9] D. O. Cowan and R. L. Drisko, Elements of Organic Photochemistry, *Plenum Press: New York*, **1976**.

[10] H. D. Roth, The beginnings of organic photochemistry, *Ang. Chem., Int. Ed.*, **1989**, 28, 1193–1207.

[11] G. Nebbia and G. B. Kauffman, Prophet of solar energy: a retrospective view of Giacomo Luigi Ciamician (1857–1922), the founder of Green Chemistry, on the 150th anniversary of his birth, *Chem. Educat.*, **2007**, 12, 362–369.

[12] E. Singer, Pioneers in photochemistry: Alexander Schönberg (1892–1985), *EPA-Newslett.*, **1986**, 1–11.

[13] K. Schaffner, Günther Otto Schenck (1913–2003): A pioneer of radiation chemistry, *Angew. Chem., Int. Ed.*, **2003**, 42, 2932–2933.

[14] H. D. Roth, Twentieth century developments in photochemistry. Brief historical sketches, *Pure Appl. Chem.*, **2001**, 73, 395–403.

[15] G. Ciamician, The photochemistry of the future, *Science*, **1912**, 36, 385–394.

[16] A. G. Griesbeck, J. Mattay (V. Ramamurthy, K. S. Schanze, Eds.), Synthetic Organic Photochemistry (Molecular and Supramolecular Photochemistry), Vol. 12; *Marcel Dekker: New York*, **2005**.

[17] N. Hoffmann, Photochemical reactions as key steps in organic synthesis, *Chem. Rev.*, **2008**, 108, 1052–1103.

[18] *Molecular and Supramolecular Photochemistry*; V. Ramamurthy, K. S. Schanze, Eds.; *Marcel Dekker: New York*, **1997**; Vol. 1: Organic Photochemistry. *Molecular and Supramolecular Photochemistry*; V. Ramamurthy, K. S. Schanze, Eds.; *Marcel Dekker: New York*, **1998**; Vol. 2: Organic and Inorganic Photochemistry. *Molecular and Supramolecular Photochemistry*; V. Ramamurthy, K. S. Schanze, Eds.; *Marcel Dekker: New York*, **1999**; Vol. 3: Organic Molecular Photochemistry. *Molecular and Supramolecular Photochemistry*; V. Ramamurthy, K. S. Schanze, Eds.; *Marcel Dekker: New York*, **2000**; Vol. 6: Organic, Physical and Materials Photochemistry. *Molecular and Supramolecular Photochemistry*; V. Ramamurthy, K. S. Schanze, Eds.; *Marcel Dekker: New York*, **2001**; Vol. 8: Understanding and Manipulating Excited-State Processes. *Molecular and Supramolecular Photochemistry*; V. Ramamurthy, K. S. Schanze, Eds.; *Marcel Dekker: New York*, **2003**; Vol. 9: Photochemistry of Organic Molecules in Isotropic and Anisotropic Media. *Molecular and Supramolecular Photochemistry*; V. Ramamurthy, K. S. Schanze, Eds.; *Marcel Dekker: New York*, **2004**; Vol. 11: Chiral Photochemistry. *Molecular and Supramolecular Photochemistry*; Ramamurthy, K. S. Schanze, Eds.; *Marcel Dekker: New York*, **2002**; A. G. Griesbeck, J. Mattay; Vol. 12: Synthetic Organic Photochemistry. *Molecular and Supramolecular Photochemistry*; V. Ramamurthy, K. S. Schanze, Eds.; *Marcel Dekker: New York*, **2005**.

[19] G. Stochel, M. Brindell, W. Macyk, Z. Stasicka, K. Szacilowski, Bioinorganic Photochemistry, *Wiley: Chichester*, **2009**.

[20] P. Klán and J. Wirz, Photochemistry of organic compounds: from concepts to practice, *Wiley: Chichester*, **2009**.

[21] E. E. Coyle and M. Oelgemöller, Micro-photochemistry: photochemistry in microstructured reactors. The new photochemistry of the future?, *Photochem. Photobiol. Sci.*, **2008**, 7, 1313–1322.

[22] J. W. Verhoeven, Glossary of terms used in photochemistry (IUPAC Recommendations 1996), *Pure Appl. Chem*., **1996**, 68, 2223–2286.

[23] http://www.wikipidea.com

[24] P. Suppan, Principles of Photochemistry, *Royal Society of Chemistry: Cambridge*, **1973**.

[25] D. C. Neckers, Mechanistic Organic Photochemistry, *Reinhold Publishing Corp.: New York,* **1967**.

[26] P. J. Wagner, R. J. Truman, A. E. Puchalski, R. Wake, Extent of charge transfer in the photoreduction of phenyl ketones by alkylbenzenes, *J. Am. Chem. Soc.*, **1986**, 108 (24), 7727–7738.

[27] J. D. Coyle, Introduction to Organic Photochemistry, *Wiley: Chichester*, **1986**.

[28] S. Protti, D. Dondi, M. Fagnoni and A. Albini, Assessing photochemistry as a green synthetic method. Carbon–carbon bond forming reactions, *Green Chem.*, **2009**, 11, 239–249.

[29] C. L. Ciana and C.G. Bochet, Clean and easy photochemistry, *Chimia*, **2007**, 61, 650–654.

[30] P. T. Anastas, J. C. Wagner, Green Chemistry. Theory and Practice, *Oxford University Press: Oxford*, **1998**.

[31] J. J. Lerou, A. L. Tonkovich, L. Silva, S. Perry, J. McDaniel, Microchannel reactor architecture enables greener processes, *Chem. Eng. Sci.*, **2010**, 65, 380–385.

[32] K. Porter and D. H. Volman, Microphotochemistry in liquid systems. The photolysis of propionaldehyde in aqueous solutions, *Bull. Soc. Chim. Belg.*, **1962**, 71, 831–836.

[33] K. Jähnisch and U. Dingerdissen, Photochemical generation and [4 + 2]-cycloaddition of singlet oxygen in a falling-film microreactor, *Chem. Eng. Technol.*, **2005**, 28, 426–427.

[34] H. Ehrich, D. Linke, K. Morgenschweis, M. Baerns and K. Jähnisch, Application of microstructured reactor technology for the photochemical chlorination of alkylaromatics, *Chimia*, **2002**, 56, 647–653.

[35] K. Jähnisch, M. Baerns, V. Hessel, W. Ehrfeld, V. Haverkamp, H. Löwe, Ch. Wille, A. Cuber, Direct fluorination of toluene using elemental fluorine in gas/liquid microreactors, *J. Fluorine Chem.*, **2000**, 105, 117–128.

[36] N. Steinfeldt, R. Abdallah, U. Dingerdissen and K. Jähnisch, Ozonolysis of acetic acid 1-vinyl-hexyl ester in a falling film microreactor, *Org. Process Res. Dev.*, **2007**, 11, 1025–1031.

[37] Mikroglas chemtech GmbH, Galileo-Galilei-Str. 28 55129 Mainz, Germany (http://www.mikroglas.de).

[38] A. Sugimoto, T. Fukuyama, Y. Sumino, M. Takagi, I. Ryu, Microflow photo-radical reaction using a compact light source: application to the Barton reaction leading to a key intermediate for myriceric acid A, *Tetrahedron*, **2009**, 65, 1593–1598.

[39] The Dolomite Centre Ltd, Unit 1, Anglian Business Park, Orchard Road, Royston, Hertfordshire, SG8 5TW, UK (www.dolomite-centre.com).

[40] Institut fur Mikrotechnik Mainz GmbH, Carl-Zeiss-Strasse 18–20, 55129 Mainz, Germany (http://www.imm-mainz.de). V. Hessel, H. Lowe and T. Stange, Micro chemical processing at IMM – from pioneering work to customer-specific services, *Lab Chip*, 2002, **2**, 14N–21N.

[41] Micronit Microfluidics, Colosseum 15, 7521 PV Enschede, Netherlands (www.micronit.com).

[42] O. Shvydkiv, A. Yavorskyy, K. Nolan, A. Youssef, E. Riguet, N. Hoffmann, M. Oelgemöller, Photosensitized addition of isopropanol to furanones in a 365 nm UV-LED microchip, *Photochem. Photobiol. Sci.*, **2010**, 9, 1601–1603.

[43] Y. Matsushita, N. Ohba, S. Kumada, K. Sakeda, T. Suzuki and T. Ichimura, Photocatalytic reactions in microreactors, *Chem. Eng. J.*, **2008**, 135, S303–S308.

[44] K. Jähnisch, V. Hessel, H. Löwe and M. Baerns, Chemistry in microstructured reactors, *Ang. Chem., Int. Ed.*, **2004**, 43, 406–446.

[45] A. de Mello and R. Wootton, But what is it good for? Applications of microreactor technology for the fine chemical industry, *Lab Chip*, **2002**, 2, 7N–13N.

[46] B. Ahmed-Omer, J. C. Brandt and T. Wirth, Advanced organic synthesis using microreactor technology, *Org. Biomol. Chem.*, **2007**, 5, 733–740.

[47] B. P. Mason, K. E. Price, J. L. Steinbacher, A. R. Bogdan and D. T. McQuade, Greener approaches to organic synthesis using microreactor technology, *Chem. Rev.*, **2007**, 107, 2300–2318.

[48] T. Van Gerven, G. Mul, J. Moulijn and A. Stankiewicz, A review of intensification of photocatalytic processes, *Chem. Eng. Process.*, **2007**, 46, 781–789.

[49] P. Watts and C. Wiles, Recent advances in synthetic micro reaction technology, *Chem. Commun.*, **2007**, 443–467.

[50] P. Watts and C. Wiles, Micro reactors: a new tool for the synthetic chemist, *Org. Biomol. Chem.*, **2007**, 5, 727–732.

[51] P. D. I. Fletcher, S. J. Haswell, E. Pombo-Villar, B. H. Warrington, P. Watts, S. Y. F. Wong and X. Zhang, Micro reactors: principles and applications in organic synthesis, *Tetrahedron*, **2002**, 58, 4735–4757.

[52] K. Geyer, J. D. C. Codèe and P. H. Seeberger, Microreactors as tools for synthetic chemists - The chemists' round-bottomed flask of the 21st century?, *Chem.–Eur. J.*, **2006**, 12, 8434–8442.

[53] A. E. Rubin, S. Tummala, D. A. Both, C. C. Wang and E. J. Delaney, Emerging technologies supporting chemical process R&D and their increasing impact on productivity in the pharmaceutical industry, *Chem. Rev.*, **2006**, 106, 2794–2810.

[54] V. Hessel and H. Löwe, Organic synthesis with microstructured reactors, *Chem. Eng. Technol.*, **2005**, 28, 267–284.

[55] P. Watts and S. J. Haswell, The application of microreactors for small scale organic synthesis, *Chem. Eng. Technol.*, **2005**, 28, 290–301.

[56] H. Pennemann, P. Watts, S. J. Haswell, V. Hessel and H. Löwe, Benchmarking of microreactor applications, *Org. Proc. Res. Devel.*, **2004**, 8, 422–439.

[57] S. J. Haswell and P.Watts, Green chemistry: synthesis in micro reactors, *Green Chem.*, **2003**, 5, 240–249.

[58] T. Fukuyama, M. T. Rahman, M. Sato and I. Ryu, Adventures in inner space: Microflow systems for practical organic synthesis, *Synlett*, **2008**, 2, 151–163.

[59] Y. Matsushita, T. Ichimura, N. Ohba, S. Kumada, K. Sakeda, T. Suzuki, H. Tanibata and T. Murata, Recent progress on photoreactions in microreactors, *Pure Appl. Chem.*, **2007**, 79 (11), 1959–1968.

[60] V. Hessel, S. Hardt, H. Löwe and F. Schönfeld, Laminar mixing in interdigital micromixers with different mixing chambers – Part 1: Experimental characterization, *AIChE J.*, **2003**, 49, 566–577.

[61] H. Lu, M. A. Schmidt and K. F. Jensen, Photochemical reactions and on-line UV detection in microfabricated reactors, *Lab Chip*, **2001**, 1, 22–28.

[62] U. Bentrup, L. Küpper, U. Budde, K. Lovis, K. Jähnisch, Mid-Infrared monitoring of gas-liquid reactions in Vitamin D analogue synthesis with a novel fiber optical diamond ATR sensor, *Chem. Eng. Technol.*, **2006**, 29, 1216–1220.

[63] A. A. Lapkin, V. M. Boddu, G. N. Aliev, B. Goller, S. Polisski and D. Kovalev, Photo-oxidation by singlet oxygen generated on nanoporous silicon in a LED-powered reactor, *Chem. Eng. J.*, **2008**, 136, 331–336.

[64] H. W. Chen, Y. Ku and A. Irawan, Photodecomposition of o-cresol by UV-LED, *Chemosphere*, **2007**, 69, 184–190.

[65] D. H. Chen, X. J. Ye and K. Y. Li, Oxidation of PCE with a UV LED photocatalytic reactor, *Chem. Eng. Technol.*, **2005**, 28, 95–97.

[66] G. Kreisel, S. Meyer, D. Tietze, T. Fidler, R. Gorges, A. Kirsch, B. Schäfer and S. Rau, Leuchtdioden in der chemie - eine hochzeit verschiedener technologien, *Chem.-Ing.-Tech.*, **2007**, 79, 153–159.

[67] S. Abele, F.-Q. Nie, F. Foret, B. Paull and M. Macka, UV-LED photopolymerised monoliths, *Analyst*, **2008**, 133, 864–866.

[68] S. Landgraf, Application of semiconductor light sources for investigations of photochemical reactions, *Spectrochim. Acta, Part A*, **2001**, 57, 2029–2048.

[69] S. Vilhunen, E. V. Rokhina and J. Virkutyte, Evaluation of UV LEDs performance in photochemical oxidation of phenol in the presence of H_2O_2, *J. Environ. Eng.*, **2010**, 136, 274–280.

[70] S. Füldner, R. Mild, H. I. Siegmund, J. A. Schroeder, M. Gruber and B. König, Green-light photocatalytic reduction using dye-sensitized TiO_2 and transition metal nanoparticles, *Green Chem.*, **2010**, 12, 400–406.

[71] S. Marre, J. Baek, J. Park, M. G. Bawendi and K. F. Jensen, High-pressure/high-temperature microreactors for nanostructure synthesis, *JALA*, **2009**, 367–373.

[72] S. Werner, R. Seliger, H. Rauter, F. Wissmann, *EP-2065387A2*, **2009**.

[73] J. P. McMullen and K. F. Jensen, Integrated microreactors for reaction automation: new approaches to reaction development, *Annu. Rev. Anal. Chem.*, **2010**, 3, 19–42.

[74] Optical Building Blocks Cooperation, http://www.obb1.com.

[75] Institut für Mikrosystemtechnic, Department of Microsystems Engineering – IMTEK, University of Freiburg, Georges-Koehler-Allee 106, 79110 Freiburg, Germany (http://www.imtek.de).

[76] M-H. Wu, S-B. Huang and Gwo-Bin Lee, Microfluidic cell culture systems for drug research, *Lab Chip*, **2010**, 10, 939–956.

[77] T-H. Yoon, S-H. Park, K-I. Min, X. Zhang, S.J. Haswell and D-P. Kim, Novel inorganic polymer derived microreactors for organic microchemistry application, *Lab Chip*, **2008**, 8, 1454–1459.

[78] BOLA - Bohlender GmbH - Waltersberg 8 - 97947 Grünsfeld – Germany (http://www.bola.de).

[79] T. Horie, M. Sumino, T. Tanaka, Y. Matsushita, T. Ichimura and J. Yoshida, Photodimerization of maleic anhydride in a microreactor without clogging, *Org. Process Res. Dev.*, **2010**, 14, 405–410.

[80] B. D. A. Hook, W. Dohle, P. R. Hirst, M. Pickworth, M. B. Berry and K. I. Booker-Milburn, A practical flow reactor for continuous organic photochemistry, *J. Org. Chem.*, **2005**, 70, 7558–7564.

[81] S. V. Ley and I. R. Baxendale, The changing face of organic synthesis, *Chimia*, **2008**, 62, 162–168.

[82] C. H. Hornung, B. Hallmark, M. Baumann, I. R. Baxendale, S. V. Ley, P. Hester, P. Clayton and M. R. Mackley, Multiple microcapillary reactor for organic synthesis, *Ind. Eng. Chem. Res.*, **2010**, 49, 4576–4582.

[83] R. Gorges, S. Meyer and G. Kreisel, Photocatalysis in microreactors, *J. Photochem. Photobiol., A*, **2004**, 167, 95–99.

[84] S. Teekateerawej, J. Nishino and Y. Nosaka, Photocatalytic microreactor study using TiO_2- coated porous ceramics, *J. Appl. Electrochem.*, **2005**, 35, 693–697.

[85] S. Teekateerawej, J. Nishino and Y. Nosaka, Design and evaluation of photocatalytic micro-channel reactors using TiO_2-coated porous ceramics, *J. Photochem. Photobiol., A*, **2006**, 179, 263–268.

[86] B. Dunk and R. Jachuck, A novel reactor for UV irradiated reactions, *Green Chem.*, **2000**, 2, G13–G14.

[87] H. C. Yatmaz, C. Wallis and C. R. Howarth, The spinning disc reactor - studies on a novel TiO_2 photocatalytic reactor, *Chemosphere*, **2001**, 42, 397–403.

[88] V. Hessel, P. Angeli, A. Gavriilidis and H. Löwe, Gas-liquid and gas-liquid-solid microstructured reactors: contacting principles and applications, *Ind. Eng. Chem. Res.*, **2005**, 44, 9750–9769.

[89] B. Borderie, D. Lavabre, G. Levy, J. P. Laplante and J. C. Micheau, Single run benzophenone-benzhydrol actinometry in a exponential dilution photochemical microreactor, *J. Photochem. Photobiol., A*, **1991**, 56, 13–23.

[90] A. G. Griesbeck, N. Maptue, S. Bondock and M. Oelgemöller, The excimer radiation system: a powerful tool for preparative organic photochemistry. A technical note, *Photochem. Photobiol. Sci.*, **2003**, 2, 450–451.

[91] A. G. Griesbeck, W. Kramer and M. Oelgemöller, Photoinduced decarboxylation reactions. Radical chemistry in water, *Green Chem.*, **1999**, 1, 205–207.

[92] E. A. Sosnin, T. Oppenländer and V. F. Tarasenko, Applications of capacitive and barrier discharge excilamps in photoscience, *J. Photochem. Photobiol. C: Photochem. Rev.*, **2006**, 7, 145–163.

[93] G. Shama, C. Peppiatt and M. Biguzzi, A novel thin film photoreactor, *J. Chem. Technol. Biotechnol.*, **1996**, 65, 56–64.

[94] M. Oelgemöller, C. Jung, J. Ortner, J. Mattay and E. Zimmermann, Green photochemistry: solar photooxygenations with medium concentrated sunlight, *Green Chem.*, **2005**, 7, 35–38.

[95] C. Schiel, M. Oelgemöller, J. Ortner and J. Mattay, Green photochemistry: the solar-chemical 'photo-Friedel–Crafts acylation' of quinones, *Green Chem.*, **2001**, 3, 224–228.

[96] M. Oelgemöller, C. Jung and J. Mattay, Green photochemistry: production of fine chemicals with sunlight, *Pure Appl. Chem.*, **2007**, 79, 1939–1947.

[97] H. W. Chen, Y. Ku and A. Irawan, Photodecomposition of o-cresol by UV-LED, *Chemosphere*, **2007**, 69, 184–190.

[98] T. C. K. Yang, S. F. Wang, S. H. Y. Tsai and S. Y. Lin, Intrinsic photocatalytic oxidation of the dye adsorbed on TiO_2 photocatalysts by diffuse reflectance infrared Fourier transform spectroscopy, *Appl. Catal., B*, **2001**, 30, 293–301.

[99] J. M. Carney, R. J. Hammer, M. Hulce, C. M. Lomas, D. Miyashiro, High-efficiency microphotooxidation using milliwatt LED sources, *Tetrahedron Lett.*, **2011**, 52, 352–355.

[100] P. Ciambelli, D. Sannino, V. Palma, V. Vaiano and R. S. Mazzei, Improved performances of a fluidized bed photoreactor by a microscale illumination system, *Int. J. Photoenergy*, **2009**, doi:10.1155/2009/709365.

[101] USHIO, Excimer irradiation unit, Brochure (http://www.ushio.co.jp).

[102] Sci-Tech Encyclopedia, McGraw-Hill Encyclopedia of Science and Technology: Laser photochemistry, 5th edition, *McGraw-Hill Companies*, **2005**.

[103] A. Sugimoto, Y. Sumino, M. Takagi, T. Fukuyama and H. Ryu, The Barton reaction using a microreactor and black light. Continuousflow synthesis of a key steroid intermediate for an endothelin receptor antagonist, *Tetrahedron Lett.*, **2006**, 47, 6197–6200.

[104] T. Fukuyama, Y. Hino, N. Kamata and I. Ryu, Quick execution of [2 + 2] type photochemical cycloaddition reaction by continuous flow system using a glass-made microreactor, *Chem. Lett.*, **2004**, 33, 1430–1431.

[105] T. Fukuyama, Y. Kajihara, Y. Hino, I. Ryu, Continuous microflow [2 + 2] photocycloaddition reactions using energy-saving compact light sources, *J. Flow Chem.*, **2011**, 1, 40–45.

[106] K. Tsutsumi, K. Terao, H. Yamaguchi, S. Yoshimura, T. Morimoto, K. Kakiuchi, T. Fukuyama and I. Ryu, Diastereoselective [2 + 2] photocycloaddition of chiral cyclic enone and cyclopentene using a microflow reactor system, *Chem. Lett.*, **2010**, 39, 828–829.

[107] H. Maeda, H. Mukae and K. Mizuno, Enhanced efficiency and regioselectivity of intramolecular (2π + 2π) photocycloaddition of 1-cyanonaphthalene derivative using microreactors, *Chem. Lett.*, **2005**, 34, 66–67.

[108] H. Mukae, H. Maeda, S. Nashihara and K. Mizuno, Intramolecular photocycloaddition of 2-(2-alkenyloxymethyl)naphthalene-1-carbonitriles using glass-made microreactors, *Bull. Chem. Soc. Jpn.*, **2007**, 80, 1157–1161.

[109] A. Vasudevan, C. Villamil, J. Trumbull, J. Olson, D. Sutherland, J. Pan, S. Djuric, LOPHTOR: a convenient flow-based photochemical reactor, *Tetrahedron Lett.*, **2010**, 51, 4007–4009.

[110] M. D. Lainchbury, M. I. Medley, P. M. Taylor, P. Hirst, W. Dohle and K. I. Booker-Milburn, A protecting group free synthesis of (±)-neostenine via the [5 + 2] photocycloaddition of meleimides, *J. Org. Chem.*, **2008**, 73, 6497–6505.

[111] K. Sakeda, K. Wakabayashi, Y. Matsushita, T. Ichimura, T. Suzuki, T. Wada, Y. Inoue, Asymmetric photosensitized addition of methanol to (*R*)-(+)-(*Z*)-limonene in a microreactor**,** *J. Photochem. Photobiol., A*, **2007**, 192, 166–171.

[112] S. Fuse, N. Tanabe, M. Yoshida, H. Yoshida, T. Doi and T. Takahashi, Continuous-flow synthesis of vitamin D_3, *Chem. Commun.*, **2010**, 46, 8722–8724.

[113] D. R. Rafael and P. Andreas, WO, 2008128783, 2008.

[114] V. Belluau, P. Noeureuil, E. Ratzke, A. Skvortsov, S. Gallagher, C. A. Motti, M. Oelgemöller, Photodecarboxylative benzylations of phthalimide in pH 7 buffer: a simple access to 3-arylmethyleneisoindolin-1-ones, *Tetrahedron Lett.*, **2010**, 51, 4738–4741.

[115] K. Ueno, F. Kitagawa and N. Kitamura, Photocyanation of pyrene across an oil/water interface in a polymer microchannel chip, *Lab Chip*, **2002**, 2, 231–234.

[116] R. C. R. Wootton, R. Fortt and A. J. de Mello, A microfabricated nanoreactor for safe, continuous generation and use of singlet oxygen, *Org. Proc. Res. Devel.*, **2002**, 6, 187–189.

[117] S. Meyer, D. Tietze, S. Rau, B. Schäfer, G. Kreisel, Photosensitized oxidation of citronellol in microreactors, *J. Photochem. Photobiol. A: Chem.,* **2007**, 186, 248–253.

[118] F. Levesque, P. H. Seeberger, Highly efficient continuous flow reactions using singlet oxygen as a "green" reagent, *Org. Lett.*, **2011**, 13 (19), 5008–5011.

[119] C. P. Park, R. A. Maurya, J. H. Lee, D.-P. Kim, Efficient photosensitized oxygenations in phase contact enhanced microreactors, *Lab Chip*, **2011**, 11, 1941–1945.

[120] R. A. Maurya, C. P. Park, D.-P. Kim, Triple-channel microreactor for biphasic gas-liquid reactions: photosensitized oxygenations, *Beilstein J. Org. Chem.*, **2011**, 7, 1158–1163.

[121] H. Matsubara, Y. Hino, M. Tokizane, I. Ryu, Microflow photo-radical chlorination of cycloalkanes, *Chem. Eng. J.*, **2011**, 167, 567–571.

[122] J.-M. Herrmann, Heterogeneous photocatalysis: state of the art and present applications, *Top. Catal.*, **2005**, 34, 49–65.

[123] H. C. Aran, D. Salamon, T. Rijnaarts, G. Mul, M. Wessling, R. G. H. Lammertink, Porous photocatalytic membrane microreactor (P2M2): A new reactor concept for photochemistry, *J. Photochem. Photobiol. A: Chem.,* **2011**, 225, 36–41.

[124] F. Dionigi, P. C. K. Vesborg, T. Pedersen, O. Hansen, S. Dahl, A. Xiong, K. Maeda, K. Domen, I. Chorkendorff, Gas phase photocatalytic water splitting with $Rh_{2-y}Cr_yO_3$/GaN:ZnO in μ-reactors, *Energy Environ. Sci*, **2011**, 4, 2937–2942.

[125] H. Nakamura, X. Li, H. Wang, M. Uehara, M. Miyazaki, H. Shimizu, H. Maeda, A simple method of self assembled nano-particles deposition on the micro-capillary inner walls and the reactor application for photo-catalytic and enzyme reactions, *Chem. Eng. J.*, **2004**, 101, 261–268.

[126] N. Kitamura, K. Yamada, K. Ueno, S. Iwata, Photodecomposition of phenol by silica-supported porphyrin derivative in polymer microchannel chips, *J. Photochem. Photobiol., A*, **2006**, 184, 170–176.

[127] T. Kirner, J. Albert, M. Günther, G. Mayer, K. Reinhäckel, J. M. Köhler, Static micromixers for modular chip reactor arrangements in two-step reactions and photochemical activated processes, *Chem. Eng. J.*, **2004**, 101, 65–74.

[128] Y. Matsushita, M. Iwasawa, T. Suzuki and T. Ichimura, Multiphase photocatalytic oxidation in a microreactor, *Chem. Lett.*, **2009**, 38 (8), 846–847.

[129] Z. He, Y. Li, Q. Zhang, H. Wang, Capillary microchannel-based microreactors with highly durable ZnO/TiO_2 nanorod arrays for rapid, high efficiency and continuous-flow photocatalysis, *Appl. Catal. B: Environ.*, **2010**, 93, 376–382.

[130] G. Takei, T. Kitamori, H.-B. Kim, Photocatalytic redox-combined synthesis of L-pipecolinic acid with a titania-modified microchannel chip, *Catal. Commun.*, **2005**, 6, 357–360.

[131] Y. Matsushita, N. Ohba, S. Kumada, T. Suzuki, T. Ichimura, Photocatalytic N-alkylation of benzylamine in microreactors, *Catal. Commun.*, **2007**, 8, 2194–2197.

[132] B. Ohtani, H. Osaki, S. Nishimoto, T. Kagiya, A novel photocatalytic process of amine N-alkylation by platinized semiconductor particles suspended in alcohols, *J. Am. Chem. Soc.*, **1986**, 108, 308–310.

[133] Y. Matsushita, N. Ohba, T. Suzuki, T. Ichimura, N-Alkylation of amines by photocatalytic reaction in a microreaction system, *Catal. Today*, **2008**, 132, 153–158.

[134] Y. Matsushita, S. Kumada, K. Wakabayashi, K. Sakeda and T. Ichimura, Photocatalytic reduction in microreactors, *Chem.Lett.*, **2006**, 35 (4), 410–411.

[135] F. Levesque, P. H. Seeberger, Continuous-flow synthesis of the anti-malaria drug artemisinin, *Angew. Chem. Int. Ed.*, **2012**, 51, 1706–1709.

[136] Y. S. M. Vaske, M. E. Mahoney, J. P. Konopelski, D. L. Rogow, W. J. McDonald, Enantiomerically pure *trans-β*-lactams from α-amino acids via compact fluorescent light (CFL) continuous-flow photolysis, *J. Am. Chem. Soc.*, **2010**, 132, 11379–11385.

[137] M. Neumann, S. Füldner, B. König, K. Zeitler, Metal-free, cooperative asymmetric organophotoredox catalysis with visible light, *Angew. Chem. Int. Ed.*, **2011**, 50, 951–954.

[138] A. C. Gutierrez, T. F. Jamison, Scalable and robust synthesis of $CpRu(MeCN)_3PF_6$ via continuous flow photochemistry, *J. Flow Chem.*, **2011**, 1, 24–27.

[139] F. R. Bou-Hamdan, P. H. Seeberger, Visible-light-mediated photochemistry: accelerating $Ru(bpy)_3^{2+}$-catalyzed reactions in continuous flow, *Chem. Sci.*, **2012**, 3, 1612–1616.

[140] A. Ouchi, H. Sakai, T. Oishi, M. Kaneda, T. Suzuki, A. Saruwatari, T. Obata, Photochemical reduction of flavone with $NaBH_4$ in batch and micro-channel reactors using excimer lasers, *J. Photochem. Photobiol. A: Chem.*, **2008**, 199, 261–266.

[141] F. R. Bou-Hamdan, F. Levesque, A. G. O'Brien, P. H. Seeberger, Continuous flow photolysis of aryl azides: preparation of *3H*-azepinones, *Beilstein J. Org. Chem.*, **2011**, 7, 1124–1129.

[142] M. Nettekoven, B. Püllmann, R. E. Martin, D. Wechsler, Evaluation of a flow-photochemistry platform for the synthesis of compact modules, *Tetrahedron Lett.*, **2012**, 53, 1363–1366.

[143] S. Gallagher, F. Hatoum, N. Zientek, M. Oelgemöller, Photodecarboxylative additions of N-protected α-amino acids to *N*-methylphthalimide, *Tetrahedron Lett.*, **2010**, 51, 3639–3641.

[144] F. Hatoum, S. Gallagher, M. Oelgemöller, Photodecarboxylative additions of phenoxyacetates to N-methylphthalimide, *Tetrahedron Lett.*, **2009**, 50, 6593–6596.

[145] F. Hatoum, S. Gallagher, L. Baragwanath, J. Lex, M. Oelgemöller, Photodecarboxylative benzylations of phthalimides, *Tetrahedron Lett.*, **2009**, 50, 6335–6338.

[146] M. Oelgemöller, P. Cygon, J. Lex, A. G. Griesbeck, The photodecarboxylative addition of carboxylates to phthalimides: scope and limitations, *Heterocycles*, **2003**, 59, 669–684.

[147] A. G. Griesbeck, M. Oelgemöller, J. Lex, Photodecarboxylative additions of α-Keto carboxylates to phthalimides alkylation, acylation and ring expansion, *Synlett*, **2000**, 10, 1455–1457.

[148] A. G. Griesbeck, M. Oelgemöller, Decarboxylative photoadditions of heteroatom-substituted carboxylates to phthalimides, *Synlett*, **2000**, 1, 71–72.

[149] A. G. Griesbeck, M. Oelgemöller, Photodecarboxylative addition of carboxylates and α-keto carboxylates to phthalimides, *Synlett*, **1999**, 492–494.

[150] S. B. Tan, O. Shvydkiv, J. Fielder, F. Hatoum, K. Nolan, M. Oelgemöller, Photodecarboxylative additions of α-Thioalkyl-substituted carboxylates to alkyl phenylglyoxylates, *Synlett*, **2010**, 2240–2243.

[151] P. Perlmutter, Conjugate Addition Reactions in Organic Synthesis (Tetrahedron Organic Chemistry), *Pergamon Press: Oxford*, **1992**.

[152] D. J. Crouse, M. M. Wheeler, M. Goemann, P. S. Tobin, S. K. Basu, D. M. S. Wheeler, Oxidation of 1,5-naphthalenediol and its methyl ether: preparation of Juglone methyl ether monoacetal, *J. Org. Chem.*, **1981**, 46, 1814–1817.

[153] C. Grundmann, A new synthesis of Juglone**,** *Synthesis*, **1977**, 644–645.

[154] J. March, Advanced Organic Chemistry (Reaction Mechanisms and Structures, 4th ed, chp 7), *Wiley Interscience: New York*, **1992**.

[155] K. Yoshiaki, T. Masumi and K. Achiwa, Prostanoids and related compounds. VII. Synthesis 1-isoindolinone derivatives possessing inhibitory activity against thromboxane A_2 analog (U-46619)-induced vasoconstriction, *Chem. Pharm. Bull.*, **1999**, 47, 529–535.

[156] Y. Hatanaka, Y. Sato, H. Nakai, M. Wada, T. Mizoguchi, Y. Kanaoka, Regioselective remote photocyclization: examples of a photochemical macrocyclic synthesis with sulphide-containing phthalimides, *Liebigs Ann. Chem.*, **1992**, 1113–1123.

[157] M. Oelgemöller and A. G. Griesbeck, Photoinduced electron transfer chemistry of phthalimides: an efficient tool for C-C bond formation, *J. Photochem. Photobiol. C: Photochem. Rev.*, **2002**, 3, 109–127.

[158] A. G. Griesbeck, M. Oelgemöller, J. Lex, A Haeuseler and M. Schmittel, Synthesis of sulfur-containing tricyclic ring systems by means of photoinduced decarboxylative cyclizations, *Eur. J. Org. Chem.*, **2001**, 1831–1843.

[159] J. Barluenga, J. L. Fernandez-Simon, J. M. Concellon, M. Yus, Chloromethyl-lithium and 1-chloro-2-methylprop-1-enyl-lithium: useful intermediates in the synthesis of unsaturated and bifunctionalized compounds, *J. Chem. Soc., Perkin Trans. 1*, **1988**, 12, 3339–3343.

[160] U. C. Yoon, P. S. Mariano, The synthetic potential of phthalimide SET photochemistry, *Acc. Chem. Res.*, **2001**, 34, 523–533.

[161] A. Bartoschek, A. G. Griesbeck, M. Oelgemöller, Photoinduced electron transfer reactions of phthalimides, *J. Inf. Rec.*, **2000**, 26, 119–126.

[162] J. D. Coyle, Synthetic Organic Photochemistry, W. M. Horspool, Ed., *Plenum Press: New York*, **1984**.

[163] W. S. Ang and B. Halton, Configuration of alkylidenephthalimidine derivatives, *Aust. J. Chem.*, **1971**, 24, 851–856.

[164] H. Görner, M. Oelgemöller, A. G. Griesbeck, Photodecarboxylation study of carboxy-substituted *N*-alkylphthalimides in aqueous solution: time resolved UV-Vis spectroscopy and conductometry, *J. Phys. Chem. A*, **2002**, 106, 1458–1464.

[165] U. C. Yoon, C. W. Lee, S. W. Oh, H. J. Kim, S. J. Lee, Photocyclization reactions of (ω-phthalimidoalkoxy)acetic acids via sequential single electron transfer decarboxylation pathways, *J. Photosci.*, **2000**, 7, 143–148.

[166] A. G. Griesbeck, T. Heinrich, M. Oelgemöller, A. Molis, J. Lex, A photochemical route to cyclopeptides with a minimum of activation and protection chemistry, *J. Am. Chem. Soc.*, **2002**, 124, 10972–10973.

[167] M. Oelgemöller, A. G. Griesbeck, W. Kramer, F. Nerowski, Photochemical macrocyclization: synthesis of lactones, lactames, ethers and thioethers, *J. Inf. Rec.*, **1998**, 24, 87–94.

[168] A. G. Griesbeck, A. Henz, W. Kramer, J. Lex, F. Nerowski, M. Oelgemöller, K. Peters, E.-M. Peters, Synthesis of medium- and large-ring compounds initiated by photochemical decarboxylation of ω-phthalimido alkylcarboxylates, *Helv. Chim. Acta*, **1997**, 80, 912–933.

[169] M. Oelgemöller, A. G. Griesbeck, J. Lex, A. Haeuseler, M. Schmittel, M. Niki, D. Hesek, Y. Inoue, Structural, CV- and IR-spectroscopic evidences for preorientation in PET-active phthalimido carboxylic acids, *Org. Lett.*, **2001**, 3, 1593–1596.

[170] Y. Takahashi, T. Miyashi, U. C. Yoon, S. W. Oh, M. Mancheno, Z. Su, D. F. Falvey, P. S. Mariano, Mechanistic studies of the azomethine Ylide-forming photoreactions of *N*-(silylmethyl)phthalimides and *N*-Phthaloylglycine, *J. Am. Chem. Soc.*, **1999**, 121, 3926–3932.

[171] A. G. Griesbeck, A. Henz, Synthesis of α-[^{2}H]-amines via photodecarboxylation of N-phthaloyl α-amino acids, *Synlett*, **1994**, 931–932.

[172] Y. Sato, H. Nakai, T. Mizoguchi, M. Kawanishi, Y. Hatanaka, Y. Kanaoka, Photodecarboxylation of N-phthaloyl-α-amino acids, *Chem. Pharm. Bull.*, **1982**, 30, 1263–1270.

[173] J. O. Metzger in Houben-Weyl. (Methoden der organischen Chemie), C-Radikale, Vol. E19a; M. Regitz and B. Giese, Eds.; *Thieme: Stuttgart*, **1989**.

[174] A. G. Griesbeck, W. Kramer and M. Oelgemöller, Synthetic applications of photoinduced electron transfer decarboxylation reactions, *Synlett,* **1999**, 1169–1178.

[175] W. Kramer, A. G. Griesbeck, F. Nerowski and M. Oelgemöller, Synthetic potential of the pet-decarboxylation of ω-phthalimido carboxylic acids, *J. Inf. Rec.*, **1998**, 24, 81–85.

[176] L. Eberson (K. Hafner, Ed.), in Electron Transfer Reactions in Organic Chemistry (Reactivity and Structure-Concepts in Organic Chemistry), Vol. 25; *Springer-Verlag: Berlin*, **1987**.

[177] E. Baciocchi, T. D. Giacco, F. Elisei and A. Lapi, Sulfur radical cations. Kinetic and product study of the photoinduced fragmentation reactions of (Phenylsulfanylalkyl)-trimethylsilanes and Phenylsulfanylacetic acid radical cations, *J. Org. Chem.*, **2006**, 71, 853–860.

[178] N. J. Pienta (M. A. Fox, M. Chanon, Eds.), Amines, thiols and thioethers: heteroaromatic electron donors (Photoinduced Electron Transfer), *Elservier: Amsterdam,* **1988**, 421–486.

[179] G. McDermott, D. J. Yoon and M. Oelgemöller, Photochemical addition reactions involving phthalimides, *Heterocycles*, **2005**, 65, 2221–2257.

[180] H. Görner, M. Oelgemöller, A. G. Griesbeck, Photodecarboxylation study of carboxy-substituted *N*-Alkylphthalimides in aqueous solution: time resolved UV-Vis spectroscopy and conductometry, *J. Phys. Chem. A*, **2002**, 106 (7), 1458–1464.

[181] H. Görner, A. G. Griesbeck, T. Heinrich, W. Kramer, M. Oelgemöller, Time-resolved spectroscopy of sulphur- and carboxy-substituted *N*-Alkylphthalimides, *Chem.-Eur. J.*, **2001**, 7 (7), 1530–1538.

[182] S. Bertrand, N. Hoffmann, J.-P. Pete, Highly efficient and stereoselective radical addition of tertiary amines to electron-deficient alkenes – application to the enantioselective synthesis of Necine bases, *Eur. J. Org. Chem.*, **2000**, 2000 (12), 2227–2238.

[183] V. Wintgens, P. Valat, J. Kossanyi, L. Biczok, A. Demeter, T. Berces, Spectroscopic properties of aromatic dicarboximides. Part1.–N–H and *N*-methyl-substituted naphthalimides, *J. Chem. Soc., Faraday Trans.*, **1994**, 90 (3), 411–421.

[184] W. Ando, J. Suzuki, T. Migita, The photoreduction of benzophenone by thioethers, *Bull. Chem. Soc. Jpn.*, **1971**, 44, 1987–1989.

[185] R. S. Davidson, P. R. Steiner, Mechanism of the photoinduced decarboxylation of carboxylic acids sensitised by aromatic ketones and quinones, *J. Chem. Soc., Perkin Trans. 2*, **1972**, 10, 1357–1362.

[186] C. N. Koshelev, A. V. Mashkina and N. G. Kalinina, Decomposition of dimethyl sulphide in the presence of Al_2O_3 and catalyst deactivation, *React. Kinet. Catal. Lett.*, **1989**, 39 (2), 367–372.

[187] N. J. Pitts Jr., R. L. Letsinger, R. P. Taylor, J. M. Patterson, G. Recktenwald and R. B. Martin, Photochemical reactions of benzophenone in alcohols, *J. Am. Chem. Soc.*, **1959**, 81 (5), 1068–1077.

[188] P. Perlmutter, Conjugate Addition Reactions in Organic Synthesis (Tetrahedron Organic Chemistry), *Pergamon Press: Oxford*, **1992**.

[189] J. F. G. A. Jansen, B. L. Feringa (G. Helmchen, R. W. Hoffmann, J. Mulzer, E. Schaumann, Eds.), Addition of Enolates and Azaenolates to α,β-Unsaturated Carbonyl Compounds (Methoden der Organischen Chemie), chapter 1.5.2.4; *Thieme Verlag: Stuttgart*, **1995**.

[190] F. A. Carey, R. J. Sundberg, Advanced Organic Chemistry: Reactions and Synthesis, *Springer Science + Business Media: New York*, **2007**.

[191] N. Hoffmann, Highly diastereoselective addition of photochemically generated radicals to (5*R*)-(-)-menthyloxy-2[5*H*]-furanone – synthesis of (-)-terebic acid, *Tetrahedron: Asym.*, **1994**, 5, 879–886.

[192] N. Hoffmann, H. Buschmann, G. Raabe, H.-D. Scharf, Chiral induction in photochemical reactions – 15.: Detection of stereoelectronic effects by temperature dependent measurements of the diastereoselectivity in the photosensitized [2+2]-cycloaddition, *Tetrahedron*, **1994**, 50 (38), 11167–11186.

[193] R. Alibes, J. L. Bourdelande, J. Font, T. Parella, Highly efficient and diastereoselective approaches to (+)- and (-)-grandisol, *Tetrahedron*, **1996**, 52 (4), 1279–1292.

[194] A. I. Hashem, A. Senning, A.-S. S. Hamad, Photochemical transformations of 2(5*H*)-furanones. A review, *Org. Prep. Proc. Int.: New J. Org. Synth.*, **2009**, 30 (4), 401–425.

[195] M. V. N. De Souza, The furan-2(5*H*)-ones: recent synthetic methodologies and its application in total synthesis of natural products, *Mini-Rev. Org. Chem.*, **2005**, 2, 139–145.

[196] A. Gassama, C. Ernenwein, N. Hoffmann, Synthesis of surfactants from furfural derived 2[5*H*]-furanone and fatty amines, *Green Chem.*, **2010**, 12, 859–865.

[197] S. Marinkovic, C. Brule, N. Hoffmann, E. Prost, J.-M. Nuzillard, V. Bulach, Origin of chiral induction in radical reactions with the diastereoisomers (5*R*)- and (5*S*)-5-*1*-menthyloxyfuran-2[5*H*]-one, *J. Org. Chem.*, **2004**, 69, 1646–1651.

[198] J. Mann, A. Weymouth-Wilson, The stereoselective photochemical addition of alcohols to 5-substituted furan-2(5*H*)-ones, *Synlett*, **1992**, 1, 67–69.

[199] G. O. Schenck, G. Koltzenburg, H. Grossmann, Durch benzophenon photosensibilisierte synthese der terebinsäure, *Angew. Chem.*, **1957**, 69 (5), 177–178.

[200] D. Dondi, I. Caprioli, M. Fagnoni, M. Mella, A. Albini, A convenient route to 1,4-monoprotected dialdehydes, 1,4-ketoaldehydes, γ-lactols and γ-lactones through radical alkylation of α,β-unsaturated aldehydes in organic and organic-aqueous media, *Tetrahedron*, **2003**, 59, 947–957.

[201] M. Oelgemöller and O. Shvydkiv, Recent advances in microflow photochemistry, *Molecules*, **2011**, 16, 7522–7550.

[202] K. Ohga, T. Matsuo, Photoinduced addition of isopropyl alcohol to .alpha., .beta.-unsaturated lactones, *J. Org. Chem.*, **1974**, 39, 106–108.

[203] D. Harakat, J. Pesch, S. Marinković and N. Hoffmann, Thiocarbonyl compounds as regulating reagent in the radical addition of tertiary amines with alkenes using photoelectron transfer conditions, *Org. Biomol. Chem.*, **2006**, 4, 1202–1205.

[204] S. Bertrand, N. Hoffmann, S. Humbel and J. P. Pete, Diastereoselective tandem addition-cyclization reactions of unsaturated tertiary amines initiated by photochemical electron transfer (PET), *J. Org. Chem.*, **2000**, 65, 8690–8703.

[205] S. Bertrand, C. Glapski, N. Hoffmann and J. P. Pete, Highly efficient photochemical addition of tertiary amines to electron deficient alkenes.

Diastereoselective addition to (5R)-5-Menthyloxy-2[5H]-furanone, *Tetrahedron Lett.*, **1999**, 40, 3169–3172.

[206] P. Chin, W. S. Barney, B. A. Pindzola, Microstructured reactors as tools for the intensification of pharmaceutical reactions and processes, *Curr. Opin. Drug Discovery & Dev.*, **2009**, 12, 848–861.

[207] S. L. Murov, Handbook of Photochemistry, *Marcel Dekker: New York*, **1973**.

[208] A. Schönberg and A. Mustafa, Photo-reactions. Part VII. Reactions in sunlight involving (a) rupture of the ethane linkage, (b) dehydrogenation effected by quinone and benzophenone derivatives, (c) addition reactions between ketones and methanes, *J. Chem. Soc.*, **1944**, 67–71.

[209] C. Manfrotto, M. Mella, M. Freccero, M. Fagnoni and A. Albini, Photochemical synthesis of 4-oxobutanal acetals and of 2-hydroxycyclobutanone ketals, *J. Org. Chem.*, **1999**, 64, 5024–5028.

[210] M. Fagnoni, D. Dondi, D. Ravelli and A. Albini, Photocatalysis for the formation of the C-C bond, *Chem. Rev.*, **2007**, 107 (6), 2725–2756.

[211] A. Oeveren, C. A. J. H. Oeveren, 5-Alkoxy-2(*5H*)-furanones in asymmetric synthesis, *Groningen*, **1996**.

[212] Y. S. Rao, Recent advances in the chemistry of unsaturated lactones, *Chem. Rev.*, **1976**, 76 (5), 625–694.

[213] W. Smadja, Acyclic diastereofacial selection in intermolecular radical reactions steric *vs* electronic controls, *Synlett*, **1994**, 1, 1–26.

[214] H.-D. Becker, Photochemical reactions with phenols. V. The photochemical oxidative-reductive dimerization of acetophenones, *J. Org. Chem.*, **1967**, 32 (7), 2140–2144.

[215] Y. Takaguchi, Y. Yanagimoto, S. Fujima, S. Tsuboi, Photooxygenation of olefins, phenol, and sulfide using Fullerodendrimer as catalyst, *Chem. Lett.*, **2004,** 33 (9), 1142–1143.

[216] A. W. Jensen, C. Daniels, Fullerene-coated beads as reusable catalysts, *J. Org. Chem.*, **2003**, 68, 207–210.

[217] H. M. Chawla, K. Kaul, M. Kaul, Methylene blue sensitized photooxygenation of 2-aminonaphthalene, *Indian J. Chem., Sect. B,* **1993**, 32 (7), 733–737.

[218] A. S. Amarasekara, A new synthesis of quinoline-5,8-quinone, *Synth. Commun.*, **1999**, 29 (18), 3063–3066.

[219] J. Cossy, D. Belotti, Efficient synthesis of substituted quinoline-5,8-quinones from 8-hydroxyquinolines by photooxygenation**,** *Tetrahedron Lett.*, **2001**, 42 (26), 4329–4331.

[220] M. Oelgemöller, C. Jung, J. Ortner, M. Mattay, C. Schiel and E. Zimmermann, Green photochemistry with moderately concentrated sunlight, *The Spectrum*, **2005**, 18 (1), 28–33.

[221] E. L. Clennan and A. Pace, Advances in singlet oxygen chemistry**,** *Tetrahedron*, **2005**, 61(28), 6665–6691.

[222] V. G. O. Schenck, K. G. Kinkel, H.-J. Mertens, Über die Photosynthese des Askaridols und verwandter Endoperoxyde, *Liebigs Ann. Chem.*, **1953**, 584, 125–155.

[223] Y. Pollack, R. Segal and J. Golenser, The effect of ascaridole on the in vitro development of *Plasmodium falciparum*, *Parasitol Res.*, **1990**, 76 (7), 570–572.

[224] Y.-P. Yen, M.-J. Yeh, W.-F. Hsiao, Synthesis and nematocidal activity of ascaridole derivatives against Meloidogyne incognita and Aphelenchoides besseyi, *J. Pestic. Sci*, **2007**, 32 (1), 49–52.

[225] C. W. Jefford, A. Jaber, J. Boukouvalas, The regio- and stereo-controlled synthesis of *cis*-p-Menth-3-ene-1,2-diol by means of a 1,2,4-trioxane intermediate, *J. Chem. Soc., Chem. Commun.*, **1989**, 1916–1917.

[226] L. F. R. Cafferata, R. Jeandupeux, A. I. Canizo, Kinetics of the thermal decomposition reaction of ascaridole in solution, *Afinidad LXII*, **2005**, 62 (518), 285–289.

[227] J. Boche, O. Runquist, Kinetics of the thermal rearrangement of ascaridole, *J. Org. Chem.*, **1968**, 33 (11), 4285–4286.

[228] M. Catir, H. Kilic, Transient formation of hydrogen tetraoxide from hydrogen peroxide with *Bis*(trifluoroacetoxyiodo)benzene: a chemical generator of singlet oxygen for organic synthesis, *Synlett*, **2003**, 8, 1180–1182.

[229] W. G. Jary, T. Ganglberger, P. Pöchlauer, H. Falk, Generation of singlet oxygen from ozone catalysed by phosphinoferrocenes, *Monatshefte für Chemie*, **2005**, 136, 537–541.

[230] A. M. Braun, M. T. Maurette and E. Oliveros, *Photochemical technology*, Wiley, Chichester, West Sussex, England: New York, **1991**.

[231] L. Chen, L. A. Lucia, E. R. Gaillard, D. G. Whitten, Photooxidation of a conjugated diene by an exciplex mechanism: amplification via radical chain reactions in the perylene diimide-photosensitized oxidation of α-terpinene, *J. Phys. Chem. A*, **1998**, 102, 9095–9098.

[232] C. Karapire, H. Kolancilar, Ü. Oyman, S. Icli, Fluorescence emission and photooxidation studies with 5,6- and 6,7-benzocoumarins and a 5,6-benzochromone under direct and concentrated sun light, *J. Photochem. Photobiol. A: Chem.*, **2002**, 153, 173–184.

[233] S. Alp, S. Erten, C. Karapire, B. Köz, A. O. Doroshenko, S. Içli, Photoinduced energy-electron transfer studies with naphthalene diimides, *J. Photochem. Photobiol. A: Chem.*, **2000**, 135, 103–110.

[234] X. Han, R. A. Bourne, M. Poliakoff, M. W. George, Immobilised photosensitisers for continuous flow reactions of singlet oxygen in supercritical carbon dioxide, *Chem. Sci.*, **2011**, 2, 1059–1067.

[235] R. A. Bourne, X. Han, A. O. Chapman, N. J. Arrowsmith, H. Kawanami, M. Poliakoff, M. W. George, Homogeneous photochemical oxidation *via* singlet O_2 in supercritical CO_2, *Chem. Commun.*, **2008**, 4457–4459.

[236] R. A. Bourne, X. Han, M. Poliakoff, M. W. George, Cleaner continuous photo-oxidation using singlet oxygen in supercritical carbon dioxide, *Angew. Chem. Int. Ed.*, **2009**, 48, 5322–5325.

[237] N. Avcibasi, S. Icli, Photochemical reactions of α-terpinene and acenaphthene under concentrated sunlight, *Turk. J. Chem.*, **2003**, 27, 1–7.

[238] M. Al-Rawashdeh, V. Hessel, P. Löb, K. Mevissen, F. Schönfeld, Pseudo 3-D simulation of a falling film microreactor based on realistic channel and film profiles, *Chem. Eng. Sci.*, **2008**, 63, 5149–5159.

[239] R. H. Perry, D. W. Green, Eds., Perry's Chemical Engineers' Handbook, 7th ed., *McGraw-Hill: New York*, **1997**.

[240] M. H. H. Van Dam, J.-P. Corriou, N. Midoux, A.-S. Lamine, C. Roizard, Modelling and measurement of sulphur dioxide absorption rate in a laminar falling film reactor, *Chem. Eng. Sci.*, **1999**, 54 (21), 5311–5318.

[241] L. D. Schmidt, Eds., The engineering of chemical reactions, 2nd ed., *Oxford University Press: Oxford*, **2004**.

[242] K. Fischer and M Wilken, Experimental determination of oxygen and nitrogen solubility in organic solvents up to 10 MPa at temperatures between 298 K and 398 K, *J. Chem. Thermodynamics*, **2001**, 33, 1285–1308.

[243] F. Wilkinson, W. P. Helman and A. B. Ross, Rate constants for the decay and reactions of the lowest electronically excited singlet state of molecular oxygen in solution. An expanded and revised compilation, *J. Phys. Chem. Ref. Data*, **1995**, 24 (2), 663–678.

[244] L. M. Stephenson, D. G. Whitten, G. F. Vesley, G. S. Hammond, Conjugated dienes as quenchers for excited singlet states of aromatic hydrocarbons[1], *J. Am. Chem. Soc.*, **1996**, 88, 3665–3666.

[245] G. O. Schenck, K. Ziegler, Die synthese des ascaridols, *Naturwissenschaften*, **1944**, 32, 157.

[246] D. Murtinho, M. Pineiro, M. M. Pereira, A. M. D. Gonsalves, L. G. Arnaut, M. D. Miguel and H. D. Burrows, Novel porphyrins and a chlorin as efficient singlet oxygen photosensitizers for photooxidation of naphthols or phenols to quinones, *J. Chem. Soc., Perkin Trans. 2*, **2000**, 12, 2441–2447.

[247] S. Croux, M. T. Maurette, M. Hocquaux, A. Ananides, A. M. Braun and E. Oliveros, Kinetic parameters of the reactivity of dihydroxynaphthalenes with singlet oxygen, *New J. Chem.*, **1990**, 14, 161–167.

[248] For *rac*-Juglomycin A, see: G. A. Kraus and P. Liu, A racemic synthesis of the novel antibacterial agent Juglomycin A**,** *Synth. Commun.*, **1996**, 26 (23), 4501–4506.

[249] For Urdamycinone B, see: G. Matsuo, Y. Miki, M. Nakata, S. Matsumura and K. Toshima, Total synthesis of C-Glycosylangucycline, Urdamycinone B, using an unprotected sugar, *J. Org. Chem.*, **1999**, 64 (19), 7101–7106.

[250] For *rac*-Frenolicin B, see: P. Contant, M. Haess, J. Riegl, M. Scalone and M. Visnick, Synthesis of racemic frenolicin B and 5-epi-frenolicin B via intramolecular palladium-catalyzed aryloxycarbonylation, *Synthesis*, **1999**, 5, 821–828.

[251] For (+)-Nocardione A, see: D. L. J. Clive, S. P. Fletcher, L. Dazhan, Formal radical cyclization onto benzene rings: a general method and its use in the synthesis of ent-nocardione A**,** *J. Org. Chem.*, **2004**, 69 (10), 3282–3293.

[252] For Aloesaponarin I, see: S. J. Bingham and J. H. P. Tyman, The synthesis of kermesic acid and isokermesic acid derivatives and of related dihydroxyanthraquinones*, J. Chem. Soc., Perkin Trans. 1*, **1997**, 24, 3637–3642

[253] For (+)-Rubiginone B_2, see: J. Motoyoshiya, Y. Masue, G. Iwayama, S. Yoshioka, Y. Nishii and H. Aoyama, A facile synthesis of the angucyclinone antibiotic (+)-rubiginone B_2 involving the BF_3-mediated Diels-Alder reaction of Juglone, *Synthesis*, **2004**, 13, 2099–2102.

[254] For Angucyclines in general, see: M. C. Carreno and A. Urbano, Recent advances in the synthesis of angucyclines, *Synlett*, **2005**, 1, 1–25.

[255] T. Wakamatsu, T. Nishi, T. Ohnuma and Y. Ban, A Convenient synthesis of Juglone via neutral salcomine oxidation, *Synth. Commun.*, **1984**, 14, 1167–1173.

[256] O. Suchard, R. Kane, B. J. Roe, E. Zimmermann, C. Jung, P. A. Waske, J. Mattay and M. Oelgemöller, Photooxygenations of 1-naphthols: an environmentally friendly access to 1,4-naphthoquinones, *Tetrahedron*, **2006**, 62, 1467–1473.

[257] M. Oelgemöller, N. Healy, L. de Oliveira, C. Jung and J. Mattay, Green photochemistry: solar-chemical synthesis of Juglone with medium concentrated sunlight, *Green Chem.*, **2006**, 8, 831–834.

[258] P. Esser, B. Pohlmann, H.-D. Scharf, The photochemical synthesis of fine chemicals with sunlight, *Angew. Chem., Int. Ed.*, **1994**, 33 (20), 2009–2023.

[259] M. Luiz, A. T. Soltermann, A. Biasutti and N. A. Garcia, A kinetic study on singlet molecular oxygen ($O_2(^1\Delta_g)$) generation and quenching by dihydroxynaphthalenes, *Can. J. Chem.*, **1996**, 74 (1), 49–54.

[260] H. J. Duchstein and G. Wurm, Juglone formation, an indicator reaction for molecular activated oxygen in the singlet state, *Arch. Pharm.*, **1984**, 317 (9), 809–812.

[261] K. Gollnick, A. Griesbeck, Singlet oxygen photooxygenation of furans: isolation and reactions of (4+2)-cycloaddition products (unsaturated sec.-ozonides), *Tetrahedron*, **1985**, 41 (11), 2057–2068.

[262] G. O. Schenck, Photochemische reaktionen II. Über die unsensibilisierte und photosensibilisierte autoxydation von furanen, *Justus Liebigs Ann. Chem.*, **1953**, 584 (1), 156–176.

[263] M. E. Bouamri, J. P. Gorrichon, A. M. Braun, E. Oliveros, The reactivity of citronellol and α-thujene with singlet oxygen. Rate constants of chemical reaction and physical quenching, *Photochem. Photobiol.*, **1991**, 54 (4), 619–623.

[264] G. Ohloff, E. Klein, G. O. Schenck, Darstellung von "rosenoxyden" und anderen hydropyran-derivaten über photohydroperoxyde, *Angew. Chem.*, **1961**, 73 (16), 578.

[265] H. Görner, Photoreactions of 1,4-Naphthoquinones: effects of substituents and water on the intermediates and reactivity, *Photochem. Photobiol.*, **2005**, 81 (2), 376–383.

[266] H. Görner, Photoprocesses of *p*-naphthoquinones and vitamin K_1: effects of alcohols and amines on the reactivity in solution, *Photochem. Photobiol. Sci.*, **2004**, 3 (1), 71–78.

[267] C. W. Rees and C. R. Sabet, The condensation of phthalaldehydic acid and related compounds with various heterocyclic systems, *J. Chem. Soc.*, **1965**, 687–691.

[268] K. Heidenbluth, H. Tönjes and R. Scheffler, Isoindolines. III. Grignard reaction of phthalimides, *J. Parkt. Chem.*, **1965**, 30, 204–217.

[269] Y. J. Lee, R. Ling, P. S. Mariano, U. C. Yoon, D. U. Kim, S. W. Oh, Exploratory studies of H-atom abstraction and silyl-transfer photoreactions of silylalkyl ketones and (silylalkyl)phthalimides, *J. Org. Chem.*, **1996**, 61, 3304–3314.

[270] N. J. Miles, P. G. Sammes, P. D. Kennewell and R. Westwood, On the double bond isostere of the peptide bond: preparation of modified di- and tripeptides incorporating praline and alanine analogues, *J. Chem. Soc. Perkin. Trans. 1*, **1985**, 2299–2305.

[271] O. M. Moradei and L. A. Paquette, Reaction type: acetal formation, *Org. Synth.*, **2003**, 80, 66.

[272] Y. Morita, H. Tokuyama, T. Fukuyama, Stereocontrolled total synthesis of (–)-kainic acid. Regio- and stereoselective lithiation of pyrrolidine ring with the (+)-sparteine surrogate, *Org. Lett.*, **2005**, 7 (20), 4337–4340.

[273] S. M. Ribeiro, A. C. Serra, A. M. d'A. R. Gonsalves, Covalently immobilized porphyrins on silica modified structures as photooxidation catalysts, *J. Mol. Catal. A: Chem.*, **2010**, 326, 121–127.

Appendix

List of Publications

Refereed publications:

1. A. Yavorskyy, **O. Shvydkiv**, N. Hoffmann, K. Nolan, M. Oelgemöller, "Parallel microflow-photochemistry: process optimization, scale-up and library synthesis", *Org.Lett.*, **2012**, 14 (17), 4342–4345.
2. **O. Shvydkiv**, C. Limburg, K. Nolan, M. Oelgemöller, "Synthesis of Juglone (5-hydroxy-1,4-naphthoquinone) in a falling film microreactor", *J. Flow Chem.*, **2012**, 2, 52–55.
3. A. Yavorskyy, **O. Shvydkiv**, C. Limburg, K. Nolan, Y. M. C. Delauré, M. Oelgemöller, "Photooxygenations in a bubble column reactor", *Green Chem.*, **2012**, 14, 888–892.
4. M. Oelgemöller and **O. Shvydkiv**, "Recent advances in microflow photochemistry", *Molecules*, **2011**, 16, 7522–7550.
5. **O. Shvydkiv**, K. Nolan, M. Oelgemöller, "Microphotochemistry – 4,4'-Dimethyoxybenzophenone mediated photodecarboxylation reactions of phthalimides", *Beilstein J. Org. Chem.*, **2011**, 7, 1055–1063 (by invitation, special issue on Microflow Chemistry).
6. **O. Shvydkiv**, A. Yavorskyy, S. B. Tan, K. Nolan, N. Hoffmann, A. Youssef, M. Oelgemöller, "Microphotochemistry – a reactor comparison study using the photosensitized addition of isopropanol to furanones as a model reaction", *Photochem. Photobiol. Sci.*, **2011**, 10, 1399–1404.
7. A. Yavorskyy, **O. Shvydkiv**, K. Nolan, N. Hoffmann, M. Oelgemöller, "Photosensitized addition of isopropanol to furanones in a continuous-flow dual capillary microreactor", *Tetrahedron Lett.*, **2011**, 52, 278–280.
8. **O. Shvydkiv**, A. Yavorskyy, K. Nolan, A. Youssef, E. Riguet, N. Hoffmann, M. Oelgemöller, "Photosensitized addition of isopropanol to furanones in a 365 nm UV-LED microchip", *Photochem. Photobiol. Sci.*, **2010**, 9, 1601–1603.
9. **O. Shvydkiv**, S. Gallagher, K. Nolan, M. Oelgemöller, "From conventional to micro-photochemistry: photodecarboxylation reactions involving phthalimides", *Org. Lett.*, **2010**, 12, 5170–5173.
10. S. B. Tan, **O. Shvydkiv**, J. Fielder, F. Hatoum, K. Nolan, M. Oelgemöller, "Photodecarboxylative additions of α-thioalkyl-substituted carboxylates to alkyl phenylglyoxylates", *Synlett*, **2010**, 2240–2243.

Book chapter:

1. **O. Shvydkiv**, M. Oelgemöller, "Microphotochemistry – photochemical synthesis in microstructured reactors" in: Handbook of organic photochemistry and photobiology, 3. edition, A. G. Griesbeck, M. Oelgemöller, F. Ghetti (Eds.), CRC Press, Boca Raton **2012**, in print (scheduled January 2012).

List of Presentations

Chemistry seminar:

1. **O. Shvydkiv**, A. Yavorskyy, K. Nolan, M. Oelgemöller, "Microphotochemistry-photochemistry in microstructured and continuous flow devices", Chemistry Seminar, James Cook University, School of Pharmacy and Molecular sciences, Townsville (Australia), 5th August 2011.

Oral presentations:

1. **O. Shvydkiv**, A. Yavorskyy, K. Nolan, M. Oelgemöller, "Microphotochemistry: photodecarboxylations of phthalimides and photooxygenations of alpha-terpinene as model reactions in microstructured reactors", Central European Conference on Photochemistry – CECP 2010, Bad Hofgastein (Austria), 8 February 2010.
2. **O. Shvydkiv**, A. Yavorskyy, K. Nolan, M. Oelgemöller, "Micro-photochemistry - a new resources-efficient synthesis tool approach", Green Chemistry in Ireland: including highlights of Environmental Technology projects funded by the EPA, Dublin City University, Dublin (Ireland), 15 April 2010.
3. **O. Shvydkiv**, A. Yavorskyy, K. Nolan, M. Oelgemöller, "Microphotochemistry-photochemistry in microstructured and continuous flow devices", RSC Photochemistry and Photochemical Techniques meeting, University College Dublin, Trinity College Dublin, Dublin (Ireland), 16-18 May 2011.
4. **O. Shvydkiv**, A. Yavorskyy, K. Nolan, M. Oelgemöller, "Microphotochemistry-photochemistry in microstructured and continuous flow devices", 63rd Irish Universities Chemistry Research Colloquium 2011, University College Dublin, Dublin (Ireland), 23-24th June 2011.
5. **O. Shvydkiv**, A. Yavorskyy, K. Nolan, M. Oelgemöller, "Microphotochemistry-an efficient environmentally friendly technology", 9th Annual EPA Postgraduate Seminar, Gresham Hotel, Dublin (Ireland), 17th November 2011.

Poster presentations:

1. M. Oelgemöller, **O. Shvydkiv**, A. Yavorskyy, S. Gallagher, K. Nolan, "Microphotochemistry – The Photochemistry of the Future?", 6th Asian Photochemistry Conference, Wellington (New Zealand), 14-18 November 2010.
2. **O. Shvydkiv**, A. Yavorskyy, M. Macka, M. Oelgemöller, K. Nolan, "Microphotochemistry: photodecarboxylations of phthalimides and photooxygenations of alpha-terpinene as model reactions in microstructured reactors", EPA National Research Conference, Croke Park Conference Center, Dublin, Ireland, 23 June 2010.
3. A. Yavorskyy, **O. Shvydkiv**, M. Macka, M. Oelgemöller, K. Nolan, "Micro-flow photochemistry – new reactor design", EPA National Research Conference, Croke Park Conference Center, Dublin, Ireland, 23 June 2010.